SUBCOOLED FILM BOILING IN NON-AQUEOUS FLUIDS

BY

NAJMEDDINE HAMMOUDA

A dissertation submitted to the School of Graduate Studies and Research of the Ottawa-Carleton Institute for Mechanical and Aeronautical Engineering at the University of Ottawa in partial fulfilment of the requirements for the degree of Doctor of Philosophy in Mechanical Engineering.

UNIVERSITÉ D'OTTAWA
UNIVERSITY OF OTTAWA

Ottawa-Carleton Institute for Mechanical and Aeronautical Engineering
University of Ottawa, Ottawa, Ontario, Canada K1N 6N5
1996

ISBN 0-612-15721-0

UNIVERSITÉ D'OTTAWA
UNIVERSITY OF OTTAWA

ABSTRACT

Subcooled film boiling has been investigated experimentally for vertical up-flow in a directly heated tube using the refrigerants R-12, R-22 and R-134a as test fluids. The data cover a mass flux range of 530 to 3000 $kgm^{-2}s^{-1}$, an inlet subcooling range of 6 to 28°C and a pressure range of 0.83 to 1.4 MPa (corresponding to an equivalent water pressure range of 5 to 7 MPa, based on an equal liquid-to-vapour density ratio). To the author's knowledge, these are the first flow film boiling data ever obtained for R-134a and R-22. The results show strong effects of mass flux, inlet subcooling and pressure on the heat transfer coefficient. Also, the data exhibit complex trends of the heat transfer coefficient as a function of thermodynamic equilibrium quality. Because of the wide range of conditions covered in this study, a systematic examination of the effect of flow parameters and fluid properties on the heat transfer coefficient was performed, and this has provided a unique insight into the heat transfer mechanisms.

During this study, a number of post-CHF heat-transfer prediction methods have been assessed over a wide range of flow conditions. The prediction methods have been compared against the data obtained from this study and AECL PDO data bank. None of the assessed prediction methods is able to adequately predict the heated surface temperature for all flow conditions. For dispersed flow film boiling (DFFB), the Groeneveld-Delorme correlation provides accurate predictions at moderate-to-high pressures (7-20 MPa) and medium-to-high mass fluxes (1000-5000 $kgm^{-2}s^{-1}$). However, at low mass fluxes the correlation underpredicts the data and occasionally exhibits an incorrect parametric trend. The Shah correlation gives comparable prediction accuracy to the Groeneveld-Delorme correlation, but is not applicable for conditions of mass fluxes beyond

3442 $kgm^{-2}s^{-1}$ and thermodynamic qualities above 1. Furthermore, it was presented graphically and hence is difficult to apply in a computer code. However, it has the advantage of being valid for various fluids, whereas the Groeneveld-Delorme correlation is primarily applicable for steam-water flow. Phenomenological models provide worse prediction accuracy than the empirical equations. Among them, the Moose and Ganić, the Saha, and the Yoder and Rohsenow models yield relatively satisfactory agreement with the data. However, these models collapse abruptly at very high mass flux or/and high-pressure conditions. This is mainly caused by the limited applicability of the constitutive relations employed within these models. The constitutive equations often incorporate empirical parameters that are valid onlv for a narrow range of flow conditions.

For inverted annular film boiling (IAFB), none of the existing models or correlations is capable of providing accurate predictions over a wide range of flow conditions. Although a number of models have been developed for IAFB, the empirical nature of their constitutive equations prevents their application to wide ranges of flow conditions. Most models are valid only at low-pressure conditions, where data on interfacial parameters are available.

A two-fluid model has been developed to predict the wall temperature of a tube during IAFB. This model correctly accounts for the effects of flow variables such as mass flux, inlet subcooling, heat flux, and pressure. One of the major components in this model is the relations for shear stress and heat transfer rates. A unique methodology is utilized to derive these relations. This method is based on the concept of reducing the degrees of freedom of the system: relationships between relevant flow variables are established based on the physical mechanisms in IAFB that satisfy thermodynamic limits. Also, a hybrid post-CHF model is derived by combining the two-fluid model of IAFB with the slightly modified Moose and Ganić [1982] DFFB model, to predict heated

surface temperatures over the whole film boiling region.

Comparisons between the two-fluid model predictions and experimental data from four fluids (water, Freon-12, Freon-22, and Freon-134a) have shown very good agreement for a wide range of flow conditions. The comparisons have resulted in overall root-mean-square (RMS) errors of 14.90%, 5.67%, 6.58%, and 6.19% with the data of water, Freon-12, Freon-22, and Freon-134a, respectively. The model has shown better performance than all the IAFB prediction methods assessed during the course of this study. Also, predictions from the hybrid model have been compared to Freon data, and excellent agreement with the data has been obtained.

ACKNOWLEDGEMENTS

One of my most satisfying efforts in putting the finishing touches to this thesis is having the opportunity to express my gratitude to the people who have supported me during the course of this study. In that respect, I am very grateful to Professor S. C. Cheng for not only his academic support but also for caring for his students beyond professorial obligations. I am also deeply grateful to Dr. D. C. Groeneveld, adjunct professor and my co-supervisor, for his guidance during this study. Despite his hectic schedule, he could always find time to discuss my work. I also thank Dr. X. C. Huang, post-doctoral fellow, for the intelligent suggestions he provided during the experimental and theoretical stages of this study.

I am very delighted to take this opportunity to thank my friend Dr. R. -M. Tain, post-doctoral fellow and former student of Professor S. C. Cheng, for making my study at the University of Ottawa enjoyable. I will not forget the help he provided me with when I first started this program at the university.

The financial support provided by the Natural Science and Engineering Research Council of Canada and by AECL is gratefully acknowledged.

Table of Contents

NOMENCLATURE

a	Thermal diffusivity	m^2s^{-1}
A	Area	m^2
Bo	Boiling number	–
C_D	Drag coefficient	–
C_p	Specific heat capacity at constant pressure	$Jkg^{-1}K^{-1}$
D	Tube diameter	m
D_h	Equivalent hydraulic diameter	m
d	Droplet diameter	m
f	Fanning friction factor	–
F_{dc}	Enhancement factor due to droplet cooling (Eq. (7.3.1))	–
F_o	Fourier number	–
Fr	Froude number (Eq. (7.3.3))	–
g	Acceleration due to gravity	ms^{-2}
g_c	Conversion factor (= 32.2)	lbm ft/lb s^2
G	Mass flux	$kgm^{-2}s^{-1}$
Gr	Grashof number	–
h	Heat transfer coefficient	$Wm^{-2}K^{-1}$
h_{fg}	Latent heat of vaporization	Jkg^{-1}

h_l	Enthalpy of subcooled liquid	Jkg^{-1}
h_g	Enthalpy of saturated vapour	Jkg^{-1}
h_v	Enthalpy of superheated vapour	Jkg^{-1}
k	Thermal conductivity	$Wm^{-1}K^{-1}$
L	Heated length	m
n	Droplet number density	m^{-3}
Nu	Nusselt number	–
P	Pressure	Pa
P_c	Critical pressure	Pa
P_h	Heated perimeter	m
P_r	Reduced pressure ($=P/P_c$)	–
Pr	Prandtl number	–
q	Heat flux	Wm^{-2}
Q	Volumetric flow rate	m^3s^{-1}
R	Tube radius	m
Re	Reynolds number	–
T	Temperature	°C
u,U	Velocity	ms^{-1}
U_r	Relative velocity between vapour and liquid	ms^{-1}
S	Slip ratio	–
W	Mass flow rate	kgs^{-1}
W'	Rate of liquid evaporation per unit length	$kgm^{-1}s^{-1}$

W''	Rate of liquid evaporation per unit area	$kgm^{-2}s^{-1}$
We	Weber number	–
x	Flow quality (vapour weight fraction)	–
y	Radial distance from the wall	m
z	Axial distance from inlet	m

Greek

α	Void fraction	–
δ	Vapour film thickness	m
Δh	Average enthalpy difference between vapour and liquid	Jkg^{-1}
ΔT	Temperature difference (usually with respect to saturation)	°C
ϵ	Emissivity	–
ϵ_H	Turbulent diffusivity of heat transfer	m^2s^{-1}
ϵ_M	Turbulent diffusivity of momentum	m^2s^{-1}
Γ	Vapour generation source function	$kgm^{-3}s^{-1}$
λ	Enhancement parameter for interfacial disturbances	–
λ_c	Minimum wave length for Taylor instability	m
μ	Viscosity	Nsm^{-2}
ν	Kinematic viscosity	m^2s^{-1}
ξ	Velocity profile parameter in Eq. (5.6.1)	–
Θ_w	Wall superheat (T_w-T_v) in Eq. (8.4.1)	°C
Θ_v	Vapour superheat (T_v-T_{sat}) in Eq. (8.4.2)	°C

ρ	Density	kgm^{-3}
σ	Surface tension	Nm^{-1}
σ'	Stefan-Boltzman constant(=5.6697E-8)	$Wm^{-2}K^{-4}$
τ	Shear stress	Nm^{-2}

Subscripts

1Φ	Single-phase flow
2Φ	Two-phase flow
a	Actual
bulk	At bulk fluid conditions
c	Convection
crit	Critical
CHF	Critical heat flux
d	Droplet
dc	Droplet cooling
DNB	Departure from nucleate boiling
do	Dryout
eff	Effective
eq	Equilibrium
f	Saturated liquid
FB	Film boiling
g	Saturated vapour

hom	Homogeneous
i	Interface
i-l	Interface to liquid
l	Subcooled liquid
MFB	Minimum film boiling
Q	At quench front
r	Reduced
rad	Radiation
sat	Saturation
v	Superheated vapour
vf	At film temperature
v-d	Vapour to droplet
v-i	Vapour to interface
w	Wall
w-d	Wall to droplet
w-i	Wall to interface
w-v	Wall to vapour

Superscript

+	Non-dimensional parameter

LIST OF TABLES

LIST OF FIGURES

Chapter 1 INTRODUCTION

1.1 Background

Film boiling is a boiling heat transfer mode in which only the vapour phase is in contact with the heated surface. It occurs when the minimum film boiling temperature is exceeded. High surface temperatures are generally associated with this heat transfer mode in heat flux controlled systems (because of the poor heat transfer capability of vapour); an accurate prediction method is essential to assess the risk of heated-surface failure.

Flow film boiling is generally divided into inverted annular film boiling (IAFB), encountered at low qualities (usually at void fractions below 50%), and dispersed flow film boiling (DFFB), encountered at high qualities (void fractions beyond 80%). IAFB is characterized by high surface temperatures, and consists of a continuous liquid core at the centre of the channel, surrounded by a vapour blanket covering the heated surface. DFFB is characterized by a moderate surface temperature increase, and consists of a continuous vapour core with entrained liquid droplets. The DFFB regime can also be created from the break-up of the liquid core downstream of the IAFB regime. Depending on the flow conditions, thermal non-equilibrium between vapour and liquid can be a significant factor, and can result in a high vapour superheat. A transition region with churns of liquid (in various sizes) flowing in the vapour core is anticipated at void fractions between 50 and 80%. It is a highly unstable region, and has not been studied in detail.

Film boiling heat transfer is important in the safety analysis of postulated loss-of-coolant

accidents (LOCA's) of water-cooled nuclear reactors: During a LOCA, a portion of the fuel bundle can experience film boiling. Film boiling could also occur during a loss-of-regulation accident (LORA), where the reactor power accidentally increases. Therefore, the film boiling regime is important in reactor safety studies, as it is during this boiling mode that high fuel sheath temperature is usually encountered, and burnout may occur. Also, the post-CHF regime is of considerable practical interest in many other applications, such as steam generators, evaporators, cryogenic systems and metallurgical processing. Consequently, there has been a considerable interest in this regime in recent years.

This thesis discusses several aspects of film boiling. Chapter 2 describes the basic heat transfer mechanisms in film boiling. Chapter 3 describes the different types of IAFB correlations and models, and summarizes in tabular form (Tables 3.1 and 3.2) the IAFB correlations and models available in the literature. Chapter 4 examines two commonly used IAFB correlations: the Bromley equation [1950] and the Berenson equation [1961], both of which are derived for pool film-boiling conditions but are frequently extended to flow film-boiling conditions, based on some modifications. Chapter 5 describes three types of IAFB models, i.e., the Denham model [1984], based on a modification to the Bromley equation, the Dougall-Rohsenow model [1963], based on the turbulent boundary-layer theory, and the Analytis-Yadigaroglu model [1987], based on a two-fluid formulation. Chapter 6 describes three types of heat-transfer prediction methods in the DFFB regime: empirical equations, phenomenological models and mechanistic models. Chapter 7 describes three DFFB heat transfer correlations: the Dougall-Rohsenow correlation [1963], the Groeneveld-Delorme correlation [1976] and the Shah correlation [1980]. The Dougall-Rohsenow correlation is a thermal-equilibrium type of correlation, and the other two are a thermal non-equilibrium type.

Chapter 8 examines several models for the DFFB regime, including the Saha model [1980] and the Moose-Ganić model [1982]. Chapter 9 describes different experimental methods employed in subcooled film boiling experiments, and provides a summary of the parametric trends observed during subcooled film boiling. Chapter 10 provides a detailed description of the experimental equipment and procedure used during this study. Chapter 11 analyzes and discusses the experimental results obtained during this study. Chapters 12 and 13 assess the prediction accuracy of different equations and models by comparing their predictions against the Chalk River Laboratories (CRL) post-dryout (PDO) data base and the data obtained from this study. Chapter 14 provides the theoretical analysis for the development of IAFB and hybrid film boiling models. Chapter 15 discusses the IAFB model trends and the model's sensitivity to some flow parameters. Chapter 16 assesses the prediction accuracy of the IAFB and the hybrid film boiling models by comparing their predictions against the CRL data base and data from this study. Chapter 17 gives conclusions resulting from the study, and makes recommendations for future work.

1.2 Objectives

The main objectives of this thesis are:

1. To review and assess the predictive capability of selected IAFB and DFFB models and correlations. A number of heat transfer prediction methods have been suggested for both IAFB and DFFB. They vary from simple correlations considering only the single-phase heat transfer from the heated surface to vapour, to sophisticated two-fluid models that account for the detailed heat transfer mechanisms from the heated surface to both the liquid and vapour phases. In many cases, however, these prediction methods are valid only for conditions within their respective data base, and cannot be extended. In this study, several

prediction methods are reviewed and assessed using data from the CRL data bank and data obtained from this study. Their prediction accuracy and parametric trends are examined over a wide range of flow conditions, particularly at medium-to-high pressures and moderate-to-high mass fluxes (these conditions could be of interest to CANDU reactor safety analysis, i.e., LORA conditions). This study emphasizes the phenomenological models and correlations that account for thermal non-equilibrium in the vapour for DFFB, and two-fluid models for IAFB. The effect of changing system parameters (i.e., pressure, mass flux and quality) on heat transfer is examined and compared to the parametric trends displayed by the data. If vapour superheat data are available at conditions of interest, the correlations and models are assessed not only for heat flux and wall temperature predictions, but also for the vapour superheat.

2. To develop a hybrid model for prediction over the complete post-CHF region (from IAFB to DFFB). This includes the development of a new one-dimensional two-fluid model for the IAFB regime, and improvement upon an existing one-dimensional model for the DFFB regime (Moose and Ganić [1982] model).

3. To investigate subcooled film boiling experimentally for vertical up-flow in a directly heated tube using the refrigerants R-12, R-22 and R-134a as test fluids.

Figure 1.1 summarizes in a block diagram the work plan of this study.

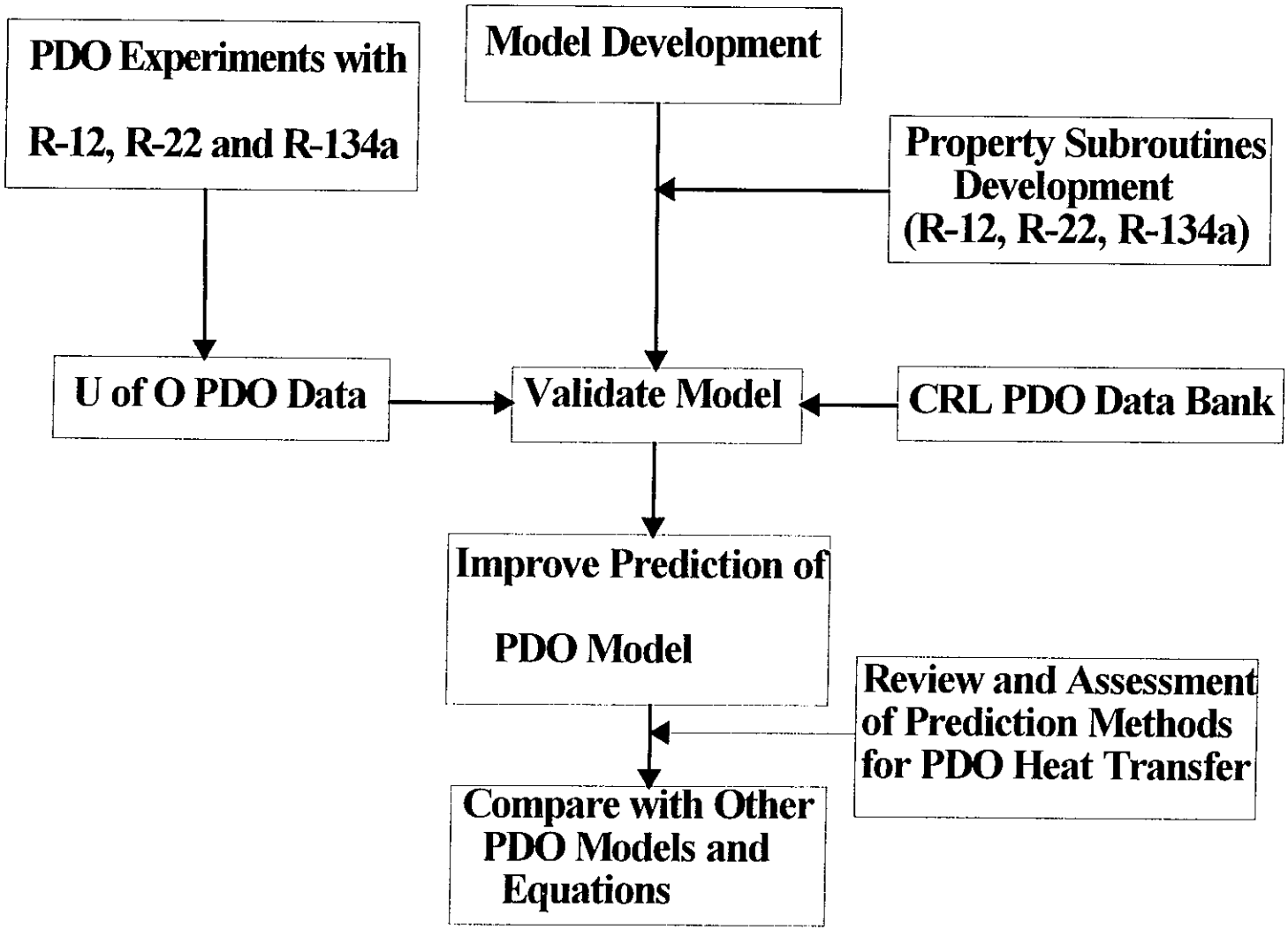

Figure 1.1 Block diagram of the thesis plan.

Chapter 2 FILM BOILING MECHANISMS

2.1 General

Figure 2.1 shows a typical pool boiling curve where the heat flux is plotted against the wall superheat. The general shape of the curve is the same for all fluids, and there are four basic regimes:

a) Single-phase natural-convection up to point A: the heat flux, q_w, is predicted by the single phase natural convection theories.

b) Nucleate boiling regime between points A and C: boiling begins at point A, where the first bubble forms at the heated surface. At point B, bubbles depart and rise to a certain distance before condensing in the subcooled liquid. At higher heat flux, beyond point B, the frequency of bubble generation increases and many columns and jets of bubbles rise at a great rate from many nucleation sites. At point C, the maximum heat flux, sometimes known as critical heat flux (CHF) or burnout, is reached. At this stage, the vapour generation rate becomes so high that it prevents the liquid from reaching the surface. The surface becomes covered with a vapour film and the heat transfer coefficient and heat flux start to decrease.

c) The transition boiling regime, which can only be achieved by a temperature controlled heater, exists between points C and L, and is characterized by unstable film boiling and nucleate boiling alternately occurring. The vapour film blanketing and collapse occur continuously, due to convection currents and surface tension. As the surface temperature is

increased, the vapour film blanketing occurs more frequently and over a large surface area until, at point L, it is continuous and lower heat flux is reached. The minimum film boiling (MFB), point L, is frequently referred to as the Leidenfrost point. At this stage, the surface is completely covered with a blanket of vapour and the heat flux reaches its minimum value.

d) The film boiling regime exists at $T>T_{MFB}$, to the right of point L, where the vapour film covers the heated surface and impedes heat transfer. At higher surface temperatures, radiation becomes important and the heat flux rate is enhanced by radiation across the vapour film.

In the single phase heat transfer region (up to point A in Fig. 2.1), experimental heat transfer data are in good agreement with free and forced convection prediction methods. Unfortunately, in the nucleate boiling range, between B and C, heat transfer prediction is subject to uncertainties, and specific experiments are needed. The heat transfer also depends strongly on surface conditions, such as the availability of vapour nucleation sites. However, the CHF at point C can be predicted reasonably well, due to the existence of general prediction methods. The prediction of the minimum heat flux at the Leidenfrost point L is also reasonably estimated by the theory. In the transition boiling region, where the boiling phenomenon alternates between nucleate boiling (with liquid-wall contact) to film boiling (no liquid-wall contact), no sound theoretical predictions are available. This is a highly unstable region and heat transfer equipment rarely operates within this region. In general, film boiling theory of pool boiling is quite adequate, due to the extensive studies conducted in this area in the past years.

The boiling regimes in pool boiling are classified as nucleate boiling, transition boiling, and film boiling. Under flow boiling conditions, the classification of boiling regimes is more complex

than for pool boiling (Fig. 2.2). At low qualities, there is resemblance between flow boiling and pool boiling. IAFB is usually observed after departure from the nucleate boiling (DNB) regime. Correlations derived for pool boiling could be used, with some modifications, to predict the heat transfer in IAFB. Under certain conditions, IAFB is succeeded by DFFB. In this regime, the heat transfer mechanism is that of interaction between the wall, the vapour, and the droplets.

At higher qualities, the behaviour of flow boiling is noticeably different from that of pool boiling or low-quality flow boiling. Here the phase distribution no longer resembles pool boiling. Suppression of nucleate boiling is possible at high flow rates. A certain point may be reached where a fundamental transition in the mechanism of heat transfer takes place: evaporation at the liquid-vapour interface replaces the process of boiling. This change of character of the heat transfer mechanism is, perhaps, caused by the high turbulence at the vapour-liquid interface due to the high vapour velocity in the core. The suppressed nucleate boiling region terminates at the CHF location. The CHF is caused by the complete depletion of the liquid film on the wall, due to the mechanisms of droplet entrainment, droplet deposition, and evaporation at the liquid-vapour interface. DFFB begins just downstream of the CHF point. In this region, at high wall temperatures, heat transfer may be due primarily to the transfer of heat from the wall to the vapour and heat transfer by radiation to droplets, whereas at lower wall temperatures heat transfer can be considerably enhanced as droplets may wet the wall. Fig. 2.3 depicts the post-dryout regimes at low quality and high quality flows.

2.2 Pool Film Boiling

In pool film boiling, a continuous blanket of vapour film covers the heated surface. Heat is conducted and radiated from the heating surface through the vapour film, which presents the major

resistance to heat transfer. Because of its simplicity, this regime is the most amenable to analysis.

In this region, the minimum value of the heat flux occurs at the lower limit of stable film boiling (or at the end of the transition boiling region). At this point, the breakdown of the continuous vapour film and the onset of liquid-solid interaction (wetting) is observed. Based on hydrodynamic stability theory, Berenson [1961] modified Zuber's [1958] analysis and arrived at the following relation for the minimum heat flux from a horizontal surface:

$$q_{MFB} = 0.09\ \Delta h\ \rho_{vf}\left[\frac{g(\rho_l - \rho_v)}{\rho_l + \rho_v}\right]^{1/2}\left[\frac{\sigma}{g(\rho_l - \rho_v)}\right]^{1/4} \qquad (2.2.1)$$

For definition of the symbols, please refer to the nomenclature.

Also, Berenson [1961] arrived at the following relation for ΔT_{MFB} at the minimum heat flux point:

$$\Delta T_{MFB} = 0.127\ \frac{\rho_{vf}\ \Delta h}{k_{vf}}\left[\frac{g(\rho_l - \rho_v)}{\rho_l + \rho_v}\right]^{2/3}\left[\frac{\sigma}{g(\rho_l - \rho_v)}\right]^{1/2}\left[\frac{\mu_f}{(\rho_l - \rho_v)}\right]^{1/3} \qquad (2.2.2)$$

Under some conditions, a jump to the nucleate boiling region may occur before q_{MFB} is reached as an object cools down from the film boiling region [Witte and Lienhard, 1982].

2.3 Minimum Film Boiling (MFB)

For temperature controlled system, the MFB temperature defines the boundary between the high temperature region, where inefficient film boiling heat transfer takes place, and the lower temperature region, where the more efficient transition boiling occurs. For heat flux controlled system, MFB defines the point at which a jump from film boiling to nucleate boiling occurs as heat flux is lowered. Hence determination of the MFB temperature is of great importance in many industrial applications. Also, it provides a lower limit to the application of film boiling correlations.

In the literature, a variety of terms have been used to describe the MFB phenomenon. Among these terms are minimum film boiling, rewetting, film boiling collapse, Leidenfrost phenomena, sputtering and departure from film boiling.

Groeneveld [1984] gave a brief summary of the main theories proposed for the mechanisms of MFB phenomenon. One theory considers the MFB temperature as a thermodynamic property of the fluid, hence it is primarily a function of pressure. The other theory suggests that the MFB temperature is hydrodynamically controlled: the liquid-vapour interface remains separated from the heated surface as long as the vapour generation rate exceeds the vapour removal rate. Further, Groeneveld [1984] pointed out that these theories do not take into consideration the flow and geometry effects. Fig. 2.4 depicts the different types of film boiling termination.

MFB data pertaining to a vapour film collapse, during stationary IAFB, were obtained by Stewart and Groeneveld[1982], Cheng et al. [1985] and Chen et al. [1989]. Stewart and Groeneveld studied the vapour film collapse during IAFB, and film boiling termination following dispersed droplet cooling during steady state experiments. These types of MFB, also known as "true quench temperature", are unaffected by transient axial conduction, since no propagating rewetting front was present. Stewart and Groeneveld have shown that at high qualities and high flows no distinct MFB temperature could be obtained, due to the absence of a minimum in the boiling curve. They derived for water a correlation for the MFB temperature as follows:

For $x_{eq} \leq 0$ and $P \leq 9$ MPa

$$T_{MFB}\ (^{\circ}C) = 284.7 + 0.0441\,P - 3.72.10^{-6}P^2 - \frac{x_{eq}.10^4}{2.82+0.00122\,P} \qquad (2.3.1)$$

For $x_{eq} > 0$ and $P \leq 9$ MPa

$$T_{MFB}\ (^{\circ}C) = 284.7 + 0.0441\,P - 3.72\ 10^{-6}P^{2} \qquad (2.3.2)$$

For P > 9 MPa

$$T_{MFB}\ (^{\circ}C) = (\Delta T_{MFB}\ ,\ 9MPa)\left(\frac{P_{crit} - P}{P_{crit} - 9}\right) + T_{sat} \qquad (2.3.3)$$

Cheng et al. measured the "true quench temperature" and its parametric trends for subcooled water, and derived a correlation as follows:

$$T_{MFB}\ (^{\circ}C) = 169.66 + 0.1050\,P + 0.1444\,G + 3.0347\,\Delta T_{sub} \qquad (2.3.4)$$

where ΔT_{sub} represents the inlet subcooling, in °C.

Chen et al. generated more data of the MFB temperature for water of the vapour film collapse type under steady state conditions by using the directly heated hot patch technique. From their data base, a correlation was derived for the following conditions:

P: 115-6050 kPa

G: 53-1209 $kgm^{-2}s^{-1}$

x_{eq}: -0.055-0.08

$$T_{MFB}\ (^{\circ}C) = 363.6 + 38.371\,P + 0.02844\,P - 3.86.10^{-6}P^{2} + A\ \Delta T_{sub}$$

$$A = \frac{17.1}{3.3 + 0.0013\ P} \quad for\ \Delta T_{sub} \geq 0 \qquad (2.3.5)$$

$$A = 0 \quad for\ \Delta T_{sub} < 0$$

A quench temperature known as "apparent quench temperature" is sometimes confused with the "true quench temperature". The true quench temperature is always lower than the apparent quench temperature. The apparent quench temperature is the temperature recorded due to a

propagating quench front and after the "true quench phenomenon" has taken place. It is greatly affected by the axial conduction because of the rewetting front.

In his review of IAFB of water, Johannsen [1988] made the following conclusions concerning the MFB temperature:

-the data base for MFB is too scarce, and inaccurate and hence no definite conclusions can be drawn concerning the parametric trends of the MFB temperature, and

-data from different sources are inconsistent with each other, and in some instances inconsistency exists within the same data base.

2.4 Inverted Annular Film Boiling (IAFB)

In IAFB, heat is transferred from the wall to a vapour layer, and subsequently through the vapour to the liquid-vapour interface and to the liquid. Heat transfer by radiation from the wall to the liquid is also important in IAFB, and should be accounted for. The heat transfer mode across the vapour-liquid interface is by forced convective evaporation. In general, the vapour film is assumed to have a higher velocity than the liquid core, because the low-viscosity, low-density vapour flow experiences a higher acceleration than the dense core flow. Consequently, the high interfacial velocity can cause liquid entrainment from the wavy interface. Heat transfer rates during IAFB have been predicted using the modified Bromley equation for pool film boiling, turbulent-boundary-layer theories, and two-fluid models. A review of physical mechanisms in IAFB has been performed by Groeneveld [1984].

In the IAFB regime for water-steam flow at pressures lower than 10 MPa, the CHF is usually high and wall temperatures can reach extremely high values. Thus only a temperature-controlled system can be operated safely at these conditions.

2.5 Slug Flow Film Boiling

The slug flow regime is usually observed just downstream of the inverted annular flow regime. It is assumed that its formation is the result of low flow rates and low void fractions, which are too high to support inverted annular film boiling but too low to maintain dispersed flow film boiling [Groeneveld, 1984].

Chi [1966, 1967, 1970] studied slug flow film boiling, and from his data it can be inferred that the liquid core will break up into slugs which are equal in length to the most unstable wavelength of interfacial waves. The effect of subcooling is to make the liquid-vapour interface stable, therefore reducing considerably the possibility of slug flow formation. Kalinin et al. [1970] suggested that slug flow occurs due to flow oscillation. They observed from transient tests that, after the introduction of liquid to the test section, vapour generation was so great as to cause a back pressure at the liquid front. This back pressure caused the flow to decelerate and the vapour generation to decrease due to the increase in pressure. The deceleration of the flow is accompanied by separation of a liquid slug from the liquid front. Subsequently, flow and vaporization rates increase again and the process is repeated.

2.6 Dispersed Flow Film Boiling (DFFB)

Heat transfer in the DFFB regime is generally poor, except at higher mass flow/qualities. In DFFB, the heat transfer coefficient is higher than in IAFB for the same pressure, P. In DFFB, three distinct heat transfer paths have been identified: heat transfer from the wall to the vapour, from the vapour to the entrained droplets, and from the wall to the droplets. In general, direct liquid-wall heat transfer may be neglected, except at $T_{CHF} < T < T_{MFB}$, where strong evaporation of liquid due to sputtering of liquid on the heated wall is presumed to occur [Chen et al., 1984]. The CHF

temperature, T_{CHF}, represents the surface temperature below which continuous wetting of the heated surface takes place.

In DFFB, droplets entering the thermal boundary layer are more likely to evaporate than droplets in the core, because the boundary layer is superheated well above that of the vapour core [Cumo and Farello, 1967]. If the temperature of the wall is below the minimum temperature, short-term wetting of the wall may occur. Iloeje et al. [1974] illustrated this phenomenon as shown in Fig. 2.5. At temperatures above the minimum temperature, only "dry collisions" are possible [Groeneveld and Gardiner, 1977]. Bennett et al. [1967] suggested that little heat transfer may take place to small droplets which bounce back after a "dry collision". The wall-vapour heat exchange is thus improved due to these dry collisions which disturb the boundary layer. Larger droplets have a lesser resistance to deformation than smaller droplets; therefore, they tend to spread considerably upon collisions, thus enhancing both the wall-vapour and vapour-droplet heat exchange [Groeneveld and Gardiner, 1977]. If the kinetic energy of the droplets is sufficiently high, this spreading may lead to a breakup into many smaller droplets [McGinnis and Holman, 1969].

Recently, several experiments were performed to measure the vapour temperature under DFFB conditions. Data from these experiments have provided proof of thermodynamic non-equilibrium between the phases. Many prediction methods have been proposed to account for this non-equilibrium. These methods can be classified as purely empirical or phenomenological. Prediction methods pertaining to each group will be presented in this study. Reviews of prediction methods for DFFB have been performed by Andreani and Yadigaroglu [1994] and Chen [1986]. Andreani and Yadigaroglu emphasized the physical mechanisms characterizing low mass flux conditions in DFFB, while Chen concentrated on the different approaches taken to model the

complex thermalhydraulic phenomena involved.

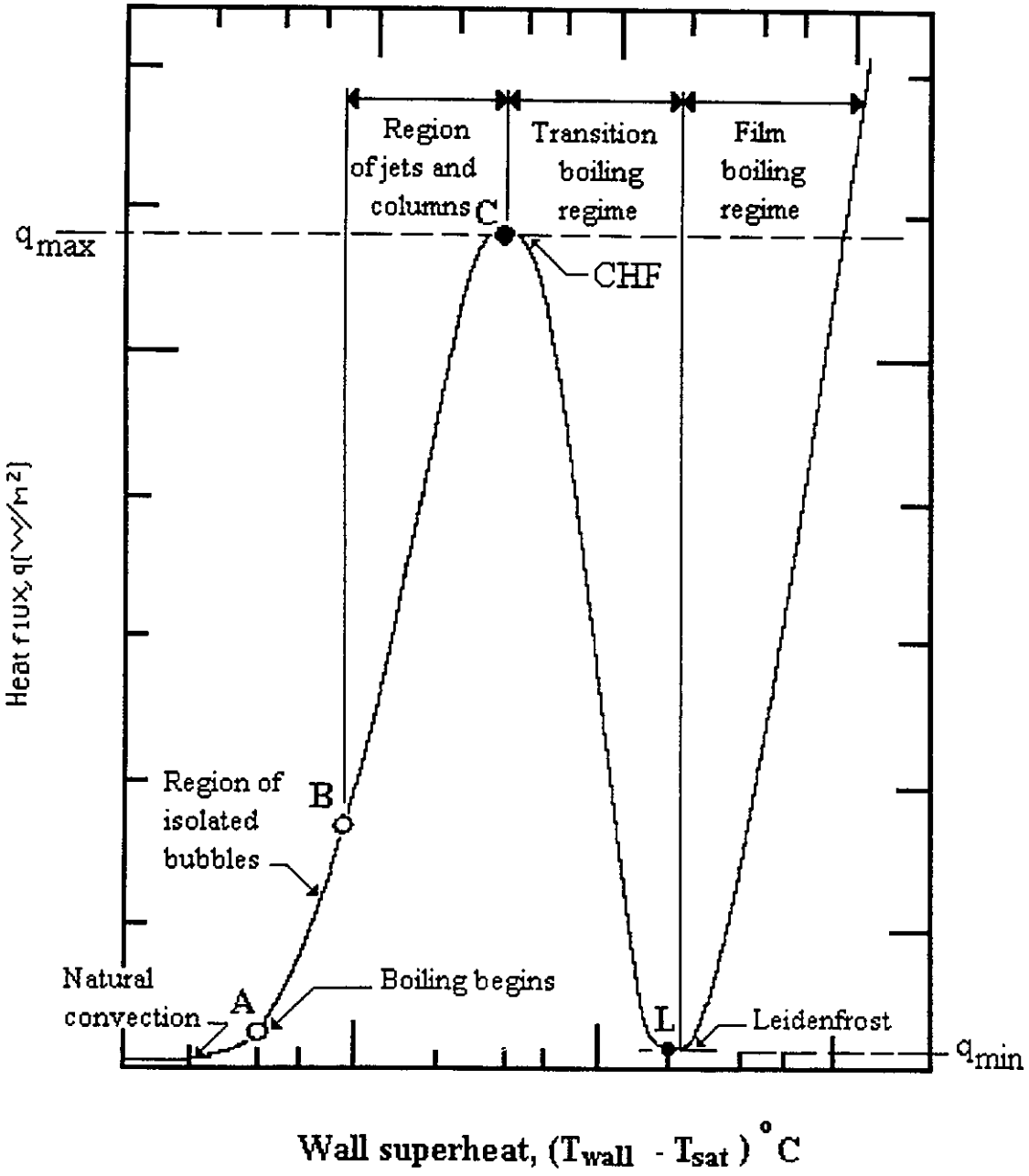

Figure 2.1 Pool boiling curve.

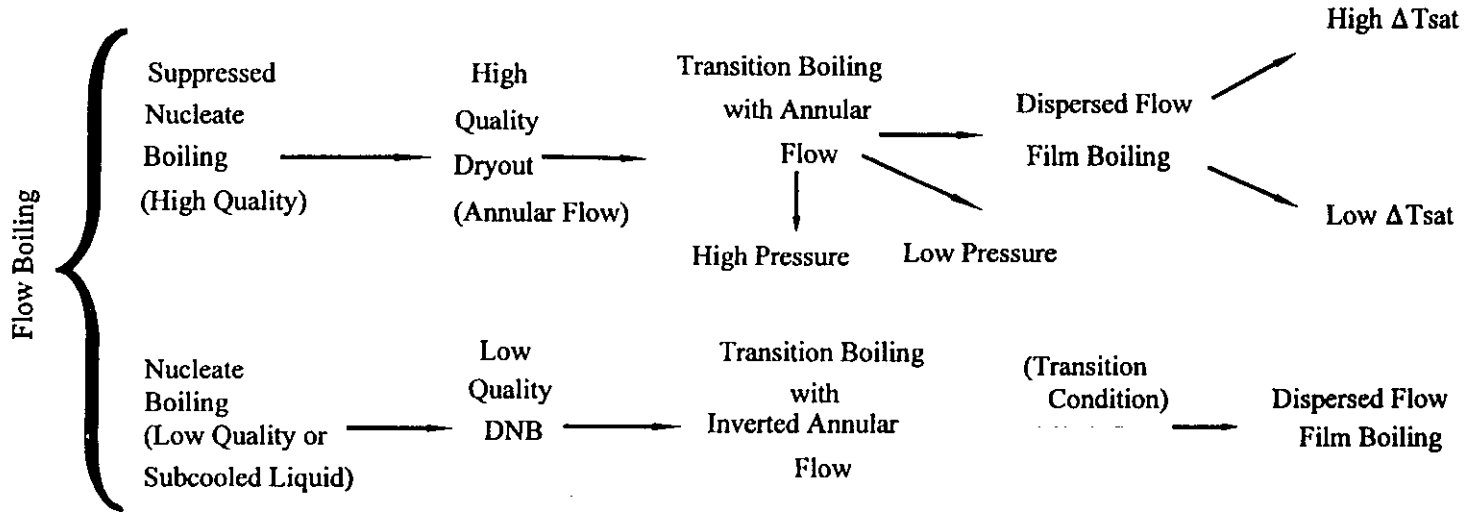

Figure 2.2 Classification of flow boiling regimes (reproduced from [Wang and Weisman, 1983]).

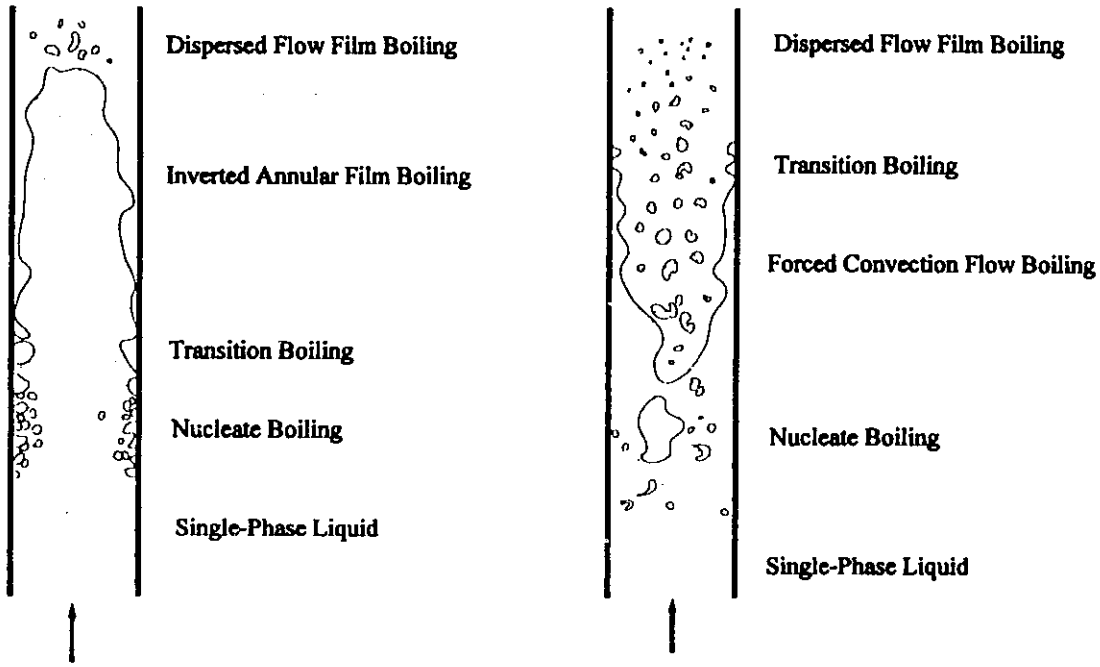

Figure 2.3 Flow boiling regimes.

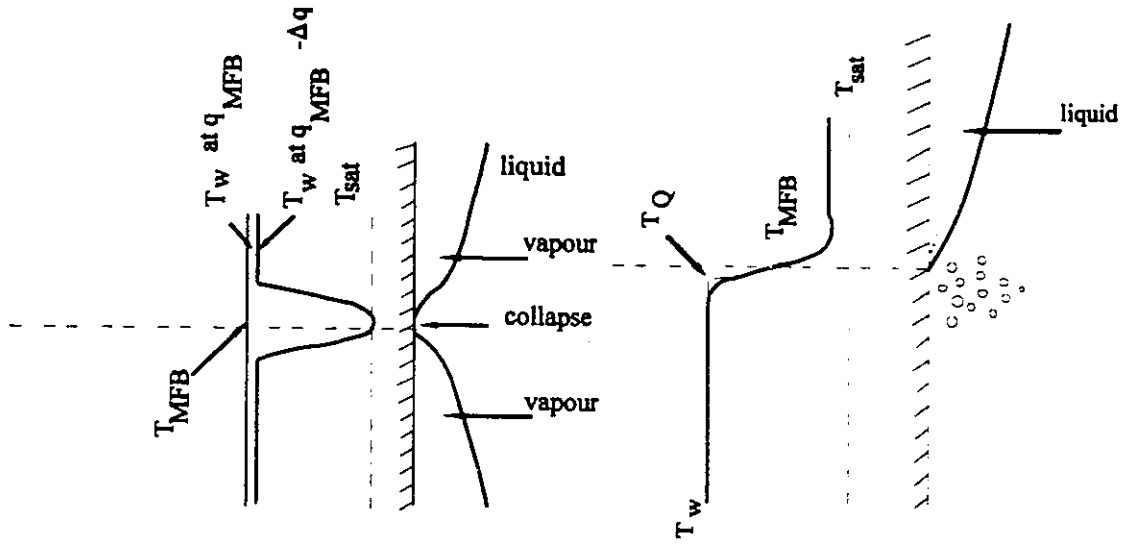

Type I : Collapse of vapour film

Type II : Top flooding

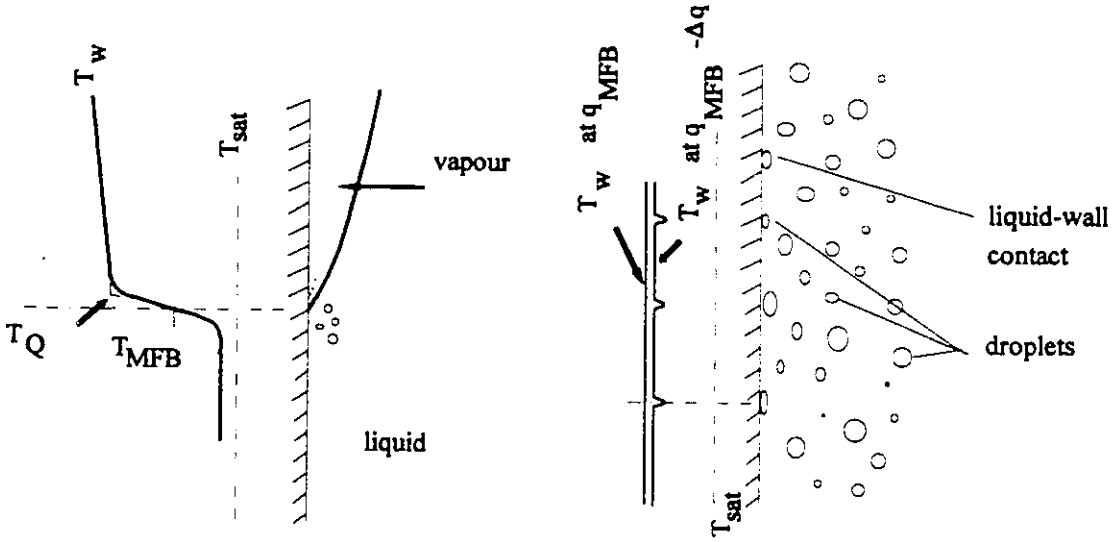

Type III : Bottom flooding

Type IV : Droplet cooling

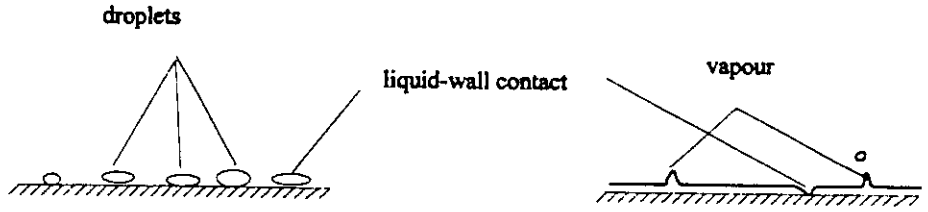

Type V : Leidenfrost boiling

Type VI : Pool boiling

Figure 2.4 Film boiling termination types (reproduced from [Groeneveld, 1984])

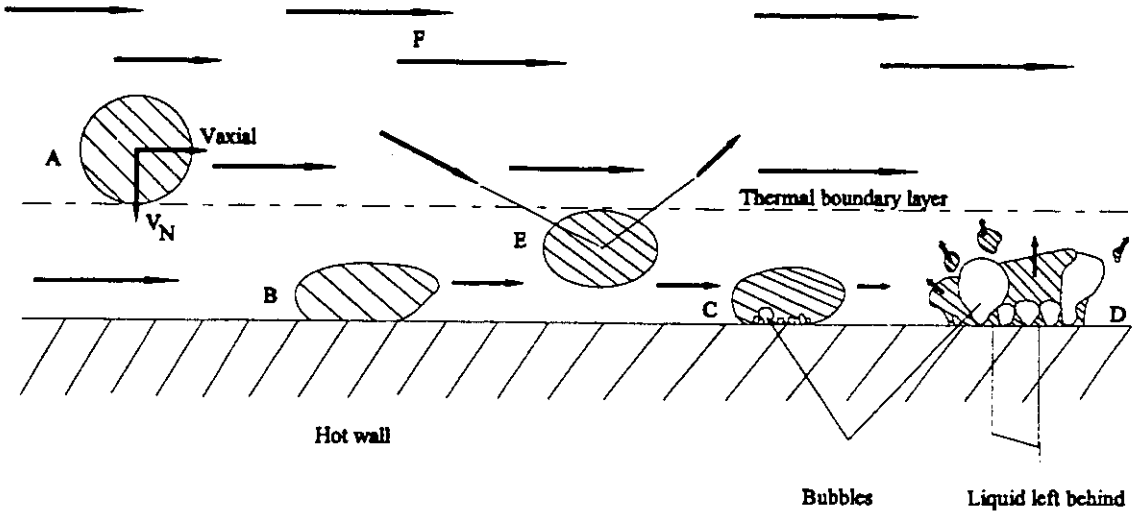

A Liquid drop entering thermal boundary layer with velocity V_N

B Liquid drop of higher kinetic energy based on V_N, arriving on wall and begining to absorb heat from wall via conduction

C Nucleation and bubble growth from liquid drop on wall

D End of bubble growth period; part of liquid drop is ejected into the mainstream by escaping vapour bubbles; part is left on wall to evaporate

E Liquid drop of lower kinetic energy being reversed into the main flow without touching the wall

F Bulk vapour flow

Figure 2.5 Wall rewet in DFFB vertical flow (reproduced from[Iloeje, 1974])

Chapter 3 IAFB PREDICTION METHODS

3.1 General

In the literature, four types of post-CHF heat-transfer prediction methods for IAFB are given:

-Correlations derived for pool boiling; they are also applied to low mass velocity flows.

-Empirical equations that take no account of the physical mechanisms involved in the heat transfer process. These equations assume that the liquid is in thermal equilibrium with the vapour, and the heated surface is cooled by forced convection to the vapour only. They are basically similar to the Dittus-Boelter [1930] type equation.

-Correlations based on the physical mechanisms governing the heat transfer process, hence they recognize the departure from a thermodynamic equilibrium condition. These types of correlations usually predict the degree of thermal non-equilibrium in the vapour, and attempt to calculate the actual vapour temperature and actual quality.

-Theoretical or semi-theoretical prediction methods, which attempt to model various individual hydrodynamic and heat transfer processes.

3.2 Equations for Low Quality and Subcooled IAFB

Since Groeneveld's [1984] last review of the IAFB correlations, there has been almost no further development of new correlations. Table 3.1 summarizes the correlations available up to the present time. This table is an updated version of Groeneveld's [1984] table for low-quality and

subcooled IAFB correlations.

IAFB equations are usually classified into three categories:

a) Modified pool-boiling equations

These equations are derived based on conduction across a vapour film whose thickness is controlled by laminar flow of the vapour film and a smooth vapour-liquid interface. Most of these equations take the following general form:

$$h_c = A\left[\frac{g\ k_v^3 \rho_v(\rho_l - \rho_v)h_{fg}}{\mu_v\ \Delta T_{sat}\ \lambda_c}\right]^{1/4} + h_{rad} \qquad (3.2.1)$$

where λ_c is the minimum wavelength for Taylor instability, and the coefficient A can be chosen to account for the velocity and subcooling effects.

b) Convection-type equations

These convective equations are used to express different heat transfer paths from the heated surface to the vapour film, from the vapour film to the vapour-liquid interface, and from the interface to the subcooled liquid core. These correlations usually have the form:

$$Nu = a\ Re^b\ Pr^c\ F \qquad (3.2.2)$$

The parameter F is introduced to fit particular data sets, and usually to approximately account for effects such as entrance-length effects.

c) Phenomenological equations

These equations are developed in an attempt to account for the physical mechanisms of heat transfer. They are basically semi-theoretical models with empirically correlated parameters. These

equations have usually more complex expressions than the other types of equations, and may be based on a combination of (a) and (b). They are easier to apply than the mechanistic models.

3.3 Phenomenological Models

Heat transfer predictions of IAFB have been analyzed by modified-Bromley [1950] equations for pool film boiling, turbulent-boundary-layer theories and two-fluid models. For the latter two theories, most of the uncertainties are related to assumptions with respect to interfacial heat and mass transfer. These assumptions are often an oversimplification of the physical mechanisms governing film boiling, in order to facilitate a mathematical solution. Table 3.2 summarizes the IAFB models existing in the literature up to the present time. This table is an updated version of Groenevelds' [1984] table for IAFB models.

Table 3.1 Low-quality and subcooled film boiling equations (updated from Groeneveld [1984])

AUTHORS	EQUATION	RANGE OF APPLICABILITY					COMMENTS
		TEST FLUID	GEOMETRY	PRESSURE MPa	FLOW RATE kgm^2s^{-1}	SUBCOOLING °C OR QUALITY	
Bromley [1952,1953]	$h_c = h_{FB} + 3/4\ h_{rad}$ $h_{FB}=0.62\left[\frac{k_v^3 g\rho_v(\rho_f-\rho_v)h'_{fg}}{D\mu_v\Delta T_{sat}}\right]^{1/4}$ $h_{rad}=\frac{5.67x10^{-8}(T_w^4-T_{sat}^4)}{\left[\frac{1}{\epsilon_w}+\frac{1}{\epsilon_f}-1\right]\Delta T_{sat}}$ $h'_{fg}=h_{fg}\left[1+\frac{0.4Cp\Delta T_{sat}}{h_{fg}}\right]^2$	Nitrogen water a-pentane benzene carbon tetra-chloride ethyl alcohol	Horizontal carbon cylinders OD- 6.4 mm - 9.5 mm - 12.7 mm	Not given	Pool boiling	Saturated	Pool film boiling from horizontal cylinders. Laminar theory.
Berenson [1961]	$h_{FB}=0.425\left[\frac{k_v^3 g\rho_v(\rho_f-\rho_v)h'_{fg}}{\mu_v\Delta T_{sat}\sqrt{\frac{\sigma}{g(\rho_f-\rho_v)}}}\right]^{1/4}$		Horizontal surface		Pool boiling	Saturated	Theory only.
Siviour and Ede [1970]	$q_v=0.613\frac{k_v}{D}\Delta T_{sat}\left[\frac{g\rho_v(\rho_l-\rho_v)h'_{fg}}{\mu_v k\Delta T_v}\right]^{1/4}+q_{rad}$ $q_{tot}=q_v+q_l$ $q_l=0.57\frac{k}{D}\Delta T_l[Gr\ Pr^2]$ $Gr=g\frac{\beta_l\Delta T_l D^3}{\nu^2}$	Water Water plus detergent	Horizontal cylinders OD- 3.2 mm - 6.4 mm	0.101	Pool boiling	0-90 °C	Correlated their data well over the entire range of subcoolings.

Table 3.1 Low-quality and subcooled film boiling equations (Continued)

AUTHORS	EQUATION	RANGE OF APPLICABILITY					COMMENTS
		TEST FLUID	GEOMETRY	PRESSURE MPa	FLOW RATE $kgm^{-2}s^{-1}$	SUBCOOLING °C OR QUALITY	
Andersen [1976]	$h_c=C_1\left[\frac{k_v^3 h_{fg}^{\prime 2}\rho_g^3(\rho_f-\rho_v)^4 g^4}{\mu_v^4 \Delta T_{sat}^2 \sigma}\right]^{1/11}$ $0.3321 \le C_1 \le 0.5498$				Low flow rates	Saturated	Gives slightly higher heat-transfer coefficient than Berenson's equation for $\Delta T_s > 200$ °C. Theory only.
Ellion [1954]	$h=4/3\left[\frac{g\rho_l\rho_v k_v^3 h_{fg}'}{12\Delta T_{sat} L\mu_v}\right]^{1/4}+q_{rad}$	water	Vertical annulus OD-63.5 mm ID-6.4 mm length-76.2 mm	0.11-0.41	(0.336-1.53)x10^3	28 °C - 56 °C	
Bailey [1972]	$h=\left[\frac{2k_g^3 g\rho_g(\rho_f-\rho_g)h_{fg}}{D\mu_g\Delta T_{sat}}\right]^{1/4}$	Theory	Vertical rods			Saturated	D=rod OD
Collier [1980]	$\left[\frac{h(z)z}{k_g}\right]=\left[\frac{z^3 g\rho_g(\rho_f-\rho_g)h_{fg}}{4k_g\mu_g\Delta T}\right]^{1/4}$	Theory	Vertical surface				Laminar vapour film
Collier [1980]	$\left[\frac{h(z)z}{k_g}\right]=0.056Re_g^{0.2}[Pr\ Gr']^{1/3}$ $Gr'=\left[\frac{z^3 g\rho_g(\rho_f-\rho_g)}{\mu_g^2}\right]$		Vertical surface				Turbulent vapour film
Mosaad and Johannsen [1988]	$h=h_{FB}+3/4\ h_{rad}$ $h_{FB}=\lambda(1+0.4\theta_x+0.075\theta_x^2)h_{sat}$ $\theta_{sat}=\Delta T_l\ h_{l-l}/\Delta T_{sat}\ h_{sat}$ $h_{sat}=[g\rho_v(\rho_l-\rho_v)h'_{fg}/16\mu_v\Delta T_{sat}h_v z]^{1/4}$ $h'_{fg}=h_{fg}[1+0.5c_{pv}(T_w-T_{sat})]$ $h_{l-l}=h_{l-l,-}[1+2.5(D/z)]$ $h_{l-l,-}=3.66k_l/(D-2\delta)$, $Re<2000$ $h_{l-l,-}=0.023k_l Re^{0.8}Pr_l^{0.4}/(D-2\delta)$, $Re\ge 2000$ $\lambda=1+7.5(\delta_{sat}/D)$ $\delta_{sat}=k_v/h_{sat}$ $h_{rad}=5.67x10^{-8}(T_w^4-T_{sat}^4)/(1/\epsilon_w+1/\epsilon_l-1)(T_w-T_{sat})$ $\epsilon_l=0.8$, $\epsilon_w=0.95$	water	vertical tube OD-12 mm ID-9 mm length- 280 mm	0.101	50-500	0-30	Laminar boundary-layer analysis

Table 3.1 Low-quality and subcooled film boiling equations (Concluded)

AUTHORS	EQUATION	RANGE OF APPLICABILITY					COMMENTS
		TEST FLUID	GEOMETRY	PRESSURE MPa	FLOW RATE kgm^2s^{-1}	SUBCOOLING °C OR QUALITY	
Lee and Kim [1987]	$q/q_w=(r_w-r_i q_{i-l}/q_w)(r^2-r_w^2)/r(r_w^2-r_i^2)+r_w/r$ $q_{i-l}=h_{i-l}(T_{sat}-T_l)$ $h_{i-l}=\rho_l c_{pl}/(1.17B+1.83D)$ $B=r_i\int_0^{r_i}\frac{\cos(\frac{r}{r_i}\frac{\pi}{2})-1}{r(\epsilon_M+\alpha)}dr$ $D=\int_0^{r_i}\frac{\sin(\frac{r}{r_i}\frac{\pi}{2})dr}{(\epsilon_M+\alpha)}$ q:heat flux distribution across the vapor layer ϵ_M:eddy diffusivity from the modified Reichardt's equations.	Theory	Vertical tube			Saturated or subcooled	Turbulent-boundary-layer analysis. Applicable to the flow region immediately downstream of the rewetting front.
Takenaka et al. [1989]	$q_v=\frac{r_w q}{r_i-y_v}\left[1-\frac{r_w q-r_i q_{i-l}}{r_w q}\frac{\int_0^{y_v}(r_i-y_v)u_v dy_v}{\int_0^{r_i}(r_i-y_v)u_v dy_v}\right]$ $q_l=\frac{r_i q_{i-l}}{r_i-y_l}\left[1-\frac{\int_0^{y_l}(r_i-y_l)u_l dy_l}{\int_o^{r_i}(r_i-y_l)u_l dy_l}\right]$ $q_{i-l}=\frac{\rho_l Cp_l(T_{sat}-T_l)}{y_l}$ $1-\frac{\int_0^{r_i}(r_i-y_l)u_l dy_l}{r_i}$ $\int_0^{r_i}\frac{\int_0^{r_i}(r_i-y_l)u_l dy_l}{(r_i-y_l)(a_l+\epsilon_l)}dy_l$	R-113	Vertical tube OD-11 mm ID-10 mm length 900-1485 mm	0.10	136-1280	10-40	Turbulent-boundary-layer analysis using modified Reichardt equations. This analysis is limited to the region where the actual quality >> 0. q_v and q_l are the heat fluxes retained by the vapour and the liquid phases, respectively.

Table 3.2 IAFB models (updated from Groeneveld [1984])

REFERENCE	ASSUMPTIONS	HEAT FLUX COMPONENTS	COMMENTS
Kalinin et al. [1970]	$U_v=U_l$ $T_v=T_{sat}$	$Nu_{w,v}=f(Re_v,Pr_v,T_w/T_{sat})$ $Nu_{i,l}=f(Re_l,Pr_l,Z/De)$	Model was compared to nitrogen data.
Groeneveld [1972]	At dryout $U_v=U_l$ $\tau_i=k\delta_v(U_v-U_l)^2$ $T_l=T_v=T_{sat}$	$Nu_{w,v}=aRe_v^bPr_v^c(\mu_v/\mu_w)^dC_r$ C_r=enhancement in $h_{w,v}$ due to liquid-wall interactions and turbulence in vapour film.	Model permits entrained vapour in liquid core. Compared to Freon data.
Kaufman [1976]	$T_v=(T_w+T_{sat})/2$ $f_i=0.005(1+300\delta/D)$	$Re_v<100: Nu_{w,v}=1$, else $Nu_{w,v}=f(Re,Pr)$ $Re_l<2000: Nu_{i,l}=3.66$, else $Nu_{i,l}=f(Re,Pr)$	Interfacial heat transfer and friction enhanced by factor $1+300\delta/D$.
Chan [1980]	$\tau_i=0$ $h'_{fg}=h_{fg}+0.34Cp_v(T_v-T_{sat})$	$q_{w,tot}=q_{rad,w-i}+q_{w-i}$ q_{w-i}:conduction across laminar vapour film $Nu_{i,l}=0.023Re_l^{0.8}Pr_l^{0.4}.C$, C=1.5-2.0	Vapour entrained in liquid core.
Elias [1981]	Vapour entirely generated at the quench front. Constant vapor film thickness. $T_i \le T_{sat}$, T_w=const.	$q_{w,tot}=q_{rad,w-i}+q_{w-i}$ $q_{w-i}=f(Pe_v,U_v,\delta,k_v)$ Pe_v:vapor Peclet number. q_{i-l}:from boundary layer in the liquid at the interface	Model is restricted to the entrance subcooled region. Compared to Fung's data.
Han and Bankoff [1982]	τ_i according to Barathan [1979]	q_{w-i}:conduction across laminar sublayer q_{i-l}:use one-seventh power law in liquid core	Entrained droplets in vapour phase.
Fung [1981]	$T_v=(T_w+T_{sat})/2$ $U_i=U_l$	$q_{i-l}=k_{eff}\,dT/dr$ k_{eff} includes eddy diffusivity $q_{w-i}=k_v(T_w-T_{sat})/\delta_{sat}$	Compare well with Fung's low P data. δ_{sat}=laminar vapour film or thermal sublayer thickness.
Laperrière [1983]	$T_v=(T_w+T_{sat})/2$ $U_i=(U_v+U_l)/2$	$N_{w,v}$, $Nu_{v,i}$ and $Nu_{i,l}$ all have form $Nu=a.Re^b.Pr^c.C$	C=heat transfer enhancement factor. Results compared to Stewart's [1982] and Laperrière's [1983] data.
Denham [1984]	$T_v=(T_w+T_{sat})/2$	$q_{w-i}=k_v(T_w-T_{sat})/\delta$ $q_{i-l}=k_l(T_{sat}-T_l).f(U_i,U_Q,F_o)$ $k_l=k_{l,laminar}$ Nu (turb) / Nu (laminar)	δ from Bromley's laminar flow theory. F_o=Fourier number
Kawaji and Banerji [1983]	laminar flow in core $U_i=U_l$	q_{i-l} from thermal entry problem in laminar flow q_{w-v} and q_{v-i} from formulation of convection between parallel plates.	Stability analysis predicts transition to slug or dispersed flow film boiling.
Wang and Shi [1984]	Similarity to single-phase turbulent boundary layer flow is assumed. U_l=const. $U_v \sim (1/\delta)^{1/7}$	$q_{w,tot}=q_v+q_{i-l}$ $q_{w,tot}$ from turbulent boundary layer using Karman's theory. q_v:heat flux to evaporate the liquid. $q_{w,tot}=A(T_w-T_{sat})$, $A=f(\tau_w,Pr_v,U_i)$ $q_v=f(h_{fg},U_l,\delta)$ $q_{i-l}=k_{eff}\,dT_l/dr$, k_{eff} includes eddy diffusivity.	Model valid for turbulent flow on horizontal plate. Compared to water data.

Table 3.2 IAFB models (Concluded)

REFERENCE	ASSUMPTIONS	HEAT FLUX COMPONENTS	COMMENTS
Yan [1987]	Laminar flow in vapor film T_w=const. two boundary conditions for interface are considered: τ_i=0 or U_i=U_l turbulent flow in vapor film T_w=const. τ_i=0, τ_w=$\delta(\rho_l-\rho_v)g$	$q_{w,tot}=q_{rad,w-i}+q_{w-i}$ $q_{w-i}=k_v(T_w-T_{sat})/\delta$ $q_{i-l}=h(T_l-T_{sat})$ Re_l<2200:h=f(Re_l,Pr_l,Gr_l) Re_l>2200:h=f(Re_l,Pr_l) $q_{w-i}=-\rho_v c_{pv}(k_v+\epsilon_v)dT/dy$	Model is applicable to laminar and turbulent flow. Compared to water data.
Analytis [1987]	In core both laminar and turbulent flow are considered. U_l=U_l	$q_{i-l}=H_l(T_{sat}-T_l)$ Re_l<2000:H_l=3.66k_lF/(R-δ) Re_l>2000:H_l=f(Re.Pr).F F=1+1.4R/z $q_{w,v}$ and q_{v-i} from formulation of convection between parallel plates.	Interfacial heat transfer and friction enhancement factor 1+300δ/D.
Wang [1988]	U_l=const.=U_{inlet} δ_v=bx^n no vapor superheat	$q_{w,tot}=q_v+q_{i-l}$ q_v:heat flux to evaporate the liquid. $q_{w,tot}=0.023\rho_v c_{pv}(T_w-T_s).f(U_i,\delta)$ $q_v=d\delta/dx$ .f(h_{fg},U_i,δ) $q_{i-l}=-\rho_l c_{pl}\epsilon_{M,l}dT_l/dr$ ϵ_M:turbulent diffusivity of momentum exchange.	Model is restricted to liquid flowing with high velocity. Compared to R11 data and Dougall's data [1963].
Chen [1988]	T_v=(T_w+T_b)/2 T_b:bulk liquid temperature Uniform liquid velocity	$q_{v-i}+q_{rad,w-i}=q_{i-l}+q_v$ q_v:heat flux to evaporate the liquid. $q_v=h_{fg}/2\pi r_i$ dΓ/dz Γ:vapor flow rate $q_{v-i}=\rho_v c_{pv}(\epsilon_v+\alpha_v)dT/dr$ $q_{i-l}=\rho_l c_{pl}(\epsilon_l+\alpha_l)dT/dr$ ϵ_v=f(U_v,δ,ΔT_{sat},h_{fg}) ϵ_l=C$U_l\delta$, C=0.05	Model was compared to water data.
Hsu [1984]	Turbulent flow in both vapor film and liquid core U_l=U_l=U_v at interface flow field is divided into two regions: -region (I):δ=const. and interface slightly subcooled -region (II):δ=f(z) and interface at saturation	$q_{w,tot}=q_{w-i}+q_{rad,w-i}$ $q_{w-i}=k_v dT/dr$ $q_{i-l}=k_l dT/dr$ k_v=f(k_{vL},U_v,ρ_v,c_{pv}) in region (I) $k_v=k_v|_{region(II)}$+f(T_{sat},T_l,k_{vL}) in region (II) k_l=f(k_{lL},δ,U_l,c_{pl}) k_{vL}:vapor thermal conductiviy in laminar flow k_{lL}:liquid thermal conductivity in laminar flow	Model is two-dimenional, two-region and two-fluid model.Compared to Stewart's[1982] data.

Chapter 4 IAFB EMPIRICAL EQUATIONS

4.1 The Bromley Correlation [1950]

For stable film boiling in horizontal tubes, Bromley [1950] derived an expression for the heat transfer coefficient as

$$h_c = 0.62\left[\frac{g(\rho_f - \rho_v)\ \rho_{vf}\ h_{fg}'\ k_{vf}^3}{D\ \mu_{vf}\ (T_w - T_{sat})}\right]^{1/4} \qquad (4.1.1)$$

where h_{fg}' and D are the effective latent heat of vaporization allowing for the effect of superheat and the tube diameter, respectively. The effective latent heat is given by

$$h_{fg}' = h_{fg}\left[1 + 0.68\frac{C_{pv}(T_w - T_{sat})}{h_{fg}}\right] \qquad (4.1.2)$$

Based on Eq. (4.1.1), the heat transfer coefficient approaches zero for very large tubes and horizontal flat surfaces. To correct this trend, Breen and Westwater [1962] modified Bromley's equation to

$$h_c = [0.59 + 0.069\frac{\lambda_c}{D}]\left[\frac{g(\rho_f - \rho_v)\rho_{vf}\ k_{vf}^3\ h_{fg}'}{\lambda_c\ \mu_{vf}\ \Delta T}\right]^{1/4} \qquad (4.1.3)$$

where the minimum wavelength for Taylor instability, λ_c, is given by

$$2\pi\left[\frac{\sigma}{g(\rho_f - \rho_v)}\right]^{1/2} \qquad (4.1.4)$$

In film boiling, surface temperatures are usually high and hence radiation heat transfer can be a significant component. Therefore, Bromley suggested that the total heat transfer rate should be combined with the effects of convection and radiation, i.e.,

$$h_{tot} = h_c + 0.75\, h_{rad} \qquad (4.1.5)$$

where h_c and h_{rad} represent the convective heat transfer coefficient and the radiative heat transfer coefficient, respectively.

4.2 The Berenson Correlation [1961]

Berenson [1961] derived a heat transfer coefficient for pool film boiling by applying a hydrodynamic instability analysis with the Taylor-Helmholtz instability theory. Based on the experimental data for a horizontal surface, the heat transfer coefficient for pool film boiling on a horizontal surface is expressed as

$$h = 0.425\left[\frac{k_{vf}^{3}\,(h_v - h_f)\rho_{vf}\,g(\rho_f - \rho_v)}{\mu_{vf}\,(T_w - T_{sat})\sqrt{\dfrac{\sigma}{g(\rho_f - \rho_v)}}}\right]^{1/4} \qquad (4.2.1)$$

A number of assumptions are utilized in the analysis:

- in pool film boiling from a horizontal surface, bubbles are located in a square regular lattice, where bubble spacing is unaffected by vapour velocity and vapour film thickness,
- vapour flows radially into the bubble,

- the flow is laminar,

- the vapour layer located between the bubbles has an average constant thickness,

- average vapour properties are evaluated at the average of the wall temperature and the saturation liquid temperature,

- the dominant heat transfer mode is conduction; radiation is negligible, and

- vapour is generated in an area equal to $\lambda^2/2$ (the wavelength, λ, is the most dangerous wavelength of the disturbances at the liquid-vapour interface).

Justifications for the above assumptions were provided by Berenson [1961].

Strictly speaking, this analysis is only valid for low wall superheats (values of the temperature difference near the minimum). Berenson, however, suggested that it can be extended to a much wider range of applicability (e.g., at high superheats), due to the insensitivity of the heat transfer coefficient to the characteristic length. The characteristic length, which is represented by λ, is derived based on conditions for the heat flux being near the minimum value on the boiling curve. This correlation is also often employed, with some modifications to the constant, for flow film boiling from different geometries, such as vertical upward flow in a tube. In most cases, no justification is provided for this practice. For example, Leung and Groeneveld [1988] modified the constant in Eq. (4.2.1) to account for inlet subcooling effects in flow film boiling. The constant is modified as

$$C = 0.425 \left(1 + 8.3 \frac{T_{sat} - T_{bulk}}{T_{bulk} + 273.15} \right) \qquad \textbf{(4.2.2)}$$

T_{bulk} is calculated from the equilibrium quality as

$$T_{bulk} = T_{sat} \qquad for \quad x_{eq} \geq 0$$

$$T_{bulk} = T_{sat} + \frac{h_{fg}}{Cp_l} x_{eq} \qquad for \quad x_{eq} < 0 \tag{4.2.3}$$

Chapter 5 IAFB PHENOMENOLOGICAL MODELS

This chapter describes several theoretical analyses pertinent to IAFB. Heat transfer predictions of IAFB frequently employ modified Bromley [1950] equations for pool film boiling, turbulent-boundary-layer theories and two-fluid models. For the latter two theories, most of the uncertainties are related to assumptions with respect to interfacial heat and mass transfer. These assumptions are often an oversimplification of the physical mechanisms governing film boiling, in order to facilitate a mathematical solution.

5.1 The Dougall and Rohsenow Model [1963]

Dougall and Rohsenow [1963] applied a turbulent flow model for predicting heat transfer in saturated inverted annular flow of low qualities inside vertical tubes. They used a universal three-layer velocity model of Von Karman, and showed good agreement between predictions and their experimental data of Freon-113 flow.

The thermal resistance of half of the vapour layer near the wall was computed using the three-layer model of Von Karman: a laminar thermal resistance next to the wall, $0 \le y^+ \le 5$; a buffer thermal resistance, $5 \le y^+ \le 30$; and a turbulent thermal resistance near the middle of the vapour film. The thermal resistance near the interface was calculated for three cases: (i) three-layer film, where the interface resistance is equal to the complete resistance in the other half of the film (laminar, buffer, and turbulent thermal resistances), (ii) two-layer film, where the interface resistance is equal to the sum of the buffer and turbulent layers in the other half of the film, and (iii) one-layer film,

where the thermal resistance is equal to the turbulent resistance. For the thermal resistance near the interface, comparison with experimental results of Freon-113 showed that:

- for low-vapour Reynolds numbers near the start of film boiling, the use of a two-layer film analysis gives good prediction, and

- for higher-vapour Reynolds numbers, the turbulent layer predicts the experimental results best.

The total shear stress and heat flux are assumed to be given by

$$\frac{\tau}{\rho_{vf}} = (\nu_{vf} + \epsilon_M)\frac{du}{dy} \qquad (5.1.1)$$

and

$$\frac{q}{\rho_{vf} C_{pvf}} = -(a_{vf} + \epsilon_H)\frac{dT}{dy} \qquad (5.1.2)$$

where y is the distance from the wall. By assuming that the Reynolds analogy holds ($\epsilon_M = \epsilon_H = \epsilon$), the eddy diffusivity, ϵ, is calculated with Eq. (5.1.1) using the universal velocity profile. The following equation is then used to calculate the Nusselt numbers for the inverted annular flow regime based on the buffer-turbulent layers and the turbulent-layer theories:

$$Nu_{vf} = \frac{h_c D}{k_{vf}} = \frac{0.794\left[\frac{\rho_{vf}(\rho_f - \rho_{vf})gD^3}{\mu_{vf}^2}\right]^{1/3}(\delta^*)^{1/3}}{\int_0^{\delta^*}\frac{dy^*}{1+Pr\frac{\epsilon}{\nu_{vf}}}} \qquad (5.1.3)$$

For definitions of the symbols used above, please see the nomenclature.

5.2 The Kalinin et al. Model [1977]

Kalinin et al. developed a one-dimensional steady-state flow model for subcooled inverted annular flow film boiling. They assumed that:

- the liquid moves in the form of a turbulent jet, which is separated from the heated surface by a turbulent vapour film,

-the interface is smooth,

-the interfacial temperature is equal to the saturation temperature, and

-the vapour and the liquid are moving at the same velocity.

In addition to these assumptions, Kalinin et al. presented some further constraints and assumptions. For instance, the heat transfer from the wall to the vapour and from the vapour into the liquid core are assumed to obey the following equations:

$$Nu_v = A\ Re_v^{\ m} \tag{5.2.1}$$

$$Nu_l = B\ Re_l^{\ n} \tag{5.2.2}$$

In this analysis, only the continuity and energy equations are needed, because of the assumption of zero interface slip. The authors stated that this assumption is valid for large flow velocities and small pressure drop along the channel. By combining the continuity and energy equations, a differential equation describing the variation of film thickness is obtained:

$$\frac{db}{dH} - \phi_1(b) - E\ \phi_2(b) = 0$$
$$b = \frac{2\delta}{D} \tag{5.2.3}$$

where H represents the prior history of the flow and is expressed as a function of Nu_v and the axial wall temperature, and E represents the fraction of heat that goes into the liquid and is a function of Nu_v and Nu_l. The functions Φ_1 and Φ_2 are shown below

$$\phi_1(b) = \frac{\left[(1-b)^2 + \frac{\rho_v}{\rho_l}(2-b)b\right]^{2-m}}{2b^{1-m}(1-b)} \qquad (5.2.4)$$

$$\phi_2(b) = \frac{\left[(1-b)^2 + \frac{\rho_v}{\rho_l}(2-b)b\right]^{2-n}}{2(1-b)^{1-n}} \qquad (5.2.5)$$

The constants A and B of Eqs. (5.2.1) and (5.2.2) are obtained from empirical film boiling heat transfer correlations proposed by Kalinin et al. [1977]. The exponents m and n are assigned the values of 0.75 and 1, respectively.

5.3 The Analytis and Yadigaroglu Model [1987]

Analytis and Yadigaroglu [1987] developed an analytical two-phase flow model of IAFB with the two-fluid hydrodynamic equations having a frame of reference moving with the quench front. Although the equations are written in steady-state form, they claimed that their model is also adaptable to a fully transient formulation. The mass, momentum and energy conservation equations for the liquid and vapour are given as

$$\frac{d}{dz}[\rho_l U_l(1-\alpha)] = -W'' \frac{P_l}{A} \qquad (5.3.1)$$

$$\frac{d}{dz}[\rho_v U_v \alpha] = W'' \frac{P_i}{A} \tag{5.3.2}$$

$$(1-\alpha)\frac{dP}{dz} - (1-\alpha)\rho_l U_l \frac{dU_l}{dz} = (1-\alpha)\rho_l g - \frac{\tau_i P_i}{A} - W'' \frac{(U_l - U_i)P_i}{A} \tag{5.3.3}$$

$$-\alpha\frac{dP}{dz} - \rho_v \alpha U_v \frac{dU_v}{dz} = \rho_v \alpha g + \frac{\tau_w P_w}{A} + \frac{\tau_i P_i}{A} + W'' \frac{(U_v - U_i)P_i}{A} \tag{5.3.4}$$

$$(1-\alpha)U_l \frac{dT_l}{dz} = \frac{q_{i\text{-}l} P_i}{C_{p_l}\rho_l A} - W'' \frac{(h_f - h_l)P_i}{C_{p_l}\rho_l A} \tag{5.3.5}$$

$$\alpha U_v \frac{dT_v}{dz} = \frac{q_v P_i}{C_{p_v}\rho_v A} + W'' \frac{(h_g - h_v)P_i}{C_{p_v}\rho_v A} \tag{5.3.6}$$

For definitions of the symbols used above, please see the nomenclature.

In their analysis, they assumed a turbulent flow in the vapour film, but a laminar flow for Re<2000 and turbulent flow otherwise in the liquid core. The heat transfer from the wall to the vapour and from the vapour to the liquid interface were modelled by treating the vapour flow as flow between two parallel plates (the wall and the liquid interface). Heat transfer equations given by Kays and Crawford [1980] for flow between parallel planes are used to give expressions for the heat fluxes $q_{w\text{-}v}$ and $q_{v\text{-}i}$, from the wall to the vapour and from the vapour to the interface. To account for the waviness and disturbances at the interface, an enhancement factor λ and an interfacial friction factor f were introduced. Closure relations for the vapour generation W", radiation heat transfer q_{rad} and interfacial shear stresses are given by the authors and will not be listed here.

Analytis and Yadigaroglu compared the predictions of their model against experimental data obtained from the UC-Berkely single-tube reflood tests [Seban et al., 1978; Seban, 1983]. They

claimed that very good agreement was found for all runs except for two cases. These two cases are the case of very low wall temperature and the case of very high flooding rate and wall temperature. In the latter, the model underpredicted the heat transfer coefficient, especially near the quench front. The authors gave detailed discussion of these two cases. Overall, their model predicts the dependency of the heat transfer coefficient on flooding rate, subcooling and pressure correctly.

5.4 The Johannsen and Mosaad Model [1989]

Johannsen and Mosaad [1989] recently developed a semi-empirical two-fluid model, based on a laminar boundary-layer analysis of the vapour film. The liquid core was treated by considering cross-sectional averages of its characteristics as a function of the axial coordinate only. Their analysis is based on some further simplifying assumptions, such as no entrained liquid in the vapour film and no entrained vapour in the liquid core. The governing continuity and momentum equations for the vapour film were solved with the one-dimensional integral technique. A detailed formulation of this model is given by Mosaad and Johannsen [1988]. The constitutive equations used for this model are summarized in Table 5.1. An enhancement parameter λ was introduced to account for interfacial disturbances. The enhancement parameter is given as a function of the local film thickness and the liquid jet Reynolds number. The parameter λ is given as

$$\lambda = 1 + a\left(\frac{\delta}{D}\right) Re_l^{\,b} \qquad (5.4.1)$$

where δ is the film thickness. The two adjustable constants a and b were determined from empirical data.

5.5 The Elias and Chambré Model [1981]

Elias and Chambré developed a model based on the photographic study of Goodman and

Elias [1978], who observed the existence of two distinct regions in IAFB. The first region is found immediately above the quench front. This region is characterized by a smooth vapour film of constant thickness. The thickness of this vapour layer depends on flow velocity and subcooling. The second region is located further downstream, and is characterized by a wavy and unstable vapour-liquid interface.

Elias and Chambré based their modelling study on the above observations. In their model, the energy equation for the first region is solved analytically. The vapour layer thickness has been considered as a parameter in their model, and was correlated as a function of the equilibrium quality at the quench front position.

Elias and Chambré introduced several assumptions for modelling the heat transfer in the region near the quench front "entrance region":

-the vapour is entirely generated in the entrance section at the quench front,

-the vapour-liquid interface is slightly below the saturation temperature, T_{sat}, and hence little or no evaporation occurs,

-the vapour temperature at the quench front is equal to the saturation temperature,

-the wall temperature is maintained constant, $T_w > T_{sat}$, and the vapour layer has a constant film thickness, δ,

-vapour film has a constant velocity profile; it is also assumed that the heat is transported through the vapour layer by conduction,

-above the quench front, a heat flux, $q_{i-l}(z)$, is generated at the vapour-liquid interface, and at $z=0$ the liquid is uniformly subcooled at a mixed mean temperature, T_o, and the heat flux, $q_{i-l}(z)$, causes the interface surface temperature to rise up to the saturation

temperature, T_{sat}, at the position where the entrance region terminates, and

-a thin boundary layer exists in the liquid core at the interface, in which the temperature distribution can be determined from the boundary-layer theory.

By solving the equation of the heat flow in the vapour layer for the entrance section

$$u_v \frac{\partial T}{\partial z} = a_v^2 \frac{\partial^2 T}{\partial y^2} \qquad (5.5.1)$$

Elias and Chambré determined the temperature profile and the wall heat flux as a function of distance along the tube. They concluded that the wall heat flux in the entrance region is a more complicated function of z (the heat flux varies exponentially) than the commonly used equation in Bromley-type equations, $q_w = (k_v/\delta)\,\Delta T$. The entrance region length was calculated by using only the thermal conditions in the channel, since it is assumed that no boiling takes place at the entrance region.

5.6 The Denham Model [1984]

Denham noted that the Bromley model does not include certain effects, such as liquid subcooling, liquid velocity, turbulence in the liquid or vapour and instability of the vapour-liquid interface. However, he concluded that not all of these effects are important, and included only the effects of liquid subcooling and liquid velocity in his model. Subcooling of the liquid core results in an increase in the heat transfer rate, especially at higher flow rates. It is generally assumed that part of the heat flux to the core is used to raise the liquid temperature, instead of generating vapour at the interface. This results in an increase in the heat transfer rate, since the vapour film is thinner.

Denham adopted the same relation for the vapour film thickness, δ, as used in Bromley model

$$\delta = \left(\frac{\xi m_v \mu_v}{g(\rho_l - \rho_v)\rho_v} \right)^{1/3} \qquad (5.6.1)$$

The heat flux from the wall and radiation heat flux are calculated with

$$q_{w\text{-}l} = k_v \frac{(T_w - T_{sat})}{\delta} \qquad (5.6.2)$$

$$q_{rad} = \frac{\sigma'(T_w^4 - T_{sat}^4)}{\frac{D_w}{D_l}\frac{1}{\epsilon_l} + (\frac{1}{\epsilon_w} - 1)} \qquad (5.6.3)$$

Denham's model differs from the Bromley model because of the inclusion of the heat transfer from the vapour-liquid interface into the bulk of the liquid. By neglecting axial conduction and assuming the conduction of heat into a circular cylinder (liquid core), with a sudden change of surface temperature, the heat flux to the liquid core is calculated with

$$q_{l\text{-}l} = - k_l \left[\frac{\partial T}{\partial r} \right]_l = k_l \frac{T_{sat} - T_l}{\sqrt{\pi \alpha_l t}} \frac{1}{1 + 3.75 F_o} \qquad (5.6.4)$$

Further, Denham assumed that at the quench front, the liquid core temperature is uniform. Then the rate of evaporation of liquid at the interface is given as

$$W'' = \frac{(q_{w\text{-}l} + q_{rad} - q_{l\text{-}l})}{h_{fg}} \qquad (5.6.5)$$

A non-linear differential equation was obtained from Eqs. (5.6.1) to (5.6.5), which was integrated numerically starting from the quench front.

When comparing this model prediction with reflooding experiment data, good agreement

was obtained up to about a 10 cm distance from the quench front. Beyond this distance, the heat fluxes predicted by the model gradually deviated from experimental heat fluxes. Denham stipulated that this is due to the beginning of the breakdown of the inverted annular flow regime. His model presented correctly the effect of subcooling and flow rate.

5.7 The Cachard Model [1994]

This model is basically a modified version of the Analytis-Yadigaroglu [1987] model. Cachard has used the same assumptions and conservation equations given by Analytis and Yadigaroglu, but he has derived new closure relationships. Mainly, he changed the equations for the heat transfer components $q_{w\text{-}v}$, $q_{v\text{-}i}$, and $q_{i\text{-}l}$, and introduced new correlations for the shear stress at the wall and at the liquid-vapour interface.

In the vapour film, the wall shear stress is expressd by

$$\tau_w = f_w \, \rho_v |U_v + U_{qf}| \frac{(U_v + U_{qf})}{2} \qquad (5.7.1)$$

where U_{qf} is the quench front velocity. Cachard expressed the friction factor, f_w, as follows

$$f_w = \frac{24}{Re_v} \quad for \; Re_v < 2000$$

$$and \qquad (5.7.2)$$

$$f_w = \frac{0.085}{Re_v^{0.25}} \quad for \; Re_v > 2000$$

where the Reynolds number is defined by

$$Re_v = \rho_v |U_v + U_{gf}| \frac{2\delta}{\mu_v} \qquad (5.7.3)$$

The above expressions are identical to those given by Analytis and Yadigaroglu [1987], with the exception of the laminar-turbulent flow transition criteria, where turbulent flow in the vapour film is assumed to exist at a Re_v larger than 2000, instead of 100 as Analytis and Yadigaroglu assumed. Cachard used the argument that turbulent flow correlations lead to unrealistic values when applied at such low Re_v (=100), since they are extrapolated beyond their intended range. He gave similar expression for the interfacial shear stress as

$$\tau_{vi} = f_{vi}\rho_v |U_v - U_l| \frac{(U_v - U_l)}{2} \qquad (5.7.4)$$

where τ_{vi} is the interfacial shear stress from the vapour side. The friction factor f_{vi} is expressed by

$$f_{vi} = \lambda_{fv} \frac{24}{Re_{vi}}$$

and (5.7.5)

$$Re_{vi} = \rho_v |U_v - U_l| \frac{2\delta}{\mu_v}$$

λ_{fv} is a momentum enhancement factor accounting for interfacial disturbances. An empirical equation was derived for λ_{fv} from Fung's [1981] data covering atmospheric conditions.

$$\lambda_{fv} = c_1(\delta^*)^{c_2}$$

$$c_1 = 0.0362 \qquad (5.7.6)$$

$$c_2 = 1.96$$

δ^* is a dimensionless film thickness given as

$$\delta^* = \delta\left[\frac{\rho_v(\rho_l - \rho_v)g}{\mu_v^2}\right]^{1/3} \qquad (5.7.7)$$

In the liquid core, the interfacial shear stress is given by

$$\tau_{li} = -f_l\rho_l|U_l - U_i|\frac{U_l - U_i}{2} \qquad (5.7.8)$$

The friction factor f_l is expressed by

$$f_l = \lambda_l\frac{16}{Re_{li}} \quad \textit{for laminar flow}$$

$$\textit{and} \qquad (5.7.9)$$

$$f_l = \lambda_l\frac{0.079}{Re_{li}^{0.25}} \quad \textit{for turbulent flow}$$

where Re_{li} is defined by

$$Re_{li} = \rho_l|U_l - U_i|\frac{(D - 2\delta)}{\mu_l}$$

Again, Cachard gave an empirical equation for λ_l as

$$\lambda_l = c_5(1 + c_6\frac{D}{z})$$
$$c_5 = 4.18 \qquad (5.7.10)$$
$$c_6 = 0.7$$

For heat transfer in the vapour film, Cachard modified Kays' [1980] equations for heat transfer of flow between parallel plates by introducing a heat transfer enhancement factor, λ_{hv}, which is empirically determined from Fungs' data. The resulting expressions are

$$q_{w\text{-}v} = \lambda_{hv}\frac{k_v Nu_v}{2\delta(1 - \theta^2)}\frac{P_w + P_l}{2}[(T_w - T_v') - \theta(T_v' - T_{sat})]$$
$$q_{v\text{-}l} = \lambda_{hv}\frac{kv Nu_v}{2\delta(1 - \theta^2)}\frac{P_w + P_l}{2}[(T_v' - T_{sat}) - \theta(T_w - T_v')] \qquad (5.7.11)$$

λ_{hv} is expressed by

$$\lambda_{hv} = c_3(\delta^*)^{c_4}$$
$$c_3 = 0.679 \qquad (5.7.12)$$
$$c_4 = 0.509$$

Nu_v and θ are the Nusselt number and the influence coefficient given by Kays [1980] in a tabular form. T'_v is the mean vapour temperature in a vapour wall-sublayer written as

$$T_v' = T_v + (\lambda_{hv} - 1)(T_v - T_{sat}) \qquad (5.7.13)$$

In the liquid core, heat transfer from the interface to the liquid is expressed by

$$q_{i-l} = h_{i-l} P_i (T_{sat} - T_l) \qquad \textbf{(5.7.14)}$$

where the interface-liquid heat transfer coefficient, h_{i-l}, is given by

$$h_{i-l} = 3.66 \lambda_l \frac{k_l}{2(R - \delta)} \left(\frac{\mu_f}{\mu_l} \right)^{-0.14} \quad \textit{for laminar flow}$$

$$h_{i-l} = \frac{|\tau_{il}| Cp_l}{|U_l - U_i| Pr_l^{2/3}} \quad \textit{for turbulent flow} \qquad \textbf{(5.7.15)}$$

The empirical factors λ_{fv}, λ_{fw} and λ_l are derived from steam-water data obtained at low flow and low pressure (atmospheric pressure), hence the model should not be expected to be valid for elevated pressures, high mass fluxes and for fluids other than water.

Table 5.1 Constitutive relations used with the model of Mosaad and Johannsen [1989]

HEAT-TRANSFER RELATIONS	EQUATIONS
Wall heat flux	$q_{w\text{-}i} = q_{w\text{-}i,c} + q_{w\text{-}i,rad}$
Wall to vapour conduction	$q_{w\text{-}i,c} = \frac{k_v}{\delta}(T_w - T_s)$
Wall to vapour radiation $q_{w\text{-}v,rad} = 0$	$q_{w\text{-}v,rad} = 0$
Wall to liquid radiation	$q_{w\text{-}i,rad} = \frac{\sigma'(T_w^4 - T_{sat}^4)}{(1/\epsilon_w + 1/\epsilon_L)}$ $\epsilon_w = 0.95; \quad \epsilon_l = 0.8$
Liquid heating	$q_{i\text{-}l} = h_{i\text{-}l}(T_{sat} - T_l) = h_{i\text{-}l,\infty}\Delta T_l F$ $h_{i\text{-}l,\infty} = 3.66\frac{k_l}{(D\text{-}2\delta)}$, *if* $Re_l < 2000$ $h_{i\text{-}l,\infty} = 0.023\frac{k_l}{(D\text{-}2\delta)} Re_l^{0.8} Pr_l^{0.4}$, *if* $Re_l \geq 2000$ $F = 1 + 0.7(D/z)$
Heat flux for vaporization and vapour heating	$q_{ev} = q_{w\text{-}i,c} + q_{w\text{-}i,\,rad} - q_{i\text{-}l} = (\frac{d\Gamma_v}{dz})h_{fg}$

Chapter 6 DFFB PREDICTION METHODS

6.1 General

DFFB heat transfer models can be grouped into three categories: empirical equations, phenomenological models (accounting for the vapour superheat) and mechanistic models. Phenomenological models can be further subdivided into local-condition and history-dependent models. Local-condition models use existing heat-transfer correlations to estimate the vapour superheat at any location downstream from the CHF point, in terms of local parameters such as quality, pressure and wall temperature or heat flux. History-dependent or integral models use a step-by-step integration procedure of the conservation equation for the vapour, and an actual volumetric vapour source to calculate the thermal non-equilibrium.

6.2 Empirical Equations

The majority of empirical equations are modifications of the Dittus-Boelter equation for single-phase heat transfer. Usually, there are two types of empirical equations: thermal equilibrium correlations and thermal non-equilibrium correlations. Thermal equilibrium correlations are based on two major assumptions: thermodynamic equilibrium between the phases and turbulent convective heat transfer from the heated wall to the vapour phase. They generally take no account of the physical phenomena involved, but are relatively easy to implement for computer calculations. Probably the best-known equilibrium correlation is that of Dougall and Rohsenow [1963], and the best-known thermal non-equilibrium correlation is that of Groeneveld and Delorme [1976]. It has

been reported by Andreani and Yadigaroglu [1994] and shown by Gottula et al. [1985] that the Dougall-Rohsenow correlation can give surprisingly good agreement with the data. For that reason, this correlation will also be examined in this study. However, in general, thermal equilibrium correlations have only a limited range of validity and should not be used outside their database. In addition to empirical equilibrium equations, Leung and Groeneveld [1988] recently proposed a post-dyout (PDO) look-up table. Basically, the PDO look-up table is a 4-D normalized data bank based on 20 000 tube PDO data, and provides PDO heat transfer coefficients as a function of pressure, mass flux, thermodynamic equilibrium quality and heat flux.

Thermal non-equilibrium equations are based on two major assumptions: thermodynamic non-equilibrium between the phases, and turbulent convective heat transfer from the heated wall to the vapour phase. The most popular thermal non-equilibrium equation is the Groeneveld-Delorme correlation. Predictions from the Groeneveld-Delorme correlation are in good agreement with data from a variety of sources. Occasionally, however, this correlation is used for heat transfer calculations at low pressure and low mass flux conditions, which are well outside its data base range and can result in large prediction errors. Probably one reason for this practice is that Groeneveld and Delorme have noted that the correlation exhibits correct asymptotic trends. Good performance of this correlation under high mass flux conditions has been reported by Kumamaru et al. [1987]. The Groeneveld-Delorme correlation is presently implemented in the ASSERT [Rowe et al., 1988] subchannel code. Recently, a non-equilibrium equation was provided by Hein and Kohler [1984]. This equation gives very good agreement with data from three fluids (water, Freon-12 and hydrogen), as reported by Andreani and Yadigaroglu [1994]. It is applicable at high pressures ($P \geq 3$ MPa) and moderate to high mass fluxes ($G \geq 300$ kgm^{-2}s^{-1}) and high qualities ($x_{eq} \geq 0.2$).

Comprehensive reviews of published heat transfer correlations were presented by Groeneveld and Gardiner [1977] and Mayinger and Langner [1978]. Table 6.1 summarizes the empirical equilibrium equations found in the published literature, while Table 6.2 summarizes the empirical non-equilibrium equations. Table 6.1 is reproduced from Groeneveld and Snoek [1986], while Table 6.2 is an updated version of Groenevelds' and Snoeks' [1986] table for non-equilibrium post-dryout equations.

6.3 Phenomenological Models

The main goal in these models is the calculation of vapour superheat based on the physical processes involved. In most of these models the wall-liquid and radiative heat transfer are neglected.

6.3.1 Local-Condition Models

The local-condition models calculate the vapour superheat and the wall heat transfer at any location downstream from the dryout point based on local thermalhydraulic parameters, such as x_{eq}, P, G, and T_W or q_w. The best-known models in this category are those of Chen, Ozkaynak and Sundaram [1979] (known as the CSO model), Yoder and Rohsenow [1983] and Varone and Rohsenow [1984]. At very low mass flux conditions, the CSO model fails to predict the data trends, and the same model in a refined form [Webb and Chen, 1984] gives a better prediction accuracy when compared to data [Andreani and Yadigaroglu, 1994]. This model includes several empirical factors, which are derived from regression analysis of data obtained at low flow, low pressure and low-to-moderate quality. Therefore, this model is not valid for elevated pressures and high mass fluxes. The Yoder and Rohsenow [1983] model (and its improved version by Varone and Rohsenow [1984]) compared fairly well with the data, as reported by Kumamaru et al. [1987] and Andreani and Yadigaroglu [1994]. However, it gives large errors at low pressure and low mass flux

conditions. Testing of the accuracy and applicability of the CSO model and the Yoder-Varone-Rohsenow model with high mass flux and high pressure data will be carried out in this study.

6.3.2 History-Dependent Models

The history-dependent models estimate the vapour superheat at any location downstream from the dryout point, recognizing that thermal non-equilibrium is dependent on the upstream conditions starting from the CHF point. Thermal non-equilibrium is calculated from a stepwise integration of the conservation equation for the vapour phase, which includes an actual volumetric vapour-generation function, Γ. These models differ mainly in the method used in attempting to estimate Γ. Examples of such models are those of Jones and Zuber [1977], Webb et al. [1982] and Webb and Chen [1984]. This class of models is not recommended for predictive purposes by Andreani and Yadigaroglu [1994], who argue that more experimental work is needed to improve these phenomenological models.

Table 6.3 summarizes the main features of the local-condition and history-dependent models.

Table 6.1 DFFB empirical equations (reproduced from [Groeneveld and Snoek, 1986])

EQUATION AND REFERENCE	RANGE OF APPLICABILITY OF EQUATION				EQUATION AGREES WITH DATA FROM REFERENCE	COMMENTS
	P MPa	G $Mgm^{-2}s^{-1}$	X	GEOMETRY		
$Nu_{vf}=0.00136Re_{vf}^{0.853}Pr_{vf}^{1/3}\left(\frac{x}{1-x}\right)^{0.147}\left(\frac{\rho_f}{\rho_g}\right)^{2/3}$ *Polomik* [1961]	5.60-10.2	1.00-2.45	0.40-0.70	Annulus	Polomik [1961]	Exponents and coefficients for these equations are obtained from least-square error analysis using data from Polomik [1961].
$Nu_{vf}=0.416Re_{vf}^{0.509}Pr_{vf}^{1/3}\left(\frac{\rho_g}{\rho_f}\right)^{0.208}\left(\frac{1-x}{x}\right)^{0.616}$ *Polomik* [1961]	5.60-10.2	1.00-2.45	0.40-0.70	Annulus	Polomik [1961]	
$Nu_{vf}=0.023Re_{vf}^{0.292}Pr_{vf}^{1/3}\left(\frac{1-x}{x}\right)^{0.01}q^{0.417}\left(\frac{\rho_f}{\rho_g}\right)^{0.091}$, q *in* $Btu/h.ft^2$ *Polomik* [1961]	5.60-10.2	1.00-2.45	0.40-0.70	Annulus	Polomik [1961]	
$Nu_g=0.00115Re_g^{0.9}Pr_g^{0.3}\left(\frac{T_w}{T_f}1\right)^{-0.15}$, T *in* °F *Polomik* [1967]	4.08-10.2	0.70-2.70	0.20-1.00	2-rod	Hench [1964]	Has additional temperature parameter to allow for property variations at the heater wall ±20% variation with data from Hench [1964].
$Nu_g=0.0039\left[Re_g\left(x+\frac{\rho_g}{\rho_f}(1-x)\right)\right]^{0.9}$ *Polomik* [1967]	4.08-10.2	0.70-2.70	0.20-1.00	2-rod	Hench [1964]	±10% variation with data from Hench [1964]. Better than above equation.
$q\left[D_e^{0.2}/(Gx)^{0.8}\right]=C(T_w-T_s)^m$, $m=1.284-0.00312G$ $C=\frac{1}{389}e^{0.01665G}$ *Collier* [1962]	7.03	>1.00	0.15-1.00	Round tubes and annuli	Polomik [1961] Bertoletti [1961]	T_w-T_{sat} must be below 200 °C.

Table 6.1 DFFB empirical equations (Continued)

EQUATION AND REFERENCE	RANGE OF APPLICABILITY OF EQUATION				EQUATION AGREES WITH DATA FROM REFERENCE	COMMENTS
	P MPa	G $Mgm^{-2}s^{-1}$	X	GEOMETRY		
$q\left[D_e^{0.2}/(Gx)^{0.8}\right]=0.018(T_w-T_{sat})^{0.921}$ *Collier* [1962]	7.03	see comments	0.15-1.00	Round tubes and annuli	Polomik [1961] Bertoletti [1961]	Correlation may be used if either $G < 1$ $Mgm^{-2}s^{-1}$ or $T_w-T_{sat} > 200$ °C.
$Nu_{vf}=0.0193Re_{vf}^{0.8}Pr_{vf}^{1.23}\left(\frac{\rho_g}{\rho_f}\right)^{0.068}\left[x+\frac{\rho_g}{\rho_f}(1-x)\right]^{0.68}$ *Bishop* [1965]	4.80-21.9	0.70-3.40	0.07-1.00	Round Tubes	Polomik [1961] Bishop [1965] Swenson [1961] Bishop [1962] Bishop [1964]	
$Nu_w=0.033Re_w^{0.8}Pr_w^{1.25}\left(\frac{\rho_g}{\rho_f}\right)^{0.197}\left[x+\frac{\rho_g}{\rho_f}(1-x)\right]^{0.738}$ *Bishop* [1965]	4.80-21.9	0.70-3.40	0.07-1.00	"	Polomik [1961] Bishop [1965] Swenson [1961] Bishop [1962] Bishop [1964]	
$Nu_w=0.098\left[Re_w\frac{\rho_w}{\rho_g}\left(x+\frac{\rho_g}{\rho_f}(1-x)\right)\right]^{0.8}Pr_w^{0.83}\left(\frac{\rho_g}{\rho_f}\right)^{0.50}$ *Bishop*[1964]	16.8-21.9	1.35-3.40	0.10-1.00	"	Swenson [1961] Bishop [1964] Miropol'skiy [1963]	Based on high-pressure data.
$Nu_w=0.055\left[Re_w\frac{\rho_w}{\rho_g}\left(x+\frac{\rho_g}{\rho_f}(1-x)\right)\right]^{0.82}Pr_w^{0.96}\left(\frac{\rho_g}{\rho_f}\right)^{0.34}\left(1+\frac{26.9}{L/D}\right)$ *Bishop*[1964]	16.8-21.9	1.35-3.40	0.10-1.00	"	Bishop [1964]	
$T_w-T_{sat}=1.915\left[\frac{q}{G\left[x+\frac{1-x}{4.15}\right]}\right]^2$ *Lee*[1970]	14.2-18.2	1.00-4.00	0.30-0.75	Tubes	Lee [1970]	Based on data obtained with 1.3 cm ID indirectly heated tube.

Table 6.1 DFFB empirical equations (Continued)

EQUATION AND REFERENCE	RANGE OF APPLICABILITY OF EQUATION				EQUATION AGREES WITH DATA FROM REFERENCE	COMMENTS
	P MPa	G $Mgm^{-2}s^{-1}$	X	GEOMETRY		
$Nu_g=0.023\left[Re_g\left[x+\frac{\rho_g}{\rho_f}(1-x)\right]\right]^{0.8} Pr_w^{0.8} Y,\ Y=1-0.1\left(\frac{\rho_f}{\rho_g}-1\right)^{0.4}(1-x)^{0.4}$ *Miropol'skiy*[1963]	4.05-22.3	0.70-2.00	0.06-1.00	Tubes	Swenson [1960] Schmidt [1960] Miropol'skly [1963]	Factor Y was determined empirically.
$Nu_{sf}=0.0089\left(Re_{sf}\frac{x}{\alpha}\right)^{0.84} Pr_{sf}^{1/3}\left(\frac{1-x_{do}}{x-x_{do}}\right)^{0.124}$ *Brevi*[1969]	5.06	0.50-3.00	0.40-1.00	"	Brevi [1969]	
$Nu_w=0.06\left\{\left[Re_w\left[x+\frac{\rho_G}{\rho_L}(1-x)\right]\right]\left(\frac{\rho_w}{\rho_G}\right)Pr_w\right\}^{0.8}\left(\frac{G}{G_0}\right)^{0.4}\left(\frac{P}{P_c}\right)^{2.7}$ $G_0=10^3 kg\ m^{-2}\ s^{-1}$ *Herkenrath*[1967]	14.2-22.3	0.75-4.10	0.10-1.00	"	Herkenrath [1967] Bishop [1964] Swenson [1961]	
$Nu_w=0.005\left[\frac{DsU_m\rho_w}{\mu_w}\right]^{0.8} Pr_G^{0.5}$ *Tong*[1964]	> 14.0	> 0.70	< 0.10	"	Bishop [1964] Bishop [1962]	Design equation. To be used only at low-quality or subcooled conditions.
$Nu_g=1.604.10^{-4}\left[Re_g\left(x+\frac{\rho_g}{\rho_f}(1-x)\right)\right]^{0.838} Pr_w^{1.81} q^{0.278}\left[\frac{k_g}{k_{crit}}\right]^{0.508}$ *q in Btu/h.ft*^{2} *Slaughterbeck*[1973]	6.88-20.2	1.05-5.30	0.12-0.90	"	Bennet [1967] Bishop [1965] Bertoletti [1964]	
$h=0.023\frac{k_g}{D}Re_g^{0.8}Pr_g^{0.4},\ Re_g=\frac{GD}{\mu_g}\left(\frac{\rho_g}{\rho_f}(1-x_{eq})+x_{eq}\right)$ *Dougall*[1963]	< 3.5	1.66-3.65	< 0.5	Tubes	Dougall [1963]	

Table 6.1 DFFB empirical equations (Continued)

EQUATION AND REFERENCE	RANGE OF APPLICABILITY OF EQUATION				EQUATION AGREES WITH DATA FROM REFERENCE	COMMENTS
	P MPa	G $Mgm^{-2}s^{-1}$	X	GEOMETRY		
$Nu_g = a\left[Re_g\left(x+\frac{\rho_g}{\rho_f}(1-x)\right)\right]^b Pr_w{}^c Y^d q^e$, *qin Btu/h.ft²*					Bennett [1967] Era [1967] Bishop [1964] Bishop [1965] Bertoletti [1961] Bertoletti [1964] Swenson [1961] Schmidt [1960]	
$Y = 1-0.1\left(\frac{\rho_f}{\rho_g}1\right)^{0.4}(1-x)^{0.4}$						
i) $a=1.85.10^{-4}$ $b=1.00$ $c=1.57$ $d=-1.12$ $e=0.131$	6.88-21.8	0.70-5.30	0.10-0.90	"		
$a=1.09.10^{-3}$ $b=0.989$ $c=1.41$ $d=-1.15$ $e=0$					Era [1967] Benett [1964] Groeneveld [1969] Polomik [1961]	
ii) $a=1.30.10^{-2}$ $b=0.664$ $c=1.68$ $d=-1.12$ $e=0.133$	3.44-10.1	0.80-4.10	0.10-0.90	Annuli	Bennett [1967] Era [1967] Bennett [1964] Groeneveld [1969] Bishop [1964] Bishop [1965] Bertoletti [1961] Bertoletti [1964]	
$a=5.20.10^{-2}$ $b=0.688$ $c=1.26$ $d=-1.06$ $e=0$						
iii) $a=7.75.10^{-4}$ $b=0.902$ $c=1.47$ $d=-1.54$ $e=0.112$	3.44-21.8	0.70-5.30	0.10-0.90	Tubes and Annuli		
$a=3.27.10^{-3}$ $b=0.901$ $c=1.32$ $d=-1.50$ $e=0$						
Groeneveld[1973]						
$q=q_{TB}+0.023(T_w-T_v)\frac{k_v}{De}\left(\frac{\rho_v V_m De}{\mu_v}\right)^{0.8} Pr_v^{0.333}$						
q_{TB} *transition boiling heat flux* V_m *near wall mixture velocity* *Tong*[1974]	4.05-10.1	0.40-5.15	0.2-1.45	Tubes	Bennet [1967] Era [1967] Keeys [1971]	Correlation also valid for transition boiling region if q_{TB} reported in Tong [1974] is used.

Table 6.1 DFFB empirical equations (Concluded)

EQUATION AND REFERENCE	RANGE OF APPLICABILITY OF EQUATION				EQUATION AGREES WITH DATA FROM REFERENCE	COMMENTS
	P MPa	G $Mgm^{-2}s^{-1}$	X	GEOMETRY		
$h=0.114Re_g^{0.244}Pr_{g,w}^{2.54}D_e^{-0.304}k_g^{0.554}$ *Mattson*[1974]	4.18-9.88	1.00-4.10	0.10-0.90	Annuli	Groeneveld [1969] Polomik [1967]	RMS error: 17.5%
$Nu_{vf}=0.0089\left(\frac{GxD}{\alpha\mu_{vf}}\right)^{0.84}\left(\frac{Cp_{vf}\mu_{vf}}{k_{vf}}\right)^{1/3}\left(\frac{1-x_{do}}{x-x_{do}}\right)^{1/8}$ *Cumo*[1974]	7	1.03-2.00	0.45-1.20	"	Cumo [1974]	Error: 10-25%

Table 6.2 Non-equilibrium post-dryout equations (updated from [Groeneveld and Snoek, 1986])

REFERENCE	NON-EQUILIBRIUM EQUATION	TO BE USED IN CONJUNCTION WITH:	COMMENTS
Chen [1979]	$\frac{x_{eq}-x_a}{x_{eq}} = \frac{0.26}{1.15-\left(\frac{P}{P_c}\right)^{0.65}} \frac{T_v-T_{sat}}{T_w-T_v}$	$h_{w,v} = \frac{f}{2} G x_a Cp_{vf} Pr_{vf}^{-\frac{2}{3}}$ $f = 0.037\left[\frac{DG}{\mu_v}\left(x_a - \frac{\rho_v}{\rho_f}(1-x_a)\right)\right]^{0.17}$	Underpredicts T_v measured by Nijhawan [1980].
Groeneveld and Delorme [1976]	$\frac{h_v-h_{veq}}{h_{fg}} = \exp(-\tan\psi)$ $\psi = a_1 Pr_{veq}^{a_2} Re_{hom}^{a_3}\left(\frac{qDCp_{veq}}{k_{veq}h_{fg}}\right)^{a_4} \sum_{i=0}^{i=2} b_i (x_{eq})^i$, a_1=0.13864, a_2=0.2031, a_3=0.20006 a_4=-0.09232, b_0=1.3072, b_1=-1.0833, b_2=0.8455, *if* $\psi < 0 \rightarrow \psi = 0$, *if* $\psi > \frac{\pi}{2} \rightarrow \psi = \frac{\pi}{2}$ $Re_{hom} = GDx_1/\mu_{veq}\alpha_{hom}$, $x_1 = \min(x_{eq}, 1)$	$Nu_{vf} = 0.008348\left[\frac{GD}{\mu_{vf}}\left(x_a + \frac{\rho_v}{\rho_f}(1-x_a)\right)\right]^{0.8774} Pr_{vf}^{0.6112}$	Overpredicts T_v measured by Nijhawan [1980]: x_a = max (predicted value, x_{do}),i.e., just downstream of dryout $x_a = x_{do}$ until T_v reaches
Tong [1974]	$\frac{x_a}{x_{eq}} = 1 + aB - 0.12\left[x_{eq} - \exp(bB^{0.8})\right]$ $B = 0.05 G/1350$ $G < 945$ $kgm^{-2}s^{-1}$ $a = -0.49$, $b = -0.26$ $1080 < G < 3375$ $a = -0.29$, $b = -0.57$ $945 < G < 1080$ *interpolate*	$q = q_{TB} + q_{FB}$, $q_{TB} = q_{NB}\exp[f(\Delta T, x_{eq}, q)]$ q_{FB} *from:* $Nu_v = 0.023\left[\frac{GD}{\mu_v}\left\{\frac{x_a\frac{\rho_v}{\rho_g} + S(1-x_a)\frac{\rho_v}{\rho_f}}{x_a + S(1-x_a)}\right\}\right]^{0.8} Pr_v^{0.4}$	Non-equilibrium is assumed to disappear for $\Delta T <$ 111 °C or $G > 3375$ $kg.m^2.s^{-1}$.
Shah [1980]	*for* $\frac{q}{h_{fg}G} > 4.5\ x10^{-4}$ $x_a = f(x_{do}, x_{eq}, Fr_f)$ $Fr_f G^2/(\rho_f^2 gD)$; *f- graphical relationship may also be obtained from table*	$Nu_{vf} = 0.008348\left[\frac{GD}{\mu_{vf}}\left(x_a + \frac{\rho_v}{\rho_f}(1-x_a)\right)\right]^{0.8774} Pr_{vf}^{0.6112}$	F_{DC} = droplet cooling factor.
Plummer [1976]	$\frac{x_a - x_{do}}{x_{eq} - x_{do}} = K = 0.07\ln\left[G(1-x_{do})^5\sqrt{\frac{D}{\rho_v}}\right] + 0.4$	$q = h_{w,v}(T_w - T_v) + h_{w,d}(T_w - T_{sat})$ $h_{w,v}$ *from:* $Nu_v = 0.23\left[\frac{Gx_aD}{\mu_v\alpha}\right]^{0.8} Pr_v^{1/3}\left[\frac{\mu_v}{\mu_w}\right]^{0.14}\left[1 + 0.3\left[\frac{D}{0.01D + L_{FB}}\right]^{0.7}\right]$ $h_{w,d} = \frac{k_{vf}}{d}(1-\alpha)\exp(-2\frac{D}{L_{FB}})$; $d = 1.22\ x10^{-4} m$	To evaluate the slip ratio, S, use an iterative procedure: $S = f(D_{do}, K, x_{eq}, x_{do})$. S needed to calculate the void. L_{FB} is the film-boiling length.

Table 6.2 Non-equilibrium post-dryout equations (Concluded)

REFERENCE	NON-EQUILIBRIUM EQUATION	TO BE USED IN CONJUNCTION WITH:	COMMENTS
Hein [1984]	$\frac{x_a}{x_{eq}}=\frac{2}{\sqrt{1+\frac{4Cp_v q}{h_{fg}(h_t F)}}-1}$ $T_v=T_{sat}+\frac{h_{fg}}{2Cp_v}\left[\sqrt{1+\frac{4Cp_v q}{h_{fg}(h_t F)}}-1\right]$	$(h_t F)=\begin{cases}1.473\ x10^{-7}(G/L_{La})^{1.33} & for\ \ G/L_{La}<1767x10^3\\ 3.078\ x10^{-24}(G/L_{La})^{4} & for\ \ G/L_{La}>1767x10^3\end{cases}$ $Nu_{w-v}=\frac{(f_w/8)(Re_v-1000)Pr_v}{1+12.7\sqrt{f_w/8}(Pr_v^{2/3}-1)}$ $f_w=(1.82\log_{10}Re_v-1.64)^{-2}$ $Re_v=\frac{GD}{\mu_v}\left[x_a+(1-x_a)\frac{\rho_v}{\rho_L}\right]$ $L_{La}=\sqrt{\frac{\sigma}{g(\rho_L-\rho_v)}}$	$(h_i F)$ expressed in kWm^{-2} q expressed in kWm^{-2} G expressed in $kgm^{-2}s^{-1}$

Table 6.3 Non-equilibrium post-dryout models

REFERENCE	NON-EQUILIBRIUM EQUATION	TO BE USED IN CONJUNCTION WITH:	COMMENTS
Saha [1980]	$\frac{dx_a}{dx_{eq}}=\frac{\Gamma_v}{qP_h/Ah_{fg}}$ $\Gamma_v=K_1\frac{k_v(1-\alpha)(T_v-T_{sat})}{D^2h_{fg}}$ *or* $\Gamma_v=\left[\frac{6(1-\alpha)}{d}\right]\left[\frac{h_{v-d}(T_v-T_{sat})}{h_{fg}}\right]$ $(1-\alpha)=\frac{1-x_a}{\left[1+\frac{x_a(\rho_f-\rho_v)}{\rho_v}\right]+\rho_f\frac{V_{Lj}}{G}}$ $V_{Lj}=1.41\left[\frac{g\sigma(\rho_f-\rho_v)}{\rho_v^2}\right]^{0.25}$ $K_1=6300\left(1-\frac{P}{P_c}\right)^2\left[\left(\frac{Gx_a}{\alpha}\right)^2\frac{D}{\rho_v\sigma}\right]^{0.5}$ $h_{v-d}=\frac{k_v}{d}\left[2+0.459\left\{\frac{\rho_v(U_v-U_f)d}{\mu_v}\right\}^{0.55}Pr_v^{0.33}\right]$ $\frac{d}{D}=1.47\left[\frac{\rho_v j_{v,do}^2\left(\frac{\sigma}{g(\rho_f-\rho_v)}\right)^{0.5}}{\sigma}\right]+0.675\left(\frac{1-x_a}{1-x_{do}}\right)^{\frac{1}{3}}$	$h_{w-v}=0.0157\frac{k_{vf}}{D}Re_{vf}^{0.84}Pr_{vf}^{0.33}\left(\frac{L}{D}\right)^{-0.04}\quad 6<\frac{L}{D}<60$ $h_{w-v}=0.0133\frac{k_{vf}}{D}Re_{vf}^{0.84}Pr_{vf}^{0.33}\quad \frac{L}{D}>60$ $Re_{vf}=\frac{\rho_vU_vD}{\mu_{vf}}=\frac{GxD}{\alpha\mu_{vf}}$	Either the d-correlation or the K_1-correlation can be used to find Γ_v.

Table 6.3 Non-equilibrium post-dryout models (Continued)

REFERENCE	NON-EQUILIBRIUM EQUATION	TO BE USED IN CONJUNCTION WITH:	COMMENTS
Varone [1984]	$\frac{dx_a}{dz}=-3\frac{(1-x_a)}{d}\frac{dd}{dz}$ $\frac{dd}{dz}=-2\left[\frac{h_{v-d}(T_v-T_{sat})}{V_f\rho_f h_{fg}}+\frac{1}{3}\frac{d}{D}\frac{V_p}{V_f}\epsilon\right]$ $\frac{dV_f}{dz}=\frac{-g}{V_f}\left(1-\frac{\rho_v}{\rho_f}\right)+\frac{3}{4}C_D\frac{\rho_v}{\rho_f}V_f(S-1)^2\frac{1}{d}$ $\frac{dT_v}{dz}=\frac{4q}{DGx_aCp_v}\left[(T_v-T_{sat})+\frac{h_{fg}}{Cp_v}\right]\frac{1}{x_a}\frac{dx_a}{dz}$ $T_w-T_v=\frac{q}{h_{w-v}\alpha}\frac{1}{2}\frac{(1-\alpha)h_{fg}V_p\rho_f}{h_{w-v}\alpha}\frac{\beta_1}{\beta_2}\epsilon$ $V_v=\frac{Gx_a}{\rho_v\alpha},\quad V_f=\frac{V_v}{S}$ $S=\frac{\frac{Gx_a}{\rho_v}}{\left[V_f-\frac{G(1-x_a)}{\rho_f}\right]}$ $\alpha=\frac{1}{\left[\frac{1-x_a}{x_a}\frac{\rho_v}{\rho_f}S+1\right]}$	$\frac{d_{do}}{D}=\frac{\rho_v\sigma}{G^2D}\frac{We_c}{(S_{do}-1)^2\left(\frac{\rho_v}{\rho_f}+\left(\frac{1}{S_{do}}-\frac{\rho_v}{\rho_f}\right)x_{do}\right)^2}$ $\alpha_{do}=\frac{1}{\frac{\rho_v}{\rho_f}S_{do}\frac{1-x_{do}}{x_{do}}+1}$ $S_{do}=1+\sqrt{1-\left(1-\frac{4}{3}\frac{\rho_f\rho_v g(1-\rho_v/\rho_f)}{G^2C_D}d_{do}\frac{\alpha^2}{x_{do}^2}\right)\left(1-\frac{16}{3}\frac{qd_{do}}{Gh_{fg}D}\frac{\rho_f}{\rho_v}\frac{1}{x_{do}}\right)}$ $S_f=\frac{V_v}{V_f}=\left(\frac{\rho_f}{\rho_v}\right)^{0.205}\left(\frac{GD}{\mu_f}\right)^{-0.016}$ $x_a=\left(\frac{S_{do}-1}{S_f-1}\right)\frac{\frac{\rho_v}{\rho_f}+\left(\frac{1}{S_{do}}-\frac{\rho_v}{\rho_f}\right)x_{do}}{\frac{\rho_v}{\rho_f}+\left(\frac{1}{S_f}-\frac{\rho_v}{\rho_f}\right)}$ $\frac{\bar{D}}{D}=\frac{1}{x_{do}-0.1}\left\{\left(\frac{d_{do}}{D}(x_a-0.1)+\left(\frac{\rho_f}{\rho_v}\right)^2\frac{We_c}{(S_f-1)^2}\frac{\rho_v\sigma}{G^2D}\right)\left[\frac{1}{\left(\frac{\rho_f}{\rho_v}\frac{1}{S_f}-1\right)}\left[1+x_a\left(\frac{\rho_f}{\rho_v}\frac{1}{S_f}-1\right)-1+x_{do}\left(\frac{\rho_f}{\rho_v}\frac{1}{S_f}-1\right)\right]\right]\right\}$ $We_c=6.5$ *properties evaluated at* T_{sat} $\epsilon=2.6\left(\frac{\rho_v}{\rho_f}\right)^{\frac{1}{2}}\left(\frac{\bar{R}}{D}\right)\left(\frac{\rho_f V_p^2 D}{\sigma}\right)^{\frac{1}{8}}\left(\frac{\beta_2 k_v(T_w-T_{sat})}{h_{fg}(\rho_v\sigma D)^{\frac{1}{2}}}\right)^{\frac{1}{2}}\left(I_2\frac{\mu_f h_{fg}}{\beta_2 k_v(T_w-T_{sat})}+I_1\right)^{-\frac{1}{4}}$ $I_1=0.225,\quad I_2=1.5$ $\bar{R}=(R_{max}+0.43D)/2$ $\frac{R_{max}^2}{D^2}=\frac{2}{3}(1+\frac{We_p}{12})\cos^2\left\{\frac{1}{3}\left[\arccos\left(\frac{-1.225}{(1+\frac{We_p}{12})^{\frac{3}{2}}}\right)\right]\right\}$ $We_p=\frac{\rho V_p^2 D}{\sigma}$ *if* $We_p < 1.74$ *then* $R_{max}=0.43D$ $\beta_1=\left(1+0.43\frac{Cp_v(T_w-T_{sat})}{h_{fg}}\right)\Big/\left(1+0.3\frac{Cp_v(T_w-T_{sat})}{h_{fg}}\right)$ $\beta_2=\frac{1}{1+0.3\frac{Cp_v(T_w-T_{sat})}{h_{fg}}}$	V_{lf} is the velocity of the liquid film. $\bar{D}$ is the mass weighted average droplet diameter at dryout. To calculate α_{do} and S_{do} iteration is required. After the first iteration step, replace d_{do} with $\bar{D}$ in S_{do} equation. ϵ is the drop cooling effectiveness, defined as the ratio of the actual drop-wall heat transfer to that completely required to evaporate drops colliding with the wall. W_p is the Weber number for drop direction perpendicular to tube wall.

Table 6.3 Non-equilibrium post-dryout models (Continued)

REFERENCE	NON-EQUILIBRIUM EQUATION	TO BE USED IN CONJUNCTION WITH:	COMMENTS
Varone [1984](cont'd)		$\delta^4=0.45\pi\bar{R}^4\left(\frac{1}{We_p}\right)^{1/2}\left[\frac{\beta_2 k_v\mu_v(T_w-T_{sat})}{\rho_v h_{fg}\sigma d}\right]\left[I_2+\frac{\beta_2 k_v(T_w-T_{sat})}{\mu_v h_{fg}}I_1\right]$ $\frac{\delta_c}{D}=\frac{\beta_1}{Nu_w}\left[\frac{T_w-T_{sat}}{T_w-T_v}\right]$ *vapour properties evaluated at* $T_f=\frac{T_v+T_{sat}}{2}$ $\frac{h_{v-d}d}{k_v}=\frac{[2+0.6Re^{1/2}Pr_v^{1/3}]}{[1+\frac{Cp_v(T_v-T_{sat})}{h_{fg}}]}$ $Re=\frac{(V_v-V_f)\rho_v D}{\mu_v}$ *properties evaluated at* T_f $C_D=\frac{27}{Re^{0.84}}$, $Re < 150$, $C_D=0.4$, $Re \geq 150$ $\frac{V_p}{V_v}=\frac{0.023}{Re^{0.1}}, Re=\frac{V_v\rho_v D}{\mu_v}$ *properties evaluated at the bulk temperature,* T_v $h_{w-v}=0.00834R_{Nu}\frac{k_v}{D}Re^{0.8774}Pr_v^{0.6112}$, $Re=\frac{Gx_e D}{\mu_v\alpha}$ *properties evaluated at the film temperature,* T_f	if $\delta > \delta_c$ drop wall interaction is not included in the wall energy balance. if $\delta < \delta_c$ drop wall interaction is included in the wall energy balance. R_{Nu} is the ratio of Nusselt number with droplets present to that without droplets.

Table 6.3 Non-equilibrium post-dryout models (Continued)

REFERENCE	NON-EQUILIBRIUM EQUATION	TO BE USED IN CONJUNCTION WITH:	COMMENTS
Yoder [1983]	$K\frac{x_a^{3/4}x_{eq}}{(1-x_a)^{7/12}}\frac{dx_a}{dx_{eq}}=(x_{eq}-x_a)$ $\frac{Cp_v(T_v-T_{sat})}{h_{fg}}=\frac{x_{eq}-x_a}{x_a}$	$K=0.0013\frac{f\Phi Pr_v^{\frac{2}{3}}\left(\sqrt{\frac{\rho_f}{\rho_v}x_{do}+1}\right)^{\frac{5}{2}}\left(\frac{\mu_v}{\mu_f}\right)^{\frac{5}{6}}A_c^{\frac{3}{4}}Re_{do}^{\frac{4}{3}}}{(1-x_{do})^{\frac{5}{12}}x_{do}^{\frac{7}{4}}\left(\frac{\rho_f}{\rho_v}\right)^{\frac{1}{12}}We_{do}^{\frac{5}{4}}}$ $A_c=\frac{q}{Gh_{fg}}, \quad Re_{do}=\frac{GD}{\mu_v}[x_{do}+\frac{\rho_v}{\rho_f}(1-x_{do})]$ $We_{do}=\frac{G^2x_{do}^2D}{\rho_v\sigma}$ $\lambda x_{do}=\frac{0.0338x_{do}}{Re_{do}^{\frac{1}{8}}A_c}$ $\frac{hD}{k_v}=0.008348\left(\frac{Gx_aD}{\mu_v\alpha}\right)^{0.8774}Pr_v^{0.6112}$ *properties evaluated at* T_f $\frac{1}{\alpha}=1+\frac{1-x_a}{x_a}\frac{\rho_v}{\rho_f}$ $T_w=T_v+q/h$	Requires the use of charts (not suitable for computer calculations). f and Φ are drop diameter functions, which are read from charts. λx_{do} is the product of the deposition parameter and dryout quality, which is read from charts.

Table 6.3 Non-equilibrium post-dryout models (Concluded)

REFERENCE	NON-EQUILIBRIUM EQUATION	TO BE USED IN CONJUNCTION WITH:	COMMENTS
Chen [1984]	$G\frac{dx_a}{dz}=\Gamma$ $\Gamma=\Gamma_{NF}+\Gamma_{FF}$ $\Gamma_{NF}=\Gamma_{eq}\exp(-0.0016\frac{\Theta_w L/D}{G(1-x_a)})$ $\Gamma_{eq}=\frac{4q}{Dh_{fg}}$, $\Theta_w=T_w-T_{sat}$ $\Gamma_{FF}=0.02\frac{G^2}{\rho_v^2}\frac{(1-\alpha_h)^{\frac{2}{3}}\Theta_v}{Dh_{fg}}$, $\Theta_v=T_v-T_s$	$h_{w\text{-}v}=h_{modCSO}(1+F_s)(1+0.8(L/D)^{-1})$ $F_s=250\left(\frac{P}{P_c}\right)^{0.69}\left(\frac{1-x_a}{x_a}\right)^{0.49}Re_v^{-0.55}$ $h_{modCSO}=\frac{f}{2}Cp_{vf}Gx_aPr_{vf}^{-\frac{2}{3}}$ $f=f_{cp}\left(\frac{T_w}{T_v}\right)^{-0.1}$ $\frac{1}{f_{cp}^{0.5}}=3.48-4\log_{10}\left(\frac{2\epsilon}{D}+\frac{9.35}{Re(f_{cp})^{0.5}}\right)$ $\epsilon=1.5\ \mu m$ *(drawn tubing)*	Low mass flux conditions $G \leq 100\ kgm^{-2}s^{-1}$ $0.21 \leq P \leq 7$ MPa $0.0 \leq x_{CHF} \leq 0.66$

Chapter 7 DFFB EMPIRICAL EQUATIONS

This chapter describes in detail the most important empirical equations. It also describes important assumptions underlying their formulation, along with the range of data on which they are based.

7.1 The Dougall-Rohsenow Correlation [1963]

This correlation was derived assuming complete thermodynamic equilibrium between the phases. Dougall and Rohsenow postulated that if the amount of liquid present is small, a modified form of the Dittus-Boelter equation should give a fairly accurate representation of the heat transfer in DFFB. Due to the presence of liquid droplets, however, the velocity used in the definition of the Reynolds number should be selected properly, to represent the flow field. Accordingly, Dougall and Rohsenow defined a two-phase flow velocity as

$$U = \frac{Q_l + Q_v}{A} \tag{7.1.1}$$

where Q_l, Q_v and A represent the average volumetric flow rate of liquid, average volumetric flow rate of vapour in the test section and the fluid-flow cross-sectional area, respectively. Physically, this velocity represents the total volumetric flow rate of the fluid per unit cross-sectional area. Hence, introducing Eq. (7.1.1) into the Dittus-Boelter equation yields

$$Nu = 0.023\left[\frac{\rho_g D}{\mu_g}\left(\frac{Q_l + Q_v}{A}\right)\right]^{0.8} Pr_g^{0.4} \qquad (7.1.2)$$

or, in terms of a two-phase Reynolds number,

$$Nu = 0.023\, Re_{2\Phi}^{0.8}\, Pr_g^{0.4}$$

$$Re_{2\Phi} = Re_g\left[x_{eq} + \frac{\rho_g}{\rho_f}(1 - x_{eq})\right] \qquad (7.1.3)$$

where the fluid properties are evaluated at the saturation temperature. Dougall and Rohsenow noted that the correlation should be most accurate at moderate qualities, and less accurate at higher qualities, where the bulk vapour temperature can deviate considerably from saturation conditions. Although not mentioned by the authors, it is assumed that this equation should not be used at low flow, where non-equilibrium becomes very significant. Also, it is assumed that the accuracy of the correlation diminishes considerably at low qualities, where the flow regime might be that of the inverted annular flow.

7.2 The Groeneveld-Delorme Correlation [1976]

This non-equilibrium correlation falls in the category of local-condition correlations. Although the correlation is empirical in nature, it has been developed based on the physical phenomena involved. It provides correct asymptotic trends of heat-transfer coefficient and calculation of the actual vapour temperature. Groeneveld and Delorme estimated the vapour superheat at any location downstream from the dryout point using a suitable single-phase heat

transfer correlation for superheated steam modified for two-phase flow. It is argued that this choice is reasonable based on the following assumptions:

-direct droplet-wall contact is insignificant,

-radiative heat transfer from the wall is negligible, and

-flow is homogeneous.

The authors have justifications for these assumptions.

The range of conditions for the correlation's database is: mass flux from 130 to 5200 kgm^2s^{-1}, pressure from 6.9 to 21.5 MPa, and equilibrium quality from -0.12 to 3.09.

At the time of the development of the correlation, data for the actual vapour temperatures at post-dryout conditions were not available. Hence, to estimate the actual vapour qualities, Groeneveld and Delorme inferred values of x_a from data of wall temperature measurements. The Hadaller and Banerjee [1969] correlations for superheated steam, modified for two-phase flow, were employed for that purpose. Then, the inferred value of actual quality were utilized to obtain a correlation for the vapour enthalpy. The relations derived for the wall heat transfer coefficient, the actual quality and the vapour enthalpy are expressed as follows:

$$\frac{q_w}{T_w - T_v} = h = 0.008348 \frac{k_{vf}}{D} \left[\frac{GD}{\mu_{vf}} \left(x_a + \frac{\rho_v}{\rho_f} (1 - x_a) \right) \right]^{0.8774} Pr_{vf}^{0.6112} \qquad (7.2.1)$$

$$\frac{x_a}{x_{eq}} = \frac{h_{fg}}{h_v(P,T_v) - h_f} \qquad (7.2.2)$$

$$\frac{h_v(P,T_v) - h_v(P,T_{sat})}{h_{fg}} = \exp(-\tan\ \psi), \qquad (7.2.3)$$

$$\psi = a_1 Pr_v^{a_2}\ Re_{hom}^{a_3} \left(\frac{q_w\ D\ Cp_{v_{eq}}}{k_{v_{eq}}\ h_{fg}} \right)^{a_4} \sum_{i=0}^{2} b_i\ (x_{eq})^i \qquad (7.2.4)$$

$$(if\ \psi < 0\ then\ \psi = 0,\ if\ \psi > \frac{\pi}{2}\ then\ \psi = \frac{\pi}{2})$$

$$Re_{hom} = \frac{GD}{\mu_{v_{eq}}} \left[x_1 + \frac{\rho_v}{\rho_f}(1 - x_1) \right] \qquad (7.2.5)$$

$$(0 < x_1 = x_{eq} < 1\ )$$

where

$a_1 = 0.13864$, $b_0 = 1.3072$,

$a_2 = 0.2031$, $b_1 = -1.0833$,

$a_3 = 0.20006$, $b_2 = 0.8455$,

$a_4 = -0.09232$

7.3 The Shah Correlation [1980]

Shah developed a non-equilibrium-based prediction method applicable to various fluids, based on the following assumptions:

-DFFB is the post-dryout flow regime,

- thermodynamic equilibrium exists between the phases at the dryout location,

-at low-to-moderate reduced pressures, heat transfer from the wall to liquid droplets due

to droplet-wall direct contact is negligible,

-at high reduced pressures, heat transfer by droplet-wall direct contact is important, and

-radiative heat transfer from the wall is neglected.

The range of conditions for the correlation covers mass flux from 30 to 3442 $kgm^{-2}s^{-1}$, pressure from 0.14 to 21.5 MPa, and equilibrium quality from 0.1 to 2.9.

The total heat flux from the wall is written as

$$q_w = q_c + q_{dc} = F_{dc}\, h_{w\text{-}v}(T_w - T_v) \qquad \textbf{(7.3.1)}$$

where q_c, q_{dc}, F_{dc} and $h_{w\text{-}v}$ represent the heat flux removed from the wall through convection by vapour, the heat flux removed from the wall through liquid droplet cooling, the enhancement factor due to droplet cooling of the heated wall, and the vapour heat-transfer coefficient, respectively. The vapour temperature is obtained from a heat balance and is expressed by

$$\frac{x_{eq} - x_a}{x_a} h_{fg} = \int_{T_{sat}}^{T_v} Cp_v \, dT = h_v - h_g \qquad \textbf{(7.3.2)}$$

Two expressions are presented for the actual quality:

$$\begin{aligned} &For\ Bo \le 4.5\ x10^{-4} \\ &x_a = x_{eq} \\ &For\ Bo > 4.5\ x10^{-4} \\ &x_a = f(x_{do},\ x_{eq},\ Fr_f) \end{aligned} \qquad \textbf{(7.3.3)}$$

where Bo and Fr_f are the boiling number and the Froude number ($= G^2/\rho^2_f gD$), respectively. The

functional relation for x_a in Eq. (7.3.3) is presented in a graphical form. Shah provides a step-by-step procedure for the calculation of actual quality. The enhancement factor, F_{dc}, for steam-water flow is expressed as

$$F_{dc} = \begin{cases} 1.5\ x_a^{0.14}, & P_r > 0.8 \text{ and } x_a \geq x_{do} + 0.30 \\ 1.0, & \text{otherwise} \end{cases} \qquad (7.3.4)$$

and is 1 for other fluids. The Hadaller correlation, modified for two-phase flow, is employed to estimate the heat transfer from the wall to the vapour. The correlation is expressed as

$$h_{w\text{-}v} = \frac{k_{vf}}{D}\ 0.00834 \left(\frac{G\ D\ x_a}{\mu_{vf}\ \alpha} \right)^{0.8774} Pr_{vf}^{\ 0.6112} \qquad (7.3.5)$$

The properties in Eq. (7.3.5) are evaluated at the film temperature. For other fluids, the Dittus-Boelter equation is chosen:

$$h_{w\text{-}v} = \frac{k_v}{D}\ 0.023 \left(\frac{G\ D\ x_a}{\mu_v\ \alpha} \right)^{0.8} Pr_v^{\ 0.4} \qquad (7.3.6)$$

The vapour properties in Eq. (7.3.6) are evaluated at the actual vapour temperature. In both Eqs. (7.3.5) and (7.3.6), the void fraction is needed to calculate the heat transfer coefficients. Thus, by assuming no slip between the phases, Shah suggested the use of the homogeneous void fraction:

$$\alpha = \frac{x_a\ \rho_f}{(1 - x_a)\rho_v + \rho_f\ x_a} \qquad (7.3.7)$$

7.4 Other Correlations

Other empirical non-equilibrium equations of interest have been developed by Nishikawa et al. [1982] and Koizumi et al. [1988], for tubes and rod bundles, respectively. Also, empirical relations for the calculation of thermal non-equilibrium have been developed by Chen and Chen [1993].

Chapter 8 DFFB PHENOMENOLOGICAL MODELS

This chapter outlines the formulation of various models. Most of these phenomenological models comprise several empirical factors. Therefore, their applicability will be limited to the range of data base from which these factors are derived.

8.1 The Chen-Ozkaynak-Sundaram Model [1979]

This model is based on a simplified description of the physical phenomena. It presents correlations for estimating the vapour superheat and the wall-to-vapour heat-transfer coefficient. First, the authors used the turbulent analogy between heat and momentum transfer (based on the Colburn modification of Reynolds analogy), and expressed the heat-transfer coefficient as:

$$h = G\, x_a\, Cp_{vf}\, Pr_{vf}^{-2/3}\, \frac{f}{2} \qquad \textbf{(8.1.1)}$$

where the factor, f, is the Fanning friction factor, approximated from Beattie's [1975] correlation for post-CHF dispersed flow. The properties are evaluated at the film temperature. To calculate the heat transfer from the wall to the vapour, the actual vapour temperature, T_v, and the actual quality, x_a, are needed. In attempting to predict the degree of non-equilibrium, Chen et al. used the fact that thermal non-equilibrium (expressed usually as the ratio or the difference between actual quality and thermodynamic quality) depends mostly on the dynamic balance in heat transfer between the vapour phase and liquid phase (dispersed droplets). Then, based on a comparison against data, Chen et al. established a dependency relationship between quality ratio and a non-dimensional temperature, T_d:

$$\frac{x_a}{x_{eq}} = 1 - B(P)\ T_d \qquad \textbf{(8.1.2)}$$

where

$$T_d = \frac{T_v - T_{sat}}{T_w - T_v} \qquad \textbf{(8.1.3)}$$

The coefficient B was obtained from regression analysis and is given as

$$B(P) = \frac{0.26}{1.15 - (P/P_{crit})^{0.65}} \qquad \textbf{(8.1.4)}$$

$$for\ 0 < P < 2830\ psia.$$

Finally, to obtain the actual vapour temperature, T_v, Eq. (8.1.2) is solved, along with a second independent relationship for quality ratio. This relation is obtained from a heat balance and is given as

$$\frac{x_a}{x_{eq}} = \frac{h_{fg}}{h_v(P,T_v) - h_f(P,T_{sat})} \qquad \textbf{(8.1.5)}$$

Equations (8.1.2) and (8.1.5) are solved to determine T_v and x_a. Therefore, given the local input parameters P, G, x_{eq}, and T_w, the wall heat flux can be predicted using Eq. (8.1.1), the vapour temperature and the actual quality,

$$q_{w\text{-}v} = h_{w\text{-}v}\ (T_w - T_v) \qquad \textbf{(8.1.6)}$$

8.2 The Saha Model [1980]

This model is based on a mechanistic modelling of the heat-transfer phenomena involved. The main goal is to develop a constitutive relation for the volumetric vapour generation. Then, the local vapour temperature and the actual quality are found from mass and energy conservation. The following assumptions have been employed in the development of the model:

-one-dimensional flow field, i.e., at any flow cross section, the velocity and the temperature distributions are uniform,

-droplets have the same diameter at any given cross section,

-droplets are at saturation temperature, and

-direct wall-to-droplet and radiation heat transfer are negligible.

An expression for the mass rate of vapour generation was presented based on the conservation of mass and the heat transfer to the droplets,

$$\Gamma = \left[\frac{6(1 - \alpha)}{d} \right] \left[\frac{h_{v\text{-}d} (T_v - T_{sat})}{h_{fg}} \right] \qquad \textbf{(8.2.1)}$$

where $h_{v\text{-}d}$ is the convective heat transfer coefficient between the vapour and a droplet. The interfacial heat transfer coefficient, $h_{v\text{-}d}$, is given as

$$h_{v\text{-}d} = \frac{k_v}{d} \left[2 + 0.459 \left\{ \frac{\rho_v (U_v - U_d) d}{\mu_v} \right\}^{0.55} Pr_v^{0.33} \right] \qquad \textbf{(8.2.2)}$$

The Heineman [1960] correlation for superheated steam is utilized for the heat-transfer coefficient, $h_{w\text{-}v}$, between heated surface and vapour,

$$h_{w\text{-}v} = 0.0157 \frac{k_{vf}}{D} Re_{vf}^{0.84} Pr_{vf}^{0.33} \left(\frac{L}{D}\right)^{-0.04} \quad 6 < \frac{L}{D} < 60$$

$$h_{w\text{-}v} = 0.0133 \frac{k_{vf}}{D} Re_{vf}^{0.84} Pr_{vf}^{0.33} \quad \frac{L}{D} > 60 \tag{8.2.3}$$

The vapour continuity equation is expressed as

$$\frac{dx_a}{dx_{eq}} = \frac{\Gamma}{(q_w P_h) / A h_{fg}} \tag{8.2.4}$$

As indicated in Eq. (8.2.1), the prediction of the volumetric mass rate of vapour generation requires the void fraction, α, the vapour-to-droplet heat transfer, $h_{v\text{-}d}$, and the droplet diameter, d. Usually, the droplet diameter is the most difficult to calculate. Saha devised a procedure to circumvent this problem: two approaches are employed to obtain Γ. In the first method, Γ is rewritten as

$$\Gamma = K_1 \frac{k_v(1 - \alpha)(T_v - T_s)}{D^2 h_{fg}} \tag{8.2.5}$$

The parameter K_1 is considered as a measure of the effectiveness of vapour-to-droplet heat transfer, and is expressed in terms of local flow variables as

$$K_1 = 6300 \left(1 - \frac{p}{p_{crit}}\right)^2 \left[\left(\frac{Gx_a}{\alpha}\right)^2 \frac{D}{\rho_v \sigma}\right]^{0.5} \tag{8.2.6}$$

The void fraction is expressed as

$$(1 - \alpha) = \frac{1 - x_a}{\left[1 + \frac{x_a(\rho_f - \rho_v)}{\rho_v}\right] + \frac{\rho_f V_{Lj}}{G}} \qquad \textbf{(8.2.7)}$$

where the droplet drift velocity, V_{Lj}, is defined as follows:

$$V_{Lj} = -1.41 \left[\frac{g\ \sigma(\rho_f - \rho_v)}{\rho_v^2}\right]^{0.25} \qquad \textbf{(8.2.8)}$$

In the second method, the droplet diameter d is correlated in terms of the actual quality, x_a, and an average droplet diameter at dryout, d_{do},

$$\frac{d}{d_{do}} = \left[\frac{1 - x_a}{1 - x_{do}}\right]^{1/3} \qquad \textbf{(8.2.9)}$$

An expression for the average droplet diameter at dryout is obtained based on a consideration of the balance between inertia and surface tension forces, and of flow conditions for droplets entrained in the pre-dryout annular flow region. It is written as

$$\frac{d_{do}}{D} = 1.47\left[\frac{\rho_g\ j_{g,do}^2\{\sigma/[g(\rho_f - \rho_g)]\}^{1/2}}{\sigma}\right]^{-0.675} \qquad \textbf{(8.2.10)}$$

where $j_{g,do}$ is the volumetric vapour flux density at dryout, i.e., Gx_{do}/ρ_g. Therefore, the droplet diameter, d, is expressed as

$$\frac{d}{D} = 1.47 \left[\frac{\rho_g \, j_{g,do}^2 \{\sigma/[g(\rho_f - \rho_g)]\}^{1/2}}{\sigma} \right]^{-0.675} \left(\frac{1 - x_a}{1 - x_{do}} \right)^{1/2} \qquad \textbf{(8.2.11)}$$

Now, given K_1, to calculate the wall temperature for a given wall heat flux, Eqs. (8.2.5), (8.2.3), (8.2.6), (8.2.7), (8.2.8), along with

$$q_w = h_{w\text{-}v}(T_w - T_v)$$

$$\textit{and} \qquad \textbf{(8.2.12)}$$

$$h_v(P,T_v) = h_g + \frac{(x_{eq} - x_a)}{x_a} h_{fg}$$

can be solved simultaneously. Alternatively, given d from Eq. (8.2.11), Eqs. (8.2.1), (8.2.3), (8.2.8) and (8.2.2) are solved to predict the wall temperature from Eq. (8.2.12).

8.3 The Yoder-Varone-Rohsenow Model [1983, 1984]

In this model, the momentum and energy equations for both vapour and liquid were developed. An average droplet diameter at dryout and heat-transfer correlations for the vapour-to-droplet and wall-to-droplet were employed to complete the model. The solution involves a step-by-step integration down the tube from the dryout location. The model was later refined by presenting a graphical solution for the actual quality versus the equilibrium quality. The main assumptions of the model are that:

-at dryout the quality is equal to the equilibrium quality,

-droplet size distribution can be characterized by one average drop size, and

-liquid droplets are at saturation.

The model requires knowledge of the drop size at dryout. Yoder and Rohsenow [1983] established

a procedure to calculate an average drop diameter at dryout. The expressions needed for the calculation of the average drop diameter are listed in Table 6.3.

The authors considered the following heat-transfer mechanisms:

-heat transfer from the heated surface to the vapour,

-heat transfer from the vapour to the liquid droplets, and

-heat transfer from the heated wall to droplets during droplet-wall collisions.

Several complex expressions were derived for the prediction of wall temperature. These equations and their constitutive relations are summarized in Table 6.3. The model requires the input values of the mass velocity, G, the wall heat flux, q, the tube diameter, D, the dryout quality, x_{do}, and the fluid properties. The authors have refined the model to simplify the solution procedure. Yoder and Rohsenow [1983], after various simplifications, arrived at the following relation:

$$K \frac{x_a^{3/4}\, x_{eq}}{(1 - x_a)^{7/12}} \frac{dx_a}{dx_{eq}} = x_{eq} - x_a \qquad \textbf{(8.3.1)}$$

where K represents a non-equilibrium constant dependent on fluid parameters. The expression for K is listed in Table 6.3. The solution of Eq. (8.3.1) is given in graphical form as x_a versus x_{eq} for various magnitudes of the non-equilibrium parameter K. One disadvantage of this relation is the graphical solution for x_a, which is convenient for hand calculations, but not for computer applications.

8.4 The Webb-Chen Model [1984]

The main purpose of the analysis is to determine correlations for the vapour generation source function, Γ. Based on observations of some vapour superheat data, Webb and Chen concluded

that the vapour generation rate is high near the quench front (near-field region), but becomes low further downstream (far-field region). Since the vapour superheat is low near the CHF point, the postulated higher vapour generation rate in the near-field region can only be attributed to direct wall-to-liquid contact. The authors hypothesized that the wall-to-liquid contact is due to the sputtering action of the liquid film at the CHF location. Then, it is assumed that the near-field vapour generation rate, Γ_{NF}, is related to the wall superheat, Θ_w, the distance from the quench front, L/D, and the liquid mass flux, $G(1-x_a)$. Accordingly, an expression for Γ_{NF} is derived and is written as

$$\Gamma_{NF} = \Gamma_{eq} \exp\left(- 0.0016 \frac{\Theta_w \; L/D}{G(1 - x_a)} \right) \qquad \textbf{(8.4.1)}$$

where Γ_{eq} is the vapour generation rate function such that the equilibrium quality, x_{eq}, is maintained. In the far-field region, the vapour generation Γ_{FF} is assumed to occur mainly due to droplet evaporation, and the evaporation rate is dependent on the local vapour superheat. The expression for Γ_{FF} is

$$\Gamma_{FF} = 0.02 \; \frac{G^2}{\rho_v^2} \frac{(1 - \alpha)^{2/3} \Theta_v}{h_{fg} D} \qquad \textbf{(8.4.2)}$$

where α represents the homogeneous void fraction. Hence, the total vapour generation rate is given as the sum of the near-field and the far-field generation rates,

$$\Gamma = \Gamma_{NF} + \Gamma_{FF} \qquad \textbf{(8.4.3)}$$

Next, a correlation for the convective heat-transfer coefficient at the heated surface is needed

to predict the wall temperature given the heat flux, or vice versa. The authors have postulated that the enhancement in wall heat transfer in dispersed flow compared to single-phase superheated steam is due to the liquid droplets, which act as distributed heat sinks in the vapour. Consequently, a two-phase heat-transfer coefficient is defined as

$$h_{2\Phi} = h_{1\Phi}(1 + F_s)\ (1 + 0.8\ (L/D)^{-1}) \tag{8.4.4}$$

where F_s, the sink factor, is written as

$$F_s = 250\ (P/P_{crit})^{0.69} \left(\frac{1 - x_a}{x_a} \right)^{0.49} Re_v^{-0.55} \tag{8.4.5}$$

and the two-phase heat transfer coefficient is given as

$$h_{2\Phi} = h_{\text{mod CSO}}\ (1 + F_s)\ (1 + 0.8\ (L/D)^{-1}) \tag{8.4.6}$$

The coefficient $h_{\text{mod CSO}}$ ($=h_{1\Phi}$) is the heat transfer coefficient used in the modified CSO correlation (Webb and Chen [1983]). Therefore, given Γ and $h_{2\Theta}$, the wall temperature can be obtained by solving the steady-state one-dimensional continuity and energy equations:

$$\begin{gathered} G dx_a = \Gamma dz \\ \text{and} \\ \frac{x_a}{x_{eq}} = \frac{h_{fg}}{h_v(P,T_v) - h_f} \end{gathered} \tag{8.4.7}$$

8.5 The Nishikawa et al. Model [1986]

Nishikawa et al. [1986] attempted to determine the non-equilibrium between the phases by

introducing a non-dimensional parameter, Kn, which was empirically obtained with Freon-22 data. As a consequence, this formulation is assumed to be mainly valid for DFFB with Freon. The parameter, Kn, is considered as a measure of the degree of thermodynamic non-equilibrium in dispersed flow. The non-equilibrium equation is obtained from the conservation of energy equation for the two-phase flow mixture as

$$\frac{dx_a}{dx_{eq}} = \frac{h_{v\text{-}d}\, A_d\, (T_v - T_{sat})}{q_w} \qquad \textbf{(8.5.1)}$$

where A_d is the total surface area of droplets per unit area of the inside wall surface of the tube, q_w is the inside wall heat flux, and h_d is the heat-transfer coefficient from the vapour to the liquid droplets given as

$$h_{v\text{-}d} = \frac{k_v}{d}\,\frac{1}{1+B}(2 + 0.6\, Re_d^{1/2}\, Pr_v^{1/3})$$

and

$$Re_d = \frac{\rho_v(U_v - U_d)d}{\mu_v} \qquad \textbf{(8.5.2)}$$

$$B = \frac{h_v - h_g}{h_{fg}}$$

From the energy equation for a liquid droplet, the droplet diameter d can be expressed as

$$\frac{dd}{dx_{eq}} = -\frac{GDh_{v\text{-}d}}{2q_w\rho_f U_d}(T_v - T_{sat}) \qquad \textbf{(8.5.3)}$$

and from the equation of motion:

$$\frac{dU_d}{dx_{eq}} = \frac{GDh_{fg}}{4q_w}\left[\frac{3}{4}\frac{C_D\rho_v(U_v - U_d)^2}{\rho_l U_d D_d} - \frac{(\rho_l - \rho_v)}{\rho_l U_d}g\right] \tag{8.5.4}$$

The actual quality is related to the actual vapour enthalpy and the equilibrium quality as follows:

$$x_a = \frac{h_{fg}}{h_v(p,T_v) - h_f}\, x_{eq} \tag{8.5.5}$$

The equation is rewritten to express explicitly the vapour temperature, T_v

$$T_v - T_s = \frac{h_{fg}}{Cp_v}\left(\frac{x_{eq}}{x_a} - 1\right) \tag{8.5.6}$$

The drag coefficient C_D is obtained from

$$C_D = \frac{C_{Do}}{1 + B}$$

$$C_{Do} = \begin{cases} 24Re_d^{-1}, & Re_d \le 2 \\ 18.5Re_d^{-0.6}, & 2 < Re_d \le 5\ x10^2 \\ 0.44, & 5\ x10^2 < Re_d < 2\ x10^5 \end{cases} \tag{8.5.7}$$

Then, by substituting Eq. (8.5.2) into Eq. (8.5.1), one can obtain the following expression:

$$\frac{dx_a}{dx_{eq}} = \frac{1}{B_o Kn}\left(\frac{x_{eq}}{x_a} - 1\right) \tag{8.5.8}$$

where B_o represents the boiling number and is given as

$$B_o = \frac{q_w}{G h_{fg}} \tag{8.5.9}$$

and the non-equilibrium parameter Kn is written as

$$Kn = \frac{G\ Cp_v}{h_{v\text{-}d}\ A_d} \tag{8.5.10}$$

Alternatively, Nishikawa et al. correlated Kn as a function of local non-dimensional parameters:

$$Kn = 4.26 \times 10^3 \left(\frac{GD}{\mu_v}\right)^{0.52} \left(\frac{G^2 D}{\sigma \rho_v}\right)^{-0.73} Pr_v^{0.3} \left(\frac{\rho_v}{\rho_l}\right)^{0.3} x_a^{\,n} \times (1 - x_a)^{-0.20} \left(\frac{x_{eq}}{x_a} - 1\right)^{0.83} \tag{8.5.11}$$

where n is defined as

$$n = 2.0 \exp\left[-1.3 \left(G \frac{\mu_v}{\sigma} \rho_v\right) \left(\frac{\rho_f}{\rho_v} - 1\right)^{1.7}\right] - 1 \tag{8.5.12}$$

A heat transfer correlation for superheated vapour Freon is introduced. The correlation is written as

$$h_{w\text{-}v} = \frac{k_v}{D} 0.0048 \left\{ \left(\frac{GD}{\mu_v} \right) \left[x_a + \frac{\rho_v}{\rho_f}(1 - x_a) \right] \right\}^{0.92} \times Pr^{0.4} \left[1 + \frac{2}{(L/D)^{1.1}} \right] \tag{8.5.13}$$

and the wall heat flux as

$$q_w = h_{w\text{-}v} \, (T_w - T_v) \tag{8.5.14}$$

Then, the prediction of the wall temperature for a given heat flux can be obtained from Eq. (8.5.14) by solving Eq. (8.5.8) numerically together with Eqs. (8.5.11), (8.5.12), (8.5.2) and (8.5.3).

8.6 The Jones-Zuber Model [1977]

Jones and Zuber [1977] derived a simplified procedure to reduce the calculation of thermal non-equilibrium to the solution of a single equation. The major assumptions in this model are that

-droplets have spherical shape, and are at saturation temperature,

-heat transfer is in two steps: (i) from the heated wall to the vapour, and (ii) from the vapour to liquid droplets,

-distribution of droplet concentration at any flow cross-section is uniform, and

-flow field is one-dimensional.

From an energy conservation for the vapour phase, the vapour generation rate, Γ, is given as

$$\Gamma = \frac{6 \, h_{v\text{-}d} \, (T_v - T_{sat})(1 - \alpha)}{d \, h_{fg}} \tag{8.6.1}$$

where $h_{v\text{-}d}$, α and d represent the droplet heat transfer coefficient, the void fraction and the droplet diameter, respectively. The thermal equilibrium and non-equilibrium qualities are related through the mixture enthalpies

$$\frac{(x_{eq} - x_a)}{x_a} = \frac{(h_v - h_g)}{h_{fg}} = \frac{Cp_v(T_v - T_{sat})}{h_{fg}} \tag{8.6.2}$$

Hence, the vapour superheat temperature is expressed as

$$(T_v - T_{sat}) = \frac{(x_{eq} - x_a)\, h_{fg}}{x_a\, Cp_v} \tag{8.6.3}$$

Mass and energy conservation of the vapour phase give

$$\frac{dx_a}{dz} = \frac{\Gamma}{G}$$

$$and \tag{8.6.4}$$

$$\frac{dx_{eq}}{dz} = \frac{\Gamma_{eq}}{G} = \frac{qP_h}{GAh_{fg}}$$

where P_h is the heated wall perimeter. Alternatively, the non-equilibrium can be expressed as

$$\frac{d(x_a - x_{eq})}{dz} = \frac{\Gamma - \Gamma_{eq}}{G} \tag{8.6.5}$$

Then, using Eq. (8.6.1) for Γ in Eq. (8.6.5) yields

$$\frac{d(x_{eq} - x_a)}{dz} + \frac{(x_{eq} - x_a)}{\left[\frac{G\ d\ Cp_v x_a}{6h_{v\text{-}d}(1 - \alpha)}\right]} = \frac{q\ P_h}{GAh_{fg}} \qquad \textbf{(8.6.6)}$$

Equation (8.6.6) is rewritten in non-dimensional form so that

$$\frac{d(x_{eq} - x_a)}{dx_{eq}} + N_{sr}\ (x_{eq} - x_a) = 1 \qquad \textbf{(8.6.7)}$$

where the superheat relaxation number, N_{sr}, is given as

$$N_{sr} = \frac{3}{2}\left(\frac{n\pi}{6}\right)^{2/3} \frac{k_v D h_{fg}}{Cp_v q_w x_a}\ Nu_{v\text{-}d}\ (1 - \alpha)^{1/3} \qquad \textbf{(8.6.8)}$$

Jones and Zuber employed a Dittus-Boelter type correlation for heat transfer from the wall to the vapour phase:

$$Nu_{w\text{-}v} = 0.023\left(\frac{GD}{\mu_v}\frac{x_a}{\alpha}\right)^{0.8} Pr_v^{0.4} \qquad \textbf{(8.6.9)}$$

By assuming that the drag and buoyancy forces are balanced, a relation for the droplet diameter is derived:

$$d = \frac{3C_D \rho_v U_r^2}{\alpha g \Delta\rho} \qquad \textbf{(8.6.10)}$$

where U_r is the relative velocity between droplets and vapour, and $\Delta\rho$ is the density difference

between liquid and vapour. The drag coefficient, C_D, is obtained from

$$C_D = \frac{24}{Re_d}(1+ 0.1Re_d)^{0.7}$$
$$Re_d = \frac{(U_v - U_d)d\rho_v}{\mu_v} \qquad \textbf{(8.6.11)}$$

In the original paper the droplet Reynolds number, Re_d, in Eq. (8.6.11) was expressed as a function of the vapour velocity, U_v, instead of the relative velocity, $(U_v - U_f)$. Physically, that is not correct, and hence the relative velocity between the phases was employed.

The droplet size is related to the droplet size at dryout, to give

$$d = d_{do}\left(\frac{1 - \alpha}{1 - \alpha_{do}}\right)^{1/2}$$
and $$\textbf{(8.6.12)}$$
$$d_{do} = \left(\frac{27}{4}\right)^{1/6}\left(\frac{C_D\sigma We_{do}}{\alpha g\Delta\rho}\right)^{1/2}$$

The slip ratio can be given as

$$\frac{U_v}{U_f} = \left(1 - \frac{\alpha\rho_v U_r}{Gx_a}\right)^{-1} \qquad \textbf{(8.6.13)}$$

A correlation for the heat-transfer coefficient from the vapour to a droplet is given as

$$Nu_d = 2 + 0.74\ Re_d^{1/2}\ Pr_v^{1/3} \qquad \textbf{(8.6.14)}$$

Thus, at any location downstream from the dryout point, Eqs. (8.6.12)-(8.6.14) can be used to solve

for the drop diameter, relative velocity, slip ratio and void fraction. The actual quality is calculated with Eq. (8.6.7) and (8.6.8) in conjunction with Eq. (8.6.9), and the wall temperature is obtained with Eq. (8.6.9).

Jones and Zuber showed that the agreement is poor between predictions of this model and data. To improve the prediction accuracy, they derived an empirical relaxation number, N_{sr}, which is written as

$$N_{sr} = \begin{cases} 14.3\ Bou\left(\dfrac{S}{P_r^{0.5}}\right)^2, & \dfrac{S}{P_r^{0.5}} < 0.22 \\ 1.23\ Bou\left(\dfrac{S}{P_r^{0.5}}\right)^{3/8}, & \dfrac{S}{P_r^{0.5}} > 0.22 \end{cases} \qquad \textbf{(8.6.15)}$$

where P_r, S and Bou represent the reduced pressure, the slip ratio and the Boussinesque number, $G/\rho_L(gd_{do})^{0.5}$, respectively.

8.7 The Moose-Ganić Model [1982]

Moose and Ganić presented a DFFB mechanistic model that is based on the same approach taken by other researchers (Laverty and Rohsenow [1964], Forslund and Rohsenow [1968], and Hynek et al. [1969]). The heat transfer from the heated wall is assumed to follow three heat-transfer paths: heat transfer from wall to vapour, from wall to droplets and from vapour to liquid droplets. This model is very similar to that of Hynek et al. [1969], but includes equations developed by Ganić and Rohsenow [1976] for homogeneous droplet distribution and Leidenfrost heat-transfer correlation from the heated surface to impinging liquid droplets. Further refinements are introduced for the droplet size distribution and droplet diameter at the dryout location. In general, formulation of mechanistic models of this type results in several equations of flow-parameter gradients, such as the

bulk vapour temperature, vapour quality, droplet size and vapour velocities. The same gradient equations derived by Hynek et al. [1969] are employed in this model.

The model is based on the following assumptions:

-thermodynamic equilibrium holds at dryout,

-superheating of the vapour downstream of the dryout location is possible,

-the liquid phase takes the form of spherical droplets, characterized by statistical distribution,

-liquid droplets are at saturation,

-there are three heat transfer paths: wall to vapour, vapour to liquid and wall to liquid, and

-radiation heat transfer is negligible.

The equations for the gradients utilized in the model are given next. The droplet velocity gradient is written as

$$\frac{dU_f}{dz} = \frac{3C_D\ \rho_v\ (U_v - U_f)^2}{4d_{32}\ \rho_f\ U_f} - \left[1 - \frac{\rho_v}{\rho_f}\right]\frac{g}{U_f} \qquad \textbf{(8.7.1)}$$

where C_D and d_{32} represent the drag coefficient and the Sauter mean diameter for a characteristic mean droplet size, respectively. The Sauter mean diameter, d_{32}, was chosen by the authors as the characteristic droplet size, and is defined as

$$d_{32} = 4d_* \qquad \textbf{(8.7.2)}$$

where d_* represents the most probable droplet diameter. Next, the droplet diameter gradient is given as

$$\frac{dd_{32}}{dz} = \frac{-2q_{v\text{-}d}}{h_{fg}\ \rho_f\ U_f} - \frac{4d_{32}\ q_{w\text{-}d}}{3(1 - x_a)D\ G\ h_{fg}} \tag{8.7.3}$$

where $q_{v\text{-}d}$, $q_{w\text{-}d}$ and D are the heat flux from the vapour to the droplet, heat flux from the wall to the droplet and the tube diameter, respectively. The actual quality and the equilibrium quality gradients are:

$$\frac{dx_a}{dz} = \frac{-3(1 - x_{do})d_{32}^{\ 2}}{d_{do}^{\ 3}}\frac{dd_{32}}{dz}$$

$$\frac{dx_{eq}}{dz} = \frac{4q_w}{G\ h_{fg}\ D} \tag{8.7.4}$$

where q_w denotes the total heat flux from the wall defined as

$$q_w = q_{w\text{-}v} + q_{w\text{-}d} \tag{8.7.5}$$

Finally, the vapour temperature gradient is written as

$$\frac{dT_v}{dz} = \frac{h_{fg}\ \frac{dx_{eq}}{dz} - [h_{fg} + Cp_v(T_v - T_{sat})]\frac{dx_a}{dz}}{x_a\ Cp_v} \tag{8.7.6}$$

At the dryout location, the Hynek et al. [1969] procedure was used to determine the initial liquid and vapour velocities, $(U_f)_{do}$ and $(U_v)_{do}$. Also, the velocity gradient at dryout is taken as

$$\frac{dU_f}{dz} = \frac{4q_w\ x_a}{h_{fg}\ D\ \rho_v} \tag{8.7.7}$$

Further, Hynek's Weber number at dryout ($We=We_c=7.5$) is replaced by the following expression:

$$We = \frac{\rho_v(U_v - U_f)^2 d_{32}}{\sigma} \tag{8.7.8}$$

Other constitutive relations are presented for the heat transfer from the vapour to a droplet, from the wall to the vapour and from the wall to a droplet:

$$q_{v\text{-}d} = \frac{2(T_v - T_{sat})k_v}{d_{32}}\left(1 + 0.276 Re_d^{0.8} Pr_v^{0.33}\right)$$

$$h_{w\text{-}v} = \frac{k_v}{d}\left(0.023 Re_v^{0.8} Pr_v^{0.33}\right)\left(\frac{\mu_v}{\mu_w}\right)^{0.14} \tag{8.7.9}$$

$$q_{w\text{-}d} = V_o(1 - \alpha)\rho_f h_{fg}' f_c \epsilon$$

In Eq. (8.7.9), V_o, h_{fg}', f_c and ε represent the droplet deposition velocity, the effective heat of vaporization, the fraction of the liquid mass that impinges on the heated surface and the efficiency of evaporation of an impinging liquid droplet, respectively. Equations for V_o, h_{fg}', f_c and ε are given below:

$$V_o = 0.17U^* \tag{8.7.10}$$

$$h_{fg}' = h_{fg} + Cp_v(T_w - T_v) \tag{8.7.11}$$

$$f_c = \frac{1}{24}\,[\bar{d}^4 + 4\bar{d}^3 + 24\bar{d} + 24]\exp(-\bar{d}), \qquad \bar{d} = \frac{d_c}{d_*} \tag{8.7.12}$$

$$\varepsilon = 8.44\ x10^{-4}\left(\frac{\rho_f^2\ V_o^2\ \bar{d}_{10}}{\rho_{fv}\sigma}\right)^{0.341} \exp\left[1 - \left(\frac{T_w}{T_{sat}}\right)^2\right] \tag{8.7.13}$$

where U^*, d_c, and d_{10} are the friction velocity, the deposition cutoff diameter (droplets smaller than d_c cannot reach the heated surface) and the average droplet size striking the wall, respectively. The average droplet size striking the wall is written as

$$\bar{d}_{10} = \left[\frac{\bar{d}^2 + 2\bar{d} + 2}{\bar{d} + 1}\right] d_* \tag{8.7.14}$$

The wall temperature is determined from

$$\begin{aligned} q_{w\text{-}v} &= h_{w\text{-}v}(T_w - T_v) \\ q_w &= q_{w\text{-}v} + q_{w\text{-}d} \end{aligned} \tag{8.7.15}$$

which give

$$T_w = \frac{q_w - q_{w\text{-}d}}{h_{w\text{-}v}} + T_v \tag{8.7.16}$$

8.8 Other models

Other attempts to establish mechanistic models have been made by Styrikovich et al. [1982],

Koizumi et al. [1979], Kaminaga [1981], and Mastanaiah and Ganić [1981].

Chapter 9 REVIEW OF EXPERIMENTAL METHODS AND PARAMETRIC TRENDS OF SUBCOOLED FILM BOILING

9.1 General

Interest in subcooled film boiling was initially limited to cryogenic applications. Before 1978, IAFB experimental data obtained with water as the working fluid were virtually non-existent, since the CHF phenomenon would result in wall temperatures in excess of the melting point of the test section material. To avoid the problem of a large temperature rise normally associated with the transition from subcooled nucleate boiling to subcooled film boiling, Groeneveld [1978] proposed the so-called "hot-patch" technique to perform IAFB experiments. Since then, two versions of the hot-patch technique have been developed and successfully applied, and a large amount of data have been generated for water flowing upwards in a vertically mounted circular tube. These are: the data of Fung [1981]; the data of Stewart and Groeneveld [1982]; the data of Laperriere [1983]; the data of Swinnerton, Hood and Pearson [1988]; the data of Mosaad and Johannsen [1988]; and the data of Chen, Fu and Chen [1988].

A close look at the recent literature reveals that the current low-quality film boiling research is directed towards obtaining more data with water as the working fluid to predict coolant behaviour during a LOCA . This trend will lead to the narrowing of the large gaps existing in the water data base. Although the gaps in the available data base of water might be continuously filled in the

future, the gaps in the data base of cryogenic or refrigerant fluids will probably remain unfilled, or at best will fill at a much slower pace. To provide a thorough check of the reliability of existing models and correlations, the heat transfer characteristics of film boiling should be investigated in greater detail with various kinds of liquids (besides water), such as refrigerants, organic liquids, and so on. With water as the working fluid, it is still difficult to reach the high heat flux required for higher subcooling, higher flow rate and higher pressure flow conditions with the hot-patch technique, due to restrictions imposed by the performance of the cartridge heaters: CHF may reach a high value to cause failure of the cartridge heaters of the hot patch. On the other hand, this problem will not be encountered if a refrigerant liquid is used.

The IAFB characteristics of water can be investigated by direct experimentation in water (usually requiring expensive thermalhydraulic test facilities operating at high pressures, temperatures and power), or by using refrigerant fluids, as in this study at water equivalent conditions (i.e., same Re, Nu, ρ_l/ρ_g, x); this is more cost effective, as it requires much lower power, pressure and temperature. Furthermore, refrigerant data permits a more thorough check of the reliability of existing film boiling models and equations: since the physical mechanisms of IAFB are the same for all fluids, a reliable IAFB model or equation should give reasonable agreement with data obtained in any fluid.

9.2 The Indirectly Heated Hot-Patch Technique Experiments

The indirectly heated hot-patch consists of a hollow copper cylinder brazed to the electrically heated test section. Heat to the hot patch is supplied by cartridge heaters embedded in the copper block. Recently, experimental data of water using the indirectly heated hot-patch technique have been obtained by several authors. Table 9.1 summarizes the test conditions of IAFB studies that

have used the indirectly heated hot-patch technique.

9.3 The Directly Heated Hot-Patch Technique Experiments

More data using water as the test fluid have been generated by applying the directly heated hot-patch technique. In these experiments the wall thickness of the test section tube is reduced over a short length at both ends, to increase the local electrical resistance of the tube. Power to the hot patch and the test section maybe controlled separately. This experimental method was first applied by Chen and Li [1984]. Table 9.2 summarizes the test conditions of IAFB experiments that have used the directly heated hot-patch technique.

9.4 Parametric Trends in Subcooled Film Boiling

9.4.1 Mass Flux Effect

The observed mass flux effect on the heat transfer coefficient during steady state IAFB under different experimental conditions has been summarized in Table 9.3. In general, at higher mass flow rates, the vapour layer is thinner and turbulence intensity is higher. Consequently, the heat transfer coefficient increases. The increase in heat transfer coefficient with mass flux in the positive quality region ($x_{eq}>0$) is due to the higher vapour velocities. At low mass flux values and in the subcooled region, the mass flux effect is, generally, small.

9.4.2 Inlet Subcooling Effect

In general, an increase of the heat transfer coefficient with an increased inlet subcooling was observed (Table 9.4). At low inlet subcooling, higher vapour generation will result in a higher Re_v, which will improve the convective heat transfer. At high inlet subcooling, low vapour superheat and low vapour generation will result in a much thinner vapour film layer, hence higher conductive heat transfer. For a given inlet subcooling, in the subcooled region the void fraction is low. Conduction

through the vapour film is the dominant heat transfer mode. The thickness of the vapour film depends on the bulk temperature of the liquid core region. The higher the difference between the liquid core temperature and the saturation temperature at that location, the thinner the vapour film layer. In the positive quality region (x_{eq} >0), far away downstream of the hot patch, the convective heat transfer coefficient becomes more important, due to high void fraction. Hence, heat flux is higher for lower inlet subcooling.

9.4.3 Length Effect

Table 9.5 summarizes the observed axial location effect. Heat transfer coefficient near the entrance region is high, due to the entrance effect. The creation of a vapour blanket at the dryout or quench location considerably disturbs the flow. Also, the heat transfer at the entrance region (subcooled region) is mainly by conduction across a thin vapour film, and this results in higher heat transfer coefficient at the beginning of the dry patch. At the positive quality region, the vapour film becomes thicker; this initially results in an increased thermal resistance and hence a lower heat transfer coefficient. At locations further downstream, the vapour velocity also increases. This increases the convective component and the overall heat transfer coefficient increases.

9.4.4 Heat Flux Effect

Table 9.6 summarizes the heat flux effect. Conduction is the dominant mode of heat transfer in the subcooled region of IAFB. In this region, an increase in the heat flux results in an increase in the vapour film thickness, because the increased evaporation rate results in higher heat transfer resistance. In the positive quality region, a higher heat flux results in higher vapour flow, and hence a better mixing and lower vapour superheat. These effects produce a better overall heat transfer coefficient in this region.

9.4.5 Pressure Effect

The pressure effect on the heat transfer coefficient during steady state IAFB is summarized in Table 9.7. In general, the heat transfer coefficient increases with increasing pressure. The improvement in the heat transfer coefficient can be attributed to the thinner vapour film. At higher pressures, the vapour film thickness decreases, due to the increase of the vapour density. This effect improves the heat transfer across the vapour film.

Table 9.1 Summary of IAFB data obtained by the indirectly heated hot-patch technique

Reference	Test Fluid	Geometry	Pressure (MPa)	Mass Flux ($kgm^{-2}s^{-1}$)	Inlet quality
Fung [1981]	water	tube	atmospheric	50-500	-0.131 to -0.009
Laperriere [1983]	water	tube	9.6	1000-4500	-0.190 to 0.150
Stewart and Groeneveld [1982]	water	tube	2-9	110-2750	-0.160 to -0.026
Swinnerton et al. [1988]	water	tube	0.2-2	47-1010	-0.053 to -0.005
Takenaka et al. [1989]	R-113	tube	0.1	136-1280	-0.075 to -0.019

Table 9.2 Summary of IAFB data obtained by the directly heated hot-patch technique

Reference	Test Fluid	Geometry	Pressure (MPa)	Mass Flux ($kgm^{-2}s^{-1}$)	Inlet quality
Chen and Li [1984]	water	tube	atmospheric	134-646	-0.101 to 0.000
Chen [1987]	water	tube	1-5.5 atm	130-920	-0.144 to 0.000
Chen et al. [1988]	water	tube	0.105-1.024	25-512	-0.029 to 0.12
Chen et al. [1989]	water	tube	0.41-6.0	47.6-1462	-0.05 to 0.24
Mosaad and Johannsen [1989]	water	tube	atmospheric	50-500	-0.056 to 0.000

Table 9.3 Mass flux effect

Mass flux range, $kgm^{-2}.s^{-1}$	Pressure, MPa	Inlet quality	Test fluid	Effect on H.T.C.[a]	References
50-500	atmospheric	-0.13 to -0.01	water	The heat flux increases with increasing mass flux for all axial locations.	Fung [1981]
110-2750	2-9	-0.16 to -0.03	water	In general, the H.T.C. increases with increasing mass flux. At high inlet subcooling mass flux effect is strong. At lower inlet subcooling mass flux effect is much smaller.	Stewart [1982]
1000-4500	9.6	-0.19 to 0.15	water	At low subcooling and positive inlet quality, the H.T.C. is strongly affected by mass flux.	Laperrière [1983]
20-160	0.2	-0.11 to 0.10	water	The H.T.C. increases with increasing mass flux.	Denham [1984]
130-880	2 atm	-0.14 to 0.00	water	The H.T.C. increases with increasing mass flux.	Chen [1987]
90-476	0.4	-0.12 to -0.03	water	The H.T.C. increases with increasing mass flux.	Chen [1988]
100-400	0.110	-0.06 to 0.00	water	The H.T.C. increases with increasing mass flux.	Mosaad [1988]
106-1266	0.10	-0.08 to -0.02	R-113	The H.T.C. increases with mass flux for G>320 $kgm^{-2}.s^{-1}$ with large gradient. For G<210 $kgm^{-2}.s^{-1}$ the increase is very small. The flow pattern for G<210 probabily is different from G>320.	Takenaka [1989]
98.3-1460	6-7.4	-0.24 to -0.05	water	The H.T.C. increases with increasing mass flux.	Chen [1990]

[a] H. T. C. is an abreviation for heat transfer coefficient.

Table 9.4 Inlet subcooling effect

Inlet quality	Pressure, MPa	Mass flux, $kgm^{-2}s^{-1}$	Test fluid	Effect on H.T.C.[a]	References
-0.131 to -0.009	atmospheric	50-500	water	Heat flux increased with increased subcooling near DNB location (subcooled region). The effect on heat flux is reduced or even reversed far away downstream from dryout location (positive quality region).	Fung [1981]
-0.160 to -0.026	2-9	110-2750	water	Little effect at low G and x_{eq}>0.05. Strong effect at high G, especially, at high P and low x_{eq}.	Stewart [1982]
-0.190 to 0.150	9.6	1000-4500	water	Subcooling effect is stronger for low mass flux than at higher mass flux. The H.T.C. increases with x_{eq} for low mass flux at low inlet subcooling.	Laperrière [1983]
-0.110 to 0.100	0.2	40	water	The H.T.C. increased with lower inlet quality.	Denham [1984]
-0.120 to -0.029	0.105-1.024	25-512	water	H.T.C. increased significantly with increased inlet subcooling. This increase seems less steep at lower inlet subcooling.	Chen [1987]
-0.240 to -0.050	0.41-6.0	47.6-1462	water	Inlet quality effect is most significant over a short region near the dryout point (subcooled region). Generally, the H.T.C. increases with a high inlet subcooling increase.	Chen et al. [1989]

[a] H. T. C is an abreviation for heat transfer coefficient.

Table 9.5 Axial location effect

Pressure, MPa	Mass flux, $kgm^{-2}s^{-1}$	Inlet quality	Test fluid	Effect on H.T.C.[a]	Reference
0.1	300	-0.13 to -0.01	water	H.T.C. decreases initially, then levels off towards the end and, under certain conditions, it may increase.	Fung [1981]
atmospheric	134-646	-0.10 to 0.00	water	The H.T.C. decreases continuously at low inlet subcooling. At higher inlet subcooling, the H.T.C. increases initially to a maximum, then it decreases further downstream.	Chen and Li[1984]
0.2	20-160	-0.11 to -0.05	water	From negative to positive quality, the H.T.C. showed a continuous decrease along the axial direction downstream of the quench front.	Denham [1984]
3.6,5.5 atm	420,880	-0.14 to 0.00	water	At very low inlet subcooling, the H.T.C. distribution is rather uniform. At higher subcooling and mass flux, the H.T.C. increases to a maximum, then it decreases. At lower mass flux, the H.T.C. decreases along the heated length.	Chen [1987]
atmospheric	100,500	-0.06 to 0.00	water	The H.T.C. decreases steeply along the heated length.	Mosaad and Johannsen[1988]
0.6-0.74	110-1460	-0.01 to -0.001	water	At lower mass flux, the H.T.C. decreases continuously along the heated length. As mass flux increa,ses the H.T.C. levels off, then it increases at higher mass flux.	Chen et al. [1989]

[a] H. T. C. is an abreviation for heat transfer coefficient.

Table 9.6 Heat flux effect

Heat flux range, kWm^{-2}	Pressure, MPa	Mass flux, $kgm^{-2}s^{-1}$	Inlet quality (Inlet subcooling)	Test fluid	Effect on H.T.C.[a]	References
112-245	2-9	359,923	-0.16,-0.03	water	Generally, the H.T.C. is reduced as the heat flux is increased. This effect is strongest at higher mass fluxes and lower qualities. At positive qualities ($x_{eq}\geq 0.005$), a slight reversal in the trend (at 2-4 MPa) was observed.	Stewart [1982]
133-589	9	1000-4500	-0.19 to 0.15	water	Generally, the H.T.C. increases with decreasing heat flux. For higher mass fluxes, the heat flux effects are more noticeable at the upstream region of IAFB, especially at lower heat flux. In the downstream region, this effect decreases.	Laperrière [1983]
307-598	atmospheric	270,624	-0.06	water	The H.T.C. decreases with increasing heat flux.	Chen and Li [1984]
61-200	5.8,6.0	410,920	-0.008,-0.054	water	In general, in the subcooled region an increase in the heat flux produces a decrease on the H.T.C.; however, the trend is reversed at positive qualities.	Chen et al.[1989]

[a] H. T. C. is an abreviation for heat transfer coefficient.

Table 9.7 Pressure effect

Pressure range, MPa	Mass flux, $kgm^{-2}s^{-1}$	Inlet quality	Test fluid	Effect on H.T.C.[a]	References
2,4,6,8	359,923	-0.05,-0.06,-0.06,-0.07	water	In general, the H.T.C. decreases with decreasing pressure. At higher pressures the axial temperature distribution is more uniform than at lower pressures.	Stewart and Groeneveld [1982]
1,5.5 atm	130,830	0,-0.08	water	At low subcooling and low flow rates, the H.T.C. increases with pressure. At higher subcooling and lower flow rates the trend is reversed.	Chen [1987]
0.136,0.402,1.004	195	-0.008,0.005,0.007	water	Generally, the H.T.C. increases with increasing pressure.	Chen et al. [1988]
0.59-5.88	420	-0.029 to 0.00	water	The H.T.C. increases with increasing pressure.	Chen et al. [1989]

[a] H. T. C. is an abreviation for heat transfer coefficient.

Chapter 10 EXPERIMENTAL SETUP AND PROCEDURE

10.1 Loop and Test Conditions

A small multi-fluid loop was constructed for studying the subcooled film boiling regime. A schematic diagram of the apparatus is shown in Fig. 10.1. The loop was originally designed to perform CHF tests for non-aqueous fluids, but later was modified to accommodate post-CHF experiments. The volume of the loop was approximately 2.6 litres. The maximum pressure of the film boiling experiments was 1.4 MPa . For safety purposes, the loop was designed to withstand a pressure up to 3.3 MPa .

The major components of the loop were the secondary coolant water supply, the recirculating gear pumps (two pumps mounted in series), the coriolis mass flow meter, the preheater, the heat exchanger, the test section and the pressurizer. The loop was constructed from stainless steel, with the main tubing being of 1/2 inch nominal diameter. The heat exchanger and a few minor parts in the loop were made from brass. The heat exchanger was of the tube and tube type rated at 3.3 MPa, and made by Packless Industries. The heat exchanger and the preheater can be operated together, to provide a wide range of subcooling. The secondary side of the loop was a once-through open loop, providing cooling water from taps on-site. The loop pressure was adjusted by varying the power to a 500-W tubular heater mounted at the bottom of the pressurizer to boil the liquid, and by controlling the cooling water flow rate through a cooling coil located at the top of the pressurizer to condense the vapour.

In this study, three different refrigerants were used as working fluids: (i) Freon-12, as it is the refrigerant used widely in air-conditioning equipment, and has been used as a thermalhydraulic modelling fluid for many years, (ii) Freon-22, an alternative refrigerant having only 1/20th of the ozone depletion potential (ODP) of Freon-12, and (iii) Freon-134a, the currently recommended replacement for Freon-12, having an ODP value of zero. Because of the low latent heat of these fluids (about 10-15 times less than water), the maximum power required was only 2.0 kW. To prevent flow instability, the flow was throttled at the test section inlet; the mass flow rate was also controlled by this throttle valve. The generated vapour in the test section was condensed in the heat exchanger. The experimental conditions were as follows: (1) exit pressures of 0.83, 1.14 and 1.40 MPa; mass velocities between 530 and 3000 $kgm^{-2}s^{-1}$; and inlet subcoolings between 8 and 28°C. A total of 290 runs were performed at different combinations of inlet subcooling, mass flux and pressure.

10.2 Test Section

The test section was made of Inconel-718 tubing with a 4.38 mm ID and 5.46 mm OD; it is shown schematically in Fig. 10.2. The test section was heated by D.C. electric power supplied through copper power electrodes clamped tightly onto the tube. The power supply was capable of delivering a maximum power of 2.5 kW. The heated length of the test section was 0.90 m.

The indirectly heated hot-patch technique was used. The hot patch was silver-brazed to the Inconel tube, and equipped with six 250-watt cartridge heaters. The purpose of the hot patch was to stop the quench front from propagating downstream. Also, by using the hot patch the low-temperature region of the film boiling curve was easily covered, and Freon decomposition, due to high surface temperatures, was avoided. For a heat flux controlled system, and without the hot

patch, only the high-temperature region of the film boiling curve can be covered. Furthermore, with the hot patch the power required to reach CHF was much lower than that for a uniformly heated tube without the hot patch (approximately 6 to 8 times lower). Figure 10.3 shows a schematic of the hot patch.

The test section was equipped with thirty bare-wire chromel-alumel thermocouples, of 0.13 mm diameter, to measure the axial temperature distribution during film boiling. The thermocouples were fixed to the outside surface and electrically isolated from it by a thin layer of Teflon tape. Preliminary tests indicated that the maximum temperature drop across the Teflon layer was about 0.3°C. The tube wall inside temperature was determined from a one-dimensional (radial) conduction equation for the tube (see Appendix A for details). The entire test section was insulated with high-temperature fibre glass insulation; the heat loss through it (up to 3% of the total heat input) was experimentally determined by means of heat balance tests and zero flow runs, and included in the data reduction. Appendix A provides the details of the heat loss and heat balance calculations. Appendix B gives the details of error analyses for temperature, mass flow rate, pressure, and power measurements.

10.3 Controls and Instrumentation

Controls were located at the front panel of the loop, which also served as a protection shield. Controls performed the following functions:

-controlled temperatures (at the inlet and outlet of pumps, at the inlet of test section, etc.),

-controlled loop pressure to 3 MPa,

-controlled loop mass flow rate to 4000 $kgm^{-2}s^{-1}$, and

-controlled the flow rate, temperature and pressure to the secondary side of the heat

exchanger.

The instrumentation required to perform post-CHF experiments provided the following measurements:

-test section mass flow rate,

-coolant temperature at the inlet and outlet of the test section,

-total pressure at the inlet and outlet of the test section,

-temperature in different sections of the loop,

-total D.C. power to the test section and the hot patch, and

-test section outside wall temperatures.

The D.C. power applied to the test section was measured by monitoring the voltage across the test section and the hot patch, and the current across a calibrated shunt in series with the tube. The voltage was read by a Fluke 45 dual display multimeter, and the current calculated from the shunt, which has a voltage drop of 50 millivolts at a full value of 250 Amperes. Temperatures at the test section inlet and exit were measured with calibrated sheathed thermocouples in the flow stream. Flow around the loop was provided by two 350-W gear pumps manufactured by Micropump Corporation. Each pump had its own flow bypass, to prevent flow instabilities. The flow through the test section and mass flow meter was varied by means of a flow control valve manually operated from the front control panel of the loop. The mass flow rate was measured directly by a high-precision coriolis-type mass flowmeter, covering a range from 0 to 300 kgh^{-1}. The mass flow meter signal was converted to D.C. voltage and processed by the data acquisition system. The absolute pressure at the exit of the tube was measured by a pressure transducer, and the pressure at the inlet of the tube was measured by a pressure gauge. The fluid temperature at the inlet and outlet of the

heat exchanger and pumps was measured with chromel-alumel thermocouples. These measurements were made to monitor loop operation and aid in loop control. Measurements of wall temperatures of the test section were made with ungrounded chromel-alumel thermocouples. The outputs of the thermocouples were directly connected to the data acquisition system for permanent recording. All sensor outputs were displayed on a CRT monitor.

The data acquisition system is composed of an IBM PC compatible (386) as the host computer for data processing and analysis, a high-speed analog-to-digital converter (Model 236), a 32-channel analog expansion module (Model 252), an IBM PC /XT/AT/386 interface card (Model 802) and a table-top chassis (Model 293) to encase the 236 and 252 modules. Modules 236, 252, 802 and 293 were manufactured by Sciemetric Instruments Inc. GEN 200 (version 4.1) was the software used for controlling the data acquisition process. It is a menu-driven package that has various controlling and scanning features.

10.4 Procedure

Steady film boiling was achieved in the test section as follows. Flow conditions at the test section inlet were established. The hot patch was then heated to the desired film boiling temperature, which was predetermined from preliminary tests. Once stable film boiling was established at the hot patch, the test section power was gradually increased until the dry patch started to propagate from the hot patch in the downstream direction. When the dry patch arrived at the upper power clamp, the test section power was reduced to a safe level in order to avoid Freon decomposition. Sufficient time was allowed for test conditions to stabilize. Data were then recorded and stored in a computer disk for later processing. The power was subsequently reduced in steps, and data scans were taken at each power level until rewetting of the test section occurred. One data scan consisted of

measurements of the thirty outside wall thermocouple signals and mass flow rate signals. Pressures and fluid temperatures at the test section inlet and outlet were measured. The temperature and mass flow rate measurements were automatically averaged by the data acquisition system, to eliminate any electronic noise that might be present.

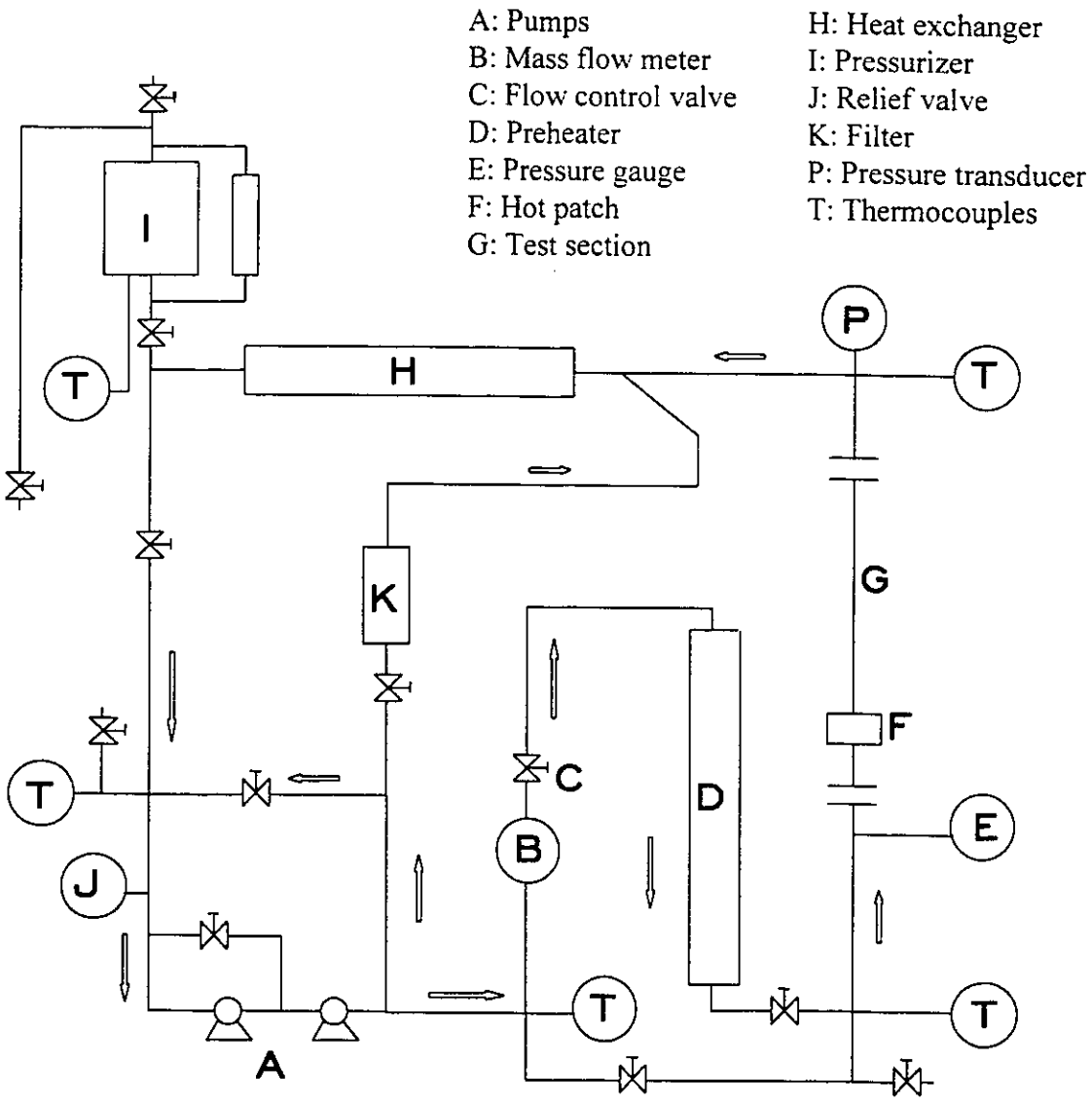

Figure 10.1 Schematic diagram of the experimental apparatus.

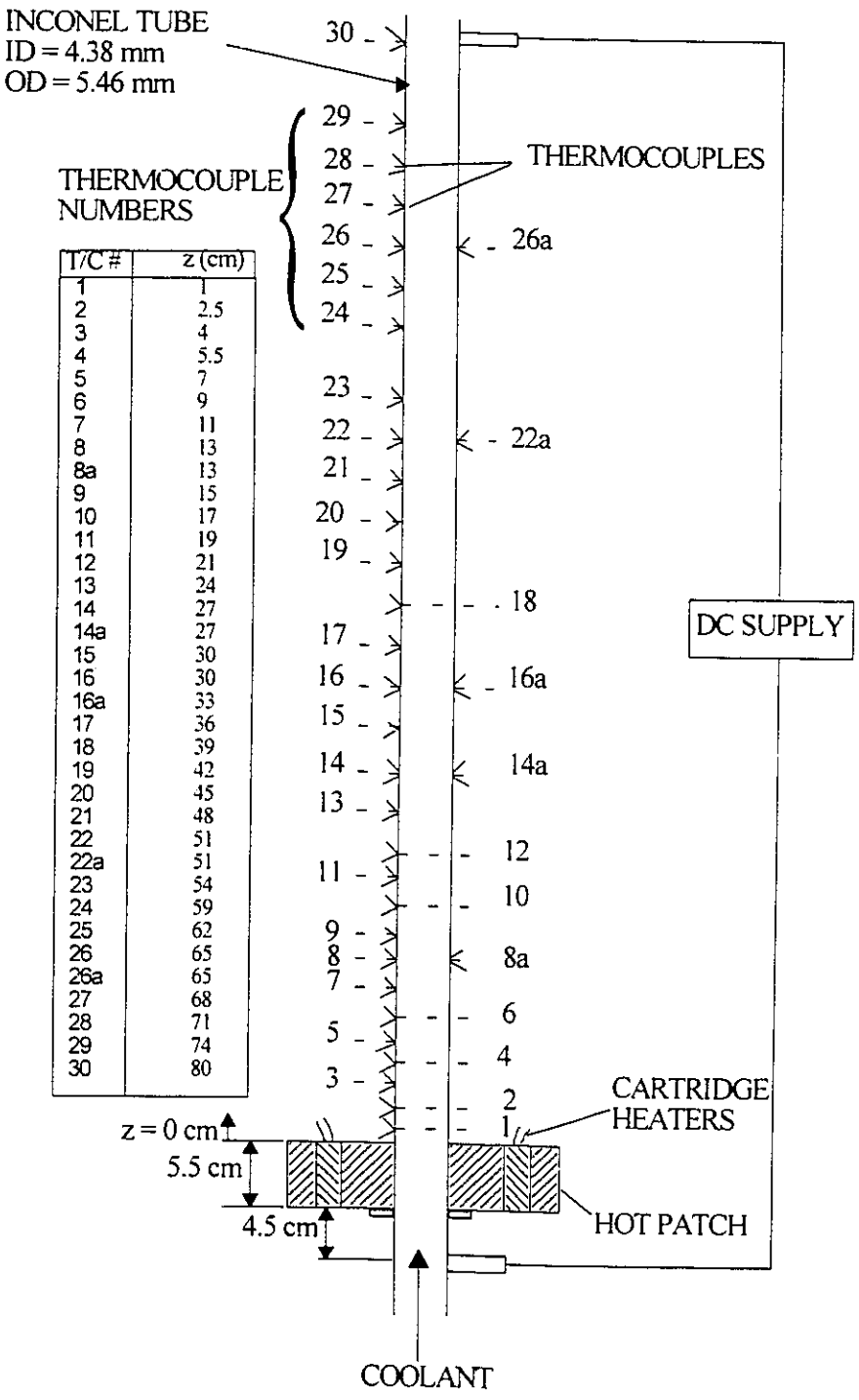

Figure 10.2 Test section.

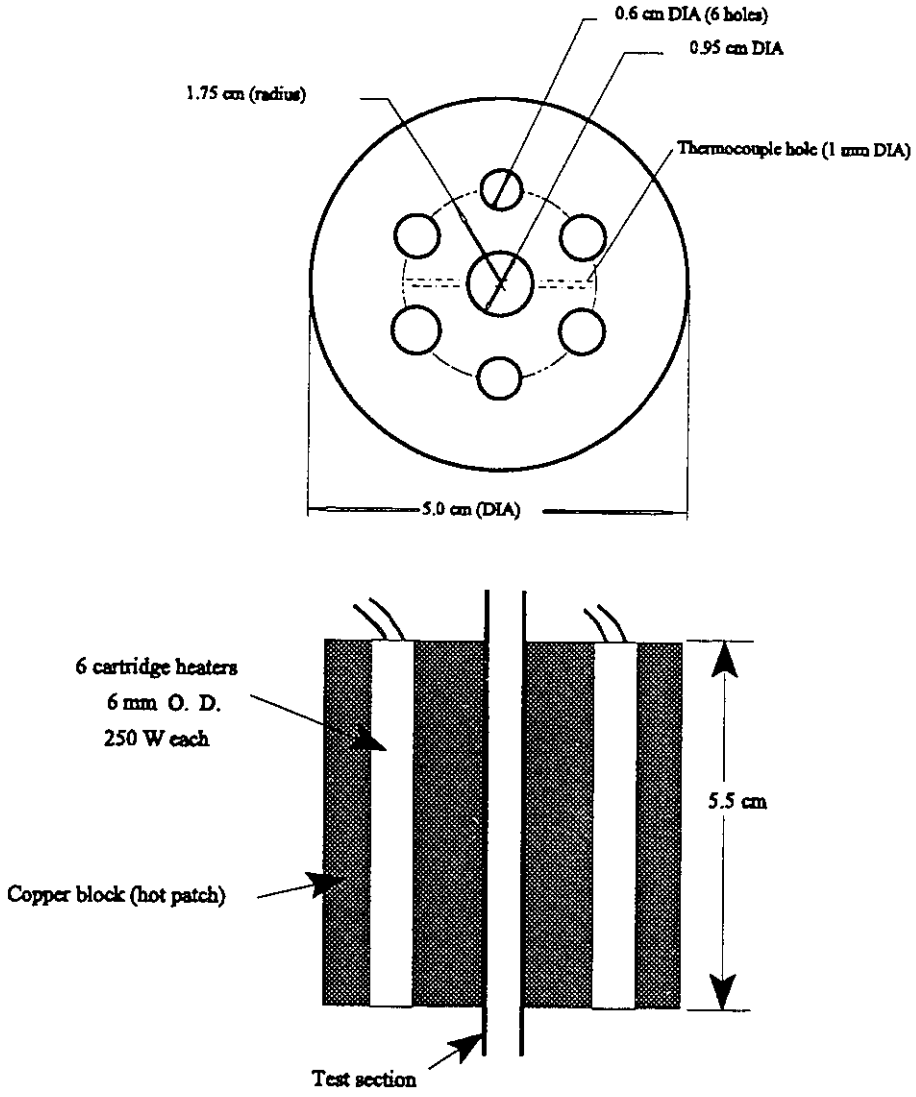

Figure 10.3 Schematic of hot patch.

Chapter 11 EXPERIMENTAL RESULTS AND DISCUSSION

11.1 Experimental Results

11.1.1 Data Reduction

For each run, the test section current, voltage and thermocouple signals were recorded, and the measurements carefully processed. Any inconsistencies in the results were removed, corrections for heat loss to the surroundings were made, and the final data were used to calculate the heat flux. After the heat flux was determined, the fluid enthalpy and the thermodynamic equilibrium quality were calculated along the test section length from a heat balance. The heat transfer coefficient was then determined based on the difference between the inside wall temperature and the saturation temperature. Since the pressure drop over the film boiling length was considered negligible when compared to the absolute pressure of the loop, the saturation temperature was based on the pressure at the exit of the test section.

11.1.2 Data Tabulation

A total of 8 120 post-CHF data points were compiled: 2300 data points obtained with Freon-12, 2500 with Freon-134a, and 1200 with Freon-22. The reduced data are described and tabulated in Appendix C.

11.2 Discussion of Results

The results are tabulated in Appendix C for the inside wall temperatures. Also, in this chapter results of the heat transfer coefficients are shown graphically, where the heat transfer

coefficients have been plotted against the thermodynamic equilibrium quality, which is conventional practice in film boiling studies; e.g., see Fig. 11.1(a). Figure 11.1(b) shows the corresponding axial wall temperature (corrected for temperature drop across the heated wall) at four heat flux levels. The heat transfer coefficient trends shown in the figures are typical of all the data trends observed during this study. Parametric effects on the heat transfer coefficient have been investigated previously for water; in the present study, it is found that these effects are more complicated than observed before. The following sections will discuss the parametric effects on the heat transfer coefficient.

11.2.1 CHF Location Inside the Hot Patch

The CHF location inside the hot patch was not measured during the experiments; however, it can be accurately estimated. This information is necessary for the comparison of prediction methods against this data. History-dependent models, such as two-fluid models, require initial conditions (conditions at the CHF location) as input. Therefore, it is important to know this information.

For all experiments conducted during this study, it was ascertained that the CHF location was very near the hot-patch inlet. Two sheathed chromel-alumel thermocouples were inserted in the hot patch through holes of 1 mm diameter (see Fig. 10.3). The junction of each thermocouple touched the outside surface of the test section. One thermocouple was placed at 1 cm from the top surface of the hot patch, and the other at 1 cm from the bottom surface. When power was applied to the hot patch and gradually increased, the CHF first occurred at the outlet. Further increase in power caused the drypatch to slowly propagate upstream of the hot patch. The power was then increased until the dry patch front reached the top thermocouple location, which was indicated by

a rapid temperature increase. The power was gradually increased until the dry patch arrived at the bottom thermocouple location. Then the power was further increased to make sure that the dry patch front began very near the inlet of the hot patch. Then, power was adjusted until the desired hot-patch temperature was reached. At this point, the two thermocouples usually showed steady and identical temperature readings.

11.2.2 Reproducibility of Results

During the experiments it was observed that Freon-134a, Freon-12 and Freon-22 decomposed to some extent at the wall temperatures occurring in film boiling. Decomposition, however, occurred at different temperatures for the different refrigerants. The decomposed Freon was a serious problem, since it incurred a drastic change in the test section temperature distribution. Further, once decomposition occurred, it was found that stable film boiling would not take place under identical conditions to those for which it was stable earlier in the runs. When the inside of the tube was cleaned thoroughly with acetone, stable film boiling could be established again. Also, it was found that after several hours running in the film boiling regime, if Freon in the loop was not replaced, the results of previous runs were not repeatable. This meant that either the Freon characteristics (physical properties) had changed or the characteristics of the inside surface of the test section had changed (rougher surface due to decomposition deposits). However, if the Freon in the loop was replaced regularly, after a few runs, the repeatability of the results was very good. Several experiments were conducted to examine the extent of Freon decomposition for different run time periods. During these experiments, the maximum test section wall temperature was kept low, to avoid decomposition due to high wall temperatures. The inside surface of the test section was thoroughly checked before and after each extended run time period. One important result was

obtained: a black flaky deposit on the tube wall was observed for all extended run time periods, if the Freon in the loop was not replaced; however, no such deposit was found if the Freon was replaced after each run. The above observations are true for all the tested refrigerants (Freon-134a, Freon-12 and Freon-22); however, the extent of the decomposition and the temperature at which it occurred varied from Freon to Freon. For instance, it was found that Freon-22 was more susceptible to decomposition than either Freon-134a or Freon-12, and Freon-134a was the most stable thermally. In fact, Freon-134a was subjected to more severe experimental conditions (longer running time periods and higher tube wall temperatures) and decomposition was not observed for most tests. No effort was made to quantify the temperatures at which decomposition occurred for each Freon.

In order to check the reproducibility of the data, several runs, having similar test conditions, were performed at different time periods. During these experiments, precautions were taken to avoid problems associated with Freon decomposition. Figure 11.2 shows comparisons between the outside wall temperature vs axial locations of Freon-134a for sevaral runs. The results show very close similarity between the data. In Fig. 11.2(a), test conditions were not exactly matched for the mass flux, but overall these runs have very close matching conditions.

Figure 11.3 shows comparisons of the Freon-12 heat transfer coefficient vs thermodynamic equilibrium quality for several runs having very closely matching conditions. These results show that the data are quite reproducible.

11.2.3 Heat Transfer Regions

Figure 11.4(a) and 11.4(b) shows a distinctive variation in the distribution of the heat transfer coefficient vs equilibrium quality at various mass flux values. At low mass fluxes (530-

1000 $kgm^{-2}s^{-1}$), the heat transfer coefficient was almost constant near the hot patch, then it increased with a moderate gradient with increasing quality. At very high mass fluxes (2000-3000 $kgm^{-2}s^{-1}$), the heat transfer coefficient reduced sharply initially to a minimum, then it increased steeply. Following this steep increase, it remained almost constant, and sometimes showed either a small increase or decrease, with increasing quality. After that, it again increased with a moderate gradient to the end of the heated length. At moderate mass fluxes (1000-2000 $kgm^{-2}s^{-1}$), the characteristics of the heat transfer coefficient were similar to those of high mass flux conditions, except that no initial sharp decrease was observed.

The above observations indicate two distinct heat transfer trends: one at high mass fluxes, and the other at low mass fluxes. At high mass fluxes, the heat transfer characteristics are divided into four regions (see Fig. 11.4(c)), which are assumed to correspond to different flow patterns. Regions I and II usually appeared in the subcooled IAFB region ($x_{eq}<0$). Regions III and IV could extend from the negative quality region to the positive quality region. At low mass fluxes, the x_{eq} values were higher, and often only regions III and IV could be observed; the distinction between these two regions was not as simple as in the high mass flux case. Takenaka et al. [1989] observed similar heat transfer regions in their experiments of steady IAFB in a vertical tube using Freon R-113. Three heat transfer regions, which corresponded to different flow patterns (subcooled IAFB, saturated IAFB and agitated inverted annular film boiling (AIAFB)), were identified (see Fig. 11.5). Ishii and Denton [1988] observed similar flow patterns in their experimental study of two-phase flow behaviour at post-dryout conditions. They classified the observed flow patterns into four regimes: smooth, rough wavy, agitated and dispersed regimes. These four flow pattern regimes correspond approximately to the heat transfer regions I-IV described above. Details of the heat

transfer mechanisms encountered in these heat transfer regions will be discussed in Section 11.2.5.

11.2.4 Parametric Trends

11.2.4.1 Mass Flux Effect

As expected, the heat transfer coefficient increased with increasing mass flux. A careful examination of the mass flux effect showed that the number of so-called heat transfer regions decreased as the mass flux decreased. This is clearly shown in Fig. 11.4(a) and 11.4(b). Region I started to disappear when the mass flux was reduced from 3000 to 2000 $kgm^{-2}s^{-1}$, while region II vanished with a further reduction in mass flux. This may be explained as follows. Film boiling initially occurs near the upstream end of the hot patch. Under high mass flux and high subcooling conditions, a thin vapour blanket extends from under the hot patch to a region downstream of the hot patch (regions I and II). However, at lower mass fluxes, region I (where conduction heat transfer is dominant) may start and terminate under the hot patch, due to a higher vapour generation rate and higher x_{eq} values, thus promoting an earlier transition to region II, where heat transfer is convection controlled. Further, if the hot-patch heat flux is very high, regions I and II may start and terminate under the hot patch.

11.2.4.2 Inlet Subcooling Effect

Figure 11.6 shows the effect of inlet subcooling on a h vs x_{eq} curve with other flow parameters held constant. The liquid subcooling was varied from 8 to 28°C during the experiments. An increase in inlet subcooling shifted the lower quality section of the heat transfer coefficient curve to the left. Also, subcooling affected the formation of the different heat transfer regions, as the previous section described.

At high mass flux, the inlet subcooling affected the length of region I. Figure 11.6(c) shows

that reduction in the inlet subcooling resulted in a reduction of the length of region I. At very low inlet subcoolings, vapour generation is high and region I may begin and terminate under the hot patch. At low mass fluxes and low inlet subcoolings, fluid conditions at the hot patch may be at saturation and the CHF mechanism could approach dryout, instead of DNB (departure from nucleate boiling) type at the hot patch; hence the flow regime may be similar to that of region III and/or region IV (DFFB or slug flow regime).

Figure 11.6(a) shows that at high inlet subcooling and high mass flux conditions, the equilibrium quality stayed negative along the whole film boiling length, and that region IV could hardly be obtained. Therefore, high inlet subcooling impeded the formation of region IV, but encouraged the formation of region I. Also, as the inlet subcooling was reduced, region I and possibly region III became shorter. Figure 11.6(a) and 11.6(b) clearly shows that the effect of inlet subcooling disappeared altogether at positive qualities. This was not true at negative x_{eq} values; Fig. 11.6(a) suggests that at the same mass flux and x_{eq}, the flow regime could be different for different inlet subcoolings. Also, Fig. 11.6(a) and 11.6(c) shows that the minimum point of the h vs x_{eq} and h vs z curves occurred at different x_{eq} and different axial locations, respectively.

Figure 11.6(b) shows that at low mass flux, reducing the inlet subcooling caused a considerable decrease in h at low x_{eq} values, and the steep slope of h vs x_{eq} curve suggested the presence of region IV. Because of the higher x_{eq} values usually encountered at low mass flux, the inlet subcooling in general had a small effect on h in region IV (DFFB regime).

In region I, for a highly subcooled liquid core, a large fraction of the wall heat flux is used to increase the liquid core bulk temperature. Under these conditions the vapour generation rate is low, and hence the vapour layer is very thin and the heat transfer coefficient is high, as shown in

Fig. 11.6(c). The shift in curves in Fig. 11.6(a) can be explained by the greater degree of non-equilibrium at high inlet subcoolings. In regions II-IV, higher inlet subcooling gave a greater degree of non-equilibrium between the phases, and produced lower heat transfer rates, except maybe at low mass flux conditions and high positive x_{eq}, as shown in Fig. 11.6(b).

11.2.4.3 Pressure Effect

Figure 11.7 shows that the heat transfer coefficient increased with increasing pressure, except at low mass flux conditions, where the effect may have been less pronounced. Also, the higher pressure shifted the minimum of the heat transfer curve to the right. These trends are consistent with reported studies in the literature. In general, the shape of the h vs x_{eq} curve did not change much with pressure.

The effect of pressure on the heat transfer coefficient in region I can be explained in terms of a change in thermophysical properties of the vapour as a function of pressure. The increase in the vapour thermal conductivity with increasing pressure is relatively small at low to moderate reduced pressures (P_r<0.4), as Fig. 11.8 shows. Therefore, such an increase can be ignored. However, in many film boiling studies, where P_r is usually less than 0.5, the improvement in the heat transfer coefficient is attributed to the higher thermal conductivity of the vapour at higher reduced pressures. On the other hand, the decrease of density ratio (ρ_l / ρ_v) with increasing pressure must be considered, since it affects the void fraction distribution. The void fraction increases with increasing density ratio. The decrease of void with pressure implies a thinner vapour layer, and hence better heat transfer in region I. This may also explain the longer length of region I at higher pressure. At higher pressure, the critical vapour layer thickness, at which convection becomes important, occurred farther downstream along the heated length.

At higher pressure, the improvement in the heat transfer coefficient in regions II-IV can only be attributed to the lower thermodynamic non-equilibrium between vapour and liquid at higher pressure. For the same x_{eq}, there are two competing mechanisms that may control the heat transfer rate from the heated surface. In the first mechanism, the actual quality (x_a) and the void fraction decrease with increasing pressure. Since convection is the dominant heat transfer mechanism in these regions, this decrease in quality results in lower vapour velocities (lower Reynolds number), which induces a lower heat transfer rate. In the second mechanism, higher pressure leads to lower vapour superheat, hence better heat transfer from the wall, since heat transfer from the wall is mainly controlled by convection to the vapour phase. Figure 11.7 shows that the second mechanism is the dominant one in regions II-IV. This effect, however, is not very pronounced in region IV, as Fig. 11.7(c) shows. This implies that the first mechanism is starting to become as important as the second mechanism in region IV.

11.2.4.4 Heat Flux Effect

Figure 11.9(a) and 11.9(b) shows that, in general, increasing the heat flux had little effect on the heat transfer coefficient (h vs x_{eq}) in region I, but increased the heat transfer coefficient in regions II-IV. The shape of the h vs x_{eq} curve stayed virtually the same for regions II-IV. At high mass flux, for a given fluid, the transition point from region I to region II (which corresponds to a minimum in the heat transfer coefficient curve) always occurred at the same quality, and it was not affected by the variation in heat flux. This is quite different from the results of Section 11.2.4.2, which showed that the transition point varied with x_{eq} and z for different inlet subcoolings. Figure 11.9(c) shows that, locally, the heat transfer coefficient (h vs z) was lower for higher q_w in region I, but it was higher for higher q_w in regions II-IV.

In region I, an increase in the heat flux led to an increase in the vapour film thickness, because of the increased evaporation rate. In regions II-IV for the same x_{eq}, higher heat flux produced lower subcooling in the liquid core. This implies a higher evaporation rate, which may cause a desuperheating effect on the vapour. These effects produce a better overall heat transfer coefficient in these regions.

The effect of heat flux on the heat transfer coefficient in region IV was not as pronounced as in regions II and III, as Fig. 11.9(a) and 11.9(b) shows. Region IV may begin from the transition region (AIAFB regime or slug flow regime) and extend to the DFFB region. In general, for the same x_{eq} and in the DFFB regime, increasing the heat flux causes a reduction in the heat transfer coefficient, due to the increase in vapour superheat as well as the corresponding lower x_a value. This effect has been very well established from experimental data of DFFB. Consequently, one would assume that the vapour superheat increases as the heat flux increases in region IV. Nevertheless, Fig. 11.9(a) and 11.9(b) shows that the heat transfer coefficient increased as q_w increased. This may have been caused by the influence of thermophysical properties of the vapour on the heat transfer coefficient. For instance, Fig. 11.8 shows a large increase in thermal conductivity of vapour at higher vapour temperatures (higher vapour superheat). Generally, it is assumed that convective heat transfer is directly proportional to $Re_v^{0.8}$and $Pr_v^{0.4}$. Both of these non-dimensional numbers are functions of vapour properties (e.g., k_v, Cp_v, μ_v, ρ_v), which in turn are a function of the vapour temperature for a given pressure. Figure 11.10 shows that the group ($k_v\ Pr_v^{0.4}\ \mu_v^{-0.8}$), which is proportional to the convective heat transfer coefficient, increases continuously with vapour temperature. This increase may well compensate for the expected decrease in h with increasing q_w, especially for Freon-134a, and thus explains the observed increase of Fig. 11.9.

Many qualitative analyses regarding the physical mechanisms in IAFB have been presented in the literature. Most of these analyses give a reasonable explanation of the heat transfer characteristics of regions I, II and IV, but not for the transition region III.

11.2.4.5 Fluid Effect

Figure 11.10 shows that Freon-134a appears to be the more effective heat transfer fluid, based on its vapour heat transport properties. To eliminate the impact of differences in heat transport properties on the heat transfer coefficient, the ratios of the measured post-CHF heat transfer coefficient (h) to the homogeneous two-phase flow heat transfer coefficient (h_{hom}) were plotted against the thermal equilibrium quality for a reduced pressure, P_r, of 0.28. The homogeneous two-phase flow heat transfer coefficient is based on a single phase heat transfer equation for vapour modified for two-phase flow, and is defined as:

$$h_{hom} = \left(\frac{k_g}{D}\right) 0.023 \; Re_{TP}^{0.8} \; Pr_g^{0.4}$$

where

$$Re_{TP} = Re_g \left[x_{eq} + \frac{\rho_g}{\rho_f}(1 - x_{eq}) \right] \qquad \textbf{(11.2.1)}$$

and

$$Re_g = \frac{GD}{\mu_g}$$

Figure 11.11 shows that R-12, R-22 and R-134a display very similar parametric trends in film boiling. Note that the differences (as displayed, for example in Fig. 11.7(c), where for similar conditions, R-134a had a much higher heat transfer coefficient than R-12) have virtually disappeared. Figure 11.11 suggests, at least within the experimental conditions of this study, that

this ratio (h/h_{hom}) is not strongly dependent on the type of fluid, and in the development of a heat transfer correlation or model this ratio could serve as a suitable parameter.

11.2.5 Physical Mechanisms

This section describes the physical mechanisms of subcooled IAFB, based on experimental observations both from this study and from others.

11.2.5.1 General

It is expected that DNB occurs at the inlet of the hot patch due to the high heat flux (see Fig. 11.12). The lower-density vapour generated at the hot patch begins to accelerate rapidly downstream relative to the subcooled liquid core. The vapour is initially confined to a thin vapour layer at the wall, and bubbles are absent in the subcooled liquid core [Kawaji and Banerji, 1983]. For a highly subcooled liquid core, evaporation plays a minor role and some condensation of the vapour at the interface is possible. This region is usually referred to as the subcooled IAFB region. In this region, the interface is smooth and stable, and significant non-equilibrium between the phases is present.

Further downstream, the vapour velocity increases, due to the increased vapour generation rate. Also, the liquid subcooling is reduced considerably, because of the significant increase in the liquid bulk temperature. In this region, as the vapour layer thickness increases, the vapour-liquid interface becomes wavy and unstable, and entrainment of liquid in the vapour is possible. This region forms the start of the saturated IAFB region (occasionally referred to as the wavy region of IAFB).

Downstream of the wavy region, the flow regime might be that of slug flow or of AIAFB flow. At low flow velocities, slug flow is expected to be present; i.e., most of the liquid is in the

form of slugs of liquid in the centre of the flow channel. At higher flow velocities, AIAFB may be present [Takenaka et al., 1989]. In this region, the liquid core may have a helical appearance, or consist of sheet-like segments as a result of large-amplitude roll waves [Ishii, 1992]. The flow is usually highly agitated, due to the high turbulence level, and the vapour phase is distributed across the channel flow area.

Both slug flow and AIAFB flow represent transitions to the DFFB regime. Liquid droplets of various sizes are formed from the liquid slugs or sheets of the transition regime. The vapour phase moves at a higher velocity than the liquid droplets. The droplets reduce in size, due to evaporation and droplet break-up, which occurs when the critical Weber number is reached.

11.2.5.2 Interfacial Characteristics

For the subcooled IAFB regime, a strong effect of subcooling on the interface was reported by many workers. It is likely that most of the heat added to the fluid is used for heating the subcooled liquid core. This in turn results in low or zero vapour generation rates, and consequently in a low slip velocity. Stability between the phases is mainly dependent on the slip velocity, hence this mechanism may explain the stabilizing effect of subcooling. As the bulk liquid core temperature approaches saturation, the vapour-liquid interface becomes unstable, because of the increased vapour generation rate and hence increased slip velocity. The instability and waviness of the vapour-liquid interface is usually accompanied by considerable turbulence in the vapour film. The heat transfer coefficient at the interface depends strongly on the interface roughness and the local slip velocity between the phases.

Kawaji and Banerjee [1983] observed the formation and growth of waves at the liquid-vapour interface downstream of the quench front. The same phenomenon was observed by Hsu and

Westwater [1959] from photographic studies in pool film boiling. Oscillation of the vapour flow in the lateral direction (normal to the wall) was observed by Baum et al. [1978]. When the vapour-liquid interface approaches the heat transfer surface, heat transfer to the liquid is augmented significantly and the evaporation rate increases. Subsequently, the vapour-liquid interface is pushed away from the hot surface due to the vapour thrust force.

11.2.5.3 Liquid Core Break-Up and Flow-Regime Transition

The similarity between the hydrodynamics of a confined jet and the subcooled liquid core of IAFB has prompted several workers to apply jet break-up methods to predict the disintegration of the liquid core. Several studies of the hydrodynamic behaviour of the liquid core, such as flow characteristics and flow pattern transitions, have been conducted by De Jarlais and Ishii [1983, 1983a], and Ishii and De Jarlais [1987]. They established that the two predominant mechanisms of liquid core disintegration are roll wave entrainment and jet instability. The transition from IAFB to DFFB is believed to be related to Kelvin-Helmholtz instability at the liquid-vapour interface. The increased evaporation rate results in a larger increase in the low-inertia vapour velocity compared to the liquid velocity; at some point, the slip velocity reaches a critical value, at which the liquid core breaks into droplets and filaments.

Dougall and Rohsenow [1963] and Laverty and Rohsenow [1964] measured the heat transfer and the actual quality during post-dryout heat transfer in vertical tubes for Freon-113 and nitrogen. They observed that the transition between the low-quality region (IAFB) and the high-quality region (DFFB) occurred at a quality of around 10%. Ottosen [1980] used γ-rays to measure the void fraction in a vertical tube for nitrogen in the IAFB regime, and concluded that the flow pattern changed from IAFB to DFFB at a void fraction of 0.8.

11.2.5.4 Thermodynamic Non-Equilibrium

The thermodynamic non-equilibrium in the IAFB regime is different from that in the DFFB regime, as shown schematically in Fig. 11.13. In the subcooled IAFB region, the actual quality (x_a) is always positive, but the equilibrium quality (x_{eq}) is negative. In the saturated IAFB region, x_{eq} increases above zero and gradually approaches x_a. When the liquid temperature approaches saturation, the thermodynamic non-equilibrium reverses direction and x_a becomes lower than x_{eq}. The latter type of non-equilibrium is typical of the DFFB regime.

No measurements have been taken of T_{va} in the IAFB regime. It is expected that initially, in the subcooled IAFB region (region I), $T_{va} \approx (T_w + T_{sat})/2$ for region I, where conduction dominates. Subsequently, the vapour superheat levels off and starts to decrease in the saturated IAFB region, as a result of convection becoming the dominant heat transfer mode. This trend will continue in the transition region (AIAFB or slug flow regime), because of the strong mixing, high level of turbulence and larger interfacial area. The reduction in wall temperature in this region can be attributed to the improvement in h due to higher vapour velocities, and lower vapour superheat due to improved vapour-liquid heat transfer at higher x_{eq} values. It is assumed that the bulk liquid temperature in region III is at or close to saturation; this also results in lower vapour superheat, due to the increase in evaporation rate compared to the subcooled IAFB regime.

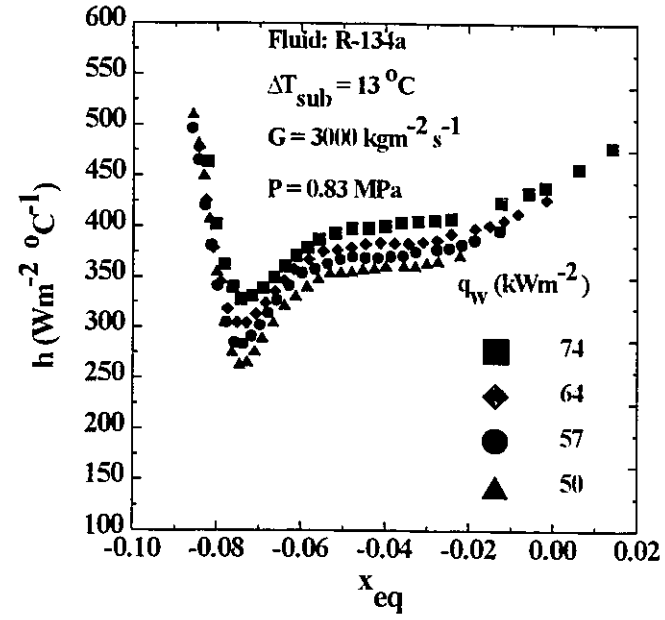

(a)

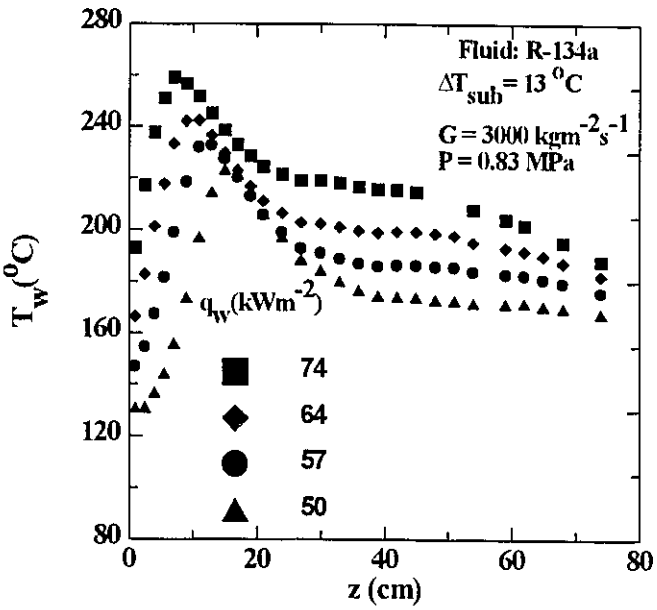

(b)

Figure 11.1 (a) Heat transfer coefficient vs thermodynamic equilibrium quality and (b) inside wall temperature vs axial distance at different heat flux levels.

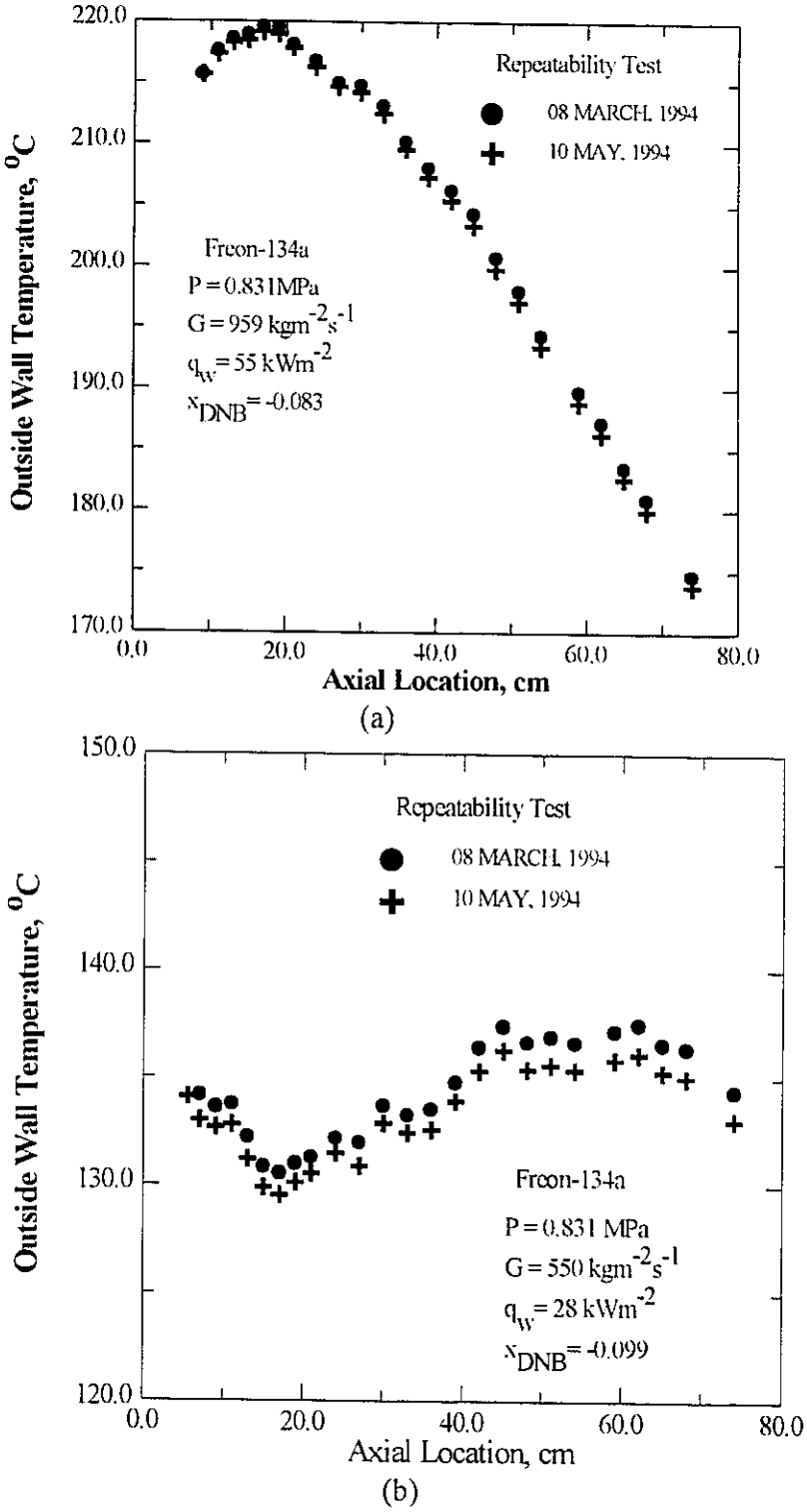

Figure 11.2 Reproducibility of data of outside wall temperature vs axial distance.

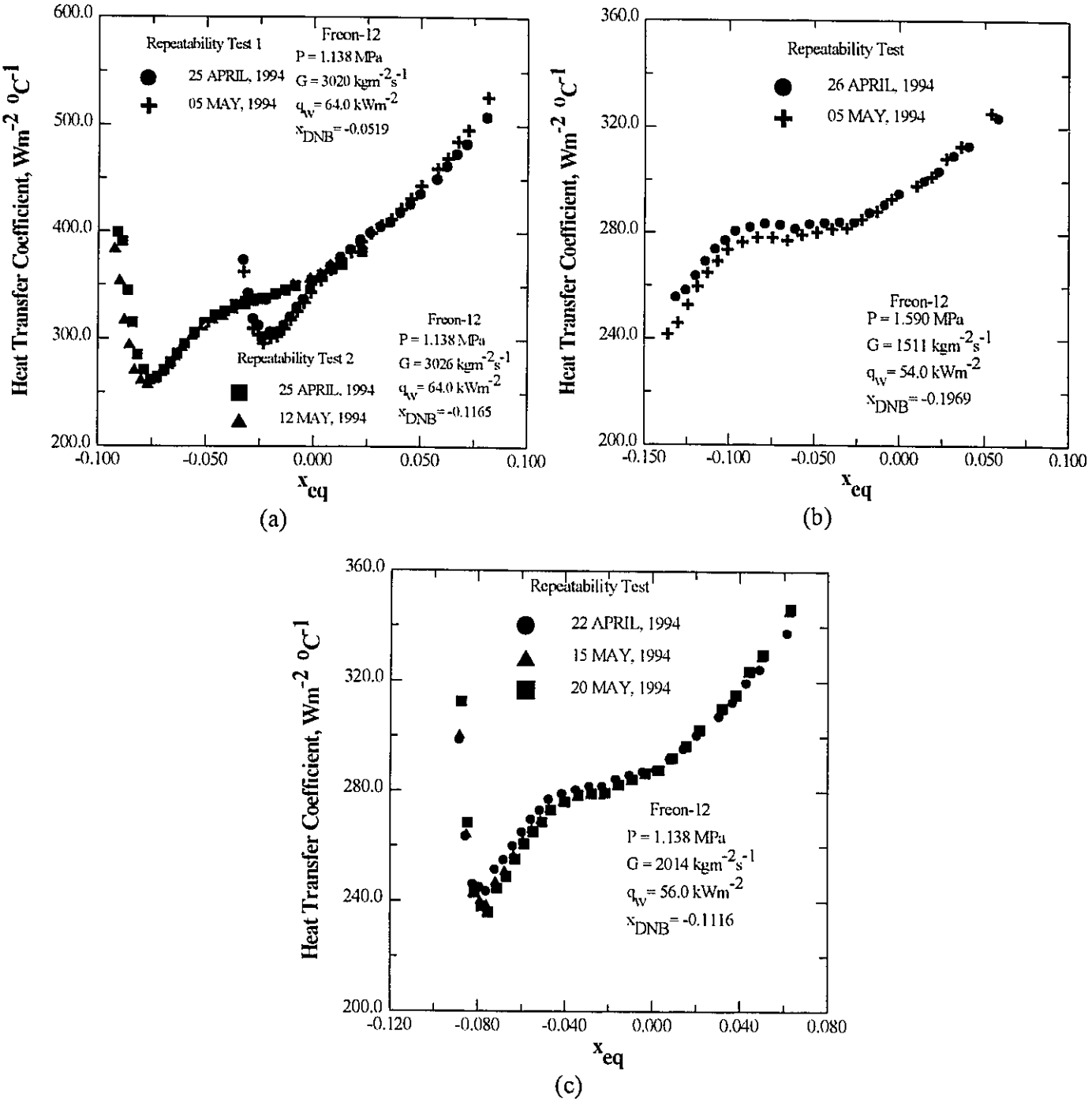

Figure 11.3 Reproducibility of data of heat transfer coefficient vs thermodynamic equilibrium quality.

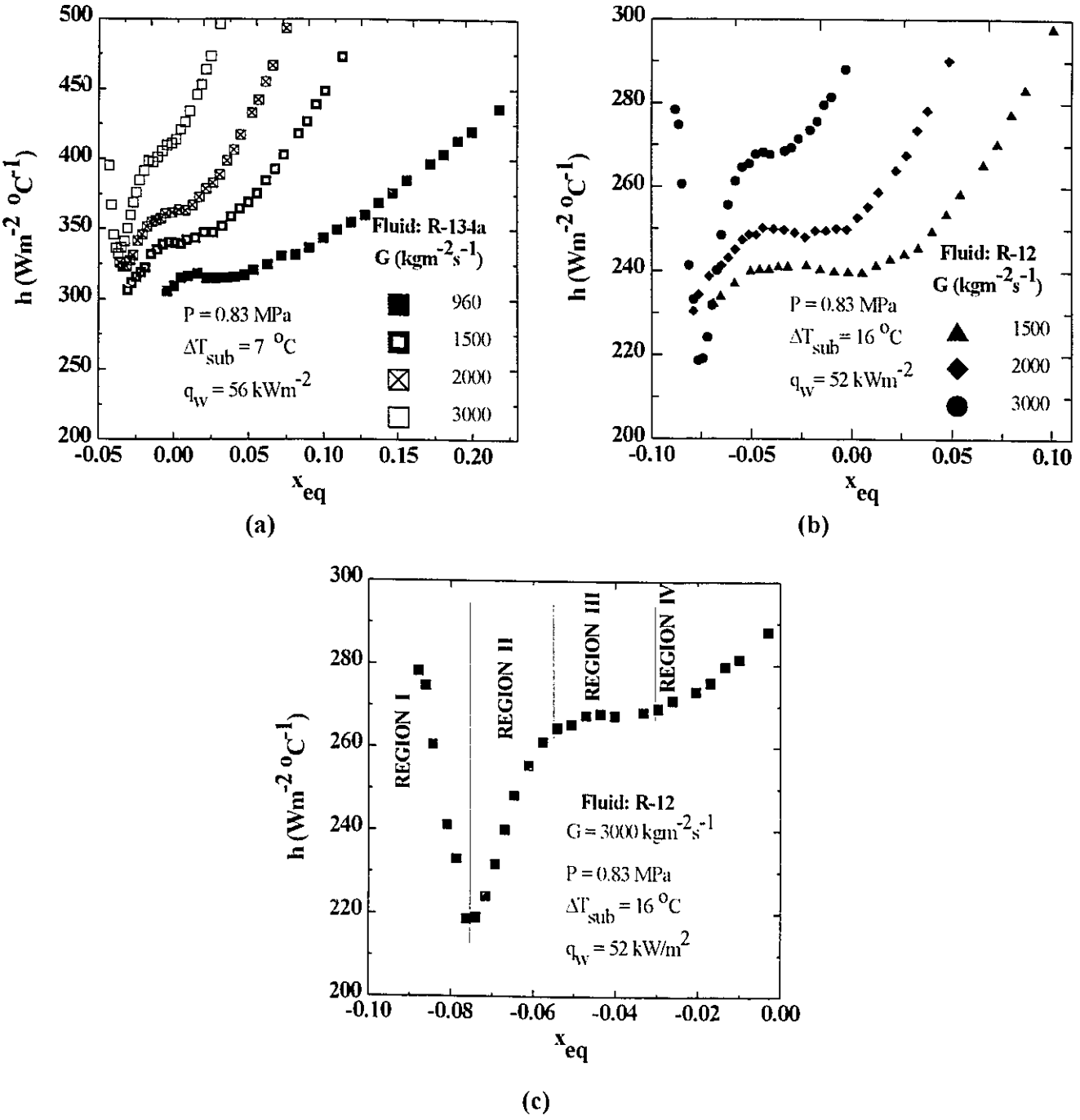

Figure 11.4 Heat transfer coefficient vs thermodynamic equilibrium quality with mass flux as a parameter (a) for R-134a, (b) for R-12 and (c) in different heat transfer regions.

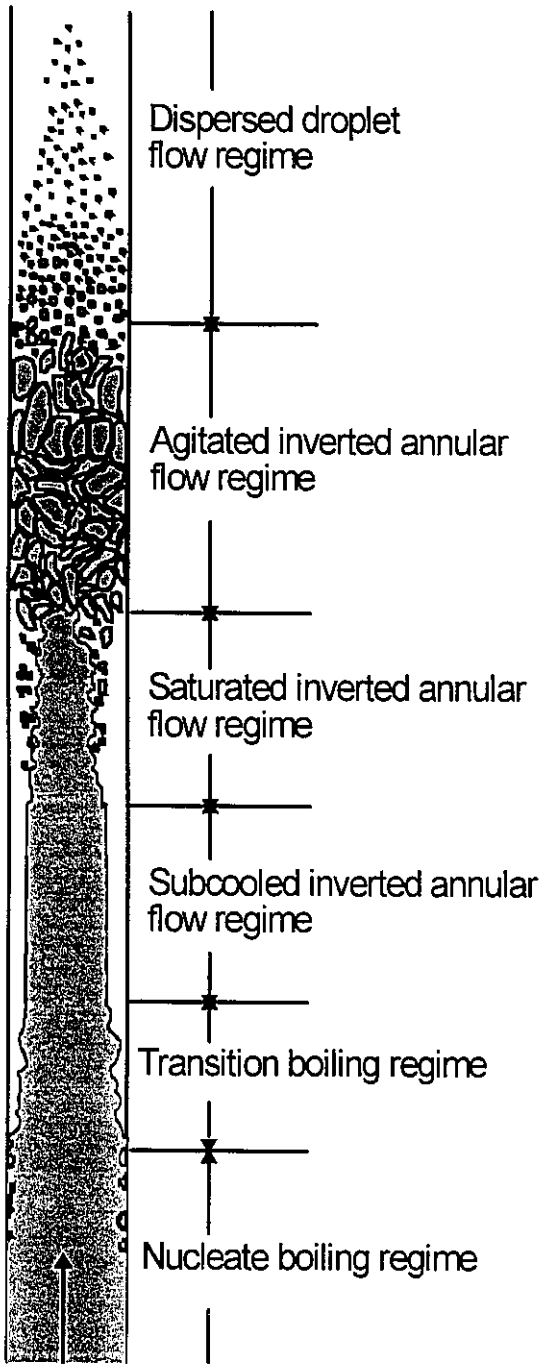

Figure 11.5 Flow regimes in low-quality film boiling.

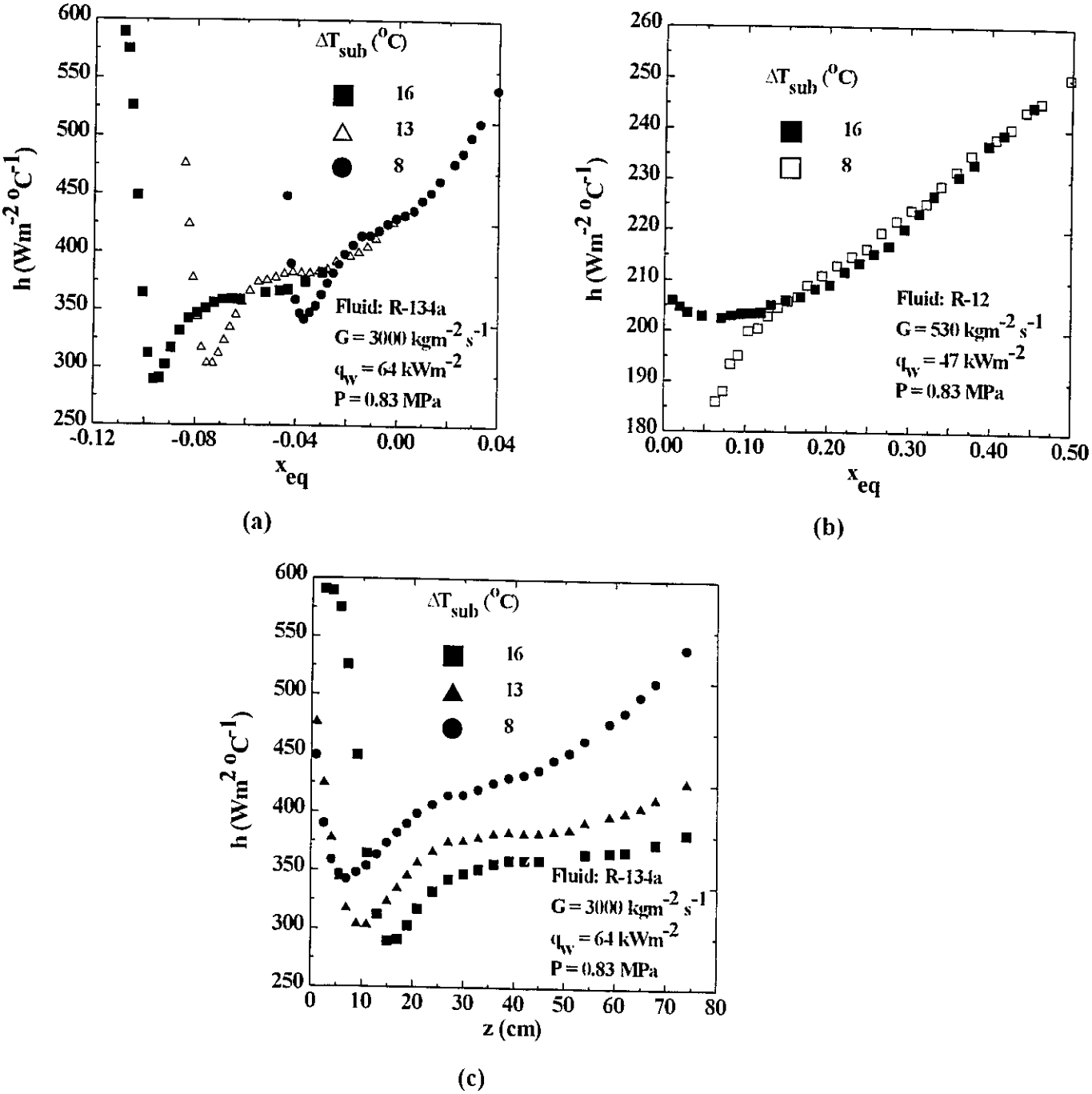

Figure 11.6 Effect of inlet subcooling on the heat transfer coefficient (a) at high mass flux, (b) at low mass flux and (c) vs axial distance.

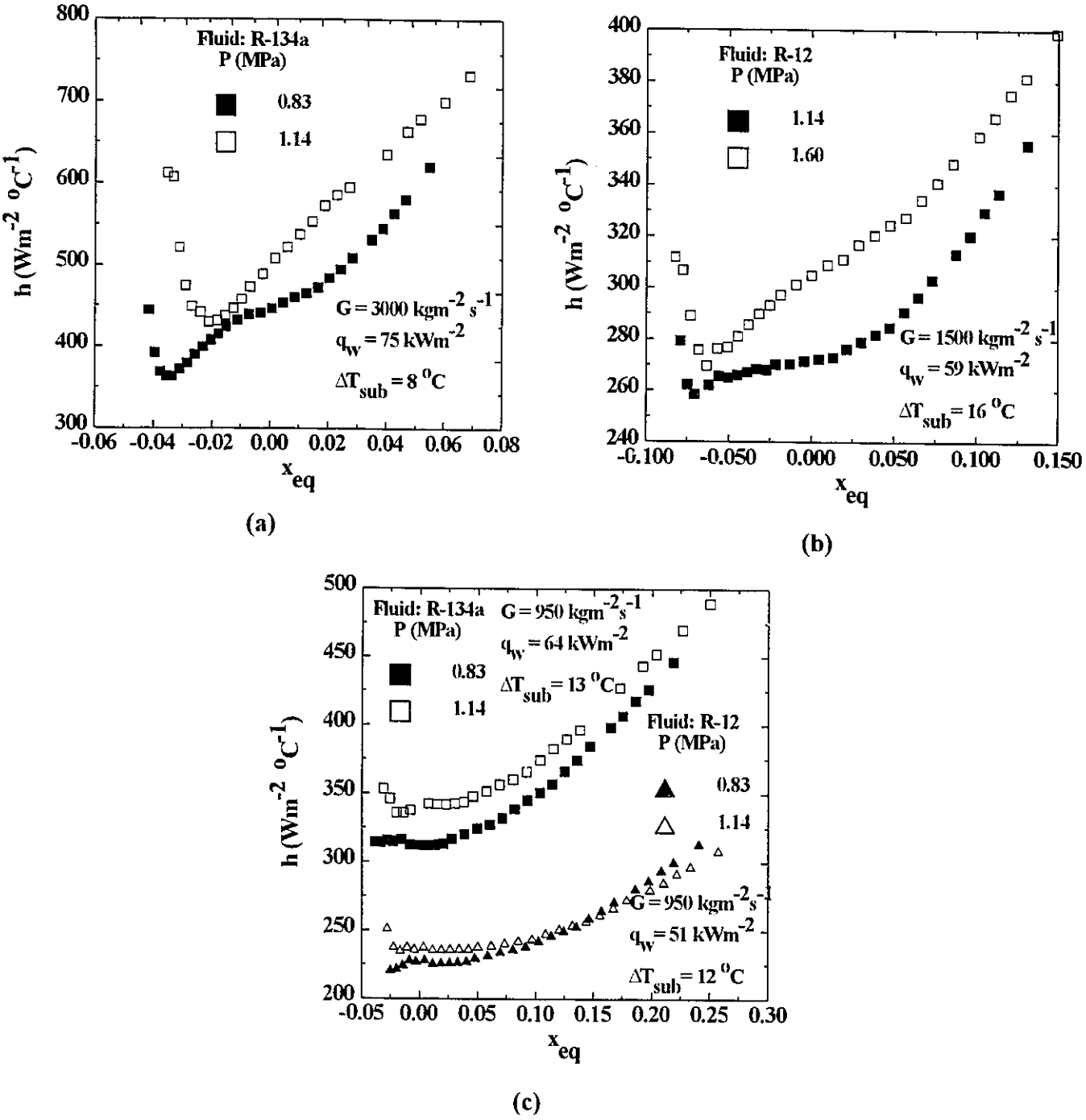

Figure 11.7 Effect of pressure on the heat transfer coefficient (a) at high mass flux, (b) at moderate mass flux and (c) at low mass flux.

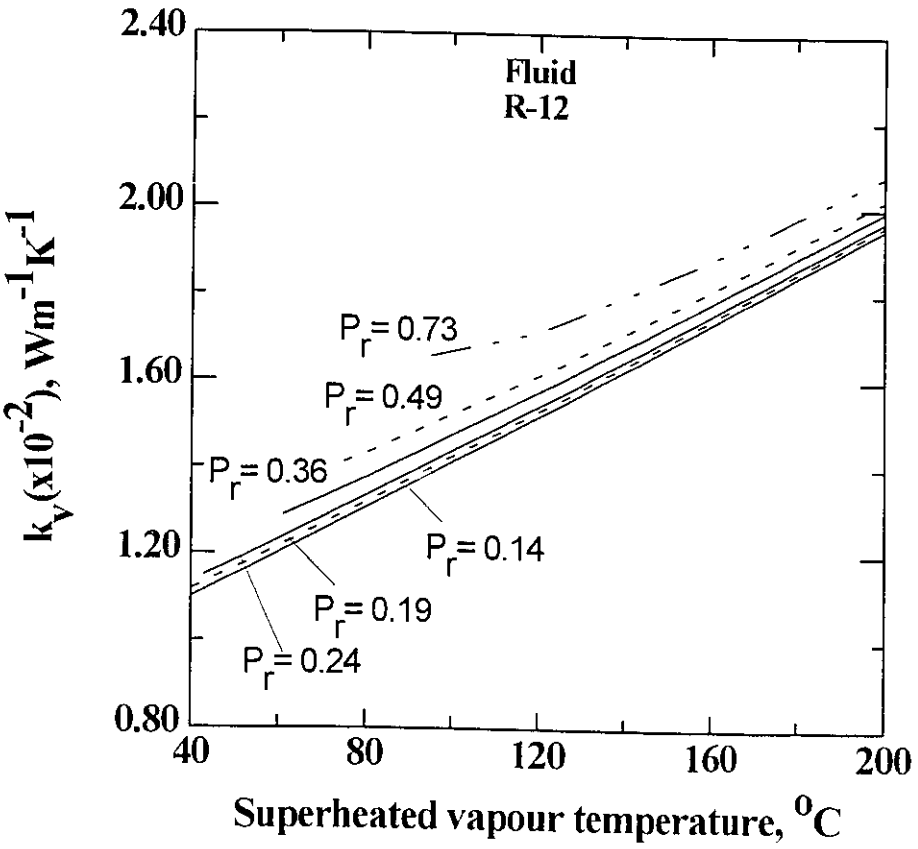

Figure 11.8 Effect of pressure on vapour thermal conductivity of R-12.

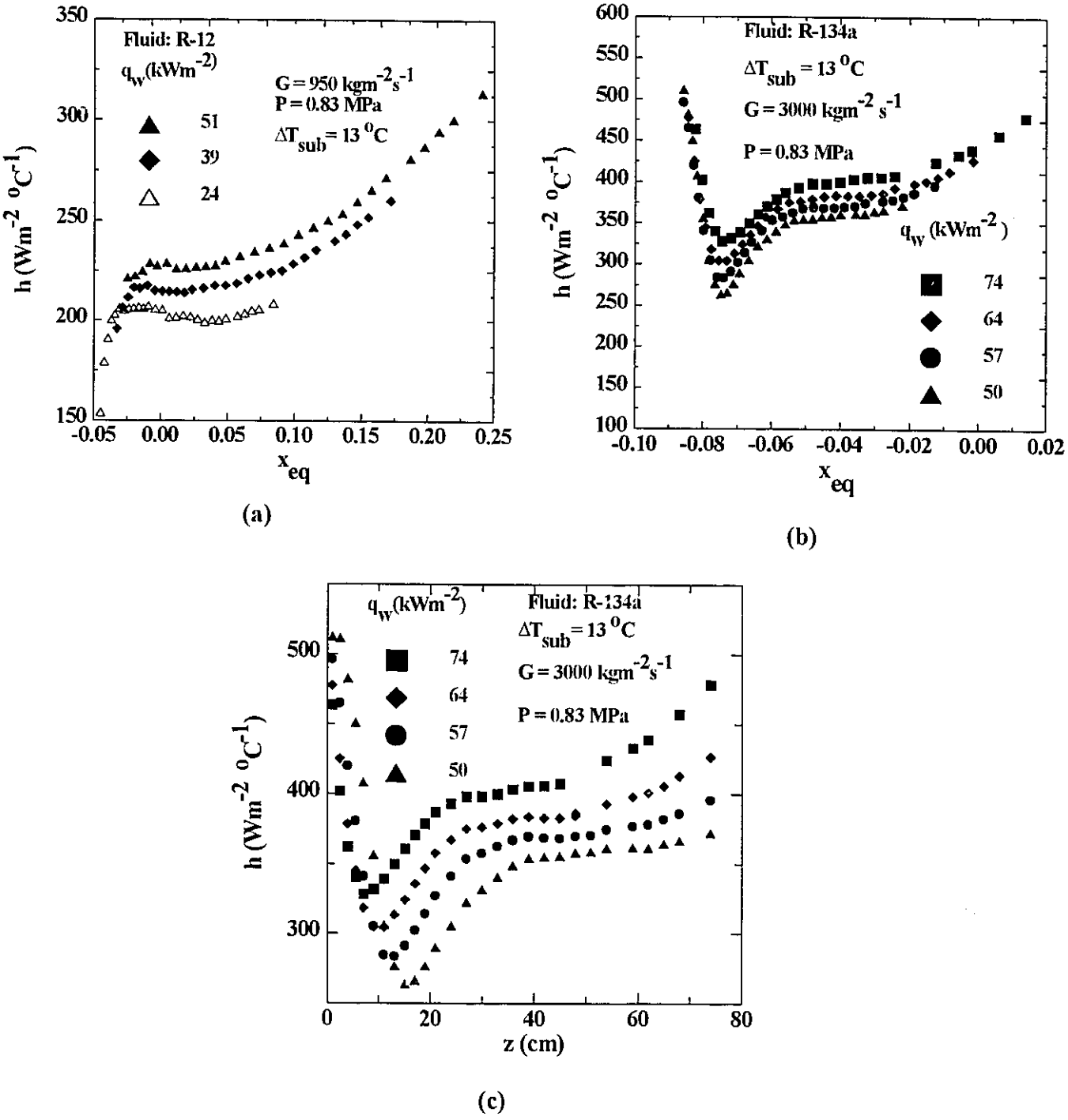

Figure 11.9 Effect of heat flux on the heat transfer coefficient (a) at low mass flux, (b) at high mass flux and (c) for heat transfer coefficient vs axial distance.

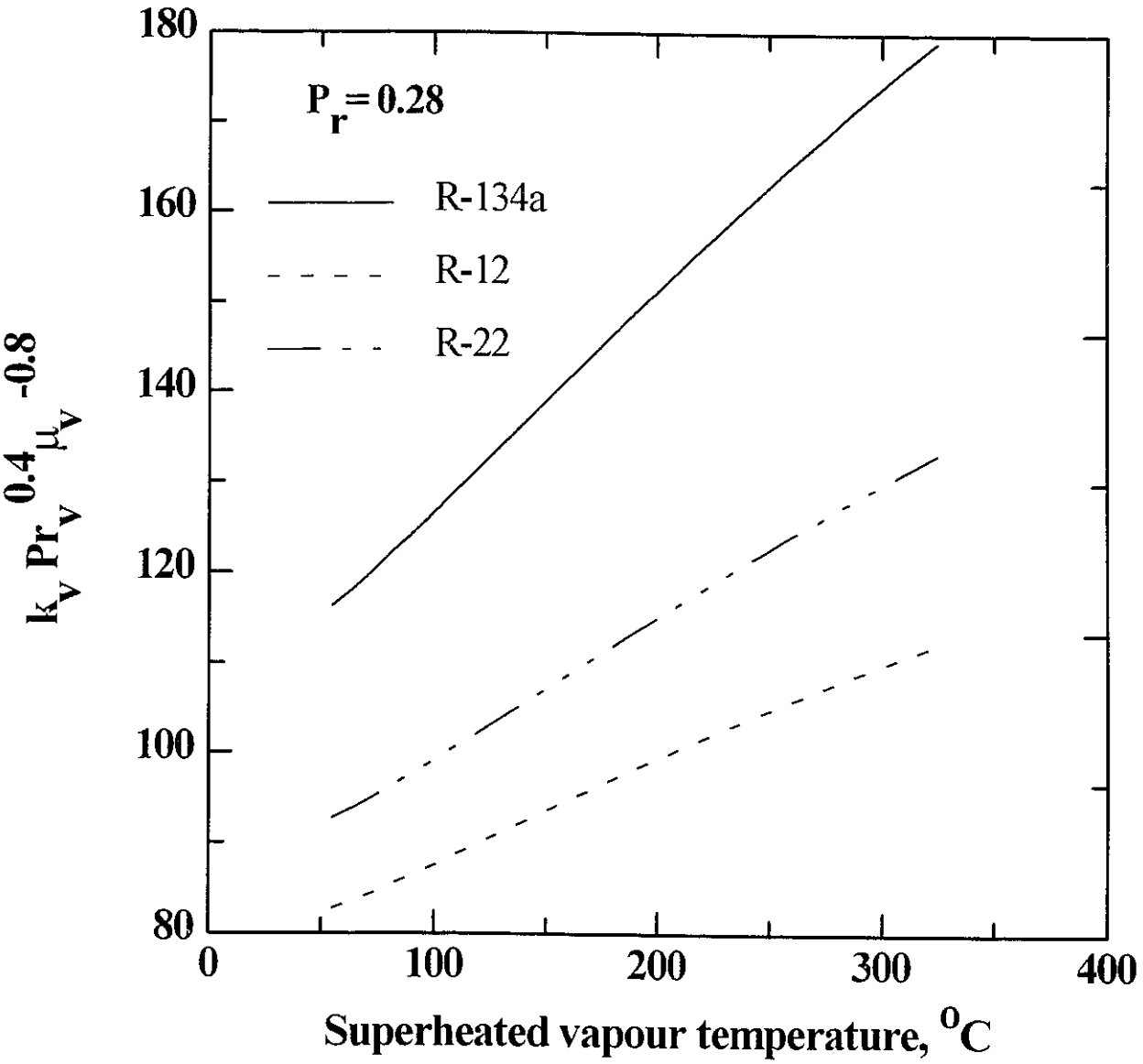

Figure 11.10 The property group $k_v Pr_v^{0.4} \mu_v^{-0.8}$ as a function of vapour temperature.

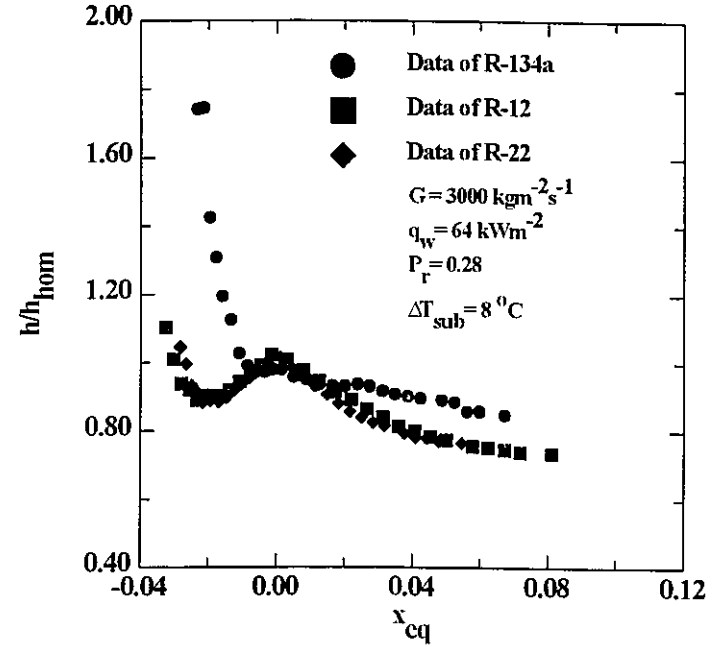

(a)

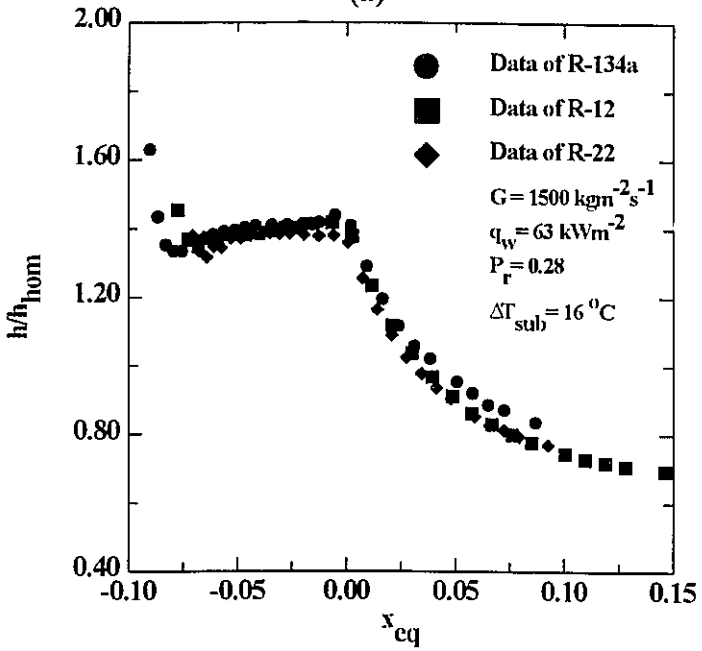

(b)

Figure 11.11 Comparison of the heat transfer coefficient for different fluids (a) at high mass flux and (b) at moderate mass flux.

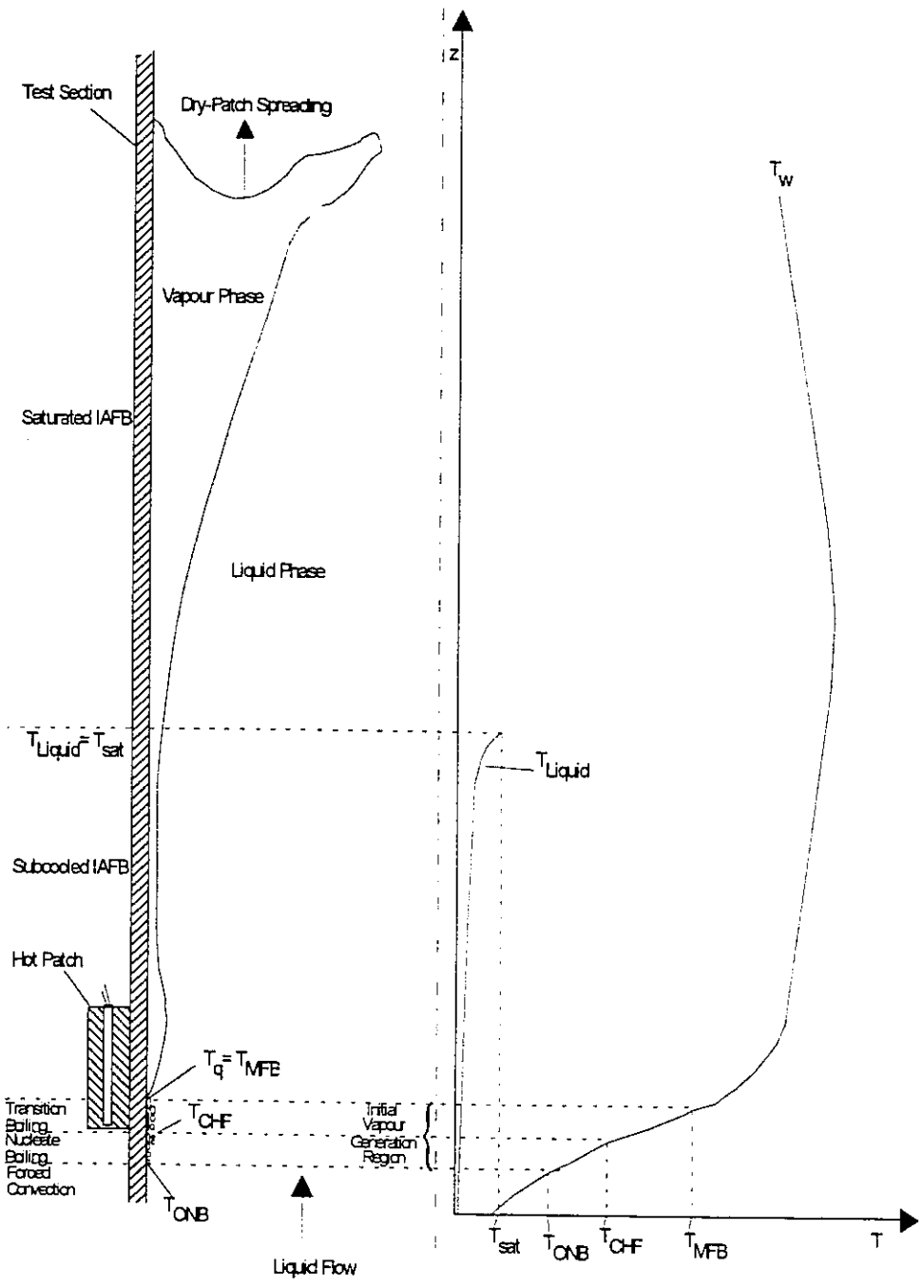

Figure 11.12 Schematic illustration of dry patch spreading and initial vapour generation at the quench front.

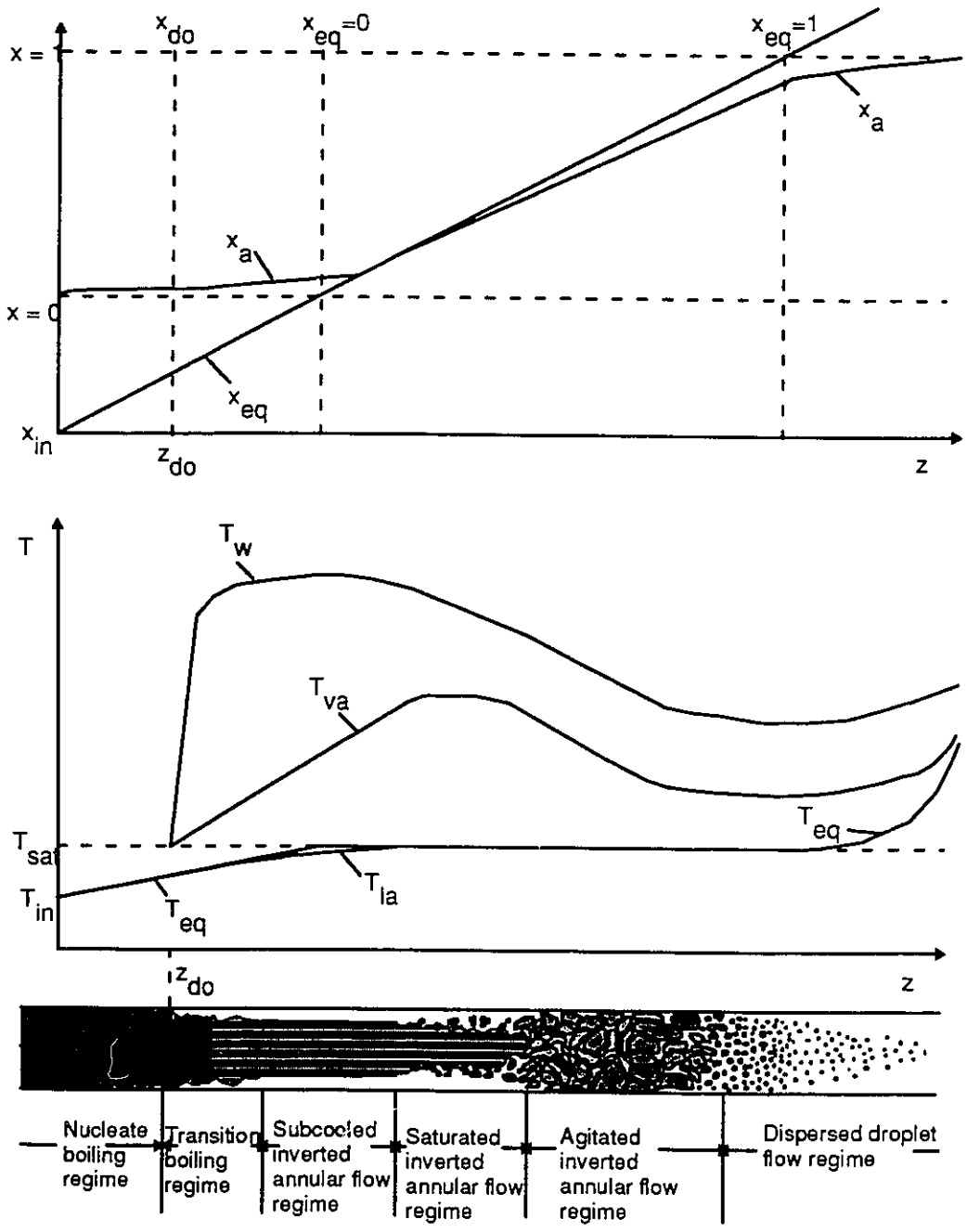

Figure 11.13 Schematic illustration of thermodynamic non-equilibrium in subcooled film boiling.

Chapter 12 COMPARISON OF THE DFFB PREDICTION METHODS TO WATER DATA

This chapter compares the predictive capability of the most promising DFFB prediction methods against data sets from the AECL-PDO data base and PDO-lookup table data. The parametric and asymptotic trends of the prediction methods are also examined. The results of the comparison are shown on plots of wall temperatures versus thermal equilibrium qualities. The approach followed first compares the models and correlations to Bennett's [1967] PDO data. Bennett's data is widely used in the literature for comparison purposes, and is considered reliable. Next, prediction methods that yield satisfactory agreement with Bennett's data are further examined against several other data sets from AECL's data base. The methods that give adequate overall predictions of the experimental data are compared to the PDO-lookup table data.

12.1 Wall Temperature Prediction

Figure 12.1 shows the comparison of nine DFFB prediction methods with the PDO water data. In general, the Dougall and Rohsenow correlation performs satisfactorily at very high mass flow rates, low heat flux levels and high pressures, where the thermal non-equilibrium is minimum, and the bulk vapour temperature is at saturation. However, at low mass flow rates and high heat flux, the correlation underpredicts the wall temperatures by a large margin, presumably due to the presence of thermal non-equilibrium in vapour.

Figures 12.1 and 12.2 illustrate the comparison of Shah's multi-fluid correlation predictions with the PDO data. In most cases, the correlation performs very well. Surprisingly, it yields

reasonable predictions even outside its range of applicability. The correlation tends to overpredict the wall temperatures at low mass flow rates, but agrees with the data at higher mass flow rates. At pressures near the critical pressure (>20 MPa) and at low mass flow rates, the correlation overpredicts the wall temperatures and occasionally exhibits an incorrect trend. On the whole, this correlation predicts the correct parametric trends.

Figures 12.1 and 12.2 compare the Groeneveld-Delorme correlation predictions with the PDO data. Predictions from this correlation are similar to those of Shah's correlation; however, the Groeneveld-Delorme correlation is applicable to a wider range of mass flow rates (up to 5200 $kgm^{-2}s^{-1}$, compared to Shah's 3492 $kgm^{-2}s^{-1}$). Further, the Groeneveld-Delorme correlation yields better predictions than Shah's correlation at high pressures (> 17 MPa). Nevertheless, at low flow rates, the correlation tends to underpredict the wall temperature, and at high pressures it shows the correct trend but differs from the data.

At low mass flow rates, the correlation of Hein and Koehler shows an incorrect parametric trend, because it tends to predict a rapid increase of the wall temperature immediately downstream from the dryout point, until the hypothesized "fully-developed" thermal non-equilibrium is attained. Afterwards, it predicts either a continuous decrease of the wall temperature due to increasing quality (which results in a higher heat-transfer coefficient from the wall), or a constant wall temperature when the quality reaches a limit value, above which superheated steam flow is assumed to exist. Nevertheless, in many cases the wall temperature increases continuously far downstream from the dryout location, as the low flow data in Figure 12.1 show. Further, the correlation is only applicable for mass fluxes of 300-2500 $kgm^{-2}s^{-1}$.

The Webb and Chen model was examined against the data of Bennett, and consistently

underpredicts the wall temperatures, as Figure 12.1 shows. In this assessment, it was necessary to omit the entrance-region factor introduced in the wall-to-vapour heat-transfer correlation. Otherwise, the model yields values of actual quality that are higher in magnitude than those of equilibrium quality. This is obviously in contrast to the physical phenomena involved in DFFB, and is caused by the empirical coefficients derived from data obtained at very low pressures and very low mass flow rates.

The Yoder and Rohsenow model is assessed against Bennett's data; fairly good agreement is obtained with the data of Figure 12.1. However, the model completely collapsed at high mass flow rates ($G > 3000$ $kgm^{-2}s^{-1}$), where it gives unrealistic average droplet diameters at the dryout location (negative droplet size!).

The Saha model was first compared to the data of Bennett. Excellent results are obtained over a wide range of mass flow rates and dryout qualities, as Figure 12.1 shows. Unfortunately, the model failed when compared to Becker's [1983] high-pressure data, as Figure 12.2 shows. This is partly due to the void fraction correlation employed with the model, which yields values greater than unity in some cases [Chen, 1986].

The Jones and Zuber model is assessed with Bennett's data. Unfortunately, Jones and Zuber did not provide the procedure for the evaluation of some parameters that are used in the derivation of the relaxation equation described in Section 8.6. This leads to some uncertainty in implementing the model in a computer code. Nevertheless, in most cases, the model gives the correct data trend; however, it considerably overpredicts the wall temperature, as Figure 12.1 shows.

Limited success was obtained with the Moose and Ganić model. An extensive comparison of the model predictions with the PDO data was conducted. The model performs extremely well

when compared to Bennett's data, as Figure 12.1 shows. However, in several instances the model failed to replicate the data trend at high-pressure conditions.

No attempt was made to validate the Nishikawa model and the CSO model described in Chapter 8. The former utilizes empirical heat transfer correlations developed with Freon-22 data, and hence is not expected to be valid for steam-water flow. For the latter, several revised versions of the same model were introduced in the literature, such as the Webb and Chen [1983] model discussed previously, and are considered to be improvements of the original model.

The above comparisons demonstrate that no existing model or correlation is able to adequately predict the heated surface temperature over the complete range of flow conditions.

12.2 Vapour Superheat Prediction

It is not possible to make direct comparison between the predicted vapour temperatures and the experimental vapour temperatures at conditions of interest, since no data are available at high flow rate and high-pressure conditions. Instead, the vapour temperatures predicted by various models and correlations are presented in the same figures of the wall temperature distributions, as Figs. 12.3-12.6 show. Also, the equilibrium vapour temperature, $T_{v,eq}$, is shown to give an indication of the lower bound to the superheat predicted by various methods.

Most prediction methods exhibit the anticipated trend of vapour superheat: higher vapour superheat at low mass flow rates, and negligible vapour superheat at high mass flow rates and pressures. The Webb and Chen model, however, shows unrealistic values of the vapour temperatures when the entrance-region factor employed in the wall to the vapour heat transfer correlation is utilized. For equilibrium qualities less than unity, the model gives vapour temperatures slightly lower than the saturation temperature. For equilibrium qualities exceeding unity, the model predicts

vapour temperatures much lower than the bulk fluid temperature. On the other hand, the Jones and Zuber model yields extremely high vapour superheats at low mass flow rates. In some instances, the predicted vapour temperatures are higher than the experimental wall temperature data. However, the model exhibits the correct trends at high flow rates.

12.3 Parametric Trends

12.3.1 Pressure

Figure 12.7 depicts the effect of pressure on the wall temperature distribution as given by the PDO-lookup table [Leung and Groeneveld,1988] at a mass flux of 4000 $kgm^{-2}s^{-1}$. Predictions from the Shah and the Groeneveld-Delorme correlations are also presented. At high mass flux, the PDO table shows the following trends with pressure. The wall temperature increases with increasing pressure (0.2 MPa - 10 MPa). At high pressures (> 10 MPa) the trend may reverse. The figures show a crossover trend for pressures of 10 and 17 MPa. The Shah correlation follows the correct pressure trend for equilibrium qualities less than one. However, the correlation is applicable up to a mass flux of 3442 $kgm^{-2}s^{-1}$. This may explain the discrepancies between the correlation prediction and the PDO table for equilibrium qualities larger than unity. The Groeneveld and Delorme correlation exhibits the same trends as those of Shah's correlation; however, at equilibrium qualities larger than unity, the Groeneveld and Delorme correlation gives the correct trend and order of magnitude of the data.

12.3.2 Mass Flux

Figure 12.8 shows the mass flux effect on wall temperature. The PDO-lookup table shows an increase in the wall temperature with decreasing mass flux. Again, Shah's correlation succeeds in displaying the correct data trend, except at equilibrium qualities greater than one, and mass flux

outside its range of applicability. The Groeneveld and Delorme correlation gives almost a perfect match of the PDO-table data. This is not surprising, since this correlation was partially employed for the construction of the PDO-table.

12.3.3 Heat Flux

Figure 12.9 illustrates the heat flux effect on wall temperature. The PDO-lookup table shows decreasing wall temperatures with decreasing heat flux. Shah's correlation gives the correct trend and magnitude of the data, except at equilibrium qualities higher than unity. Again, as expected, the Groeneveld and Delorme correlation agrees with the PDO-table data.

12.4 Discussion

The Groeneveld-Delorme correlation gives accurate predictions at moderate-to-high pressures (7-20 MPa) and medium-to-high mass fluxes (1000-5000 $kgm^{-2}s^{-1}$). However, at low mass fluxes the correlation underpredicts the data and occasionally exhibits an incorrect data trend. Further, the Groeneveld-Delorme correlation was developed from a data base covering a large number of data sets available in the open literature. This might put this correlation at an advantage when its predictions are compared to others. Hence, Becker's data [1983], which was not used in the development of the correlation, was chosen to further investigate the performance of the correlation. Again, the Groeneveld-Delorme correlation performed extremely well, as Fig. 12.2 shows. The Shah correlation gives prediction accuracy comparable to the Groeneveld-Delorme correlation, except it is not applicable for mass fluxes higher than 3442 $kgm^{-2}s^{-1}$ or equilibrium qualities greater than one. However, the Shah correlation is developed from data of various fluids, whereas the Groeneveld-Delorme correlation has been tested mostly for water.

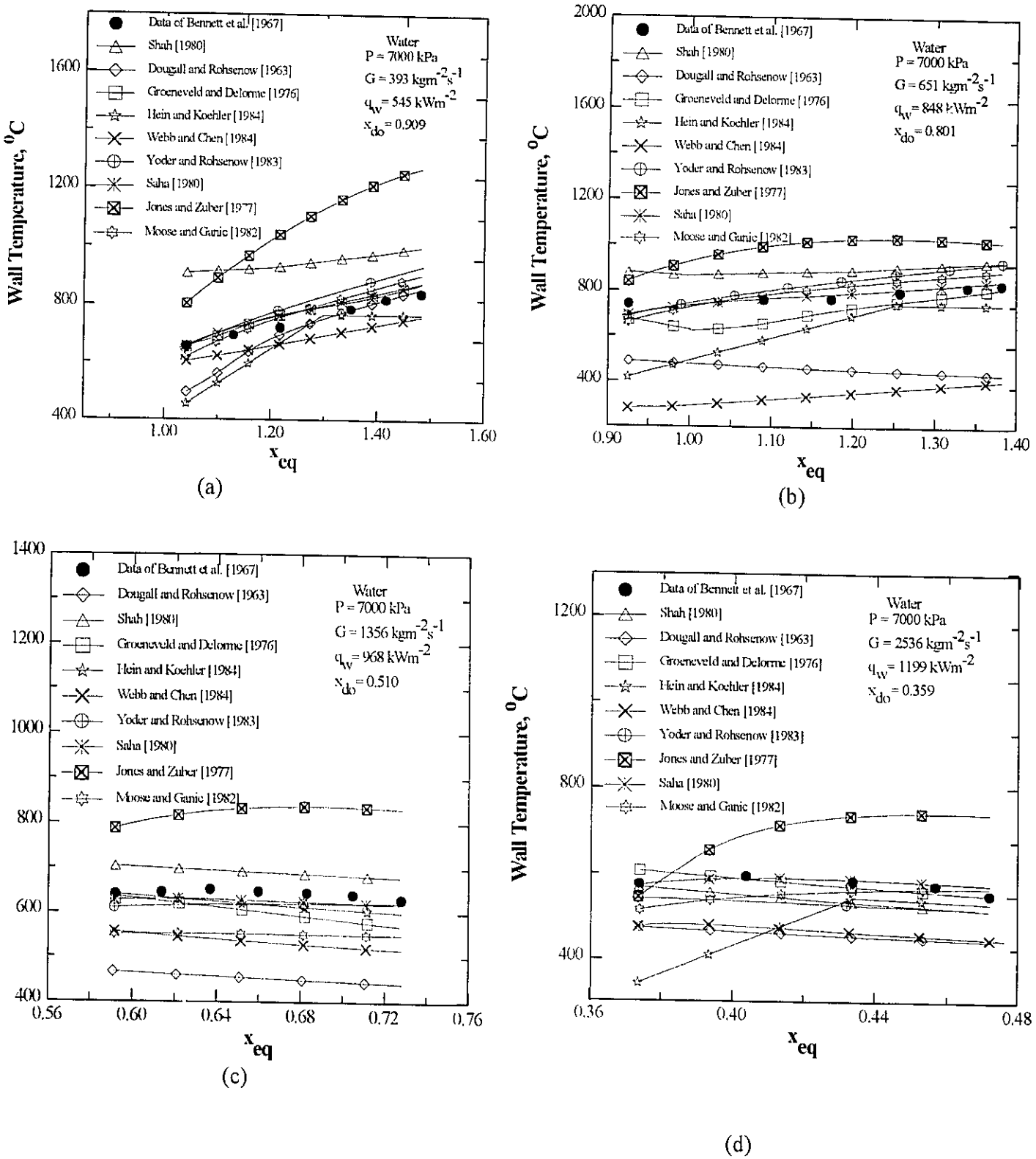

Figure 12.1 Comparison of DFFB prediction methods with Water data.

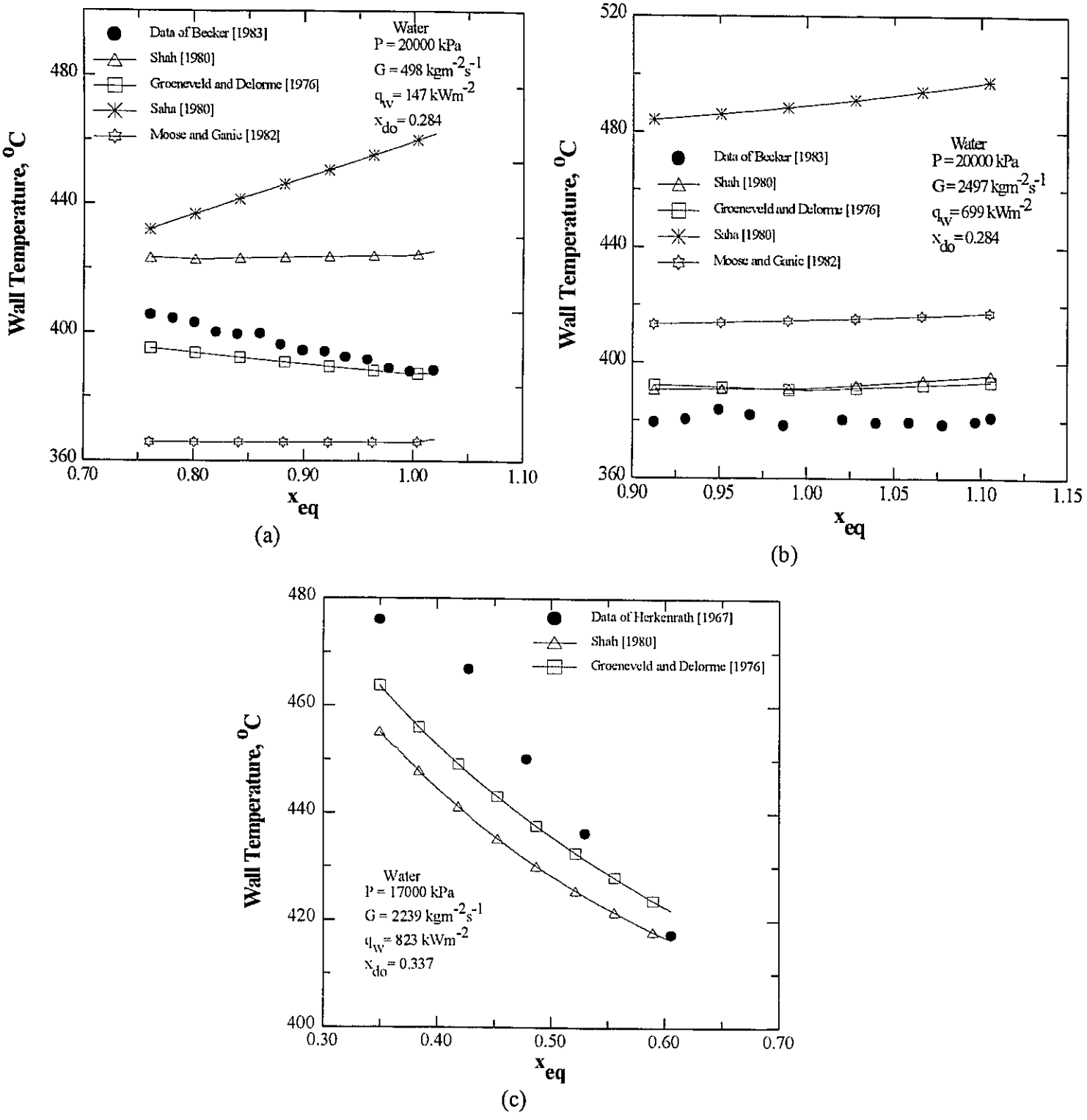

Figure 12.2 Comparison of DFFB prediction methods with water data.

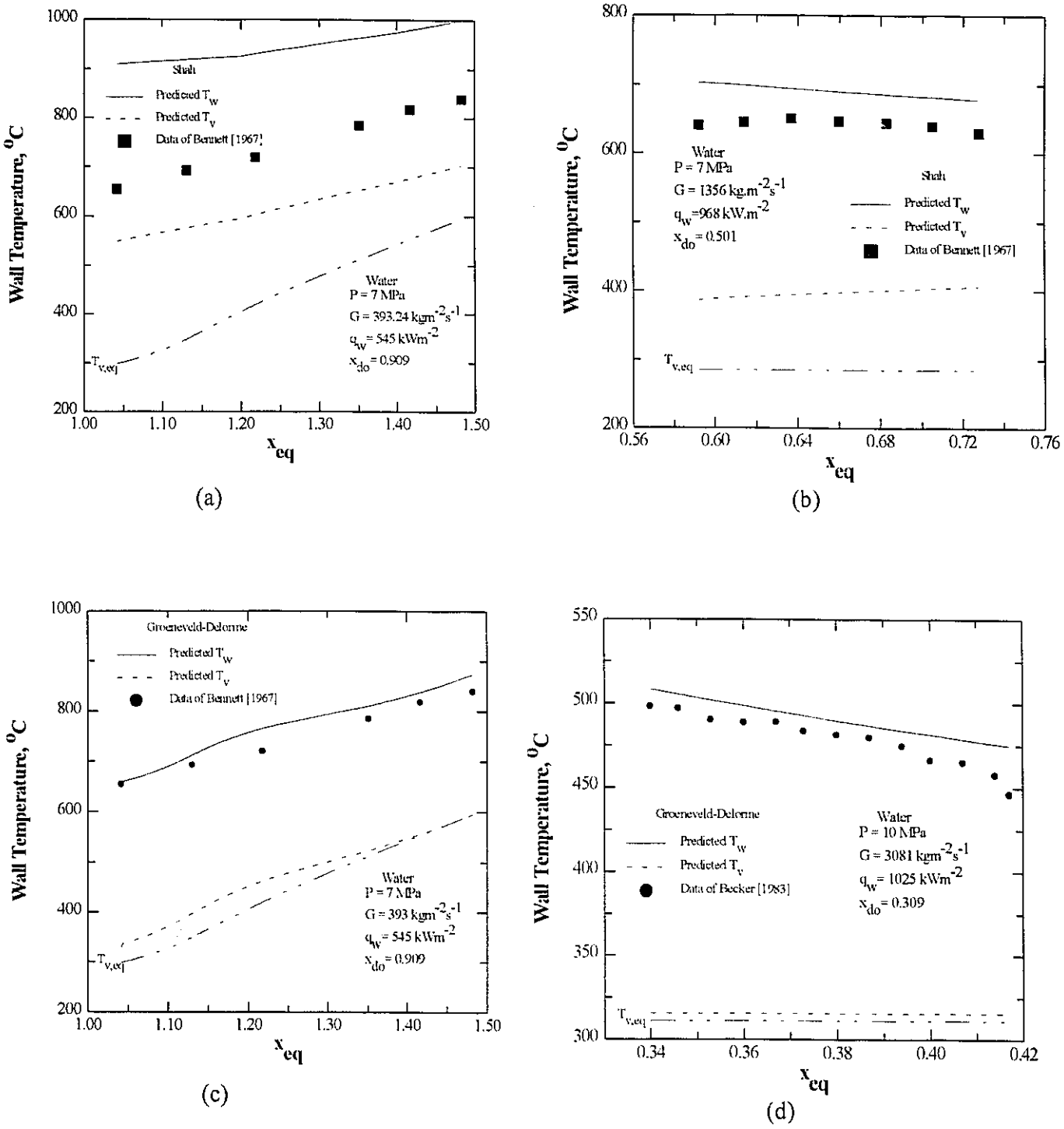

Figure 12.3 Wall and vapour temperatures predicted by the Shah correlation [1980] and the Groeneveld and Delorme correlation [1976].

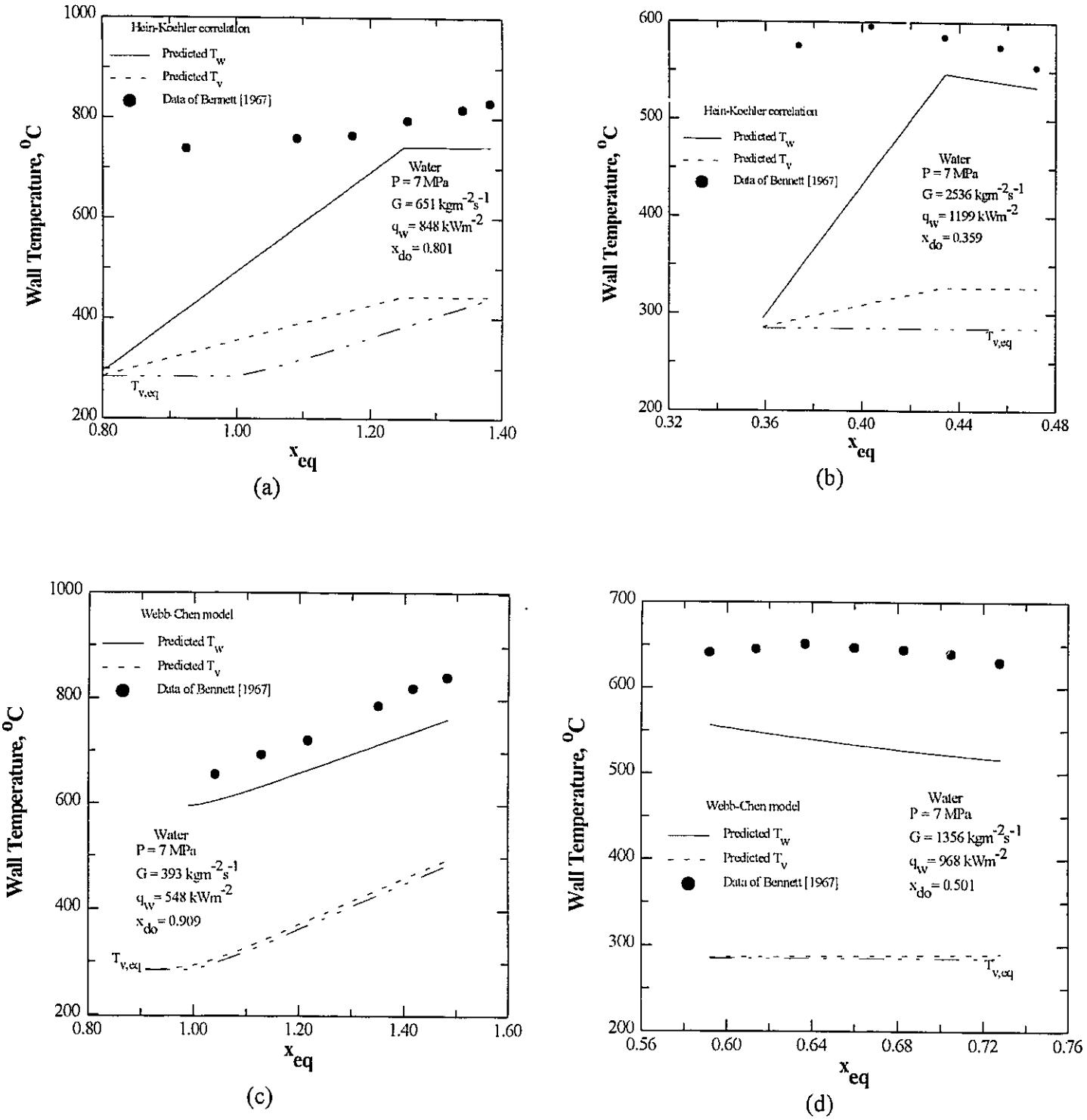

Figure 12.4 Wall and vapour temperatures predicted by the Hein and Koehler correlation [1984] and the Webb and Chen model [1984].

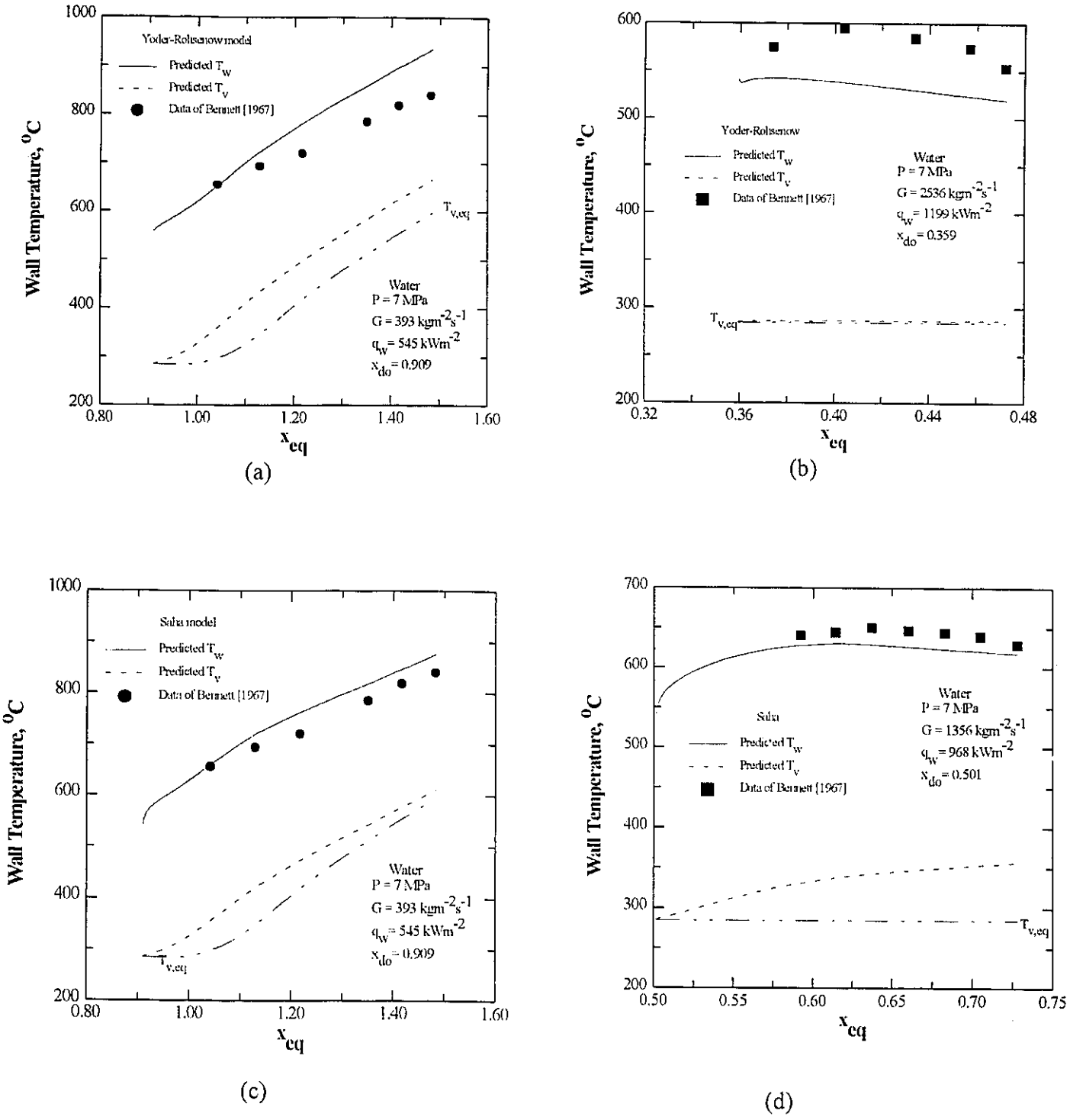

Figure 12.5 Wall and vapour temperatures predicted by the Yoder and Rohsenow model [1983] and the Saha model [1980].

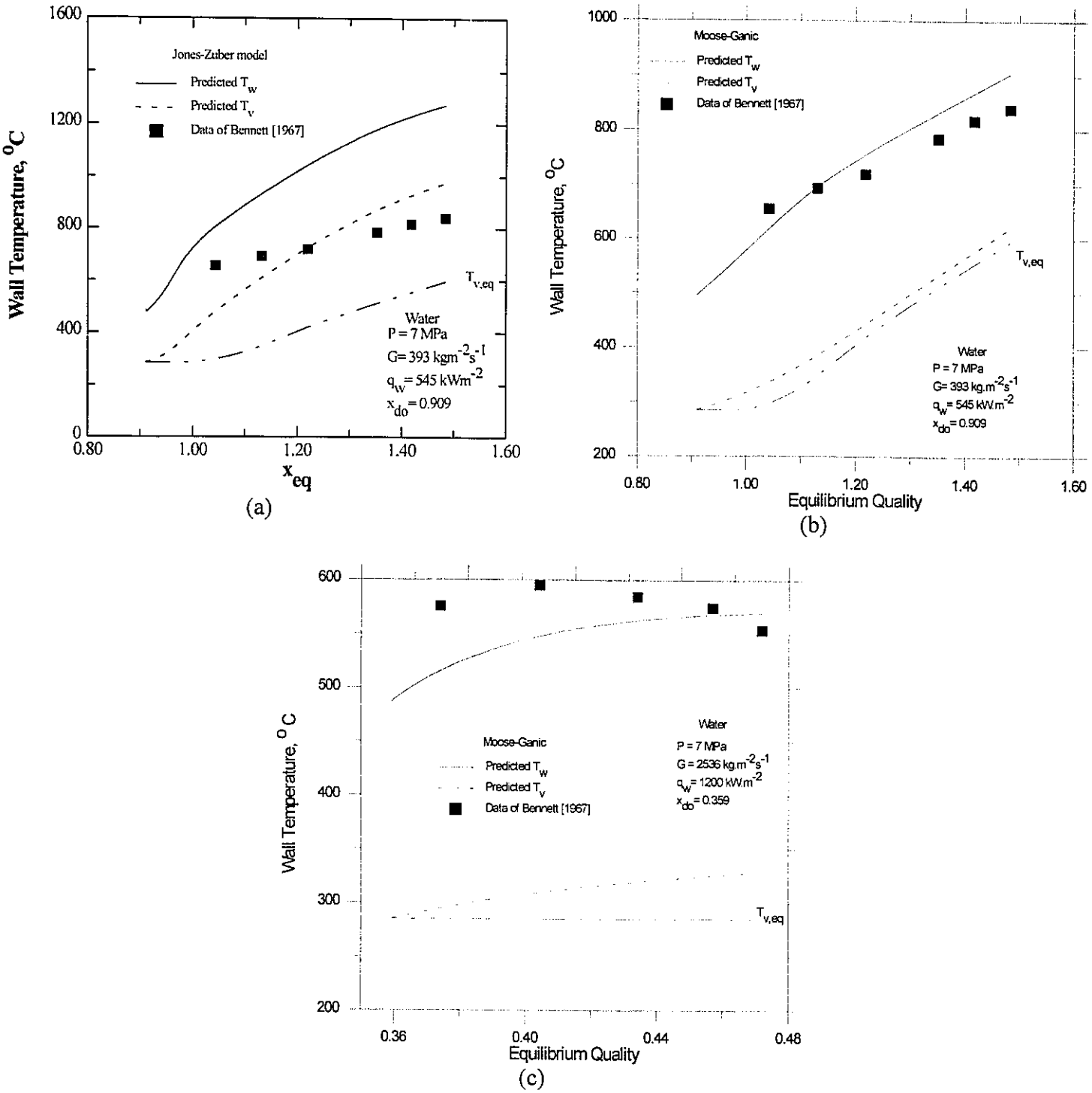

Figure 12.6 Wall and vapour temperatures predicted by the Jones and Zuber model [1977] and the Moose and Ganić model [1982].

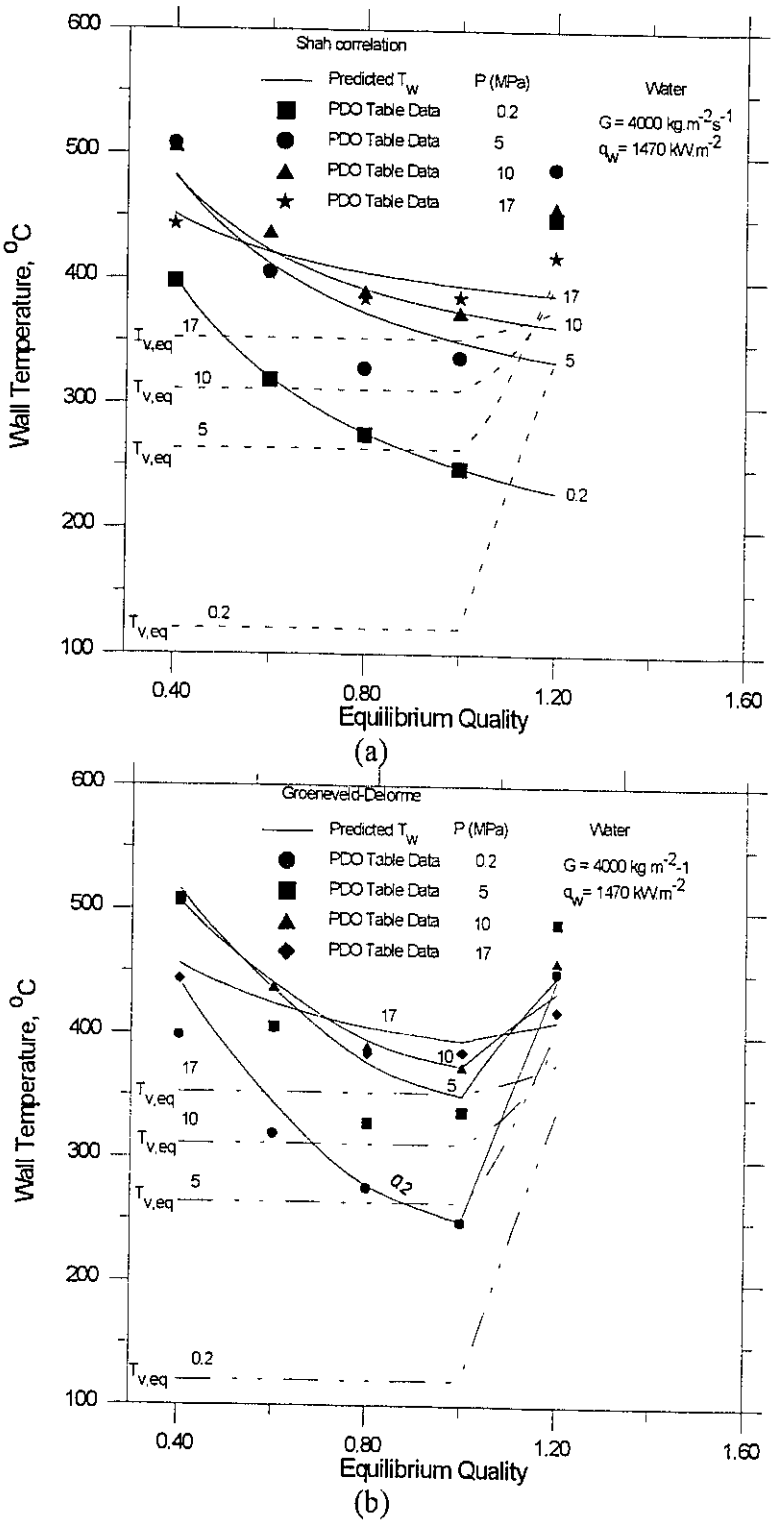

Figure 12.7 The effect of pressure on the wall temperature distribution as predicted by the PDO-lookup table and (a) the Shah and (b) the Groeneveld-Delorme correlations.

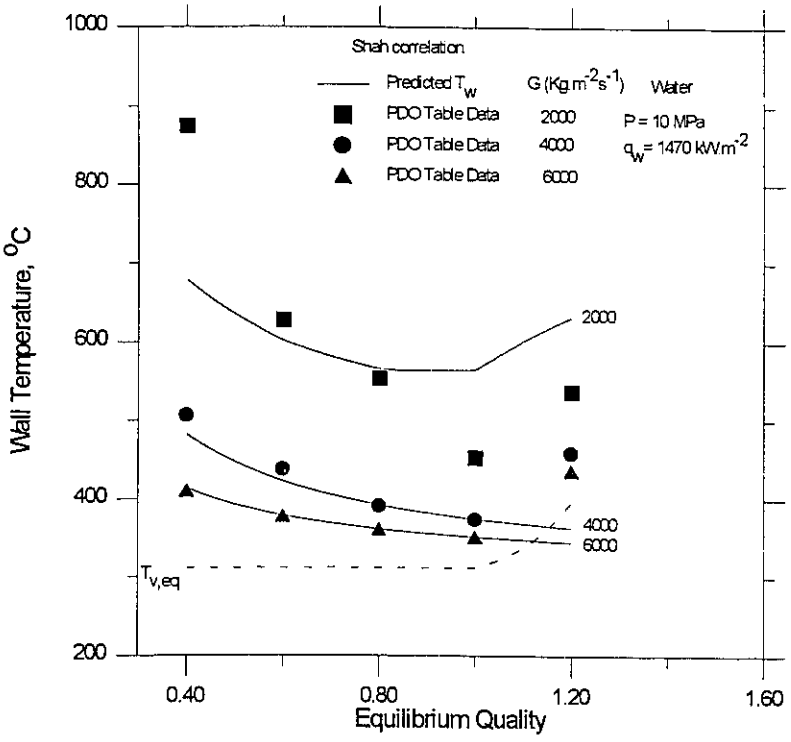

(a)

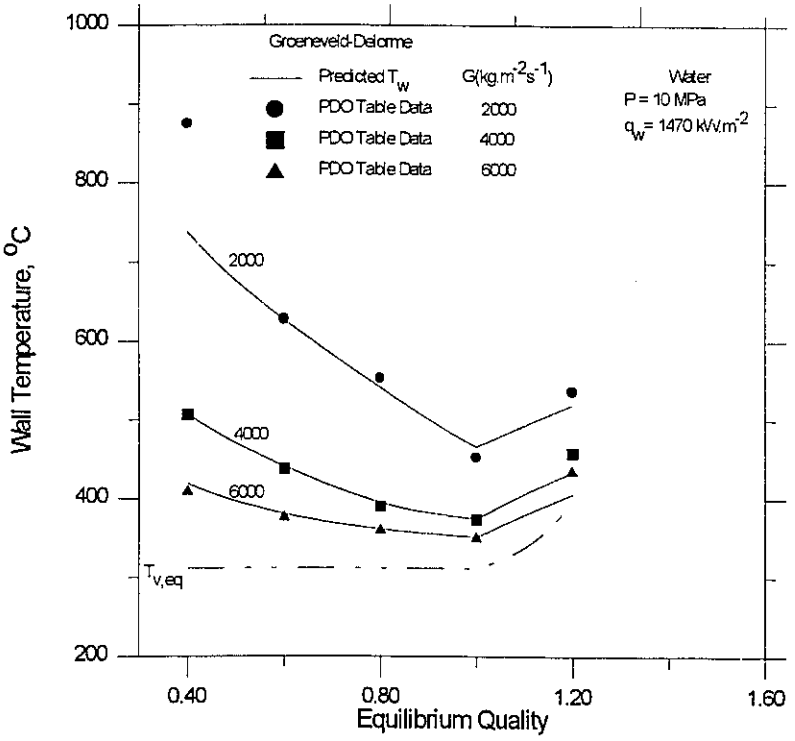

(b)

Figure 12.8 The effect of mass flux on the wall temperature distribution as predicted by the PDO-lookup table and (a) the Shah and (b) the Groeneveld-Delorme correlations.

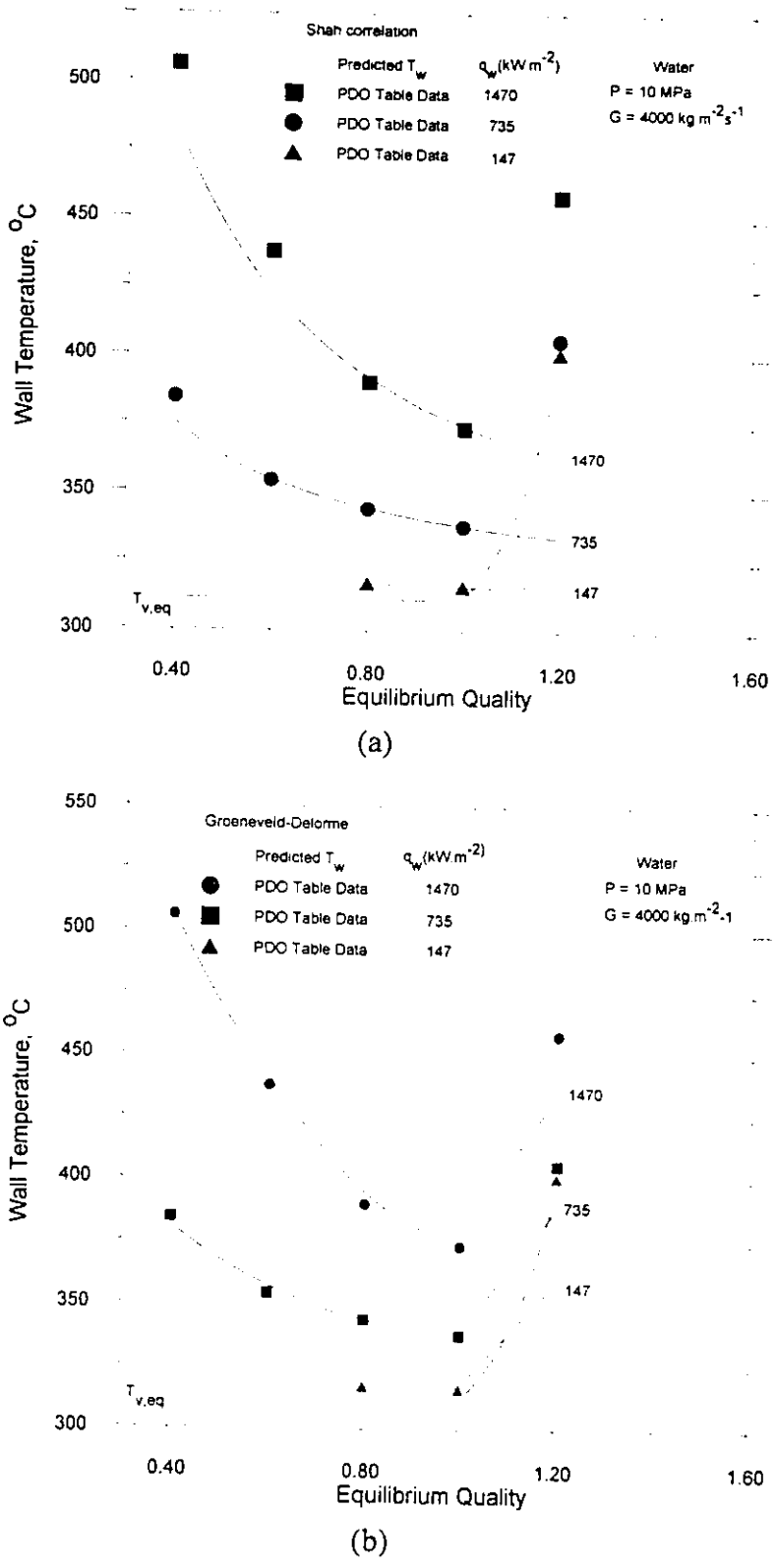

Figure 12.9 The effect of heat flux on the temperature distribution as predicted by the PDO-lookup table and (a) the Shah and (b) the Goeneveld-Delorme correlations.

Chapter 13 COMPARISON OF THE IAFB PREDICTION METHODS TO DATA

This chapter compares predictions from selected IAFB prediction methods against data sets from the AECL PDO data base and data generated during this study. The results of the comparison are displayed as plots of wall temperature versus thermodynamic equilibrium quality.

13.1 Wall Temperature Prediction

13.1.1 Comparison to Water Data

Figures 13.1-13.3 show the comparison of five prediction methods predictions with the PDO water data. Qualitatively, the Analytis-Yadigaroglu model provides the correct trend of wall temperature distribution as a function of equilibrium quality for a wide range of flow conditions. Quantitatively, it overpredicts the wall temperatures by a large margin, especially at low mass flux conditions ($G < 1000$ kgm^{-2}s^{-1}), but gives reasonable predictions at atmospheric conditions. Analytis and Yadigaroglu [1987] proposed an enhancement factor, λ, for the heat flux component, $q_{v\text{-}l}$, and the interfacial shear stress, τ_i. This factor is defined as

$$\lambda = 1 + 150\frac{\delta}{R} \quad for \ \delta \ll R \tag{9.1.1}$$

From this study, however, it was found that a value of 1.0 for λ gives the best predictions, and hence no enhancement is required.

The Denham model underpredicts the data at low pressure ($P < 2$ MPa) conditions, but it

overpredicts the data at high inlet subcoolings, high mass fluxes, and high pressures. Occasionally, the model yields fairly good predictions. In general, the Johannsen and Mosaad model overpredicts the data. The model consistently collapses at high inlet subcoolings, where it usually predicts higher heat transfer rates to the subcooled liquid core than the total heat transfer rate from the heated surface. This is obviously in defiance to conservation of energy principle.

In general, the modified Berenson [1988] equation underpredicts the data, especially at atmospheric conditions. In addition, it predicts incorrectly the trend of the wall temperature distribution versus equilibrium quality. The Cachard model gives the worst predictions. This is expected since the model contains a large number of empirical factors derived from steam-water data obtained at atmospheric conditions. Also, it predicts very rapid increase of void fraction along the channel heated length; hence earlier transition to the DFFB regime compared to the other prediction methods.

13.1.2 Comparison to Freon Data

Figures 13.4-13.7 show the comparison of five prediction methods predictions with the Freon data obtained during this study. In general, the Analytis-Yadigaroglu model overpredicts the wall temperatures, but it gives the correct trend of wall temperature versus thermodynamic equilibrium quality for a wide range of flow conditions. On the other hand, the modified Berenson equation underpredicts the wall temperatures at low mass flux and/or high inlet subcooling conditions, but overpredicts the wall temperatures at high mass fluxes. Occasionally, it predicts correctly the trend and the order of magnitude of the data.

The Denham model predicts incorrectly the trend of wall temperature distribution as a function of thermal equilibrium quality for a wide range of flow conditions. However, it provides

reasonable predictions at high inlet subcoolings. The Johannsen and Mosaad model consistently overpredicts the data by a large margin. Also, as noted in the previous section, it collapses at very high inlet subcooling conditions. This model contains several empirical factors that are derived from IAFB water data, and hence it should not be expected to perform satisfactory when compared to data obtained with other fluids. These same restrictions apply to the Cachard model; however, it overpredicts the data to a lesser degree compared to the Johannsen and Mosaad model predictions.

13.2 Vapour Temperature Prediction

In all cases, the Analytis-Yadigaroglu model predicts extremely high vapour temperatures. In some cases, the predicted vapour temperatures are higher than the experimental wall temperatures, as Figure 13.8 shows. Since the prediction of the wall heat flux is dependent on the difference between the wall and the vapour temperatures, the model yields very high wall temperatures for a given heat flux. Figure 13.8 suggests that the wall temperature predictions could be considerably improved if the model was modified to yield lower vapour temperature predictions.

The rest of the prediction methods discussed in Section 13.1, except the cachard model, approximate the vapour temperature by the vapour film temperature ($T_{vf} = (T_w + T_{sat})/2$). This approximation usually yields a higher vapour temperature than the actual vapour temperature in IAFB.

13.3 Discussion

Low quality and subcooled film boiling is of particular interest for the reflood phases of a LOCA. This flow regime usually precedes the arrival of the quench front and influences its rate

of progression. As a consequence, the majority of subcooled film-boiling prediction methods existing in the literature deal with Loss Of Coolant Accident (LOCA) conditions at low pressures (up to 0.4 MPa) and low mass fluxes (up to 300 $kgm^{-2}s^{-1}$). It has been shown in this study that mechanistic models such as two-fluid models (e.g., the Analytis-Yadigaroglu model) are the most suitable to apply for subcooled film boiling. Two-fluid models, however, need constitutive relations to predict momentum and heat transfer. These relations are usually approximated (or inferred) from data relevant to LOCA conditions (low pressures and low mass fluxes). This restricts the models to the same conditions. Therefore, to extend and improve the prediction accuracy of such models, a more generalized constitutive relations based on theoretical derivation should be sought. This requires experimental measurements of momentum and heat transport through the interface. Unfortunately, this is very difficult to achieve at high pressures and/or high mass fluxes.

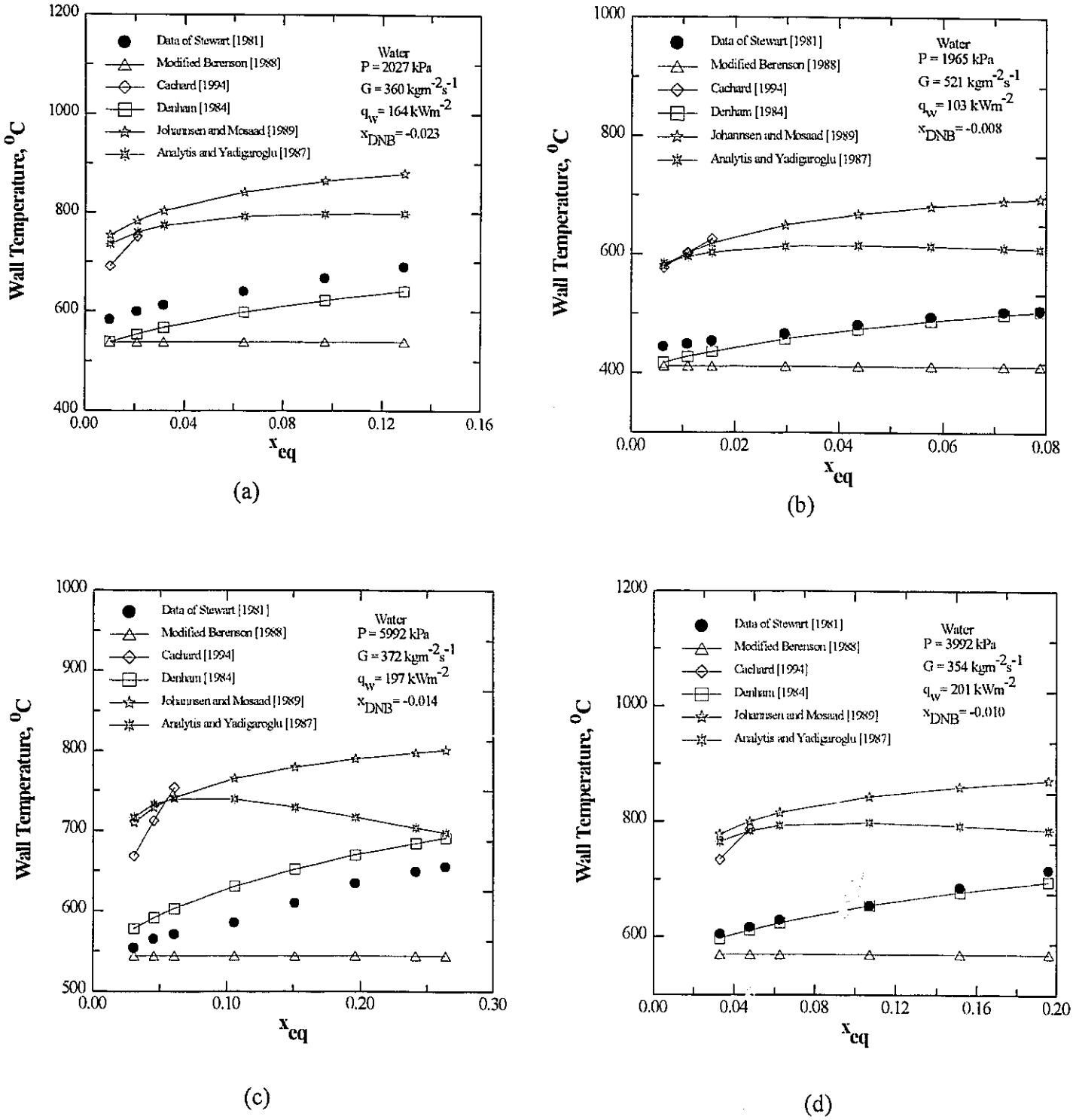

Figure 13.1 Comparison of five IAFB prediction methods with water data.

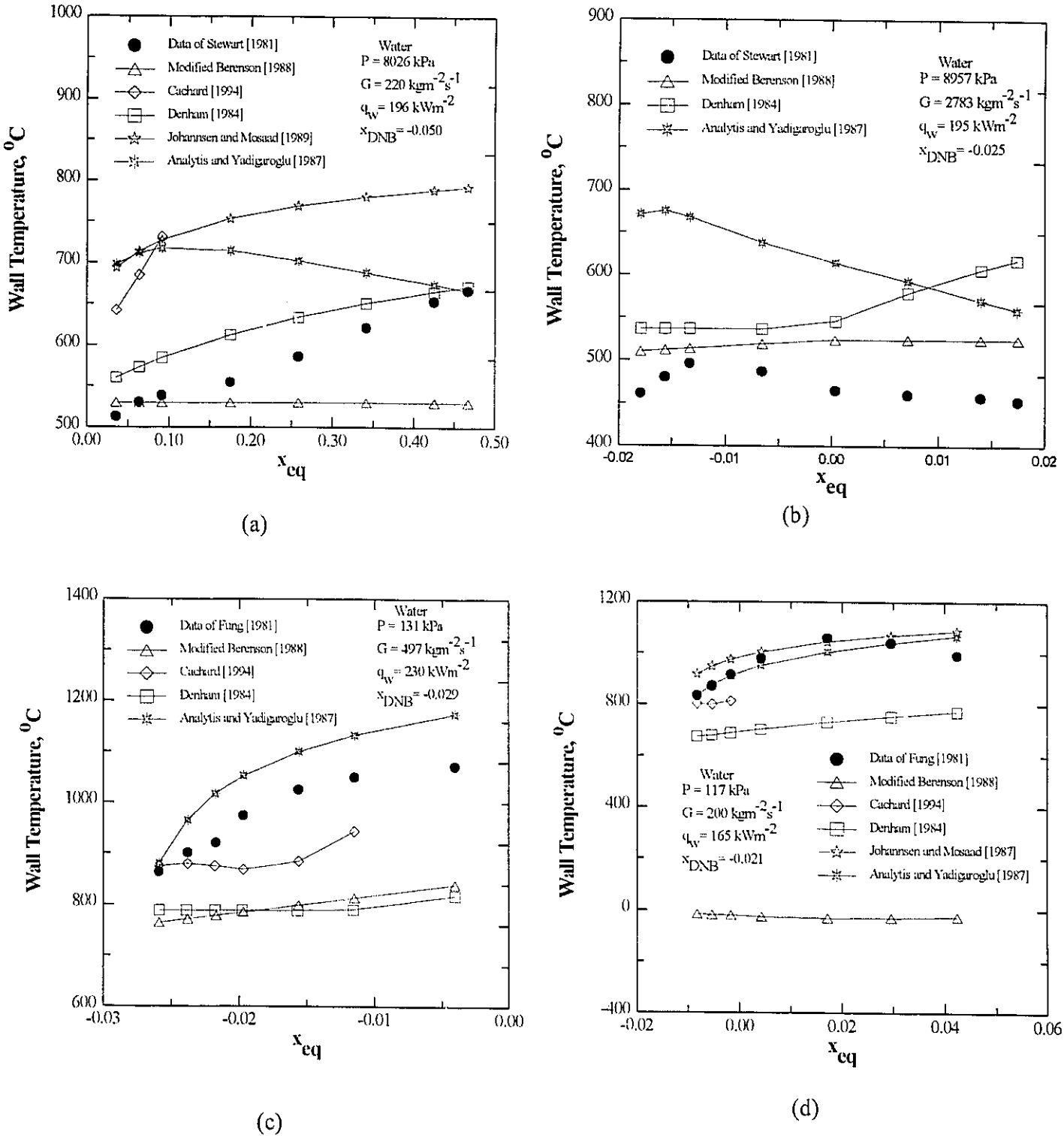

Figure 13.2 Comparison of five IAFB prediction methods with water data.

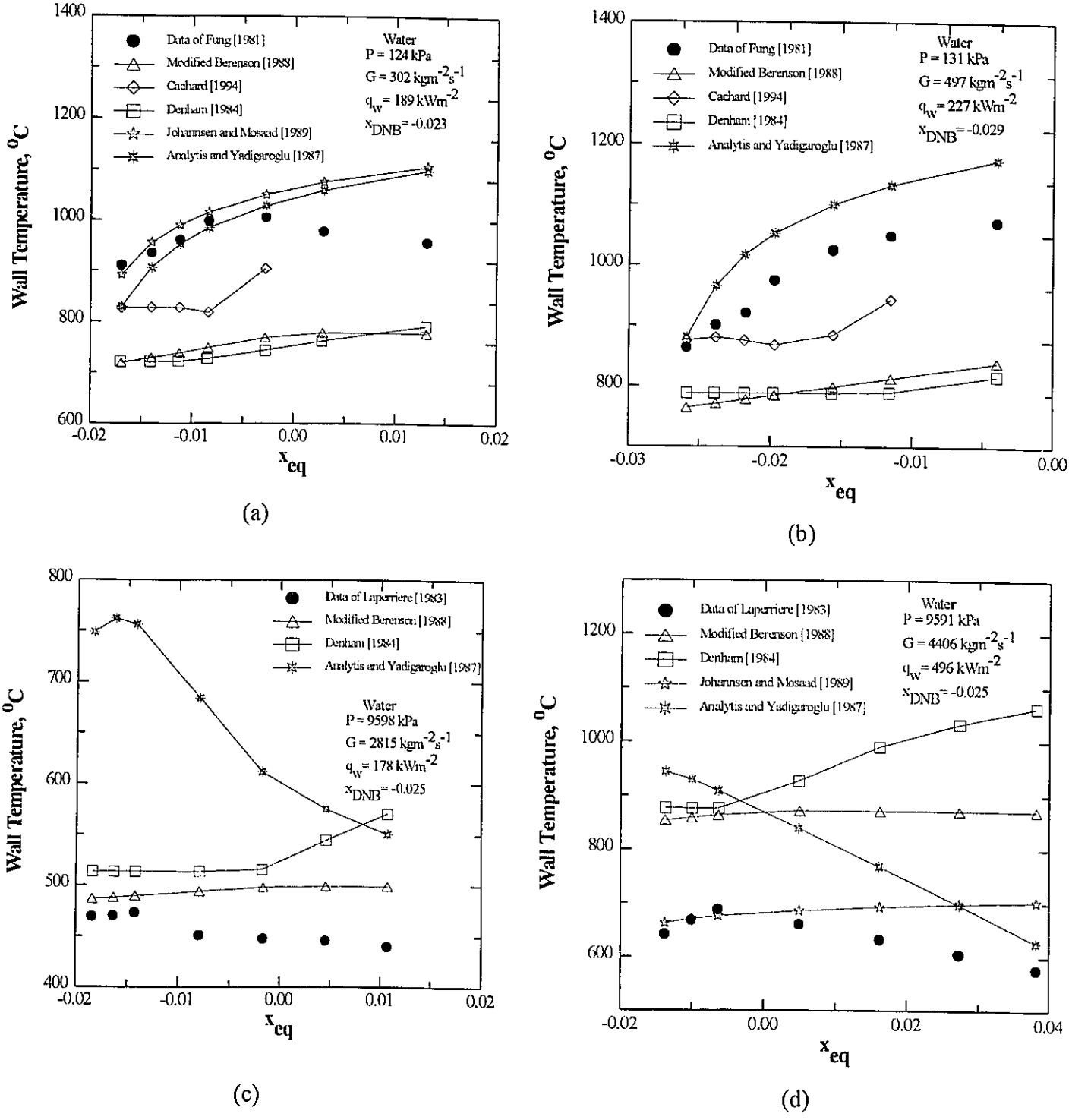

Figure 13.3 Comparison of five IAFB prediction methods with water data.

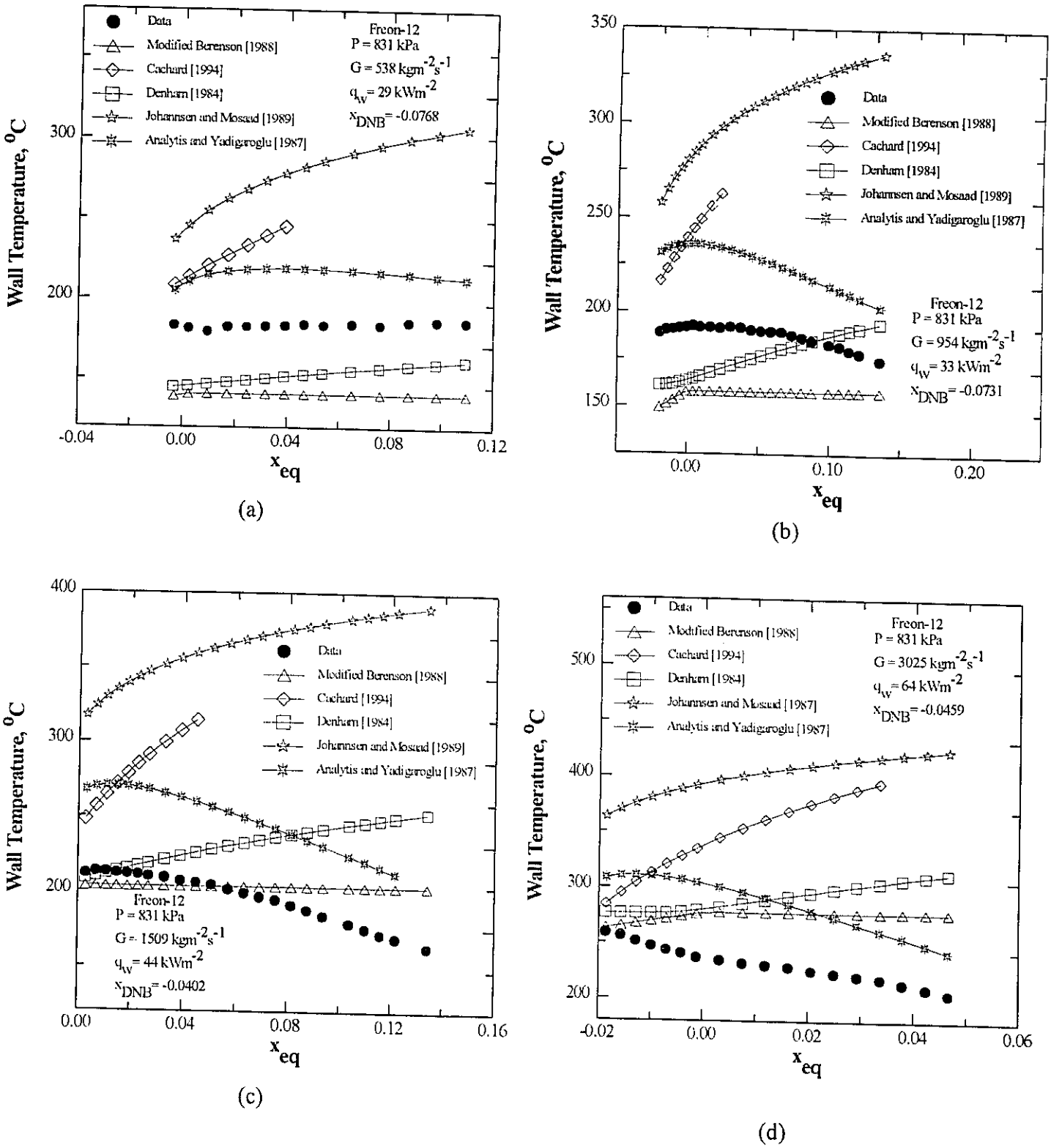

Figure 13.4 Comparison of five IAFB prediction methods with Freon-12 data.

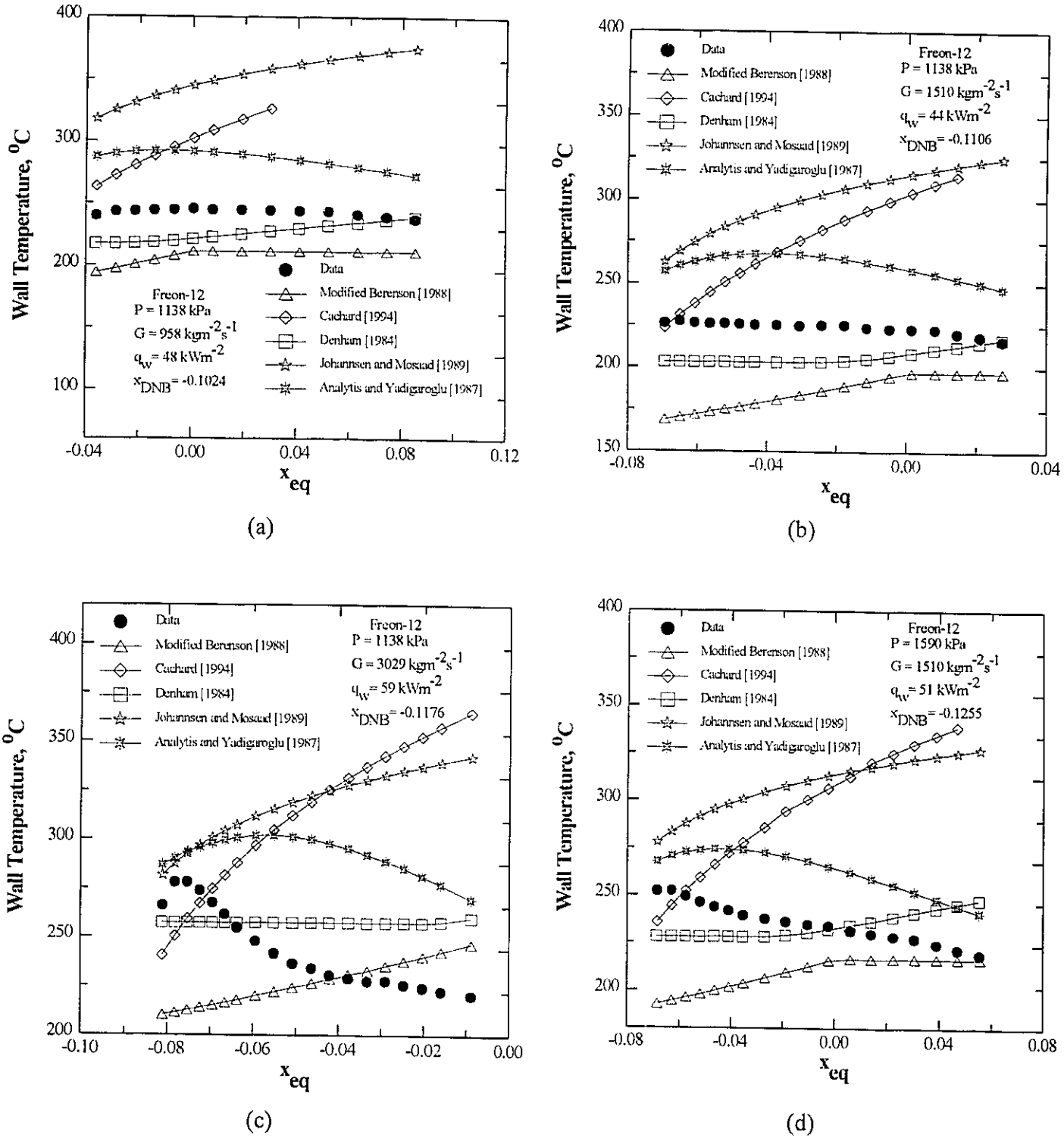

Figure 13.5 Comparison of five IAFB prediction methods with Freon-12 data.

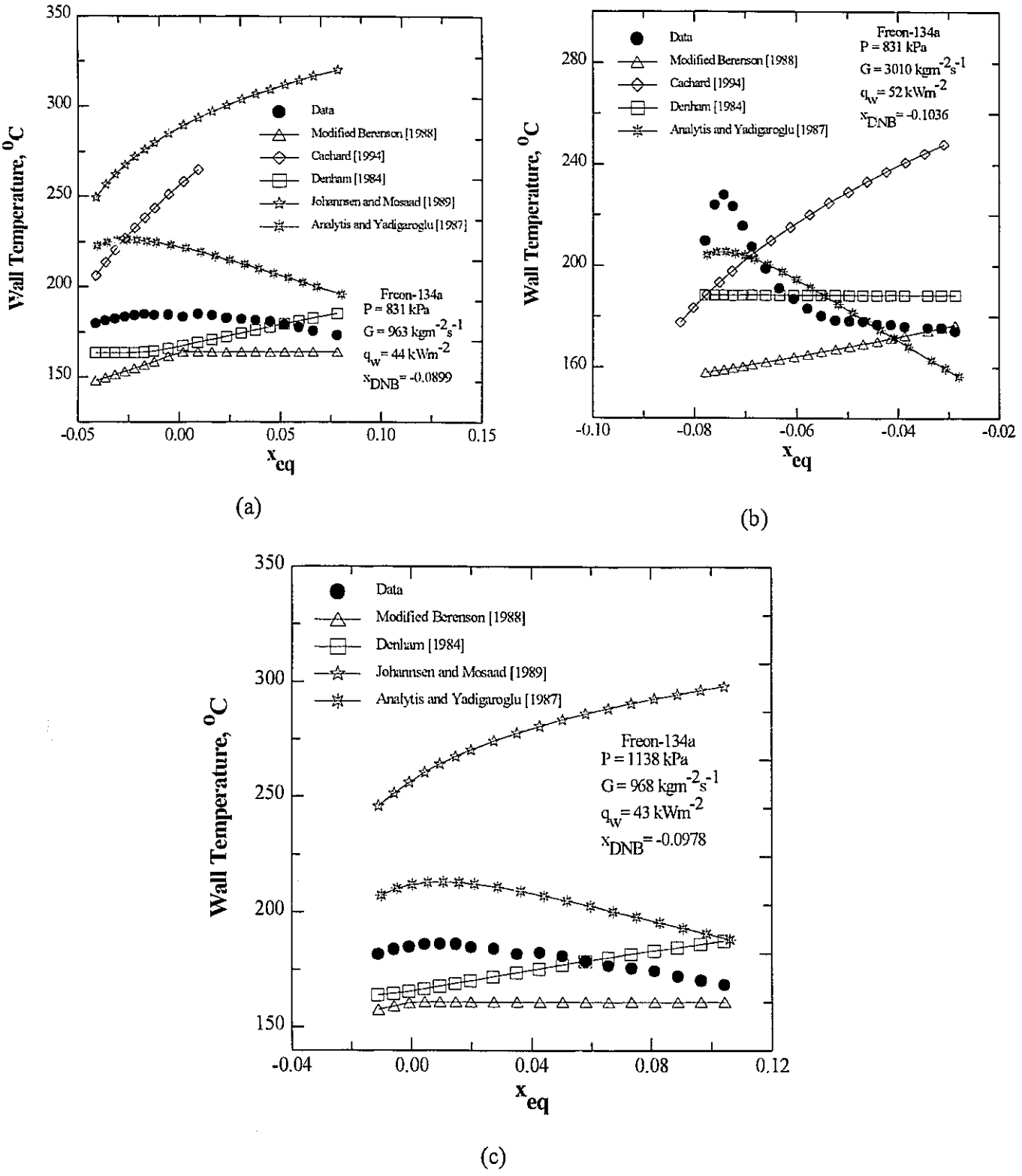

Figure 13.6 Comparison of five IAFB prediction methods with Freon-134a data.

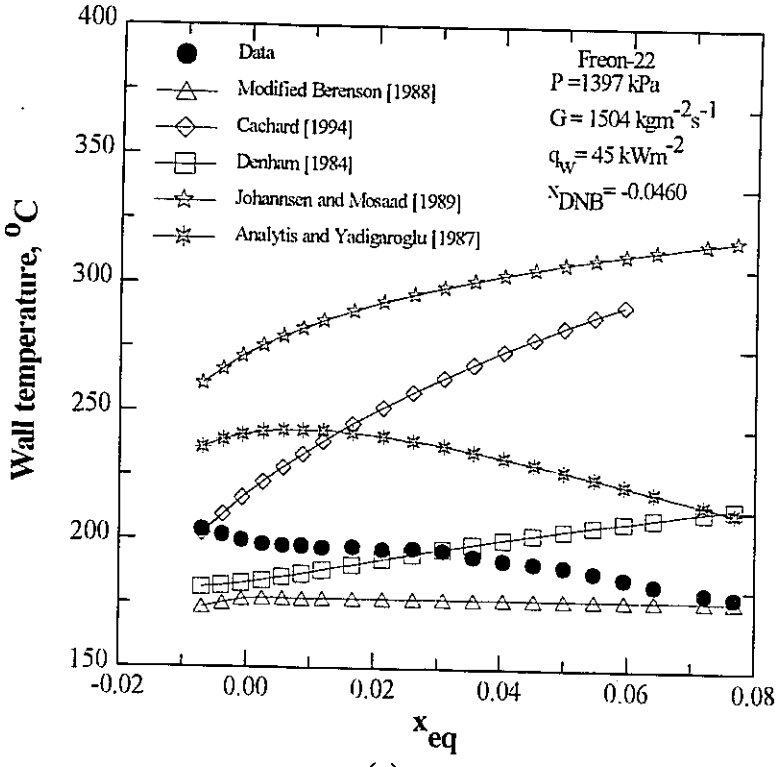

(a)

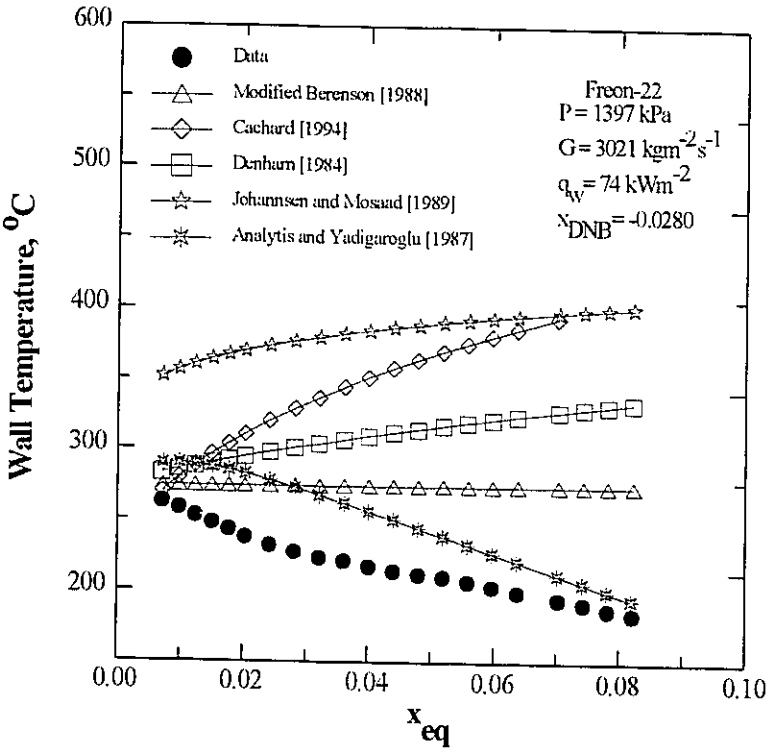

(b)

Figure 13.7 Comparison of five IAFB prediction methods with Freon-22 data.

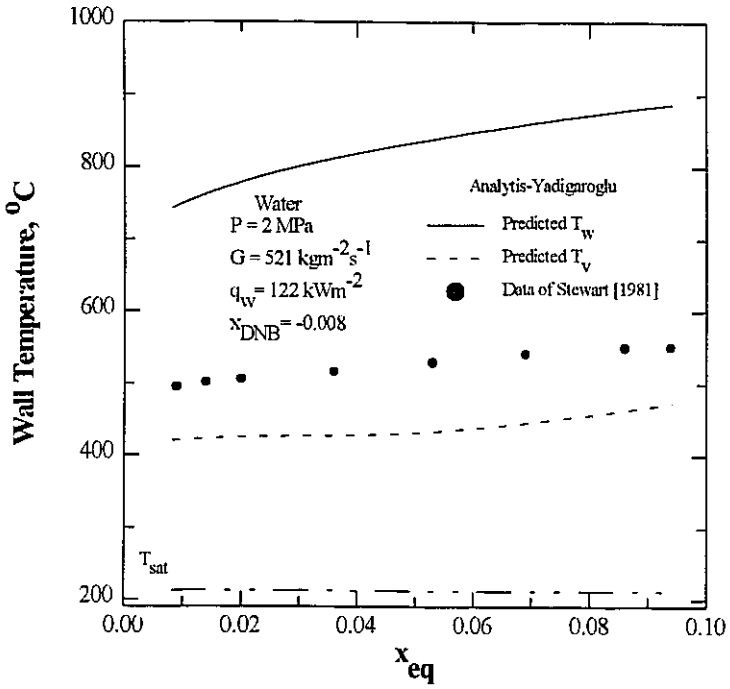

(a)

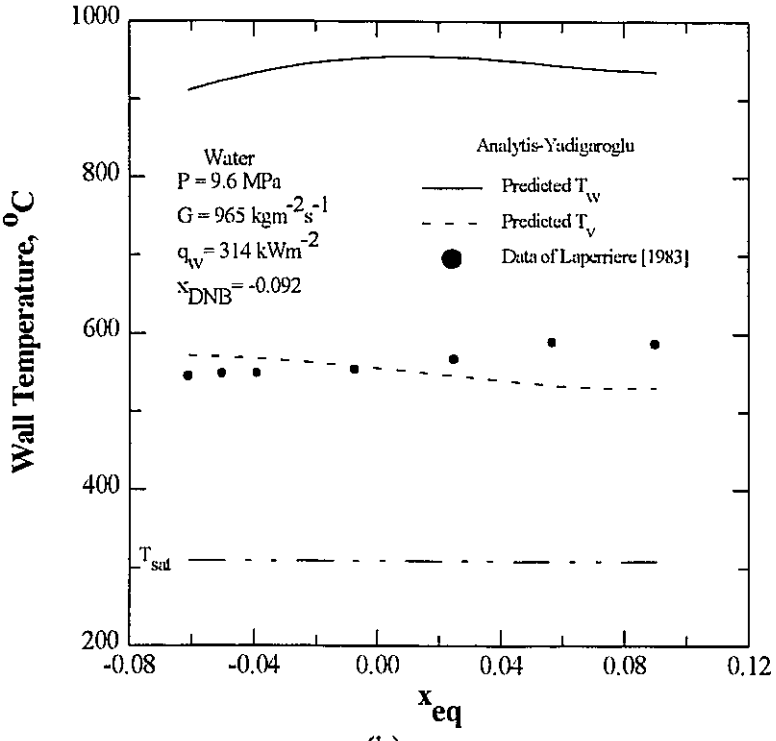

(b)

Figure 13.8 Wall and vapour temperatures predicted by the Analytis and Yadigaroglu model [1987].

Chapter 14 THEORETICAL ANALYSIS

14.1 General

Presently, there is no general prediction method, applicable to a wide range of conditions, for the complete post-CHF region (i.e., from the IAFB to DFFB regime). This is mainly due to the difficulty of developing a single general model capable of representing all or most of the physical mechanisms of post-CHF heat transfer: the geometry of the interface during film boiling can be continuous (IAFB) or discrete (DFFB). The transition from one shape of the interface to another can be very difficult to express mathematically. Hence, it is necessary to develop a hybrid model for prediction over the complete region. For instance, Leung and Groeneveld [1988] utilized a combination of the modified Berenson equation and the Groeneveld-Delorme correlation to construct a PDO look-up table applicable for both the IAFB and DFFB regions.

A number of heat transfer prediction methods have been suggested for both IAFB and DFFB. They vary from simple correlations considering only the single-phase heat transfer from the heated surface to vapour, to sophisticated two-fluid models that account for the detailed heat transfer mechanisms from the heated surface to both the liquid and vapour phases. In many cases, however, these prediction methods are valid only for conditions within their respective data base, and cannot be extended. In Chapters 3 to 6 and 12 and 13, several prediction methods are reviewed and assessed using data from this study and data from the Chalk River Laboratories (CRL) data bank. Their prediction accuracy and parametric trends are examined over a wide range of flow

conditions, particularly at medium-to-high pressures and moderate-to-high mass fluxes.

None of the existing models and correlations is able to adequately predict the heated surface temperature for all flow conditions. In general, phenomenological models provide worse prediction accuracy than the empirical correlations. This is mainly caused by the limited applicability of the constitutive relations employed within these models. The constitutive equations often incorporate empirical parameters that are valid only for a narrow range of flow conditions.

Low quality and subcooled film boiling is of particular interest for the blowdown and reflood phases of a LOCA. As a consequence, the majority of subcooled film-boiling prediction methods existing in the literature deal with LOCA conditions at low pressures (up to 0.4 MPa) and low mass fluxes (up to 300 $kgm^{-2}s^{-1}$). It has been shown in this study that mechanistic models such as two-fluid models are the most suitable to apply for subcooled film boiling. Two-fluid models, however, need constitutive relations to predict momentum and heat transfer. These relations are usually approximated (or inferred) from data relevant to LOCA conditions (low pressures and low mass fluxes). This restricts the models to the same conditions. Therefore, to extend and improve the prediction accuracy of such models, more generalized constitutive relations, based on theoretical derivation, should be sought. This requires experimental measurements of momentum and heat transport through the interface. Unfortunately, this is very difficult to achieve at high pressures and/or high mass fluxes.

In the present analysis, a two-fluid model for the IAFB regime in which more general constitutive relations, with a minimum of empirical parameters, is presented. This task has been achieved in this study by deriving simple relations for mass, momentum, and energy transfer based on the physical phenomena involved. Also, a hybrid post-CHF model is derived by combining the

present IAFB model with a modified Moose and Ganić [1982] DFFB model.

14.2 Approach and Assumptions

14.2.1 Methodology

The objective of this theoretical investigation is to develop a hybrid post-CHF model applicable over the complete post-CHF region (from the IAFB regime to the DFFB regime). The approach followed here is to derive the conservation equations for each phase separately. First, the one-dimensional two-fluid model equations for the IAFB regime are considered in detail. Then, for the DFFB regime, a model similar to that of Moose and Ganić [1982] will be presented. Therefore, by combining these two models together, the flow field is completely specified by performing axial integration of the model equations.

For the one-dimensional two-fluid model of IAFB, it is assumed that the vapour and liquid parameters change only along the length of the channel, but they are constant over the channel cross section. In general, mathematical modelling of a two-fluid model involves the following:

-conservation equations for mass, momentum, and energy for each phase,

-relevant constitutive relations of mass, momentum, and energy transfer, and

-boundary and initial conditions.

The development of constitutive relations is a critical step in a two-fluid model: it is these relations that distinguish one two-fluid model from another, since the basic conservation equations are the same for any two-fluid model.

14.2.2 Assumptions

For the IAFB regime, the mass, momentum and energy equations are derived based on the following assumptions:

-The mean flow is steady. This assumption permits the direct use of post-CHF heat transfer data obtained with the hot-patch technique.

-The flow in the liquid core is turbulent. This assumption is reasonable for high mass flow rates.

-The velocity profile of the liquid core is uniform. This is justified, since turbulent flow is assumed.

-The density of each phase within any cross-sectional area is considered to be uniform. For most practical two-phase flow problems, this assumption is valid, since the transverse pressure gradient within a channel is relatively small.

-No vapour bubbles in the liquid core. This assumption is reasonable in the subcooled IAFB region. However, some entrainment of vapour into the liquid core may be possible in the saturated IAFB region.

-No liquid entrained in the vapour layer. This is more likely to be true for the subcooled IAFB region, where the interface is relatively smooth.

-Thermodynamic non-equilibrium holds for the complete IAFB regime.

-In the vapour film, the flow is turbulent for vapour Reynolds numbers, Re_v, larger than 100 and laminar otherwise. It has been shown by Hsu and Westwater [1959] that transition to turbulent flow in the vapour film occurs at a Re_v value of 100.

-The vapour-liquid interface is at saturation.

-No direct liquid-wall contact.

-Both the liquid and vapour phases are incompressible.

-Liquid flows in the centre of the flow channel and is separated from the heated wall by a

thin vapour film.

-The vapour film thickness is very small with respect to the tube radius (which will usually be the case). Therefore, the vapour is treated as flow between two parallel plates, the heated wall and the liquid-vapour interface. This allows the use of a Cartesian coordinate system, instead of a cylindrical coordinate system.

Further assumptions and conditions are discussed as they appear in the analysis.

14.3 Derivation of the Conservation Equations

The basic conservation equations of two-phase flow can be derived in many different ways. The derivation of these equations have been the subject of interest for many years, and several authors have provided a rigorous and systematic study of their correct forms ([Ishii, 1975]; [Delhaye, 1969]; [Delhaye, 1981]; [Ishii and Mishima, 1984]; [Yadigaroglu and Lahey, 1975]). The one-dimensional two-fluid equations relevant to the IAFB regime can be readily obtained from these general two-phase flow equations. However, it is preferred here to rederive these equations directly using the previous assumptions. This derivation method of the equations is preferred because it conveys a physical understanding of the hydrodynamics and heat transfer phenomena in IAFB, since the derivations are phenomenologically based. The equations are all assumed to contain some level of space and time averaging. In all the derivations that follow, it is implicitly assumed that the cross-sectional average of products of the dependent variables is approximately equal to the product of the averages. Strictly speaking, this assumption is not valid for the general case of two-phase flow; however, it is a good assumption for separated or slip flows, such as the IAFB regime [Yadigaroglu and Lahey, 1975]. In the following sections, the conservation equations are derived with reference to the differential control volume shown in Fig. 14.1.

14.3.1 Mass Conservation

For the control volume shown in Fig. 14.1, we consider the mass conservation equations written separately for each phase,

$$\frac{d}{dz}\left[\rho_v \, \alpha \, A \, U_v \right] = W' \qquad \textbf{(14.3.1)}$$

$$\frac{d}{dz}\left[\rho_l \, (1 - \alpha) \, A \, U_l \right] = - W' \qquad \textbf{(14.3.2)}$$

where W', α, A, U_v and U_l represent the vapour source per unit axial length in the differential control volume, the void fraction, the tube cross-sectional area, the vapour mean velocity and the liquid core mean velocity, respectively. For one-dimensional flow, the void fraction α is defined as the fraction of flow area occupied by the vapour phase. For a constant tube cross-sectional area the mass conservation equations become

$$\frac{d}{dz}\left[\rho_v \, \alpha \, U_v \right] = \frac{W'}{A} \qquad \textbf{(14.3.3)}$$

$$\frac{d}{dz}\left[\rho_l \, (1 - \alpha) \, U_l \right] = - \frac{W'}{A} \qquad \textbf{(14.3.4)}$$

4.3.2 Momentum Conservation

The momentum conservation equations for the liquid and vapour phases are considered next. For the control volume shown in Fig. 14.1, a force balance can be written over the liquid phase cross-sectional area to give

$$-\frac{d}{dz}[P_l\,(1\ -\ \alpha)\ A]\Delta z + p_i\frac{d\ [(1\ -\ \alpha)\ A]}{dz}\Delta z\ -\ g\rho_l(1\ -\ \alpha)A\Delta z\ +\ \tau_i P_i\Delta z$$
$$=\ \frac{d}{dz}[\rho_l\,A(1\ -\ \alpha)U_l^2]\Delta z\ +\ W'U_i\Delta z \qquad \textbf{(14.3.5)}$$

The four terms on the L.H.S. of this equation can be designated as external forces at the ends of the control volume due to pressure, force due to liquid flow area variation and interfacial pressure, p_i, gravitational force and shear stress force at the liquid-vapour interface (P_i denotes interface perimeter), respectively. The terms on the R.H.S. represent the spacial acceleration term and the momentum exchange due to mass transfer between the phases, respectively.

The interfacial velocity, U_i, is generally different from the vapour and liquid velocities, hence to maintain generality it can be expressed as

$$U_i\ =\ \eta U_l\ +\ (1\ -\ \eta)U_v \qquad \textbf{(14.3.6)}$$

The parameter η can be assigned any value between 0 and 1. By assuming that the interfacial pressure, p_i, is equal to the liquid pressure, P_l, on the liquid side, the first two terms on the L.H.S. of the momentum equation can be combined to yield,

$$-(1\ -\ \alpha)A\frac{dP_l}{dz}\Delta z \qquad \textbf{(14.3.7)}$$

Thus simplifying and rearranging, the liquid-phase momentum equation becomes

$$-(1\ -\ \alpha)\frac{dP_l}{dz}\ -\ g\rho_l(1\ -\ \alpha)\ +\ \frac{\tau_i P_i}{A}\ =\ \frac{1}{A}\frac{d}{dz}[\rho_l\,A(1\ -\ \alpha)U_l^2]$$
$$+\ \frac{W'}{A}[\eta U_l\ +\ (1\ -\ \eta)U_v] \qquad \textbf{(14.3.8)}$$

The momentum equation for the vapour phase can be treated in a similar manner to yield,

$$-\alpha\frac{dP_v}{dz} - g\rho_v\alpha - \frac{\tau_i P_i}{A} - \frac{\tau_w P_w}{A} = \frac{1}{A}\frac{d}{dz}[\rho_v A\alpha U_v^2] - \frac{W'}{A}[\eta U_l + (1-\eta)U_v] \tag{14.3.9}$$

The momentum equations can be further simplified by using the mass conservation equations, and by expanding the acceleration terms to give

$$-(1-\alpha)\frac{dP_l}{dz} - g\,\rho_l(1-\alpha) + \frac{\tau_i P_i}{A} = \rho_l(1-\alpha)U_l\frac{dU_l}{dz} + \frac{\delta W'}{A}[(\eta-1)U_l + (1-\eta)U_v] \tag{14.3.10}$$

$$-\alpha\frac{dP_v}{dz} - g\,\rho_v\alpha - \frac{\tau_i P_i}{A} - \frac{\tau_w P_w}{A} = \rho_v\alpha U_v\frac{dU_v}{dz} + \eta\frac{\delta W'}{A}[U_v - U_l] \tag{14.3.11}$$

In Eqs. (14.3.10) and (14.3.11) it was assumed that p_i is equal to P_l on the liquid side, and equal to P_v on the vapour side.

14.3.3 Energy Conservation

In this derivation, shear induced dissipation and axial conduction are neglected. Hence, for the control volume of Fig. 14.1, conservation of energy for the liquid phase results in

$$\frac{d}{dz}[\rho_l(1-\alpha)A\,U_l\,e_l]\Delta z + W'e_i\Delta z - q_{i-l}P_i\Delta z = 0 \tag{14.3.12}$$

the specific energy term, e_l (or e_v for vapour phase), is defined by

$$e_k = h_k + \frac{U_k^2}{2} + gz \qquad k = l\ (\textit{liquid phase})\ \textit{or}\ v\ (\textit{vapour phase}) \tag{14.3.13}$$

where h_k is the local enthalpy of phase k.

The first term in Eq. (14.3.12) is the convective energy transfer. The second term is the energy

transfer due to change of phase, where the specific interfacial energy, e_i, is given by

$$e_i = h_{ki} + \frac{U_i^2}{2} + gz \qquad k = f\ (liquid\ \ phase\ )\ or\ g\ (vapour\ \ phase\ ) \tag{14.3.14}$$

where h_{ki} is the local specific enthalpy at the interface. The third term in Eq. (14.3.12) is the heat transfer used to heat up the liquid core.

In a similar manner, conservation of energy for the vapour control volume yields

$$\frac{d}{dz}[\rho_v U_v e_v \alpha A]\Delta z + q_{v\text{-}i} P_i \Delta z - W' e_i \Delta z - q_{w\text{-}v} P_w \Delta z = 0 \tag{14.3.15}$$

where $q_{w\text{-}v}$ and $q_{v\text{-}i}$ represent the heat flux terms from the heated wall to the vapour phase and from the vapour to the liquid-vapour interface, respectively. Alternatively, a global energy equation can be derived by considering a single control volume for the liquid and vapour phases. That yields

$$W'(e_v - e_l) + \alpha A \rho_v U_v \frac{de_v}{dz} + (1 - \alpha) A \rho_l U_l \frac{de_l}{dz} = q_{w\text{-}v} P_w \tag{14.3.16}$$

14.3.4 Further Simplifications of the Conservation Equations

In order to further simplify Eqs. (14.3.3-14.3.16), the following assumptions are made:

-The phasic pressures at the two sides of the interface are equal. Fung [1981] has shown that the difference between P_l and P_v across the interface is very small. Further, it is a common practice to assume that $p_i = P_l = P_v$. Nevertheless, it should be noted that though the pressure difference term across the interface is very small, this small difference is very important in interfacial instability analysis.

-Kinetic energy is negligible. This is valid at low Mach numbers.

-The interfacial velocity, U_i, is equal to the liquid average velocity, U_l. That yields a value

of one for η (see Eq. (14.3.6)) . Yadigaroglu and Lahey [1975] recommended the value of one for η, because of the flat velocity profiles typical of highly turbulent flows. Further, as will be shown in Chapter 17, the present model yields more accurate predictions when a value of one is used for η.

Making these assumptions, the above equations can be reduced to simpler forms:

$$\frac{d}{dz}\left[\ \rho_v\ \alpha\ U_v\ \right] = \frac{W'}{A} \tag{14.3.17}$$

$$\frac{d}{dz}\left[\ \rho_l\ (1\ -\ \alpha)\ U_l\ \right] = -\ \frac{W'}{A} \tag{14.3.18}$$

$$-\ (1\ -\ \alpha)\frac{dP}{dz}\ -\ g\ \rho_l(1\ -\ \alpha)\ +\ \frac{\tau_i P_i}{A} = \rho_l(1\ -\ \alpha)U_l\frac{dU_l}{dz} \tag{14.3.19}$$

$$-\ \alpha\frac{dP}{dz}\ -\ g\ \rho_v\alpha\ -\ \frac{\tau_i P_i}{A}\ -\ \frac{\tau_w P_w}{A} = \rho_v\alpha U_v\frac{dU_v}{dz}\ +\ \frac{W'}{A}[U_v\ -\ U_l] \tag{14.3.20}$$

$$(1\ -\ \alpha)U_l\frac{dh_l}{dz} = \frac{q_{i\text{-}l}\ P_i}{\rho_l\ A}\ -\ \frac{W'\ (h_f\ -\ h_l)}{\rho_l\ A} \tag{14.3.21}$$

$$\alpha\ U_v\ \frac{dh_v}{dz} = \frac{q_{w\text{-}v}\ P_w}{\rho_v\ A}\ -\ \frac{q_{v\text{-}i}\ P_i}{\rho_v\ A}\ +\ \frac{W'\ (h_g\ -\ h_v)}{\rho_v\ A} \tag{14.3.22}$$

For definitions of the symbols used in the above equations, please refer to the nomenclature.

Other relations

The vapour layer thickness can be expressed as a function of the tube radius and the void fraction,

$$\delta = R(1-\sqrt{1-\alpha}) \qquad (14.3.23)$$

and the cross sectional area, interfacial and inside tube wall peripheral lengths as

$$A = \pi R^2, \qquad R = \textit{tube radius} \qquad (14.3.24)$$

$$P_i = 2\pi(R - \delta) \qquad (14.3.25)$$

$$P_w = 2\pi R \qquad (14.3.26)$$

14.3.5 Constitutive Relations

14.3.5.1 Approach

The Eulerian area averaging procedure over the liquid and vapour phase cross-sections lead to the practical quasi-one dimensional field equations (Eqs. (14.3.17-14.3.22)). These equations are applicable to various flow situations, provided the interfacial mass, momentum, and energy transfer terms are expressed by appropriate constitutive relations for a particular flow regime. However, due to the averaging procedure, gradients of variables in the direction normal to the flow (in the radial direction) are basically lost. This information is needed to provide equations for shear and heat transfer components, and to close the set of Eqs. (14.3.17-14.3.22). Therefore, transfer of momentum and energy at the interface and the wall can only be specified by empirical equations or

by simplified models. Presently, no data base of interfacial transport parameters exists to allow development of appropriate constitutive relations for the IAFB regime. Hence, due to this limitation, relations developed for single-phase flows or adiabatic two-phase flows are often employed. Despite the considerable uncertainties in these constitutive relations, there is, however, no substitute to two-fluid models for modelling accurately the heat transfer in the IAFB regime.

This analysis describes a fundamentally different approach to finding constitutive relations for two-fluid models. The purpose is to present an alternative approach to the problem of providing constitutive relations for two-fluid models of IAFB; and to show that this approach works well when applied to systems having several degrees of freedom, which are caused by the thermal and mechanical non-equilibrium between the phases, such as in IAFB. It is not intended here to rigorously develop or to demonstrate the overall capability of developed correlations, but to simply show that heat transfer predictions in the IAFB regime can be physically described based on the idea of reduction of degrees of freedom of the system. This can be achieved by properly identifying and establishing physically sound relationships between the system variables. For instance, instead of attempting to provide independent equations for the shear stresses at the wall and the interface based on single-phase or adiabatic annular two-phase flow relations, as is usually done in two-fluid models of IAFB, effort should first be concentrated on finding the physical relationship between the wall shear stress and interfacial shear stress first. Then, it becomes only necessary to provide a single equation for either the shear stress at the wall or at the interface, hence reducing the degrees of freedom of the system. The same concept is applied to the heat transfer relations discussed in the next section.

To this author's knowledge, the present approach has not been offered previously to describe

the hydrodynamics and heat transfer in the IAFB regime. In the following sections, closure relations for the various heat transfer and shear stress components are proposed in order to complete the one-dimensional two-fluid model of the IAFB.

14.3.5.2 Heat Flux

The heat transfer process in IAFB is a three-step process: heat transfer from wall-to-vapour ($q_{w\text{-}v}$), from vapour-to-interface ($q_{v\text{-}i}$), and from interface-to-liquid core ($q_{i\text{-}l}$). The heat transfer components $q_{w\text{-}v}$, $q_{v\text{-}i}$, and $q_{i\text{-}l}$ are schematically shown in Fig. 14.2. One main limitation of two-fluid models is the large degree of uncertainties involved in specifying relations for the heat transfer components. In most two-fluid models, single-phase convective heat transfer correlations are often used to evaluate the heat transfer components $q_{w\text{-}v}$, $q_{v\text{-}i}$, and $q_{i\text{-}l}$. These empirical equations are usually independently developed for single-phase flow situations, and often there is little justification and consistency in their application to a two-phase flow situation, such as the IAFB. As a result, frequently they give irrational heat transfer predictions when applied to two-fluid models of IAFB. For example, the model may give higher heat transfer rates from the interface-to-liquid core ($q_{i\text{-}l}$) than the total heat transfer rate to the vapour-liquid interface, or/and higher heat transfer rates from vapour-to-interface ($q_{v\text{-}i}$) than from wall-to-vapour ($q_{w\text{-}v}$). This situation is encountered in many two-fluid models, such as those of Analytis and Yadigaroglu [1987], Mosaad and Johannsen [1988], and others. This deficiency is frequently the cause of failure of these models. Obviously, it is caused by the neglect of first attempting to establish physical relationships between the different heat transfer processes (wall-to-vapour, vapour-to-interface, and interface-to-liquid). As previously noted, the approach of establishing physically sound relations between $q_{w\text{-}v}$, $q_{v\text{-}i}$, and $q_{i\text{-}l}$ reduces the number of degrees of freedom in the system, and enables the two-fluid model to give heat transfer

predictions within thermodynamic limits. The heat transfer relations described in this section are based on this concept.

A number of these relations can be readily obtained based on conservation of energy:

$$Q_w = q_w P_w = q_{w\text{-}v} P_w + q_{rad} P_w \qquad \textbf{(14.3.27)}$$

$$Q_v = q_{w\text{-}v} P_w - q_{v\text{-}i} P_i \qquad \textbf{(14.3.28)}$$

$$Q_{ev} = q_{ev} P_i = q_{v\text{-}i} P_i + q_{rad} P_w - q_{i\text{-}l} P_i \qquad \textbf{(14.3.29)}$$

where Q_w, Q_v and Q_{ev} are the wall heat transfer rate, vapour heating rate and evaporation heat transfer rate per unit axial length, respectively. Equation (14.3.27) simply states that the heat transfer mechanism from the wall is by wall-to-vapour convection and wall-to-liquid radiation (q_{rad}). Equation (14.3.28) expresses the vapour heating source, Q_v, causing superheating of the vapour phase. Equation (14.3.29) states that the total heat transfer to the liquid is used partially for evaporation at the interface and partially for reduction of subcooling in the liquid core.

Equations (14.3.27)-(14.3.29) are derived based on first principles; other relations between $q_{w\text{-}v}$, $q_{v\text{-}i}$, and $q_{i\text{-}l}$ can be derived based on phenomenological reasoning of the heat transfer process that satisfies thermodynamic limits. For given flow conditions, the predicted heat fluxes $q_{w\text{-}v}$, $q_{v\text{-}i}$, and $q_{i\text{-}l}$ must satisfy the following thermodynamic limits:

$$\frac{q_{v\text{-}i}\,P_i}{q_{w\text{-}v}\,P_w} \le 1 \qquad \textbf{(14.3.30)}$$

$$\frac{q_{i\text{-}l}\,P_i}{q_{v\text{-}i}\,P_i + q_{rad}\,P_w} \le 1 \qquad \textbf{(14.3.31)}$$

$$\frac{q_{i\text{-}l}\,P_i}{q_{w\text{-}v}\,P_w + q_{rad}\,P_w} \le 1 \qquad \textbf{(14.3.32)}$$

As mentioned earlier, a large number of IAFB models, the most important of them assessed in Chapter 13, do not satisfy these limits under certain flow conditions; i.e., high subcooling, high mass flux, etc.

a) Relation for $q_{v\text{-}i}/q_{w\text{-}v}$

The heat transfer rates from wall-to-vapour ($q_{w\text{-}v}$) and from vapour-to-interface ($q_{v\text{-}i}$) are directly dependent on two parameters: (i) the temperature differences between the wall and the vapour (T_w - T_v) and the vapour and interface (T_v - T_{sat}), respectively, and (ii) the heat transfer coefficients from wall-to-vapour ($h_{w\text{-}v}$) and from vapour-to-interface ($h_{v\text{-}i}$), respectively. Thus, the ratio $q_{v\text{-}i}/q_{w\text{-}v}$ may be expressed as follows:

$$\frac{q_{v\text{-}i}}{q_{w\text{-}v}} = \left(\frac{h_{v\text{-}i}}{h_{w\text{-}v}}\right)\left(\frac{T_v - T_{sat}}{T_w - T_v}\right) \qquad \textbf{(14.3.33)}$$

For turbulent flow in the vapour, the heat transfer coefficients $h_{w\text{-}v}$ and $h_{v\text{-}i}$ are directly dependent on the Reynolds numbers, $Re_{w\text{-}v}$ and $Re_{v\text{-}i}$, and the Prandtl numbers, $Pr_{w\text{-}v}$ and $Pr_{v\text{-}i}$. Therefore, the ratio $h_{w\text{-}v}/h_{v\text{-}i}$ must also be dependent on these dimensionless numbers. By definition, the $Re_{w\text{-}v}$ and $Re_{v\text{-}i}$ can be expressed as follows:

$$Re_{w\text{-}v} = \frac{\rho_v U_v 2\delta}{\mu_v}$$
$$Re_{v\text{-}i} = \frac{\rho_v |U_v - U_l| 2\delta}{\mu_v} \qquad \textbf{(14.3.34)}$$

and $Pr_{w\text{-}v}$ and $Pr_{v\text{-}i}$ as

$$Pr_{w\text{-}v} = \frac{\mu_v Cp_v}{k_v} = Pr_{v\text{-}i} \qquad \textbf{(14.3.35)}$$

Here, it is assumed that $h_{w\text{-}v}$ and $h_{v\text{-}i}$ take a similar functional form as that of the Dittus-Boelter relation, such that

$$h_{w\text{-}v} = \frac{k_v}{2\delta} C_{w\text{-}v} Re_{w\text{-}v}^{\ m} Pr_{w\text{-}v}^{\ n}$$
$$h_{v\text{-}i} = \frac{k_v}{2\delta} C_{v\text{-}i} Re_{v\text{-}i}^{\ m} Pr_{v\text{-}i}^{\ n} \qquad \textbf{(14.3.36)}$$

and the ratio $(h_{v\text{-}i}/h_{w\text{-}v})$ becomes

$$\frac{h_{v\text{-}i}}{h_{w\text{-}v}} = \frac{C_{v\text{-}i}}{C_{w\text{-}v}} \left(\frac{U_v - U_l}{U_v} \right)^m \qquad \textbf{(14.3.37)}$$

The heat transfer near the vapour-liquid interface is considerably enhanced due to interfacial waves and turbulence. Hence, the coefficient $C_{v\text{-}i}$ is expected to be higher than $C_{w\text{-}v}$. However, since U_v is larger than $(U_v - U_l)$, this is assumed to compensate for the higher values of $C_{v\text{-}i}$. Therefore, this implies that $h_{w\text{-}v}$ and $h_{v\text{-}i}$ are of the same order of magnitude, and the ratio $h_{v\text{-}i}/h_{w\text{-}v}$ is assumed to approach one. Chapter 16 provides further discussion and validation of this assumption. Also, this means that $q_{v\text{-}i}/q_{w\text{-}v}$ is predominantly controlled by the temperature difference ratio, and

$$\frac{q_{v\text{-}i}}{q_{w\text{-}v}} \cong \frac{T_v - T_{sat}}{T_w - T_v} \qquad \textbf{(14.3.38)}$$

The lower limit of the heat transfer rate from wall-to-vapour, $q_{w\text{-}v}$, is that of pure conduction through a vapour film of thickness δ with the vapour temperature evaluated at the average value between wall and saturation temperatures (film temperature):

$$T_{vf} = \frac{T_w + T_{sat}}{2} \qquad \textbf{(14.3.39)}$$

This results in $q_{w\text{-}v} = q_{v\text{-}i}$ in Eq. (14.3.38). However, due to evaporation, the value of the vapour temperature is lower than the value of the film temperature $((T_v - T_{sat})/(T_w - T_v) < 1)$. This is significant in that it influences the value of the thermophysical properties of the vapour. The upper limit of the heat transfer rate from the vapour-to-interface, $q_{v\text{-}i}$, is restricted by the thermodynamic limit (Eq. (14.3.30)), such that

$$q_{v\text{-}l}\, P_t = q_{w\text{-}v}\, P_w \qquad \textbf{(14.3.40)}$$

b) Relation for $(q_{v\text{-}i} + q_{rad})/q_{i\text{-}l}$

The ratio $(q_{v\text{-}i} + q_{rad})/q_{i\text{-}l}$ can be treated in a similar manner as in section (a), namely

$$\frac{q_{v\text{-}l} + q_{rad}}{q_{t\text{-}l}} \cong f\left(\frac{T_v - T_{sat}}{T_{sat} - T_l}, \frac{T_w - T_{sat}}{T_{sat} - T_l}, \frac{h_{v\text{-}l}}{h_{t\text{-}l}}, \frac{h_{rad}}{h_{t\text{-}l}}\right) \qquad \textbf{(14.3.41)}$$

The specific functional relationship of Eq. (14.3.41) can be found from data of IAFB for $q_{v\text{-}i}$ and $q_{i\text{-}l}$; however, such data are not available. Therefore, based on the results of section (a), the following relationship is assumed to apply

$$\frac{q_{v\text{-}l} + q_{rad}}{q_{t\text{-}l}} = \Phi_1 \frac{T_v - T_{sat}}{T_{sat} - T_l} + \Phi_2 \frac{T_w - T_{sat}}{T_{sat} - T_l} \qquad \textbf{(14.3.42)}$$

where

$$\Phi_1 = \frac{h_{v\text{-}l}}{h_{t\text{-}l}}$$

$$\textit{and} \qquad \textbf{(14.3.43)}$$

$$\Phi_2 = \frac{h_{rad}}{h_{t\text{-}l}}$$

Expressions for these two parameters will be given shortly. Due to Eqs. (14.3.38) and (14.3.42), only a reliable equation for $q_{w\text{-}v}$ is needed to determine $q_{v\text{-}i}$ and $q_{i\text{-}l}$. This will be the focus of the next

section.

c) Heat Transfer from the Wall, q_{w-v}

There are two choices for providing an equation for q_{w-v}: (i) to use a single-phase vapour equation, or (ii) to develop a heat transfer equation based on IAFB data. The latter is very difficult to achieve, since it requires measurements of actual vapour temperatures for a wide range of flow conditions. The former, however, is easier to implement, as long as modifications for two-phase flow conditions are included, and hence it is adopted here. There is a multitude of relations for single-phase convective heat transfer from a wall to a fluid. Probably the best-known of these, and widely employed in two-fluid models of IAFB, are the Dittus-Boelter equation and the various modified versions of it. The Dittus-Boelter relation is derived for tube flow, but it is used indiscriminately in IAFB models. Probably the best-suited single-phase equations for q_{w-v} in the IAFB regime are those derived for concentric annulus geometry, because of the close geometrical resemblance of the vapour flow cross-sectional area and flow in a concentric annulus. In that respect, Kays' [1980] equations for heat transfer rates in a concentric annulus are applicable for a wide range of flow conditions.

In their two-fluid model, Analytis and Yadigaroglu [1987] treated the vapour as flow between two parallel plates, the tube wall and the liquid-vapour interface, and they used Kays equations for q_{w-v} and q_{v-i}. They introduced a so-called enhancement factor into the q_{v-i} equation to account for interfacial disturbances. Also, Cachard [1994] modified the Analytis and Yadigaroglu model by introducing enhancement factors to both the q_{w-v} and q_{v-i} equations. Cachard then derived expressions for the enhancement factors based on IAFB data at atmospheric conditions. The Analytis and Yadigaroglu model and the Cachard model are reviewed and assessed in Chapters 5

and 13, and the results of the assessment clearly show that the approach of modifying q_{w-v} and q_{v-i} equations by introducing enhancement factors is not sufficient, since it limits the range of applicability of the models.

For flow between parallel planes, Kays [1980] gives the following expressions:

$$q_{w-v} = \frac{k_v Nu_v}{2\delta} \frac{(T_w - T_v)}{1 - \frac{q_{v-i}}{q_{w-v}}\theta}$$

$$q_{v-i} = \frac{k_v Nu_v}{2\delta} \frac{(T_v - T_{sat})}{1 - \frac{q_{w-v}}{q_{v-i}}\theta} \qquad \textbf{(14.3.44)}$$

where Nu_v is the Nusselt number and θ the influence coefficient. For laminar flow between two parallel planes, Nu_v and θ are given by $Nu_v = 5.385$ and $\theta = 0.346$. For turbulent flow between two parallel planes, Kays gives Nu_v and θ in tabular form up to a Reynolds number of 10^6, and Prandtl numbers from 0 to 1000.

In this study, the above equations are modified to account for the differences between flow between parallel planes and the vapour flow in the vapour layer of the IAFB regime. These differences are mainly due to the following:

-The boundary condition of a fluid-to-fluid, instead of fluid-to-wall, may play an important role in affecting the turbulence structure near the interface, due to the complex wave patterns at the liquid-vapour interface, which present some sort of roughness to the vapour flow.

-It has been observed that the liquid core oscillates in the lateral direction perpendicular to the flow [Baum et al., 1978]. This implies that there might be variations in heat flux around

the periphery of the liquid core. This effect may be similar to the effect of eccentricity on turbulent-flow heat transfer in circular annuli. It is difficult to measure and account for this effect, but since in one-dimensional two-fluid models interest is in the time-averaged and area-averaged quantities, rather than on the instantaneous values, it can be assumed that on the average this effect is much less pronounced.

The main modification introduced here is to replace the ratio $q_{v\text{-}i}/q_{w\text{-}v}$ in Eq. (14.3.44) by Eq. (14.3.38). This renders the second equation in Eq. (14.3.44) redundant, since $q_{v\text{-}i}$ can be directly obtained from Eq. (14.3.38). This approach of modifying Eq. (14.3.44) should be better than the approach of introducing empirically derived factors into the equation, because the expression used for the $q_{v\text{-}i}/q_{w\text{-}v}$ (Eq. (14.3.38)) is based on physical grounds.

After substituting for $q_{v\text{-}i}/q_{w\text{-}v}$ and using Eq. (14.3.23) for δ, Eq. (14.3.44) becomes

$$q_{w\text{-}v} = \frac{Nu_v}{\left[1 - \frac{T_v - T_{sat}}{T_w - T_v}\theta\right]} \frac{k_v}{D[1 - \sqrt{1 - \alpha}]} (T_w - T_v) \qquad \textbf{(14.3.45)}$$

After substituting Eq. (14.3.45) in Eq. (14.3.38), an expression for $h_{v\text{-}i}$ can be written as

$$h_{v\text{-}i} = \frac{Nu_v}{\left[1 - \frac{T_v - T_{sat}}{T_w - T_v}\theta\right]} \frac{k_v}{D[1 - \sqrt{1 - \alpha}]} \qquad \textbf{(14.3.46)}$$

Next, $h_{i\text{-}l}$ is expressed as

$$h_{i\text{-}l} = 0.023 \frac{k_l}{D\sqrt{1 - \alpha}} Re_l^{0.8} Pr_l^{0.4} F \qquad \textbf{(14.3.47)}$$

This is basically the Dittus-Boelter equation for the heat transfer coefficient for turbulent flow in a circular tube of radius (R-δ) subjected to a constant temperature boundary condition (T_{sat} in this case). The parameter F is introduced to approximately account for entrance-length effects, and is given as

$$F = 1 + 1.4 \frac{R}{z} \qquad \textbf{(14.3.48)}$$

In Eq. (14.3.47) the liquid velocity, U_l, is employed for calculating h_{i-l}, since using $(U_l - U_i)$ gives zero values for h_{i-l}, due to the assumption of $U_i = U_l$. This method is similar to that of Analytis and Yadigaroglu [1987]. This approach may not seem logical, but the results are not strongly affected by this assumption, as will be shown later in Chapter 16. Further, Analytis and Yadigaroglu argue that the interfacial velocity can be determined only by solving the two-dimensional Navier-Stokes equations in the liquid and the vapour phases, a difficult task that is further complicated by a turbulent-flow entrance-length problem.

By assuming that the vapour film is transparent and that the wall is grey, radiation to the liquid core interface q_{rad} can be expressed as

$$q_{rad} = \frac{\sigma (T_w^4 - T_{sat}^4)}{\frac{1}{\varepsilon_w} + \frac{1}{\varepsilon_l \sqrt{1 - \alpha}} - 1} \qquad \textbf{(14.3.49)}$$

Thus the radiation heat transfer coefficient, h_{rad}, is

$$h_{rad} = \frac{\sigma (T_w^4 - T_{sat}^4)}{(\frac{1}{\varepsilon_w} + \frac{1}{\varepsilon_l \sqrt{1 - \alpha}} - 1)(T_w - T_{sat})} \qquad \textbf{(14.3.50)}$$

From Eqs. (14.3.46) and (14.3.50), an approximate expressions for Φ_1 and Φ_2 can be obtained as

$$\Phi_1 = \frac{Nu_v}{\left[1 - \frac{T_v - T_{sat}}{T_w - T_v}\theta\right]} \frac{k_v}{k_l} \frac{\sqrt{1 - \alpha}}{(1 - \sqrt{1 - \alpha})} \frac{1}{0.023\,F} Re_l^{-0.8} Pr_l^{-0.4}$$

$$\Phi_2 = \frac{\sigma\,(T_w^4 - T_{sat}^4)\,D\sqrt{1 - \alpha}}{0.023\,F\,k_l\left(\frac{1}{\varepsilon_w} + \frac{1}{\varepsilon_l\sqrt{1 - \alpha}} - 1\right)(T_w - T_{sat})} Re_l^{-0.8} Pr_l^{-0.4} \qquad \textbf{(14.3.51)}$$

In applying the model in the suggested manner, two things are found. First, the ratio q_{rad}/q_{i-l} is very small compared to q_{v-i}/q_{i-l}, except at extremely high wall temperatures. Second, the model predictions are insensitive to the h_{v-i}/h_{i-l} ratio (see Chapter 16), except probably near the CHF location, and at very high inlet subcoolings and low heat fluxes. Thus a value of one for Φ_1 was chosen, since, in general, it gives the best prediction accuracy for most of the flow conditions examined. This implies that q_{v-i}/q_{i-l} is strongly controlled by the temperature difference ratio. Consequently, it is decided to simplify Eq. (14.3.42) to the following form

$$\frac{q_{i-l}}{q_{v-i}} = \frac{T_{sat} - T_l}{T_v - T_{sat}} \qquad \textbf{(14.3.52)}$$

which is very similar to the form of Eq. (14.3.38). Although Eq. (14.3.52) appears to be too simple, it allows a strikingly accurate prediction of the model. In addition, it has the advantage of being free of empirical factors that might need tuning to different data sets.

d) Vapour Generation

For the vapour generation per unit axial length, W', the following expression is given

$$W' h_{fg} = q_{ev} P_i \qquad (14.3.53)$$

where the evaporation heat flux, q_{ev}, can be written as

$$q_{ev} P_i = q_{v-i} P_i + q_{rad} P_w - q_{l-i} P_i \qquad (14.3.54)$$

14.3.5.3 Shear Stress

In general, interfacial and wall shear stresses are expressed in terms of friction factors, which can be obtained by solving the Navier-Stokes equations in the vapour film and in the liquid core , or extrapolated from shear stress correlations in the annular flow regime.

(a) Interfacial Shear Stress

Many of the most important features of the flow in the IAFB regime stem from the complex waves at the liquid-vapour interface. However, accounting for wave effects may not be easy or practical for an IAFB model. Hence, IAFB two-fluid models are often developed by making the assumption that the liquid-vapour interface is smooth, and single-phase shear stress relations are applicable. In general, interfacial shear stress in the IAFB should be expected to be higher than what would be expected if the vapour film was actually smooth, due to the hydrodynamic drag of interfacial waves (this is similar to the roughness effect). Therefore, correction factors are often introduced to account for this effect. The constitutive relation for τ_i can be expressed in terms of a friction factor, as is done in single-phase flows:

$$\tau_i = \frac{f_i \rho_v U_r |U_r|}{2} \qquad \textbf{(14.3.55)}$$

where U_r is the relative velocity at the interface. Many empirical equations have been developed for the interfacial shear stress, τ_i, and a number of these have been reviewed by Donevski et al. [1992]. Table 14.1, similar to Table 2 in Donevski et al. [1992], summarizes the most important equations of interfacial shear stress used in many IAFB models. A class of these equations uses relations derived for single-phase flow and modified for two-phase annular flow. These modifications are frequently based on the observation that the thicker the vapour film, the larger the wave amplitudes at the interface. The best-known relation of this class is that by Wallis [1969], where the friction factor, f_i, in Eq. (14.3.55) is given as

$$f_i = 0.005 \left[1 + 300 \frac{\delta}{D}\right] \qquad \textbf{(14.3.56)}$$

Eq. (14.3.56) implies a constant friction factor in the absence of liquid flow.

In this study, instead of expressing τ_i in terms of a friction factor, a different approach is used based on the following reasons:

(i) No data are available to allow calculation of f_i, and if τ_i is expressed in terms of f_i, correction factors, usually referred to as enhancement factors, are used with this equation. These enhancement factors are tuned to fit a particular data set, thus, limiting the range of applicability of the models to the range of the data base from which these factors are derived.

(ii) The momentum interaction between the phases is directly affected by the wall shear stress through the interfacial shear, and hence, there must be a specific relationship between

τ_w and τ_i expressing this physical mechanism. Nevertheless, the use of independently derived empirical equations for τ_i such as Eq. (14.3.56) can alter this relation and thus distort the picture of the actual physical phenomenon.

Therefore, in this study, attention will be focused on finding a relation between τ_w and τ_i, rather than on using or modifying empirical equations derived for other flow situations, such as annular flow. Further, such a relationship allows the reduction of the degrees of freedom in the system. Once such a relationship is determined, the problem reduces to finding an appropriate relation for the wall shear stress. Since only the vapour phase is in contact with the heated surface in IAFB, wall shear stress expression(s) for single-phase vapour can be employed.

Next, a relationship between τ_i and τ_w is approximated from consideration of the momentum equation of the vapour phase. From Eq. (14.3.20), the equation for the interfacial shear is

$$\frac{\tau_i P_i}{A} = -\alpha \frac{dP}{dz} - g \rho_v \alpha - \frac{\tau_w P_w}{A} - \rho_v \alpha U_v \frac{dU_v}{dz} + \frac{W'(U_l - U_v)}{A} \qquad \textbf{(14.3.57)}$$

This equation is the basic equation for the evaluation of τ_i, but the information required in this equation is difficult to provide. However, since the intention is to find a simple approximate relationship between τ_i and τ_w, some simplifying assumptions must be made to facilitate the handling of this equation. The most straightforward assumption is to assume constant shear stress, equal to the wall shear stress, within the vapour film. This would be a good approximation when the vapour film is very thin and τ_i very high in comparison to the gravitational, accelerative, and pressure gradient forces exerted on the film. These conditions can be closely satisfied in the subcooled IAFB region, where the vapour generation rate is very low and the acceleration term is

small. This approximation is similar to the assumption made in turbulent single-phase flow for the near-wall region in the boundary layer theory, where it is assumed that shear stress in the region near the wall is equal to the wall shear stress.

The model predictions, however, should be expected to deviate from the data in the saturated and agitated IAFB regions, where the vapour generation rate is high (thicker vapour film), and the acceleration term in Eq. (14.3.57) may become dominant. Nevertheless, Cachard [1994] has shown (based on numerical results) that this term is negligible, even with significant vaporization. Thus, making these assumptions, it follows that:

$$|\tau_i| \cong |\tau_w| \qquad \textbf{(14.3.58)}$$

b) Wall Shear Stress

Assuming turbulent flow in the vapour film, any wall shear stress relation in single-phase vapour flow can be used to find τ_w. In general, the shape of the flow cross section has little effect on the shear stress at the wall, because most of the velocity change in a turbulent flow takes place very close to the wall, and is relatively independent of the proximity of other wall surfaces (the vapour-liquid interface in this case). Therefore, empirical equations derived for friction coefficients in turbulent flow in tubes can be employed, provided that some kind of equivalent tube diameter could be defined for evaluating the Reynolds number. The usual practice is to use the hydraulic diameter, which for flow between parallel plates (the wall and the interface) reduces to

$$D_h = 2\delta \qquad \textbf{(14.3.59)}$$

where δ is the vapour film thickness given by Eq. (14.3.23). The wall shear stress is then expressed

as follows:

$$\tau_w = \frac{f_w}{2} \rho_v U_v |U_v| \qquad \textbf{(14.3.60)}$$

During this study, several equations for the friction factor, f_w, recommended by Bhatti and Shah [1987] were examined. It was found that the model gives best prediction accuracy with the following equation.

$$f_w = (1 + 0.0925\ r^*) f_c$$

where

$$\frac{1}{\sqrt{f_c}} = 1.7372\ \ln\left(\frac{Re_v}{1.964\ \ln(Re_v) - 3.8215}\right) \quad 5x10^3 \le Re_v \le 10^7 \qquad \textbf{(14.3.61)}$$

and

$$r^* = \frac{R_i}{R} = \frac{R(1-\alpha)^{1/2}}{R} = (1-\alpha)^{1/2}$$

This equation is due to Bahatti and Shah [1987], and for turbulent flow in concentric annuli based on the laminar equivalent diameter, D_l, in the definition of Re_v defined as

$$\frac{D_l}{D_h} = \frac{1 + r^{*2} + \dfrac{(1 - r^{*2})}{\ln(r^*)}}{(1 - r^*)^2} \qquad \textbf{(14.3.62)}$$

For laminar flow between parallel plates (the wall and the interface), f_w is expressed as

$$f_w = \frac{24}{Re_v} \qquad (14.3.63)$$

Table 14.2 summarizes the constitutive relations for the IAFB model. It should be remembered that no attempt at refining these relations has been tried, since it is only desired to demonstrate the adequacy of this modelling approach, which emphasizes the correct physics combined with a minimum amount of empiricism. Chapter 15 gives a detailed step-by-step procedure for implementing the two-fluid model in a computer code.

14.4 Hybrid Post-CHF Model

The present IAFB two-fluid model is capable of predictions up to a void fraction of 60%. Above this value, model predictions start to deviate from the data, because the flow regime is no longer that of IAFB. Commonly, it is presumed that the transition to the DFFB regime occurs at a void fraction of 80%. Between void fraction values of 50 and 80%, a transition regime such as the slug flow regime or AIAFB regime is present. This section describes a method by which to combine an existing DFFB model, with the present IAFB model to predict wall temperatures for the whole subcooled film boiling region. The Moose and Ganić [1982] DFFB model is the model chosen for this purpose. This model is based on the three-path heat transfer concept. Mainly, it assumes heat transfer from the heated surface to vapour, from the heated surface to droplets in contact with the wall, and from vapour to liquid droplets in the vapour core. Section 8.7 gives a detailed description of the model derivation. This section discusses only the modifications introduced into the original model.

14.4.1 Approximation of Initial Conditions of the DFFB Model

The main difficulty in combining the IAFB and DFFB models is in determining the initial conditions of the DFFB model. For the DFFB regime resulting from high-quality flow (named here the type I DFFB regime), and where annular flow is the pre-dryout flow regime, the dryout quality at CHF is usually known, and thermodynamic equilibrium is assumed to exist at the CHF location. For the DFFB regime resulting from the break-up of the liquid core of the IAFB regime (named here the type II DFFB regime), the actual quality is undetermined at the start of DFFB, and thermodynamic non-equilibrium is generally present. Hynek et al. [1969] have shown that wall temperatures of type II DFFB are higher than wall temperatures of type I DFFB, given equal heat and mass fluxes and for the same x_{eq}. This is mainly due to the greater non-equilibrium that type II DFFB has. For type I DFFB, thermodynamic equilibrium between the liquid and the vapour phases is present upstream of the dryout point, whereas for type II DFFB non-equilibrium is already established before its initiation.

The parameters that are needed at the start of DFFB are the droplet diameter, d, and the vapour and droplet velocities. Moose and Ganić adopted Hynek et al's [1969] initialization technique, with few changes, to calculate the initial liquid and vapour velocities. Hynek et al. assume thermodynamic equilibrium at dryout, and solve the momentum and continuity equations, along with the assumption that the liquid acceleration is related to the vapour acceleration and the heat flux under isothermal conditions. Knowing the liquid and vapour velocities at dryout the droplet diameter is obtained from a critical Weber number, We_c. Although Hynek et al. used a value of 7.5 for We_c, Moose and Ganić left the Weber number as an unknown parameter to be determined, along with the droplet size, during the iteration for the initial liquid and vapour velocities. Clearly,

the Hynek et al. initialization technique does not apply to type II DFFB, where the assumption of thermodynamic equilibrium is no longer valid. Also, an energy conservation equation for the vapour has to be considered, since now the vapour temperature is different from the saturation temperature, as is assumed in Hynek et al's technique.

To circumvent this difficulty the following method is employed. The calculations of the IAFB model are allowed to proceed to a void fraction of 60% (50% is commonly taken as the upper value for which the IAFB regime persists). Then, the predicted values of the liquid velocity and vapour velocity are used as initial values for the DFFB model. Since the DFFB regime is presumed to exist at void fraction values beyond 80%, this procedure is transforming part of the transition region to a hypothetical dispersed flow regime, whose initial droplet size and velocities are given by the values predicted from the IAFB model. It will be shown in Chapter 17 that this transformation technique works quite well. For the critical Weber number, a value of 7.5, as used by Hynek et al., leads to a very small droplet size and the model predicts values of actual quality slightly higher than those of equilibrium quality. Obviously this is not correct, and hence a higher critical Weber number value is used. From comparison with the data, a Weber number of 25 gives the best results for all the data sets tested. This gives a relatively large droplet size (~0.4 mm) at the start of the DFFB regime; however, it seems consistent with the method of hypothetically transforming the transition region, where slugs of liquid are present, to a DFFB region.

Comparing the hybrid model predictions with the data, the model overpredicts the wall temperatures in the transition region, but it gives excellent agreement with the data for void fraction values larger than 70%. This implies that the DFFB model is not very sensitive to the initial conditions far away from the start of the DFFB regime; besides, at these values of void fraction the

flow regime is truly that of DFFB. Consequently, in the transition region, the wall temperatures are approximated by linearly interpolating between the temperature values predicted by the IAFB model at a void fraction of 60%, and by the DFFB model at a void fraction of 70%. As will be shown in Chapter 17, this method gives satisfactory predictions of wall temperatures in the transition region.

14.4.2 Further Discussion on Flow Regime Transition in the Post-CHF Region

In general, transitions from the IAFB regime to the AIAFB regime or slug flow regime, and from the AIAFB regime or slug flow regime to the DFFB regime are dependent on flow variables, such as mass flow rate, heat flux, pressure, etc. Consequently, the use of constant values of void fraction to denote transition to the AIAFB regime or DFFB regime is not justified, and it may result in large errors in predicting the wall temperatures. However, there is no alternative to this approach, due to the absence of detailed hydrodynamic data of flow regime transition in the post-CHF region.

There are very limited studies on the hydrodynamic mechanisms of flow regime transition of post-CHF two-phase flow. The most important of these studies are those made by Ishii and co-workers [1983, 1983a, 1987]. A comprehensive review of flow regime transition of post-CHF two-phase flow was presented by Ishii [1992]. Also, Ishii [1992] presented several correlations for various post-CHF flow regime transition, where the break-up length (L_B) of each post-CHF regime is correlated in terms of the liquid core Webber number (We_l) and Reynolds number (Re_l) as

$$\frac{L_B}{D_l} = f(Re_l, We_l) \qquad (14.4.1)$$

where D_l is the liquid core diameter. All these correlations, however, are based on data obtained from flow visualization of idealized IAFB regime (central jet core surrounded by a coaxial annulus

of gas), and their application to an actual IAFB situation is still to be determined. In this study, no attempt was made to use these correlations in the hybrid model to predict the transition between the flow regimes. This task is left for a future study which could then lead to an improvement of the hybrid model.

Table 14.1 Summary of interfacial shear stress equations used with IAFB models (updated from Donevski et al. [1992])

EQUATIONS	REFERENCE
$\tau_i = \frac{4\sqrt{1-\alpha}}{D}\frac{f_i}{2}\rho_v\lvert U_v-U_l\rvert(U_v-U_l)$ $f_i = \frac{0.085}{Re_v^{0.25}};\ Re_v = \frac{\rho_v\lvert U_v-U_l\rvert 2\delta}{\mu_v}$	Kawaji and Banerjee [1983]
$\tau_i = \frac{f_i}{2}\rho_m U_r\lvert U_r\rvert$ $U_r = U_m-U_l;\ f_i = 0.005\cdot A(\delta^*)^B;\ \log_{10}A = 0.56-9.07/D^*$ $B = 1.63-\frac{4.74}{D^*};\ D^* = \frac{D}{(\sigma/g\Delta\rho)^{1/2}};\ \delta^* = \frac{\delta}{(\sigma/g\Delta\rho)^{1/2}};\ m \equiv mixture$	Han and Bankoff [1982]
$\tau_i = \frac{f_i}{2}\rho_v(U_v-U_l)^2$ $f_i = \frac{31}{Re_l^{0.25}}\frac{\delta}{D};\ Re_l = \frac{\rho_v(U_v-U_l)(D-2\delta)}{\mu_v}$	Inoue et al. [1982]
$\tau_i = \frac{f_i}{2}\rho_v(U_v-U_l)^2$ $f_i = 0.005(1+300\frac{\delta}{D})$	Kaufman [1976]
$\tau_i = \frac{f_i}{2}\rho_v(U_v-U_l)^2$ $f_i = 0.01$	Thurgood et al. [1981]
$\tau_i = \frac{f_i}{2}\rho_v(U_v-U_l)^2\lambda$ $f_i = \frac{0.085}{Re_l^{0.25}};\ Re_l = \frac{\rho_v\lvert U_v-U_l\rvert 2\delta}{\mu_v};\ \lambda = 1+150\frac{\delta}{R}$	Analytis and Yadigaroglu [1987]

Table 14.2 Summary of constitutive relations used with the present IAFB model

RELATIONS	EQUATIONS	COMMENTS
Wall heat transfer	$q_w P_w = q_{w-v} P_w + q_{rad} P_i$	
Wall-to-vapour heat transfer	$q_{w-v} = \frac{Nu_v}{\left[1 - \frac{T_v - T_{sat}}{T_w - T_v}\theta\right]} \frac{k_v}{D[1 - \sqrt{1 - \alpha}]}(T_w - T_v)$ $Nu_v = \frac{5.071}{Pr_v^{0.0439}} + 0.0028\ Pr_v^{0.645}\ Re_v$ $\theta = 0.3476\ Pr_v^{0.0026} - \frac{0.146\ Pr_v^{0.5418}\ Re_v}{9900}$	Modified Kays' equations [1980] for flow between parallel planes
Vapour-to-interface heat transfer	$q_{v-i} = \frac{T_v - T_{sat}}{T_w - T_v} q_{w-v}$	For laminar flow ($Re_v < 100$), conduction across the vapour film is assumed, and $q_{v-i} = q_{w-v}$
Wall-to-liquid radiation	$q_{rad} = \frac{\sigma(T_w^4 - T_{sat}^4)}{\frac{1}{\varepsilon_w} + \frac{1}{\varepsilon_l\sqrt{1 - \alpha}} - 1}$	Siegel and Howell [1972]
Interface-to-liquid heat transfer	$q_{i-l} = q_{v-i} \frac{T_v - T_{sat}}{T_{sat} - T_l}$	
Vaporization heat flux	$q_{ev} P_i = q_{v-i} P_i + q_{rad} P_w - q_{i-l} P_i$	

Table 14.2 Summary of constitutive relations used with the present IAFB model (Concluded)

RELATIONS	EQUATIONS	COMMENTS
Interfacial mass transfer	$$\Gamma = \frac{q_{ev} P_I}{h_{fg}}$$	
Wall-vapour shear stress	$$\tau_w = \frac{f_w}{2} \rho_v U_v^2$$ *Laminar flow:* $$f_w = \frac{24}{Re_v}$$ $$Re_v = \frac{\rho_v U_v 2\delta}{\mu_v}$$ *Turbulent flow:* $$f_w = (1 - 0.0925\, r')\, f_c$$ $$\frac{1}{\sqrt{f_c}} = 1.7372 \ln\left(\frac{Re_v}{1.964 \ln (Re_v) - 3.8215}\right)$$ $$Re_v = \frac{\rho_v U_v D_I}{\mu_v}; \quad r' = (1 - \alpha)^{1/2};$$ $$D_I = \frac{1 - r'^2 - \frac{(1 - r'^2)}{\ln(r')}}{(1 - r')^2} 2\delta$$	Based on flow between parallel planes. Based on flow in concentric annuli. Bhatti and Shah [1987]
Interfacial shear stress	$$\tau_I = \tau_w$$	
Transition to DFFB regime	$$\alpha \geq 0.5$$	

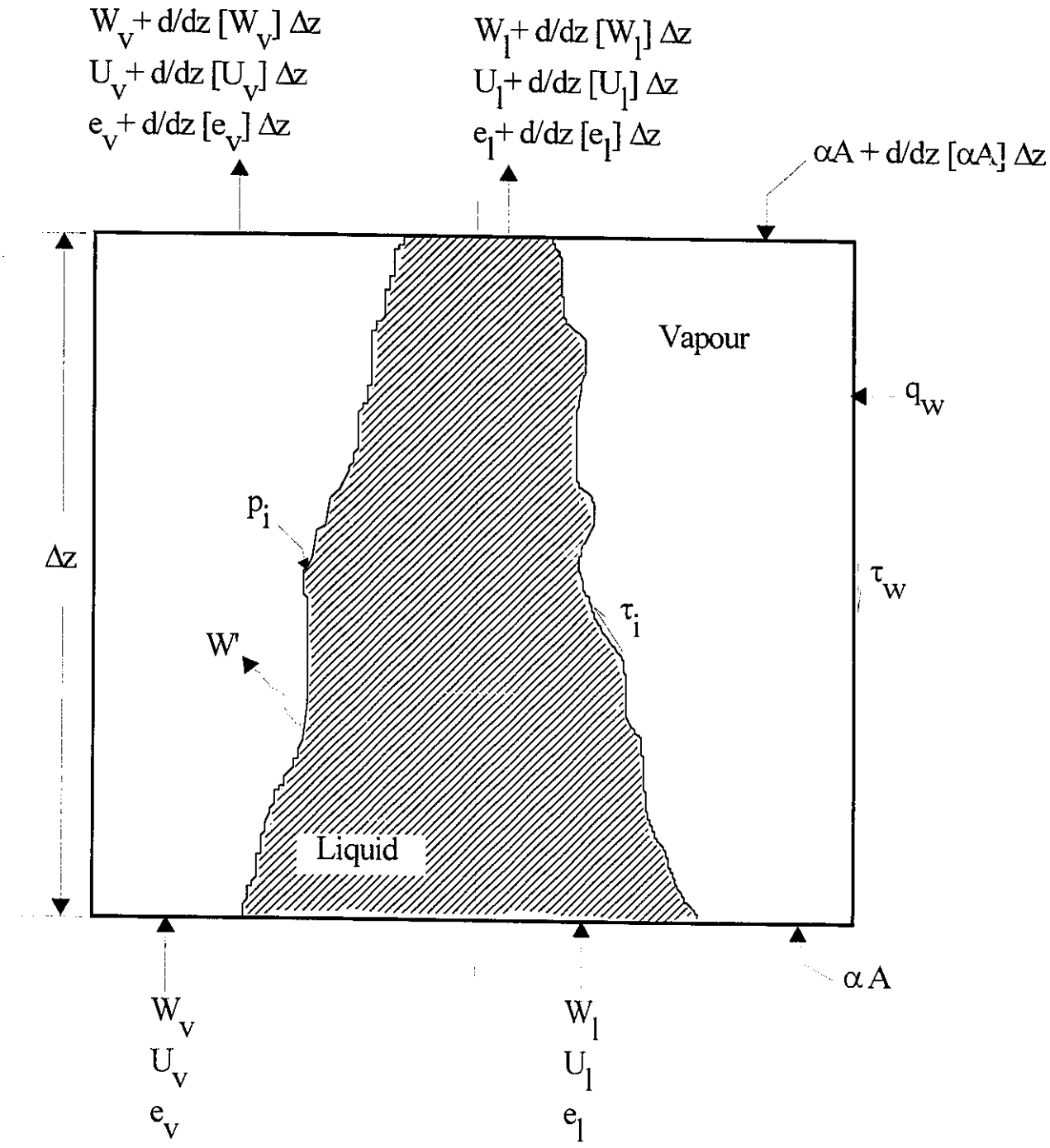

Figure 14.1 Control volume for the IAFB model.

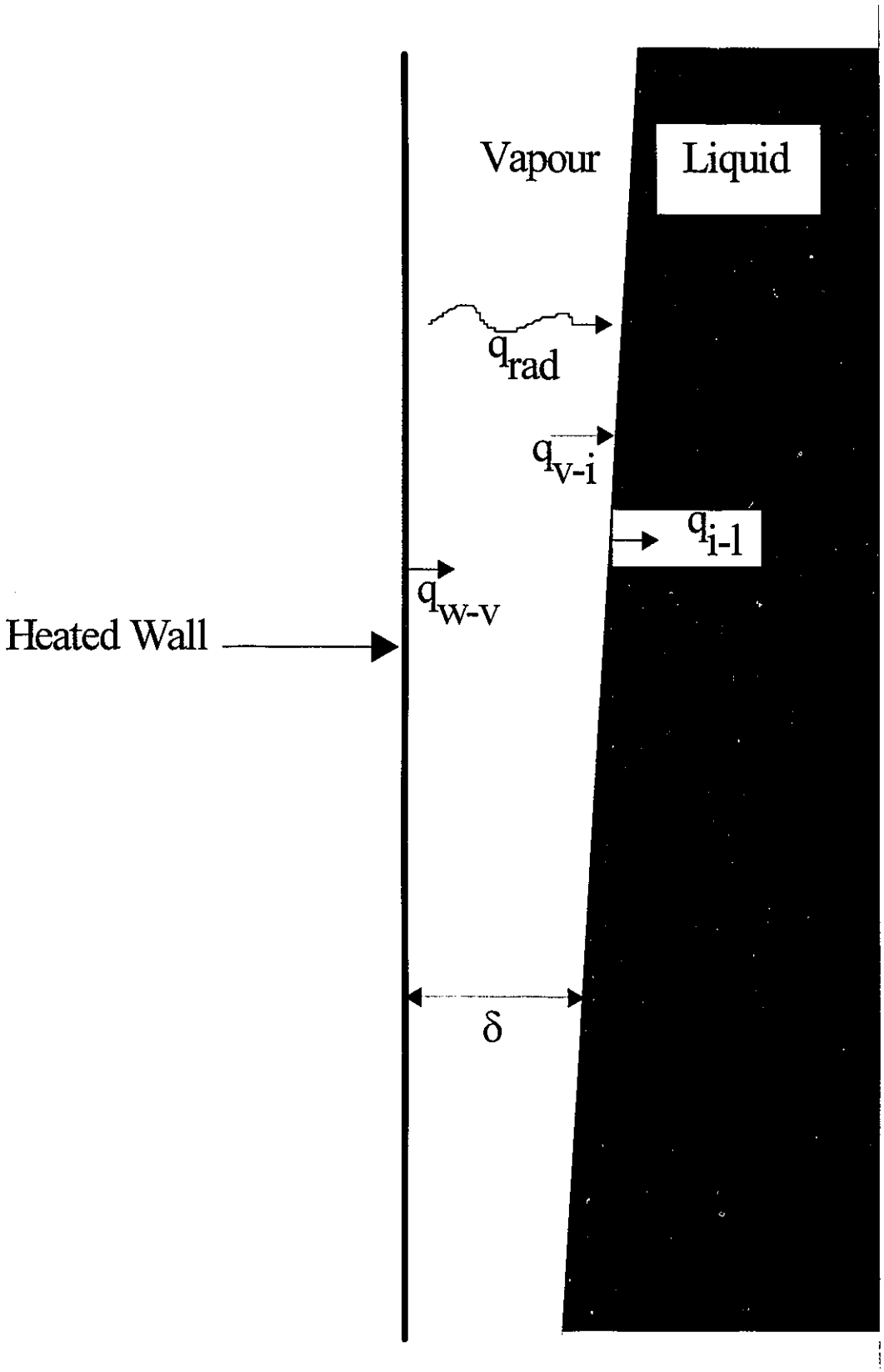

Figure 14.2 Heat flux components in IAFB.

Chapter 15 COMPUTER IMPLEMENTATION OF THE IAFB MODEL

15.1 Model Equations

The conservation equations and the constitutive relations for the two-fluid model for IAFB are derived in Chapter 14, and they are shown here again for convenience.

$$\frac{d}{dz}\left[\ \rho_v\ \alpha\ U_v\ \right] = \frac{W'}{A} \tag{15.1.1}$$

$$\frac{d}{dz}\left[\ \rho_l\ (1\ -\ \alpha)\ U_l\ \right] = -\ \frac{W'}{A} \tag{15.1.2}$$

$$-\alpha\frac{dP}{dz} - g\ \rho_v\alpha - \frac{\tau_i P_i}{A} - \frac{\tau_w P_w}{A} = \rho_v\alpha U_v\frac{dU_v}{dz} + \frac{W'}{A}[U_v - U_l] \tag{15.1.3}$$

$$-(1\ -\ \alpha)\frac{dP}{dz} - g\ \rho_l(1\ -\ \alpha) + \frac{\tau_i P_i}{A} = \rho_l(1\ -\ \alpha)U_l\frac{dU_l}{dz} \tag{15.1.4}$$

$$\alpha\ U_v\ \frac{dh_v}{dz} = \frac{q_{w\text{-}v}\ P_w}{\rho_v\ A} - \frac{q_{v\text{-}l}\ P_i}{\rho_v\ A} + \frac{W'\ (h_g\ -\ h_v)}{\rho_v\ A} \tag{15.1.5}$$

$$(1\ -\ \alpha)U_l\frac{dh_l}{dz} = \frac{q_{i\text{-}l}\ P_i}{\rho_l\ A} - \frac{W'\ (h_f\ -\ h_l)}{\rho_l\ A} \tag{15.1.6}$$

$$q_{w\text{-}v} = \frac{Nu_v}{\left[1 - \frac{T_v - T_{sat}}{T_w - T_v}\theta\right]} \frac{k_v}{D[1 - \sqrt{1 - \alpha}]}(T_w - T_v)$$

$$Nu_v = \frac{5.071}{Pr_v^{0.0439}} + 0.0028\ Pr_v^{0.645}\ Re_v \qquad \textbf{(15.1.7)}$$

$$\theta = 0.3476\ Pr_v^{0.0026} - \frac{0.146\ Pr_v^{0.5418}\ Re_v}{9900}$$

$$\frac{q_{v\text{-}l}}{q_{w\text{-}v}} = \frac{T_v - T_{sat}}{T_w - T_v} \qquad \textbf{(15.1.8)}$$

$$\frac{q_{v\text{-}l}}{q_{l\text{-}l}} = \frac{T_v - T_{sat}}{T_{sat} - T_l} \qquad \textbf{(15.1.9)}$$

$$q_{rad} = \frac{\sigma\ (T_w^4 - T_{sat}^4)}{\frac{1}{\varepsilon_w} + \frac{1}{\varepsilon_l\sqrt{1 - \alpha}} - 1} \qquad \textbf{(15.1.10)}$$

$$W'\ h_{fg} = q_{ev}\ P_l \qquad \textbf{(15.1.11)}$$

$$q_{ev}\ P_l = q_{v\text{-}l}\ P_l + q_{rad}\ P_w - q_{l\text{-}l}\ P_l \qquad \textbf{(15.1.12)}$$

$$\tau_w = \frac{f_w}{2} \rho_v U_v^2$$

$$\textit{Laminar flow}: \; f_w = \frac{24}{Re_v}$$

$$Re_v = \frac{\rho_v U_v 2\delta}{\mu_v}$$

$$\textit{Turbulent flow}: \; f_w = (1 + 0.0925 \; r^*) f_c$$

$$\frac{1}{\sqrt{f_c}} = 1.7372 \; \ln\left(\frac{Re_v}{1.964 \; \ln (Re_v) - 3.8215} \right) \qquad \textbf{(15.1.13)}$$

$$Re_v = \frac{\rho_v U_v D_l}{\mu_v}; \quad r^* = (1 - \alpha)^{1/2};$$

$$D_l = \frac{1 + r^{*2} + \dfrac{(1 - r^{*2})}{\ln(r^*)}}{(1 - r^*)^2} 2\delta$$

The specific enthalpies, h_l and h_v, in the conservation of energy equations can be expressed in terms of the temperatures T_l and T_v as follows:

$$dh_l = Cp_l \, dT_l$$

$$dh_v = Cp_v \, dT_v \qquad \textbf{(15.1.14)}$$

where Cp_l and Cp_v are the specific heats of the liquid and the vapour at constant pressure, respectively. Hence, Eqs. (15.1.5) and (15.1.6) become

$$\frac{dT_v}{dz} = \frac{q_{w\text{-}v} P_w}{\alpha \; \rho_v U_v Cp_v A} - \frac{q_{v\text{-}l} P_i}{\alpha \; \rho_v U_v Cp_v A} + \frac{W' (h_g - h_v)}{\alpha \; \rho_v U_v Cp_v A} \qquad \textbf{(15.1.15)}$$

$$\frac{dT_l}{dz} = \frac{q_{t-l}\, P_t}{(1 - \alpha)\rho_l\, U_l\, Cp_l\, A} - \frac{W'\,(h_f - h_l)}{(1 - \alpha)\rho_l\, U_l\, Cp_l\, A} \qquad \textbf{(15.1.16)}$$

15.2 Final Form of Model Equations

At this stage the model equations are arranged in a manner to allow easy programming for computer computation. The equations are listed below.

$$-\rho_l\, U_l \frac{d\alpha}{dz} + (1 - \alpha)\rho_l \frac{dU_l}{dz} = \frac{-4W'\sqrt{1 - \alpha}}{D} \qquad \textbf{(15.2.1)}$$

$$\rho_v\, U_v \frac{d\alpha}{dz} + \rho_v\, \alpha \frac{dU_v}{dz} = \frac{4W'\sqrt{1 - \alpha}}{D} \qquad \textbf{(15.2.2)}$$

$$-(1 - \alpha)\frac{dP}{dz} - (1 - \alpha)\rho_l\, U_l \frac{dU_l}{dz} = (1 - \alpha)\rho_l\, g - \frac{4\tau_i\sqrt{1 - \alpha}}{D} \qquad \textbf{(15.2.3)}$$

$$-\alpha \frac{dP}{dz} - \rho_v\, \alpha\, U_v \frac{dU_v}{dz} = \alpha\, \rho_v\, g + \frac{4\tau_i\sqrt{1 - \alpha}}{D} + \frac{4\tau_w}{D} + \frac{4W'\,(U_v - U_l)\sqrt{1 - \alpha}}{D} \qquad \textbf{(15.2.4)}$$

$$\frac{dT_l}{dz} = \frac{q_{t-l}\, P_t}{(1 - \alpha)\rho_l\, U_l\, Cp_l\, A} - \frac{W'\,(h_f - h_l)}{(1 - \alpha)\rho_l\, U_l\, Cp_l\, A} \qquad \textbf{(15.2.5)}$$

$$\frac{dT_v}{dz} = \frac{q_{w-v} P_w}{\alpha \rho_v U_v Cp_v A} - \frac{q_{v-i} P_i}{\alpha \rho_v U_v Cp_v A} + \frac{W'(h_g - h_v)}{\alpha \rho_v U_v Cp_v A} \qquad (15.2.6)$$

Also, the hydrodynamics equations can be expressed in a matrix form as follows:

$$\begin{bmatrix} 0 & -\rho_l U_l & 0 & (1-\alpha)\rho_l \\ 0 & \rho_v U_v & \rho_v \alpha & 0 \\ -(1-\alpha) & 0 & 0 & -(1-\alpha)\rho_l U_l \\ -\alpha & 0 & -\rho_v \alpha U_v & 0 \end{bmatrix} \begin{bmatrix} \frac{dP}{dz} \\ \frac{d\alpha}{dz} \\ \frac{dU_v}{dz} \\ \frac{dU_l}{dz} \end{bmatrix} = \begin{bmatrix} \frac{-4W''\sqrt{1-\alpha}}{D} \\ \frac{4W''\sqrt{1-\alpha}}{D} \\ (1-\alpha)\rho_l g - \frac{4\tau_i\sqrt{1-\alpha}}{D} \\ \rho_v \alpha g + \frac{4\tau_i\sqrt{1-\alpha}}{D} - \frac{4\tau_w}{D} - \frac{4W''(U_v-U_l)\sqrt{1-\alpha}}{D} \end{bmatrix} \qquad (15.2.7)$$

15.3 Numerical Solution

This section presents the numerical method used to solve the IAFB model equations. The numerical solution is separated into three steps: (i) in the first step the momentum and mass equations are solved for the flow variables (i.e., the velocities, pressure, and void fraction), (ii) in the second step the energy equations are solved for the temperatures of the vapour and the liquid phases, and (iii) in the third step the inside wall temperature is obtained by iteration. Hence, given the initial conditions, the steady-state solution involves a process of direct matrix and iteration solutions at each step.

Equations (15.2.1)-(15.2.6) form a system of ordinary differential equations (ODEs). They are solved as an initial value problem in z-direction using a fourth-order Runge-Kutta method, and the initial values of the independent variables specified at the CHF location. Figure 15.1 shows an overall diagram of the model's computer code structure and logic. This subroutine contains the

iteration controls and calls all the subroutines required for the model equations solution.

The main program is divided into three principal parts: constants and initial conditions at the quench front, section to solve the ODE's, and an output section. The initial conditions for the void fraction, vapour velocity, liquid velocity, vapour temperature, liquid temperature, and wall temperature at the CHF location are not readily available. Therefore, they are approximated using the subroutine INIT shown in Figure 15.2. The solution of the ODE's involves two steps. First, the derivatives of the flow variables P, U_l, U_v, and α (given by Eq. (15.2.7)) are obtained by direct matrix inversion using the Gauss-Jordan subroutine. Second, these derivatives, along with the initial conditions, are used by the Runge-Kutta subroutine to give the solution for P, U_l, U_v, and α for one step. Next, the liquid and vapour temperatures are calculated from Eqs. (15.2.5) and (15.2.6) by the Runge-Kutta subroutine. The Runge-Kutta subroutine makes three calls to the subroutine DERIVA (see Fig. 15.3), where all the derivatives of the dependent variable are evaluated. In the main program and in the DERIVA subroutine several calls to the subroutine PROPER are made. The subroutine PROPER evaluates the thermophysical properties of the specified fluid for a given temperature and pressure. Appendix D describes in detail the subroutine PROPER.

15.3.1 Prediction of Wall Temperature

At each axial level (or step), an iterative procedure is used to evaluate the wall temperature. The iteration starts with an initial guess of the wall temperature. Iteration continues until an iteration limit is reached. The iteration limit is based on comparison between the experimental heat flux and the heat flux predicted by the model. If the iteration limit is not satisfied, the wall temperature is increased when the predicted heat flux is lower than the experimental flux, or decreased in the opposite case. The total predicted heat transfer rate at the wall is given as

$$q_w P_w = q_{w\text{-}v} P_w + q_{rad} P_w \qquad \textbf{(15.3.1)}$$

where the heat transfer components $q_{w\text{-}v}$ and q_{rad} are given by Eqs. (15.1.7) and (15.1.10), respectively. The radiation absorption in the vapour film is neglected. For the emissivity of the wall, ε_w, values recommended in the experimental data sources analyzed are employed. For the test section used in this study a value of 0.6 for ε_w is used. For the liquid core, a value of 1.0 for ε_l is used.

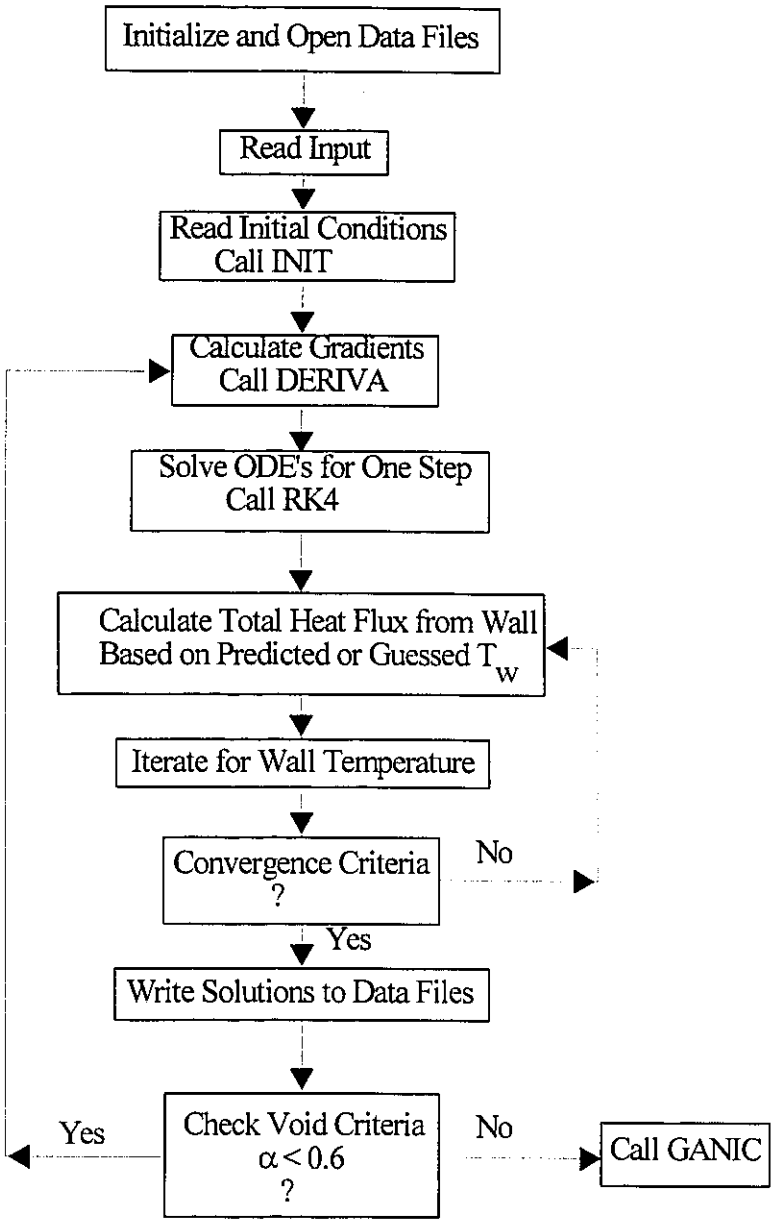

Figure 15.1 Schematic diagram for program NAJR.

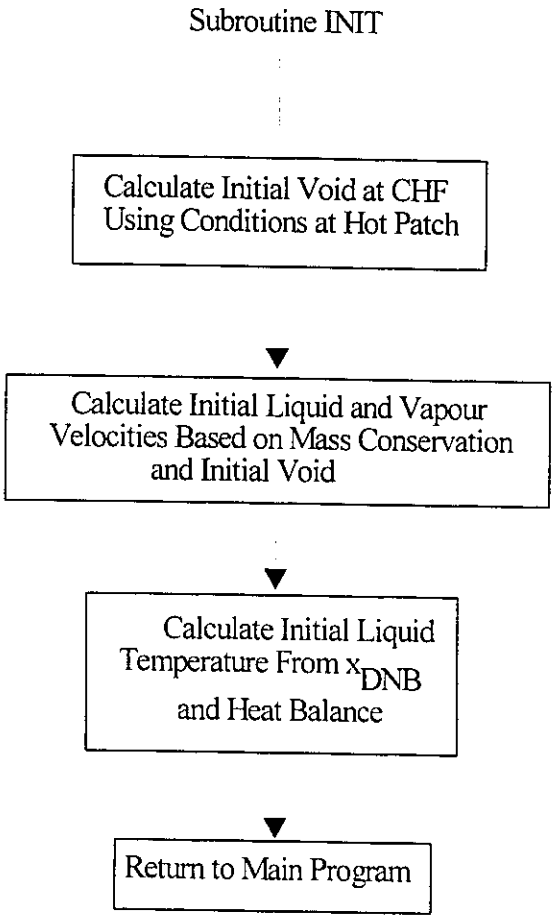

Figure 15.2 Schematic diagram for subroutine INIT.

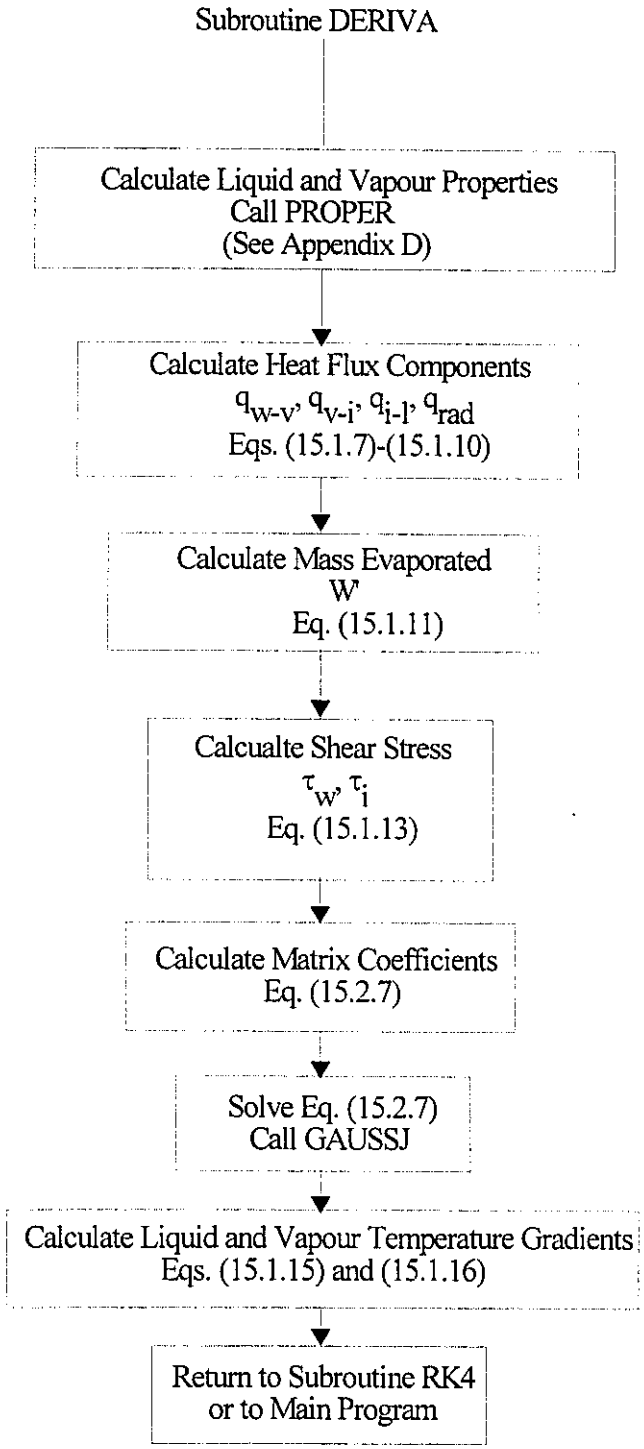

Figure 15.3 Schematic diagram of subroutine DERIVA.

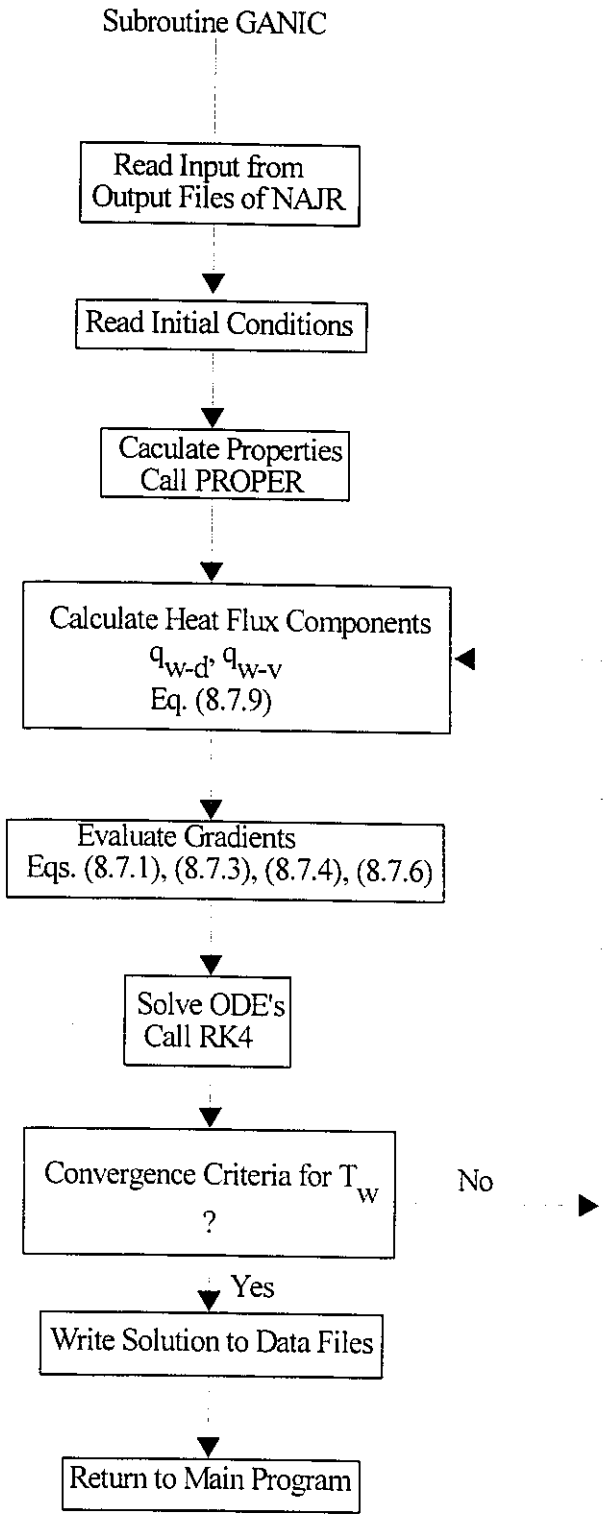

Figure 15.4 Schematic diagram for subroutine GANIC.

Chapter 16 DISCUSSION OF THE IAFB MODEL

16.1 General

Chapters 14 and 15 described the development of the two-fluid model of IAFB. The model is expected to account for the effects of flow variables such as mass flux, pressure, heat flux, and inlet subcooling. Also, it is expected to apply to a wide range of flow conditions, since it does not contain parameters derived from particular data sets. Most of the uncertainties in the model predictions lie in the constitutive equations for interfacial shear stress, interfacial velocity, and interfacial heat transfer. The interfacial shear stress is directly related to the shear stress at the wall. Consequently, any dependence of the wall shear on the flow field is directly influencing the interfacial shear stress. The interfacial heat transfer is dependent on the validity and sensitivity of the IAFB model to the assumptions made in Chapter 14.

It should be noted that the model calculations are stopped at a void fraction of 60%, since IAFB is unlikely to exist beyond this value. Also, it is thought that data points just downstream of the hot patch might be affected by the hot patch's presence (i.e., axial heat conduction); hence, they are not used in the comparison with the model predictions. Further, in this chapter only a limited number of figures are shown, as they are typical of the many data sets that are used.

Chapter 9 provided a general description of the effect of flow field variables such as mass flux, pressure, heat flux, and inlet subcooling on the heat transfer coefficient of IAFB, based on trends from data of other studies. Chapter 11 described in detail these effects based on the data of

this study. The following sections compare the two-fluid model predicted trends with those observed from the data of this study. Also, the model sensitivity to the interfacial velocity, shear stress, and heat transfer is discussed.

16.2 Effect of Mass Flux

Figures 16.1 and 16.2 show a comparison of predicted and measured mass flux effect on the wall temperature distribution at various flow conditions and for three fluids. In general, the model correctly predicts the trend and the magnitude of the wall temperatures. It gives better predictions at low mass flux values. At high mass fluxes, initially the data has a sharp peak, then a steep rapid decrease, and then a smooth moderate decrease in wall temperatures downstream. These are the characteristics of the axial wall temperature distribution at high mass flux values, which are discussed in Chapter 11. Initially, the model seems unable to follow the rapid changes in the data, but it does a better job as x_{eq} increases. It predicts a lower temperature peak and a lower rate of decrease in wall temperatures at lower x_{eq} values (in heat transfer region II, described in Chapter 11). Errors in predicting the peak temperatures (the maximum wall temperatures in the T_w vs x_{eq} curves) can be as high as 20°C-- approximately a 12% relative error. Despite this discrepancy, at high mass flux values, this is still considered a good prediction for the IAFB regime.

No attempt was made to discover what might be causing the discrepancies in the measured and predicted wall temperatures at high mass flux values, since the procedure can only be one of trial and error, due to the many variables involved. Nevertheless, in a future attempt to deal with this matter, the primary concern should not be so much the magnitude of the error in the predicted wall temperatures, but the shape of the axial temperature profiles, especially in heat transfer regions I and II.

Figures 16.3 and 16.4 show the effect of mass flux on the heat transfer components per unit length, $q_{w\text{-}v}P_w$, $q_{v\text{-}i}P_i$, $q_{i\text{-}l}P_i$, and $q_{rad}P_w$, as predicted by the model. It can be seen from these figures that the convective heat transfer per unit length $q_{v\text{-}i}P_i$ and $q_{i\text{-}l}P_i$ increase with mass flux, while $q_{w\text{-}v}P_w$ increases only slightly and $q_{rad}P_i$ decreases. The increase in $q_{w\text{-}v}P_w$, $q_{v\text{-}i}P_i$, and $q_{i\text{-}l}P_i$ is mainly due to the increase in the vapour and liquid velocities. Figure 16.5 shows the predicted vapour and liquid velocities at four different mass flux values. It indicates that the magnitude and the slope of the vapour and liquid velocities increase with increasing mass flux. The decrease in $q_{rad}P_w$ is due to the lower wall temperatures at higher mass flux.

16.3 Effect of Inlet Subcooling

Figure 16.6 shows the effect of inlet subcooling on the wall temperature distribution. In this figure, the critical quality (quality at CHF, x_{DNB}) is used to indicate the degree of subcooling at the start of IAFB, instead of using the temperature difference at the inlet of the test section (T_{sat} - T_l). This is thought to be a better choice, due to the presence of the hot patch: for different inlet temperatures, it was difficult to maintain the same hot-patch power, since this resulted in either rewetting at the hot patch for lower hot-patch powers and lower inlet temperatures, or Freon decomposition for higher hot-patch powers and higher inlet temperatures.

As described in Chapter 11, the mere effect of inlet subcooling is to shift the T_w vs x_{eq} curves to lower x_{eq} range. The model correctly predicted this trend. Again, as mentioned in the previous section, the model appears to give better agreement with the data at lower mass flux values. Figure 16.6(b) shows that at low mass flux values the wall temperatures for different inlet subcooling approach each other. At higher mass flux values, and in the same heat transfer region, the wall temperatures are lower for higher x_{DNB} values, as Fig. 16.6(c) shows.

Figure 16.7 shows the fraction of the total heat flux transferred to the liquid core at two different inlet subcoolings. As expected, at higher inlet subcooling a larger fraction of the total heat flux goes to heating up the liquid core. Also, the fraction of liquid core heat flux decreases gradually along the boiling length, due to the continuous decrease in $(T_{sat} - T_l)$, which is the main driving potential for the heat transfer from the interface to the liquid core.

16.4 Effect of Heat Flux

Figures 16.8 and 16.9 show the effect of heat flux on the wall temperature distribution. The model predictions are in good agreement with the data. The data shows that wall temperatures are higher for higher heat fluxes. Chapter 11 provided some physical explanations for the effect of heat flux on heat transfer in the IAFB regime.

16.5 Effect of Pressure

Figures 16.10 and 16.11 show the effect of pressure on the wall temperature distributions. In general, the model correctly predicted the effect of pressure on T_w vs x_{eq}. As expected, wall temperatures are lower at higher pressures. Detailed discussion of this trend was provided in Chapter 11 and will not be repeated here.

16.6 Actual Quality Prediction

Section 11.4 provided a qualitative description of the thermodynamic non-equilibrium in subcooled film boiling. Figures 16.12-16.15 show quantitative results of thermal non-equilibrium in the IAFB regime, expressed in plots of x_a vs x_{eq}.

Figure 16.12 shows that, for the same x_{eq}, the actual quality x_a is higher for higher mass flux. Higher x_a implies lower vapour superheat, and higher vapour velocities. This results in a higher convective heat transfer in the vapour layer. On the other hand, for the same x_a, x_{eq} is lower for

higher mass flux values, indicating higher liquid core subcooling. This gives higher heat transfer rates from the interface to the liquid core, since q_{i-l} depends strongly on $(T_{sat} - T_l)$. All these effects result in lower wall temperatures at higher mass flux values, as Figs.16.1 and 16.2 show. Increasing the mass flux has two opposing effects on the thermodynamic non-equilibrium : (i) it reduces the vapour superheat, but (ii) it increases the liquid subcooling.

Figure 16.13 shows that the effect of inlet subcooling on the thermodynamic non-equilibrium is similar to that of mass flux. Mainly, higher inlet subcooling results in lower vapour superheat and higher liquid core subcooling.

Figure 16.14 shows that the pressure has little effect on the thermodynamic non-equilibrium. Overall, however, thermodynamic non-equilibrium is lower for higher pressure, especially at positive x_{eq} values.

Figure 16.15 shows the effect of heat flux on the thermodynamic non-equilibrium. For the same x_{eq}, x_a is higher at lower q_w values, indicating lower vapour superheat. For the same x_a, x_{eq} is lower for lower q_w. This effect is similar to those of increasing the mass flux or increasing the inlet subcooling.

The slip ratio, defined as the ratio of the average vapour velocity (U_v) to the average liquid velocity (U_l), is important in the calculation of the void fraction from the actual quality, as shown below:

$$\alpha = \frac{x_a}{x_a + \frac{\rho_v}{\rho_l}(1 - x_a)\frac{U_v}{U_l}} \qquad \textbf{(16.6.1)}$$

Also, it gives an indication of the degree of mechanical non-equilibrium between the phases. Figure

16.16(a) shows the predicted slip at four different mass flux values with other flow parameters held unchanged. It indicates that the slip decreases with increasing mass flux. This suggests that at low mass flux values, the vapour velocity increases rapidly, due to the high rate of vapour generation.

Figure 16.16(b) shows the predicted effect of pressure on the slip. The model predicts lower slip at higher pressure; this is in compliance with other observations in the literature, where the slip reduces as the pressure increases. Figure 16.16(c) shows that just downstream of the hot patch (in the subcooled IAFB region) the slip reduces as the inlet subcooling is increased, but this effect disappears at greater distances from the hot patch (saturated IAFB region). Figure 16.16 shows that the rate of increase of slip along the axial direction reduces gradually. This means that the slip will eventually reach a maximum value, then gradually will decrease to a value close to one in the DFFB regime, where the flow field is more homogeneous.

16.7 Fluid Effect

In Section 11.2.4.5, it was shown that the ratio of (h/h_{hom}) is not strongly dependent on the type of fluid. In order to check wether the model predicts this trend correctly, (h/h_{hom}) values predicted by the model are compared to those calculated from the experimental data, and the comparison is shown in Fig. 16.17 for (h/h_{hom}) vs x_{eq}. The model provides the correct data trend, but overpredicts (h/h_{hom}) for $x_{eq} < 0$. For $x_{eq} > 0$, the model gives the correct order of magnitude and trend for the data. Note that test conditions were not exactly matched for the mass flux, heat flux, and inlet subcooling, as there were slight differences. Apart from an inherent prediction error of the model, these differences might have a more pronounced effect on the model predictions for $x_{eq} < 0$, since, in general, history-dependent models are very sensitive to flow conditions in the subcooled IAFB region.

16.8 Sensitivity Analysis

This section discusses the sensitivity of the IAFB model to the interfacial shear stress, interfacial velocity, the ratio of $(h_{v\text{-}i}/h_{w\text{-}v})$, and the ratio of $(h_{i\text{-}l}/h_{v\text{-}i})$.

16.8.1 Model Sensitivity to Interfacial Shear Stress

When comparing the model predictions to the data, it was observed that the model consistently and systematically underpredicts the wall temperatures. This is primarily attributed to the low friction factor, f_w, used to evaluate the wall shear stress. In effect, a higher wall shear stress retards the vapour flow, resulting in a thicker vapour layer and higher wall temperatures, especially in the subcooled IAFB region, where conduction heat transfer is presumed to dominate. Indeed, the model underpredicts the wall temperatures mainly in the subcooled IAFB region ($x_{eq}<0$).

Also, experimental observations from this study seem to support the notion that f_w should take higher value than the one predicted from Eq. (14.3.61). Equation (14.3.61) gives a friction factor for a smooth surface; however, the condition of the inside surface of the test section used during this study is believed to have changed from a smooth to a rougher surface. Section 11.2.2 discussed problems associated with Freon decomposition. It was necessary to clean the inside surface of the test section every time decomposition of Freon occurred, but it was difficult to completely restore the inside surface of the test section to its original state. This implies that decomposition might have changed the test section inside-surface roughness, resulting in a higher friction factor than would be expected for a smooth tube. In fact, when f_w is increased (multiplied by a roughness factor, C_f), the model predictions improve considerably, as Figure 16.18 shows. Figure 16.18 shows that the model gives the best predictions at a C_f value of 1.4, for the flow conditions indicated in the figure. This result suggests that the model is quite sensitive to the value

of friction factor f_w, and roughness effects of the test section surface should be taken in consideration. Unfortunately, from the data of this study, there is no easy way to measure or approximate the effect of Freon decomposition on the test section inside surface. Further, to keep the model free from empirical factors, it was opted not to attempt to derive a correlation for C_f from the data of this study, and Eq. (14.3.61) is used as-is. As will be shown in the next chapter, the model would still give good predictions when compared to data, and gives lower RMS errors than other prediction methods.

16.8.2 Model Sensitivity to Interfacial Velocity

Part of the uncertainties of the theoretical model lie in the relation for the interfacial velocity U_i. No measurements have been taken of U_i in the IAFB regime. Consequently, there are few limited methods to approximate it. The easiest method is to express U_i in terms of the average liquid velocity U_l and the average vapour velocity U_v, as given by Eq. (14.3.6). For the two-fluid model of this study, it is assumed that U_i is close to the liquid core velocity, U_l. In several other two-fluid models, U_i is taken as the average of U_v and U_l.

Figure 16.19 shows the effect of changing the interfacial velocity on the wall temperature distribution. These figures clearly show that approximating U_i by U_l is better than taking the average of U_l and U_v, and that the model predictions are not very sensitive to variations in U_i.

16.8.3 Model Sensitivity to the Ratios of $(h_{v\text{-}i}/h_{w\text{-}v})$ and $(h_{i\text{-}l}/h_{v\text{-}i})$

In Section 14.3.5.2(a), it was argued that $h_{w\text{-}v}$ and $h_{v\text{-}i}$ are approximately of the same order of magnitude, and that the ratio $(h_{v\text{-}i}/h_{w\text{-}v})$ approaches one. This section validates this assumption through comparison of model prediction of wall temperatures with experimental data for various values of $(h_{v\text{-}i}/h_{w\text{-}v})$. Figures 16.20-16.22 clearly show that the model gives best predictions at $(h_{v\text{-}}$

$_i/h_{w-v}$) values approaching one. Figure 16.21 provides root-mean-square (RMS) error distributions versus (h_{v-i}/h_{w-v}), for the model predictions shown in Fig. 16.20. Figure 16.22 shows the total RMS error resulting from comparison with 2407 data points of Freon-12, and for a wide range of flow conditions. Note that the results of this comparison are typical of all the model predictions.

For (h_{v-i}/h_{w-v}) values above one, the model tends to underpredict the wall temperatures. This is expected, because a higher heat transfer from vapour-to-interface results in lower vapour superheat (lower T_v), as Fig. 16.20 shows. Since heat transfer from the wall is mainly controlled by convection to the vapour phase, the model underpredicts the data. Similar argument applies to (h_{v-i}/h_{w-v}) values less than one, except this time the model tends to overpredict the data.

Actual data of the ratio (h_{v-i}/h_{w-v}) are not available, due to the experimental difficulty in determining the interfacial heat transfer coefficient, h_{i-l}. Nevertheless, in view of the better agreement obtained between model predictions and data for (h_{v-i}/h_{w-v}) values approaching one, it is reasonable to approximate the ratio of (h_{v-i}/h_{w-v}) to a value of one. It should be cautioned, however, that though this approximation works well within the frame of the present model, it may lead to poor prediction accuracy when applied to other prediction methods, if the actual physical mechanism at the interface leads to much different values of (h_{v-i}/h_{w-v}) from one.

Figure 16.23 shows the effect of varying the ratio of (h_{i-l}/h_{v-i}) on the model prediction of wall temperatures distribution. The ratio of (h_{i-l}/h_{v-i}) was varied from a value of 0.4 to 4.0, for the flow conditions shown in Fig. 16.23. In Fig. 16.23(a) the maximum value of (h_{i-l}/h_{v-i}) was 9.0, as predicted by Eq. (14.3.51). Figure 16.23 shows that the impact of changing the values of (h_{i-l}/h_{v-i}) on the wall temperatures distribution is insignificant. In general, the heat transfer from the interface to the liquid core, q_{i-l}, becomes less and less important with increasing x_{eq} values along the heated

length of the flow channel, because the bulk liquid core temperature rapidly approaches saturation. Consequently, the contribution of q_{i-l} to the total heat transfer from the wall becomes less significant, except probably near the CHF location and for high inlet subcoolings.

16.8.4 Model Sensitivity to the Thin Vapour Film Assumption

As mentioned in Section 16.1, the model calculations are stopped at a void fraction of 60%. At this void fraction value, the δ/R ratio reaches values of about 0.37, and the vapour film is no longer thin. At a void fraction of 60%, the flow regime is that of the AIAFB or slug flow film boiling (transition regimes), and a large fraction of the vapour is entrained in the liquid core. Under these conditions, the thin film assumption for the vapour film becomes questionable, and the IAFB model is not expected to give good agreements with the data in the AIAFB or slug flow film boiling regimes.

The model, however, still gives satisfactory predictions at such high void fractions, as seen from Figs. 16.1-16.17. This relative good agreement with the data may be explained as follows: The data show an improvement in heat transfer in the transition region, due to the increase in the heat transfer interfacial area. In the transition region, the main heat transfer mechanisms are the heat transfer from the wall-to-vapour and from the vapour-to-liquid, where the liquid is assumed to be at saturation. Under these conditions, the IAFB model still considers all the vapour to be contained in a layer near the heated wall. Nevertheless, it accounts correctly for the heat transfer mechanisms: heat transfer from wall-to-vapour and from vapour-to-liquid. Therefore, the agreement of the model predictions with the data implies that the model is overpredicting the vapour-to-liquid heat transfer (Eq. 14.3.52), in order to compensate for the actual enhancement of heat transfer from the increased interfacial heat transfer area.

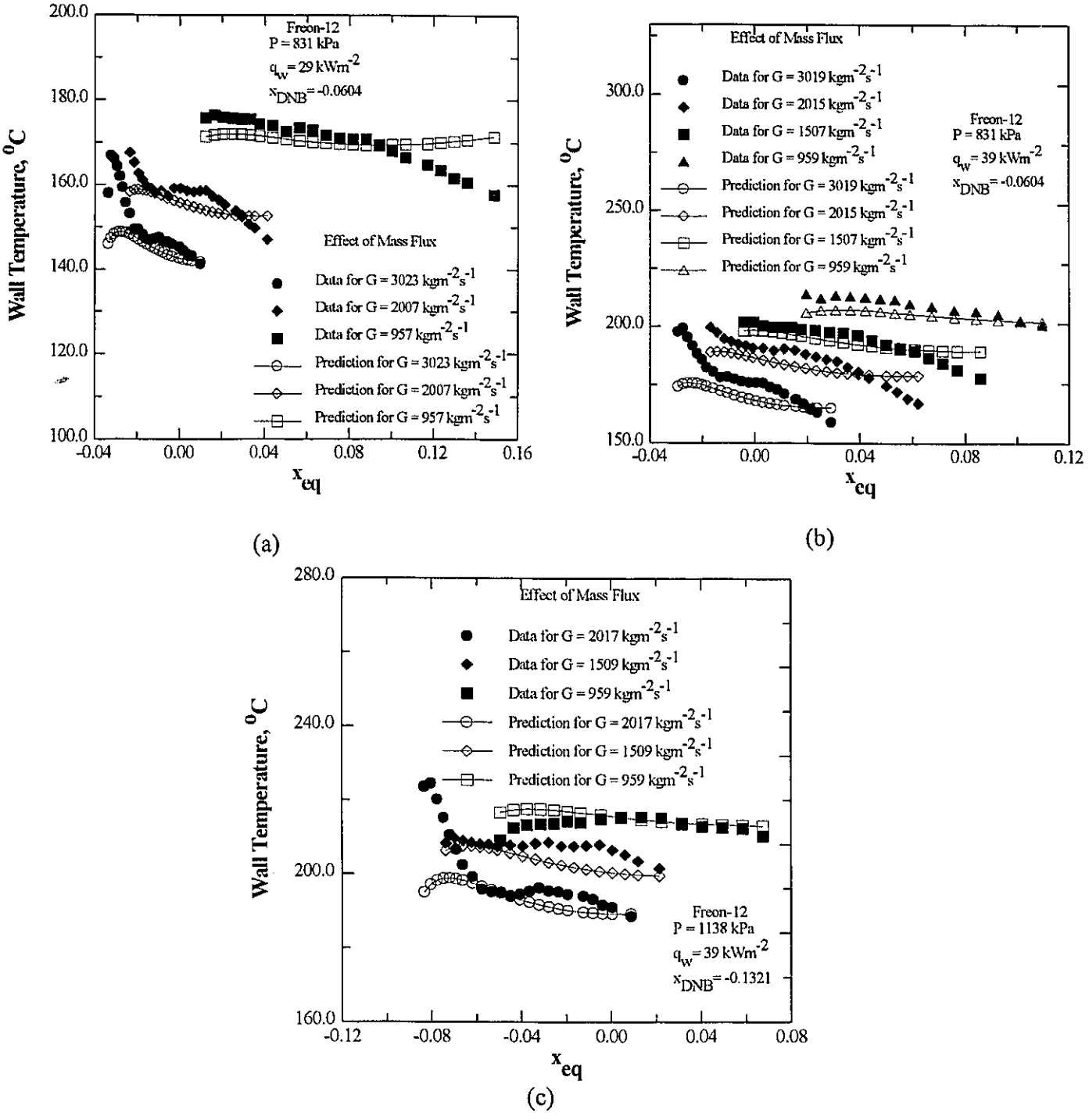

Figure 16.1 Comparison of measured mass flux effect with model predictions.

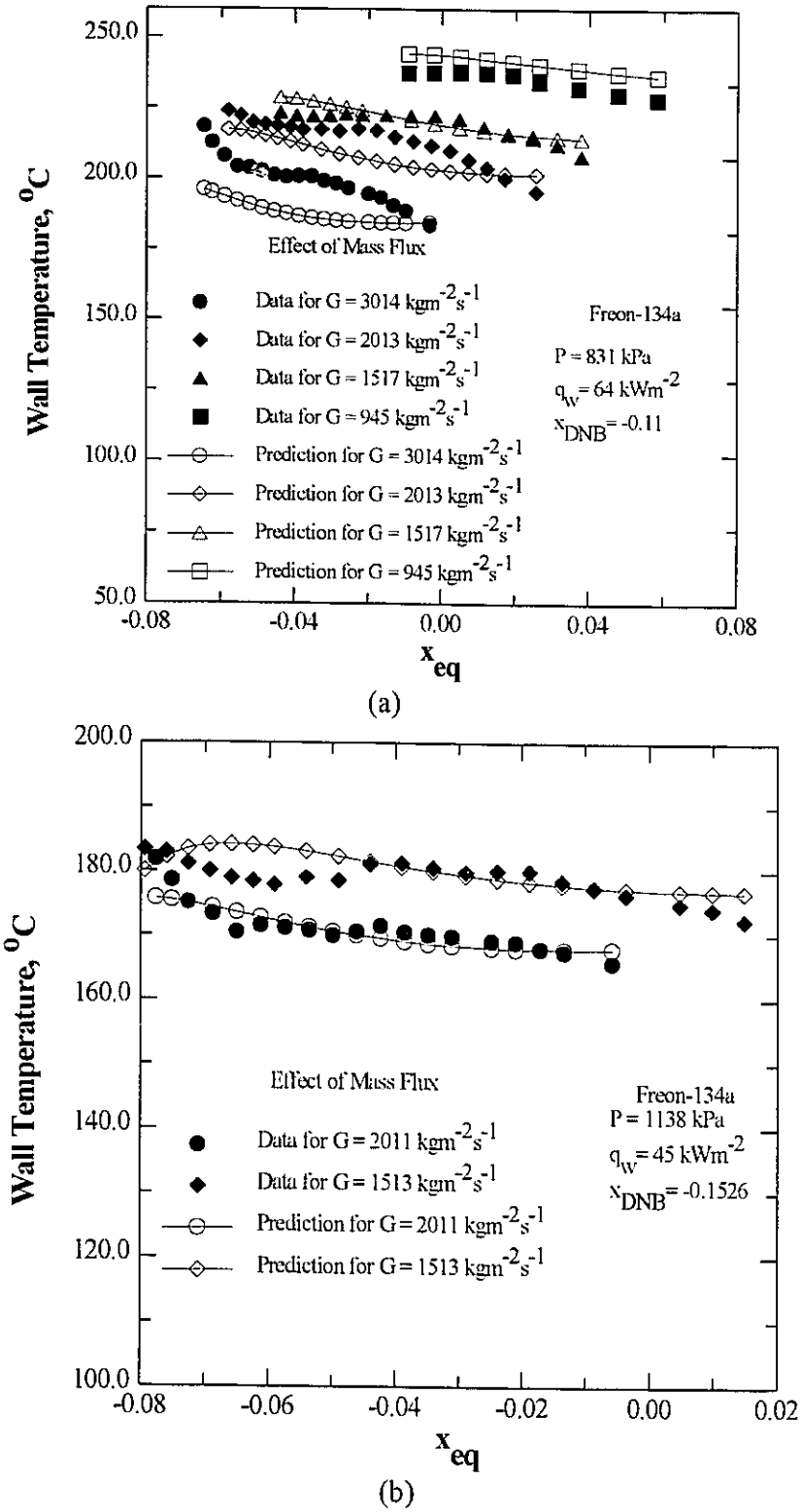

Figure 16.2 Comparison of measured mass flux effect with model predictions.

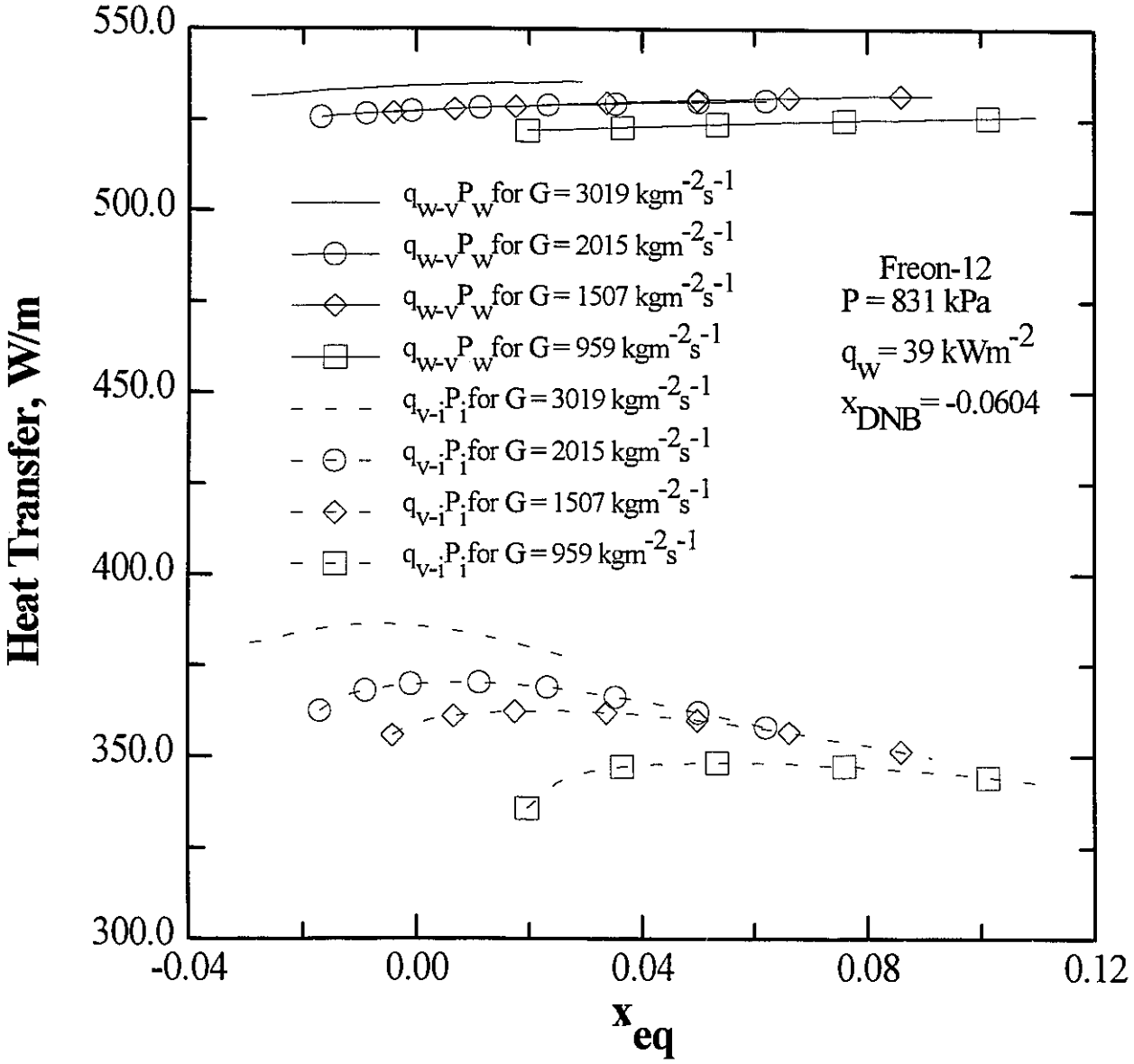

Figure 16.3 Model predictions of heat transfer from wall-to-vapour and from vapour-to-liquid.

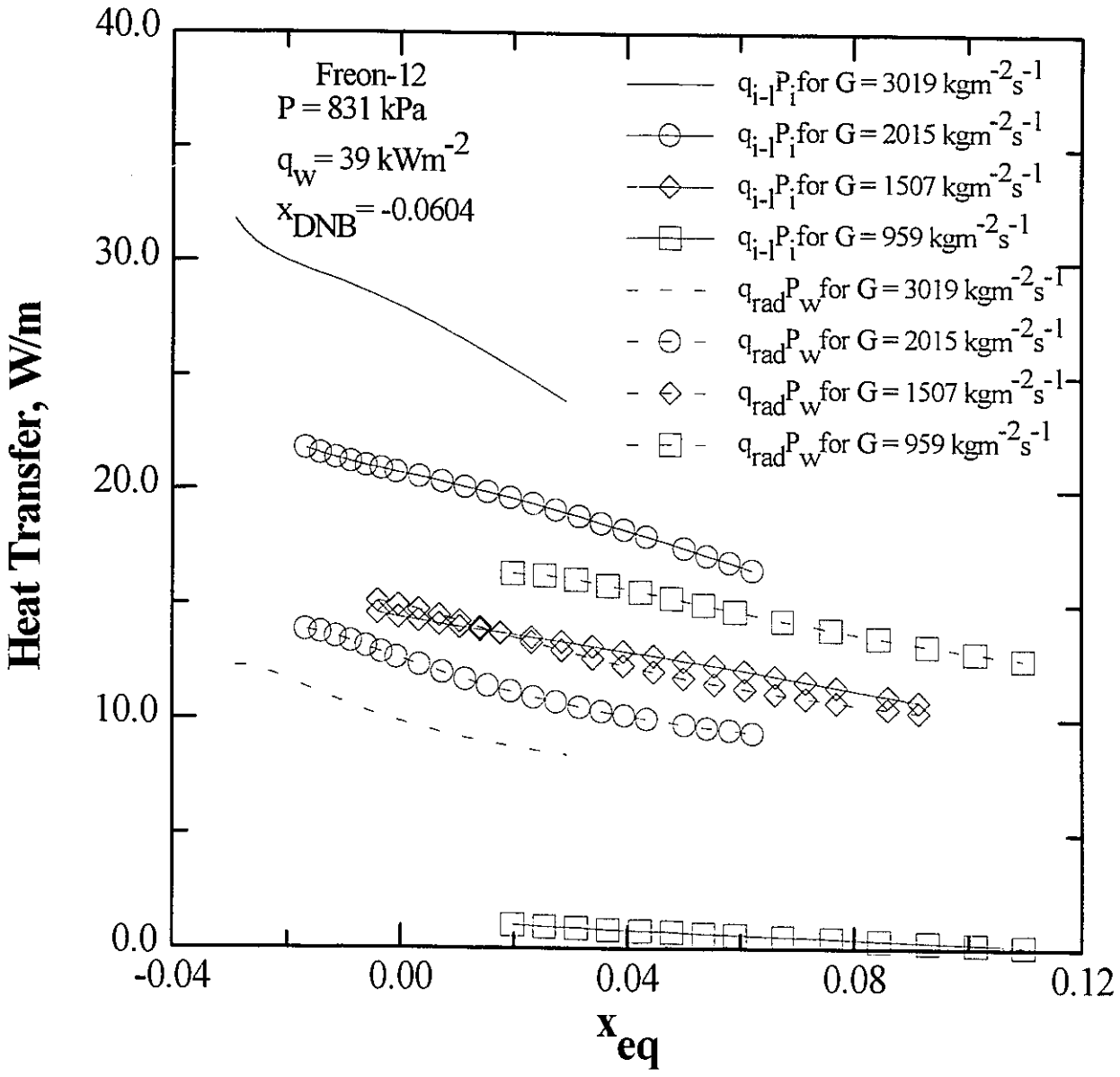

Figure 16.4 Model predictions of heat transfer from interface-to-liquid and radiative heat transfer from wall-to-liquid.

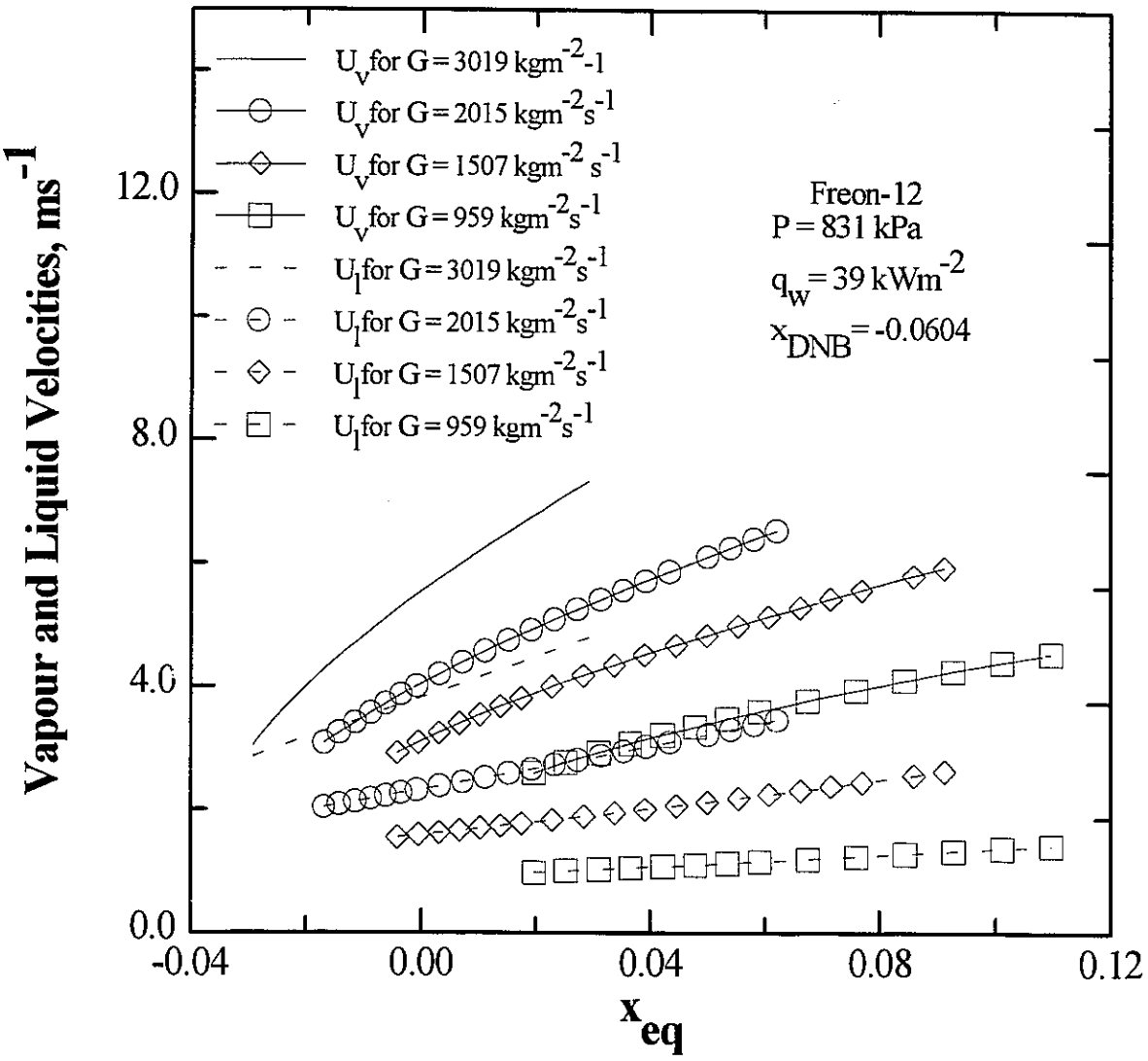

Figure 16.5 Model predictions of vapour and liquid velocities.

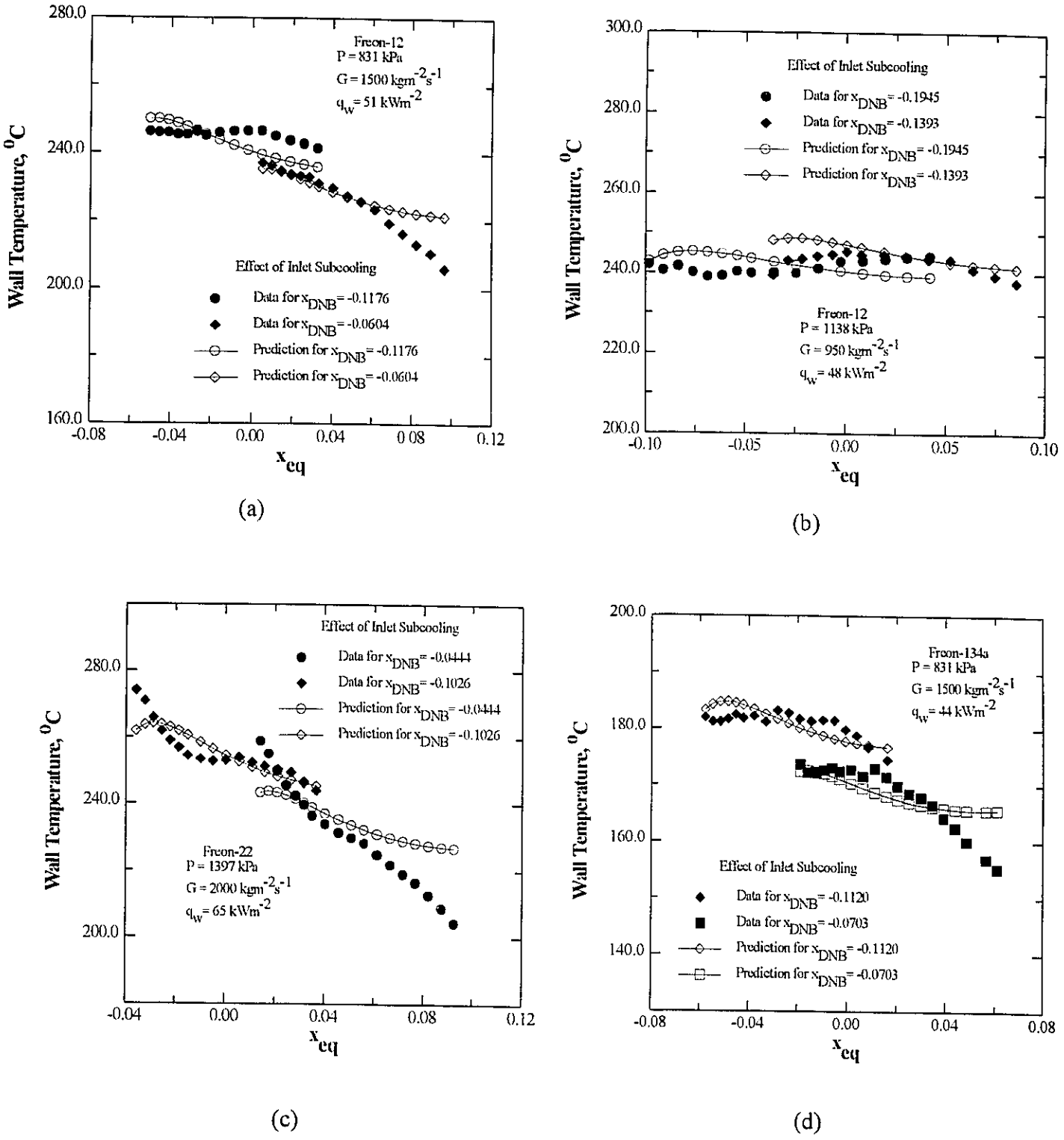

Figure 16.6 Comparison of measured inlet subcooling effect with model predictions.

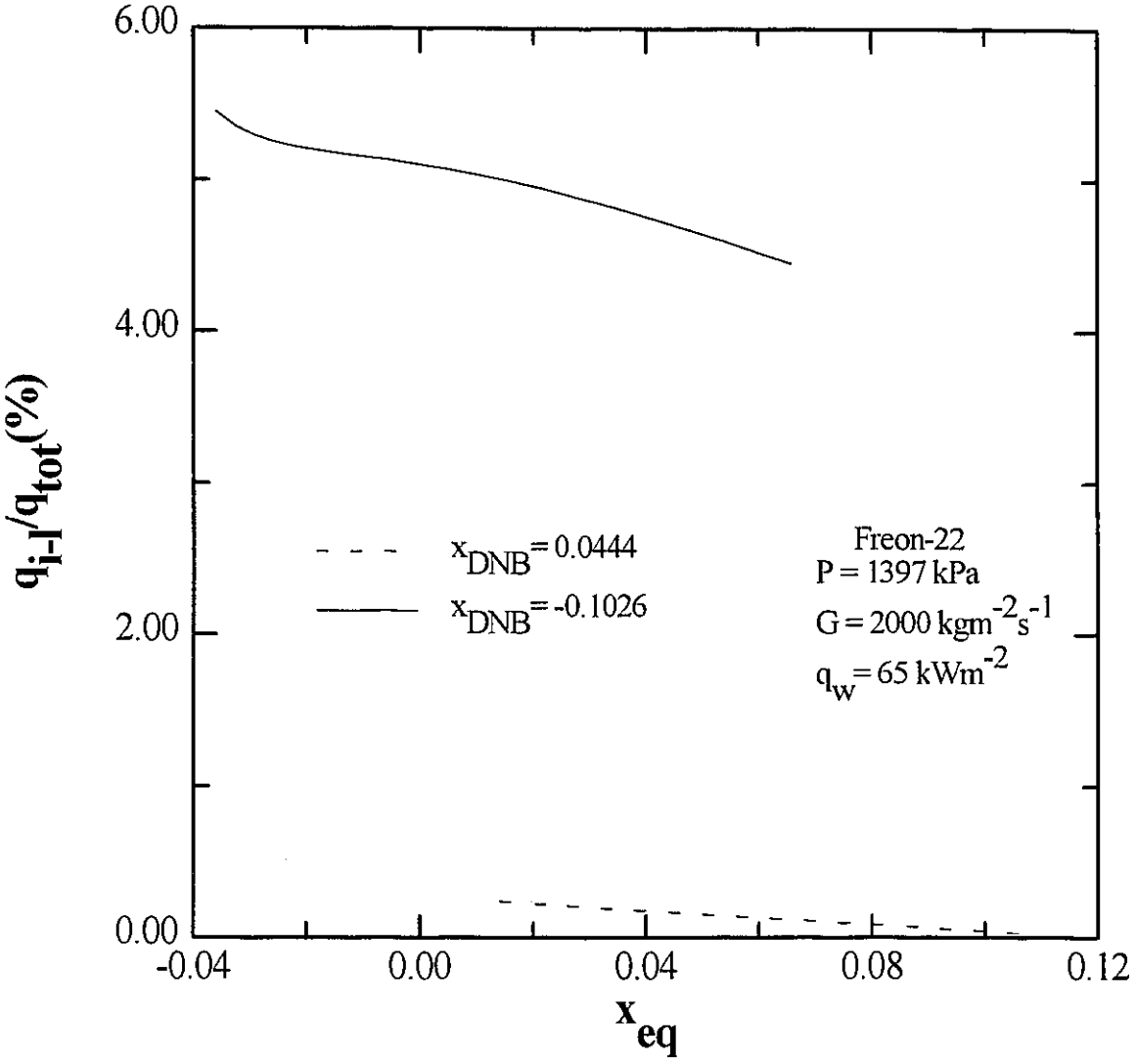

Figure 16.7 Model prediction of the fraction of total heat flux transferred to the liquid core.

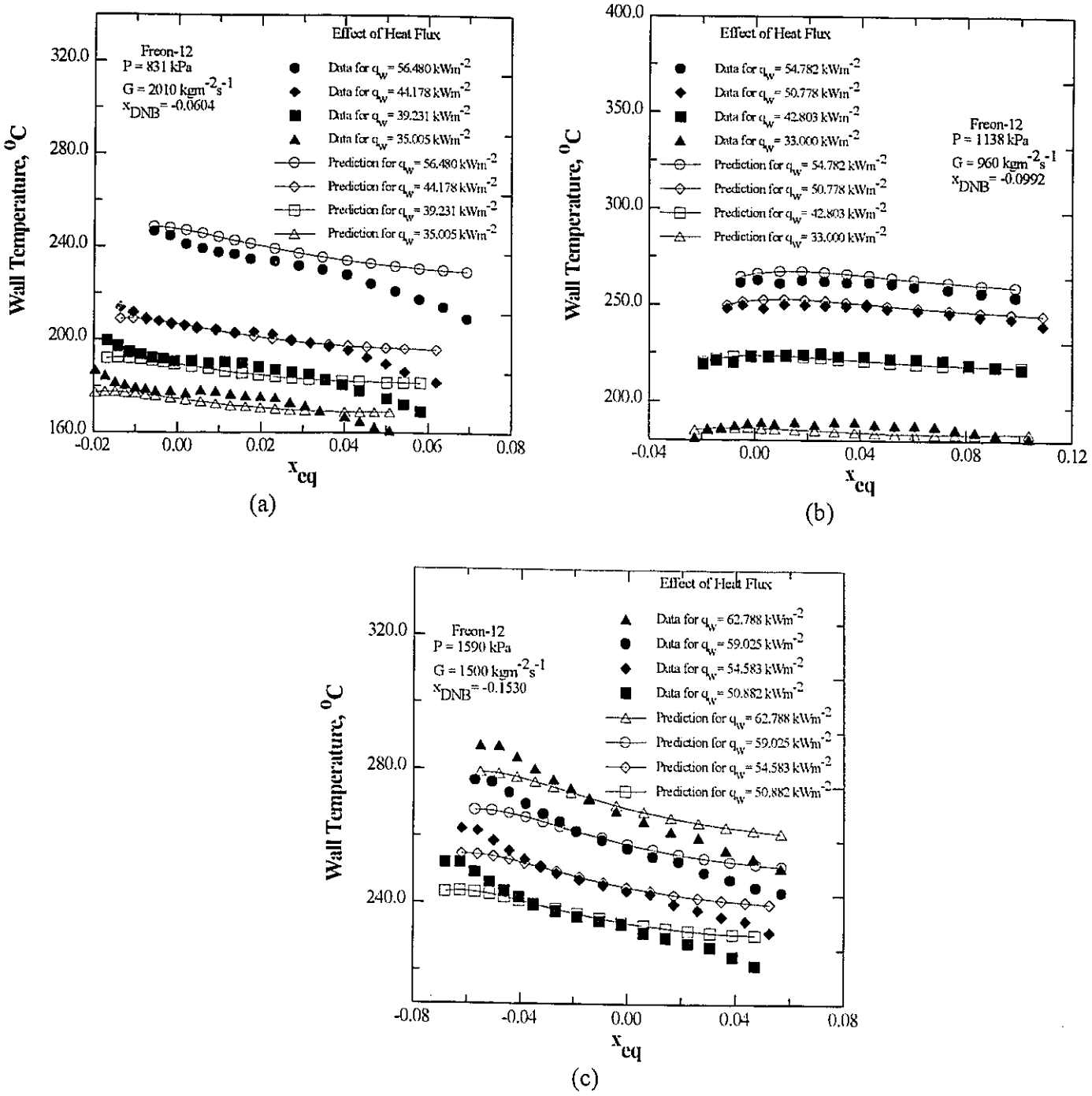

Figure 16.8 Comparison of measured heat flux effect with model predictions.

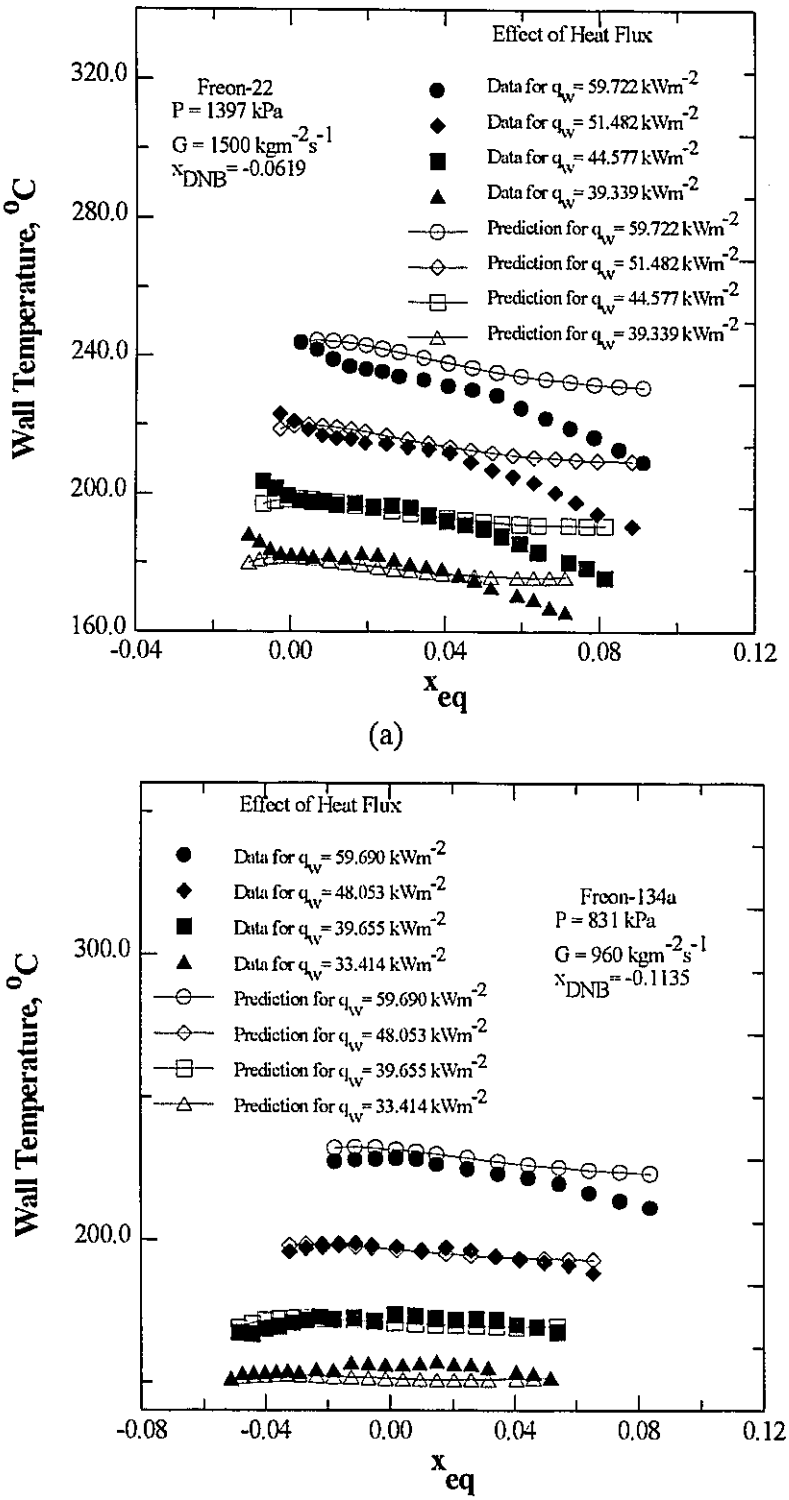

Figure 16.9 Comparison of measured heat flux effect with model predictions.

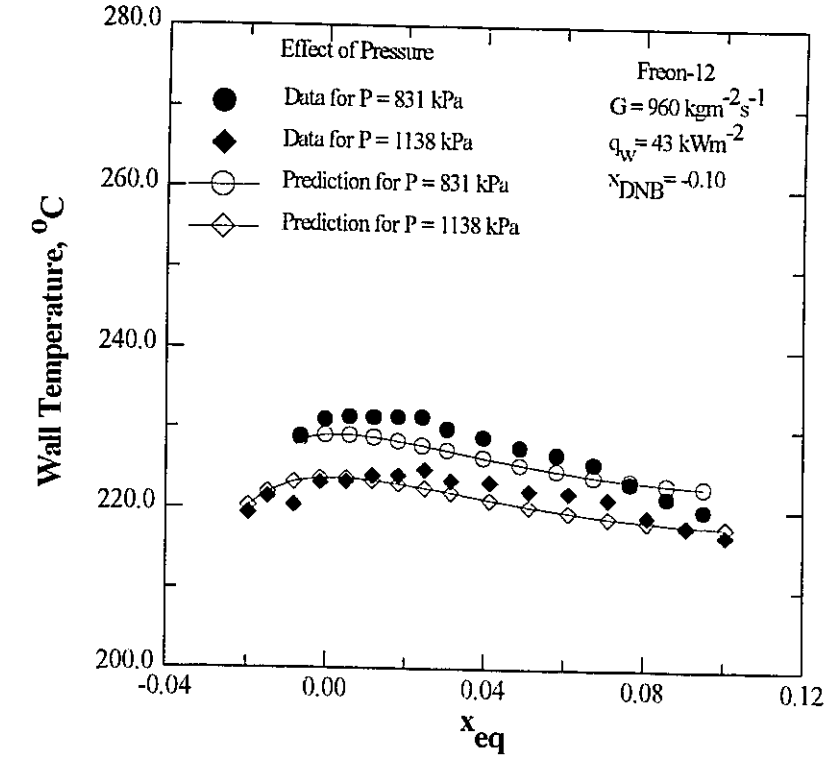

(a)

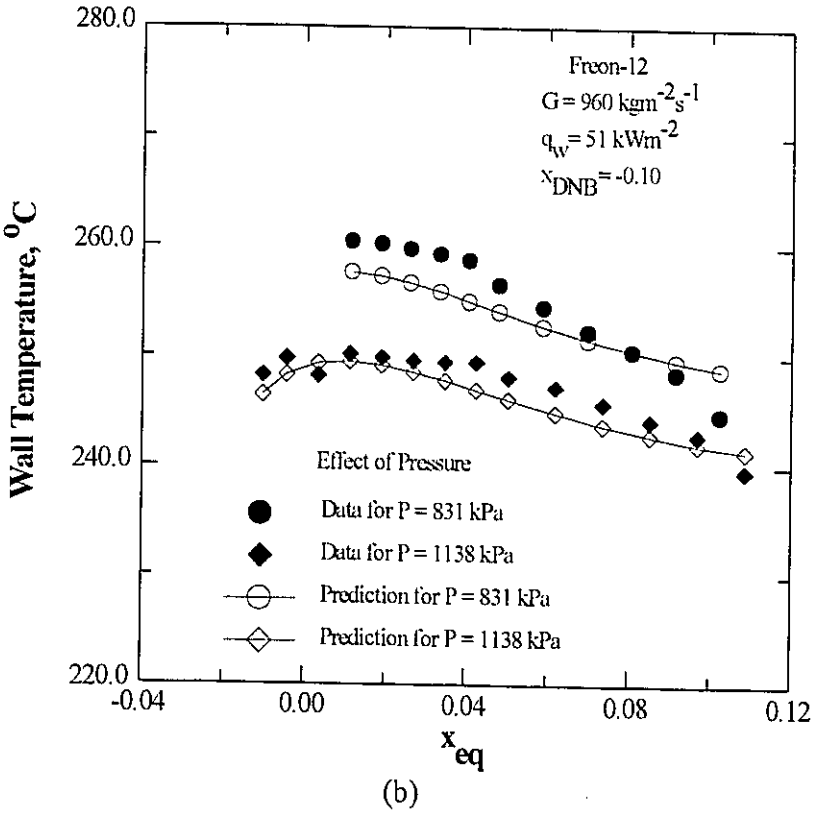

(b)

Figure 16.10 Comparison of measured pressure effect with model predictions.

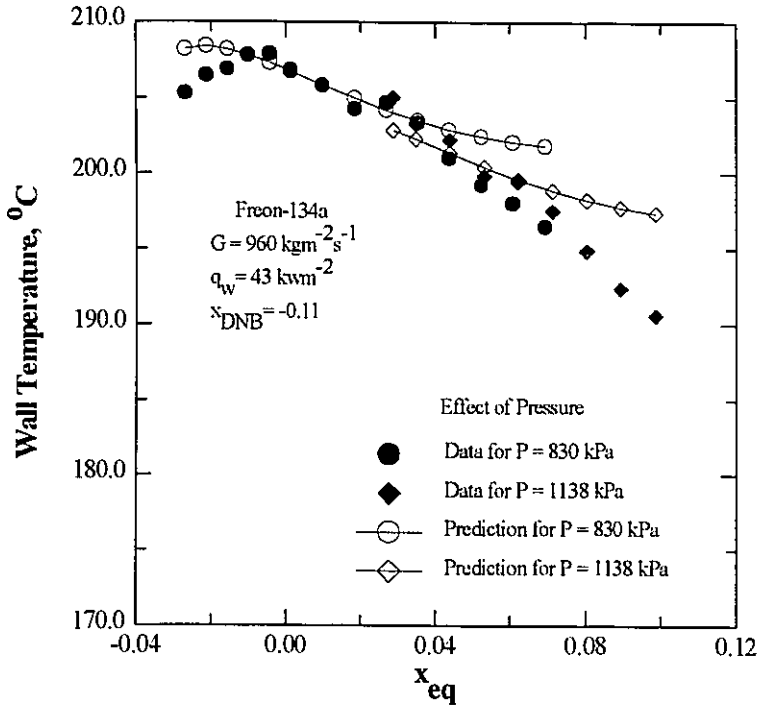

(a)

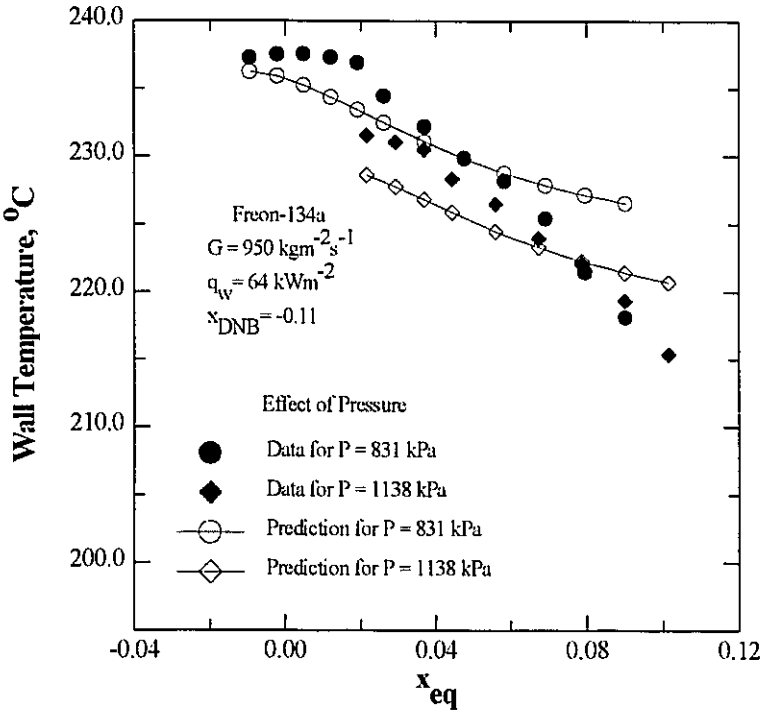

(b)

Figure 16.11 Comparison of measured pressure effect with model predictions.

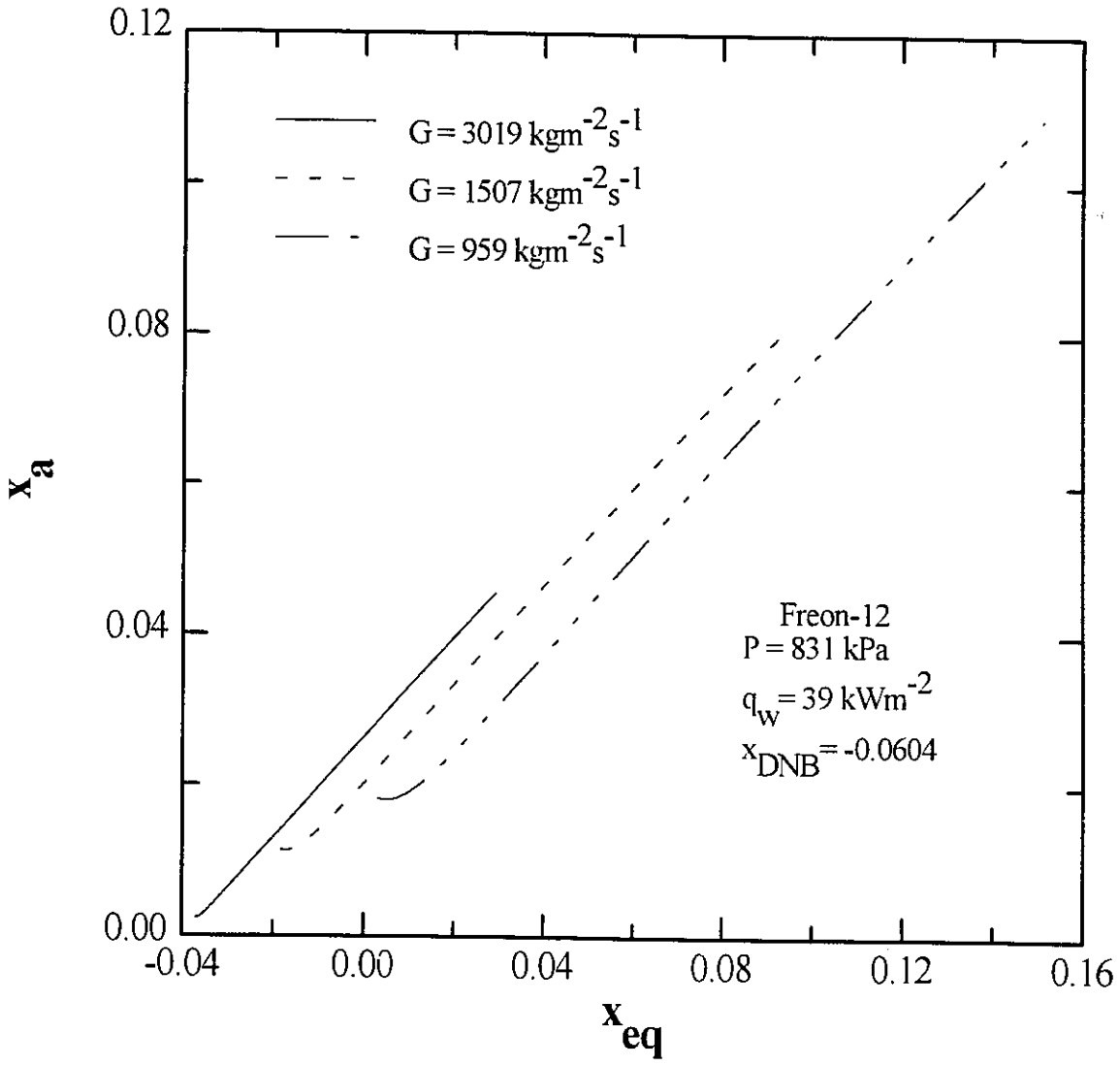

Figure 16.12 Model predictions of mass flux effect on the thermodynamic non-equilibrium.

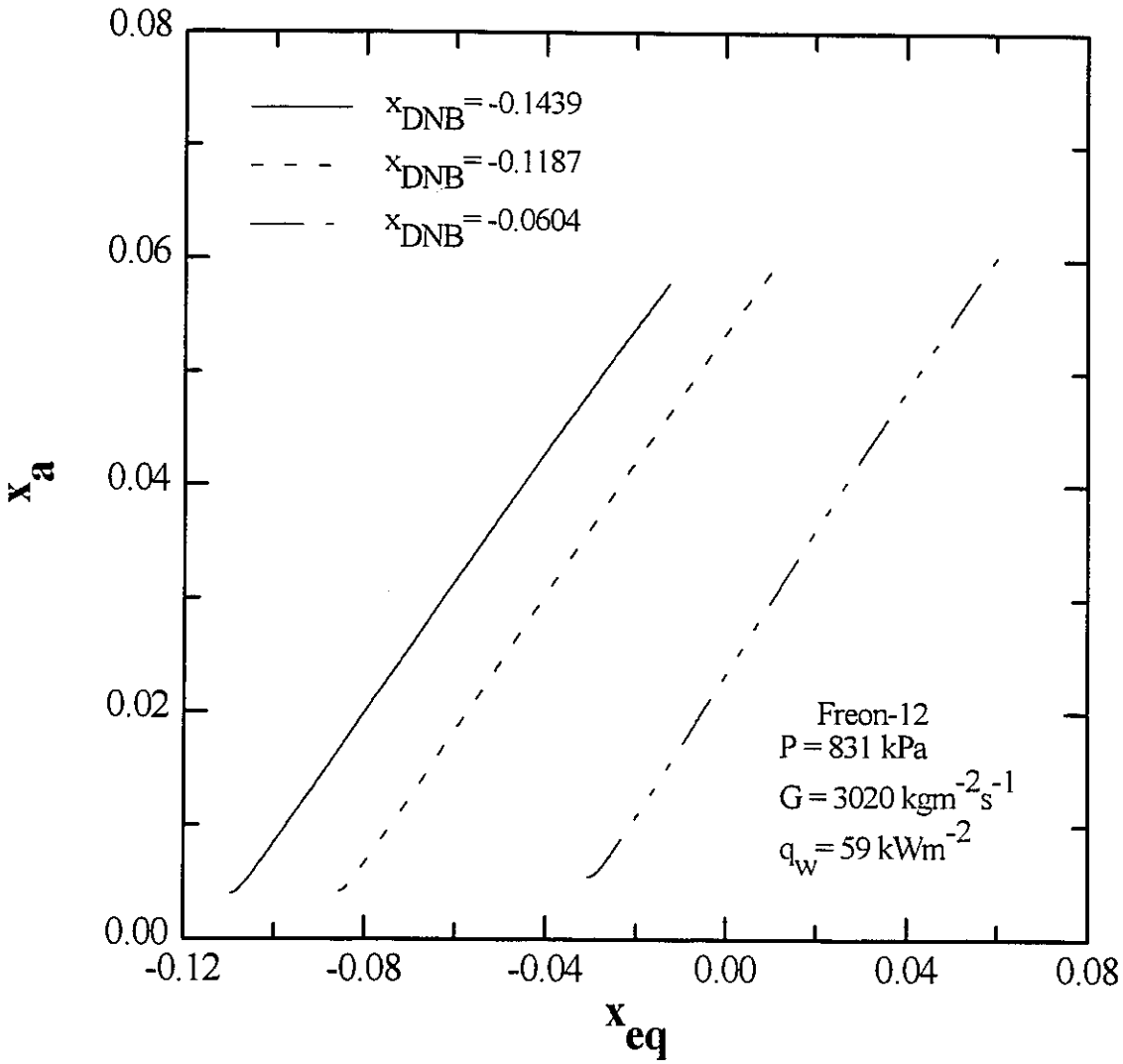

Figure 16.13 Model predictions of inlet subcooling effect on the thermodynamic non-equilibrium.

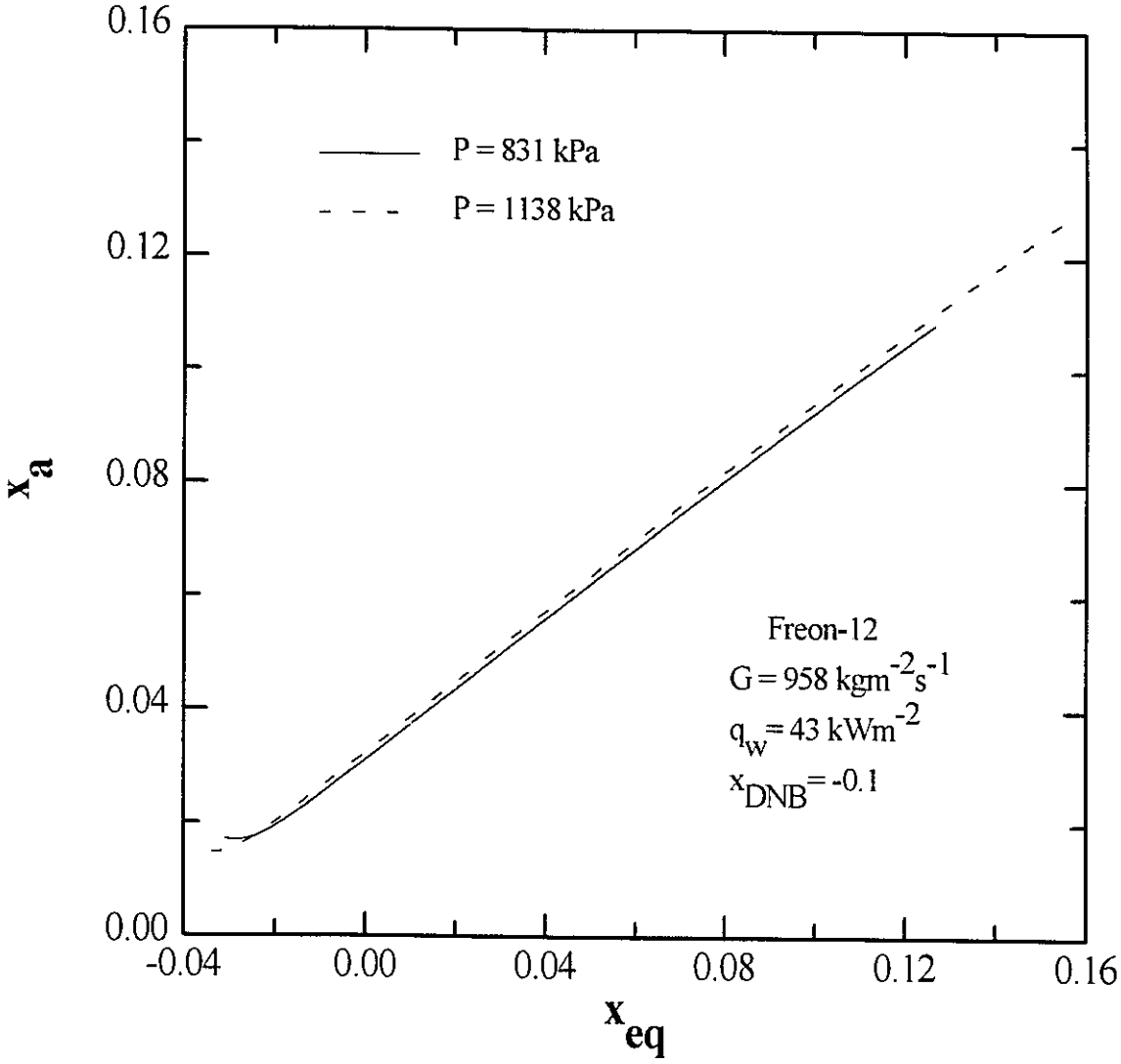

Figure 16.14 Model predictions of pressure effect on the thermodynamic non-equilibrium.

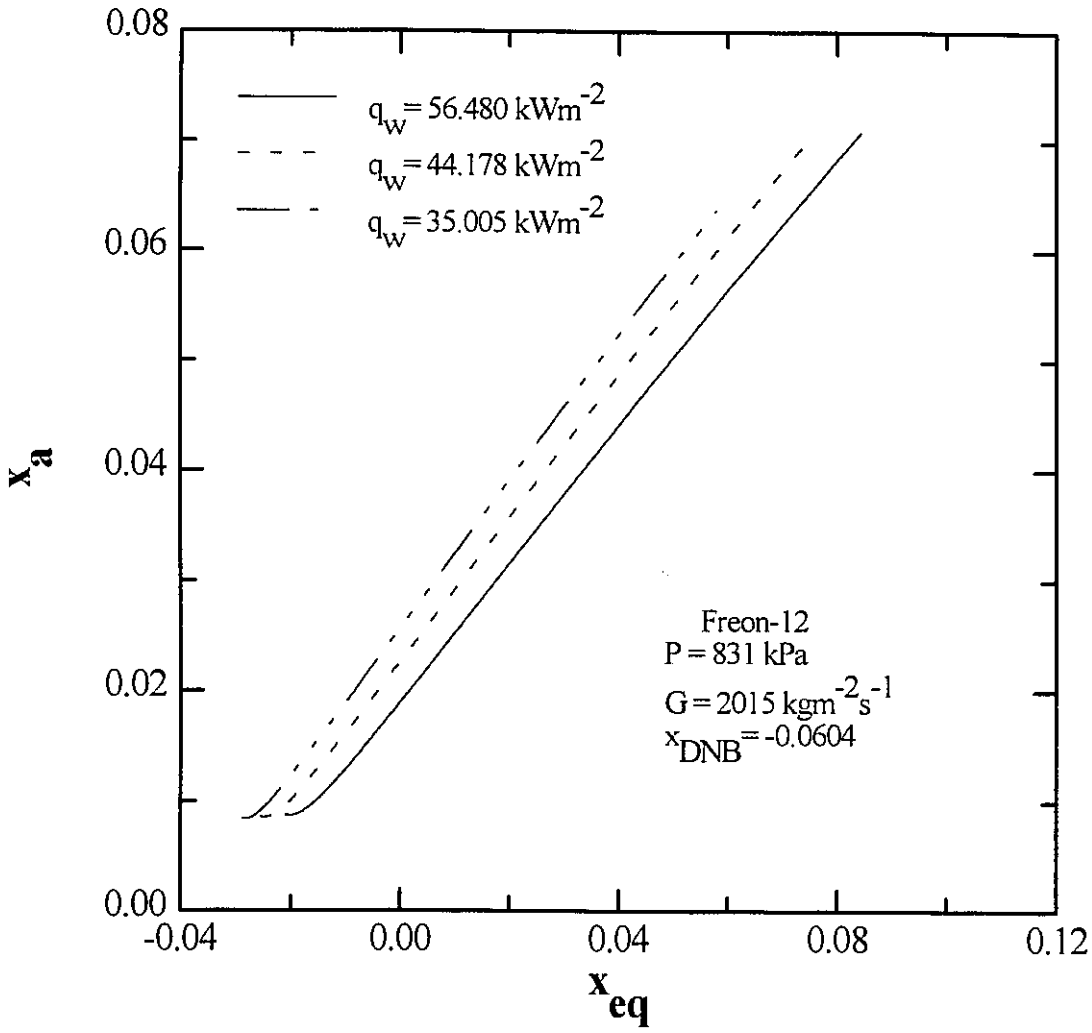

Figure 16.15 Model predictions of heat flux effect on the thermodynamic non-equilibrium.

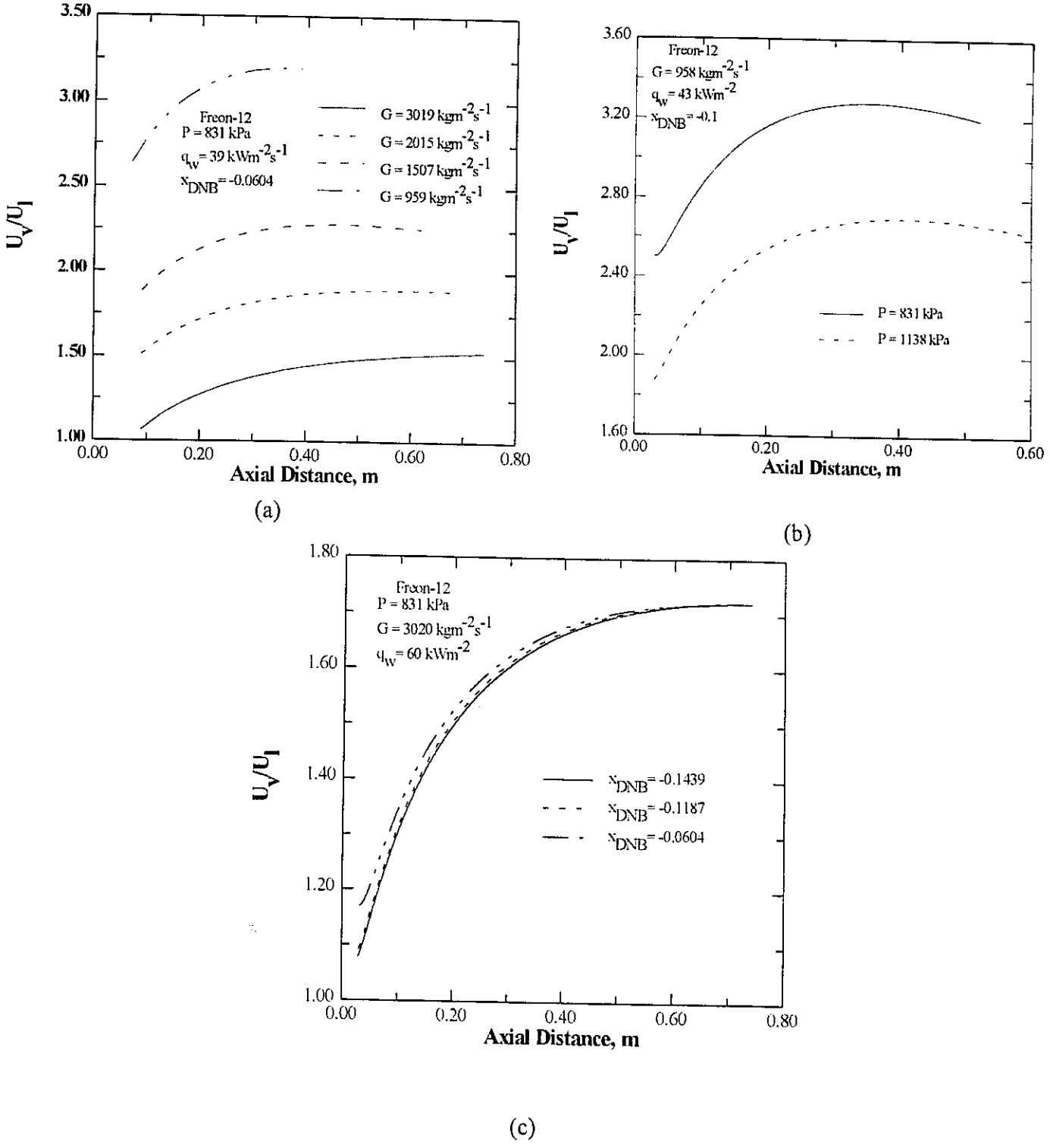

Figure 16.16 Effect of (a) mass flux, (b) pressure and (c) inlet subcooling on the slip.

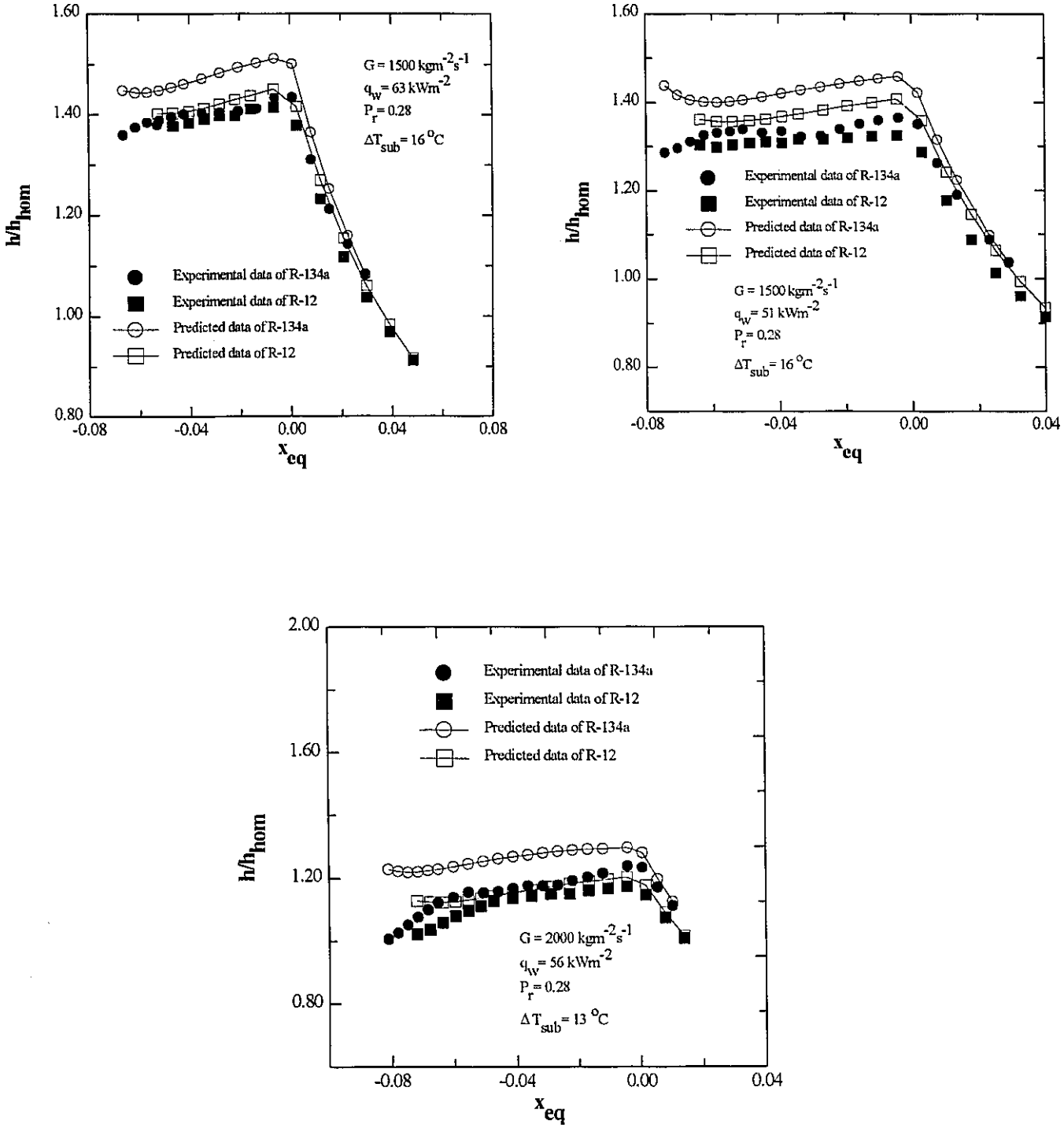

Figure 16.17 Model predictions of fluid effect on the (h/h_{hom}) ratio.

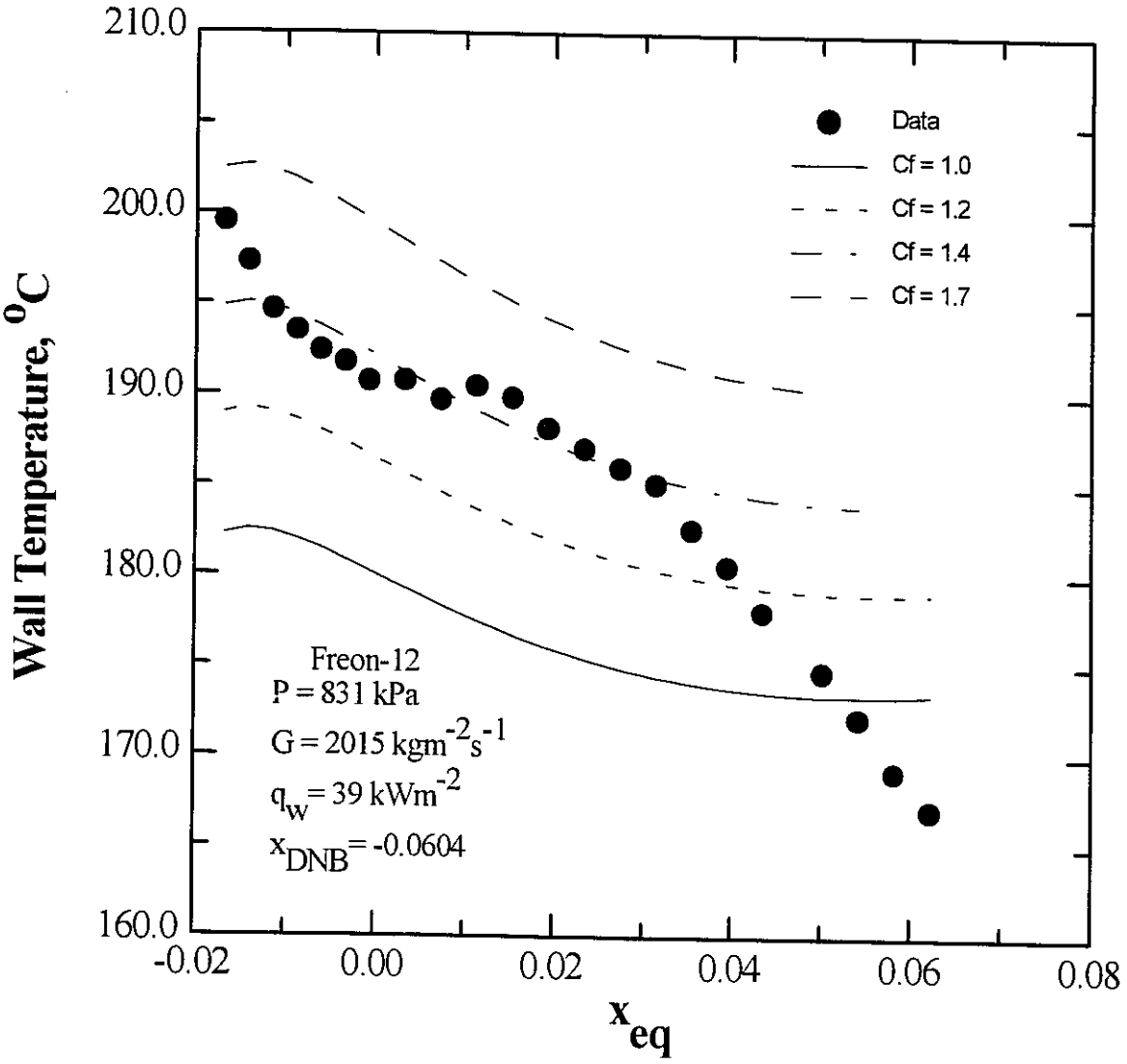

Figure 16.18 Model sensitivity to wall friction factor.

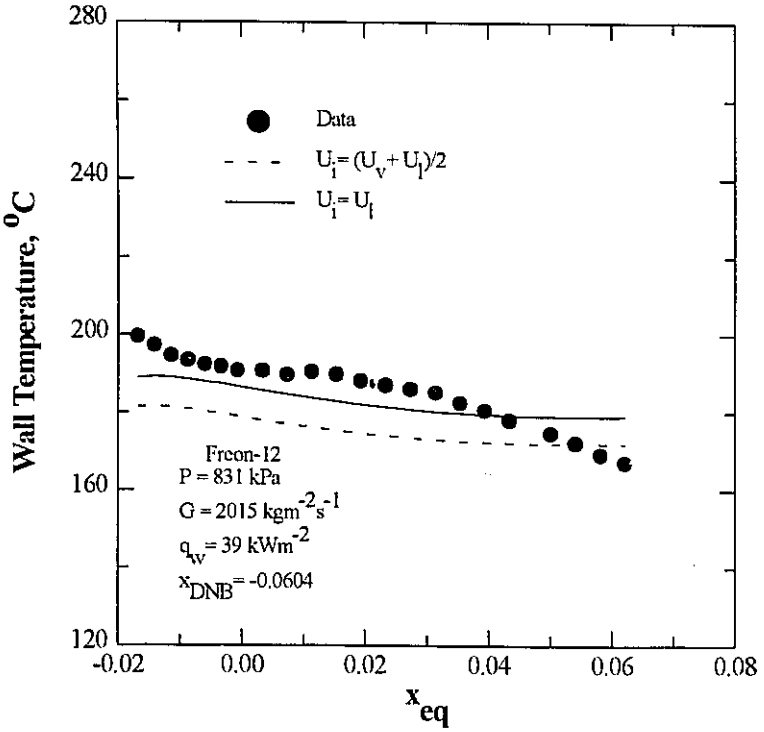

(a)

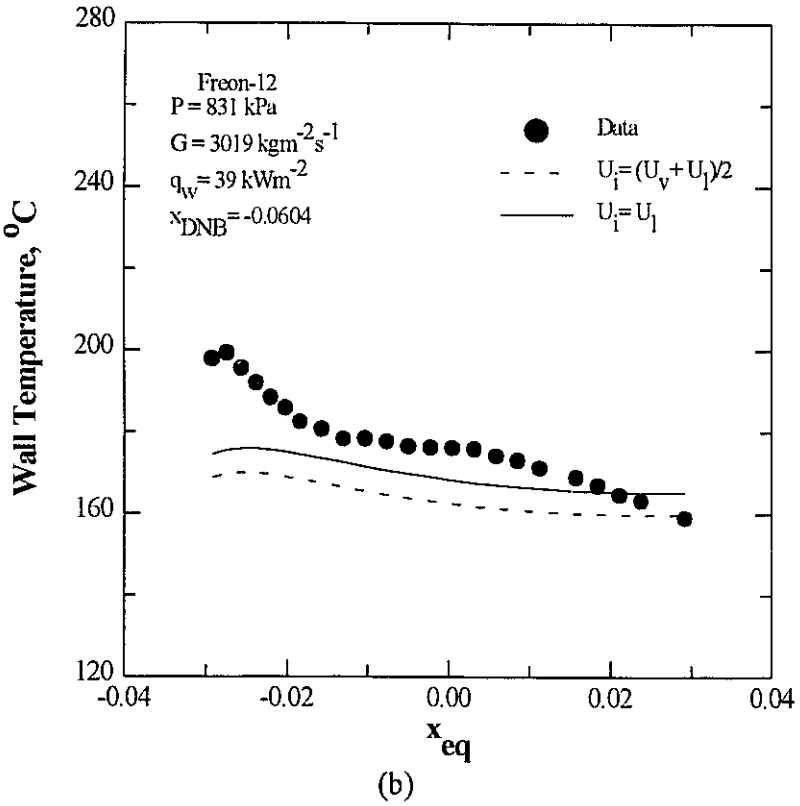

(b)

Figure 16.19 Model sensitivity to interfacial velocity.

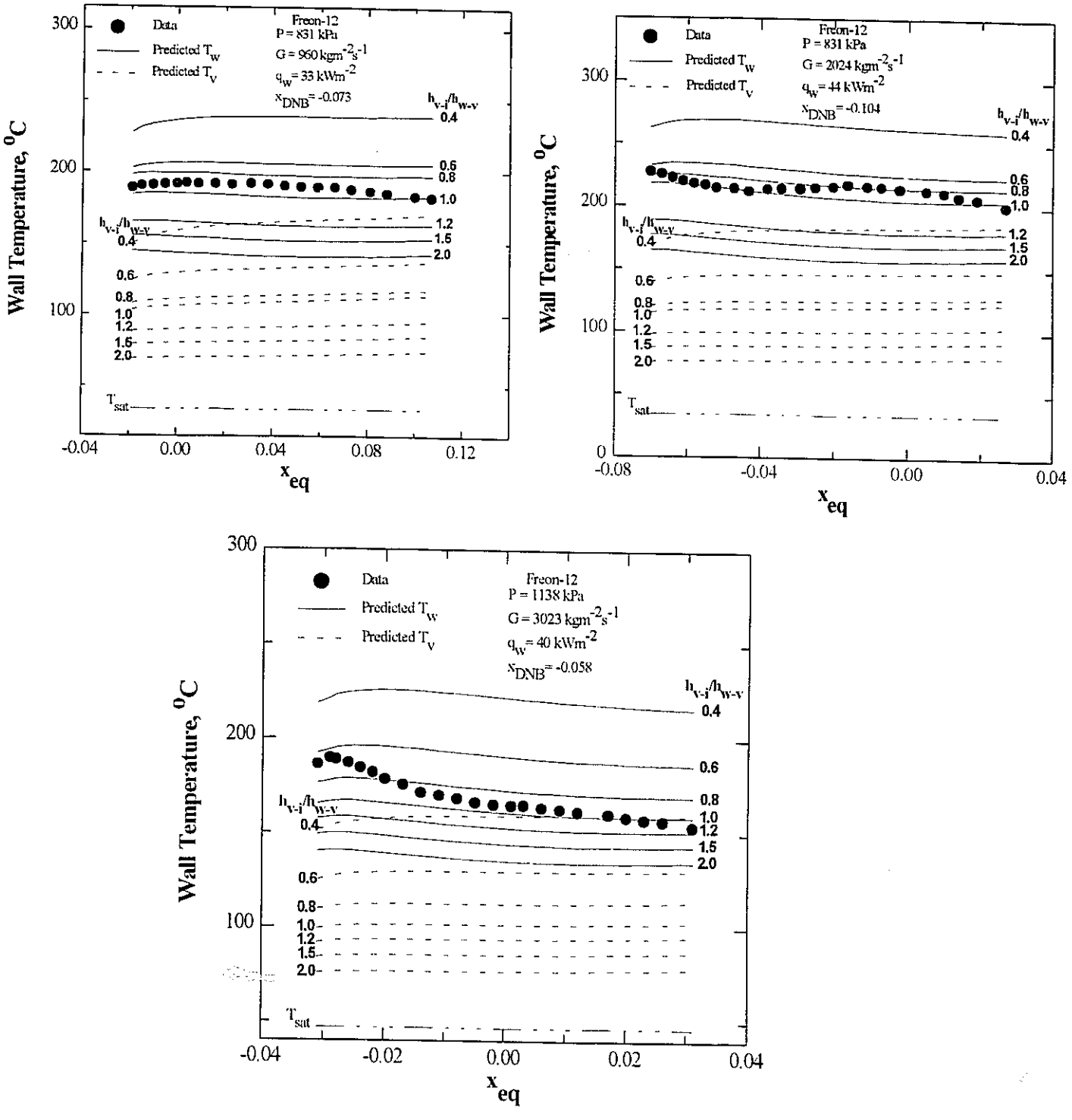

(c)

Figure 16.20 Model sensitivity to the (h_{v-i}/h_{w-v}) ratio.

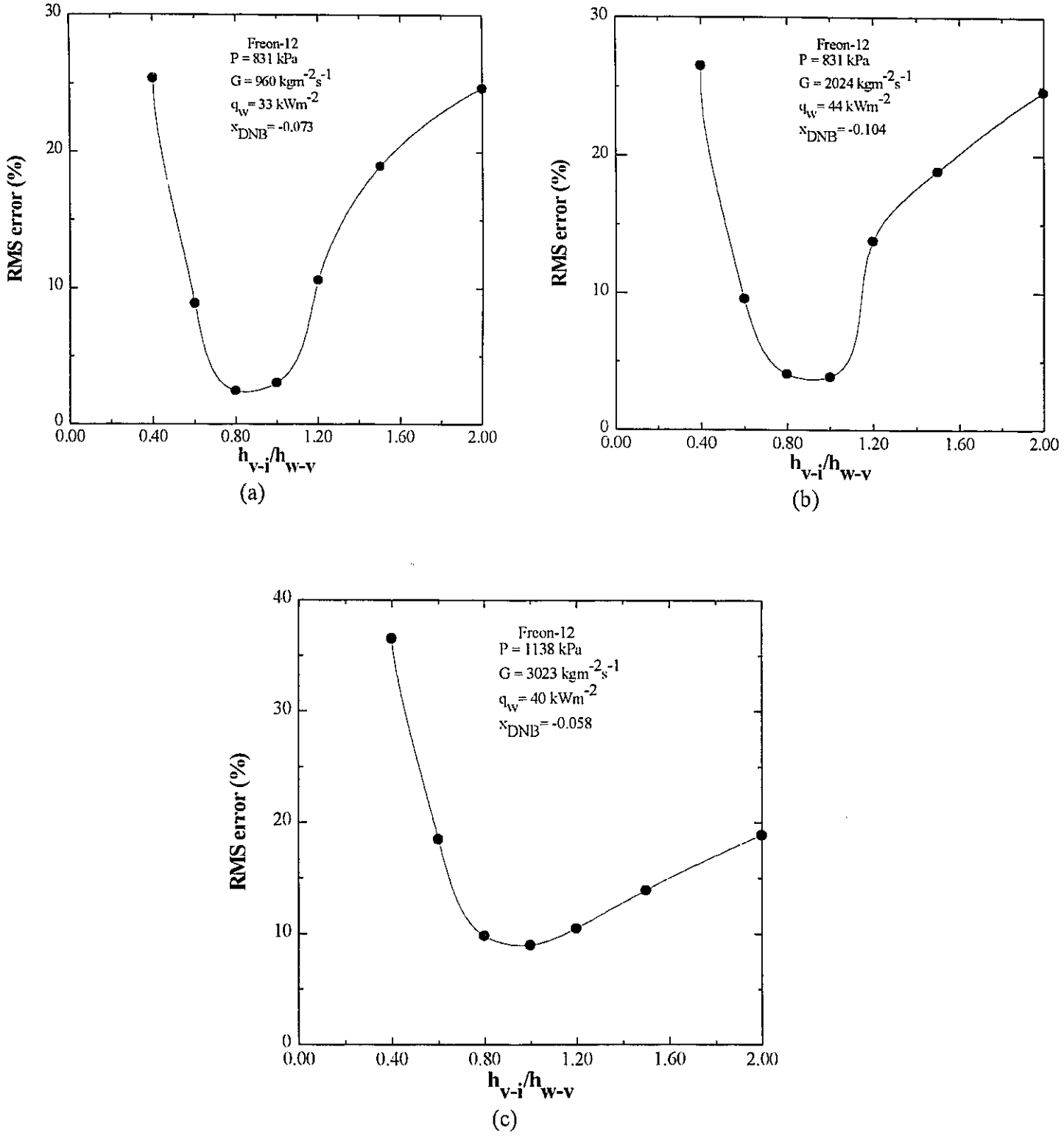

Figure 16.21 Model sensitivity to the ($h_{v\text{-}i}/h_{w\text{-}v}$) ratio.

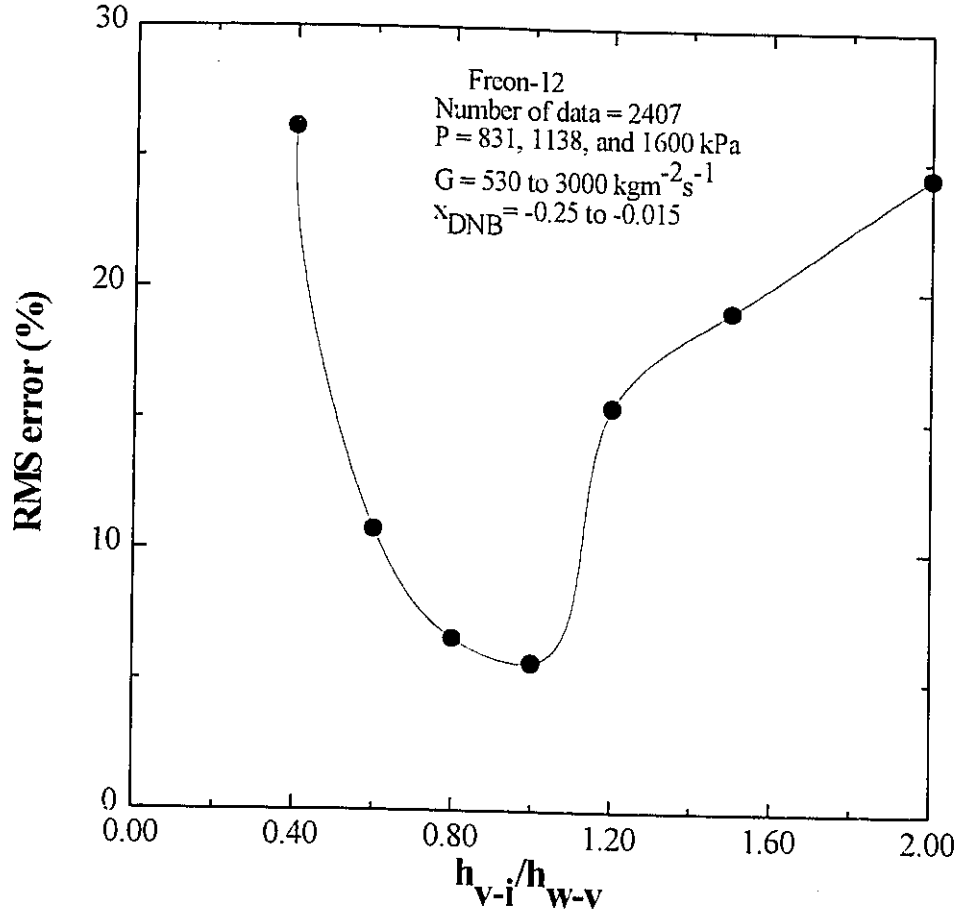

Figure 16.22 Deviation of predicted wall temperatures from experimental data of Freon-12 at various values of $h_{v\text{-}i}/h_{w\text{-}v}$.

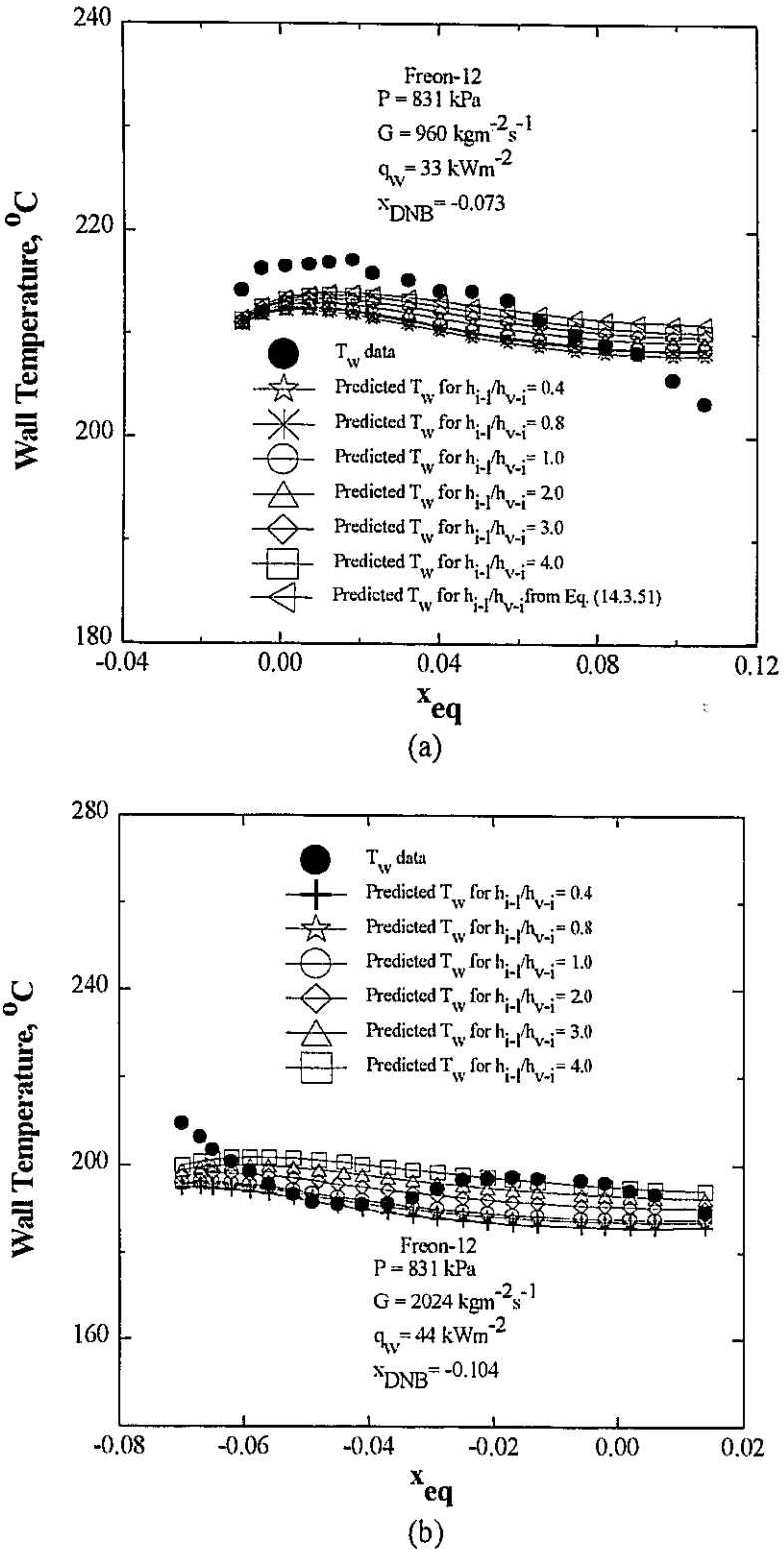

Figure 16.23 Model sensitivity to the (h_{i-l}/h_{v-i}) ratio.

Chapter 17 COMPARISON OF MODEL PREDICTION TO DATA

17.1 General

Chapter 16 compared the two-fluid model predicted trends with those observed from the data of this study. Chapter 17 compares predictions from the two-fluid model to the data of this study and data from the AECL PDO data base. The results of the comparison are displayed as plots of wall temperature versus thermodynamic equilibrium quality. Also, these same plots show predictions from the various prediction methods discussed in Chapter 13, in order to compare them to the new model.

17.2 Comparison to Freon Data

Figures 17.1-17.4 show predictions of wall temperatures for three fluids (Freon-12, Freon-134a, and Freon-22), and for a wide range of flow conditions. The new model predicts the trend and the magnitude of the wall temperatures correctly, and it gives much better prediction accuracy than the other prediction methods. In general, the model performs best at lower mass fluxes. At high mass fluxes, none of the prediction methods, including this model, is capable of accurate predictions in heat transfer regions I and II, as Figs. 17.2(c) and 17.3(b) show.

17.3 Comparison to Water Data

Figures 17.5-17.7 show predictions of wall temperature for pressure conditions ranging from atmospheric to 9 MPa for water. It is interesting to notice that, in general, the prediction methods have a worse prediction accuracy for the water data than for the refrigerant data of this

study.

It is understood that the physical mechanisms of heat transfer in subcooled film boiling are the same for all fluids. Consequently, the greater discrepancies in the predictions for the water data can only be attributed to uncertainties in the water data itself. In fact, it was found that in all low-quality water data given in AECL's PDO data base, the quality at CHF (x_{DNB}) is not the same as the critical quality reported in the original works. For instance, Fung [1981], in his P.h. D. thesis, gives the location of the CHF very near the inlet of the hot patch; however, AECL's data base gives the CHF location close to the outlet of the hot patch. This discrepancy could considerably affect the prediction accuracy of history-dependent models, especially in the subcooled IAFB region. Also, Stewart's data [1981] lists only the outside wall temperatures, whereas prediction methods provide predictions of the inside wall temperatures. Furthermore, Stewart's [1981] data lists two thermocouple readings of wall temperatures at the same axial location along the heated length. His data shows that the difference between these readings could be as high as 100°C at temperatures of 700°C; however, AECL's data base gives the average of these values. Also, some data sets from different sources, which cover very similar flow conditions, do not agree with each other. Nevertheless, overall the new model still provides the most accurate predictions among the prediction methods examined in this study.

17.4 Overall Comparison

Table 17.1 lists the root-mean-square (RMS) and the average errors of the prediction methods examined during this study. The average error and the RMS error are defined as follows.

$$RMS\ \ Error\ \ = \left[\frac{1}{n}\sum_{i=1}^{n}(Error)^2_i\right]^{1/2} \qquad (17.4.1)$$

$$Average\ \ Error\ \ = \frac{1}{n}\sum_{i=1}^{n}(Error)_i \qquad (17.4.2)$$

where Error is a relative error defined as

$$Error\ \ = \frac{Predicted\ \ T_w\ \ -\ Experimental\ \ T_w}{Experimental\ \ T_w} \qquad (17.4.3)$$

where T_w is the inside tube surface temperature in °C and n is the number of data points. The data of water are from Stewart [1981], Laperriere [1983], and Fung [1981]. Table 9.1 summarizes the test conditions of the data.

Overall, for water data, the present model gives conservative predictions of wall temperatures, as indicated by the average error of 5.20%, which has resulted from a total of 2809 data points. Also, the model gives an overall RMS error of 14.88%, which is the lowest. It is of interest to see that the present model provides better prediction accuracy than the modified Berenson correlation, which was modified based on the same water data base used for comparison in this study.

For Freon data, the present model gives the lowest RMS errors among all the prediction methods, as Table 17.1 shows. Overall, the new model yields the lowest RMS errors, and the Mosaad and Johannsen [1989] and Cachard [1994] models the highest. This is not surprising, since the new model applies to all flow conditions and uses minimum amount of empiricism, while the

others contain a large number of empirically determined factors, which are evaluated from water data covering a narrow range of flow conditions.

17.5 Comparison of Hybrid Model Predictions to Freon Data

Figures 17.8-17.11 show a comparison between the hybrid model predictions and the data. Overall, the model provides the correct trend and magnitude of wall temperatures from the IAFB region to the DFFB region. As explained in Section 14.4, predictions in the transition region are based on interpolation of wall temperatures between the values predicted by the IAFB model at a void fraction of 60% and the DFFB model at a void fraction of 70%. Figures 17.8-17.11 show that this simple approximation yields very satisfactory predictions.

17.6 Discussion

Low quality and subcooled film boiling is of particular interest for the reflood phases of a LOCA. This flow regime usually precedes the arrival of the quench front and influences its rate of progression. As a consequence, the majority of subcooled film boiling prediction methods existing in the literature deal with LOCA conditions at low pressures (up to 0.4 MPa) and low mass fluxes (up to 300 $kgm^{-2}s^{-1}$). The constitutive relations used within these models contain parameters that are approximated (or inferred) from data relevant to LOCA conditions (low pressures and low mass fluxes). This restricts the models to the same conditions. This may explain the poor performance of the prediction methods discussed in Chapter 13, when compared to the data of this study and to the high-pressure data of water ($P \geq 2$ MPa). For example, the Mosaad and Johannsen [1989] and Cachard [1994] models give very poor prediction accuracy when compared to the moderate-to-high mass flow rate and moderate-to-high pressure water data. This is because these models were adjusted to predict heat transfer rates during LOCA conditions.

Table 17.1 Deviation of predicted wall temperatures from experimental values

Prediction Method	RMS %	Average deviation %	Number of data	Fluid
Analytis-Yadigaroglu [1987]	21.70	20.44	2407	Freon-12
Denham [1984]	16.79	3.54	2407	
Johannsen-Mosaad[a] [1989]	61.65	56.23	1676	
Modified Berenson [1988]	16.94	-7.70	2407	
Cachard [1994][a]	34.34	28.24	1518	
New model	5.67	-3.11	2407	
Analytis-Yadigaroglu [1987]	19.44	17.96	705	Freon-22
Denham [1984]	26.31	11.91	705	
Johannsen-Mosaad[a] [1989]	68.22	64.29	481	
Modified Berenson [1988]	18.82	-0.81	705	
Cachard[a] [1994]	41.57	33.64	309	
New model	6.58	-1.87	705	
Analytis-Yadigaroglu [1987]	17.15	11.59	2083	Freon-134a
Denham [1984]	15.78	4.55	2083	
Johannsen-Mosaad[a] [1989]	70.14	65.87	1172	
Modified Berenson [1988]	15.39	-4.07	2083	
Cachard[a] [1994]	35.69	31.25	657	
Present model	6.19	-3.14	2083	
Analytis-Yadigaroglu [1987]	26.90	19.90	2809	Water
Denham [1984]	22.1	-0.51	2809	
Johannsen-Mosaad[a] [1989]	23.90	19.40	1294	
Modified Berenson [1988]	19.00	-8.70	2809	
Cachard[a] [1994]	26.70	11.90	1547	
Present model	14.88	5.20	2809	

[a] Unable to calculate all data points-- see Chapter 13 for explanations.

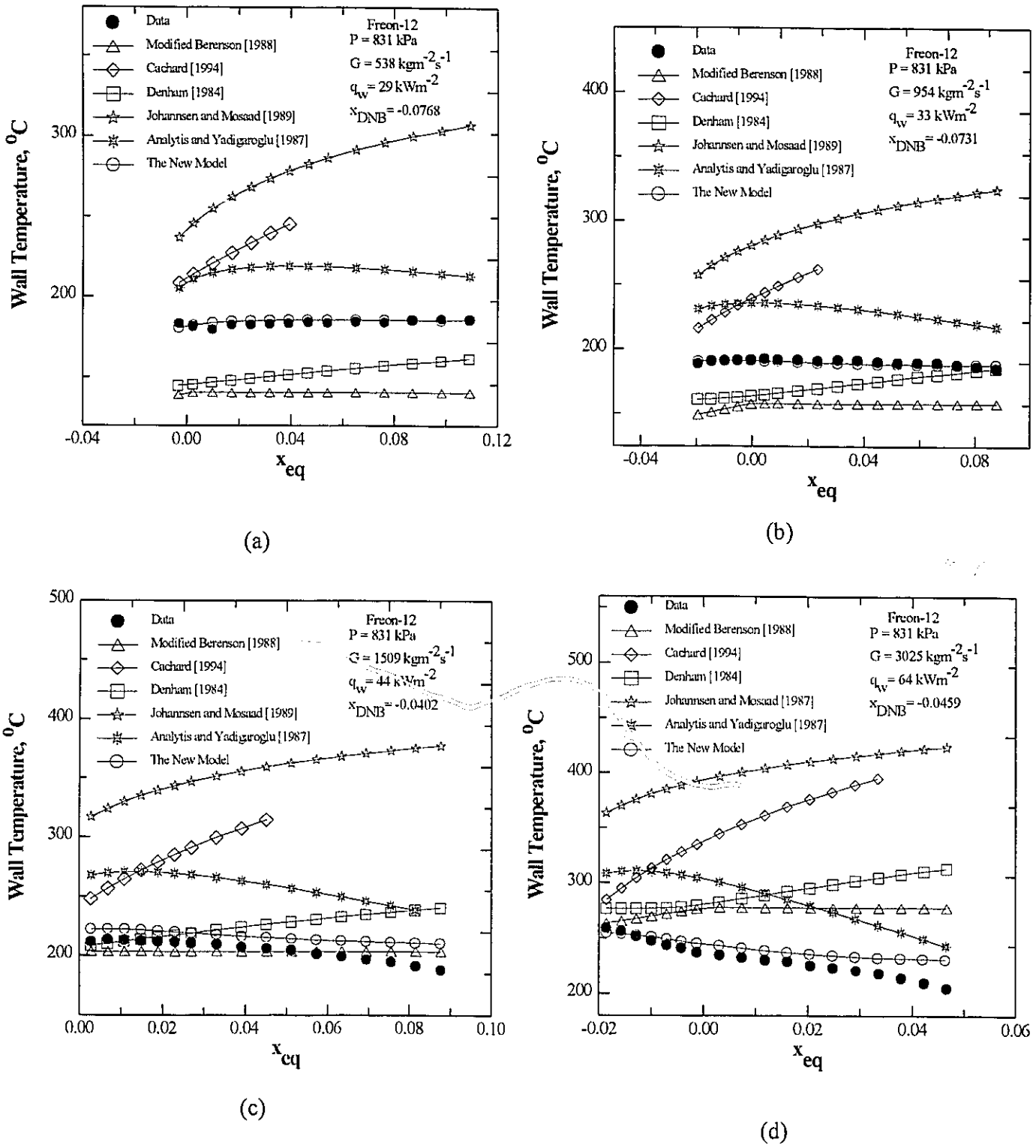

Figure 17.1 Comparison of the IAFB model predictions with Freon-12 data.

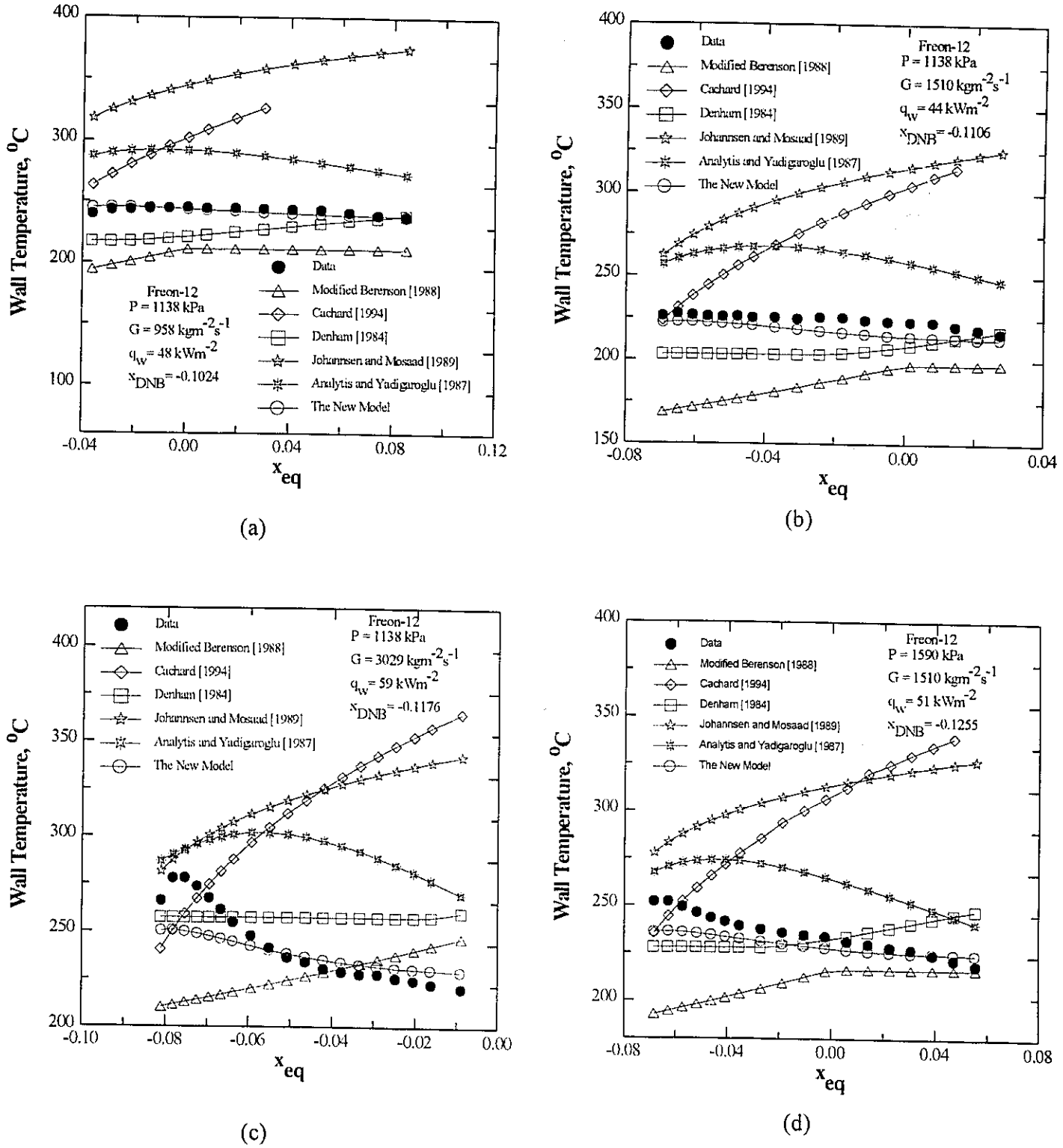

Figure 17.2 Comparison of the IAFB model predictions with Freon-12 data.

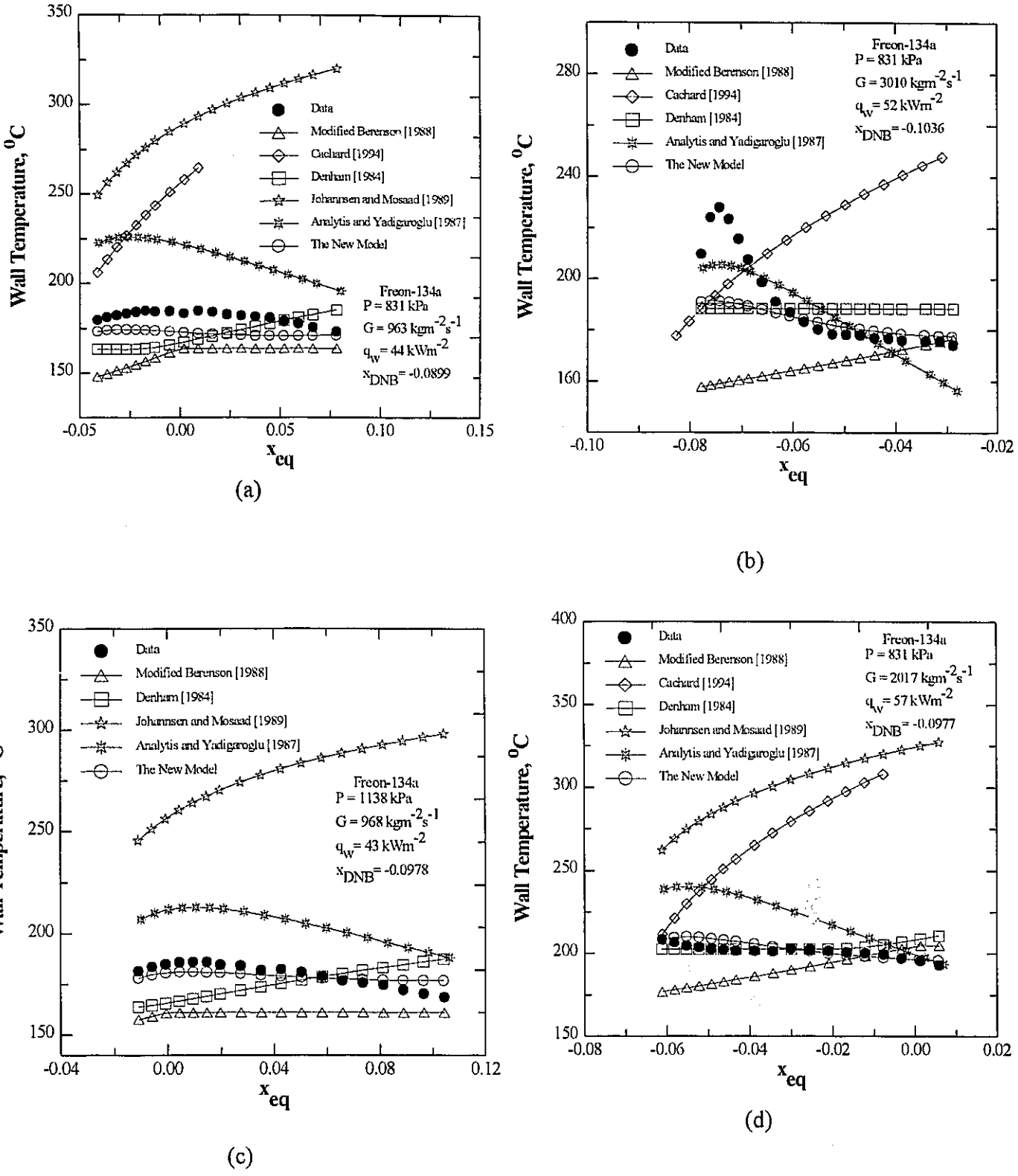

Figure 17.3 Comparison of the IAFB model predictions with Freon-134a data.

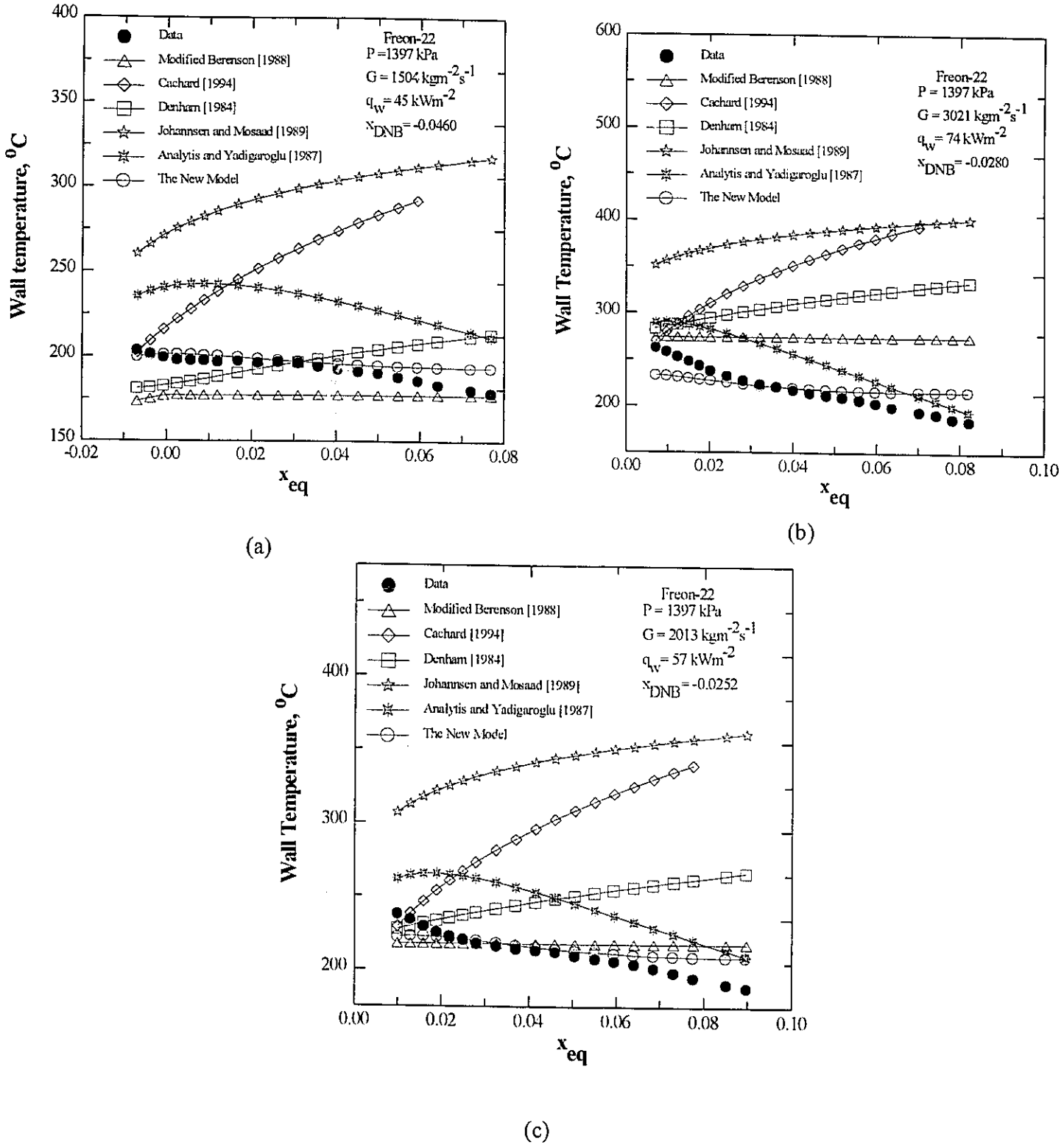

Figure 17.4 Comparison of the IAFB model predictions with Freon-22 data.

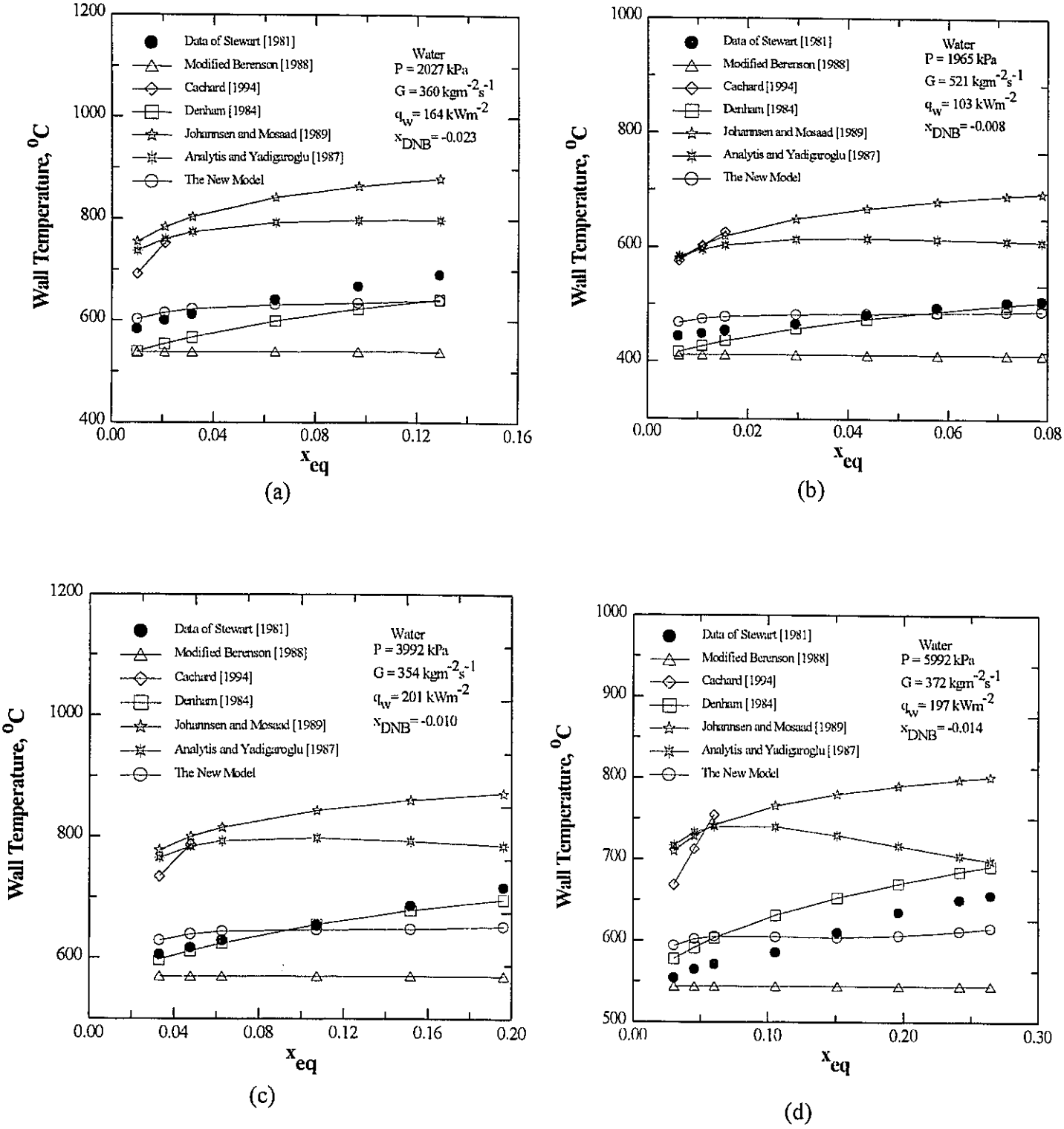

Figure 17.5 Comparison of the IAFB model predictions with water data.

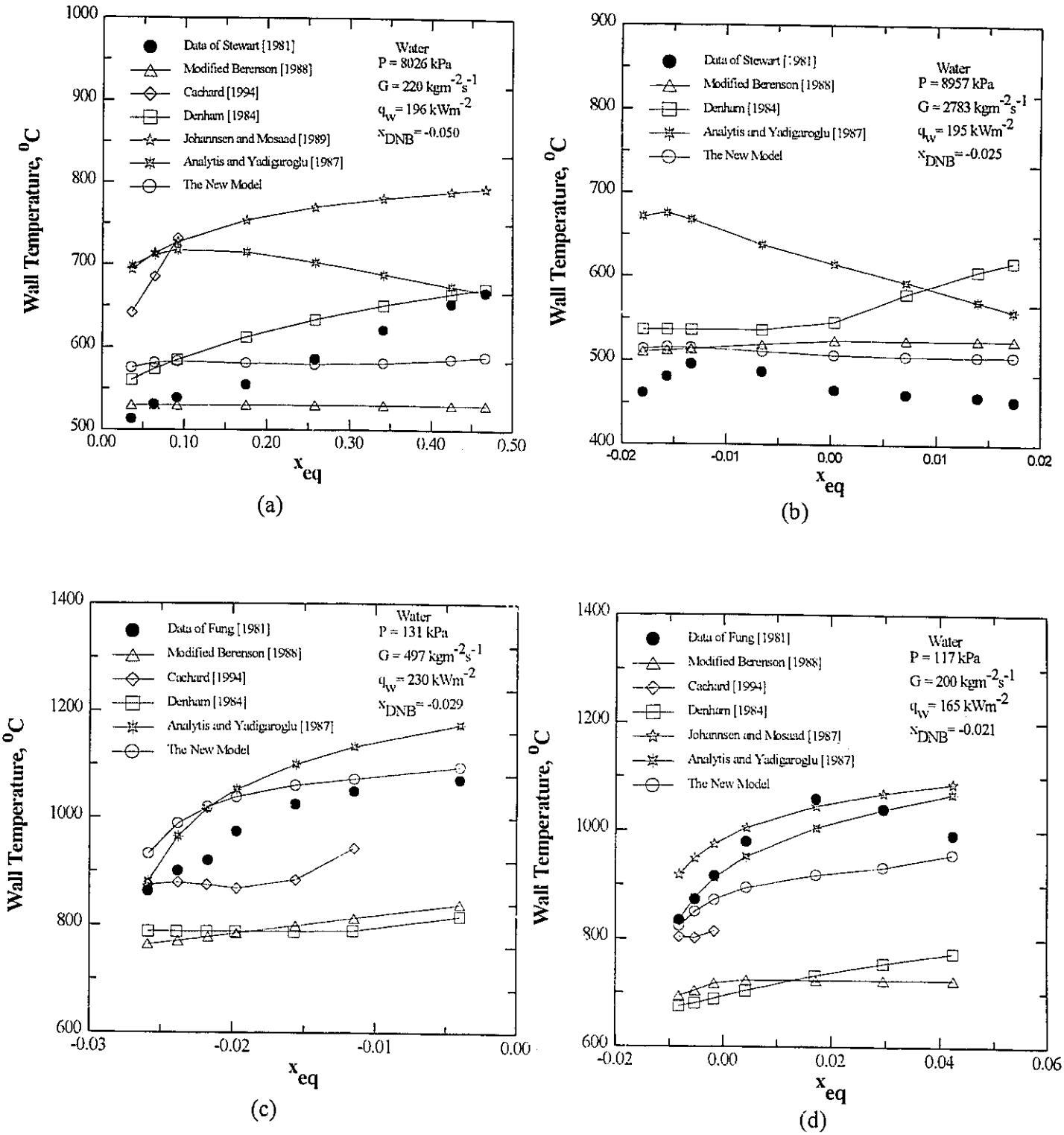

Figure 17.6 Comparison of the IAFB model predictions with water data.

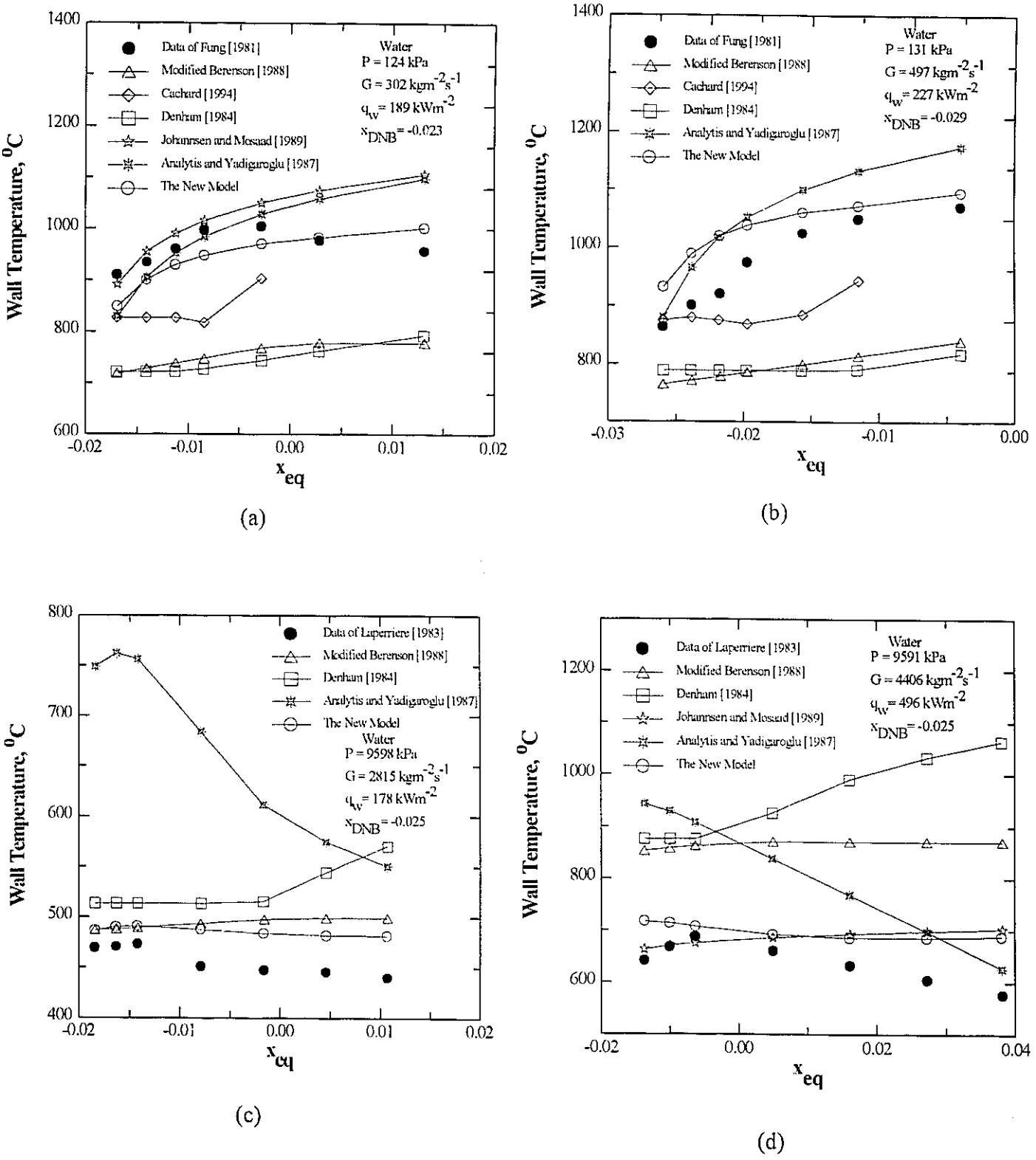

Figure 17.7 Comparison of the IAFB model predictions with water data.

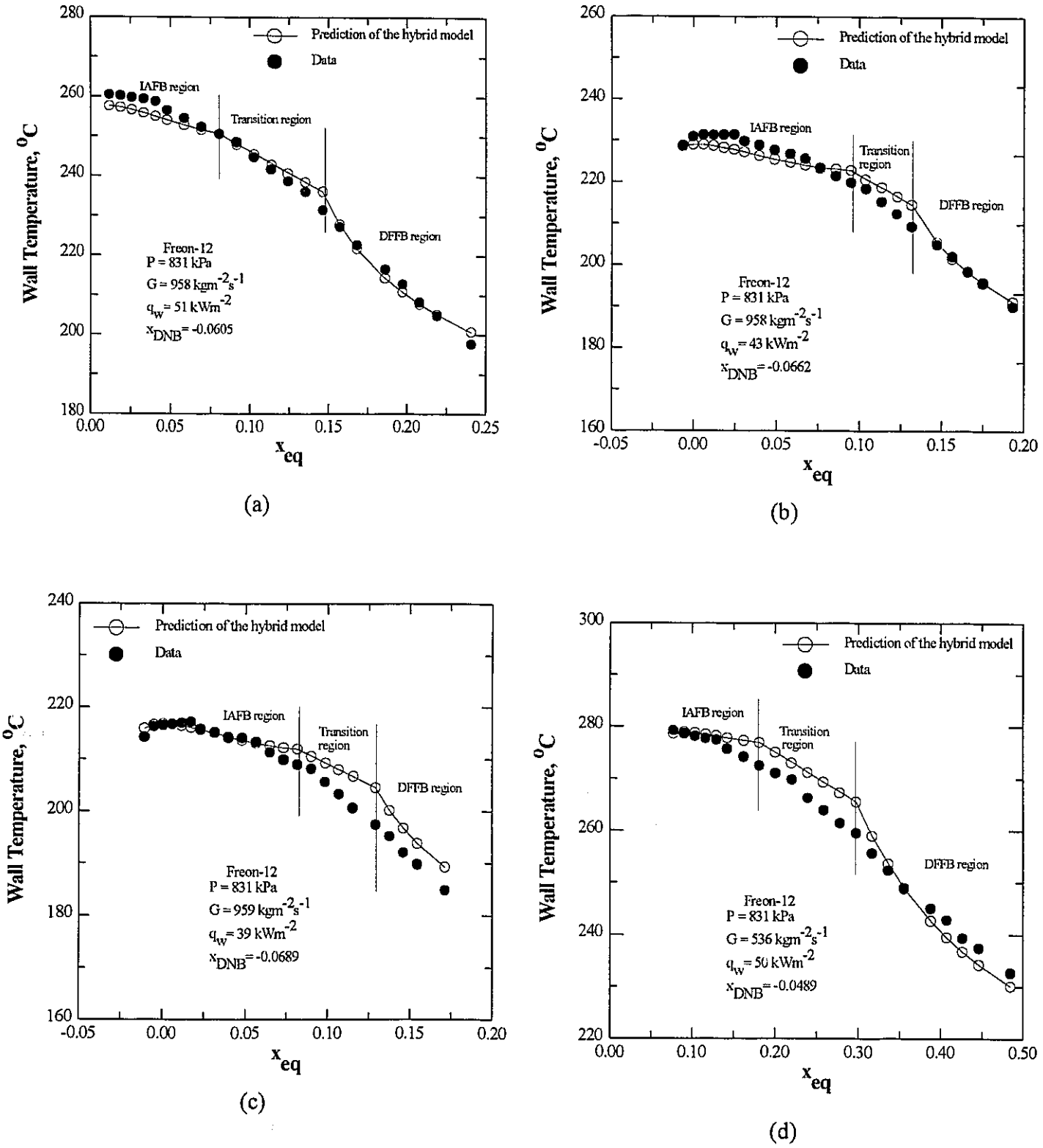

Figure 17.8 Comparison of the hybrid model predictions with Freon-12 data.

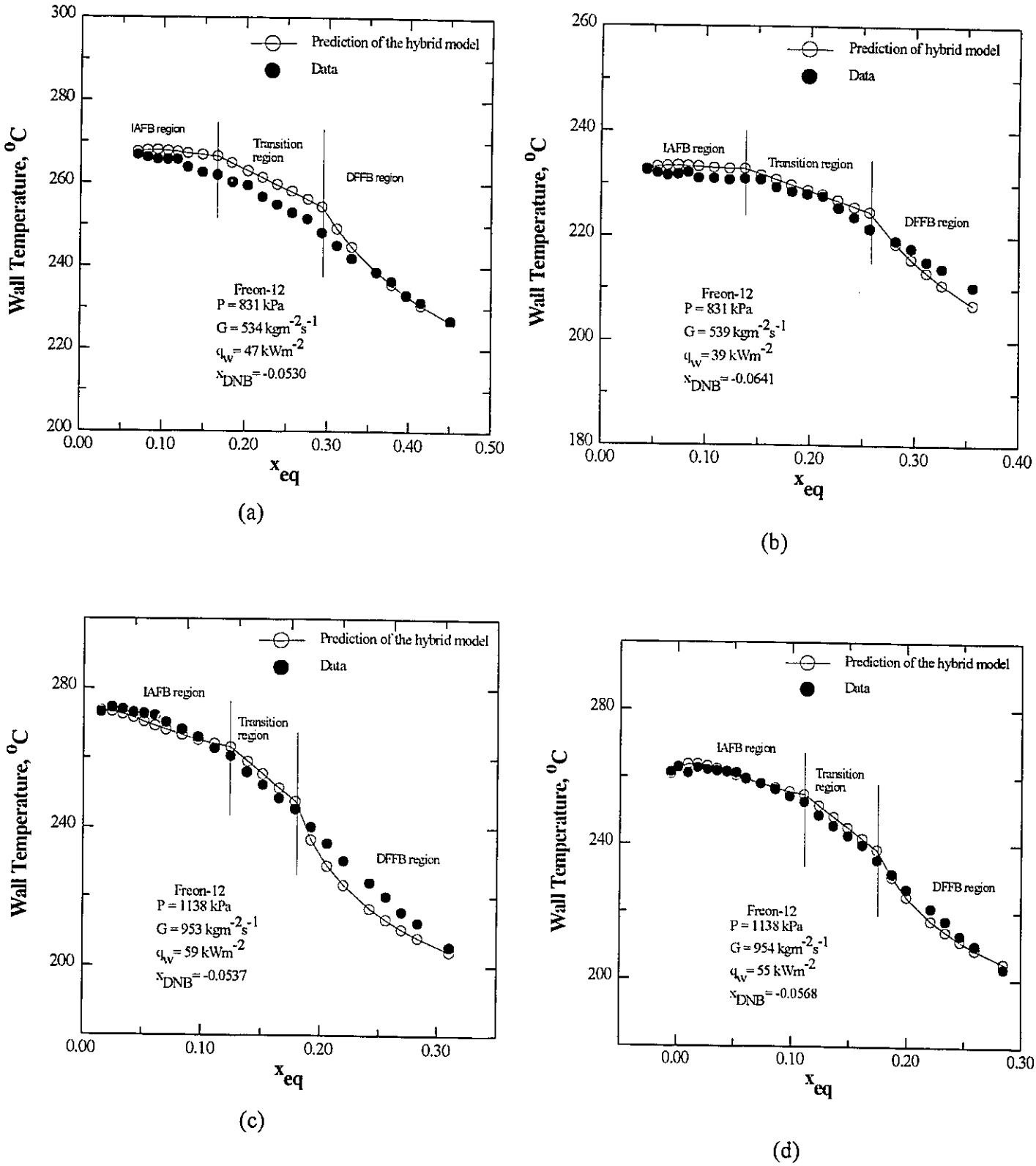

Figure 17.9 Comparison of the hybrid model predictions with Freon-12 data.

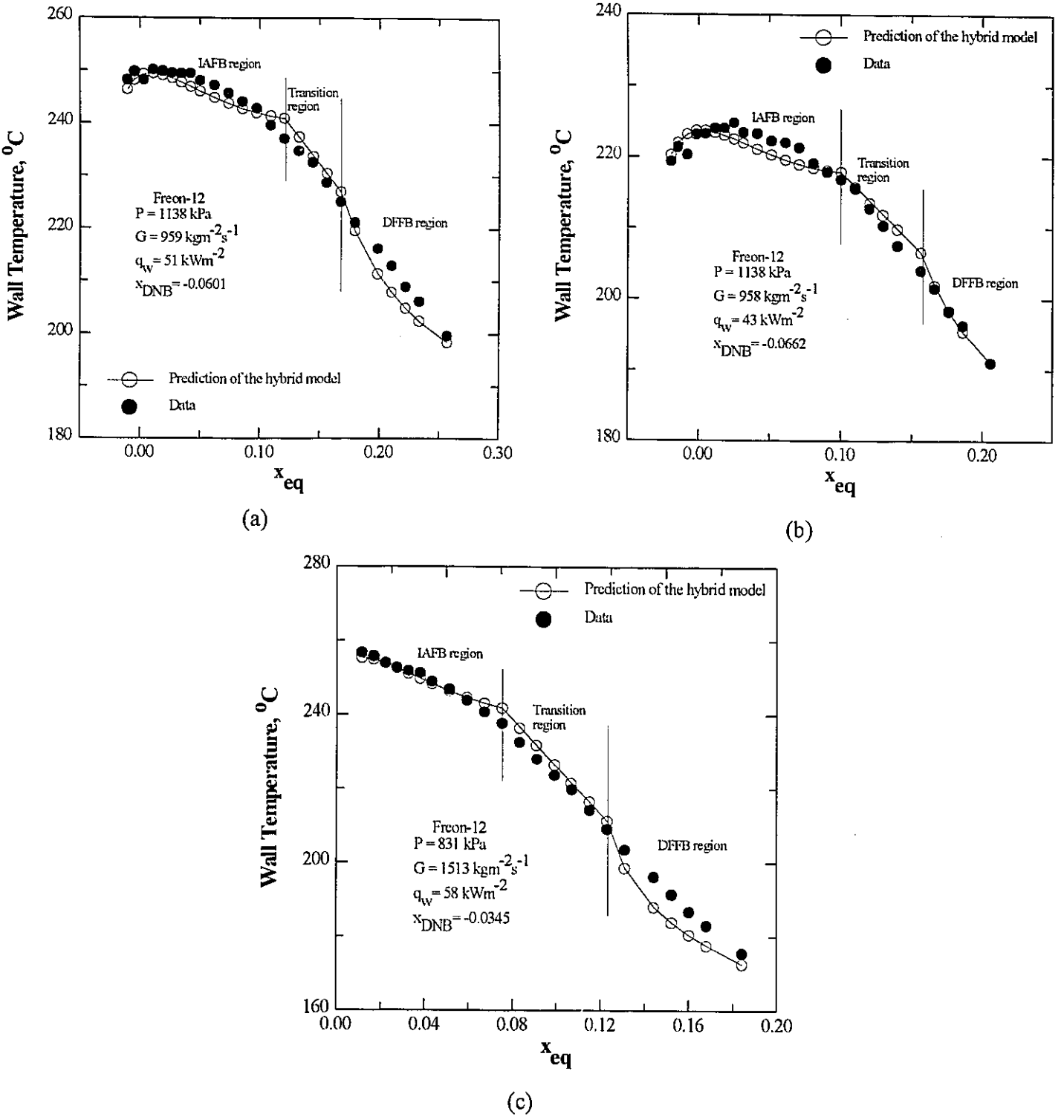

Figure 17.10 Comparison of the hybrid model predictions with Freon-12 data.

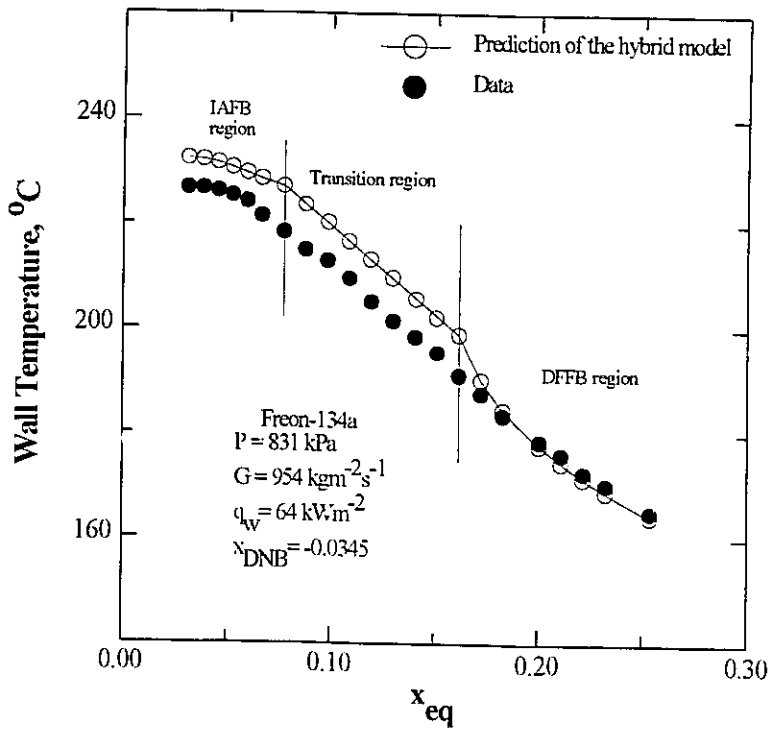

(a)

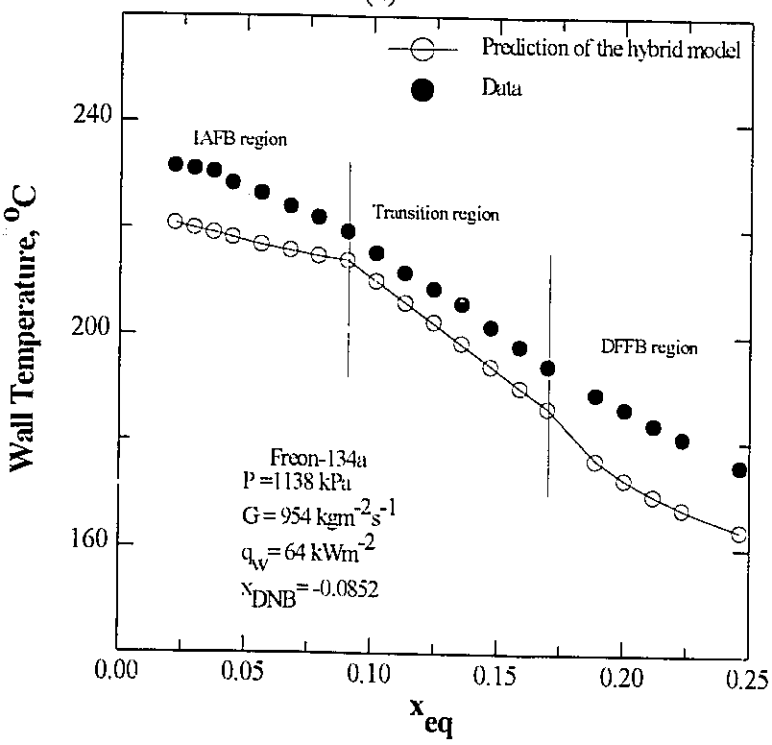

(b)

Figure 17.11 Comparison of the hybrid model predictions with Freon-134a data.

Chapter 18 CONCLUSIONS AND FINAL REMARKS

18.1 Conclusions

1. Experimental results of the heat transfer coefficients and wall temperatures for up-flow in a tube have been presented. About 8120 tube film boiling data were obtained. To the author's knowledge, the data obtained using R-134a and R-22 are the first-ever flow film boiling data covering a wide range of flow conditions. The data cover a mass flux range of 530 to 3000 $kgm^{-2}s^{-1}$, an inlet subcooling range of 6 to 28°C, and a pressure range of 0.83 to 1.4 MPa (corresponding to an equivalent water pressure range of 5 to 7 MPa, based on an equal liquid-to-vapour density ratio).

2. Results from the present study show that R-134a is a better coolant in film boiling than R-12 and R-22, and it is a suitable fluid to use in post-CHF experiments. R-134a has a zero ODP (ozone depletion potential), and for this reason has been selected as a replacement fluid for R-12.

3. The data show complex trends of the heat transfer coefficient in terms of the thermodynamic equilibrium quality. Different heat transfer regions, which correspond to different flow patterns, are identified for low and high mass flux conditions. The heat transfer coefficient decreases steeply with an increase in quality in region I, it increases slightly with quality in regions II and IV, and it may increase or decrease with quality in region III.

4. In general, the heat transfer coefficient is very sensitive to flow parameters such as pressure, mass flux, inlet subcooling and heat flux. Chapter 11 discussed in detail the parametric

trends and their effects on the heat transfer coefficient.

5. The ratio (h/h_{hom}) is a suitable post-CHF modelling parameter, as it effectively reduces the effect of differences in physical properties of the fluid on post-CHF heat transfer.

6. There is a strong non-equilibrium effect on the heat transfer coefficient in the subcooled IAFB region. This effect is less pronounced at low x_{eq} in the positive quality region.

7. The thermodynamic equilibrium quality can be used as an independent correlating variable in heat transfer regions III and IV.

8. The heat transfer coefficient exhibits a minimum in the subcooled IAFB region, where, for very high subcooling, the heat transfer becomes conduction controlled and the heat transfer coefficient increases with increasing local subcooling in the negative quality region. This minimum is not affected by the variation in wall heat flux; however, it is very sensitive to inlet subcooling.

9. Various post-CHF prediction methods have been reviewed and assessed during this study, using data generated from this study and data from the Chalk River Laboratories (CRL) PDO data bank for water. Their prediction accuracy and parametric trends have been examined over a wide range of flow conditions.

10. Results of the assessment show that for the DFFB regime, the Groeneveld-Delorme correlation provides accurate predictions for steam-water flow at moderate-to-high pressures (7-20 MPa) and medium-to-high mass fluxes (1000-5000 $kgm^{-2}s^{-1}$). The Shah correlation gives comparable prediction accuracy to the Groeneveld-Delorme correlation, but it has a narrower range of applicability. The Shah correlation has the advantage of being valid for various fluids, whereas the Groeneveld-Delorme correlation is primarily applicable to steam-

water flow. For the inverted annular flow boiling (IAFB) regime, none of the existing prediction methods is capable of providing accurate predictions for a wide range of flow conditions.

11. Due to the limited applicability of existing IAFB prediction methods, a two-fluid one-dimensional model has been developed to predict the surface temperature of a tube in IAFB at low-to-high pressure and low-to-high flow conditions. The model predictions have been compared with data from four fluids (water, Freon-12, Freon-22, and Freon-134a). The model gives the least RMS error when compared to the various IAFB prediction methods assessed during the course of this study. The overall RMS errors of the predictions are 5.67%, 6.19%, 6.58%, and 14.90% for the data of Freon-12, Freon-134a, Freon-22, and water, respectively. Also, a hybrid post-CHF model is derived by combining the two-fluid model of IAFB with the slightly modified Moose and Ganić [1982] model, to predict heated surface temperatures over the whole subcooled film boiling region. Comparison between the hybrid model predictions and experimental data showed good agreement.

12. A different approach of developing constitutive relations for two-fluid IAFB models was needed, due to the inconsistencies and limitations these relations impose on IAFB prediction methods of IAFB. In this study, a unique methodology of developing constitutive relations has been proposed, and discussed in Chapter 14. Even though the constitutive relations derived for the new two-fluid model are very approximate and crude, it is of interest to see how well the method works compared to others.

13. A computer code for the predictions of the thermophysical properties of Freon-22 has been developed during this study. This code is integrated with the University of Ottawa property

code (see Appendix D), which is now capable of predicting thermophysical properties of 24 fluids.

18.2 Final Remarks

1. Although an appreciable amount of low-quality film boiling data, with water as the working fluid, has been generated in recent years, it has been discovered during the course of this study that there are some inaccuracies and discrepancies within the data base, and in some instances data from different sources are inconsistent. Therefore, it is highly desirable to thoroughly examine the existing water data base, and to generate more data covering the same conditions as the existing one, for the purpose of comparison.

2. During this study, data of Freon-134a has been used to examine the accuracy of various IAFB prediction methods; however, it has been realized that the predictions of Freon-134a vapour superheat properties (i.e., k_v, μ_v, Cp_v, etc.) may not be accurate. Hence, a complete study of vapour superheat Freon-134a properties should be considered in the future, especially since this fluid is now a substitute for Freon-12.

3. The theoretical model of this study has been developed to demonstrate primarily the adequacy of the modelling approach proposed in Chapter 14. Consequently, the constitutive relations have not been rigorously derived. Despite the simplifying assumptions used to derive these relations, relatively good agreement has been obtained between model predictions and the data. Hence, it is suggested that refinement of these relations should be pursued in the future, to further improve the model predictions.

4. In highly subcooled film boiling, the vapour film at the heated surface is very thin over most of the IAFB length. All prediction methods, including the new model, overpredict the wall

temperatures by a significant margin. This might be an indication that the heat transfer relations used in these prediction methods are no longer applicable for a very thin film. Therefore, equations developed for heat transfer rates for flow in very small gaps should be considered. A thorough literature survey of such relations may prove very useful.

5. In the experimental program of this study, data of low-quality dispersed flow were obtained. The DFFB regime was created from the break-up of the liquid core of the IAFB regime. DFFB prediction methods are usually assessed against data of high-quality DFFB. High-quality DFFB is present downstream of an annular film dryout. It would be of practical interest to examine DFFB prediction methods against the data of low-quality DFFB, and to compare the flow characteristics of both types of DFFB regimes (i.e., drop formation and size).

REFERENCES

Adachi, Y., Lu, B. C. Y. and Sugie, H. 1983. A four parameter equation of state. *Fluid Phase Equilibria, Vol. 11, 29-48.*

Analytis, G. Th. and Yadigaroglu, G. 1987. Analytical modeling of Inverted Annular Film Boiling. *Nucl. Engrg. Des., Vol. 99, 201-212.*

Andersen, J. G. M. 1976. Low flow film boiling heat transfer on vertical surfaces -Part I: Theoretical model. *Presented at the 16th National Heat Transfer Conf., AIChE-52, St. Louis.*

Andreani, M. and Yadigaroglu, G. 1994 Prediction methods for dispersed flow film boiling. *Int. J. Multiphase Flow 20, 1-51.*

Bailey, N. A. 1972. The interaction of droplet and forced convection in post dryout heat transfer at high subcritical pressures. *European Two-Phase Flow Group Meeting, Rome.*

Baum, A. J., Purcupile, J. C. and Dougall, R. S. 1978. Transition and film boiling heat transfer from vertical surfaces. *6th Int. Heat Transfer Conf., Toronto.*

Beattie, D. R. H. 1975. Friction factors and regime transitions in high pressure steam-water flows. ASME Publication 75-WA/HT-4.

Becker, K. M., Ling C. H., Heelberg, S. and Strand G. 1983. An experimental investigation of post dryout heat transfer. *KTH-NEL-33, Sweden.*

Bennett, A. W., Kearsey, H. A. and Keeys, R. K. F. 1964. Heat transfer to mixtures of high pressure

steam and water in an annulus. *Part VI, AERE-R-4352.*

Bennett, A. W., Hewitt, G. F., Kearsey, H. A. and Keeys, R. K. F. 1967. Heat transfer to steam water mixtures flowing in uniformly heated tubes in which the critical heat flux has been exceeded. *AERE-R-5373.*

Berenson, P. J. 1961. Film-boiling heat transfer from a horizontal surface *J. Heat Transfer 83, 351-358.*

Bertoletti, S. 1961. Heat transfer and pressure drop with steam water spray. *CISE R-36.*

Bertoletti, S., Lombardi G. and Silvestri M. 1964. Heat transfer to steam water mixtures. *Topical Report #9, CISE R-78.*

Bhatti, M. S. and Shah, R. K. 1987. Turbulent and transition flow convective heat transfer in ducts. *Handbook of single-phase convective heat transfer* (Editors: Kakaç, S., Shah, R. K. and Aung, W.), John Wiley & Sons Publication, New York.

Bishop, A. A., Efferding, L. E. and Tong, L. S. 1962. A review of heat transfer and fluid flow of water in the supercritical region and during 'Once-Thru' operation. *WCAP-2040.*

Bishop, A. A., Sandberg, R. O. and Tong, L. S. 1964. High temperature supercritical pressure water loop. Part V: Forced convection heat transfer to water after the Critical Heat Flux at high supercritical pressures. *WCAP-2056.*

Bishop, A. A., Sandberg, R. O. and Tong, L. S. 1964. Forced convection heat transfer at high pressure after the critical heat flux. *ASME-65-HT-31.*

Bishop, A. A., Sandberg, R. O. and Tong, L. S. 1965. Forced convection heat transfer at high

pressure after the critical heat flux. *ASME-65-HT-31.*

Breen, B. P. and Westwater, J. W. 1962. Effect of diameter of horizontal tubes on film boiling heat transfer. *Chem. Eng. Prog., AIChE, Vol. 58, No. 7, 67-72.*

Brevi, R., Cumo, M., Palmieri, A. and Pitimada, D. 1969. Heat transfer coefficient in post-dryout two-phase mixtures. *European Two-Phase Group Meeting. Karlsruhe.*

Bromley, L. A. 1950. Heat transfer in stable film boiling. *Chem. Eng. Prog., Vol. 46, No. 5, 211-227.*

Bromley, L. A. 1952. Effect of heat capacity on condensate. *Ind. Eng. Chem., Vol. 44, 2966-2969.*

Bromley, L. A., LeRoy, N. R. and Robbers, J. A. 1953. Heat transfer in forced convective film boiling. *Ind. Eng. Chem., Vol. 45, 2639-2646.*

Cachard, de F. 1994. Development, implementation and assessment of specific closure laws for inverted-annular film-boiling in a two-fluid model. *Paul Scherrer Institute (PSI) Report 94-16.*

Chan, K. C. and Yadigaroglu, G. 1980. Calculations of film boiling heat transfer above the quench front during reflooding. *Experimental and Analytical Modelling of LWR Safety Experiments, ASME Publication HTD-Vol. 7.*

Chen, Y. and Li, J. 1984. Subcooled flow film boiling of water at atmospheric pressure. In *"Two-Phase Flow and Heat Transfer," 141-150, Eds: Chen, X. -J and Veziroglu, T. N., Hemisphere Publ. Co.*

Chen, Y. 1987. Experimental study of inverted annular flow film boiling heat transfer of water. *In "Heat Transfer Science and Technology," 627-634, Eds: Wang, B. -X, Hemisphere Publ. Co.*

Chen, Y. Z., Fu, X. Y. and Chen S. 1988. Experimental and analytical study of Inverted Annular Film Boiling with forced flow water. *1st World Conf. on Exp. Heat Transfer, Fluid Mechanics, Thermodynamics, Dubrovnik, Yugoslavia, Sept.*

Chen, Y. Z., Cheng, P., Wang, J. W. and Young, M. 1989. Experimental results of subcooled and low quality film boiling heat transfer of water in vertical tubes at moderate pressure. *Proceedings 4th Int. Topical Meeting on Nucl. Reactor Thermal-Hydraulics, Vol. 2, Oct. 10-13.*

Chen, Y., Wang, J., Yang, M. and Fu, X. 1989. Experimental measurement of the minimum film boiling temperature of flowing water. *Multiphase Flow and Heat Transfer, 2nd Int. Symp.*

Chen, Y.-Z. and Chen, H.-Y. 1993. A model of dispersed flow film boiling heat transfer of water. *Proceedings of the 10th Int. Heat transfer Conf., Vol. 7.*

Chen, J. C., Ozkaynak, F. T. and Sundaram, R. K. 1979. Vapor heat transfer in post-CHF region including the effect of thermodynamic non-equilibrium. *Nucl. Engng. Design 51, 143-155.*

Chen, J. C., Morgan, C. D. and Sundaram, R. K. 1984. A correlation of low flow, low pressure, and low-to-moderate quality post-CHF data. *In First Int. Workshop on Fundamental Aspects of Post-dryout Heat Transfer, 2-4 April, Salt Lake City, UT, U.S.A NUREG/CP-0060.*

Chen, J. C. 1986. A short review of dispersed flow heat transfer in post-dryout boiling. *Nucl. Engng Design 95, 375-383.*

Cheng, S. C., Lau, P. W. K. and Poon, K. T. 1985. Measurements of true quench temperature of subcooled water under forced convective conditions. *Int. J. Heat Mass Transfer, Vol. 28, No. 1, 235-243.*

Cheng, S.C. and Nguyen, C. 1989. U. O. Property code for light water. *Proceedings of the SCS*

Western Multiconference on Modeling and Simulation on Microcomputers, San Diego, California, 138-141, Jan. 4-6.

Chi, J. W. H. 1966. Forced convection boiling heat transfer to hydrogen. *J. Spacecr. Rockets, Vol. 3, 150.*

Chi, J. W. H. 1967. Slug flow and film boiling of hydrogen. J. *Spacecr. Rockets, Vol. 4, 1329.*

Chi, J. W. H. and Pierse, B. L. 1970. An experimental and analytical study of film boiling heat transfer to hydrogen. *AIAA Propulsion Joint Specialist Conf., 6th, San Diego.*

Collier, J. G. 1962. Heat transfer and fluid dynamic research applied to fog cooled reactors. Atomic of Energy Canada Limited, *Report AECL-1631.*

Collier, J. G. 1980. Convective boiling and condensation. *2nd Ed, McGraw-Hill, London.*

Collier, J. G. 1981. Post dryout heat transfer. *In "Two-Phase Flow and Heat Transfer in the Power and Process Industries," 282-324, Eds: Bergles, A. E., Collier, J. G., Delhaye, J. M., Hewitt, G. F. and Mayinger, F., Hemisphere publishing corporation.*

Costigan, G. and Wade, C. D. 1984. Visualization of the reflooding of a vertical tube by dynamic neutron radiography. *Int. Workshop on Post-Dryout Heat Transfer, Salt Lake City, Utah 1984, April 1-4.*

Cumo, M. and Farello, G. E. 1967. Heated wall droplet interaction for two phase flow heat transfer in liquid deficient region. *Proceedings Symposium on two phase flow dynamics. Eindhoven, Vol. II, 1325-1357.*

Cumo, M. and Urbani, G. C. 1974. Post-burnout heat transfer (Attainable precision limits of the

measured coefficient). *CNEN/RT/ING(74)24.*

De Jarlais, G. and Ishii, M. 1983a. Hydrodynamic stability of inverted annular flow in a adiabatic simulation. *Interfacial Transport Phenomena HTD 23*, ASME Proc., 75-83.

De Jarlais, G. and Ishii, M. 183b. Hydrodynamic of adiabatic inverted annular flow-an experimental study. *3rd Multiphase Flow and Heat Transfer Symposium, Miami Beach, Florida* .

Delhaye, J. M. 1969. Equations fondamentales des écoulements diphasiques. *CEA-R-3429.*

Delhaye, J. M. 1981. Basic equations for two-phase flow modeling. in *"Two-phase flow and heat transfer in the power and process industries"* (Edited by Bergles, A. E., Collier, J. G., Delhaye, J. M., Hewitt, G. F. and Mayinger, F.). Hemisphere Publishing. New York.

Denham, M. K. 1984. Inverted Annular Film Boiling and the Bromley model. *IChE Symp. Series 86, 13-23.*

Diller, D. E., Aragon, A. S. and Laesecke, A. 1991. Measurement of viscosities of saturated and compressed liquid 1,1,1,2-tetrafluoroethane (R134a), 2,2-dichloro-1,1,1-trifluoroethane (R123) and 1,1-dichloro-1-1fluoroethane (R141b). *Proceedings of the 11th Symposium on Thermophysical Properties, Boulder, Colorado, June 23-27.*

Dittus, F. W. and Boelter, L. M. K. 1930. Heat transfer in automobile radiators of the tubular type. *University of California Publications 2, 443-461.*

Donevski, B., Chang, J. S. and Groeneveld, D. C. 1992. Prediction methods for interfacial parameters used in inverted annular film boiling. *Int. J. Heat and Technology, Vol. 10, No. 3.4, 43-70.*

Dougall, R.S and Rohsenow, W. M. 1963. Film boiling in the inside of vertical tubes with upward flow of the fluid at low qualities. *MIT Report 9079-26.*

Elias, E. and Chambré, P. 1981. Inverted-Annular Film Boiling heat transfer from vertical surfaces. *Nucl. Engrg. Des., Vol. 64, 249-257.*

Ellion, M. E. 1954. A study of the mechanism of boiling heat transfer. *Ph.D. thesis, California Institute of Technology.*

Era, A., Gaspari, G. P., Hassid, A., Milani, A. and Zavattarelli, R. 1967. Heat transfer data in the liquid defficient region for steam-water mixtures at 70 kg/cm^2 flowing in tubular and annular conduits. *CISE R-184.*

Forslund, R. P. and Rohsenow, W. M. 1968. Dispersed flow film boiling. *ASME Paper No. 68-HT-44.*

Fung, K. K., Gardiner, S. R., M. and Groeneveld, D. C. 1979. Subcooled and low quality flow film boiling of water at atmospheric pressure. *Nucl. Engrg. Des., Vol. 55, 51.*

Fung, K. K. 1981. Subcooled and low quality film boiling of water in vertical flow at atmospheric pressure. *Ph.D. thesis, Univ. of Ottawa, Ottawa, Canada.*

Ganić, E. N. and Rohsenow, W. M. 1976. Dispersed flow heat transfer. *Int. J. Heat Mass Transfer 20, 855-866.*

Goodman, J. and Elias, E. 1978. *Trans. ANS, 398. CRC Press.*

Gottula, R. C., Condie, K. G., Sundaram, R. K., Neti, S., Chen, J. C., and Nelson, R. A., 1985. *Forced convective, non-equilibrium, post-CHF heat transfer. Experiment data and correlation*

comparison report. NUREG/CR-3193, March 1985.

Groeneveld, D. C. 1969. An investigation of heat transfer in the liquid defficient regime. Atomic Energy of Canada Limited, *Report AECL-3281.*

Groeneveld, D. C. 1972. The thermal behaviour of a heated surface at and beyond dryout. Atomic Energy of Canada Limited , *Report AECL-4309.*

Groeneveld, D. C. 1973. Forced convective heat transfer to superheated steam in rod bundle. Atomic Energy of Canada Limited, *Report AECL-4450.*

Groeneveld, D. C. 1975. Post-dryout heat transfer: Physical mechanisms and a survey of prediction methods. *Nucl. Engng Design 32, 283-294.*

Groeneveld, D. C. and Delorme, G. G. J. 1976. Prediction of thermal non-equilibrium in the post-dryout regime. *Nucl. Engng Design 36, 17-26.*

Groeneveld, D. C. and Gardiner, S. R. M. 1977. Post-CHF heat transfer under forced convective conditions. *ASME Symposium on the Thermal and Hydraulic Aspects of Nuclear Reactor Safety 1, 43-73*, Eds: Jones, O. C. and Bankoff, S. G.

Groeneveld, D. C. 1978. A method of obtaining flow film boiling data for subcooled water, *Int. J. Heat Mass Transfer* **21**, 664-665.

Groeneveld, D.C. 1984. Inverted annular and low quality film boiling: a state-of-the-art report. *Paper Presented at the Int. Workshop on Post-Dryout Heat Transfer, Salt Lake City, April 1-4.*

Groeneveld, D.C. and Snoek, C. W. 1986. A comprehensive examination of heat transfer correlations suitable for reactor safety analysis. Multiphase Science and Technology, Vol. II, 181-

Groeneveld, D.C. 1992. Inverted annular and low quality film boiling: a state-of-the-art report. Presented in *"Post-dryout heat transfer" book edited by Hewitt, G. F., Delhaye, J. M. and Zuber, N.*

Hadaller, G. and Banerjee, S. 1969. Heat transfer to superheated steam in round tubes. *Atomic Energy of Canada, Internal Report WDI-147.*

Hammouda, N., Cheng, S. C. and Groeneveld, D. C. 1990. Revised thermodynamic and transport properties evaluation for non-polar fluids, Special Report. *AECL contract, 94 pages, July 1990.*

Hammouda, N. and Cheng, S. C. 1991. Thermophysical properties of refrigerant 22 using the revised UO property code (MOD2). *Special Report, AECL contract, 96 pages, March 1991.*

Hammouda, N., Cheng, S. C. and Groeneveld, D. C. 1992. Thermodynamic and transport properties evaluation for nonpolar fluids. *ASME, HTD-Vol. 225, pp. 25-34.*

Hammouda, N., Cheng, S. C., Groeneveld, D. C., Tain, R. M. and Doerffer, S. 1993a. Thermodynamic and transport properties evaluation for nonpolar fluids and property code MOD3. *Special Report, AECL contract, Purchase Order C83041, March .*

Hammouda, N., Cheng, S. C. and Groeneveld, D. C. 1993b. Evaluation of thermophysical properties of Freon-22. *Wärme- und Stoffübertragung, Vol. 28, pp. 387-395.*

Han, S. H. and Bankoff, S. G. 1982. Film boiling from a vertical jet of fuel entering a water pool. *Nucl. Engrg. Des., Vol. 75, 81-86.*

Hein, D. and Kohler, W. 1984. A simple-to-use post-dryout heat transfer model accounting for

thermal non-equilibrium. *In First Int. Workshop on Fundamental Aspects of Post-dryout Heat Transfer, 2-4 April, Salt Lake City, UT, U.S.A NUREG/CP-0060.*

Heineman, J. B. 1960. An experimental investigation of heat transfer to superheated steam in round and rectangular channels. *ANL-6213.*

Hench, J. E. 1964. Forced flow transition boiling experiments in a two-rod test section at high pressures. *ASME 64-WA/HT-44.*

Herkenrath, H., Mörk-Mörkenstein, P., Jung, U. and Weckermann, F.-J. 1967. Wärmeübergang an Wasser bei Erzwungener Strömung im Druckbereich von 140 bis 250 bar. *EUR-3658d.*

Hsu, C., Guo, Z., Yan, A., and Bi, H. 1984. Low pressure and subcooled water flow film boiling research by visual method. *In "Two-Phase Flow and Heat Transfer," 471-482, Eds: Chen, X. -J. and Veziroglu, T. N., Hemisphere Publ. Co.*

Hsu, Y. Y. and Westwater, J. W. 1959. Approximate theory for film boiling on vertical surfaces. Chem. Engrg. Progress (Symposium), AIChE, Heat Transfer Conf., Storrs, Conn., Vol. 56, 15-24.

Huang, X. C., Vasic, A. and Cheng, S. C. 1995. Heat balance tests and evaluation of R-134a thermal property prediction methods. *Private communication between Huang, X. C. and Groeneveld, D. C.*

Hynek, S. J., Rohsenow, W. M. and Bergles, A. B. 1969. Forced convection dispersed flow film boiling. *MIT Heat Transfer Lab. Report No. DSR 70586-63.*

Iloeje, O. C., Plummer, D. N., Rohsenow, W. M. and Grifith, P. 1974. A Study of wall rewet and heat transfer in dispersed vertical flow. *MIT Report No. 727718-92, Sep.*

Inoue, A., Aoki, S., Aritomi, M. and Hanawa, K. 1982. Study in inverted annular flow. *19th*

National Heat Transfer Symposium of Japan, 418-420.

Ishii, M. 1975. Thermo-fluid dynamic theory of two-phase flow. Eyrolles.

Ishii, M. and Mishima, K. 1984. Two-fluid model and hydrodynamic constitutive relations. *Nucl. Eng. Des., 86.*

Ishii, M. and Denton, J. P. 1988. Experimental study of two-phase flow behaviour of the post critical heat flux region. *Japan-U.S. Seminar on Two-Phase Flow Dynamics, Ohtsu, Japan .*

Ishii, M. and De Jarlais, G. 1987. Flow visualization study of inverted annular flow of post-dryout heat transfer region. *Nucl. Engng. Design* **99**, 187-199.

Ishii, M. 1992. Flow phenomena in post-dryout heat transfer. In *Post-Dryout Heat Transfer* (Edited by Hewitt, G. F., Delhaye, J. M. and Zuber, N.), Chap. 4, CRC Press, Inc.

Johannsen, K. 1988. Low quality transition and inverted annular flow film boiling of water: An updated review. In *"Experimental Heat Transfer, Fluid Mechanics and Thermodynamics", 1416-1429, Eds: Shah, R. K., Ganic, E. N. and Young, K. T., Elsevier Science Publishing Co.*

Johannsen, K. and Mosaad, M. 1989. Assessment of heat transfer correlations for subcooled and low quality film boiling of water in a vertical tube. *Multiphase Flow and Heat Transfer, 2nd Int. Symp.*

Jones, Jr. O. C. and Zuber, N. 1977. Post-CHF heat transfer: A non-equilibrium, relaxation model. *ASME paper 77-HT-79.*

Kalinin, E. K., Koshkin, V. K., Yarkho, S. R., Berlin, I. I., Kochelov, Y. S., Kostyuk, V. V., Korolev, A. L. and Sdobnov, G. N. 1970. Investigation of film boiling in tubes with subcooled nitrogen flow. *4th Int. Heat Transfer Conf., B4.5, Paris.*

Kalinin, E. K., Balashov, G. I., Berlin, I. I., Kostyuk, V. V. and Liventsov, V.M. 1977. A mathematical model of heat transfer for forced-convective film boiling. *J. of Engrg. Phys., Vol. 99, 201-212.*

Kaminaga, F. 1981. Heat transfer model for dispersed flow regime during reflooding. *J. Nucl. Sci. Technol., Vol. 18, 6-14.*

Kaufman, J. M. 1976. Post critical heat flux heat transfer to water in a vertical tube. *M. Sc. Thesis, MIT.*

Kawaji, M. and Banerji, S. 1983. A two-fluid model for reflooding of a vertical tube: Structure and stability of the Inverted Annular Flow model. *AIChE Symp. Series 225, Vol. 79, 236-249.*

Kays, W. M. and Crawford, M. E. 1980. Convective heat and mass transfer. *2nd Edition, McGraw-Hill Book Co.*

Keeys, R. K. F., Ralph, J. C. and Roberts, D. N. 1971. Post burnout heat transfer in high pressure steam-water mixtures in a tube with a cosine heat flux distribution. *AERE-R6411.*

Koizumi, Y., Ueda, T. and Tanaka, H. 1979. Post dryout heat transfer to R-113 upward flow in a vertical tube. *Int. J. Heat Mass Transfer, Vol. 22, 669-678.*

Koizumi, Y., Yonomoto, T., Kumamaru, H. and Tasaka, K. 1988. Post-dryout heat transfer coefficient of high pressure steam-water two-phase flow in multi-rod bundle. *Nucl. Sci. Technol., Vol. 25, 104-106.*

Kumamaru, H., Koizumi, Y. and Tasaka, K. 1987. Investigation of pre- and post-dryout heat transfer of steam-water two-phase flow in a rod bundle. *Nucl. Engng Design 102, 71-84.*

Laperrière, A. 1983. An analytical and experimental investigation of forced convective film boiling. *M. Sc. thesis, Univ. of Ottawa, Ottawa, Canada.*

Laverty, W. F. and Rohsenow, W. M. 1964. Film boiling of saturated liquid nitrogen flowing in a vertical tube. *J. Heat Transfer 89, 90-98.*

Lee, D. H. 1970. Studies of heat transfer and pressure drop relevant to sub-critical once-through evaporators. IAEA-SM-130/56. *IAEA Symp. on Progress in Sodium-Cooled Fast Reactor Engineering. Monaco.*

Lee, Y. and Kim, K. H. 1987. Inverted annular flow boiling. *Int. J. Multiphase Flow, Vol. 13, 345-355.*

Leung, L. K. H. and Groeneveld, D. C. 1988. Development of post-dryout look-up table for Loss-Of-Regulation Accident conditions. *RC-34 (also CANDEV-88-68).*

Mastanaiah, K. and Ganić, E. N. 1981. Heat transfer in two-component dispersed flow. *J. Heat Transfer, Vol. 103, 300-306.*

Mattson, R. J., Condie, K. G., Bengston, S. J. and Obenchain, C. F. 1974. Regression analysis of Post-CHF flow boiling data. *Fifth Int. Heat Transfer Conf. IV, B3.8, Tokyo.*

Mayinger, F. and Langner, H. 1978. Post-dryout heat transfer. *Proceedings of Sixth International Heat Transfer Conference, Toronto, Vol. 6, 181-198.*

McGinnis, F. K. and Holman, J. P. 1969. Individual droplet heat-transfer rates for splattering on hot surfaces. *Int. J. Heat Mass Transfer, Vol. 12, 95-108.*

McLinden, M. O., Gallagher, J. S., Weber, L. A., Morrison, G., Ward, D., Goodwin, A. R. H.,

Moldover, M. R., Schmidt, J. W., Chae, H. B., Bruno, T. J., Ely, J. F. and Huber, M. L. 1989. Measurement and formulation of the thermophysical properties of refrigerants 134a (1,1,1,2-Tetrafluoroethane) and 123 (1,1-Dichloro-2,2,2-Trifluoroethane). *ASHRAE Trans., Vol. 95, Part 2, 263.*

Miropol'skiy, Z. L. 1963. Heat transfer in film boiling of a steam water mixture in steam generating tubes. *Teploenergetika 10, 49-53.*

Moose, R. A. and Ganić, E. N. 1982. On the calculation of wall temperatures in the post dryout heat transfer region. *Int. J. Multiphase Flow 8, No. 5, 525-542.*

Mosaad, M. and Johannsen, K. 1988. Subcooled film boiling heat transfer to flowing water in a vertical tube at atmospheric pressure. *Int. Symp. on Phase Change Heat Transfer, Chong Qiung, China, May 20-23.*

Mosaad, M. and Johannsen, K. 1989. A new correlation for subcooled and low quality film boiling heat transfer of water at pressures from 0.1 to 8 MPa. *Proceedings Fourth International Topical Meeting on Nuclear Reactor Thermal-Hydraulics, Vol. 2, 10-13, October.*

Nijhawan, S., Chen, J. C., Sundaram, R. K. and London, E. J. 1980. Measurement of vapour superheat in post-critical heat flux boiling. *ASME J. Heat Transfer, Vol. 102, 450-470.*

Nishikawa, K., Yoshida, S., Mori, H. and Takamatsu, H. 1982. An experiment on the heat transfer characteristics in the post-burnout region at high subcritical pressures. *Nucl. Engng Design* 74, 233-239.

Nishikawa, K., Yoshida, S., Mori, H. and Takamatsu, H. 1986. Post-dryout heat transfer to freon in a vertical tube at high subcritical pressures. *Int. J. Heat Mass Transfer 29, 1245-1251.*

Ottosen, P. 1980. Experimental and theoretical investigation of inverse annular flow, important under LOCA conditions. *Riso National Lab Denmark, Report R-424.*

Plummer, D.N., Griffith, P. and Rohsenow, W. M. 1976. Post-critical heat transfer to flowing liquid in a vertical tube. *16th National Heat Transfer Conf., 76-CSME/ChE-13, St. Louis.*

Polomik, E. E., Levy, S. and Sawochka, S. G. 1961. Heat transfer coefficients with annular flow during once through boiling of water to 100% quality at 800, 1000. and 1400 psi. *GEAP-3703.*

Polomik, E. E. 1967. Transition boiling, heat transfer program, final summary report on Program for Feb. 63 - Oct. 67. *GEAP-5563.*

Rowe, D. S., Carver, M. B., Kiteley, J. C., Tahir, A. and Banas, A. O. 1988. ASSERT-IV theory manual. *CRNL-4221.*

Saha, P. 1980. A non-equilibrium heat transfer model for dispersed droplet post-dryout regime. *Int. J. Heat and Mass Transfer 23, 483-492.*

Schmidt, K. R. 1960. Thermodynamic investigations of highly loaded boiler heating surfaces. *AEC-TR-4033.*

Seban, S. 1983. Reflooding of a vertical tube at 1, 2 and 3 atmospheres. *EPRI Report NP-3191. (Reference is Taken from Analytis and Yadigaroglu, (1987)).*

Seban, R., Greif, R., Yadigaroglu, G., Elias, E., Yo, K., Abdolhahian, D. and Peake, W. 1978. *UC-B Reflood Program; Experimental Data Report. EPRI Report NP-743 (Reference is Taken from Analytis and Yadigaroglu, (1987).*

Shah, M. M. 1980. A general predictive technique for heat transfer during saturated film boiling in

tubes. *Heat Transfer Engineering 2, 51-62.*

Siegel, R. and Howell, J. R. 1972. Thermal radiation heat transfer. *McGraw-Hill, New York.*

Siviour, J. B. and Ede, A. J. 1970.Heat transfer in subcooled pool film boiling. 4th Int. Heat Transfer Conf., B3.12, Paris.

Slaughterbeck, D. C., Ybarrondo, L. J. and Obenchain, C. F. 1973. Flow film boiling heat transfer correlations: A parametric study with data comparisons. *ASME 73-HT-50.*

Stewart, J. C. and Groeneveld, D. C. 1982. Low quality and subcooled film boiling of water at elevated pressures. *Nucl. Engrg. Des., Vol. 67, 259.*

Stewart, J. C. 1981. Low quality film boiling at intermediate and elevated pressures. *M. Sc. thesis, Univ. of Ottawa, Ottawa, Canada.*

Styrikovich, M. A., Baryshev, YU. V., Grigorieva, M. E. and Tsiklauri, G. V. 1982. Investigation of heat transfer processes during film boiling in steam generating channel. *7th Int. Heat Transfer Conf., Munich, Germany.*

Swenson, H. S., Carver, J. R. and Szoeke, G. 1961. The effect of nucleate boiling versus film boiling on heat transfer in power boiler tubes. *ASME 61-WA-201.*

Swinnerton, D., Hood, M. L. and Pearson, K. G. 1988. Steady state post-dryout (experiments) at low quality and medium pressure: Data Report. *UKAEA Report AEEW-R2267.*

Tain, R.-M. 1994. An investigation of CHF fluid-to-fluid scaling and multi-fluid prediction techniques. *Ph.D. thesis, Univ. of Ottawa, Ottawa, Canada.*

Takenaka, N., Fujii, T., Akagawa, K. and Nishida, K. 1989. Flow pattern transition and heat transfer of Inverted Annular Flow. *Int. J. Multiphase Flow, Vol. 15, 767-785.*

Thurgood, M. J., Crowell, K. R. and Kelly, J. M. 1981. COBRA-TF equations and constitutive models. *Battelle, Pacific Northwest Laboratory.*

Tong, L. S. 1965. Boiling heat transfer and two-phase flow. *John Wiley and Sons.*

Tong, L. S. and Young, J. D. 1974. A phenomenological transition and film boiling heat transfer correlation. *Fifth Int. Heat Transfer Conf. IV, B3.9, Tokyo.*

Varone, A. F. and Rohsenow, W. M. 1984. Post-dryout heat transfer prediction. *In First Int. Workshop on Fundamental Aspects of Post-dryout Heat Transfer, 2-4 April, Salt Lake City, UT, U.S.A NUREG/CP-0060.*

Wallis, G. B. 1969a. One-dimensional two-phase flow. McGraw-Hill, New York.

Wallis, G. B. 1969b. Annular two-phase flow-Part I: A simple theory. *ASME Publication 69-FE-45.*

Wallis, G. B. 1969c. Annular two-phase flow-Part II: Additional effects. *ASME Publication 69-FE-46.*

Wang, S. W. and Weisman, J. 1983. Post-critical heat flux heat transfer: A Survey of current correlations and their applicability. *Progress in Nuclear Energy, Vol. 12, No. 2, 149-168.*

Wang, B. X. and Shi, D. H. 1984. A semi-empirical theory for forced-flow turbulent film boiling of subcooled liquid along a horizontal plate. *Int. J. Heat Mass Transfer, Vol. 28, 1499-1505.*

Wang, B. X. and Peng, X. F. 1988. Turbulent film boiling of saturated liquid flowing with high

velocity in a circular tube, in *"Experimental Heat Transfer, Fluid Mechanics, and Thermodynamics," Edited by Shah, R. K., Ganic, E. W. and Yang, K. T., Elsevier Science Publishing Co. Inc.*

Webb, S. W., Chen, J. C. and Sundaram, R. K. 1982. Vapor generation rate in nonequilibrium convective film boiling. *7th Int. Heat Transfer Conf., Munich, Germany.*

Webb, S. W. and Chen, J. C. 1984. A two-region vapor generation rate model for convective film boiling. *In First Int. Workshop on Fundamental Aspects of Post-dryout Heat Transfer, 2-4 April, Salt Lake City, UT, U.S.A NUREG/CP-0060.*

Webb, S. W., Chen, J. C. and Sundaram, R. K. 1982. Vapor generation rate in nonequilibrium convective film boiling. *7th Int. Heat Transfer Conf., Munich, Germany.*

Webb, S. W. and Chen, J. C. 1983. Inferring nonequilibrium vapour conditions in convective film boiling. *In Thermal-hydraulics of nuclear reactors (edited by Merilo, M.), ANS, Vol. 1, 326-334.*

Witte, L. C. and Lienhard, J. H. 1982. *Int. J. Heat Mass Transfer, Vol. 25, 771.*

Wong, Y. L., Cheng, S. C. and Groeneveld, D. C. 1990. Generalized thermodynamic and transport properties evaluation for nonpolar fluids. *Heat Transfer Engineering, Vol. 11, p. 60.*

Yadigaroglu, G. and Lahey, R. T. 1975. On the various forms of the conservation equations in two-phase flow. *Int. J. Multiphase flow.*

Yan, D. 1987. Subcooled forced convection film boiling heat transfer. *In "Heat Transfer Science and Technology," by Wang, B. X., 694-700, Hemisphere Publ., Washington.*

Yoder, G. L. and Rohsenow, W. M. 1983. A solution for dispersed flow heat transfer using

equilibrium fluid conditions. *J. Heat Transfer 105, 10-17.*

Zuber, N. 1958. On the stability of boiling heat transfer. *ASME Transactions, Vol. 80, 711-720.*

APPENDIX A CORRECTIONS USED IN DATA REDUCTION

A.1 Calculation of the Inside Wall Temperature

The temperature at the inside surface of the test section is estimated from the measured outside surface temperature, using a steady-state heat conduction equation for the tube wall. It is assumed that axial heat conduction is much smaller than radial heat conduction in the test section wall. Then, the governing heat conduction equation becomes

$$\frac{d^2T}{dr^2} + \frac{1}{r}\frac{dT}{dr} + \frac{q'''}{k} = 0 \qquad \textbf{(A.1.1)}$$

where q''' is the power generated per unit volume (W/m^3). Integration of Eq. (A.1.1) gives the equation for the temperature distribution in the wall as

$$T = -\frac{r^2 q'''}{4k} + C_1 \ln r + C_2 \qquad \textbf{(A.1.2)}$$

The boundary conditions are:

$$\begin{aligned} &at \quad r = r_o \qquad T = T_o \quad and \quad -k\frac{dT}{dr}\Big|_{r=r_o} = q_{loss} \\ &at \quad r = r_i \qquad T = T_i \end{aligned} \qquad \textbf{(A.1.3)}$$

where

r_i = inside tube radius

r_o = outside tube radius

T_i = inside wall temperature

T_o = outside wall temperature

From Eq. (A.1.3) it follows that

$$C_1 = \frac{q'''r_o^2 - 2q_{loss}r_o}{2k}$$

$$C_2 = T_o + \frac{q'''r_o^2}{4k} + \frac{2q_{loss}r_o - q'''r_o^2}{2k} lnr_o \qquad \textbf{(A.1.4)}$$

where q_{loss} is the heat loss from the outside surface of the tube wall through the insulation, and is calculated in section A.2.

The solution for T_i, in terms of T_o, q''' and q_{loss} is:

$$T_i = T_o + \frac{2q_{loss}r_o - q'''r_o^2}{2k} \ln\frac{r_o}{r_i} + (r_o^2 - r_i^2)\frac{q'''}{4k} \qquad \textbf{(A.1.5)}$$

where q''' can be expressed in terms of the inside wall heat flux, q_w, as

$$q''' = \frac{2q_w r_i + 2q_{loss}r_o}{(r_o^2 - r_i^2)} \qquad \textbf{(A.1.6)}$$

and

$$q_{loss} = f(T_o) \qquad \textbf{(A.1.7)}$$

L is the heated length (0.9 m).

The thermal conductivity, k, of Inconel 718 is evaluated from the manufacturer's data. A fit to this

data is given as

$$k\left(\frac{W}{m.^{o}C}\right) = 10.87101 + 0.016156\ T_o - 1.4x10^{-7}\ T_o^2 \qquad \textbf{(A.1.8)}$$

Typically, the temperature drop between the inside and outside surfaces of the tube is always less than 2 °C.

A.2 Test Section Heat Loss and Heat Balance

In order to accurately evaluate the heat flux at the inside surface of the test section, a heat balance test was conducted to determine the amount of heat lost to the surroundings. Two main heat losses were recognized: radial conduction through the insulation and axial conduction from the test section through the power clamps. A dry test was carried out in which the loop was first put under high vacuum using a high-capacity vacuum pump, then the test section was heated to the desired temperature. At each power level, sufficient time was allowed for the test section temperature to stabilize; the power to the test section is then equal to the heat loss. Near the end and start of the heated length, axial conduction was significant. Hence, only the heat loss at the location of zero axial temperature gradient was taken and a correlation of heat loss in terms of the outside wall temperature was derived:

$$Q_{loss}(W) = q_{loss}\ 2\pi r_o L = -0.66494 + 0.062663\ T_o + 216x10^{-6}T_o^2 \qquad \textbf{(A.2.1)}$$

For all the experiments conducted, the heat loss was always less than 3% of the total test section power.

The axial conduction losses at the ends of the test section were difficult to control and

determine. However, the experiments indicated that these losses influenced the temperature distribution only very near the ends of the test section. Therefore, thermocouple readings at the ends of the test section were not used in the data reduction.

A similar dry test was conducted to determine the heat loss in the hot patch. The equation derived is given as

$$Q_{hp}(W) = 2.732213 - 0.02757\,T_{hp} + 287.35x10^{-6}\,T_{hp}^{2} - 5.5x10^{-7}\,T_{hp}^{3} + 4.79x10^{-10}\,T_{hp}^{4} \qquad \text{(A.2.2)}$$

where T_{hp} is the hot-patch temperature in °C.

In order to verify the flow measurement, heat balance tests were later carried out by Huang et al. [1995] on the same loop and test section using Freon-22. Results showed good agreement, as shown in Tables A.1 (this table is reproduced from [Huang et al., 1995]). In Table A.1, P, m, T_{in}, T_{out}, Δh, Q, Q_{loss}, and P_{elec} represent the pressure, the mass flow rate, inlet temperature, outlet temperature, enthalpy difference between inlet and outlet, heat convected to the fluid, heat loss to the ambient, and the measured electric power, respectively.

Table A.1 Heat balance results for Freon-22

P (kPa)	m ($kgmin^{-1}$)	T_{in} (°C)	T_{out} (°C)	Δh (Jkg^{-1})	Q (W)	Q_{loss} (W)	P_{elec} (W)	Error (W)	Error %
1723	2.0	12.2	17.5	6318	210	7.2	219	1.8	0.8
1723	2.0	12.2	28.0	19165	636	11.1	647	0.9	0.14
1723	2.0	11.4	32.0	25259	838	15.7	873	19.3	2.21
1723	2.0	11.9	38.1	32650	1083	17.4	1116	15.6	1.40
1723	2.0	12.1	42.9	38967	1279	15.9	1323	28.1	2.12
1723	2.0	12.7	43.4	39030	1294	15.9	1329	18.1	1.36

APPENDIX B ERROR ANALYSIS

Detailed error analysis requires the determination of system variables that are most important for the experimental study. For this study, these variables are the mass flow rate, the pressure, the test section and hot patch powers, and the temperature. The uncertainties in these variables are related to the independent quantities that enter into their evaluation. In this appendix, error estimates for mass flow rate, pressure, power and temperature are presented. The combined uncertainties in measuring a dependent variable G can be obtained from the uncertainties in measuring the n-independent variables g_1, g_2, ..., g_n as follows:

$$(\delta G)^2 = \left(\frac{\partial G}{\partial g_1}\delta g_1\right)^2 + \left(\frac{\partial G}{\partial g_2}\delta g_2\right)^2 + \ldots + \left(\frac{\partial G}{\partial g_n}\delta g_n\right)^2 \qquad \textbf{(B.1)}$$

B.1 Temperature Measurement

There are two temperature measurements requiring estimation of their error: the liquid temperature at the inlet of the test section and the outside wall temperatures of the test section. The liquid temperature is measured by a sheathed K-type thermocouple. Errors in the inlet thermocouple are as follows:

1. Calibration. The standard limit of error for K-type thermocouple, as specified by the ASTM standard, is ± 0.75% or ± 2.2 °C, whichever is greater.

2. Reference junction error. Using an electronic ice point reference (an electric-equivalent ice bath), the reference junction error is estimated to be ± 0.0 °C.

3. Data acquisition error. The uncertainty in the data acquisition system is estimated to be ± 0.024% of full range.

Hence, the uncertainty in T_{in} is given by

$$Uncertainty \quad in \quad T_{in} = \left[(0.75)^2 + (0.024)^2\right]^{1/2} = \pm 0.75\% \qquad \textbf{(B.1.1)}$$

The temperature of the outside surface of the test section is measured by fine-wire gauge K-type thermocouples. The errors in these thermocouples are as follows:

1. Calibration. Each thermocouple is individually calibrated, and the uncertainty in all the calibrated thermocouples is estimated to be ± 0.5% (within the experimental temperature range of 80 °C to 310 °C). The ASTM standard specifies the special limits of error to be ± 0.4% or ± 1.1 °C, whichever is greater.

2. Reference junction. The reference junction error is estimated to be ±0.0 °C.

3. Data acquisition error. The uncertainty is estimated to be ± 0.024% of full range.

Hence, the uncertainty in T_w is given by

$$Uncertainty \quad in \quad T_{w} = \left[(0.5)^2 + (0.024)^2\right]^{1/2} = \pm 0.50\% \qquad \textbf{(B.1.2)}$$

B.2 Pressure Measurement

Errors associated with pressure transducer measurement are

1. Uncertainty in current, specified by the manufacturer as ± 0.25% of full scale.

2. Uncertainty in digital display meter, specified by the manufacturer as ± 1.0%.

Hence, the probable error in full scale is

$$\textit{Uncertainty in } P = \left[(0.25)^2 + (1)^2\right]^{1/2} = \pm 1.063\ \% \qquad \textbf{(B.2.1)}$$

B.3 Mass Flow Rate Measurement

Errors associated with the Coriolis mass flow meter are

1. Uncertainty in voltage specified by the manufacturer to be ± 0.25% of full scale.

2. Uncertainty in data acquisition system estimated to be± 0.024% of full range.

Hence, the uncertainty in W is

$$\textit{Uncertainty in } W = \left[(0.25)^2 + (0.024)^2\right]^{1/2} = \pm 0.25\ \% \qquad \textbf{(B.3.1)}$$

B.4 Power Measurement

Power to the test section is calculated from the measured current and voltage, and is given as

$$Q = V \cdot I \qquad \textbf{(B.4.1)}$$

where

Q = test section power

V = test section voltage

I = test section current

Then, the uncertainty interval, δQ, is given by

$$(\delta Q)^2 = \left(\frac{\partial Q}{\partial V}\delta V\right)^2 + \left(\frac{\partial Q}{\partial I}\delta I\right)^2 \qquad \textbf{(B.4.2)}$$

or

$$\left(\frac{\delta Q}{Q}\right)^2 = \left(\frac{\delta V}{V}\right)^2 + \left(\frac{\delta I}{I}\right)^2 \qquad \textbf{(B.4.3)}$$

Errors associated with current measurements are

1. Shunt error. The shunt has an estimated uncertainty of ± 0.25% of full scale.

2. Uncertainty in the Fluke 45 Multimeter, specified by the manufacturer to be ± 0.031% of full range.

Hence, the uncertainty in current measurement is

$$\textit{Uncertainty in } I = [(0.25)^2 + (0.031)^2]^{1/2} = \pm 0.25\% \qquad \textbf{(B.4.4)}$$

Errors associated with voltage measurements are

1. Uncertainty in voltage leads, estimated to be ± 0.4% (within the experimental range of 4.0 volts to 12 volts).

2. Uncertainty in the Multimeter, estimated to be ± 0.025% of full scale.

Thus, the uncertainty in V is

$$\textit{Uncertainty in } V = [(0.4)^2 + (0.025)^2]^{1/2} = \pm 0.40\% \qquad \textbf{(B.4.5)}$$

Errors associated with test section power measurement are

1. Error in current measurement.

2. Error in voltage measurement.

Hence, the uncertainty in power measurement is given from Eq. (B.4.3) as

$$\textit{Uncertainty in } Q = [(0.25)^2 + (0.40)^2]^{1/2} = \pm 0.47\% \qquad \textbf{(B.4.6)}$$

Power to the hot patch is calculated from the measured voltage and resistance, and is given as

$$Q_{hp} = \frac{V^2}{R} \qquad \textbf{(B.4.7)}$$

Then, applying Eq. (B.1) δQ_{hp} is

$$(\delta Q_{hp})^2 = \left(\frac{2V}{R}\delta V\right)^2 + \left(\frac{-V^2}{R^2}\delta R\right)^2 \qquad \textbf{(B.4.8)}$$

or

$$\left(\frac{\delta Q_{hp}}{Q_{hp}}\right)^2 = \left(2\frac{\delta V}{V}\right)^2 + \left(\frac{\delta R}{R}\right)^2 \qquad \textbf{(B.4.9)}$$

Errors associated with hot-patch power measurement are

1. Uncertainty in resistance measurement, estimated to be ± 1.3%.

2. Uncertainty in voltage measurement, which is the same as for the test section power measurement.

Hence, the uncertainty in hot-patch power measurement is

$$\textit{Uncertainty in } Q_{hp} = \left[(1.3)^2 + (2x0.40)^2\right]^{1/2} = \pm 1.53\,\% \qquad \textbf{(B.4.10)}$$

APPENDIX C DATA TABULATION

Due to the large volume of the data obtained during this study (over 8 000 data points), only part of it is listed here. This appendix presents three tables:

-Table C.1 lists the inside wall temperature data for Freon-12.

-Table C.2 lists the inside wall temperature data for Freon-134a.

-Table C.3 lists the inside wall temperature data for Freon-22.

Each table contains 12 colums, the format of which is shown below:

RUN	D	P OUT	G	Q_w	HOTP POW	X_{in}	X_{DNB}	Z	X_{eq}	T_w	T_{HP}
	(m)	(kPa)	(kg/m^2.s)	(W/m^2)	(W)			(cm)		(°C)	(°C)

The first column gives the run name. Each data run is identified by a run name composed of seven characters. The first five numbers in the run name give the month, the day and the year of the run, respectively. The last two characters serve as indices specific to a particular run. Columns two through twelve give the tube diameter (D), the mass flux (G), the heat flux (Q_w), the hot-patch power, the inlet quality (X_{in}), the CHF quality (X_{DNB}), the axial distance (Z), the equilibrium quality (X_{eq}), the tube inside wall temperature (T_w), and the hot-patch temperature (T_{HP}), respectively.

Table C.1 Inside Wall Temperature Data for Freon-12

RUN	D	P OUT	G	Q_w	HOTP POW	X_{in}	X_{exp}	Z	X_{eq}	T_w	T_{sat}
	(m)	(kPa)	(kg/m².s)	(W/m²)	(W)			(cm)		(°C)	(°C)
41294A1	0.00438	830.811	964.537	50960.68	61.509	-0.0970	-0.0605	1.0	-0.0249	265.22	266.3
41294A1	0.00438	830.811	964.537	50960.68	61.509	-0.0970	-0.0605	2.5	-0.0194	264.13	266.3
41294A1	0.00438	830.811	964.537	50960.68	61.509	-0.0970	-0.0605	4.0	-0.0140	261.62	266.3
41294A1	0.00438	830.811	964.537	50960.68	61.509	-0.0970	-0.0605	5.5	-0.0085	257.80	266.3
41294A1	0.00438	830.811	964.537	50960.68	61.509	-0.0970	-0.0605	7.0	-0.0030	259.01	266.3
41294A1	0.00438	830.811	964.537	50960.68	61.509	-0.0970	-0.0605	9.0	0.0042	257.82	266.3
41294A1	0.00438	830.811	964.537	50960.68	61.509	-0.0970	-0.0605	11.0	0.0115	260.41	266.3
41294A1	0.00438	830.811	964.537	50960.68	61.509	-0.0970	-0.0605	13.0	0.0188	260.18	266.3
41294A1	0.00438	830.811	964.537	50960.68	61.509	-0.0970	-0.0605	15.0	0.0261	259.74	266.3
41294A1	0.00438	830.811	964.537	50960.68	61.509	-0.0970	-0.0605	17.0	0.0334	259.27	266.3
41294A1	0.00438	830.811	964.537	50960.68	61.509	-0.0970	-0.0605	19.0	0.0407	258.71	266.3
41294A1	0.00438	830.811	964.537	50960.68	61.509	-0.0970	-0.0605	21.0	0.0480	256.48	266.3
41294A1	0.00438	830.811	964.537	50960.68	61.509	-0.0970	-0.0605	24.0	0.0589	254.46	266.3
41294A1	0.00438	830.811	964.537	50960.68	61.509	-0.0970	-0.0605	27.0	0.0698	252.31	266.3
41294A1	0.00438	830.811	964.537	50960.68	61.509	-0.0970	-0.0605	30.0	0.0808	250.49	266.3
41294A1	0.00438	830.811	964.537	50960.68	61.509	-0.0970	-0.0605	33.0	0.0917	248.52	266.3
41294A1	0.00438	830.811	964.537	50960.68	61.509	-0.0970	-0.0605	36.0	0.1026	244.72	266.3
41294A1	0.00438	830.811	964.537	50960.68	61.509	-0.0970	-0.0605	39.0	0.1136	241.69	266.3
41294A1	0.00438	830.811	964.537	50960.68	61.509	-0.0970	-0.0605	42.0	0.1245	238.75	266.3
41294A1	0.00438	830.811	964.537	50960.68	61.509	-0.0970	-0.0605	45.0	0.1354	236.01	266.3
41294A1	0.00438	830.811	964.537	50960.68	61.509	-0.0970	-0.0605	48.0	0.1464	231.38	266.3
41294A1	0.00438	830.811	964.537	50960.68	61.509	-0.0970	-0.0605	51.0	0.1573	227.14	266.3
41294A1	0.00438	830.811	964.537	50960.68	61.509	-0.0970	-0.0605	54.0	0.1682	222.59	266.3
41294A1	0.00438	830.811	964.537	50960.68	61.509	-0.0970	-0.0605	59.0	0.1865	216.47	266.3
41294A1	0.00438	830.811	964.537	50960.68	61.509	-0.0970	-0.0605	62.0	0.1974	212.73	266.3
41294A1	0.00438	830.811	964.537	50960.68	61.509	-0.0970	-0.0605	65.0	0.2083	208.16	266.3
41294A1	0.00438	830.811	964.537	50960.68	61.509	-0.0970	-0.0605	68.0	0.2193	204.75	266.3
41294A1	0.00438	830.811	964.537	50960.68	61.509	-0.0970	-0.0605	74.0	0.2411	197.64	266.3
41294A2	0.00438	830.811	958.544	42765.24	61.749	-0.0970	-0.0662	1.0	-0.0308	244.33	266.9
41294A2	0.00438	830.811	958.544	42765.24	61.749	-0.0970	-0.0662	2.5	-0.0262	237.02	266.9
41294A2	0.00438	830.811	958.544	42765.24	61.749	-0.0970	-0.0662	4.0	-0.0216	233.25	266.9
41294A2	0.00438	830.811	958.544	42765.24	61.749	-0.0970	-0.0662	5.5	-0.0170	229.30	266.9
41294A2	0.00438	830.811	958.544	42765.24	61.749	-0.0970	-0.0662	7.0	-0.0124	229.95	266.9
41294A2	0.00438	830.811	958.544	42765.24	61.749	-0.0970	-0.0662	9.0	-0.0062	228.82	266.9
41294A2	0.00438	830.811	958.544	42765.24	61.749	-0.0970	-0.0662	11.0	-0.0000	230.97	266.9
41294A2	0.00438	830.811	958.544	42765.24	61.749	-0.0970	-0.0662	13.0	0.0061	231.34	266.9
41294A2	0.00438	830.811	958.544	42765.24	61.749	-0.0970	-0.0662	15.0	0.0123	231.26	266.9
41294A2	0.00438	830.811	958.544	42765.24	61.749	-0.0970	-0.0662	17.0	0.0184	231.34	266.9
41294A2	0.00438	830.811	958.544	42765.24	61.749	-0.0970	-0.0662	19.0	0.0246	231.36	266.9
41294A2	0.00438	830.811	958.544	42765.24	61.749	-0.0970	-0.0662	21.0	0.0307	229.85	266.9
41294A2	0.00438	830.811	958.544	42765.24	61.749	-0.0970	-0.0662	24.0	0.0400	228.86	266.9
41294A2	0.00438	830.811	958.544	42765.24	61.749	-0.0970	-0.0662	27.0	0.0492	227.64	266.9
41294A2	0.00438	830.811	958.544	42765.24	61.749	-0.0970	-0.0662	30.0	0.0584	226.76	266.9
41294A2	0.00438	830.811	958.544	42765.24	61.749	-0.0970	-0.0662	33.0	0.0677	225.67	266.9
41294A2	0.00438	830.811	958.544	42765.24	61.749	-0.0970	-0.0662	36.0	0.0769	223.26	266.9
41294A2	0.00438	830.811	958.544	42765.24	61.749	-0.0970	-0.0662	39.0	0.0861	221.51	266.9
41294A2	0.00438	830.811	958.544	42765.24	61.749	-0.0970	-0.0662	42.0	0.0954	219.94	266.9
41294A2	0.00438	830.811	958.544	42765.24	61.749	-0.0970	-0.0662	45.0	0.1046	218.43	266.9
41294A2	0.00438	830.811	958.544	42765.24	61.749	-0.0970	-0.0662	48.0	0.1138	215.30	266.9
41294A2	0.00438	830.811	958.544	42765.24	61.749	-0.0970	-0.0662	51.0	0.1231	212.39	266.9
41294A2	0.00438	830.811	958.544	42765.24	61.749	-0.0970	-0.0662	54.0	0.1323	209.33	266.9
41294A2	0.00438	830.811	958.544	42765.24	61.749	-0.0970	-0.0662	59.0	0.1477	204.92	266.9
41294A2	0.00438	830.811	958.544	42765.24	61.749	-0.0970	-0.0662	62.0	0.1569	202.18	266.9
41294A2	0.00438	830.811	958.544	42765.24	61.749	-0.0970	-0.0662	65.0	0.1661	198.51	266.9
41294A2	0.00438	830.811	958.544	42765.24	61.749	-0.0970	-0.0662	68.0	0.1754	195.90	266.9
41294A2	0.00438	830.811	958.544	42765.24	61.749	-0.0970	-0.0662	74.0	0.1938	189.97	266.9
41294A3	0.00438	830.811	959.477	38979.22	63.901	-0.0970	-0.0689	1.0	-0.0328	234.11	267.1
41294A3	0.00438	830.811	959.477	38979.22	63.901	-0.0970	-0.0689	2.5	-0.0286	223.76	267.1
41294A3	0.00438	830.811	959.477	38979.22	63.901	-0.0970	-0.0689	4.0	-0.0243	219.10	267.1
41294A3	0.00438	830.811	959.477	38979.22	63.901	-0.0970	-0.0689	5.5	-0.0201	214.89	267.1
41294A3	0.00438	830.811	959.477	38979.22	63.901	-0.0970	-0.0689	7.0	-0.0159	215.17	267.1
41294A3	0.00438	830.811	959.477	38979.22	63.901	-0.0970	-0.0689	9.0	-0.0103	214.15	267.1
41294A3	0.00438	830.811	959.477	38979.22	63.901	-0.0970	-0.0689	11.0	-0.0047	216.23	267.1
41294A3	0.00438	830.811	959.477	38979.22	63.901	-0.0970	-0.0689	13.0	0.0009	216.47	267.1
41294A3	0.00438	830.811	959.477	38979.22	63.901	-0.0970	-0.0689	15.0	0.0065	216.71	267.1
41294A3	0.00438	830.811	959.477	38979.22	63.901	-0.0970	-0.0689	17.0	0.0121	216.92	267.1
41294A3	0.00438	830.811	959.477	38979.22	63.901	-0.0970	-0.0689	19.0	0.0177	217.13	267.1
41294A3	0.00438	830.811	959.477	38979.22	63.901	-0.0970	-0.0689	21.0	0.0233	215.79	267.1
41294A3	0.00438	830.811	959.477	38979.22	63.901	-0.0970	-0.0689	24.0	0.0317	215.15	267.1
41294A3	0.00438	830.811	959.477	38979.22	63.901	-0.0970	-0.0689	27.0	0.0401	214.09	267.1
41294A3	0.00438	830.811	959.477	38979.22	63.901	-0.0970	-0.0689	30.0	0.0485	214.05	267.1
41294A3	0.00438	830.811	959.477	38979.22	63.901	-0.0970	-0.0689	33.0	0.0569	213.23	267.1
41294A3	0.00438	830.811	959.477	38979.22	63.901	-0.0970	-0.0689	36.0	0.0653	211.29	267.1
41294A3	0.00438	830.811	959.477	38979.22	63.901	-0.0970	-0.0689	39.0	0.0737	209.87	267.1
41294A3	0.00438	830.811	959.477	38979.22	63.901	-0.0970	-0.0689	42.0	0.0821	208.91	267.1
41294A3	0.00438	830.811	959.477	38979.22	63.901	-0.0970	-0.0689	45.0	0.0905	208.13	267.1
41294A3	0.00438	830.811	959.477	38979.22	63.901	-0.0970	-0.0689	48.0	0.0990	205.58	267.1
41294A3	0.00438	830.811	959.477	38979.22	63.901	-0.0970	-0.0689	51.0	0.1074	203.25	267.1
41294A3	0.00438	830.811	959.477	38979.22	63.901	-0.0970	-0.0689	54.0	0.1158	200.59	267.1
41294A3	0.00438	830.811	959.477	38979.22	63.901	-0.0970	-0.0689	59.0	0.1298	197.39	267.1
41294A3	0.00438	830.811	959.477	38979.22	63.901	-0.0970	-0.0689	62.0	0.1382	195.16	267.1
41294A3	0.00438	830.811	959.477	38979.22	63.901	-0.0970	-0.0689	65.0	0.1466	191.98	267.1
41294A3	0.00438	830.811	959.477	38979.22	63.901	-0.0970	-0.0689	68.0	0.1550	189.82	267.1
41294A3	0.00438	830.811	959.477	38979.22	63.901	-0.0970	-0.0689	74.0	0.1718	184.84	267.1

Table C.1 Inside Wall Temperature Data for Freon-12 (Cont'd)

RUN	D	P OUT	G	Q_w	HOTP POW	X_{in}	X_{out}	Z	X_{eq}	T_w	T_{sp}
	(m)	(kPa)	(kg/m².s)	(W/m²)	(W)			(cm)		(°C)	(°C)
41294A4	0.00438	830.811	954.345	32972.74	61.476	-0.0970	-0.0731	1.0	-0.0385	217.34	267.0
41294A4	0.00438	830.811	954.345	32972.74	61.476	-0.0970	-0.0731	2.5	-0.0349	201.95	267.0
41294A4	0.00438	830.811	954.345	32972.74	61.476	-0.0970	-0.0731	4.0	-0.0313	196.00	267.0
41294A4	0.00438	830.811	954.345	32972.74	61.476	-0.0970	-0.0731	5.5	-0.0277	190.93	267.0
41294A4	0.00438	830.811	954.345	32972.74	61.476	-0.0970	-0.0731	7.0	-0.0242	190.21	267.0
41294A4	0.00438	830.811	954.345	32972.74	61.476	-0.0970	-0.0731	9.0	-0.0194	188.78	267.0
41294A4	0.00438	830.811	954.345	32972.74	61.476	-0.0970	-0.0731	11.0	-0.0146	190.34	267.0
41294A4	0.00438	830.811	954.345	32972.74	61.476	-0.0970	-0.0731	13.0	-0.0099	190.83	267.0
41294A4	0.00438	830.811	954.345	32972.74	61.476	-0.0970	-0.0731	15.0	-0.0051	191.44	267.0
41294A4	0.00438	830.811	954.345	32972.74	61.476	-0.0970	-0.0731	17.0	-0.0003	191.83	267.0
41294A4	0.00438	830.811	954.345	32972.74	61.476	-0.0970	-0.0731	19.0	0.0044	192.60	267.0
41294A4	0.00438	830.811	954.345	32972.74	61.476	-0.0970	-0.0731	21.0	0.0092	191.93	267.0
41294A4	0.00438	830.811	954.345	32972.74	61.476	-0.0970	-0.0731	24.0	0.0164	191.91	267.0
41294A4	0.00438	830.811	954.345	32972.74	61.476	-0.0970	-0.0731	27.0	0.0235	191.39	267.0
41294A4	0.00438	830.811	954.345	32972.74	61.476	-0.0970	-0.0731	30.0	0.0307	192.05	267.0
41294A4	0.00438	830.811	954.345	32972.74	61.476	-0.0970	-0.0731	33.0	0.0378	191.65	267.0
41294A4	0.00438	830.811	954.345	32972.74	61.476	-0.0970	-0.0731	36.0	0.0450	190.53	267.0
41294A4	0.00438	830.811	954.345	32972.74	61.476	-0.0970	-0.0731	39.0	0.0521	189.89	267.0
41294A4	0.00438	830.811	954.345	32972.74	61.476	-0.0970	-0.0731	42.0	0.0593	189.63	267.0
41294A4	0.00438	830.811	954.345	32972.74	61.476	-0.0970	-0.0731	45.0	0.0664	189.61	267.0
41294A4	0.00438	830.811	954.345	32972.74	61.476	-0.0970	-0.0731	48.0	0.0736	187.87	267.0
41294A4	0.00438	830.811	954.345	32972.74	61.476	-0.0970	-0.0731	51.0	0.0807	186.64	267.0
41294A4	0.00438	830.811	954.345	32972.74	61.476	-0.0970	-0.0731	54.0	0.0879	185.06	267.0
41294A4	0.00438	830.811	954.345	32972.74	61.476	-0.0970	-0.0731	59.0	0.0998	183.20	267.0
41294A4	0.00438	830.811	954.345	32972.74	61.476	-0.0970	-0.0731	62.0	0.1069	181.98	267.0
41294A4	0.00438	830.811	954.345	32972.74	61.476	-0.0970	-0.0731	65.0	0.1141	179.72	267.0
41294A4	0.00438	830.811	954.345	32972.74	61.476	-0.0970	-0.0731	68.0	0.1212	178.41	267.0
41294A4	0.00438	830.811	954.345	32972.74	61.476	-0.0970	-0.0731	74.0	0.1355	174.73	267.0
41294A5	0.00438	830.811	959.337	27984.18	61.784	-0.0970	-0.0768	1.0	-0.0426	202.41	266.1
41294A5	0.00438	830.811	959.337	27984.18	61.784	-0.0970	-0.0768	2.5	-0.0395	183.67	266.1
41294A5	0.00438	830.811	959.337	27984.18	61.784	-0.0970	-0.0768	4.0	-0.0365	176.64	266.1
41294A5	0.00438	830.811	959.337	27984.18	61.784	-0.0970	-0.0768	5.5	-0.0335	171.08	266.1
41294A5	0.00438	830.811	959.337	27984.18	61.784	-0.0970	-0.0768	7.0	-0.0305	169.75	266.1
41294A5	0.00438	830.811	959.337	27984.18	61.784	-0.0970	-0.0768	9.0	-0.0265	167.89	266.1
41294A5	0.00438	830.811	959.337	27984.18	61.784	-0.0970	-0.0768	11.0	-0.0224	169.24	266.1
41294A5	0.00438	830.811	959.337	27984.18	61.784	-0.0970	-0.0768	13.0	-0.0184	169.41	266.1
41294A5	0.00438	830.811	959.337	27984.18	61.784	-0.0970	-0.0768	15.0	-0.0144	169.68	266.1
41294A5	0.00438	830.811	959.337	27984.18	61.784	-0.0970	-0.0768	17.0	-0.0104	170.05	266.1
41294A5	0.00438	830.811	959.337	27984.18	61.784	-0.0970	-0.0768	19.0	-0.0063	170.65	266.1
41294A5	0.00438	830.811	959.337	27984.18	61.784	-0.0970	-0.0768	21.0	-0.0023	170.04	266.1
41294A5	0.00438	830.811	959.337	27984.18	61.784	-0.0970	-0.0768	24.0	0.0037	170.64	266.1
41294A5	0.00438	830.811	959.337	27984.18	61.784	-0.0970	-0.0768	27.0	0.0098	170.57	266.1
41294A5	0.00438	830.811	959.337	27984.18	61.784	-0.0970	-0.0768	30.0	0.0158	172.41	266.1
41294A5	0.00438	830.811	959.337	27984.18	61.784	-0.0970	-0.0768	33.0	0.0218	172.45	266.1
41294A5	0.00438	830.811	959.337	27984.18	61.784	-0.0970	-0.0768	36.0	0.0279	171.77	266.1
41294A5	0.00438	830.811	959.337	27984.18	61.784	-0.0970	-0.0768	39.0	0.0339	171.67	266.1
41294A5	0.00438	830.811	959.337	27984.18	61.784	-0.0970	-0.0768	42.0	0.0399	171.81	266.1
41294A5	0.00438	830.811	959.337	27984.18	61.784	-0.0970	-0.0768	45.0	0.0460	172.30	266.1
41294A5	0.00438	830.811	959.337	27984.18	61.784	-0.0970	-0.0768	48.0	0.0520	171.07	266.1
41294A5	0.00438	830.811	959.337	27984.18	61.784	-0.0970	-0.0768	51.0	0.0581	170.52	266.1
41294A5	0.00438	830.811	959.337	27984.18	61.784	-0.0970	-0.0768	54.0	0.0641	169.67	266.1
41294A5	0.00438	830.811	959.337	27984.18	61.784	-0.0970	-0.0768	59.0	0.0742	168.87	266.1
41294A5	0.00438	830.811	959.337	27984.18	61.784	-0.0970	-0.0768	62.0	0.0802	168.09	266.1
41294A5	0.00438	830.811	959.337	27984.18	61.784	-0.0970	-0.0768	65.0	0.0862	166.35	266.1
41294A5	0.00438	830.811	959.337	27984.18	61.784	-0.0970	-0.0768	68.0	0.0923	165.31	266.1
41294A5	0.00438	830.811	959.337	27984.18	61.784	-0.0970	-0.0768	74.0	0.1043	162.38	266.1
41294A6	0.00438	830.811	954.876	24472.22	62.015	-0.0970	-0.0793	1.0	-0.0450	193.72	267.0
41294A6	0.00438	830.811	954.876	24472.22	62.015	-0.0970	-0.0793	2.5	-0.0423	171.18	267.0
41294A6	0.00438	830.811	954.876	24472.22	62.015	-0.0970	-0.0793	4.0	-0.0397	162.78	267.0
41294A6	0.00438	830.811	954.876	24472.22	62.015	-0.0970	-0.0793	5.5	-0.0370	156.88	267.0
41294A6	0.00438	830.811	954.876	24472.22	62.015	-0.0970	-0.0793	7.0	-0.0344	155.20	267.0
41294A6	0.00438	830.811	954.876	24472.22	62.015	-0.0970	-0.0793	9.0	-0.0308	153.29	267.0
41294A6	0.00438	830.811	954.876	24472.22	62.015	-0.0970	-0.0793	11.0	-0.0273	153.94	267.0
41294A6	0.00438	830.811	954.876	24472.22	62.015	-0.0970	-0.0793	13.0	-0.0238	153.49	267.0
41294A6	0.00438	830.811	954.876	24472.22	62.015	-0.0970	-0.0793	15.0	-0.0202	153.25	267.0
41294A6	0.00438	830.811	954.876	24472.22	62.015	-0.0970	-0.0793	17.0	-0.0167	152.96	267.0
41294A6	0.00438	830.811	954.876	24472.22	62.015	-0.0970	-0.0793	19.0	-0.0131	153.26	267.0
41294A6	0.00438	830.811	954.876	24472.22	62.015	-0.0970	-0.0793	21.0	-0.0096	152.69	267.0
41294A6	0.00438	830.811	954.876	24472.22	62.015	-0.0970	-0.0793	24.0	-0.0043	153.65	267.0
41294A6	0.00438	830.811	954.876	24472.22	62.015	-0.0970	-0.0793	27.0	0.0010	153.72	267.0
41294A6	0.00438	830.811	954.876	24472.22	62.015	-0.0970	-0.0793	30.0	0.0063	156.11	267.0
41294A6	0.00438	830.811	954.876	24472.22	62.015	-0.0970	-0.0793	33.0	0.0116	155.98	267.0
41294A6	0.00438	830.811	954.876	24472.22	62.015	-0.0970	-0.0793	36.0	0.0169	155.45	267.0
41294A6	0.00438	830.811	954.876	24472.22	62.015	-0.0970	-0.0793	39.0	0.0222	155.80	267.0
41294A6	0.00438	830.811	954.876	24472.22	62.015	-0.0970	-0.0793	42.0	0.0275	156.60	267.0
41294A6	0.00438	830.811	954.876	24472.22	62.015	-0.0970	-0.0793	45.0	0.0328	157.55	267.0
41294A6	0.00438	830.811	954.876	24472.22	62.015	-0.0970	-0.0793	48.0	0.0381	156.90	267.0
41294A6	0.00438	830.811	954.876	24472.22	62.015	-0.0970	-0.0793	51.0	0.0434	157.06	267.0
41294A6	0.00438	830.811	954.876	24472.22	62.015	-0.0970	-0.0793	54.0	0.0487	156.41	267.0
41294A6	0.00438	830.811	954.876	24472.22	62.015	-0.0970	-0.0793	59.0	0.0576	155.68	267.0
41294A6	0.00438	830.811	954.876	24472.22	62.015	-0.0970	-0.0793	62.0	0.0629	154.92	267.0
41294A6	0.00438	830.811	954.876	24472.22	62.015	-0.0970	-0.0793	65.0	0.0682	154.00	267.0
41294A6	0.00438	830.811	954.876	24472.22	62.015	-0.0970	-0.0793	68.0	0.0735	153.64	267.0
41294A6	0.00438	830.811	954.876	24472.22	62.015	-0.0970	-0.0793	74.0	0.0841	152.00	267.0

Table C.1 Inside Wall Temperature Data for Freon-12 (Cont'd)

RUN	D	P OUT	G	Q_w	HOTP POW	X_{in}	X_{out}	Z	X_{eq}	T_w	T_{sat}
	(m)	(kPa)	(kg/m^2.s)	(W/m^2)	(W)			(cm)		(°C)	(°C)
41394A1	0.00438	830.811	2009.947	53333.09	82.590	-0.1187	-0.1004	1.0	-0.0780	261.31	298.2
41394A1	0.00438	830.811	2009.947	53333.09	82.590	-0.1187	-0.1004	2.5	-0.0752	259.10	298.2
41394A1	0.00438	830.811	2009.947	53333.09	82.590	-0.1187	-0.1004	4.0	-0.0725	249.86	298.2
41394A1	0.00438	830.811	2009.947	53333.09	82.590	-0.1187	-0.1004	5.5	-0.0697	254.77	298.2
41394A1	0.00438	830.811	2009.947	53333.09	82.590	-0.1187	-0.1004	7.0	-0.0670	257.05	298.2
41394A1	0.00438	830.811	2009.947	53333.09	82.590	-0.1187	-0.1004	9.0	-0.0633	252.44	298.2
41394A1	0.00438	830.811	2009.947	53333.09	82.590	-0.1187	-0.1004	11.0	-0.0597	251.06	298.2
41394A1	0.00438	830.811	2009.947	53333.09	82.590	-0.1187	-0.1004	13.0	-0.0560	249.55	298.2
41394A1	0.00438	830.811	2009.947	53333.09	82.590	-0.1187	-0.1004	15.0	-0.0523	247.86	298.2
41394A1	0.00438	830.811	2009.947	53333.09	82.590	-0.1187	-0.1004	17.0	-0.0487	246.81	298.2
41394A1	0.00438	830.811	2009.947	53333.09	82.590	-0.1187	-0.1004	19.0	-0.0450	247.23	298.2
41394A1	0.00438	830.811	2009.947	53333.09	82.590	-0.1187	-0.1004	21.0	-0.0414	246.01	298.2
41394A1	0.00438	830.811	2009.947	53333.09	82.590	-0.1187	-0.1004	24.0	-0.0359	246.20	298.2
41394A1	0.00438	830.811	2009.947	53333.09	82.590	-0.1187	-0.1004	27.0	-0.0304	246.47	298.2
41394A1	0.00438	830.811	2009.947	53333.09	82.590	-0.1187	-0.1004	30.0	-0.0249	246.87	298.2
41394A1	0.00438	830.811	2009.947	53333.09	82.590	-0.1187	-0.1004	33.0	-0.0194	247.59	298.2
41394A1	0.00438	830.811	2009.947	53333.09	82.590	-0.1187	-0.1004	36.0	-0.0139	246.15	298.2
41394A1	0.00438	830.811	2009.947	53333.09	82.590	-0.1187	-0.1004	39.0	-0.0084	245.86	298.2
41394A1	0.00438	830.811	2009.947	53333.09	82.590	-0.1187	-0.1004	42.0	-0.0029	245.16	298.2
41394A1	0.00438	830.811	2009.947	53333.09	82.590	-0.1187	-0.1004	45.0	0.0026	244.70	298.2
41394A1	0.00438	830.811	2009.947	53333.09	82.590	-0.1187	-0.1004	48.0	0.0081	241.88	298.2
41394A1	0.00436	830.811	2009.947	53333.09	82.590	-0.1187	-0.1004	51.0	0.0135	239.48	298.2
41394A1	0.00438	830.811	2009.947	53333.09	82.590	-0.1187	-0.1004	54.0	0.0190	236.33	298.2
41394A1	0.00438	830.811	2009.947	53333.09	82.590	-0.1187	-0.1004	59.0	0.0282	231.91	298.2
41394A1	0.00438	830.811	2009.947	53333.09	82.590	-0.1187	-0.1004	62.0	0.0337	228.86	298.2
41394A1	0.00438	830.811	2009.947	53333.09	82.590	-0.1187	-0.1004	65.0	0.0392	224.35	298.2
41394A1	0.00438	830.811	2009.947	53333.09	82.590	-0.1187	-0.1004	68.0	0.0447	221.06	298.2
41394A1	0.00438	830.811	2009.947	53333.09	82.590	-0.1187	-0.1004	74.0	0.0556	212.64	298.2
41394A2	0.00438	830.811	2012.508	50804.44	83.156	-0.1187	-0.1013	1.0	-0.0788	255.65	299.3
41394A2	0.00438	830.811	2012.508	50804.44	83.156	-0.1187	-0.1013	2.5	-0.0762	251.90	299.3
41394A2	0.00438	830.811	2012.508	50804.44	83.156	-0.1187	-0.1013	4.0	-0.0736	243.24	299.3
41394A2	0.00438	830.811	2012.508	50804.44	83.156	-0.1187	-0.1013	5.5	-0.0710	247.96	299.3
41394A2	0.00438	830.811	2012.508	50804.44	83.156	-0.1187	-0.1013	7.0	-0.0684	250.08	299.3
41394A2	0.00438	830.811	2012.508	50804.44	83.156	-0.1187	-0.1013	9.0	-0.0649	245.64	299.3
41394A2	0.00438	830.811	2012.508	50804.44	83.156	-0.1187	-0.1013	11.0	-0.0614	244.14	299.3
41394A2	0.00438	830.811	2012.508	50804.44	83.156	-0.1187	-0.1013	13.0	-0.0579	242.39	299.3
41394A2	0.00438	830.811	2012.508	50804.44	83.156	-0.1187	-0.1013	15.0	-0.0545	240.47	299.3
41394A2	0.00438	830.811	2012.508	50804.44	83.156	-0.1187	-0.1013	17.0	-0.0510	239.41	299.3
41394A2	0.00438	830.811	2012.508	50804.44	83.156	-0.1187	-0.1013	19.0	-0.0475	239.51	299.3
41394A2	0.00438	830.811	2012.508	50804.44	83.156	-0.1187	-0.1013	21.0	-0.0440	238.19	299.3
41394A2	0.00438	830.811	2012.508	50804.44	83.156	-0.1187	-0.1013	24.0	-0.0388	238.39	299.3
41394A2	0.00438	830.811	2012.508	50804.44	83.156	-0.1187	-0.1013	27.0	-0.0336	238.50	299.3
41394A2	0.00438	830.811	2012.508	50804.44	83.156	-0.1187	-0.1013	30.0	-0.0283	239.09	299.3
41394A2	0.00438	830.811	2012.508	50804.44	83.156	-0.1187	-0.1013	33.0	-0.0231	239.91	299.3
41394A2	0.00438	830.811	2012.508	50804.44	83.156	-0.1187	-0.1013	36.0	-0.0179	238.67	299.3
41394A2	0.00438	830.811	2012.508	50804.44	83.156	-0.1187	-0.1013	39.0	-0.0127	238.69	299.3
41394A2	0.00438	830.811	2012.508	50804.44	83.156	-0.1187	-0.1013	42.0	-0.0074	238.20	299.3
41394A2	0.00438	830.811	2012.508	50804.44	83.156	-0.1187	-0.1013	45.0	-0.0022	238.42	299.3
41394A2	0.00438	830.811	2012.508	50804.44	83.156	-0.1187	-0.1013	48.0	0.0030	236.12	299.3
41394A2	0.00438	830.811	2012.508	50804.44	83.156	-0.1187	-0.1013	51.0	0.0082	234.13	299.3
41394A2	0.00438	830.811	2012.508	50804.44	83.156	-0.1187	-0.1013	54.0	0.0135	231.41	299.3
41394A2	0.00438	830.811	2012.508	50804.44	83.156	-0.1187	-0.1013	59.0	0.0222	227.58	299.3
41394A2	0.00438	830.811	2012.508	50804.44	83.156	-0.1187	-0.1013	62.0	0.0274	225.01	299.3
41394A2	0.00438	830.811	2012.508	50804.44	83.156	-0.1187	-0.1013	65.0	0.0326	220.84	299.3
41394A2	0.00438	830.811	2012.508	50804.44	83.156	-0.1187	-0.1013	68.0	0.0378	217.77	299.3
41394A2	0.00438	830.811	2012.508	50804.44	83.156	-0.1187	-0.1013	74.0	0.0483	210.28	299.3
41394A3	0.00438	830.811	2023.754	43993.45	82.910	-0.1187	-0.1037	1.0	-0.0817	238.97	298.0
41394A3	0.00438	830.811	2023.754	43993.45	82.910	-0.1187	-0.1037	2.5	-0.0794	230.60	298.0
41394A3	0.00438	830.811	2023.754	43993.45	82.910	-0.1187	-0.1037	4.0	-0.0772	222.32	298.0
41394A3	0.00438	830.811	2023.754	43993.45	82.910	-0.1187	-0.1037	5.5	-0.0749	228.09	298.0
41394A3	0.00438	830.811	2023.754	43993.45	82.910	-0.1187	-0.1037	7.0	-0.0727	230.67	298.0
41394A3	0.00438	830.811	2023.754	43993.45	82.910	-0.1187	-0.1037	9.0	-0.0697	227.03	298.0
41394A3	0.00438	830.811	2023.754	43993.45	82.910	-0.1187	-0.1037	11.0	-0.0667	225.24	298.0
41394A3	0.00438	830.811	2023.754	43993.45	82.910	-0.1187	-0.1037	13.0	-0.0637	222.48	298.0
41394A3	0.00438	830.811	2023.754	43993.45	82.910	-0.1187	-0.1037	15.0	-0.0607	219.81	298.0
41394A3	0.00438	830.811	2023.754	43993.45	82.910	-0.1187	-0.1037	17.0	-0.0577	217.95	298.0
41394A3	0.00438	830.811	2023.754	43993.45	82.910	-0.1187	-0.1037	19.0	-0.0547	216.85	298.0
41394A3	0.00438	830.811	2023.754	43993.45	82.910	-0.1187	-0.1037	21.0	-0.0517	214.72	298.0
41394A3	0.00438	830.811	2023.754	43993.45	82.910	-0.1187	-0.1037	24.0	-0.0472	213.97	298.0
41394A3	0.00438	830.811	2023.754	43993.45	82.910	-0.1187	-0.1037	27.0	-0.0427	212.00	298.0
41394A3	0.00438	830.811	2023.754	43993.45	82.910	-0.1187	-0.1037	30.0	-0.0382	213.80	298.0
41394A3	0.00438	830.811	2023.754	43993.45	82.910	-0.1187	-0.1037	33.0	-0.0337	214.47	298.0
41394A3	0.00438	830.811	2023.754	43993.45	82.910	-0.1187	-0.1037	36.0	-0.0292	214.36	298.0
41394A3	0.00438	830.811	2023.754	43993.45	82.910	-0.1187	-0.1037	39.0	-0.0247	215.28	298.0
41394A3	0.00438	830.811	2023.754	43993.45	82.910	-0.1187	-0.1037	42.0	-0.0202	216.20	298.0
41394A3	0.00438	830.811	2023.754	43993.45	82.910	-0.1187	-0.1037	45.0	-0.0157	217.62	298.0
41394A3	0.00438	830.811	2023.754	43993.45	82.910	-0.1187	-0.1037	48.0	-0.0112	216.42	298.0
41394A3	0.00438	830.811	2023.754	43993.45	82.910	-0.1187	-0.1037	51.0	-0.0067	216.03	298.0
41394A3	0.00438	830.811	2023.754	43993.45	82.910	-0.1187	-0.1037	54.0	-0.0022	214.63	298.0
41394A3	0.00438	830.811	2023.754	43993.45	82.910	-0.1187	-0.1037	59.0	0.0053	213.06	298.0
41394A3	0.00438	830.811	2023.754	43993.45	82.910	-0.1187	-0.1037	62.0	0.0098	211.56	298.0
41394A3	0.00438	830.811	2023.754	43993.45	82.910	-0.1187	-0.1037	65.0	0.0143	208.50	298.0
41394A3	0.00438	830.811	2023.754	43993.45	82.910	-0.1187	-0.1037	68.0	0.0188	206.64	298.0
41394A3	0.00438	830.811	2023.754	43993.45	82.910	-0.1187	-0.1037	74.0	0.0278	200.78	298.0
41394A4	0.00438	830.811	2012.019	38956.61	83.792	-0.1187	-0.1054	1.0	-0.0831	224.52	292.9

Table C.1 Inside Wall Temperature Data for Freon-12 (Cont'd)

RUN	D	P OUT	G	Q_w	HOTP POW	X_{in}	X_{out}	Z	X_{eq}	T_w	T_{sat}
	(m)	(kPa)	(kg/m².s)	(W/m²)	(W)			(cm)		(°C)	(°C)
41394A4	0.00438	830.811	2012.019	38956.61	83.792	-0.1187	-0.1054	2.5	-0.0811	213.51	292.9
41394A4	0.00438	830.811	2012.019	38956.61	83.792	-0.1187	-0.1054	4.0	-0.0791	213.68	292.9
41394A4	0.00438	830.811	2012.019	38956.61	83.792	-0.1187	-0.1054	5.5	-0.0771	212.88	292.9
41394A4	0.00438	830.811	2012.019	38956.61	83.792	-0.1187	-0.1054	7.0	-0.0751	213.03	292.9
41394A4	0.00438	830.811	2012.019	38956.61	83.792	-0.1187	-0.1054	9.0	-0.0725	210.74	292.9
41394A4	0.00438	830.811	2012.019	38956.61	83.792	-0.1187	-0.1054	11.0	-0.0698	209.49	292.9
41394A4	0.00438	830.811	2012.019	38956.61	83.792	-0.1187	-0.1054	13.0	-0.0671	206.30	292.9
41394A4	0.00438	830.811	2012.019	38956.61	83.792	-0.1187	-0.1054	15.0	-0.0644	203.39	292.9
41394A4	0.00438	830.811	2012.019	38956.61	83.792	-0.1187	-0.1054	17.0	-0.0618	200.78	292.9
41394A4	0.00438	830.811	2012.019	38956.61	83.792	-0.1187	-0.1054	19.0	-0.0591	198.63	292.9
41394A4	0.00438	830.811	2012.019	38956.61	83.792	-0.1187	-0.1054	21.0	-0.0564	195.56	292.9
41394A4	0.00438	830.811	2012.019	38956.61	83.792	-0.1187	-0.1054	24.0	-0.0524	193.21	292.9
41394A4	0.00438	830.811	2012.019	38956.61	83.792	-0.1187	-0.1054	27.0	-0.0484	191.48	292.9
41394A4	0.00438	830.811	2012.019	38956.61	83.792	-0.1187	-0.1054	30.0	-0.0444	190.99	292.9
41394A4	0.00438	830.811	2012.019	38956.61	83.792	-0.1187	-0.1054	33.0	-0.0404	190.94	292.9
41394A4	0.00438	830.811	2012.019	38956.61	83.792	-0.1187	-0.1054	36.0	-0.0364	191.19	292.9
41394A4	0.00438	830.811	2012.019	38956.61	83.792	-0.1187	-0.1054	39.0	-0.0324	192.49	292.9
41394A4	0.00438	830.811	2012.019	38956.61	83.792	-0.1187	-0.1054	42.0	-0.0284	194.56	292.9
41394A4	0.00438	830.811	2012.019	38956.61	83.792	-0.1187	-0.1054	45.0	-0.0244	196.66	292.9
41394A4	0.00438	830.811	2012.019	38956.61	83.792	-0.1187	-0.1054	48.0	-0.0204	196.93	292.9
41394A4	0.00438	830.811	2012.019	38956.61	83.792	-0.1187	-0.1054	51.0	-0.0164	197.20	292.9
41394A4	0.00438	830.811	2012.019	38956.61	83.792	-0.1187	-0.1054	54.0	-0.0124	196.91	292.9
41394A4	0.00438	830.811	2012.019	38956.61	83.792	-0.1187	-0.1054	59.0	-0.0057	196.50	292.9
41394A4	0.00438	830.811	2012.019	38956.61	83.792	-0.1187	-0.1054	62.0	-0.0017	195.96	292.9
41394A4	0.00438	830.811	2012.019	38956.61	83.792	-0.1187	-0.1054	65.0	0.0023	194.11	292.9
41394A4	0.00438	830.811	2012.019	38956.61	83.792	-0.1187	-0.1054	68.0	0.0063	193.33	292.9
41394A5	0.00438	830.811	2014.650	35143.74	82.182	-0.1187	-0.1067	74.0	0.0144	189.11	292.9
41394A5	0.00438	830.811	2014.650	35143.74	82.182	-0.1187	-0.1067	1.0	-0.0850	210.49	282.8
41394A5	0.00438	830.811	2014.650	35143.74	82.182	-0.1187	-0.1067	2.5	-0.0832	197.11	282.8
41394A5	0.00438	830.811	2014.650	35143.74	82.182	-0.1187	-0.1067	4.0	-0.0814	196.44	282.8
41394A5	0.00438	830.811	2014.650	35143.74	82.182	-0.1187	-0.1067	5.5	-0.0796	195.93	282.8
41394A5	0.00438	830.811	2014.650	35143.74	82.182	-0.1187	-0.1067	7.0	-0.0778	197.37	282.8
41394A5	0.00438	830.811	2014.650	35143.74	82.182	-0.1187	-0.1067	9.0	-0.0754	196.24	282.8
41394A5	0.00438	830.811	2014.650	35143.74	82.182	-0.1187	-0.1067	11.0	-0.0730	196.43	282.8
41394A5	0.00438	830.811	2014.650	35143.74	82.182	-0.1187	-0.1067	13.0	-0.0706	194.10	282.8
41394A5	0.00438	830.811	2014.650	35143.74	82.182	-0.1187	-0.1067	15.0	-0.0682	191.65	282.8
41394A5	0.00438	830.811	2014.650	35143.74	82.182	-0.1187	-0.1067	17.0	-0.0658	189.01	282.8
41394A5	0.00438	830.811	2014.650	35143.74	82.182	-0.1187	-0.1067	19.0	-0.0634	186.78	282.8
41394A5	0.00438	830.811	2014.650	35143.74	82.182	-0.1187	-0.1067	21.0	-0.0610	183.48	282.8
41394A5	0.00438	830.811	2014.650	35143.74	82.182	-0.1187	-0.1067	24.0	-0.0573	180.27	282.8
41394A5	0.00438	830.811	2014.650	35143.74	82.182	-0.1187	-0.1067	27.0	-0.0537	176.64	282.8
41394A5	0.00438	830.811	2014.650	35143.74	82.182	-0.1187	-0.1067	30.0	-0.0501	175.76	282.8
41394A5	0.00438	830.811	2014.650	35143.74	82.182	-0.1187	-0.1067	33.0	-0.0465	174.62	282.8
41394A5	0.00438	830.811	2014.650	35143.74	82.182	-0.1187	-0.1067	36.0	-0.0429	173.84	282.8
41394A5	0.00438	830.811	2014.650	35143.74	82.182	-0.1187	-0.1067	39.0	-0.0393	174.45	282.8
41394A5	0.00438	830.811	2014.650	35143.74	82.182	-0.1187	-0.1067	42.0	-0.0357	176.16	282.8
41394A5	0.00438	830.811	2014.650	35143.74	82.182	-0.1187	-0.1067	45.0	-0.0321	178.22	282.8
41394A5	0.00438	830.811	2014.650	35143.74	82.182	-0.1187	-0.1067	48.0	-0.0285	178.46	282.8
41394A5	0.00438	830.811	2014.650	35143.74	82.182	-0.1187	-0.1067	51.0	-0.0249	179.26	282.8
41394A5	0.00438	830.811	2014.650	35143.74	82.182	-0.1187	-0.1067	54.0	-0.0212	179.34	282.8
41394A5	0.00438	830.811	2014.650	35143.74	82.182	-0.1187	-0.1067	59.0	-0.0152	180.29	282.8
41394A5	0.00438	830.811	2014.650	35143.74	82.182	-0.1187	-0.1067	62.0	-0.0116	180.52	282.8
41394A5	0.00438	830.811	2014.650	35143.74	82.182	-0.1187	-0.1067	65.0	-0.0080	179.93	282.8
41394A5	0.00438	830.811	2014.650	35143.74	82.182	-0.1187	-0.1067	68.0	-0.0044	180.14	282.8
41394A6	0.00438	830.811	2014.503	29395.01	82.636	-0.1187	-0.1067	74.0	0.0028	178.32	282.8
41394A6	0.00438	830.811	2014.503	29395.01	82.636	-0.1187	-0.1086	1.0	-0.0871	193.25	280.2
41394A6	0.00438	830.811	2014.503	29395.01	82.636	-0.1187	-0.1086	2.5	-0.0856	173.10	280.2
41394A6	0.00438	830.811	2014.503	29395.01	82.636	-0.1187	-0.1086	4.0	-0.0841	169.26	280.2
41394A6	0.00438	830.811	2014.503	29395.01	82.636	-0.1187	-0.1086	5.5	-0.0825	167.53	280.2
41394A6	0.00438	830.811	2014.503	29395.01	82.636	-0.1187	-0.1086	7.0	-0.0810	168.26	280.2
41394A6	0.00438	830.811	2014.503	29395.01	82.636	-0.1187	-0.1086	9.0	-0.0790	168.80	280.2
41394A6	0.00438	830.811	2014.503	29395.01	82.636	-0.1187	-0.1086	11.0	-0.0770	171.05	280.2
41394A6	0.00438	830.811	2014.503	29395.01	82.636	-0.1187	-0.1086	13.0	-0.0750	171.03	280.2
41394A6	0.00438	830.811	2014.503	29395.01	82.636	-0.1187	-0.1086	15.0	-0.0730	170.63	280.2
41394A6	0.00438	830.811	2014.503	29395.01	82.636	-0.1187	-0.1086	17.0	-0.0710	169.04	280.2
41394A6	0.00438	830.811	2014.503	29395.01	82.636	-0.1187	-0.1086	19.0	-0.0690	167.29	280.2
41394A6	0.00438	830.811	2014.503	29395.01	82.636	-0.1187	-0.1086	21.0	-0.0669	164.06	280.2
41394A6	0.00438	830.811	2014.503	29395.01	82.636	-0.1187	-0.1086	24.0	-0.0639	160.53	280.2
41394A6	0.00438	830.811	2014.503	29395.01	82.636	-0.1187	-0.1086	27.0	-0.0609	155.43	280.2
41394A6	0.00438	830.811	2014.503	29395.01	82.636	-0.1187	-0.1086	30.0	-0.0579	153.54	280.2
41394A6	0.00438	830.811	2014.503	29395.01	82.636	-0.1187	-0.1086	33.0	-0.0549	150.33	280.2
41394A6	0.00438	830.811	2014.503	29395.01	82.636	-0.1187	-0.1086	36.0	-0.0518	147.29	280.2
41394A6	0.00438	830.811	2014.503	29395.01	82.636	-0.1187	-0.1086	39.0	-0.0488	145.90	280.2
41394A6	0.00438	830.811	2014.503	29395.01	82.636	-0.1187	-0.1086	42.0	-0.0458	145.39	280.2
41394A6	0.00438	830.811	2014.503	29395.01	82.636	-0.1187	-0.1086	45.0	-0.0428	145.65	280.2
41394A6	0.00438	830.811	2014.503	29395.01	82.636	-0.1187	-0.1086	48.0	-0.0398	144.82	280.2
41394A6	0.00438	830.811	2014.503	29395.01	82.636	-0.1187	-0.1086	51.0	-0.0367	146.46	280.2
41394A6	0.00438	830.811	2014.503	29395.01	82.636	-0.1187	-0.1086	54.0	-0.0337	147.81	280.2
41394A6	0.00438	830.811	2014.503	29395.01	82.636	-0.1187	-0.1086	59.0	-0.0287	151.75	280.2
41394A6	0.00438	830.811	2014.503	29395.01	82.636	-0.1187	-0.1086	62.0	-0.0257	153.82	280.2
41394A6	0.00438	830.811	2014.503	29395.01	82.636	-0.1187	-0.1086	65.0	-0.0227	155.47	280.2
41394A6	0.00438	830.811	2014.503	29395.01	82.636	-0.1187	-0.1086	68.0	-0.0196	157.23	280.2
41394A6	0.00438	830.811	2014.503	29395.01	82.636	-0.1187	-0.1086	74.0	-0.0136	147.62	280.2
41494A1	0.00438	830.811	535.857	50262.02	59.578	-0.1136	-0.0489	1.0	0.0133	267.13	257.5

Table C.1 Inside Wall Temperature Data for Freon-12 (Cont'd)

RUN	D	P OUT	G	Q_w	HOTP POW	X_{in}	X_{out}	Z	X_{eq}	T_w	T_{sat}
	(m)	(kPa)	(kg/m².s)	(W/m²)	(W)			(cm)		(°C)	(°C)
41494A1	0.00438	830.811	535.857	50262.02	59.578	-0.1136	-0.0489	2.5	0.0230	273.71	257.5
41494A1	0.00438	830.811	535.857	50262.02	59.578	-0.1136	-0.0489	4.0	0.0327	276.43	257.5
41494A1	0.00438	830.811	535.857	50262.02	59.578	-0.1136	-0.0489	5.5	0.0424	275.51	257.5
41494A1	0.00438	830.811	535.857	50262.02	59.578	-0.1136	-0.0489	7.0	0.0521	278.43	257.5
41494A1	0.00438	830.811	535.857	50262.02	59.578	-0.1136	-0.0489	9.0	0.0650	277.32	257.5
41494A1	0.00438	830.811	535.857	50262.02	59.578	-0.1136	-0.0489	11.0	0.0780	279.18	257.5
41494A1	0.00438	830.811	535.857	50262.02	59.578	-0.1136	-0.0489	13.0	0.0909	278.60	257.5
41494A1	0.00438	830.811	535.857	50262.02	59.578	-0.1136	-0.0489	15.0	0.1038	278.08	257.5
41494A1	0.00438	830.811	535.857	50262.02	59.578	-0.1136	-0.0489	17.0	0.1168	277.68	257.5
41494A1	0.00438	830.811	535.857	50262.02	59.578	-0.1136	-0.0489	19.0	0.1297	277.40	257.5
41494A1	0.00438	830.811	535.857	50262.02	59.578	-0.1136	-0.0489	21.0	0.1427	275.63	257.5
41494A1	0.00438	830.811	535.857	50262.02	59.578	-0.1136	-0.0489	24.0	0.1621	274.09	257.5
41494A1	0.00438	830.811	535.857	50262.02	59.578	-0.1136	-0.0489	27.0	0.1815	272.44	257.5
41494A1	0.00438	830.811	535.857	50262.02	59.578	-0.1136	-0.0489	30.0	0.2009	270.94	257.5
41494A1	0.00438	830.811	535.857	50262.02	59.578	-0.1136	-0.0489	33.0	0.2203	269.74	257.5
41494A1	0.00438	830.811	535.857	50262.02	59.578	-0.1136	-0.0489	36.0	0.2397	266.25	257.5
41494A1	0.00438	830.811	535.857	50262.02	59.578	-0.1136	-0.0489	39.0	0.2591	263.89	257.5
41494A1	0.00438	830.811	535.857	50262.02	59.578	-0.1136	-0.0489	42.0	0.2785	261.40	257.5
41494A1	0.00438	830.811	535.857	50262.02	59.578	-0.1136	-0.0489	45.0	0.2979	259.46	257.5
41494A1	0.00438	830.811	535.857	50262.02	59.578	-0.1136	-0.0489	48.0	0.3174	255.63	257.5
41494A1	0.00438	830.811	535.857	50262.02	59.578	-0.1136	-0.0489	51.0	0.3368	252.30	257.5
41494A1	0.00438	830.811	535.857	50262.02	59.578	-0.1136	-0.0489	54.0	0.3562	248.80	257.5
41494A1	0.00438	830.811	535.857	50262.02	59.578	-0.1136	-0.0489	59.0	0.3885	245.02	257.5
41494A1	0.00438	830.811	535.857	50262.02	59.578	-0.1136	-0.0489	62.0	0.4079	242.73	257.5
41494A1	0.00438	830.811	535.857	50262.02	59.578	-0.1136	-0.0489	65.0	0.4273	239.27	257.5
41494A1	0.00438	830.811	535.857	50262.02	59.578	-0.1136	-0.0489	68.0	0.4468	237.33	257.5
41494A1	0.00438	830.811	535.857	50262.02	59.578	-0.1136	-0.0489	74.0	0.4856	232.64	257.5
41494A2	0.00438	830.811	534.206	46931.77	60.027	-0.1136	-0.0530	1.0	0.0093	262.96	269.6
41494A2	0.00438	830.811	534.206	46931.77	60.027	-0.1136	-0.0530	2.5	0.0184	264.40	269.6
41494A2	0.00438	830.811	534.206	46931.77	60.027	-0.1136	-0.0530	4.0	0.0275	265.58	269.6
41494A2	0.00438	830.811	534.206	46931.77	60.027	-0.1136	-0.0530	5.5	0.0366	264.11	269.6
41494A2	0.00438	830.811	534.206	46931.77	60.027	-0.1136	-0.0530	7.0	0.0457	266.43	269.6
41494A2	0.00438	830.811	534.206	46931.77	60.027	-0.1136	-0.0530	9.0	0.0578	265.03	269.6
41494A2	0.00438	830.811	534.206	46931.77	60.027	-0.1136	-0.0530	11.0	0.0699	266.79	269.6
41494A2	0.00438	830.811	534.206	46931.77	60.027	-0.1136	-0.0530	13.0	0.0821	266.24	269.6
41494A2	0.00438	830.811	534.206	46931.77	60.027	-0.1136	-0.0530	15.0	0.0942	265.79	269.6
41494A2	0.00438	830.811	534.206	46931.77	60.027	-0.1136	-0.0530	17.0	0.1063	265.71	269.6
41494A2	0.00438	830.811	534.206	46931.77	60.027	-0.1136	-0.0530	19.0	0.1184	265.63	269.6
41494A2	0.00438	830.811	534.206	46931.77	60.027	-0.1136	-0.0530	21.0	0.1305	263.83	269.6
41494A2	0.00438	830.811	534.206	46931.77	60.027	-0.1136	-0.0530	24.0	0.1487	262.62	269.6
41494A2	0.00438	830.811	534.206	46931.77	60.027	-0.1136	-0.0530	27.0	0.1669	261.99	269.6
41494A2	0.00438	830.811	534.206	46931.77	60.027	-0.1136	-0.0530	30.0	0.1851	260.31	269.6
41494A2	0.00438	830.811	534.206	46931.77	60.027	-0.1136	-0.0530	33.0	0.2033	259.43	269.6
41494A2	0.00438	830.811	534.206	46931.77	60.027	-0.1136	-0.0530	36.0	0.2214	256.67	269.6
41494A2	0.00438	830.811	534.206	46931.77	60.027	-0.1136	-0.0530	39.0	0.2396	254.84	269.6
41494A2	0.00438	830.811	534.206	46931.77	60.027	-0.1136	-0.0530	42.0	0.2578	252.90	269.6
41494A2	0.00438	830.811	534.206	46931.77	60.027	-0.1136	-0.0530	45.0	0.2760	251.37	269.6
41494A2	0.00438	830.811	534.206	46931.77	60.027	-0.1136	-0.0530	48.0	0.2942	248.07	269.6
41494A2	0.00438	830.811	534.206	46931.77	60.027	-0.1136	-0.0530	51.0	0.3123	245.09	269.6
41494A2	0.00438	830.811	534.206	46931.77	60.027	-0.1136	-0.0530	54.0	0.3305	241.89	269.6
41494A2	0.00438	830.811	534.206	46931.77	60.027	-0.1136	-0.0530	59.0	0.3608	238.53	269.6
41494A2	0.00438	830.811	534.206	46931.77	60.027	-0.1136	-0.0530	62.0	0.3790	236.39	269.6
41494A2	0.00438	830.811	534.206	46931.77	60.027	-0.1136	-0.0530	65.0	0.3972	233.15	269.6
41494A2	0.00438	830.811	534.206	46931.77	60.027	-0.1136	-0.0530	68.0	0.4154	231.38	269.6
41494A2	0.00438	830.811	534.206	46931.77	60.027	-0.1136	-0.0530	74.0	0.4517	226.97	269.6
41494A3	0.00438	830.811	538.936	38693.03	58.239	-0.1136	-0.0641	1.0	-0.0050	242.00	274.2
41494A3	0.00438	830.811	538.936	38693.03	58.239	-0.1136	-0.0641	2.5	0.0024	235.47	274.2
41494A3	0.00438	830.811	538.936	38693.03	58.239	-0.1136	-0.0641	4.0	0.0099	233.97	274.2
41494A3	0.00438	830.811	538.936	38693.03	58.239	-0.1136	-0.0641	5.5	0.0173	231.31	274.2
41494A3	0.00438	830.811	538.936	38693.03	58.239	-0.1136	-0.0641	7.0	0.0247	232.47	274.2
41494A3	0.00438	830.811	538.936	38693.03	58.239	-0.1136	-0.0641	9.0	0.0346	230.84	274.2
41494A3	0.00438	830.811	538.936	38693.03	58.239	-0.1136	-0.0641	11.0	0.0445	232.48	274.2
41494A3	0.00438	830.811	538.936	38693.03	58.239	-0.1136	-0.0641	13.0	0.0544	231.93	274.2
41494A3	0.00438	830.811	538.936	38693.03	58.239	-0.1136	-0.0641	15.0	0.0643	231.56	274.2
41494A3	0.00438	830.811	538.936	38693.03	58.239	-0.1136	-0.0641	17.0	0.0742	231.73	274.2
41494A3	0.00438	830.811	538.936	38693.03	58.239	-0.1136	-0.0641	19.0	0.0841	232.07	274.2
41494A3	0.00438	830.811	538.936	38693.03	58.239	-0.1136	-0.0641	21.0	0.0940	230.97	274.2
41494A3	0.00438	830.811	538.936	38693.03	58.239	-0.1136	-0.0641	24.0	0.1089	230.97	274.2
41494A3	0.00438	830.811	538.936	38693.03	58.239	-0.1136	-0.0641	27.0	0.1238	230.71	274.2
41494A3	0.00438	830.811	538.936	38693.03	58.239	-0.1136	-0.0641	30.0	0.1386	230.88	274.2
41494A3	0.00438	830.811	538.936	38693.03	58.239	-0.1136	-0.0641	33.0	0.1535	230.76	274.2
41494A3	0.00438	830.811	538.936	38693.03	58.239	-0.1136	-0.0641	36.0	0.1683	229.29	274.2
41494A3	0.00438	830.811	538.936	38693.03	58.239	-0.1136	-0.0641	39.0	0.1832	228.47	274.2
41494A3	0.00438	830.811	538.936	38693.03	58.239	-0.1136	-0.0641	42.0	0.1981	228.01	274.2
. . .	. . .	. . .	. . .	. . .	. . .	. . .	. . .	. .	. . .	. . .	. . .
. . .	. . .	. . .	. . .	. . .	. . .	. . .	. . .	. .	. . .	. . .	. . .
. . .	. . .	. . .	. . .	. . .	. . .	. . .	. . .	. .	. . .	. . .	. . .
. . .	. . .	. . .	. . .	. . .	. . .	. . .	. . .	. .	. . .	. . .	. . .
. . .	. . .	. . .	. . .	. . .	. . .	. . .	. . .	. .	. . .	. . .	. . .
. . .	. . .	. . .	. . .	. . .	. . .	. . .	. . .	. .	. . .	. . .	. . .
. . .	. . .	. . .	. . .	. . .	. . .	. . .	. . .	. .	. . .	. . .	. . .
. . .	. . .	. . .	. . .	. . .	. . .	. . .	. . .	. .	. . .	. . .	. . .
. . .	. . .	. . .	. . .	. . .	. . .	. . .	. . .	. .	. . .	. . .	. . .
. . .	. . .	. . .	. . .	. . .	. . .	. . .	. . .	. .	. . .	. . .	. . .
. . .	. . .	. . .	. . .	. . .	. . .	. . .	. . .	. .	. . .	. . .	. . .

Table C.1 Inside Wall Temperature Data for Freon-12 (Concluded)

RUN	D	P OUT	G	Q_w	HOTP POW	X_{in}	X_{exp}	Z	X_{eq}	T_w	T_{sp}
	(m)	(kPa)	(kg/m².s)	(W/m²)	(W)			(cm)		(°C)	(°C)
41394E8	0.00438	830.811	3022.676	29350.86	85.618	-0.0604	-0.0537	30.0	-0.0194	149.41	245.7
41394E8	0.00438	830.811	3022.676	29350.86	85.618	-0.0604	-0.0537	33.0	-0.0174	148.18	245.7
41394E8	0.00438	830.811	3022.676	29350.86	85.618	-0.0604	-0.0537	36.0	-0.0154	147.08	245.7
41394E8	0.00438	830.811	3022.676	29350.86	85.618	-0.0604	-0.0537	39.0	-0.0134	146.90	245.7
41394E8	0.00438	830.811	3022.676	29350.86	85.618	-0.0604	-0.0537	42.0	-0.0114	147.25	245.7
41394E8	0.00438	830.811	3022.676	29350.86	85.618	-0.0604	-0.0537	45.0	-0.0094	147.51	245.7
41394E8	0.00438	830.811	3022.676	29350.86	85.618	-0.0604	-0.0537	48.0	-0.0074	146.54	245.7
41394E8	0.00438	830.811	3022.676	29350.86	85.618	-0.0604	-0.0537	51.0	-0.0053	146.41	245.7
41394E8	0.00438	830.811	3022.676	29350.86	85.618	-0.0604	-0.0537	54.0	-0.0033	145.85	245.7
41394E8	0.00438	830.811	3022.676	29350.86	85.618	-0.0604	-0.0537	59.0	0.0000	145.32	245.7
41394E8	0.00438	830.811	3022.676	29350.86	85.618	-0.0604	-0.0537	62.0	0.0020	144.38	245.7
41394E8	0.00438	830.811	3022.676	29350.86	85.618	-0.0604	-0.0537	65.0	0.0040	143.38	245.7
41394E8	0.00438	830.811	3022.676	29350.86	85.618	-0.0604	-0.0537	68.0	0.0060	143.08	245.7
41394E8	0.00438	830.811	3022.676	29350.86	85.618	-0.0604	-0.0537	74.0	0.0101	141.22	245.7

Table C.2 Inside Wall Temperature Data for Freon-134a

RUN	D	P OUT	G	Q_w	HOTP POW	X_{in}	X_{exp}	Z	X_{eq}	T_w	T_{sat}
	(m)	(kPa)	(kg/m².s)	(W/m²)	(W)			(cm)		(°C)	(°C)
31894A1	0.00438	830.811	3016.528	74272.37	123.471	-0.1128	-0.0996	1.0	-0.0824	194.26	201.3
31894A1	0.00438	830.811	3016.528	74272.37	123.471	-0.1128	-0.0996	2.5	-0.0804	218.64	201.3
31894A1	0.00438	830.811	3016.528	74272.37	123.471	-0.1128	-0.0996	4.0	-0.0784	239.00	201.3
31894A1	0.00438	830.811	3016.528	74272.37	123.471	-0.1128	-0.0996	5.5	-0.0764	252.31	201.3
31894A1	0.00438	830.811	3016.528	74272.37	123.471	-0.1128	-0.0996	7.0	-0.0744	260.39	201.3
31894A1	0.00438	830.811	3016.528	74272.37	123.471	-0.1128	-0.0996	9.0	-0.0718	258.02	201.3
31894A1	0.00438	830.811	3016.528	74272.37	123.471	-0.1128	-0.0996	11.0	-0.0692	253.06	201.3
31894A1	0.00438	830.811	3016.528	74272.37	123.471	-0.1128	-0.0996	13.0	-0.0665	246.30	201.3
31894A1	0.00438	830.811	3016.528	74272.37	123.471	-0.1128	-0.0996	15.0	-0.0639	239.78	201.3
31894A1	0.00438	830.811	3016.528	74272.37	123.471	-0.1128	-0.0996	17.0	-0.0612	234.29	201.3
31894A1	0.00438	830.811	3016.528	74272.37	123.471	-0.1128	-0.0996	19.0	-0.0586	230.04	201.3
31894A1	0.00438	830.811	3016.528	74272.37	123.471	-0.1128	-0.0996	21.0	-0.0560	225.81	201.3
31894A1	0.00438	830.811	3016.528	74272.37	123.471	-0.1128	-0.0996	24.0	-0.0520	222.82	201.3
31894A1	0.00438	830.811	3016.528	74272.37	123.471	-0.1128	-0.0996	27.0	-0.0481	220.47	201.3
31894A1	0.00438	830.811	3016.528	74272.37	123.471	-0.1128	-0.0996	30.0	-0.0441	220.44	201.3
31894A1	0.00438	830.811	3016.528	74272.37	123.471	-0.1128	-0.0996	33.0	-0.0401	219.59	201.3
31894A1	0.00438	830.811	3016.528	74272.37	123.471	-0.1128	-0.0996	36.0	-0.0362	218.02	201.3
31894A1	0.00438	830.811	3016.528	74272.37	123.471	-0.1128	-0.0996	39.0	-0.0322	217.08	201.3
31894A1	0.00438	830.811	3016.528	74272.37	123.471	-0.1128	-0.0996	42.0	-0.0283	216.84	201.3
31894A1	0.00438	830.811	3016.528	74272.37	123.471	-0.1128	-0.0996	45.0	-0.0243	216.13	201.3
31894A1	0.00438	830.811	3016.528	74272.37	123.471	-0.1128	-0.0996	48.0	-0.0204	213.66	201.3
31894A1	0.00438	830.811	3016.528	74272.37	123.471	-0.1128	-0.0996	51.0	-0.0164	212.02	201.3
31894A1	0.00438	830.811	3016.528	74272.37	123.471	-0.1128	-0.0996	54.0	-0.0124	209.09	201.3
31894A1	0.00438	830.811	3016.528	74272.37	123.471	-0.1128	-0.0996	59.0	-0.0058	205.41	201.3
31894A1	0.00438	830.811	3016.528	74272.37	123.471	-0.1128	-0.0996	62.0	-0.0019	203.18	201.3
31894A1	0.00438	830.811	3016.528	74272.37	123.471	-0.1128	-0.0996	65.0	0.0021	199.30	201.3
31894A1	0.00438	830.811	3016.528	74272.37	123.471	-0.1128	-0.0996	68.0	0.0060	196.44	201.3
31894A1	0.00438	830.811	3016.528	74272.37	123.471	-0.1128	-0.0996	74.0	0.0139	189.28	201.3
31894A2	0.00438	830.811	3025.184	69731.38	123.413	-0.1128	-0.1005	1.0	-0.0833	182.29	194.7
31894A2	0.00438	830.811	3025.184	69731.38	123.413	-0.1128	-0.1005	2.5	-0.0815	203.93	194.7
31894A2	0.00438	830.811	3025.184	69731.38	123.413	-0.1128	-0.1005	4.0	-0.0796	224.12	194.7
31894A2	0.00438	830.811	3025.184	69731.38	123.413	-0.1128	-0.1005	5.5	-0.0778	239.34	194.7
31894A2	0.00438	830.811	3025.184	69731.38	123.413	-0.1128	-0.1005	7.0	-0.0759	250.62	194.7
31894A2	0.00438	830.811	3025.184	69731.38	123.413	-0.1128	-0.1005	9.0	-0.0735	251.99	194.7
31894A2	0.00438	830.811	3025.184	69731.38	123.413	-0.1128	-0.1005	11.0	-0.0710	248.28	194.7
31894A2	0.00438	830.811	3025.184	69731.38	123.413	-0.1128	-0.1005	13.0	-0.0685	241.60	194.7
31894A2	0.00438	830.811	3025.184	69731.38	123.413	-0.1128	-0.1005	15.0	-0.0660	234.81	194.7
31894A2	0.00438	830.811	3025.184	69731.38	123.413	-0.1128	-0.1005	17.0	-0.0636	228.77	194.7
31894A2	0.00438	830.811	3025.184	69731.38	123.413	-0.1128	-0.1005	19.0	-0.0611	223.85	194.7
31894A2	0.00438	830.811	3025.184	69731.38	123.413	-0.1128	-0.1005	21.0	-0.0586	219.05	194.7
31894A2	0.00438	830.811	3025.184	69731.38	123.413	-0.1128	-0.1005	24.0	-0.0549	215.48	194.7
31894A2	0.00438	830.811	3025.184	69731.38	123.413	-0.1128	-0.1005	27.0	-0.0512	212.64	194.7
31894A2	0.00438	830.811	3025.184	69731.38	123.413	-0.1128	-0.1005	30.0	-0.0475	212.62	194.7
31894A2	0.00438	830.811	3025.184	69731.38	123.413	-0.1128	-0.1005	33.0	-0.0438	211.64	194.7
31894A2	0.00438	830.811	3025.184	69731.38	123.413	-0.1128	-0.1005	36.0	-0.0401	210.26	194.7
31894A2	0.00438	830.811	3025.184	69731.38	123.413	-0.1128	-0.1005	39.0	-0.0364	209.43	194.7
31894A2	0.00438	830.811	3025.184	69731.38	123.413	-0.1128	-0.1005	42.0	-0.0327	209.45	194.7
31894A2	0.00438	830.811	3025.184	69731.38	123.413	-0.1128	-0.1005	45.0	-0.0290	209.01	194.7
31894A2	0.00438	830.811	3025.184	69731.38	123.413	-0.1128	-0.1005	48.0	-0.0253	206.88	194.7
31894A2	0.00438	830.811	3025.184	69731.38	123.413	-0.1128	-0.1005	51.0	-0.0216	205.54	194.7
31894A2	0.00438	830.811	3025.184	69731.38	123.413	-0.1128	-0.1005	54.0	-0.0179	203.09	194.7
31894A2	0.00438	830.811	3025.184	69731.38	123.413	-0.1128	-0.1005	59.0	-0.0117	199.95	194.7
31894A2	0.00438	830.811	3025.184	69731.38	123.413	-0.1128	-0.1005	62.0	-0.0080	198.19	194.7
31894A2	0.00438	830.811	3025.184	69731.38	123.413	-0.1128	-0.1005	65.0	-0.0043	194.82	194.7
31894A2	0.00438	830.811	3025.184	69731.38	123.413	-0.1128	-0.1005	68.0	-0.0006	192.35	194.7
31894A2	0.00438	830.811	3025.184	69731.38	123.413	-0.1128	-0.1005	74.0	0.0068	186.11	194.7
31894A3	0.00438	830.811	3014.179	63850.21	123.263	-0.1128	-0.1015	1.0	-0.0844	167.61	189.6
31894A3	0.00438	830.811	3014.179	63850.21	123.263	-0.1128	-0.1015	2.5	-0.0827	183.96	189.6
31894A3	0.00438	830.811	3014.179	63850.21	123.263	-0.1128	-0.1015	4.0	-0.0810	202.42	189.6
31894A3	0.00438	830.811	3014.179	63850.21	123.263	-0.1128	-0.1015	5.5	-0.0793	218.92	189.6
31894A3	0.00438	830.811	3014.179	63850.21	123.263	-0.1128	-0.1015	7.0	-0.0776	234.50	189.6
31894A3	0.00438	830.811	3014.179	63850.21	123.263	-0.1128	-0.1015	9.0	-0.0753	243.28	189.6
31894A3	0.00438	830.811	3014.179	63850.21	123.263	-0.1128	-0.1015	11.0	-0.0730	243.50	189.6
31894A3	0.00438	830.811	3014.179	63850.21	123.263	-0.1128	-0.1015	13.0	-0.0708	237.60	189.6
31894A3	0.00438	830.811	3014.179	63850.21	123.263	-0.1128	-0.1015	15.0	-0.0685	230.73	189.6
31894A3	0.00438	830.811	3014.179	63850.21	123.263	-0.1128	-0.1015	17.0	-0.0662	224.05	189.6
31894A3	0.00438	830.811	3014.179	63850.21	123.263	-0.1128	-0.1015	19.0	-0.0640	217.98	189.6
31894A3	0.00438	830.811	3014.179	63850.21	123.263	-0.1128	-0.1015	21.0	-0.0617	212.29	189.6
31894A3	0.00438	830.811	3014.179	63850.21	123.263	-0.1128	-0.1015	24.0	-0.0583	207.63	189.6
31894A3	0.00438	830.811	3014.179	63850.21	123.263	-0.1128	-0.1015	27.0	-0.0549	203.93	189.6
31894A3	0.00438	830.811	3014.179	63850.21	123.263	-0.1128	-0.1015	30.0	-0.0515	203.44	189.6
31894A3	0.00438	830.811	3014.179	63850.21	123.263	-0.1128	-0.1015	33.0	-0.0481	202.24	189.6
31894A3	0.00438	830.811	3014.179	63850.21	123.263	-0.1128	-0.1015	36.0	-0.0447	200.76	189.6
31894A3	0.00438	830.811	3014.179	63850.21	123.263	-0.1128	-0.1015	39.0	-0.0413	200.10	189.6
31894A3	0.00438	830.811	3014.179	63850.21	123.263	-0.1128	-0.1015	42.0	-0.0379	200.46	189.6
31894A3	0.00438	830.811	3014.179	63850.21	123.263	-0.1128	-0.1015	45.0	-0.0345	200.44	189.6
31894A3	0.00438	830.811	3014.179	63850.21	123.263	-0.1128	-0.1015	48.0	-0.0311	198.87	189.6
31894A3	0.00438	830.811	3014.179	63850.21	123.263	-0.1128	-0.1015	51.0	-0.0276	198.05	189.6
31894A3	0.00438	830.811	3014.179	63850.21	123.263	-0.1128	-0.1015	54.0	-0.0242	196.24	189.6
31894A3	0.00438	830.811	3014.179	63850.21	123.263	-0.1128	-0.1015	59.0	-0.0186	194.19	189.6
31894A3	0.00438	830.811	3014.179	63850.21	123.263	-0.1128	-0.1015	62.0	-0.0152	192.99	189.6
31894A3	0.00438	830.811	3014.179	63850.21	123.263	-0.1128	-0.1015	65.0	-0.0118	190.19	189.6
31894A3	0.00438	830.811	3014.179	63850.21	123.263	-0.1128	-0.1015	68.0	-0.0084	188.38	189.6
31894A3	0.00438	830.811	3014.179	63850.21	123.263	-0.1128	-0.1015	74.0	-0.0015	183.40	189.6

Table C.2 Inside Wall Temperature Data for Freon-134a (Cont'd)

RUN	D	P OUT	G	Q_w	HOTP POW	X_{tt}	$X_{tt,lo}$	Z	X_{eq}	T_w	T_{sat}
	(m)	(kPa)	(kg/m^2.s)	(W/m^2)	(W)			(cm)		(°C)	(°C)
31894A4	0.00438	830.811	3020.505	60093.59	123.442	-0.1128	-0.1021	1.0	-0.0852	157.22	185.4
31894A4	0.00438	830.811	3020.505	60093.59	123.442	-0.1128	-0.1021	2.5	-0.0836	169.21	185.4
31894A4	0.00438	830.811	3020.505	60093.59	123.442	-0.1128	-0.1021	4.0	-0.0820	185.26	185.4
31894A4	0.00438	830.811	3020.505	60093.59	123.442	-0.1128	-0.1021	5.5	-0.0804	201.32	185.4
31894A4	0.00438	830.811	3020.505	60093.59	123.442	-0.1128	-0.1021	7.0	-0.0788	218.86	185.4
31894A4	0.00438	830.811	3020.505	60093.59	123.442	-0.1128	-0.1021	9.0	-0.0766	233.82	185.4
31894A4	0.00438	830.811	3020.505	60093.59	123.442	-0.1128	-0.1021	11.0	-0.0745	239.72	185.4
31894A4	0.00438	830.811	3020.505	60093.59	123.442	-0.1128	-0.1021	13.0	-0.0724	235.78	185.4
31894A4	0.00438	830.811	3020.505	60093.59	123.442	-0.1128	-0.1021	15.0	-0.0702	229.09	185.4
31894A4	0.00438	830.811	3020.505	60093.59	123.442	-0.1128	-0.1021	17.0	-0.0681	222.18	185.4
31894A4	0.00438	830.811	3020.505	60093.59	123.442	-0.1128	-0.1021	19.0	-0.0660	215.59	185.4
31894A4	0.00438	830.811	3020.505	60093.59	123.442	-0.1128	-0.1021	21.0	-0.0638	209.13	185.4
31894A4	0.00438	830.811	3020.505	60093.59	123.442	-0.1128	-0.1021	24.0	-0.0606	203.24	185.4
31894A4	0.00438	830.811	3020.505	60093.59	123.442	-0.1128	-0.1021	27.0	-0.0574	198.49	185.4
31894A4	0.00438	830.811	3020.505	60093.59	123.442	-0.1128	-0.1021	30.0	-0.0543	197.47	185.4
31894A4	0.00438	830.811	3020.505	60093.59	123.442	-0.1128	-0.1021	33.0	-0.0511	195.85	185.4
31894A4	0.00438	830.811	3020.505	60093.59	123.442	-0.1128	-0.1021	36.0	-0.0479	194.21	185.4
31894A4	0.00438	830.811	3020.505	60093.59	123.442	-0.1128	-0.1021	39.0	-0.0447	193.37	185.4
31894A4	0.00438	830.811	3020.505	60093.59	123.442	-0.1128	-0.1021	42.0	-0.0415	193.75	185.4
31894A4	0.00438	830.811	3020.505	60093.59	123.442	-0.1128	-0.1021	45.0	-0.0383	193.89	185.4
31894A4	0.00438	830.811	3020.505	60093.59	123.442	-0.1128	-0.1021	48.0	-0.0351	192.65	185.4
31894A4	0.00438	830.811	3020.505	60093.59	123.442	-0.1128	-0.1021	51.0	-0.0319	192.19	185.4
31894A4	0.00438	830.811	3020.505	60093.59	123.442	-0.1128	-0.1021	54.0	-0.0287	190.68	185.4
31894A4	0.00438	830.811	3020.505	60093.59	123.442	-0.1128	-0.1021	59.0	-0.0233	189.24	185.4
31894A4	0.00438	830.811	3020.505	60093.59	123.442	-0.1128	-0.1021	62.0	-0.0201	188.40	185.4
31894A4	0.00438	830.811	3020.505	60093.59	123.442	-0.1128	-0.1021	65.0	-0.0169	186.02	185.4
31894A4	0.00438	830.811	3020.505	60093.59	123.442	-0.1128	-0.1021	68.0	-0.0137	184.60	185.4
31894A4	0.00438	830.811	3020.505	60093.59	123.442	-0.1128	-0.1021	74.0	-0.0073	180.43	185.4
31894A5	0.00438	830.811	3027.054	56660.39	123.936	-0.1128	-0.1028	1.0	-0.0858	147.97	182.6
31894A5	0.00438	830.811	3027.054	56660.39	123.936	-0.1128	-0.1028	2.5	-0.0843	155.63	182.6
31894A5	0.00438	830.811	3027.054	56660.39	123.936	-0.1128	-0.1028	4.0	-0.0828	168.57	182.6
31894A5	0.00438	830.811	3027.054	56660.39	123.936	-0.1128	-0.1028	5.5	-0.0813	182.54	182.6
31894A5	0.00438	830.811	3027.054	56660.39	123.936	-0.1128	-0.1028	7.0	-0.0798	199.91	182.6
31894A5	0.00438	830.811	3027.054	56660.39	123.936	-0.1128	-0.1028	9.0	-0.0778	219.48	182.6
31894A5	0.00438	830.811	3027.054	56660.39	123.936	-0.1128	-0.1028	11.0	-0.0758	232.90	182.6
31894A5	0.00438	830.811	3027.054	56660.39	123.936	-0.1128	-0.1028	13.0	-0.0738	233.67	182.6
31894A5	0.00438	830.811	3027.054	56660.39	123.936	-0.1128	-0.1028	15.0	-0.0718	228.29	182.6
31894A5	0.00438	830.811	3027.054	56660.39	123.936	-0.1128	-0.1028	17.0	-0.0698	221.21	182.6
31894A5	0.00438	830.811	3027.054	56660.39	123.936	-0.1128	-0.1028	19.0	-0.0678	214.15	182.6
31894A5	0.00438	830.811	3027.054	56660.39	123.936	-0.1128	-0.1028	21.0	-0.0658	206.99	182.6
31894A5	0.00438	830.811	3027.054	56660.39	123.936	-0.1128	-0.1028	24.0	-0.0628	199.86	182.6
31894A5	0.00438	830.811	3027.054	56660.39	123.936	-0.1128	-0.1028	27.0	-0.0598	193.85	182.6
31894A5	0.00438	830.811	3027.054	56660.39	123.936	-0.1128	-0.1028	30.0	-0.0567	192.07	182.6
31894A5	0.00438	830.811	3027.054	56660.39	123.936	-0.1128	-0.1028	33.0	-0.0537	189.87	182.6
31894A5	0.00438	830.811	3027.054	56660.39	123.936	-0.1128	-0.1028	36.0	-0.0507	187.97	182.6
31894A5	0.00438	830.811	3027.054	56660.39	123.936	-0.1128	-0.1028	39.0	-0.0477	186.94	182.6
31894A5	0.00438	830.811	3027.054	56660.39	123.936	-0.1128	-0.1028	42.0	-0.0447	187.27	182.6
31894A5	0.00438	830.811	3027.054	56660.39	123.936	-0.1128	-0.1028	45.0	-0.0417	187.39	182.6
31894A5	0.00438	830.811	3027.054	56660.39	123.936	-0.1128	-0.1028	48.0	-0.0387	186.27	182.6
31894A5	0.00438	830.811	3027.054	56660.39	123.936	-0.1128	-0.1028	51.0	-0.0357	186.02	182.6
31894A5	0.00438	830.811	3027.054	56660.39	123.936	-0.1128	-0.1028	54.0	-0.0327	184.84	182.6
31894A5	0.00438	830.811	3027.054	56660.39	123.936	-0.1128	-0.1028	59.0	-0.0277	183.89	182.6
31894A5	0.00438	830.811	3027.054	56660.39	123.936	-0.1128	-0.1028	62.0	-0.0247	183.41	182.6
31894A5	0.00438	830.811	3027.054	56660.39	123.936	-0.1128	-0.1028	65.0	-0.0216	181.41	182.6
31894A5	0.00438	830.811	3027.054	56660.39	123.936	-0.1128	-0.1028	68.0	-0.0186	180.33	182.6
31894A5	0.00438	830.811	3027.054	56660.39	123.936	-0.1128	-0.1028	74.0	-0.0126	176.83	182.6
31894A6	0.00438	830.811	3009.736	51785.45	123.322	-0.1128	-0.1036	1.0	-0.0867	135.90	179.2
31894A6	0.00438	830.811	3009.736	51785.45	123.322	-0.1128	-0.1036	2.5	-0.0853	137.02	179.2
31894A6	0.00438	830.811	3009.736	51785.45	123.322	-0.1128	-0.1036	4.0	-0.0839	144.36	179.2
31894A6	0.00438	830.811	3009.736	51785.45	123.322	-0.1128	-0.1036	5.5	-0.0826	153.29	179.2
31894A6	0.00438	830.811	3009.736	51785.45	123.322	-0.1128	-0.1036	7.0	-0.0812	166.66	179.2
31894A6	0.00438	830.811	3009.736	51785.45	123.322	-0.1128	-0.1036	9.0	-0.0793	186.76	179.2
31894A6	0.00438	830.811	3009.736	51785.45	123.322	-0.1128	-0.1036	11.0	-0.0775	209.66	179.2
31894A6	0.00438	830.811	3009.736	51785.45	123.322	-0.1128	-0.1036	13.0	-0.0756	223.90	179.2
31894A6	0.00438	830.811	3009.736	51785.45	123.322	-0.1128	-0.1036	15.0	-0.0738	227.85	179.2
31894A6	0.00438	830.811	3009.736	51785.45	123.322	-0.1128	-0.1036	17.0	-0.0720	223.25	179.2
31894A6	0.00438	830.811	3009.736	51785.45	123.322	-0.1128	-0.1036	19.0	-0.0701	215.54	179.2
31894A6	0.00438	830.811	3009.736	51785.45	123.322	-0.1128	-0.1036	21.0	-0.0683	207.33	179.2
31894A6	0.00438	830.811	3009.736	51785.45	123.322	-0.1128	-0.1036	24.0	-0.0655	198.70	179.2
31894A6	0.00438	830.811	3009.736	51785.45	123.322	-0.1128	-0.1036	27.0	-0.0627	191.04	179.2
31894A6	0.00438	830.811	3009.736	51785.45	123.322	-0.1128	-0.1036	30.0	-0.0600	186.83	179.2
31894A6	0.00438	830.811	3009.736	51785.45	123.322	-0.1128	-0.1036	33.0	-0.0572	183.15	179.2
31894A6	0.00438	830.811	3009.736	51785.45	123.322	-0.1128	-0.1036	36.0	-0.0544	180.20	179.2
31894A6	0.00438	830.811	3009.736	51785.45	123.322	-0.1128	-0.1036	39.0	-0.0517	178.37	179.2
31894A6	0.00438	830.811	3009.736	51785.45	123.322	-0.1128	-0.1036	42.0	-0.0489	178.22	179.2
31894A6	0.00438	830.811	3009.736	51785.45	123.322	-0.1128	-0.1036	45.0	-0.0461	178.05	179.2
31894A6	0.00438	830.811	3009.736	51785.45	123.322	-0.1128	-0.1036	48.0	-0.0434	176.87	179.2
31894A6	0.00438	830.811	3009.736	51785.45	123.322	-0.1128	-0.1036	51.0	-0.0406	176.72	179.2
31894A6	0.00438	830.811	3009.736	51785.45	123.322	-0.1128	-0.1036	54.0	-0.0378	176.00	179.2
31894A6	0.00438	830.811	3009.736	51785.45	123.322	-0.1128	-0.1036	59.0	-0.0332	175.60	179.2
31894A6	0.00438	830.811	3009.736	51785.45	123.322	-0.1128	-0.1036	62.0	-0.0305	175.57	179.2
31894A6	0.00438	830.811	3009.736	51785.45	123.322	-0.1128	-0.1036	65.0	-0.0277	174.12	179.2
31894A6	0.00438	830.811	3009.736	51785.45	123.322	-0.1128	-0.1036	68.0	-0.0249	173.59	179.2
31894A6	0.00438	830.811	3009.736	51785.45	123.322	-0.1128	-0.1036	74.0	-0.0194	171.17	179.2

Table C.2 Inside Wall Temperature Data for Freon-134a (Cont'd)

RUN	D	P OUT	G	Q_w	HOTP POW	X_{in}	X_{out}	Z	X_{eq}	T_w	T_{sat}
	(m)	(kPa)	(kg/m².s)	(W/m²)	(W)			(cm)		(°C)	(°C)
31894A7	0.00438	830.811	3025.742	50300.67	123.110	-0.1128	-0.1039	1.0	-0.0872	131.80	175.6
31894A7	0.00438	830.811	3025.742	50300.67	123.110	-0.1128	-0.1039	2.5	-0.0858	132.03	175.6
31894A7	0.00438	830.811	3025.742	50300.67	123.110	-0.1128	-0.1039	4.0	-0.0845	137.89	175.6
31894A7	0.00438	830.811	3025.742	50300.67	123.110	-0.1128	-0.1039	5.5	-0.0832	145.17	175.6
31894A7	0.00438	830.811	3025.742	50300.67	123.110	-0.1128	-0.1039	7.0	-0.0818	156.83	175.6
31894A7	0.00438	830.811	3025.742	50300.67	123.110	-0.1128	-0.1039	9.0	-0.0800	174.82	175.6
31894A7	0.00438	830.811	3025.742	50300.67	123.110	-0.1128	-0.1039	11.0	-0.0783	197.92	175.6
31894A7	0.00438	830.811	3025.742	50300.67	123.110	-0.1128	-0.1039	13.0	-0.0765	215.46	175.6
31894A7	0.00438	830.811	3025.742	50300.67	123.110	-0.1128	-0.1039	15.0	-0.0747	224.23	175.6
31894A7	0.00438	830.811	3025.742	50300.67	123.110	-0.1128	-0.1039	17.0	-0.0729	222.49	175.6
31894A7	0.00438	830.811	3025.742	50300.67	123.110	-0.1128	-0.1039	19.0	-0.0711	215.38	175.6
31894A7	0.00438	830.811	3025.742	50300.67	123.110	-0.1128	-0.1039	21.0	-0.0693	207.05	175.6
31894A7	0.00438	830.811	3025.742	50300.67	123.110	-0.1128	-0.1039	24.0	-0.0667	198.13	175.6
31894A7	0.00438	830.811	3025.742	50300.67	123.110	-0.1128	-0.1039	27.0	-0.0640	189.46	175.6
31894A7	0.00438	830.811	3025.742	50300.67	123.110	-0.1128	-0.1039	30.0	-0.0613	185.33	175.6
31894A7	0.00438	830.811	3025.742	50300.67	123.110	-0.1128	-0.1039	33.0	-0.0587	181.19	175.6
31894A7	0.00438	830.811	3025.742	50300.67	123.110	-0.1128	-0.1039	36.0	-0.0560	177.69	175.6
31894A7	0.00438	830.811	3025.742	50300.67	123.110	-0.1128	-0.1039	39.0	-0.0533	175.50	175.6
31894A7	0.00438	830.811	3025.742	50300.67	123.110	-0.1128	-0.1039	42.0	-0.0506	175.13	175.6
31894A7	0.00438	830.811	3025.742	50300.67	123.110	-0.1128	-0.1039	45.0	-0.0480	174.89	175.6
31894A7	0.00438	830.811	3025.742	50300.67	123.110	-0.1128	-0.1039	48.0	-0.0453	173.68	175.6
31894A7	0.00438	830.811	3025.742	50300.67	123.110	-0.1128	-0.1039	51.0	-0.0426	173.50	175.6
31894A7	0.00438	830.811	3025.742	50300.67	123.110	-0.1128	-0.1039	54.0	-0.0400	172.76	175.6
31894A7	0.00438	830.811	3025.742	50300.67	123.110	-0.1128	-0.1039	59.0	-0.0355	172.58	175.6
31894A7	0.00438	830.811	3025.742	50300.67	123.110	-0.1128	-0.1039	62.0	-0.0328	172.66	175.6
31894A7	0.00438	830.811	3025.742	50300.67	123.110	-0.1128	-0.1039	65.0	-0.0302	171.28	175.6
31894A7	0.00438	830.811	3025.742	50300.67	123.110	-0.1128	-0.1039	68.0	-0.0275	170.72	175.6
31894A7	0.00438	830.811	3025.742	50300.67	123.110	-0.1128	-0.1039	74.0	-0.0221	168.63	175.6
31994A1	0.00438	830.811	2013.296	69641.20	124.251	-0.1380	-0.1194	1.0	-0.0936	245.55	200.0
31994A1	0.00438	830.811	2013.296	69641.20	124.251	-0.1380	-0.1194	2.5	-0.0908	261.50	200.0
31994A1	0.00438	830.811	2013.296	69641.20	124.251	-0.1380	-0.1194	4.0	-0.0880	262.69	200.0
31994A1	0.00438	830.811	2013.296	69641.20	124.251	-0.1380	-0.1194	5.5	-0.0852	255.10	200.0
31994A1	0.00438	830.811	2013.296	69641.20	124.251	-0.1380	-0.1194	7.0	-0.0824	249.80	200.0
31994A1	0.00438	830.811	2013.296	69641.20	124.251	-0.1380	-0.1194	9.0	-0.0787	243.15	200.0
31994A1	0.00438	830.811	2013.296	69641.20	124.251	-0.1380	-0.1194	11.0	-0.0750	240.59	200.0
31994A1	0.00438	830.811	2013.296	69641.20	124.251	-0.1380	-0.1194	13.0	-0.0713	237.89	200.0
31994A1	0.00438	830.811	2013.296	69641.20	124.251	-0.1380	-0.1194	15.0	-0.0676	236.47	200.0
31994A1	0.00438	830.811	2013.296	69641.20	124.251	-0.1380	-0.1194	17.0	-0.0639	235.69	200.0
31994A1	0.00438	830.811	2013.296	69641.20	124.251	-0.1380	-0.1194	19.0	-0.0602	235.37	200.0
31994A1	0.00438	830.811	2013.296	69641.20	124.251	-0.1380	-0.1194	21.0	-0.0565	234.64	200.0
31994A1	0.00438	830.811	2013.296	69641.20	124.251	-0.1380	-0.1194	24.0	-0.0509	235.13	200.0
31994A1	0.00438	830.811	2013.296	69641.20	124.251	-0.1380	-0.1194	27.0	-0.0454	235.77	200.0
31994A1	0.00438	830.811	2013.296	69641.20	124.251	-0.1380	-0.1194	30.0	-0.0398	236.83	200.0
31994A1	0.00438	830.811	2013.296	69641.20	124.251	-0.1380	-0.1194	33.0	-0.0343	236.37	200.0
31994A1	0.00438	830.811	2013.296	69641.20	124.251	-0.1380	-0.1194	36.0	-0.0287	234.54	200.0
31994A1	0.00438	830.811	2013.296	69641.20	124.251	-0.1380	-0.1194	39.0	-0.0231	233.14	200.0
31994A1	0.00438	830.811	2013.296	69641.20	124.251	-0.1380	-0.1194	42.0	-0.0176	231.91	200.0
31994A1	0.00438	830.811	2013.296	69641.20	124.251	-0.1380	-0.1194	45.0	-0.0120	230.16	200.0
31994A1	0.00438	830.811	2013.296	69641.20	124.251	-0.1380	-0.1194	48.0	-0.0065	226.71	200.0
31994A1	0.00438	830.811	2013.296	69641.20	124.251	-0.1380	-0.1194	51.0	-0.0009	224.22	200.0
31994A1	0.00438	830.811	2013.296	69641.20	124.251	-0.1380	-0.1194	54.0	0.0047	220.47	200.0
31994A1	0.00438	830.811	2013.296	69641.20	124.251	-0.1380	-0.1194	59.0	0.0139	215.50	200.0
31994A1	0.00438	830.811	2013.296	69641.20	124.251	-0.1380	-0.1194	62.0	0.0195	212.56	200.0
31994A1	0.00438	830.811	2013.296	69641.20	124.251	-0.1380	-0.1194	65.0	0.0251	208.06	200.0
31994A1	0.00438	830.811	2013.296	69641.20	124.251	-0.1380	-0.1194	68.0	0.0306	204.61	200.0
31994A1	0.00438	830.811	2013.296	69641.20	124.251	-0.1380	-0.1194	74.0	0.0417	196.33	200.0
31994A2	0.00438	830.811	2028.056	63632.80	125.777	-0.1380	-0.1212	1.0	-0.0953	223.00	223.0
31994A2	0.00438	830.811	2013.296	63632.80	125.777	-0.1380	-0.1212	2.5	-0.0928	234.01	223.0
31994A2	0.00438	830.811	2013.296	63632.80	125.777	-0.1380	-0.1212	4.0	-0.0903	239.75	223.0
31994A2	0.00438	830.811	2013.296	63632.80	125.777	-0.1380	-0.1212	5.5	-0.0878	239.58	223.0
31994A2	0.00438	830.811	2013.296	63632.80	125.777	-0.1380	-0.1212	7.0	-0.0853	239.10	223.0
31994A2	0.00438	830.811	2013.296	63632.80	125.777	-0.1380	-0.1212	9.0	-0.0819	235.32	223.0
31994A2	0.00438	830.811	2013.296	63632.80	125.777	-0.1380	-0.1212	11.0	-0.0785	234.61	223.0
31994A2	0.00438	830.811	2013.296	63632.80	125.777	-0.1380	-0.1212	13.0	-0.0752	232.76	223.0
31994A2	0.00438	830.811	2013.296	63632.80	125.777	-0.1380	-0.1212	15.0	-0.0718	231.23	223.0
31994A2	0.00438	830.811	2013.296	63632.80	125.777	-0.1380	-0.1212	17.0	-0.0684	230.19	223.0
31994A2	0.00438	830.811	2013.296	63632.80	125.777	-0.1380	-0.1212	19.0	-0.0651	229.68	223.0
31994A2	0.00438	830.811	2013.296	63632.80	125.777	-0.1380	-0.1212	21.0	-0.0617	228.63	223.0
31994A2	0.00438	830.811	2013.296	63632.80	125.777	-0.1380	-0.1212	24.0	-0.0567	228.53	223.0
31994A2	0.00438	830.811	2013.296	63632.80	125.777	-0.1380	-0.1212	27.0	-0.0516	228.87	223.0
31994A2	0.00438	830.811	2013.296	63632.80	125.777	-0.1380	-0.1212	30.0	-0.0466	229.67	223.0
31994A2	0.00438	830.811	2013.296	63632.80	125.777	-0.1380	-0.1212	33.0	-0.0415	229.31	223.0
31994A2	0.00438	830.811	2013.296	63632.80	125.777	-0.1380	-0.1212	36.0	-0.0365	227.58	223.0
31994A2	0.00438	830.811	2013.296	63632.80	125.777	-0.1380	-0.1212	39.0	-0.0315	226.36	223.0
31994A2	0.00438	830.811	2013.296	63632.80	125.777	-0.1380	-0.1212	42.0	-0.0264	225.33	223.0
31994A2	0.00438	830.811	2013.296	63632.80	125.777	-0.1380	-0.1212	45.0	-0.0214	223.93	223.0
31994A2	0.00438	830.811	2013.296	63632.80	125.777	-0.1380	-0.1212	48.0	-0.0163	221.17	223.0
31994A2	0.00438	830.811	2013.296	63632.80	125.777	-0.1380	-0.1212	51.0	-0.0113	219.32	223.0
31994A2	0.00438	830.811	2013.296	63632.80	125.777	-0.1380	-0.1212	54.0	-0.0062	216.30	223.0
31994A2	0.00438	830.811	2013.296	63632.80	125.777	-0.1380	-0.1212	59.0	0.0022	212.41	223.0
31994A2	0.00438	830.811	2013.296	63632.80	125.777	-0.1380	-0.1212	62.0	0.0072	210.03	223.0
31994A2	0.00438	830.811	2013.296	63632.80	125.777	-0.1380	-0.1212	65.0	0.0123	206.05	223.0
31994A2	0.00438	830.811	2013.296	63632.80	125.777	-0.1380	-0.1212	68.0	0.0173	203.17	223.0

Table C.2 Inside Wall Temperature Data for Freon-134a (Cont'd)

RUN	D	P OUT	G	Q_w	HOTP POW	X_{TT}	X_{CHB}	Z	X_{eq}	T_w	T_{HP}
	(m)	(kPa)	(kg/m².s)	(W/m²)	(W)			(cm)		(°C)	(°C)
31994A2	0.00438	830.811	2028.066	63632.80	125.777	-0.1380	-0.1212	74.0	0.0274	195.81	223.0
31994A3	0.00438	830.811	2022.459	56590.43	122.200	-0.1380	-0.1230	1.0	-0.0980	212.46	250.0
31994A3	0.00438	830.811	2022.459	56590.43	122.200	-0.1380	-0.1230	2.5	-0.0957	215.83	250.0
31994A3	0.00438	830.811	2022.459	56590.43	122.200	-0.1380	-0.1230	4.0	-0.0935	220.43	250.0
31994A3	0.00438	830.811	2022.459	56590.43	122.200	-0.1380	-0.1230	5.5	-0.0912	221.13	250.0
31994A3	0.00438	830.811	2022.459	56590.43	122.200	-0.1380	-0.1230	7.0	-0.0890	220.89	250.0
31994A3	0.00438	830.811	2022.459	56590.43	122.200	-0.1380	-0.1230	9.0	-0.0860	216.55	250.0
31994A3	0.00439	830.811	2022.459	56590.43	122.200	-0.1380	-0.1230	11.0	-0.0830	214.39	250.0
31994A3	0.00438	830.811	2022.459	56590.43	122.200	-0.1380	-0.1230	13.0	-0.0800	211.69	250.0
31994A3	0.00438	830.811	2022.459	56590.43	122.200	-0.1380	-0.1230	15.0	-0.0770	209.35	250.0
31994A3	0.00438	830.811	2022.459	56590.43	122.200	-0.1380	-0.1230	17.0	-0.0740	207.47	250.0
31994A3	0.00438	830.811	2022.459	56590.43	122.200	-0.1380	-0.1230	19.0	-0.0710	205.27	250.0
31994A3	0.00438	830.811	2022.459	56590.43	122.200	-0.1380	-0.1230	21.0	-0.0680	204.12	250.0
31994A3	0.00438	830.811	2022.459	56590.43	122.200	-0.1380	-0.1230	24.0	-0.0635	202.94	250.0
31994A3	0.00438	830.811	2022.459	56590.43	122.200	-0.1380	-0.1230	27.0	-0.0590	202.26	250.0
31994A3	0.00438	830.811	2022.459	56590.43	122.200	-0.1380	-0.1230	30.0	-0.0545	203.33	250.0
31994A3	0.00438	830.811	2022.459	56590.43	122.200	-0.1380	-0.1230	33.0	-0.0500	203.56	250.0
31994A3	0.00438	830.811	2022.459	56590.43	122.200	-0.1380	-0.1230	36.0	-0.0455	203.24	250.0
31994A3	0.00438	830.811	2022.459	56590.43	122.200	-0.1380	-0.1230	39.0	-0.0410	203.70	250.0
31994A3	0.00438	830.811	2022.459	56590.43	122.200	-0.1380	-0.1230	42.0	-0.0365	204.61	250.0
31994A3	0.00438	830.811	2022.459	56590.43	122.200	-0.1380	-0.1230	45.0	-0.0320	204.99	250.0
31994A3	0.00438	830.811	2022.459	56590.43	122.200	-0.1380	-0.1230	48.0	-0.0275	203.85	250.0
31994A3	0.00438	830.811	2022.459	56590.43	122.200	-0.1380	-0.1230	51.0	-0.0230	203.52	250.0
31994A3	0.00438	830.811	2022.459	56590.43	122.200	-0.1380	-0.1230	54.0	-0.0185	201.90	250.0
31994A3	0.00438	830.811	2022.459	56590.43	122.200	-0.1380	-0.1230	59.0	-0.0110	200.22	250.0
31994A3	0.00438	830.811	2022.459	56590.43	122.200	-0.1380	-0.1230	62.0	-0.0065	199.00	250.0
31994A3	0.00438	830.811	2022.459	56590.43	122.200	-0.1380	-0.1230	65.0	-0.0020	196.05	250.0
31994A3	0.00438	830.811	2022.459	56590.43	122.200	-0.1380	-0.1230	68.0	0.0025	194.03	250.0
31994A4	0.00438	830.811	2023.592	51460.67	97.941	-0.1388	-0.1252	74.0	0.0115	188.12	250.0
31994A4	0.00438	830.811	2023.592	51460.67	97.941	-0.1388	-0.1252	1.0	-0.1050	205.58	255.1
31994A4	0.00438	830.811	2023.592	51460.67	97.941	-0.1388	-0.1252	2.5	-0.1029	203.72	255.1
31994A4	0.00438	830.811	2023.592	51460.67	97.941	-0.1388	-0.1252	4.0	-0.1009	207.70	255.1
31994A4	0.00438	830.811	2023.592	51460.67	97.941	-0.1388	-0.1252	5.5	-0.0989	209.45	255.0
31994A4	0.00438	830.811	2023.592	51460.67	97.941	-0.1388	-0.1252	7.0	-0.0968	210.31	255.0
31994A4	0.00438	830.811	2023.592	51460.67	97.941	-0.1388	-0.1252	9.0	-0.0941	206.95	255.0
31994A4	0.00438	830.811	2023.592	51460.67	97.941	-0.1388	-0.1252	11.0	-0.0914	205.06	255.0
31994A4	0.00438	830.811	2023.592	51460.67	97.941	-0.1388	-0.1252	13.0	-0.0886	201.97	255.0
31994A4	0.00438	830.811	2023.592	51460.67	97.941	-0.1388	-0.1252	15.0	-0.0859	199.21	255.0
31994A4	0.00438	830.811	2023.592	51460.67	97.941	-0.1388	-0.1252	17.0	-0.0832	196.96	255.0
31994A4	0.00438	830.811	2023.592	51460.67	97.941	-0.1388	-0.1252	19.0	-0.0805	195.32	255.0
31994A4	0.00438	830.811	2023.592	51460.67	97.941	-0.1388	-0.1252	21.0	-0.0777	192.84	255.0
31994A4	0.00438	830.811	2023.592	51460.67	97.941	-0.1388	-0.1252	24.0	-0.0736	191.11	255.0
31994A4	0.00438	830.811	2023.592	51460.67	97.941	-0.1388	-0.1252	27.0	-0.0696	189.04	255.0
31994A4	0.00438	830.811	2023.592	51460.67	97.941	-0.1388	-0.1252	30.0	-0.0655	190.49	255.0
31994A4	0.00438	830.811	2023.592	51460.67	97.941	-0.1388	-0.1252	33.0	-0.0614	190.50	255.0
31994A4	0.00438	830.811	2023.592	51460.67	97.941	-0.1388	-0.1252	36.0	-0.0573	190.10	255.0
31994A4	0.00438	830.811	2023.592	51460.67	97.941	-0.1388	-0.1252	39.0	-0.0532	190.75	255.0
31994A4	0.00438	830.811	2023.592	51460.67	97.941	-0.1388	-0.1252	42.0	-0.0491	191.91	255.0
31994A4	0.00438	830.811	2023.592	51460.67	97.941	-0.1388	-0.1252	45.0	-0.0450	192.73	255.0
31994A4	0.00438	830.811	2023.592	51460.67	97.941	-0.1388	-0.1252	48.0	-0.0409	192.20	255.0
31994A4	0.00438	830.811	2023.592	51460.67	97.941	-0.1388	-0.1252	51.0	-0.0369	192.30	255.0
31994A4	0.00438	830.811	2023.592	51460.67	97.941	-0.1388	-0.1252	54.0	-0.0328	191.31	255.0
31994A4	0.00438	830.811	2023.592	51460.67	97.941	-0.1388	-0.1252	59.0	-0.0260	190.58	255.0
31994A4	0.00438	830.811	2023.592	51460.67	97.941	-0.1388	-0.1252	62.0	-0.0219	189.90	255.0
31994A4	0.00438	830.811	2023.592	51460.67	97.941	-0.1388	-0.1252	65.0	-0.0178	187.63	255.0
31994A4	0.00438	830.811	2023.592	51460.67	97.941	-0.1388	-0.1252	68.0	-0.0137	186.27	255.0
31994A5	0.00438	830.811	2021.640	44491.33	100.028	-0.1388	-0.1252	74.0	-0.0055	181.52	255.0
31994A5	0.00438	830.811	2021.640	44491.33	100.028	-0.1380	-0.1262	1.0	-0.1057	181.30	233.1
31994A5	0.00438	830.811	2021.640	44491.33	100.028	-0.1380	-0.1262	2.5	-0.1040	175.76	233.1
31994A5	0.00438	830.811	2021.640	44491.33	100.028	-0.1380	-0.1262	4.0	-0.1022	177.69	233.1
31994A5	0.00438	830.811	2021.640	44491.33	100.028	-0.1380	-0.1262	5.5	-0.1004	179.16	233.1
31994A5	0.00438	830.811	2021.640	44491.33	100.028	-0.1380	-0.1262	7.0	-0.0987	181.41	233.0
31994A5	0.00438	830.811	2021.640	44491.33	100.028	-0.1380	-0.1262	9.0	-0.0963	182.33	233.0
31994A5	0.00438	830.811	2021.640	44491.33	100.028	-0.1380	-0.1262	11.0	-0.0940	184.58	233.0
31994A5	0.00438	830.811	2021.640	44491.33	100.028	-0.1380	-0.1262	13.0	-0.0916	184.57	233.0
31994A5	0.00438	830.811	2021.640	44491.33	100.028	-0.1380	-0.1262	15.0	-0.0892	184.04	233.0
31994A5	0.00438	830.811	2021.640	44491.33	100.028	-0.1380	-0.1262	17.0	-0.0869	182.78	233.0
31994A5	0.00438	830.811	2021.640	44491.33	100.028	-0.1380	-0.1262	19.0	-0.0845	181.31	233.0
31994A5	0.00438	830.811	2021.640	44491.33	100.028	-0.1380	-0.1262	21.0	-0.0822	179.04	233.0
31994A5	0.00438	830.811	2021.640	44491.33	100.028	-0.1380	-0.1262	24.0	-0.0786	177.06	233.0
31994A5	0.00438	830.811	2021.640	44491.33	100.028	-0.1380	-0.1262	27.0	-0.0751	174.16	233.0
31994A5	0.00438	830.811	2021.640	44491.33	100.028	-0.1380	-0.1262	30.0	-0.0715	174.89	233.0
31994A5	0.00438	830.811	2021.640	44491.33	100.028	-0.1380	-0.1262	33.0	-0.0680	173.99	233.0
31994A5	0.00438	830.811	2021.640	44491.33	100.028	-0.1380	-0.1262	36.0	-0.0645	173.14	233.0
31994A5	0.00438	830.811	2021.640	44491.33	100.028	-0.1380	-0.1262	39.0	-0.0609	173.11	233.0
31994A5	0.00438	830.811	2021.640	44491.33	100.028	-0.1380	-0.1262	42.0	-0.0574	174.12	233.0
31994A5	0.00438	830.811	2021.640	44491.33	100.028	-0.1380	-0.1262	45.0	-0.0539	174.98	233.0
31994A5	0.00438	830.811	2021.640	44491.33	100.028	-0.1380	-0.1262	48.0	-0.0503	175.18	233.0
31994A5	0.00438	830.811	2021.640	44491.33	100.028	-0.1380	-0.1262	51.0	-0.0468	176.22	233.0
31994A5	0.00438	830.811	2021.640	44491.33	100.028	-0.1380	-0.1262	54.0	-0.0432	176.41	233.0
31994A5	0.00438	830.811	2021.640	44491.33	100.028	-0.1380	-0.1262	59.0	-0.0374	177.51	233.0
31994A5	0.00438	830.811	2021.640	44491.33	100.028	-0.1380	-0.1262	62.0	-0.0338	178.04	233.0
31994A5	0.00438	830.811	2021.640	44491.33	100.028	-0.1380	-0.1262	65.0	-0.0303	177.20	233.0
31994A5	0.00438	830.811	2021.640	44491.33	100.028	-0.1380	-0.1262	68.0	-0.0267	177.37	233.0

Table C.2 Inside Wall Temperature Data for Freon-134a (Cont'd)

RUN	D	P OUT	G	Q_w	HOTP POW	X_{in}	X_{exp}	Z	X_{eq}	T_w	T_{sp}
	(m)	(kPa)	(kg/m².s)	(W/m²)	(W)			(cm)		(°C)	(°C)
31994A5	0.00438	830.811	2021.640	44491.33	100.028	-0.1380	-0.1262	74.0	-0.0197	175.73	233.0
31994A6	0.00438	830.811	2014.957	39394.93	99.626	-0.1380	-0.1275	1.0	-0.1072	182.71	206.0
31994A6	0.00438	830.811	2014.957	39394.93	99.626	-0.1380	-0.1275	2.5	-0.1056	179.06	206.0
31994A6	0.00438	830.811	2014.957	39394.93	99.626	-0.1380	-0.1275	4.0	-0.1041	181.94	206.0
31994A6	0.00438	830.811	2014.957	39394.93	99.626	-0.1380	-0.1275	5.5	-0.1025	182.28	206.0
31994A6	0.00438	830.811	2014.957	39394.93	99.626	-0.1380	-0.1275	7.0	-0.1009	181.19	206.0
31994A6	0.00438	830.811	2014.957	39394.93	99.626	-0.1380	-0.1275	9.0	-0.0988	176.81	206.0
31994A6	0.00438	830.811	2014.957	39394.93	99.626	-0.1380	-0.1275	11.0	-0.0967	173.75	206.0
31994A6	0.00438	830.811	2014.957	39394.93	99.626	-0.1380	-0.1275	13.0	-0.0946	169.33	206.0
31994A6	0.00438	830.811	2014.957	39394.93	99.626	-0.1380	-0.1275	15.0	-0.0925	166.08	206.0
31994A6	0.00438	830.811	2014.957	39394.93	99.626	-0.1380	-0.1275	17.0	-0.0904	163.79	206.0
31994A6	0.00438	830.811	2014.957	39394.93	99.626	-0.1380	-0.1275	19.0	-0.0883	161.91	206.0
31994A6	0.00438	830.811	2014.957	39394.93	99.626	-0.1380	-0.1275	21.0	-0.0863	159.82	206.0
31994A6	0.00438	830.811	2014.957	39394.93	99.626	-0.1380	-0.1275	24.0	-0.0831	159.14	206.0
31994A6	0.00438	830.811	2014.957	39394.93	99.626	-0.1380	-0.1275	27.0	-0.0800	158.24	206.0
31994A6	0.00438	830.811	2014.957	39394.93	99.626	-0.1380	-0.1275	30.0	-0.0768	160.01	206.0
31994A6	0.00438	830.811	2014.957	39394.93	99.626	-0.1380	-0.1275	33.0	-0.0737	160.47	206.0
31994A6	0.00438	830.811	2014.957	39394.93	99.626	-0.1380	-0.1275	36.0	-0.0705	160.24	206.0
31994A6	0.00438	830.811	2014.957	39394.93	99.626	-0.1380	-0.1275	39.0	-0.0674	160.82	206.0
31994A6	0.00438	830.811	2014.957	39394.93	99.626	-0.1380	-0.1275	42.0	-0.0643	161.88	206.0
31994A6	0.00438	830.811	2014.957	39394.93	99.626	-0.1380	-0.1275	45.0	-0.0611	162.79	206.0
31994A6	0.00438	830.811	2014.957	39394.93	99.626	-0.1380	-0.1275	48.0	-0.0580	162.36	206.0
31994A6	0.00438	830.811	2014.957	39394.93	99.626	-0.1380	-0.1275	51.0	-0.0548	162.96	206.0
31994A6	0.00438	830.811	2014.957	39394.93	99.626	-0.1380	-0.1275	54.0	-0.0517	162.58	206.0
31994A6	0.00438	830.811	2014.957	39394.93	99.626	-0.1380	-0.1275	59.0	-0.0464	163.01	206.0
31994A6	0.00438	830.811	2014.957	39394.93	99.626	-0.1380	-0.1275	62.0	-0.0433	163.04	206.0
31994A6	0.00438	830.811	2014.957	39394.93	99.626	-0.1380	-0.1275	65.0	-0.0402	162.33	206.0
31994A6	0.00438	830.811	2014.957	39394.93	99.626	-0.1380	-0.1275	68.0	-0.0370	162.31	206.0
31994A6	0.00438	830.811	2014.957	39394.93	99.626	-0.1380	-0.1275	74.0	-0.0307	161.11	206.0
31994A7	0.00438	830.811	2018.848	35634.44	124.944	-0.1363	-0.1269	1.0	-0.1018	121.30	166.0
31994A7	0.00438	830.811	2018.848	35634.44	124.944	-0.1363	-0.1269	2.5	-0.1004	113.13	166.0
31994A7	0.00438	830.811	2018.848	35634.44	124.944	-0.1363	-0.1269	4.0	-0.0990	110.62	166.0
31994A7	0.00438	830.811	2018.848	35634.44	124.944	-0.1363	-0.1269	5.5	-0.0976	107.18	166.0
31994A7	0.00438	830.811	2018.848	35634.44	124.944	-0.1363	-0.1269	7.0	-0.0961	109.81	166.0
31994A7	0.00438	830.811	2018.848	35634.44	124.944	-0.1363	-0.1269	9.0	-0.0942	113.10	166.0
31994A7	0.00438	830.811	2018.848	35634.44	124.944	-0.1363	-0.1269	11.0	-0.0924	123.48	166.0
31994A7	0.00438	830.811	2018.848	35634.44	124.944	-0.1363	-0.1269	13.0	-0.0905	135.60	166.0
31994A7	0.00438	830.811	2018.848	35634.44	124.944	-0.1363	-0.1269	15.0	-0.0886	150.35	166.0
31994A7	0.00438	830.811	2018.848	35634.44	124.944	-0.1363	-0.1269	17.0	-0.0867	163.46	166.0
31994A7	0.00438	830.811	2018.848	35634.44	124.944	-0.1363	-0.1269	19.0	-0.0848	170.78	166.0
31994A7	0.00438	830.811	2018.848	35634.44	124.944	-0.1363	-0.1269	21.0	-0.0829	170.22	166.0
31994A7	0.00438	830.811	2018.848	35634.44	124.944	-0.1363	-0.1269	24.0	-0.0801	165.22	166.0
31994A7	0.00438	830.811	2018.848	35634.44	124.944	-0.1363	-0.1269	27.0	-0.0772	159.11	166.0
31994A7	0.00438	830.811	2018.848	35634.44	124.944	-0.1363	-0.1269	30.0	-0.0744	158.14	166.0
31994A7	0.00438	830.811	2018.848	35634.44	124.944	-0.1363	-0.1269	33.0	-0.0715	155.70	166.0
31994A7	0.00438	830.811	2018.848	35634.44	124.944	-0.1363	-0.1269	36.0	-0.0687	152.76	166.0
31994A7	0.00438	830.811	2018.848	35634.44	124.944	-0.1363	-0.1269	39.0	-0.0659	150.57	166.0
31994A7	0.00438	830.811	2018.848	35634.44	124.944	-0.1363	-0.1269	42.0	-0.0630	149.60	166.0
31994A7	0.00438	830.811	2018.848	35634.44	124.944	-0.1363	-0.1269	45.0	-0.0602	148.42	166.0
31994A7	0.00438	830.811	2018.848	35634.44	124.944	-0.1363	-0.1269	48.0	-0.0574	146.81	166.0
31994A7	0.00438	830.811	2018.848	35634.44	124.944	-0.1363	-0.1269	51.0	-0.0545	146.19	166.0
31994A7	0.00438	830.811	2018.848	35634.44	124.944	-0.1363	-0.1269	54.0	-0.0517	145.46	166.0
31994A7	0.00438	830.811	2018.848	35634.44	124.944	-0.1363	-0.1269	59.0	-0.0470	145.65	166.0
31994A7	0.00438	830.811	2018.848	35634.44	124.944	-0.1363	-0.1269	62.0	-0.0441	146.18	166.0
31994A7	0.00438	830.811	2018.848	35634.44	124.944	-0.1363	-0.1269	65.0	-0.0413	145.91	166.0
31994A7	0.00438	830.811	2018.848	35634.44	124.944	-0.1363	-0.1269	68.0	-0.0384	146.50	166.0
31994A7	0.00438	830.811	2018.848	35634.44	124.944	-0.1363	-0.1269	74.0	-0.0328	146.87	166.0
32094A1	0.00438	830.811	2014.870	69906.00	119.937	-0.1128	-0.0942	1.0	-0.0692	238.43	265.0
32094A1	0.00438	830.811	2014.870	69906.00	119.937	-0.1128	-0.0942	2.5	-0.0664	240.97	265.0
32094A1	0.00438	830.811	2014.870	69906.00	119.937	-0.1128	-0.0942	4.0	-0.0636	241.77	265.0
32094A1	0.00438	830.811	2014.870	69906.00	119.937	-0.1128	-0.0942	5.5	-0.0608	239.96	265.0
32094A1	0.00438	830.811	2014.870	69906.00	119.937	-0.1128	-0.0942	7.0	-0.0580	238.42	265.0
32094A1	0.00438	830.811	2014.870	69906.00	119.937	-0.1128	-0.0942	9.0	-0.0543	233.90	265.0
32094A1	0.00438	830.811	2014.870	69906.00	119.937	-0.1128	-0.0942	11.0	-0.0506	232.69	265.0
32094A1	0.00438	830.811	2014.870	69906.00	119.937	-0.1128	-0.0942	13.0	-0.0469	230.86	265.0
32094A1	0.00438	830.811	2014.870	69906.00	119.937	-0.1128	-0.0942	15.0	-0.0432	230.27	265.0
32094A1	0.00438	830.811	2014.870	69906.00	119.937	-0.1128	-0.0942	17.0	-0.0394	229.81	265.0
32094A1	0.00438	830.811	2014.870	69906.00	119.937	-0.1128	-0.0942	19.0	-0.0357	229.22	265.0
32094A1	0.00438	830.811	2014.870	69906.00	119.937	-0.1128	-0.0942	21.0	-0.0320	228.13	265.0
32094A1	0.00438	830.811	2014.870	69906.00	119.937	-0.1128	-0.0942	24.0	-0.0264	228.10	265.0
32094A1	0.00438	830.811	2014.870	69906.00	119.937	-0.1128	-0.0942	27.0	-0.0208	227.25	265.0
32094A1	0.00438	830.811	2014.870	69906.00	119.937	-0.1128	-0.0942	30.0	-0.0153	227.74	265.0
32094A1	0.00438	830.811	2014.870	69906.00	119.937	-0.1128	-0.0942	33.0	-0.0097	226.87	265.0
32094A1	0.00438	830.811	2014.870	69906.00	119.937	-0.1128	-0.0942	36.0	-0.0041	224.19	265.0
32094A1	0.00438	830.811	2014.870	69906.00	119.937	-0.1128	-0.0942	39.0	0.0015	222.18	265.0
32094A1	0.00438	830.811	2014.870	69906.00	119.937	-0.1128	-0.0942	42.0	0.0070	220.32	265.0
32094A1	0.00438	830.811	2014.870	69906.00	119.937	-0.1128	-0.0942	45.0	0.0126	217.94	265.0
32094A1	0.00438	830.811	2014.870	69906.00	119.937	-0.1128	-0.0942	48.0	0.0182	214.00	265.0
32094A1	0.00438	830.811	2014.870	69906.00	119.937	-0.1128	-0.0942	51.0	0.0238	210.72	265.0
32094A1	0.00438	830.811	2014.870	69906.00	119.937	-0.1128	-0.0942	54.0	0.0293	206.41	265.0
32094A1	0.00438	830.811	2014.870	69906.00	119.937	-0.1128	-0.0942	59.0	0.0386	200.55	265.0
32094A1	0.00438	830.811	2014.870	69906.00	119.937	-0.1128	-0.0942	62.0	0.0442	197.14	265.0
32094A1	0.00438	830.811	2014.870	69906.00	119.937	-0.1128	-0.0942	65.0	0.0498	192.32	265.0

Table C.2 Inside Wall Temperature Data for Freon-134a (Cont'd)

RUN	D	P OUT	G	Q_w	HOTP POW	X_{in}	X_{out}	Z	X_{eq}	T_w	T_{HP}
	(m)	(kPa)	(kg/m².s)	(W/m²)	(W)			(cm)		(°C)	(°C)
32094A1	0.00438	830.811	2014.870	69906.00	119.937	-0.1128	-0.0942	68.0	0.0554	188.37	265.0
32094A1	0.00438	830.811	2014.870	69906.00	119.937	-0.1128	-0.0942	74.0	0.0665	179.47	265.0
32094A2	0.00438	830.811	2012.871	63873.28	118.420	-0.1128	-0.0958	1.0	-0.0712	232.83	286.0
32094A2	0.00438	830.811	2012.871	63873.28	118.420	-0.1128	-0.0958	2.5	-0.0686	229.64	286.0
32094A2	0.00438	830.811	2012.871	63873.28	118.420	-0.1128	-0.0958	4.0	-0.0661	231.21	286.0
32094A2	0.00438	830.811	2012.871	63873.28	118.420	-0.1128	-0.0958	5.5	-0.0635	229.86	286.0
32094A2	0.00438	830.811	2012.871	63873.28	118.420	-0.1128	-0.0958	7.0	-0.0610	228.10	286.0
32094A2	0.00438	830.811	2012.871	63873.28	118.420	-0.1128	-0.0958	9.0	-0.0576	223.63	286.0
32094A2	0.00438	830.811	2012.871	63873.28	118.420	-0.1128	-0.0958	11.0	-0.0542	221.90	286.0
32094A2	0.00438	830.811	2012.871	63873.28	118.420	-0.1128	-0.0958	13.0	-0.0508	219.46	286.0
32094A2	0.00438	830.811	2012.871	63873.28	118.420	-0.1128	-0.0958	15.0	-0.0474	218.79	286.0
32094A2	0.00438	830.811	2012.871	63873.28	118.420	-0.1128	-0.0958	17.0	-0.0440	218.43	286.0
32094A2	0.00438	830.811	2012.871	63873.28	118.420	-0.1128	-0.0958	19.0	-0.0406	217.80	286.0
32094A2	0.00438	830.811	2012.871	63873.28	118.420	-0.1128	-0.0958	21.0	-0.0372	216.81	286.0
32094A2	0.00438	830.811	2012.871	63873.28	118.420	-0.1128	-0.0958	24.0	-0.0321	217.15	286.0
32094A2	0.00438	830.811	2012.871	63873.28	118.420	-0.1128	-0.0958	27.0	-0.0270	216.55	286.0
32094A2	0.00438	830.811	2012.871	63873.28	118.420	-0.1128	-0.0958	30.0	-0.0219	217.38	286.0
32094A2	0.00438	830.811	2012.871	63873.28	118.420	-0.1128	-0.0958	33.0	-0.0168	216.67	286.0
32094A2	0.00438	830.811	2012.871	63873.28	118.420	-0.1128	-0.0958	36.0	-0.0117	214.41	286.0
32094A2	0.00438	830.811	2012.871	63873.28	118.420	-0.1128	-0.0958	39.0	-0.0066	212.89	286.0
32094A2	0.00438	830.811	2012.871	63873.28	118.420	-0.1128	-0.0958	42.0	-0.0015	211.50	286.0
32094A2	0.00438	830.811	2012.871	63873.28	118.420	-0.1128	-0.0958	45.0	0.0036	209.69	286.0
32094A2	0.00438	830.811	2012.871	63873.28	118.420	-0.1128	-0.0958	48.0	0.0087	206.41	286.0
32094A2	0.00438	830.811	2012.871	63873.28	118.420	-0.1128	-0.0958	51.0	0.0138	203.82	286.0
32094A2	0.00438	830.811	2012.871	63873.28	118.420	-0.1128	-0.0958	54.0	0.0189	200.12	286.0
32094A2	0.00438	830.811	2012.871	63873.28	118.420	-0.1128	-0.0958	59.0	0.0274	195.38	286.0
32094A2	0.00438	830.811	2012.871	63873.28	118.420	-0.1128	-0.0958	62.0	0.0325	192.46	286.0
32094A2	0.00438	830.811	2012.871	63873.28	118.420	-0.1128	-0.0958	65.0	0.0376	188.33	286.0
32094A2	0.00438	830.811	2012.871	63873.28	118.420	-0.1128	-0.0958	68.0	0.0427	184.97	286.0
32094A2	0.00438	830.811	2012.871	63873.28	118.420	-0.1128	-0.0958	74.0	0.0529	177.27	286.0
32094A3	0.00438	830.811	2017.197	56697.49	121.729	-0.1128	-0.0977	1.0	-0.0727	210.60	238.0
32094A3	0.00438	830.811	2017.197	56697.49	121.729	-0.1128	-0.0977	2.5	-0.0705	214.11	238.0
32094A3	0.00438	830.811	2017.197	56697.49	121.729	-0.1128	-0.0977	4.0	-0.0682	216.04	238.0
32094A3	0.00438	830.811	2017.197	56697.49	121.729	-0.1128	-0.0977	5.5	-0.0660	214.41	238.0
32094A3	0.00438	830.811	2017.197	56697.49	121.729	-0.1128	-0.0977	7.0	-0.0637	213.06	238.0
32094A3	0.00438	830.811	2017.197	56697.49	121.729	-0.1128	-0.0977	9.0	-0.0607	208.43	238.0
32094A3	0.00438	830.811	2017.197	56697.49	121.729	-0.1128	-0.0977	11.0	-0.0577	206.55	238.0
32094A3	0.00438	830.811	2017.197	56697.49	121.729	-0.1128	-0.0977	13.0	-0.0547	204.75	238.0
32094A3	0.00438	830.811	2017.197	56697.49	121.729	-0.1128	-0.0977	15.0	-0.0517	203.70	238.0
32094A3	0.00438	830.811	2017.197	56697.49	121.729	-0.1128	-0.0977	17.0	-0.0486	202.71	238.0
32094A3	0.00438	830.811	2017.197	56697.49	121.729	-0.1128	-0.0977	19.0	-0.0456	202.24	238.0
32094A3	0.00438	830.811	2017.197	56697.49	121.729	-0.1128	-0.0977	21.0	-0.0426	201.49	238.0
32094A3	0.00438	830.811	2017.197	56697.49	121.729	-0.1128	-0.0977	24.0	-0.0381	201.41	238.0
32094A3	0.00438	830.811	2017.197	56697.49	121.729	-0.1128	-0.0977	27.0	-0.0336	201.16	238.0
32094A3	0.00438	830.811	2017.197	56697.49	121.729	-0.1128	-0.0977	30.0	-0.0291	202.88	238.0
32094A3	0.00438	830.811	2017.197	56697.49	121.729	-0.1128	-0.0977	33.0	-0.0246	202.43	238.0
32094A3	0.00438	830.811	2017.197	56697.49	121.729	-0.1128	-0.0977	36.0	-0.0200	201.46	238.0
32094A3	0.00438	830.811	2017.197	56697.49	121.729	-0.1128	-0.0977	39.0	-0.0155	200.61	238.0
32094A3	0.00438	830.811	2017.197	56697.49	121.729	-0.1128	-0.0977	42.0	-0.0110	200.17	238.0
32094A3	0.00438	830.811	2017.197	56697.49	121.729	-0.1128	-0.0977	45.0	-0.0065	199.56	238.0
32094A3	0.00438	830.811	2017.197	56697.49	121.729	-0.1128	-0.0977	48.0	-0.0020	197.17	238.0
32094A3	0.00438	830.811	2017.197	56697.49	121.729	-0.1128	-0.0977	51.0	0.0026	195.55	238.0
32094A3	0.00438	830.811	2017.197	56697.49	121.729	-0.1128	-0.0977	54.0	0.0071	192.88	238.0
32094A3	0.00438	830.811	2017.197	56697.49	121.729	-0.1128	-0.0977	59.0	0.0146	189.48	238.0
32094A3	0.00438	830.811	2017.197	56697.49	121.729	-0.1128	-0.0977	62.0	0.0191	187.58	238.0
32094A3	0.00438	830.811	2017.197	56697.49	121.729	-0.1128	-0.0977	65.0	0.0236	184.20	238.0
32094A3	0.00438	830.811	2017.197	56697.49	121.729	-0.1128	-0.0977	68.0	0.0282	181.65	238.0
32094A3	0.00438	830.811	2017.197	56697.49	121.729	-0.1128	-0.0977	74.0	0.0372	175.41	238.0
32094A4	0.00438	830.811	2008.520	51545.61	121.682	-0.1128	-0.0991	1.0	-0.0741	205.48	260.0
32094A4	0.00438	830.811	2008.520	51545.61	121.682	-0.1128	-0.0991	2.5	-0.0720	202.45	260.0
32094A4	0.00438	830.811	2008.520	51545.61	121.682	-0.1128	-0.0991	4.0	-0.0700	204.48	260.0
32094A4	0.00438	830.811	2008.520	51545.61	121.682	-0.1128	-0.0991	5.5	-0.0679	203.96	260.0
32094A4	0.00438	830.811	2008.520	51545.61	121.682	-0.1128	-0.0991	7.0	-0.0658	203.08	260.0
32094A4	0.00438	830.811	2008.520	51545.61	121.682	-0.1128	-0.0991	9.0	-0.0631	198.65	260.0
32094A4	0.00438	830.811	2008.520	51545.61	121.682	-0.1128	-0.0991	11.0	-0.0603	196.37	260.0
32094A4	0.00438	830.811	2008.520	51545.61	121.682	-0.1128	-0.0991	13.0	-0.0576	194.22	260.0
32094A4	0.00438	830.811	2008.520	51545.61	121.682	-0.1128	-0.0991	15.0	-0.0548	193.09	260.0
32094A4	0.00438	830.811	2008.520	51545.61	121.682	-0.1128	-0.0991	17.0	-0.0521	191.94	260.0
32094A4	0.00438	830.811	2008.520	51545.61	121.682	-0.1128	-0.0991	19.0	-0.0493	191.32	260.0
32094A4	0.00438	830.811	2008.520	51545.61	121.682	-0.1128	-0.0991	21.0	-0.0466	190.54	260.0
32094A4	0.00438	830.811	2008.520	51545.61	121.682	-0.1128	-0.0991	24.0	-0.0425	190.49	260.0
32094A4	0.00438	830.811	2008.520	51545.61	121.682	-0.1128	-0.0991	27.0	-0.0383	190.14	260.0
32094A4	0.00438	830.811	2008.520	51545.61	121.682	-0.1128	-0.0991	30.0	-0.0342	192.14	260.0
32094A4	0.00438	830.811	2008.520	51545.61	121.682	-0.1128	-0.0991	33.0	-0.0301	191.99	260.0
32094A4	0.00438	830.811	2008.520	51545.61	121.682	-0.1128	-0.0991	36.0	-0.0260	191.29	260.0
32094A4	0.00438	830.811	2008.520	51545.61	121.682	-0.1128	-0.0991	39.0	-0.0218	190.47	260.0
32094A4	0.00438	830.811	2008.520	51545.61	121.682	-0.1128	-0.0991	42.0	-0.0177	190.57	260.0
32094A4	0.00438	830.811	2008.520	51545.61	121.682	-0.1128	-0.0991	45.0	-0.0136	190.22	260.0
32094A4	0.00438	830.811	2008.520	51545.61	121.682	-0.1128	-0.0991	48.0	-0.0095	188.26	260.0
32094A4	0.00438	830.811	2008.520	51545.61	121.682	-0.1128	-0.0991	51.0	-0.0053	187.26	260.0
32094A4	0.00438	830.811	2008.520	51545.61	121.682	-0.1128	-0.0991	54.0	-0.0012	185.19	260.0
32094A4	0.00438	830.811	2008.520	51545.61	121.682	-0.1128	-0.0991	59.0	0.0057	182.66	260.0
32094A4	0.00438	830.811	2008.520	51545.61	121.682	-0.1128	-0.0991	62.0	0.0098	181.18	260.0
32094A4	0.00438	830.811	2008.520	51545.61	121.682	-0.1128	-0.0991	65.0	0.0139	178.40	260.0

Table C.2 Inside Wall Temperature Data for Freon-134a (Cont'd)

RUN	D	P OUT	G	Q_m	HOTP PCW	X_{IN}	X_{OUT}	Z	X_{eq}	T_w	T_{HP}
	(m)	(kPa)	(kg/m².s)	(W/m²)	(W)			(cm)		(°C)	(°C)
32094A4	0.00438	830.811	2008.520	51545.61	121.682	-0.1128	-0.0991	68.0	0.0180	176.23	260.0
32094A4	0.00438	830.811	2008.520	51545.61	121.682	-0.1128	-0.0991	74.0	0.0263	170.94	260.0
32094A5	0.00438	830.811	2013.628	44505.94	120.331	-0.1128	-0.1010	1.0	-0.0765	196.06	271.7
32094A5	0.00438	830.811	2013.628	44505.94	120.331	-0.1128	-0.1010	2.5	-0.0747	187.14	271.7
32094A5	0.00438	830.811	2013.628	44505.94	120.331	-0.1128	-0.1010	4.0	-0.0730	188.99	271.7
32094A5	0.00438	830.811	2013.628	44505.94	120.331	-0.1128	-0.1010	5.5	-0.0712	189.37	271.7
32094A5	0.00438	830.811	2013.628	44505.94	120.331	-0.1128	-0.1010	7.0	-0.0694	188.94	271.7
32094A5	0.00438	830.811	2013.628	44505.94	120.331	-0.1128	-0.1010	9.0	-0.0670	185.07	271.7
32094A5	0.00438	830.811	2013.628	44505.94	120.331	-0.1128	-0.1010	11.0	-0.0647	182.55	271.7
32094A5	0.00438	830.811	2013.628	44505.94	120.331	-0.1128	-0.1010	13.0	-0.0623	179.83	271.7
32094A5	0.00438	830.811	2013.628	44505.94	120.331	-0.1128	-0.1010	15.0	-0.0599	178.09	271.7
32094A5	0.00438	830.811	2013.628	44505.94	120.331	-0.1128	-0.1010	17.0	-0.0576	176.58	271.7
32094A5	0.00438	830.811	2013.628	44505.94	120.331	-0.1128	-0.1010	19.0	-0.0552	175.54	271.7
32094A5	0.00438	830.811	2013.628	44505.94	120.331	-0.1128	-0.1010	21.0	-0.0528	174.47	271.7
32094A5	0.00438	830.811	2013.628	44505.94	120.331	-0.1128	-0.1010	24.0	-0.0493	174.11	271.7
32094A5	0.00438	830.811	2013.628	44505.94	120.331	-0.1128	-0.1010	27.0	-0.0457	173.56	271.7
32094A5	0.00438	830.811	2013.628	44505.94	120.331	-0.1128	-0.1010	30.0	-0.0422	175.72	271.7
32094A5	0.00438	830.811	2013.628	44505.94	120.331	-0.1128	-0.1010	33.0	-0.0386	175.67	271.7
32094A5	0.00438	830.811	2013.628	44505.94	120.331	-0.1128	-0.1010	36.0	-0.0351	175.27	271.7
32094A5	0.00438	830.811	2013.628	44505.94	120.331	-0.1128	-0.1010	39.0	-0.0315	174.76	271.7
32094A5	0.00438	830.811	2013.628	44505.94	120.331	-0.1128	-0.1010	42.0	-0.0280	175.42	271.7
32094A5	0.00438	830.811	2013.628	44505.94	120.331	-0.1128	-0.1010	45.0	-0.0244	175.41	271.7
32094A5	0.00438	830.811	2013.628	44505.94	120.331	-0.1128	-0.1010	48.0	-0.0208	174.14	271.7
32094A5	0.00438	830.811	2013.628	44505.94	120.331	-0.1128	-0.1010	51.0	-0.0173	173.74	271.7
32094A5	0.00438	830.811	2013.628	44505.94	120.331	-0.1128	-0.1010	54.0	-0.0137	172.34	271.7
32094A5	0.00438	830.811	2013.628	44505.94	120.331	-0.1128	-0.1010	59.0	-0.0078	171.20	271.7
32094A5	0.00438	830.811	2013.628	44505.94	120.331	-0.1128	-0.1010	62.0	-0.0043	170.29	271.7
32094A5	0.00438	830.811	2013.628	44505.94	120.331	-0.1128	-0.1010	65.0	-0.0007	168.32	271.7
32094A5	0.00438	830.811	2013.628	44505.94	120.331	-0.1128	-0.1010	68.0	0.0028	167.03	271.7
32094A5	0.00438	830.811	2013.628	44505.94	120.331	-0.1128	-0.1010	74.0	0.0099	163.20	271.7
32094A6	0.00438	830.811	2011.207	35265.15	121.546	-0.1128	-0.1034	1.0	-0.0789	169.81	212.0
32094A6	0.00438	830.811	2011.207	35265.15	121.546	-0.1128	-0.1034	2.5	-0.0775	165.12	212.0
32094A6	0.00438	830.811	2011.207	35265.15	121.546	-0.1128	-0.1034	4.0	-0.0761	167.07	212.0
32094A6	0.00438	830.811	2011.207	35265.15	121.546	-0.1128	-0.1034	5.5	-0.0747	166.37	212.0
32094A6	0.00438	830.811	2011.207	35265.15	121.546	-0.1128	-0.1034	7.0	-0.0733	164.80	212.0
32094A6	0.00438	830.811	2011.207	35265.15	121.546	-0.1128	-0.1034	9.0	-0.0714	161.20	212.0
32094A6	0.00438	830.811	2011.207	35265.15	121.546	-0.1128	-0.1034	11.0	-0.0695	158.98	212.0
32094A6	0.00438	830.811	2011.207	35265.15	121.546	-0.1128	-0.1034	13.0	-0.0677	155.64	212.0
32094A6	0.00438	830.811	2011.207	35265.15	121.546	-0.1128	-0.1034	15.0	-0.0658	153.25	212.0
32094A6	0.00438	830.811	2011.207	35265.15	121.546	-0.1128	-0.1034	17.0	-0.0639	151.59	212.0
32094A6	0.00438	830.811	2011.207	35265.15	121.546	-0.1128	-0.1034	19.0	-0.0620	150.23	212.0
32094A6	0.00438	830.811	2011.207	35265.15	121.546	-0.1128	-0.1034	21.0	-0.0601	148.61	212.0
32094A6	0.00438	830.811	2011.207	35265.15	121.546	-0.1128	-0.1034	24.0	-0.0573	148.19	212.0
32094A6	0.00438	830.811	2011.207	35265.15	121.546	-0.1128	-0.1034	27.0	-0.0545	147.51	212.0
32094A6	0.00438	830.811	2011.207	35265.15	121.546	-0.1128	-0.1034	30.0	-0.0517	149.33	212.0
32094A6	0.00438	830.811	2011.207	35265.15	121.546	-0.1128	-0.1034	33.0	-0.0489	149.81	212.0
32094A6	0.00438	830.811	2011.207	35265.15	121.546	-0.1128	-0.1034	36.0	-0.0461	149.57	212.0
32094A6	0.00438	830.811	2011.207	35265.15	121.546	-0.1128	-0.1034	39.0	-0.0432	149.75	212.0
32094A6	0.00438	830.811	2011.207	35265.15	121.546	-0.1128	-0.1034	42.0	-0.0404	150.73	212.0
32094A6	0.00438	830.811	2011.207	35265.15	121.546	-0.1128	-0.1034	45.0	-0.0376	151.27	212.0
32094A6	0.00438	830.811	2011.207	35265.15	121.546	-0.1128	-0.1034	48.0	-0.0348	150.69	212.0
32094A6	0.00438	830.811	2011.207	35265.15	121.546	-0.1128	-0.1034	51.0	-0.0320	150.65	212.0
32094A6	0.00438	830.811	2011.207	35265.15	121.546	-0.1128	-0.1034	54.0	-0.0291	150.15	212.0
32094A6	0.00438	830.811	2011.207	35265.15	121.546	-0.1128	-0.1034	59.0	-0.0244	150.15	212.0
32094A6	0.00438	830.811	2011.207	35265.15	121.546	-0.1128	-0.1034	62.0	-0.0216	150.15	212.0
32094A6	0.00438	830.811	2011.207	35265.15	121.546	-0.1128	-0.1034	65.0	-0.0188	149.13	212.0
32094A6	0.00438	830.811	2011.207	35265.15	121.546	-0.1128	-0.1034	68.0	-0.0160	148.95	212.0
32094A6	0.00438	830.811	2011.207	35265.15	121.546	-0.1128	-0.1034	74.0	-0.0104	147.43	212.0
32094A7	0.00438	830.811	2013.642	32108.94	120.505	-0.1128	-0.1043	1.0	-0.0801	160.84	238.0
32094A7	0.00438	830.811	2013.642	32108.94	120.505	-0.1128	-0.1043	2.5	-0.0788	150.16	238.0
32094A7	0.00438	830.811	2013.642	32108.94	120.505	-0.1128	-0.1043	4.0	-0.0775	151.30	238.0
32094A7	0.00438	830.811	2013.642	32108.94	120.505	-0.1128	-0.1043	5.5	-0.0763	152.59	238.0
32094A7	0.00438	830.811	2013.642	32108.94	120.505	-0.1128	-0.1043	7.0	-0.0750	153.70	238.0
32094A7	0.00438	830.811	2013.642	32108.94	120.505	-0.1128	-0.1043	9.0	-0.0733	152.77	238.0
32094A7	0.00438	830.811	2013.642	32108.94	120.505	-0.1128	-0.1043	11.0	-0.0716	153.00	238.0
32094A7	0.00438	830.811	2013.642	32108.94	120.505	-0.1128	-0.1043	13.0	-0.0699	150.93	238.0
32094A7	0.00438	830.811	2013.642	32108.94	120.505	-0.1128	-0.1043	15.0	-0.0681	148.85	238.0
32094A7	0.00438	830.811	2013.642	32108.94	120.505	-0.1128	-0.1043	17.0	-0.0664	147.32	238.0
32094A7	0.00438	830.811	2013.642	32108.94	120.505	-0.1128	-0.1043	19.0	-0.0647	145.38	238.0
32094A7	0.00438	830.811	2013.642	32108.94	120.505	-0.1128	-0.1043	21.0	-0.0630	142.96	238.0
32094A7	0.00438	830.811	2013.642	32108.94	120.505	-0.1128	-0.1043	24.0	-0.0605	141.19	238.0
32094A7	0.00438	830.811	2013.642	32108.94	120.505	-0.1128	-0.1043	27.0	-0.0579	138.66	238.0
. . .	. . .	. . .	. . .	. . .	. . .	. . .	. . .	. .	. . .	. . .	. . .
. . .	. . .	. . .	. . .	. . .	. . .	. . .	. . .	. .	. . .	. . .	. . .
. . .	. . .	. . .	. . .	. . .	. . .	. . .	. . .	. .	. . .	. . .	. . .
. . .	. . .	. . .	. . .	. . .	. . .	. . .	. . .	. .	. . .	. . .	. . .
. . .	. . .	. . .	. . .	. . .	. . .	. . .	. . .	. .	. . .	. . .	. . .
. . .	. . .	. . .	. . .	. . .	. . .	. . .	. . .	. .	. . .	. . .	. . .
. . .	. . .	. . .	. . .	. . .	. . .	. . .	. . .	. .	. . .	. . .	. . .
. . .	. . .	. . .	. . .	. . .	. . .	. . .	. . .	. .	. . .	. . .	. . .
. . .	. . .	. . .	. . .	. . .	. . .	. . .	. . .	. .	. . .	. . .	. . .
. . .	. . .	. . .	. . .	. . .	. . .	. . .	. . .	. .	. . .	. . .	. . .
. . .	. . .	. . .	. . .	. . .	. . .	. . .	. . .	. .	. . .	. . .	. . .

Table C.2 Inside Wall Temperature Data for Freon-134a (Concluded)

RUN	D	P OUT	G	Q_w	HOTP POW	X_{in}	X_{exp}	Z	X_{eq}	T_w	T_{sat}
	(m)	(kPa)	(kg/m².s)	(W/m²)	(W)			(cm)		(°C)	(°C)
30894F8	0.00438	830.811	1507.020	20668.29	69.491	-0.0703	-0.0630	19.0	-0.0310	99.90	169.2
30894F8	0.00438	830.811	1507.020	20668.29	69.491	-0.0703	-0.0630	21.0	-0.0296	99.32	169.2
30894F8	0.00438	830.811	1507.020	20668.29	69.491	-0.0703	-0.0630	24.0	-0.0274	100.09	169.2
30894F8	0.00438	830.811	1507.020	20668.29	69.491	-0.0703	-0.0630	27.0	-0.0252	100.17	169.2
30894F8	0.00438	830.811	1507.020	20668.29	69.491	-0.0703	-0.0630	30.0	-0.0230	102.17	169.2
30894F8	0.00438	830.811	1507.020	20668.29	69.491	-0.0703	-0.0630	33.0	-0.0208	102.11	169.2
30894F8	0.00438	830.811	1507.020	20668.29	69.491	-0.0703	-0.0630	36.0	-0.0186	102.14	169.2
30894F8	0.00438	830.811	1507.020	20668.29	69.491	-0.0703	-0.0630	39.0	-0.0163	102.36	169.2
30894F8	0.00438	830.811	1507.020	20668.29	69.491	-0.0703	-0.0630	42.0	-0.0141	103.39	169.2
30894F8	0.00438	830.811	1507.020	20668.29	69.491	-0.0703	-0.0630	45.0	-0.0119	104.06	169.2
30894F8	0.00438	830.811	1507.020	20668.29	69.491	-0.0703	-0.0630	48.0	-0.0097	103.86	169.2
30894F8	0.00438	830.811	1507.020	20668.29	69.491	-0.0703	-0.0630	51.0	-0.0075	104.27	169.2
30894F8	0.00438	830.811	1507.020	20668.29	69.491	-0.0703	-0.0630	54.0	-0.0053	104.27	169.2
30894F8	0.00438	830.811	1507.020	20668.29	69.491	-0.0703	-0.0630	59.0	-0.0017	104.64	169.2
30894F8	0.00438	830.811	1507.020	20668.29	69.491	-0.0703	-0.0630	62.0	0.0006	105.06	169.2
30894F8	0.00438	830.811	1507.020	20668.29	69.491	-0.0703	-0.0630	65.0	0.0028	104.79	169.2
30894F8	0.00438	830.811	1507.020	20668.29	69.491	-0.0703	-0.0630	68.0	0.0050	105.16	169.2
30894F8	0.00438	830.811	1507.020	20668.29	69.491	-0.0703	-0.0630	74.0	0.0094	104.81	169.2

Table C.3 Inside Wall Temperature Data for Freon-22

RUN	D	P OUT	G	Q_w	HOTP POW	X_{in}	X_{exp}	Z	X_{eq}	T_v	T_{wp}
	(m)	(kPa)	(kg/m².s)	(W/m²)	(W)			(cm)		(°C)	(°C)
50394A1	0.00438	830.811	1503.556	44054.07	70.666	-0.1151	-0.0949	1.0	-0.0693	232.31	293.21
50394A1	0.00438	830.811	1503.556	44054.07	70.666	-0.1151	-0.0949	2.5	-0.0663	226.60	293.21
50394A1	0.00438	830.811	1503.556	44054.07	70.666	-0.1151	-0.0949	4.0	-0.0632	227.41	293.21
50394A1	0.00438	830.811	1503.556	44054.07	70.666	-0.1151	-0.0949	5.5	-0.0602	223.51	293.21
50394A1	0.00438	830.811	1503.556	44054.07	70.666	-0.1151	-0.0949	7.0	-0.0572	224.00	293.21
50394A1	0.00438	830.811	1503.556	44054.07	70.666	-0.1151	-0.0949	9.0	-0.0531	220.27	293.21
50394A1	0.00438	830.811	1503.556	44054.07	70.666	-0.1151	-0.0949	11.0	-0.0491	220.31	293.21
50394A1	0.00438	830.811	1503.556	44054.07	70.666	-0.1151	-0.0949	13.0	-0.0451	219.74	293.21
50394A1	0.00438	830.811	1503.556	44054.07	70.666	-0.1151	-0.0949	15.0	-0.0410	218.87	293.21
50394A1	0.00438	830.811	1503.556	44054.07	70.666	-0.1151	-0.0949	17.0	-0.0370	219.03	293.21
50394A1	0.00438	830.811	1503.556	44054.07	70.666	-0.1151	-0.0949	19.0	-0.0329	219.24	293.21
50394A1	0.00438	830.811	1503.556	44054.07	70.666	-0.1151	-0.0949	21.0	-0.0289	218.54	293.21
50394A1	0.00438	830.811	1503.556	44054.07	70.666	-0.1151	-0.0949	24.0	-0.0228	219.32	293.21
50394A1	0.00438	830.811	1503.556	44054.07	70.666	-0.1151	-0.0949	27.0	-0.0168	219.91	293.21
50394A1	0.00438	830.811	1503.556	44054.07	70.666	-0.1151	-0.0949	30.0	-0.0107	220.80	293.21
50394A1	0.00438	830.811	1503.556	44054.07	70.666	-0.1151	-0.0949	33.0	-0.0046	221.96	293.21
50394A1	0.00438	830.811	1503.556	44054.07	70.666	-0.1151	-0.0949	36.0	0.0014	221.25	293.21
50394A1	0.00438	830.811	1503.556	44054.07	70.666	-0.1151	-0.0949	39.0	0.0075	221.18	293.21
50394A1	0.00438	830.811	1503.556	44054.07	70.666	-0.1151	-0.0949	42.0	0.0136	220.73	293.21
50394A1	0.00438	830.811	1503.556	44054.07	70.666	-0.1151	-0.0949	45.0	0.0196	220.38	293.21
50394A1	0.00438	830.811	1503.556	44054.07	70.666	-0.1151	-0.0949	48.0	0.0257	218.18	293.21
50394A1	0.00438	830.811	1503.556	44054.07	70.666	-0.1151	-0.0949	51.0	0.0318	215.79	293.21
50394A1	0.00438	830.811	1503.556	44054.07	70.666	-0.1151	-0.0949	54.0	0.0378	212.75	293.21
50394A1	0.00438	830.811	1503.556	44054.07	70.666	-0.1151	-0.0949	59.0	0.0479	208.66	293.21
50394A1	0.00438	830.811	1503.556	44054.07	70.666	-0.1151	-0.0949	62.0	0.0540	206.21	293.21
50394A1	0.00438	830.811	1503.556	44054.07	70.666	-0.1151	-0.0949	65.0	0.0600	201.85	293.21
50394A1	0.00438	830.811	1503.556	44054.07	70.666	-0.1151	-0.0949	68.0	0.0661	198.93	293.21
50394A1	0.00438	830.811	1503.556	44054.07	70.666	-0.1151	-0.0949	74.0	0.0782	191.28	293.21
50394A2	0.00438	830.811	1505.070	44314.55	63.937	-0.0604	-0.0401	1.0	-0.0168	236.99	293.15
50394A2	0.00438	830.811	1505.070	44314.55	63.937	-0.0604	-0.0401	2.5	-0.0137	230.01	293.15
50394A2	0.00438	830.811	1505.070	44314.55	63.937	-0.0604	-0.0401	4.0	-0.0107	229.24	293.15
50394A2	0.00438	830.811	1505.070	44314.55	63.937	-0.0604	-0.0401	5.5	-0.0076	224.55	293.15
50394A2	0.00438	830.811	1505.070	44314.55	63.937	-0.0604	-0.0401	7.0	-0.0046	223.53	293.15
50394A2	0.00438	830.811	1505.070	44314.55	63.937	-0.0604	-0.0401	9.0	-0.0005	218.52	293.15
50394A2	0.00438	830.811	1505.070	44314.55	63.937	-0.0604	-0.0401	11.0	0.0035	217.66	293.15
50394A2	0.00438	830.811	1505.070	44314.55	63.937	-0.0604	-0.0401	13.0	0.0076	216.06	293.15
50394A2	0.00438	830.811	1505.070	44314.55	63.937	-0.0604	-0.0401	15.0	0.0117	215.07	293.15
50394A2	0.00438	830.811	1505.070	44314.55	63.937	-0.0604	-0.0401	17.0	0.0157	214.64	293.15
50394A2	0.00438	830.811	1505.070	44314.55	63.937	-0.0604	-0.0401	19.0	0.0198	214.30	293.15
50394A2	0.00438	830.811	1505.070	44314.55	63.937	-0.0604	-0.0401	21.0	0.0239	213.08	293.15
50394A2	0.00438	830.811	1505.070	44314.55	63.937	-0.0604	-0.0401	24.0	0.0299	212.24	293.15
50394A2	0.00438	830.811	1505.070	44314.55	63.937	-0.0604	-0.0401	27.0	0.0360	210.39	293.15
50394A2	0.00438	830.811	1505.070	44314.55	63.937	-0.0604	-0.0401	30.0	0.0421	209.02	293.15
50394A2	0.00438	830.811	1505.070	44314.55	63.937	-0.0604	-0.0401	33.0	0.0482	207.36	293.15
50394A2	0.00438	830.811	1505.070	44314.55	63.937	-0.0604	-0.0401	36.0	0.0543	203.86	293.15
50394A2	0.00438	830.811	1505.070	44314.55	63.937	-0.0604	-0.0401	39.0	0.0604	200.83	293.15
50394A2	0.00438	830.811	1505.070	44314.55	63.937	-0.0604	-0.0401	42.0	0.0665	198.03	293.15
50394A2	0.00438	830.811	1505.070	44314.55	63.937	-0.0604	-0.0401	45.0	0.0726	195.78	293.15
50394A2	0.00438	830.811	1505.070	44314.55	63.937	-0.0604	-0.0401	48.0	0.0787	192.18	293.15
50394A2	0.00438	830.811	1505.070	44314.55	63.937	-0.0604	-0.0401	51.0	0.0848	188.76	293.15
50394A2	0.00438	830.811	1505.070	44314.55	63.937	-0.0604	-0.0401	54.0	0.0909	184.97	293.15
50394A2	0.00438	830.811	1505.070	44314.55	63.937	-0.0604	-0.0401	59.0	0.1010	180.08	293.15
50394A2	0.00438	830.811	1505.070	44314.55	63.937	-0.0604	-0.0401	62.0	0.1071	177.35	293.15
50394A2	0.00438	830.811	1505.070	44314.55	63.937	-0.0604	-0.0401	65.0	0.1132	173.33	293.15
50394A2	0.00438	830.811	1505.070	44314.55	63.937	-0.0604	-0.0401	68.0	0.1193	170.61	293.15
50394A2	0.00438	830.811	1505.070	44314.55	63.937	-0.0604	-0.0401	74.0	0.1315	164.28	293.15
50594A1	0.00438	1137.626	3021.282	64044.58	126.232	-0.1321	-0.1164	1.0	-0.0925	214.72	243.02
50594A1	0.00438	1137.626	3021.282	64044.58	126.232	-0.1321	-0.1164	2.5	-0.0901	228.87	243.02
50594A1	0.00438	1137.626	3021.282	64044.58	126.232	-0.1321	-0.1164	4.0	-0.0878	249.46	243.02
50594A1	0.00438	1137.626	3021.282	64044.58	126.232	-0.1321	-0.1164	5.5	-0.0854	265.24	243.02
50594A1	0.00438	1137.626	3021.282	64044.58	126.232	-0.1321	-0.1164	7.0	-0.0831	284.12	243.02
50594A1	0.00438	1137.626	3021.282	64044.58	126.232	-0.1321	-0.1164	9.0	-0.0799	292.58	243.02
50594A1	0.00438	1137.626	3021.282	64044.58	126.232	-0.1321	-0.1164	11.0	-0.0768	296.38	243.02
50594A1	0.00438	1137.626	3021.282	64044.58	126.232	-0.1321	-0.1164	13.0	-0.0737	291.87	243.02
50594A1	0.00438	1137.626	3021.282	64044.58	126.232	-0.1321	-0.1164	15.0	-0.0705	285.66	243.02
50594A1	0.00438	1137.626	3021.282	64044.58	126.232	-0.1321	-0.1164	17.0	-0.0674	279.71	243.02
50594A1	0.00438	1137.626	3021.282	64044.58	126.232	-0.1321	-0.1164	19.0	-0.0643	273.48	243.02
50594A1	0.00438	1137.626	3021.282	64044.58	126.232	-0.1321	-0.1164	21.0	-0.0612	266.48	243.02
50594A1	0.00438	1137.626	3021.282	64044.58	126.232	-0.1321	-0.1164	24.0	-0.0565	259.12	243.02
50594A1	0.00438	1137.626	3021.282	64044.58	126.232	-0.1321	-0.1164	27.0	-0.0518	253.29	243.02
50594A1	0.00438	1137.626	3021.282	64044.58	126.232	-0.1321	-0.1164	30.0	-0.0471	249.11	243.02
50594A1	0.00438	1137.626	3021.282	64044.58	126.232	-0.1321	-0.1164	33.0	-0.0424	247.07	243.02
50594A1	0.00438	1137.626	3021.282	64044.58	126.232	-0.1321	-0.1164	36.0	-0.0377	243.36	243.02
50594A1	0.00438	1137.626	3021.282	64044.58	126.232	-0.1321	-0.1164	39.0	-0.0330	241.02	243.02
50594A1	0.00438	1137.626	3021.282	64044.58	126.232	-0.1321	-0.1164	42.0	-0.0283	239.10	243.02
50594A1	0.00438	1137.626	3021.282	64044.58	126.232	-0.1321	-0.1164	45.0	-0.0236	238.37	243.02
50594A1	0.00438	1137.626	3021.282	64044.58	126.232	-0.1321	-0.1164	48.0	-0.0189	235.87	243.02
50594A1	0.00438	1137.626	3021.282	64044.58	126.232	-0.1321	-0.1164	51.0	-0.0142	233.59	243.02
50594A1	0.00438	1137.626	3021.282	64044.58	126.232	-0.1321	-0.1164	54.0	-0.0095	230.57	243.02
50594A1	0.00438	1137.626	3021.282	64044.58	126.232	-0.1321	-0.1164	59.0	-0.0017	227.38	243.02
50594A1	0.00438	1137.626	3021.282	64044.58	126.232	-0.1321	-0.1164	62.0	0.0030	225.42	243.02
50594A1	0.00438	1137.626	3021.282	64044.58	126.232	-0.1321	-0.1164	65.0	0.0077	221.34	243.02
50594A1	0.00438	1137.626	3021.282	64044.58	126.232	-0.1321	-0.1164	68.0	0.0124	218.98	243.02

Table C.3 Inside Wall Temperature Data for Freon-22 (Cont'd)

RUN	D	P OUT	G	Q_w	HOTP POW	X_{in}	X_{pap}	Z	X_{eq}	T_w	T_{sat}
	(m)	(kPa)	(kg/m²·s)	(W/m²)	(W)			(cm)		(°C)	(°C)
50594A1	0.00438	1137.626	3021.282	64044.58	126.232	-0.1321	-0.1164	74.0	0.0218	212.01	243.02
50594A2	0.00438	1137.626	3021.135	64043.28	98.952	-0.0675	-0.0518	1.0	-0.0327	224.89	221.37
50594A2	0.00438	1137.626	3021.135	64043.28	98.952	-0.0675	-0.0518	2.5	-0.0303	240.47	221.37
50594A2	0.00438	1137.626	3021.135	64043.28	98.952	-0.0675	-0.0518	4.0	-0.0280	255.05	221.37
50594A2	0.00438	1137.626	3021.135	64043.28	98.952	-0.0675	-0.0518	5.5	-0.0256	259.21	221.37
50594A2	0.00438	1137.626	3021.135	64043.28	98.952	-0.0675	-0.0518	7.0	-0.0233	264.61	221.37
50594A2	0.00438	1137.626	3021.135	64043.28	98.952	-0.0675	-0.0518	9.0	-0.0202	261.14	221.37
50594A2	0.00438	1137.626	3021.135	64043.28	98.952	-0.0675	-0.0518	11.0	-0.0170	260.12	221.37
50594A2	0.00438	1137.626	3021.135	64043.28	98.952	-0.0675	-0.0518	13.0	-0.0139	255.41	221.37
50594A2	0.00438	1137.626	3021.135	64043.28	98.952	-0.0675	-0.0518	15.0	-0.0108	249.86	221.37
50594A2	0.00438	1137.626	3021.135	64043.28	98.952	-0.0675	-0.0518	17.0	-0.0076	244.81	221.37
50594A2	0.00438	1137.626	3021.135	64043.28	98.952	-0.0675	-0.0518	19.0	-0.0045	240.08	221.37
50594A2	0.00438	1137.626	3021.135	64043.28	98.952	-0.0675	-0.0518	21.0	-0.0014	234.68	221.37
50594A2	0.00438	1137.626	3021.135	64043.28	98.952	-0.0675	-0.0518	24.0	0.0033	228.71	221.37
50594A2	0.00438	1137.626	3021.135	64043.28	98.952	-0.0675	-0.0518	27.0	0.0080	223.65	221.37
50594A2	0.00438	1137.626	3021.135	64043.28	98.952	-0.0675	-0.0518	30.0	0.0127	219.27	221.37
50594A2	0.00438	1137.626	3021.135	64043.28	98.952	-0.0675	-0.0518	33.0	0.0174	216.30	221.37
50594A2	0.00438	1137.626	3021.135	64043.28	98.952	-0.0675	-0.0518	36.0	0.0221	211.94	221.37
50594A2	0.00438	1137.626	3021.135	64043.28	98.952	-0.0675	-0.0518	39.0	0.0268	208.66	221.37
50594A2	0.00438	1137.626	3021.135	64043.28	98.952	-0.0675	-0.0518	42.0	0.0315	205.76	221.37
50594A2	0.00438	1137.626	3021.135	64043.28	98.952	-0.0675	-0.0518	45.0	0.0362	203.63	221.37
50594A2	0.00438	1137.626	3021.135	64043.28	98.952	-0.0675	-0.0518	48.0	0.0409	200.13	221.37
50594A2	0.00438	1137.626	3021.135	64043.28	98.952	-0.0675	-0.0518	51.0	0.0456	196.69	221.37
50594A2	0.00438	1137.626	3021.135	64043.28	98.952	-0.0675	-0.0518	54.0	0.0503	192.66	221.37
50594A2	0.00438	1137.626	3021.135	64043.28	98.952	-0.0675	-0.0518	59.0	0.0581	187.62	221.37
50594A2	0.00438	1137.626	3021.135	64043.28	98.952	-0.0675	-0.0518	62.0	0.0628	184.68	221.37
50594A2	0.00438	1137.626	3021.135	64043.28	98.952	-0.0675	-0.0518	65.0	0.0675	180.28	221.37
50594A2	0.00438	1137.626	3021.135	64043.28	98.952	-0.0675	-0.0518	68.0	0.0722	177.42	221.37
50594A2	0.00438	1137.626	3021.135	64043.28	98.952	-0.0675	-0.0518	74.0	0.0816	169.99	221.37
50394B1	0.00438	1137.626	2013.558	56190.00	80.155	-0.1115	-0.0901	1.0	-0.0881	234.89	206.28
50394B1	0.00438	1137.626	2013.558	56190.00	80.155	-0.1115	-0.0901	2.5	-0.0850	260.30	206.28
50394B1	0.00438	1137.626	2013.558	56190.00	80.155	-0.1115	-0.0901	4.0	-0.0819	279.13	206.28
50394B1	0.00438	1137.626	2013.558	56190.00	80.155	-0.1115	-0.0901	5.5	-0.0788	281.74	206.28
50394B1	0.00438	1137.626	2013.558	56190.00	80.155	-0.1115	-0.0901	7.0	-0.0757	283.21	206.28
50394B1	0.00438	1137.626	2013.558	56190.00	80.155	-0.1115	-0.0901	9.0	-0.0716	275.25	206.28
50394B1	0.00438	1137.626	2013.558	56190.00	80.155	-0.1115	-0.0901	11.0	-0.0675	271.73	206.28
50394B1	0.00438	1137.626	2013.558	56190.00	80.155	-0.1115	-0.0901	13.0	-0.0633	266.56	206.28
50394B1	0.00438	1137.626	2013.558	56190.00	80.155	-0.1115	-0.0901	15.0	-0.0592	262.10	206.28
50394B1	0.00438	1137.626	2013.558	56190.00	80.155	-0.1115	-0.0901	17.0	-0.0551	258.81	206.28
50394B1	0.00438	1137.626	2013.558	56190.00	80.155	-0.1115	-0.0901	19.0	-0.0510	256.36	206.28
50394B1	0.00438	1137.626	2013.558	56190.00	80.155	-0.1115	-0.0901	21.0	-0.0469	253.28	206.28
50394B1	0.00438	1137.626	2013.558	56190.00	80.155	-0.1115	-0.0901	24.0	-0.0407	251.32	206.28
50394B1	0.00438	1137.626	2013.558	56190.00	80.155	-0.1115	-0.0901	27.0	-0.0345	249.82	206.28
50394B1	0.00438	1137.626	2013.558	56190.00	80.155	-0.1115	-0.0901	30.0	-0.0283	249.30	206.28
50394B1	0.00438	1137.626	2013.558	56190.00	80.155	-0.1115	-0.0901	33.0	-0.0221	249.32	206.28
50394B1	0.00438	1137.626	2013.558	56190.00	80.155	-0.1115	-0.0901	36.0	-0.0160	247.19	206.28
50394B1	0.00438	1137.626	2013.558	56190.00	80.155	-0.1115	-0.0901	39.0	-0.0098	245.80	206.28
50394B1	0.00438	1137.626	2013.558	56190.00	80.155	-0.1115	-0.0901	42.0	-0.0036	244.22	206.28
50394B1	0.00438	1137.626	2013.558	56190.00	80.155	-0.1115	-0.0901	45.0	0.0026	243.40	206.28
50394B1	0.00438	1137.626	2013.558	56190.00	80.155	-0.1115	-0.0901	48.0	0.0088	240.49	206.28
50394B1	0.00438	1137.626	2013.558	56190.00	80.155	-0.1115	-0.0901	51.0	0.0149	237.68	206.28
50394B1	0.00438	1137.626	2013.558	56190.00	80.155	-0.1115	-0.0901	54.0	0.0211	233.99	206.28
50394B1	0.00438	1137.626	2013.558	56190.00	80.155	-0.1115	-0.0901	59.0	0.0314	229.43	206.28
50394B1	0.00438	1137.626	2013.558	56190.00	80.155	-0.1115	-0.0901	62.0	0.0376	226.55	206.28
50394B1	0.00438	1137.626	2013.558	56190.00	80.155	-0.1115	-0.0901	65.0	0.0438	221.82	206.28
50394B1	0.00438	1137.626	2013.558	56190.00	80.155	-0.1115	-0.0901	68.0	0.0500	218.70	206.28
50394B1	0.00438	1137.626	2013.558	56190.00	80.155	-0.1115	-0.0901	74.0	0.0623	210.54	206.28
50394B2	0.00438	1137.626	2011.879	56186.32	81.996	-0.1115	-0.0896	1.0	-0.0875	227.75	191.05
50394B2	0.00438	1137.626	2011.879	56186.32	81.996	-0.1115	-0.0896	2.5	-0.0844	257.24	191.05
50394B2	0.00438	1137.626	2011.879	56186.32	81.996	-0.1115	-0.0896	4.0	-0.0814	279.15	191.05
50394B2	0.00438	1137.626	2011.879	56186.32	81.996	-0.1115	-0.0896	5.5	-0.0783	283.98	191.05
50394B2	0.00438	1137.626	2011.879	56186.32	81.996	-0.1115	-0.0896	7.0	-0.0752	286.04	191.05
50394B2	0.00438	1137.626	2011.879	56186.32	81.996	-0.1115	-0.0896	9.0	-0.0710	277.61	191.05
50394B2	0.00438	1137.626	2011.879	56186.32	81.996	-0.1115	-0.0896	11.0	-0.0669	273.72	191.05
50394B2	0.00438	1137.626	2011.879	56186.32	81.996	-0.1115	-0.0896	13.0	-0.0628	268.08	191.05
50394B2	0.00438	1137.626	2011.879	56186.32	81.996	-0.1115	-0.0896	15.0	-0.0587	263.35	191.05
50394B2	0.00438	1137.626	2011.879	56186.32	81.996	-0.1115	-0.0896	17.0	-0.0545	259.79	191.05
50394B2	0.00438	1137.626	2011.879	56186.32	81.996	-0.1115	-0.0896	19.0	-0.0504	256.94	191.05
50394B2	0.00438	1137.626	2011.879	56186.32	81.996	-0.1115	-0.0896	21.0	-0.0463	253.58	191.05
50394B2	0.00438	1137.626	2011.879	56186.32	81.996	-0.1115	-0.0896	24.0	-0.0401	251.44	191.05
50394B2	0.00438	1137.626	2011.879	56186.32	81.996	-0.1115	-0.0896	27.0	-0.0339	249.62	191.05
50394B2	0.00438	1137.626	2011.879	56186.32	81.996	-0.1115	-0.0896	30.0	-0.0277	249.21	191.05
50394B2	0.00438	1137.626	2011.879	56186.32	81.996	-0.1115	-0.0896	33.0	-0.0216	249.05	191.05
50394B2	0.00438	1137.626	2011.879	56186.32	81.996	-0.1115	-0.0896	36.0	-0.0154	246.93	191.05
50394B2	0.00438	1137.626	2011.879	56186.32	81.996	-0.1115	-0.0896	39.0	-0.0092	245.53	191.05
50394B2	0.00438	1137.626	2011.879	56186.32	81.996	-0.1115	-0.0896	42.0	-0.0030	244.00	191.05
50394B2	0.00438	1137.626	2011.879	56186.32	81.996	-0.1115	-0.0896	45.0	0.0032	243.14	191.05
50394B2	0.00438	1137.626	2011.879	56186.32	81.996	-0.1115	-0.0896	48.0	0.0094	240.23	191.05
50394B2	0.00438	1137.626	2011.879	56186.32	81.996	-0.1115	-0.0896	51.0	0.0155	237.41	191.05
50394B2	0.00438	1137.626	2011.879	56186.32	81.996	-0.1115	-0.0896	54.0	0.0217	233.76	191.05
50394B2	0.00438	1137.626	2011.879	56186.32	81.996	-0.1115	-0.0896	59.0	0.0320	229.07	191.05
50394B2	0.00438	1137.626	2011.879	56186.32	81.996	-0.1115	-0.0896	62.0	0.0382	226.25	191.05
50394B2	0.00438	1137.626	2011.879	56186.32	81.996	-0.1115	-0.0896	65.0	0.0444	221.53	191.05

Table C.3 Inside Wall Temperature Data for Freon-22 (Cont'd)

RUN	D	P OUT	G	Q_w	HOTP POW	X_{in}	X_{pso}	Z	X_{eq}	T_w	T_{sp}
	(m)	(kPa)	(kg/m².s)	(W/m²)	(W)			(cm)		(°C)	(°C)
50394B2	0.00438	1137.626	2011.879	56186.32	81.996	-0.1115	-0.0896	68.0	0.0506	218.39	191.05
50394B2	0.00438	1137.626	2011.879	56186.32	81.996	-0.1115	-0.0896	74.0	0.0630	210.18	191.05
50594B1	0.00438	1589.918	1510.648	54692.33	79.363	-0.1530	-0.1234	1.0	-0.0893	264.22	249.45
50594B1	0.00438	1589.918	1510.648	54692.33	79.363	-0.1530	-0.1234	2.5	-0.0849	273.67	249.45
50594B1	0.00438	1589.918	1510.648	54692.33	79.363	-0.1530	-0.1234	4.0	-0.0804	280.74	249.45
50594B1	0.00438	1589.918	1510.648	54692.33	79.363	-0.1530	-0.1234	5.5	-0.0760	277.37	249.45
50594B1	0.00438	1589.918	1510.648	54692.33	79.363	-0.1530	-0.1234	7.0	-0.0716	277.52	249.45
50594B1	0.00438	1589.918	1510.648	54692.33	79.363	-0.1530	-0.1234	9.0	-0.0657	270.64	249.45
50594B1	0.00438	1589.918	1510.648	54692.33	79.363	-0.1530	-0.1234	11.0	-0.0597	268.55	249.45
50594B1	0.00438	1589.918	1510.648	54692.33	79.363	-0.1530	-0.1234	13.0	-0.0538	264.96	249.45
50594B1	0.00438	1589.918	1510.648	54692.33	79.363	-0.1530	-0.1234	15.0	-0.0479	261.69	249.45
50594B1	0.00438	1589.918	1510.648	54692.33	79.363	-0.1530	-0.1234	17.0	-0.0420	259.41	249.45
50594B1	0.00438	1589.918	1510.648	54692.33	79.363	-0.1530	-0.1234	19.0	-0.0361	257.44	249.45
50594B1	0.00438	1589.918	1510.648	54692.33	79.363	-0.1530	-0.1234	21.0	-0.0302	254.60	249.45
50594B1	0.00438	1589.918	1510.648	54692.33	79.363	-0.1530	-0.1234	24.0	-0.0213	252.05	249.45
50594B1	0.00438	1589.918	1510.648	54692.33	79.363	-0.1530	-0.1234	27.0	-0.0125	249.95	249.45
50594B1	0.00438	1589.918	1510.648	54692.33	79.363	-0.1530	-0.1234	30.0	-0.0036	247.92	249.45
50594B1	0.00438	1589.918	1510.648	54692.33	79.363	-0.1530	-0.1234	33.0	0.0053	246.64	249.45
50594B1	0.00438	1589.918	1510.648	54692.33	79.363	-0.1530	-0.1234	36.0	0.0141	243.51	249.45
50594B1	0.00438	1589.918	1510.648	54692.33	79.363	-0.1530	-0.1234	39.0	0.0230	241.28	249.45
50594B1	0.00438	1589.918	1510.648	54692.33	79.363	-0.1530	-0.1234	42.0	0.0319	238.91	249.45
50594B1	0.00438	1589.918	1510.648	54692.33	79.363	-0.1530	-0.1234	45.0	0.0407	237.39	249.45
50594B1	0.00438	1589.918	1510.648	54692.33	79.363	-0.1530	-0.1234	48.0	0.0496	234.03	249.45
50594B1	0.00438	1589.918	1510.648	54692.33	79.363	-0.1530	-0.1234	51.0	0.0585	230.86	249.45
50594B1	0.00438	1589.918	1510.648	54692.33	79.363	-0.1530	-0.1234	54.0	0.0673	227.11	249.45
50594B1	0.00438	1589.918	1510.648	54692.33	79.363	-0.1530	-0.1234	59.0	0.0821	222.60	249.45
50594B1	0.00438	1589.918	1510.648	54692.33	79.363	-0.1530	-0.1234	62.0	0.0910	219.99	249.45
50594B1	0.00438	1589.918	1510.648	54692.33	79.363	-0.1530	-0.1234	65.0	0.0998	215.73	249.45
50594B1	0.00438	1589.918	1510.648	54692.33	79.363	-0.1530	-0.1234	68.0	0.1087	212.92	249.45
50594B1	0.00438	1589.918	1510.648	54692.33	79.363	-0.1530	-0.1234	74.0	0.1264	206.09	249.45
50594B2	0.00438	1589.918	1511.848	54161.43	87.556	-0.2261	-0.1969	1.0	-0.1596	250.97	244.31
50594B2	0.00438	1589.918	1511.848	54161.43	87.556	-0.2261	-0.1969	2.5	-0.1552	267.96	244.31
50594B2	0.00438	1589.918	1511.848	54161.43	87.556	-0.2261	-0.1969	4.0	-0.1508	285.85	244.31
50594B2	0.00438	1589.918	1511.848	54161.43	87.556	-0.2261	-0.1969	5.5	-0.1465	290.80	244.31
50594B2	0.00438	1589.918	1511.848	54161.43	87.556	-0.2261	-0.1969	7.0	-0.1421	294.24	244.31
50594B2	0.00438	1589.918	1511.848	54161.43	87.556	-0.2261	-0.1969	9.0	-0.1362	287.06	244.31
50594B2	0.00438	1589.918	1511.848	54161.43	87.556	-0.2261	-0.1969	11.0	-0.1304	283.25	244.31
50594B2	0.00438	1589.918	1511.848	54161.43	87.556	-0.2261	-0.1969	13.0	-0.1245	277.25	244.31
50594B2	0.00438	1589.918	1511.848	54161.43	87.556	-0.2261	-0.1969	15.0	-0.1187	271.60	244.31
50594B2	0.00438	1589.918	1511.848	54161.43	87.556	-0.2261	-0.1969	17.0	-0.1128	267.34	244.31
50594B2	0.00438	1589.918	1511.848	54161.43	87.556	-0.2261	-0.1969	19.0	-0.1070	264.05	244.31
50594B2	0.00438	1589.918	1511.848	54161.43	87.556	-0.2261	-0.1969	21.0	-0.1011	260.78	244.31
50594B2	0.00438	1589.918	1511.848	54161.43	87.556	-0.2261	-0.1969	24.0	-0.0924	258.83	244.31
50594B2	0.00438	1589.918	1511.848	54161.43	87.556	-0.2261	-0.1969	27.0	-0.0836	257.56	244.31
50594B2	0.00438	1589.918	1511.848	54161.43	87.556	-0.2261	-0.1969	30.0	-0.0748	257.59	244.31
50594B2	0.00438	1589.918	1511.848	54161.43	87.556	-0.2261	-0.1969	33.0	-0.0660	258.29	244.31
50594B2	0.00438	1589.918	1511.848	54161.43	87.556	-0.2261	-0.1969	36.0	-0.0573	256.81	244.31
50594B2	0.00438	1589.918	1511.848	54161.43	87.556	-0.2261	-0.1969	39.0	-0.0485	256.14	244.31
50594B2	0.00438	1589.918	1511.848	54161.43	87.556	-0.2261	-0.1969	42.0	-0.0397	255.24	244.31
50594B2	0.00438	1589.918	1511.848	54161.43	87.556	-0.2261	-0.1969	45.0	-0.0309	255.05	244.31
50594B2	0.00438	1589.918	1511.848	54161.43	87.556	-0.2261	-0.1969	48.0	-0.0222	252.68	244.31
50594B2	0.00438	1589.918	1511.848	54161.43	87.556	-0.2261	-0.1969	51.0	-0.0134	250.68	244.31
50594B2	0.00438	1589.918	1511.848	54161.43	87.556	-0.2261	-0.1969	54.0	-0.0046	247.73	244.31
50594B2	0.00438	1589.918	1511.848	54161.43	87.556	-0.2261	-0.1969	59.0	0.0100	244.54	244.31
50594B2	0.00438	1589.918	1511.848	54161.43	87.556	-0.2261	-0.1969	62.0	0.0188	242.51	244.31
50594B2	0.00438	1589.918	1511.848	54161.43	87.556	-0.2261	-0.1969	65.0	0.0275	238.52	244.31
50594B2	0.00438	1589.918	1511.848	54161.43	87.556	-0.2261	-0.1969	68.0	0.0363	236.00	244.31
50594B2	0.00438	1589.918	1511.848	54161.43	87.556	-0.2261	-0.1969	74.0	0.0539	229.30	244.31
51094B1	0.00438	1396.866	1500.932	63575.69	89.352	-0.0619	-0.0392	1.0	-0.0138	260.57	236.74
51094B1	0.00438	1396.866	1500.932	63575.69	89.352	-0.0619	-0.0392	2.5	-0.0104	263.66	236.74
51094B1	0.00438	1396.866	1500.932	63575.69	89.352	-0.0619	-0.0392	4.0	-0.0070	266.85	236.74
51094B1	0.00438	1396.866	1500.932	63575.69	89.352	-0.0619	-0.0392	5.5	-0.0037	262.06	236.74
51094B1	0.00438	1396.866	1500.932	63575.69	89.352	-0.0619	-0.0392	7.0	-0.0003	260.71	236.74
51094B1	0.00438	1396.866	1500.932	63575.69	89.352	-0.0619	-0.0392	9.0	0.0043	253.30	236.74
51094B1	0.00438	1396.866	1500.932	63575.69	89.352	-0.0619	-0.0392	11.0	0.0088	250.99	236.74
51094B1	0.00438	1396.866	1500.932	63575.69	89.352	-0.0619	-0.0392	13.0	0.0133	248.16	236.74
51094B1	0.00438	1396.866	1500.932	63575.69	89.352	-0.0619	-0.0392	15.0	0.0179	245.92	236.74
51094B1	0.00438	1396.866	1500.932	63575.69	89.352	-0.0619	-0.0392	17.0	0.0224	244.79	236.74
51094B1	0.00438	1396.866	1500.932	63575.69	89.352	-0.0619	-0.0392	19.0	0.0269	244.14	236.74
51094B1	0.00438	1396.866	1500.932	63575.69	89.352	-0.0619	-0.0392	21.0	0.0314	242.37	236.74
51094B1	0.00438	1396.866	1500.932	63575.69	89.352	-0.0619	-0.0392	24.0	0.0382	241.10	236.74
51094B1	0.00438	1396.866	1500.932	63575.69	89.352	-0.0619	-0.0392	27.0	0.0450	239.28	236.74
51094B1	0.00438	1396.866	1500.932	63575.69	89.352	-0.0619	-0.0392	30.0	0.0518	237.41	236.74
51094B1	0.00438	1396.866	1500.932	63575.69	89.352	-0.0619	-0.0392	33.0	0.0586	235.53	236.74
51094B1	0.00438	1396.866	1500.932	63575.69	89.352	-0.0619	-0.0392	36.0	0.0654	231.39	236.74
51094B1	0.00438	1396.866	1500.932	63575.69	89.352	-0.0619	-0.0392	39.0	0.0722	227.90	236.74
51094B1	0.00438	1396.866	1500.932	63575.69	89.352	-0.0619	-0.0392	42.0	0.0790	224.66	236.74
51094B1	0.00438	1396.866	1500.932	63575.69	89.352	-0.0619	-0.0392	45.0	0.0858	221.76	236.74
51094B1	0.00438	1396.866	1500.932	63575.69	89.352	-0.0619	-0.0392	48.0	0.0925	217.64	236.74
51094B1	0.00438	1396.866	1500.932	63575.69	89.352	-0.0619	-0.0392	51.0	0.0993	213.65	236.74
51094B1	0.00438	1396.866	1500.932	63575.69	89.352	-0.0619	-0.0392	54.0	0.1061	209.16	236.74
51094B1	0.00438	1396.866	1500.932	63575.69	89.352	-0.0619	-0.0392	59.0	0.1174	203.89	236.74

Table C.3 Inside Wall Temperature Data for Freon-22 (Cont'd)

RUN	D	P OUT	G	Q_n	HOTP POW	X_{in}	X_{pinch}	Z	X_{eq}	T_w	T_{sat}
	(m)	(kPa)	(kg/m².s)	(W/m²)	(W)			(cm)		(°C)	(°C)
51094B1	0.00438	1396.866	1500.932	63575.69	89.352	-0.0619	-0.0392	62.0	0.1242	200.92	236.74
51094B1	0.00438	1396.866	1500.932	63575.69	89.352	-0.0619	-0.0392	65.0	0.1310	196.51	236.74
51094B1	0.00438	1396.866	1500.932	63575.69	89.352	-0.0619	-0.0392	68.0	0.1378	193.66	236.74
51094B1	0.00438	1396.866	1500.932	63575.69	89.352	-0.0619	-0.0392	74.0	0.1514	186.71	236.74
51094B2	0.00438	1396.866	1504.850	59722.44	93.623	-0.0619	-0.0406	1.0	-0.0144	252.18	234.68
51094B2	0.00438	1396.866	1504.850	59722.44	93.623	-0.0619	-0.0406	2.5	-0.0112	254.92	234.68
51094B2	0.00438	1396.866	1504.850	59722.44	93.623	-0.0619	-0.0406	4.0	-0.0080	257.40	234.68
51094B2	0.00438	1396.866	1504.850	59722.44	93.623	-0.0619	-0.0406	5.5	-0.0048	252.65	234.68
51094B2	0.00438	1396.866	1504.850	59722.44	93.623	-0.0619	-0.0406	7.0	-0.0016	251.26	234.68
51094B2	0.00438	1396.866	1504.850	59722.44	93.623	-0.0619	-0.0406	9.0	0.0026	243.92	234.68
51094B2	0.00438	1396.866	1504.850	59722.44	93.623	-0.0619	-0.0406	11.0	0.0068	241.72	234.68
51094B2	0.00438	1396.866	1504.850	59722.44	93.623	-0.0619	-0.0406	13.0	0.0111	239.05	234.68
51094B2	0.00438	1396.866	1504.850	59722.44	93.623	-0.0619	-0.0406	15.0	0.0153	236.91	234.68
51094B2	0.00438	1396.866	1504.850	59722.44	93.623	-0.0619	-0.0406	17.0	0.0196	236.06	234.68
51094B2	0.00438	1396.866	1504.850	59722.44	93.623	-0.0619	-0.0406	19.0	0.0238	235.48	234.68
51094B2	0.00438	1396.866	1504.850	59722.44	93.623	-0.0619	-0.0406	21.0	0.0280	233.96	234.68
51094B2	0.00438	1396.866	1504.850	59722.44	93.623	-0.0619	-0.0406	24.0	0.0344	233.01	234.68
51094B2	0.00438	1396.866	1504.850	59722.44	93.623	-0.0619	-0.0406	27.0	0.0408	231.34	234.68
51094B2	0.00438	1396.866	1504.850	59722.44	93.623	-0.0619	-0.0406	30.0	0.0471	230.07	234.68
51094B2	0.00438	1396.866	1504.850	59722.44	93.623	-0.0619	-0.0406	33.0	0.0535	228.55	234.68
51094B2	0.00438	1396.866	1504.850	59722.44	93.623	-0.0619	-0.0406	36.0	0.0599	224.83	234.68
51094B2	0.00438	1396.866	1504.850	59722.44	93.623	-0.0619	-0.0406	39.0	0.0662	221.81	234.68
51094B2	0.00438	1396.866	1504.850	59722.44	93.623	-0.0619	-0.0406	42.0	0.0726	218.96	234.68
51094B2	0.00438	1396.866	1504.850	59722.44	93.623	-0.0619	-0.0406	45.0	0.0789	216.41	234.68
51094B2	0.00438	1396.866	1504.850	59722.44	93.623	-0.0619	-0.0406	48.0	0.0853	212.67	234.68
51094B2	0.00438	1396.866	1504.850	59722.44	93.623	-0.0619	-0.0406	51.0	0.0917	209.08	234.68
51094B2	0.00438	1396.866	1504.850	59722.44	93.623	-0.0619	-0.0406	54.0	0.0980	204.92	234.68
51094B2	0.00438	1396.866	1504.850	59722.44	93.623	-0.0619	-0.0406	59.0	0.1086	200.15	234.68
51094B2	0.00438	1396.866	1504.850	59722.44	93.623	-0.0619	-0.0406	62.0	0.1150	197.40	234.68
51094B2	0.00438	1396.866	1504.850	59722.44	93.623	-0.0619	-0.0406	65.0	0.1214	193.31	234.68
51094B2	0.00438	1396.866	1504.850	59722.44	93.623	-0.0619	-0.0406	68.0	0.1277	190.67	234.68
51094B2	0.00438	1396.866	1504.850	59722.44	93.623	-0.0619	-0.0406	74.0	0.1404	184.23	234.68
51094B3	0.00438	1396.866	1505.060	51482.11	95.276	-0.0619	-0.0436	1.0	-0.0172	234.89	235.48
51094B3	0.00438	1396.866	1505.060	51482.11	95.276	-0.0619	-0.0436	2.5	-0.0144	235.56	235.48
51094B3	0.00438	1396.866	1505.060	51482.11	95.276	-0.0619	-0.0436	4.0	-0.0117	236.57	235.48
51094B3	0.00438	1396.866	1505.060	51482.11	95.276	-0.0619	-0.0436	5.5	-0.0089	231.42	235.48
51094B3	0.00438	1396.866	1505.060	51482.11	95.276	-0.0619	-0.0436	7.0	-0.0062	230.12	235.48
51094B3	0.00438	1396.866	1505.060	51482.11	95.276	-0.0619	-0.0436	9.0	-0.0025	223.04	235.48
51094B3	0.00438	1396.866	1505.060	51482.11	95.276	-0.0619	-0.0436	11.0	0.0011	220.86	235.48
51094B3	0.00438	1396.866	1505.060	51482.11	95.276	-0.0619	-0.0436	13.0	0.0048	218.54	235.48
51094B3	0.00438	1396.866	1505.060	51482.11	95.276	-0.0619	-0.0436	15.0	0.0084	216.82	235.48
51094B3	0.00438	1396.866	1505.060	51482.11	95.276	-0.0619	-0.0436	17.0	0.0121	216.15	235.48
51094B3	0.00438	1396.866	1505.060	51482.11	95.276	-0.0619	-0.0436	19.0	0.0157	215.85	235.48
51094B3	0.00438	1396.866	1505.060	51482.11	95.276	-0.0619	-0.0436	21.0	0.0194	214.62	235.48
51094B3	0.00438	1396.866	1505.060	51482.11	95.276	-0.0619	-0.0436	24.0	0.0249	214.47	235.48
51094B3	0.00438	1396.866	1505.060	51482.11	95.276	-0.0619	-0.0436	27.0	0.0304	213.47	235.48
51094B3	0.00438	1396.866	1505.060	51482.11	95.276	-0.0619	-0.0436	30.0	0.0358	212.92	235.48
51094B3	0.00438	1396.866	1505.060	51482.11	95.276	-0.0619	-0.0436	33.0	0.0413	211.95	235.48
51094B3	0.00438	1396.866	1505.060	51482.11	95.276	-0.0619	-0.0436	36.0	0.0468	209.06	235.48
51094B3	0.00438	1396.866	1505.060	51482.11	95.276	-0.0619	-0.0436	39.0	0.0523	206.84	235.48
51094B3	0.00438	1396.866	1505.060	51482.11	95.276	-0.0619	-0.0436	42.0	0.0578	204.99	235.48
51094B3	0.00438	1396.866	1505.060	51482.11	95.276	-0.0619	-0.0436	45.0	0.0633	203.21	235.48
51094B3	0.00438	1396.866	1505.060	51482.11	95.276	-0.0619	-0.0436	48.0	0.0687	200.25	235.48
51094B3	0.00438	1396.866	1505.060	51482.11	95.276	-0.0619	-0.0436	51.0	0.0742	197.53	235.48
51094B3	0.00438	1396.866	1505.060	51482.11	95.276	-0.0619	-0.0436	54.0	0.0797	194.21	235.48
51094B3	0.00438	1396.866	1505.060	51482.11	95.276	-0.0619	-0.0436	59.0	0.0889	190.43	235.48
51094B3	0.00438	1396.866	1505.060	51482.11	95.276	-0.0619	-0.0436	62.0	0.0943	188.32	235.48
51094B3	0.00438	1396.866	1505.060	51482.11	95.276	-0.0619	-0.0436	65.0	0.0998	184.85	235.48
51094B3	0.00438	1396.866	1505.060	51482.11	95.276	-0.0619	-0.0436	68.0	0.1053	182.73	235.48
51094B3	0.00438	1396.866	1505.060	51482.11	95.276	-0.0619	-0.0436	74.0	0.1163	177.11	235.48
51094B4	0.00438	1396.866	1504.396	44576.68	95.919	-0.0619	-0.0460	1.0	-0.0197	219.22	236.25
51094B4	0.00438	1396.866	1504.396	44576.68	95.919	-0.0619	-0.0460	2.5	-0.0173	217.51	236.25
51094B4	0.00438	1396.866	1504.396	44576.68	95.919	-0.0619	-0.0460	4.0	-0.0149	217.51	236.25
51094B4	0.00438	1396.866	1504.396	44576.68	95.919	-0.0619	-0.0460	5.5	-0.0126	212.02	236.25
51094B4	0.00438	1396.866	1504.396	44576.68	95.919	-0.0619	-0.0460	7.0	-0.0102	210.63	236.25
51094B4	0.00438	1396.866	1504.396	44576.68	95.919	-0.0619	-0.0460	9.0	-0.0070	203.61	236.25
51094B4	0.00438	1396.866	1504.396	44576.68	95.919	-0.0619	-0.0460	11.0	-0.0038	201.52	236.25
51094B4	0.00438	1396.866	1504.396	44576.68	95.919	-0.0619	-0.0460	13.0	-0.0007	199.33	236.25
51094B4	0.00438	1396.866	1504.396	44576.68	95.919	-0.0619	-0.0460	15.0	0.0025	197.84	236.25
51094B4	0.00438	1396.866	1504.396	44576.68	95.919	-0.0619	-0.0460	17.0	0.0057	197.49	236.25
51094B4	0.00438	1396.866	1504.396	44576.68	95.919	-0.0619	-0.0460	19.0	0.0088	197.55	236.25
51094B4	0.00438	1396.866	1504.396	44576.68	95.919	-0.0619	-0.0460	21.0	0.0120	196.69	236.25
51094B4	0.00438	1396.866	1504.396	44576.68	95.919	-0.0619	-0.0460	24.0	0.0167	197.09	236.25
51094B4	0.00438	1396.866	1504.396	44576.68	95.919	-0.0619	-0.0460	27.0	0.0215	196.18	236.25
51094B4	0.00438	1396.866	1504.396	44576.68	95.919	-0.0619	-0.0460	30.0	0.0262	196.60	236.25
51094B4	0.00438	1396.866	1504.396	44576.68	95.919	-0.0619	-0.0460	33.0	0.0310	195.90	236.25
51094B4	0.00438	1396.866	1504.396	44576.68	95.919	-0.0619	-0.0460	36.0	0.0357	193.79	236.25
51094B4	0.00438	1396.866	1504.396	44576.68	95.919	-0.0619	-0.0460	39.0	0.0405	192.11	236.25
51094B4	0.00438	1396.866	1504.396	44576.68	95.919	-0.0619	-0.0460	42.0	0.0452	190.91	236.25
51094B4	0.00438	1396.866	1504.396	44576.68	95.919	-0.0619	-0.0460	45.0	0.0500	189.88	236.25
51094B4	0.00438	1396.866	1504.396	44576.68	95.919	-0.0619	-0.0460	48.0	0.0547	187.71	236.25
51094B4	0.00438	1396.866	1504.396	44576.68	95.919	-0.0619	-0.0460	51.0	0.0595	185.58	236.25
51094B4	0.00438	1396.866	1504.396	44576.68	95.919	-0.0619	-0.0460	54.0	0.0642	183.05	236.25
51094B4	0.00438	1396.866	1504.396	44576.68	95.919	-0.0619	-0.0460	59.0	0.0722	180.16	236.25

Table C.3 Inside Wall Temperature Data for Freon-22 (Cont'd)

RUN	D	P OUT	G	Q_w	HOTP POW	X_{in}	X_{out}	Z	X_{eq}	T_w	T_{sat}
	(m)	(kPa)	(kg/m².s)	(W/m²)	(W)			(cm)		(°C)	(°C)
51094B4	0.00438	1396.866	1504.396	44576.68	95.919	-0.0619	-0.0460	62.0	0.0769	178.58	236.25
51094B4	0.00438	1396.866	1504.396	44576.68	95.919	-0.0619	-0.0460	65.0	0.0817	175.63	236.25
51094B4	0.00438	1396.866	1504.396	44576.68	95.919	-0.0619	-0.0460	68.0	0.0864	173.90	236.25
51094B4	0.00438	1396.866	1504.396	44576.68	95.919	-0.0619	-0.0460	74.0	0.0959	169.35	236.25
51094B5	0.00438	1396.866	1509.781	39338.96	96.003	-0.0619	-0.0479	1.0	-0.0218	206.53	235.83
51094B5	0.00438	1396.866	1509.781	39338.96	96.003	-0.0619	-0.0479	2.5	-0.0198	202.93	235.83
51094B5	0.00438	1396.866	1509.781	39338.96	96.003	-0.0619	-0.0479	4.0	-0.0177	202.24	235.83
51094B5	0.00438	1396.866	1509.781	39338.96	96.003	-0.0619	-0.0479	5.5	-0.0156	196.24	235.83
51094B5	0.00438	1396.866	1509.781	39338.96	96.003	-0.0619	-0.0479	7.0	-0.0135	195.21	235.83
51094B5	0.00438	1396.866	1509.781	39338.96	96.003	-0.0619	-0.0479	9.0	-0.0107	188.25	235.83
51094B5	0.00438	1396.866	1509.781	39338.96	96.003	-0.0619	-0.0479	11.0	-0.0079	186.20	235.83
51094B5	0.00438	1396.866	1509.781	39338.96	96.003	-0.0619	-0.0479	13.0	-0.0051	183.99	235.83
51094B5	0.00438	1396.866	1509.781	39338.96	96.003	-0.0619	-0.0479	15.0	-0.0024	182.61	235.83
51094B5	0.00438	1396.866	1509.781	39338.96	96.003	-0.0619	-0.0479	17.0	0.0004	182.25	235.83
51094B5	0.00438	1396.866	1509.781	39338.96	96.003	-0.0619	-0.0479	19.0	0.0032	182.30	235.83
51094B5	0.00438	1396.866	1509.781	39338.96	96.003	-0.0619	-0.0479	21.0	0.0060	181.64	235.83
51094B5	0.00438	1396.866	1509.781	39338.96	96.003	-0.0619	-0.0479	24.0	0.0102	182.31	235.83
51094B5	0.00438	1396.866	1509.781	39338.96	96.003	-0.0619	-0.0479	27.0	0.0144	181.36	235.83
51094B5	0.00438	1396.866	1509.781	39338.96	96.003	-0.0619	-0.0479	30.0	0.0185	182.68	235.83
51094B5	0.00438	1396.866	1509.781	39338.96	96.003	-0.0619	-0.0479	33.0	0.0227	182.38	235.83
51094B5	0.00438	1396.866	1509.781	39338.96	96.003	-0.0619	-0.0479	36.0	0.0269	180.84	235.83
51094B5	0.00438	1396.866	1509.781	39338.96	96.003	-0.0619	-0.0479	39.0	0.0311	179.63	235.83
51094B5	0.00438	1396.866	1509.781	39338.96	96.003	-0.0619	-0.0479	42.0	0.0352	178.91	235.83
51094B5	0.00438	1396.866	1509.781	39338.96	96.003	-0.0619	-0.0479	45.0	0.0394	178.20	235.83
51094B5	0.00438	1396.866	1509.781	39338.96	96.003	-0.0619	-0.0479	48.0	0.0436	176.46	235.83
51094B5	0.00438	1396.866	1509.781	39338.96	96.003	-0.0619	-0.0479	51.0	0.0478	174.94	235.83
51094B5	0.00438	1396.866	1509.781	39338.96	96.003	-0.0619	-0.0479	54.0	0.0520	172.85	235.83
51094B5	0.00438	1396.866	1509.781	39338.96	96.003	-0.0619	-0.0479	59.0	0.0589	170.69	235.83
51094B5	0.00438	1396.866	1509.781	39338.96	96.003	-0.0619	-0.0479	62.0	0.0631	169.47	235.83
51094B5	0.00438	1396.866	1509.781	39338.96	96.003	-0.0619	-0.0479	65.0	0.0673	167.09	235.83
51094B5	0.00438	1396.866	1509.781	39338.96	96.003	-0.0619	-0.0479	68.0	0.0714	165.72	235.83
51094B5	0.00438	1396.866	1509.781	39338.96	96.003	-0.0619	-0.0479	74.0	0.0798	161.98	235.83
51094B6	0.00438	1396.866	1511.428	32920.40	95.935	-0.0619	-0.0502	1.0	-0.0244	188.65	231.62
51094B6	0.00438	1396.866	1511.428	32920.40	95.935	-0.0619	-0.0502	2.5	-0.0227	182.70	231.62
51094B6	0.00438	1396.866	1511.428	32920.40	95.935	-0.0619	-0.0502	4.0	-0.0209	181.55	231.62
51094B6	0.00438	1396.866	1511.428	32920.40	95.935	-0.0619	-0.0502	5.5	-0.0192	174.78	231.62
51094B6	0.00438	1396.866	1511.428	32920.40	95.935	-0.0619	-0.0502	7.0	-0.0174	174.39	231.62
51094B6	0.00438	1396.866	1511.428	32920.40	95.935	-0.0619	-0.0502	9.0	-0.0151	167.84	231.62
51094B6	0.00438	1396.866	1511.428	32920.40	95.935	-0.0619	-0.0502	11.0	-0.0128	165.95	231.62
51094B6	0.00438	1396.866	1511.428	32920.40	95.935	-0.0619	-0.0502	13.0	-0.0104	163.65	231.62
51094B6	0.00438	1396.866	1511.428	32920.40	95.935	-0.0619	-0.0502	15.0	-0.0081	162.12	231.62
51094B6	0.00438	1396.866	1511.428	32920.40	95.935	-0.0619	-0.0502	17.0	-0.0058	161.63	231.62
51094B6	0.00438	1396.866	1511.428	32920.40	95.935	-0.0619	-0.0502	19.0	-0.0035	161.53	231.62
51094B6	0.00438	1396.866	1511.428	32920.40	95.935	-0.0619	-0.0502	21.0	-0.0011	160.87	231.62
51094B6	0.00438	1396.866	1511.428	32920.40	95.935	-0.0619	-0.0502	24.0	0.0024	161.73	231.62
51094B6	0.00438	1396.866	1511.428	32920.40	95.935	-0.0619	-0.0502	27.0	0.0059	160.97	231.62
51094B6	0.00438	1396.866	1511.428	32920.40	95.935	-0.0619	-0.0502	30.0	0.0094	162.88	231.62
51094B6	0.00438	1396.866	1511.428	32920.40	95.935	-0.0619	-0.0502	33.0	0.0128	163.02	231.62
51094B6	0.00438	1396.866	1511.428	32920.40	95.935	-0.0619	-0.0502	36.0	0.0163	162.05	231.62
51094B6	0.00438	1396.866	1511.428	32920.40	95.935	-0.0619	-0.0502	39.0	0.0198	161.53	231.62
51094B6	0.00438	1396.866	1511.428	32920.40	95.935	-0.0619	-0.0502	42.0	0.0233	161.32	231.62
51094B6	0.00438	1396.866	1511.428	32920.40	95.935	-0.0619	-0.0502	45.0	0.0268	161.00	231.62
51094B6	0.00438	1396.866	1511.428	32920.40	95.935	-0.0619	-0.0502	48.0	0.0303	159.88	231.62
51094B6	0.00438	1396.866	1511.428	32920.40	95.935	-0.0619	-0.0502	51.0	0.0338	158.98	231.62
51094B6	0.00438	1396.866	1511.428	32920.40	95.935	-0.0619	-0.0502	54.0	0.0373	157.56	231.62
51094B6	0.00438	1396.866	1511.428	32920.40	95.935	-0.0619	-0.0502	59.0	0.0431	156.18	231.62
51094B6	0.00438	1396.866	1511.428	32920.40	95.935	-0.0619	-0.0502	62.0	0.0466	155.51	231.62
51094B6	0.00438	1396.866	1511.428	32920.40	95.935	-0.0619	-0.0502	65.0	0.0501	153.68	231.62
51094B6	0.00438	1396.866	1511.428	32920.40	95.935	-0.0619	-0.0502	68.0	0.0536	152.88	231.62
51094B6	0.00438	1396.866	1511.428	32920.40	95.935	-0.0619	-0.0502	74.0	0.0606	150.01	231.62
51094C1	0.00438	1396.866	2013.488	65819.54	111.093	-0.0444	-0.0230	1.0	-0.0212	257.20	236.41
51094C1	0.00438	1396.866	2013.488	65819.54	111.093	-0.0444	-0.0230	2.5	-0.0186	264.21	236.41
51094C1	0.00438	1396.866	2013.488	65819.54	111.093	-0.0444	-0.0230	4.0	-0.0160	269.93	236.41
51094C1	0.00438	1396.866	2013.488	65819.54	111.093	-0.0444	-0.0230	5.5	-0.0134	265.42	236.41
51094C1	0.00438	1396.866	2013.488	65819.54	111.093	-0.0444	-0.0230	7.0	-0.0107	265.86	236.41
51094C1	0.00438	1396.866	2013.488	65819.54	111.093	-0.0444	-0.0230	9.0	-0.0072	258.80	236.41
51094C1	0.00438	1396.866	2013.488	65819.54	111.093	-0.0444	-0.0230	11.0	-0.0037	254.96	236.41
51094C1	0.00438	1396.866	2013.488	65819.54	111.093	-0.0444	-0.0230	13.0	-0.0003	249.90	236.41
51094C1	0.00438	1396.866	2013.488	65819.54	111.093	-0.0444	-0.0230	15.0	0.0032	245.38	236.41
51094C1	0.00438	1396.866	2013.488	65819.54	111.093	-0.0444	-0.0230	17.0	0.0067	242.21	236.41
51094C1	0.00438	1396.866	2013.488	65819.54	111.093	-0.0444	-0.0230	19.0	0.0102	239.59	236.41
51094C1	0.00438	1396.866	2013.488	65819.54	111.093	-0.0444	-0.0230	21.0	0.0137	236.29	236.41
51094C1	0.00438	1396.866	2013.488	65819.54	111.093	-0.0444	-0.0230	24.0	0.0190	233.75	236.41
. . .	. . .	. . .	. . .	. . .	. . .	. . .	. . .	. .	. . .	. . .	. . .
. . .	. . .	. . .	. . .	. . .	. . .	. . .	. . .	. .	. . .	. . .	. . .
. . .	. . .	. . .	. . .	. . .	. . .	. . .	. . .	. .	. . .	. . .	. . .
. . .	. . .	. . .	. . .	. . .	. . .	. . .	. . .	. .	. . .	. . .	. . .
. . .	. . .	. . .	. . .	. . .	. . .	. . .	. . .	. .	. . .	. . .	. . .
. . .	. . .	. . .	. . .	. . .	. . .	. . .	. . .	. .	. . .	. . .	. . .
. . .	. . .	. . .	. . .	. . .	. . .	. . .	. . .	. .	. . .	. . .	. . .
. . .	. . .	. . .	. . .	. . .	. . .	. . .	. . .	. .	. . .	. . .	. . .
. . .	. . .	. . .	. . .	. . .	. . .	. . .	. . .	. .	. . .	. . .	. . .
. . .	. . .	. . .	. . .	. . .	. . .	. . .	. . .	. .	. . .	. . .	. . .

Table C.3 Inside Wall Temperature Data for Freon-22 (Concluded)

RUN	D	P OUT	G	Q_w	HOTP POW	X_{in}	X_{out}	Z	X_{eq}	T_w	T_{sat}
	(m)	(kPa)	(kg/m².s)	(W/m²)	(W)			(cm)		(°C)	(°C)
51094E6	0.00438	1396.866	3027.558	57165.59	165.089	-0.0518	-0.0306	51.0	0.0209	181.77	242.72
51094E6	0.00438	1396.866	3027.558	57165.59	165.089	-0.0518	-0.0306	54.0	0.0239	179.42	242.72
51094E6	0.00438	1396.866	3027.558	57165.59	165.089	-0.0518	-0.0306	59.0	0.0289	176.56	242.72
51094E6	0.00438	1396.866	3027.558	57165.59	165.089	-0.0518	-0.0306	62.0	0.0320	174.98	242.72
51094E6	0.00438	1396.866	3027.558	57165.59	165.089	-0.0518	-0.0306	65.0	0.0350	171.99	242.72
51094E6	0.00438	1396.866	3027.558	57165.59	165.089	-0.0518	-0.0306	68.0	0.0380	170.55	242.72
51094E6	0.00438	1396.866	3027.558	57165.59	165.089	-0.0518	-0.0306	74.0	0.0441	165.27	242.72
51094E7	0.00438	1396.866	3026.886	51903.07	166.496	-0.0527	-0.0313	1.0	-0.0304	178.22	240.48
51094E7	0.00438	1396.866	3026.886	51903.07	166.496	-0.0527	-0.0313	2.5	-0.0290	182.33	240.48
51094E7	0.00438	1396.866	3026.886	51903.07	166.496	-0.0527	-0.0313	4.0	-0.0277	193.30	240.48
51094E7	0.00438	1396.866	3026.886	51903.07	166.496	-0.0527	-0.0313	5.5	-0.0263	196.78	240.48
51094E7	0.00438	1396.866	3026.886	51903.07	166.496	-0.0527	-0.0313	7.0	-0.0249	204.33	240.48
51094E7	0.00438	1396.866	3026.886	51903.07	166.496	-0.0527	-0.0313	9.0	-0.0231	204.95	240.48
51094E7	0.00438	1396.866	3026.886	51903.07	166.496	-0.0527	-0.0313	11.0	-0.0213	206.97	240.48
51094E7	0.00438	1396.866	3026.886	51903.07	166.496	-0.0527	-0.0313	13.0	-0.0194	204.81	240.48
51094E7	0.00438	1396.866	3026.886	51903.07	166.496	-0.0527	-0.0313	15.0	-0.0176	202.45	240.48
51094E7	0.00438	1396.866	3026.886	51903.07	166.496	-0.0527	-0.0313	17.0	-0.0158	200.05	240.48
51094E7	0.00438	1396.866	3026.886	51903.07	166.496	-0.0527	-0.0313	19.0	-0.0139	197.40	240.48
51094E7	0.00438	1396.866	3026.886	51903.07	166.496	-0.0527	-0.0313	21.0	-0.0121	193.08	240.48
51094E7	0.00438	1396.866	3026.886	51903.07	166.496	-0.0527	-0.0313	24.0	-0.0093	189.39	240.48
51094E7	0.00438	1396.866	3026.886	51903.07	166.496	-0.0527	-0.0313	27.0	-0.0066	186.03	240.48
51094E7	0.00438	1396.866	3026.886	51903.07	166.496	-0.0527	-0.0313	30.0	-0.0038	184.25	240.48
51094E7	0.00438	1396.866	3026.886	51903.07	166.496	-0.0527	-0.0313	33.0	-0.0011	182.21	240.48
51094E7	0.00438	1396.866	3026.886	51903.07	166.496	-0.0527	-0.0313	36.0	0.0017	179.80	240.48
51094E7	0.00438	1396.866	3026.886	51903.07	166.496	-0.0527	-0.0313	39.0	0.0044	178.28	240.48
51094E7	0.00438	1396.866	3026.886	51903.07	166.496	-0.0527	-0.0313	42.0	0.0072	177.66	240.48
51094E7	0.00438	1396.866	3026.886	51903.07	166.496	-0.0527	-0.0313	45.0	0.0099	176.88	240.48
51094E7	0.00438	1396.866	3026.886	51903.07	166.496	-0.0527	-0.0313	48.0	0.0127	175.44	240.48
51094E7	0.00438	1396.866	3026.886	51903.07	166.496	-0.0527	-0.0313	51.0	0.0154	174.02	240.48
51094E7	0.00438	1396.866	3026.886	51903.07	166.496	-0.0527	-0.0313	54.0	0.0182	172.11	240.48
51094E7	0.00438	1396.866	3026.886	51903.07	166.496	-0.0527	-0.0313	59.0	0.0227	169.93	240.48
51094E7	0.00438	1396.866	3026.886	51903.07	166.496	-0.0527	-0.0313	62.0	0.0255	168.77	240.48
51094E7	0.00438	1396.866	3026.886	51903.07	166.496	-0.0527	-0.0313	65.0	0.0282	166.19	240.48
51094E7	0.00438	1396.866	3026.886	51903.07	166.496	-0.0527	-0.0313	68.0	0.0310	165.17	240.48
51094E7	0.00438	1396.866	3026.886	51903.07	166.496	-0.0527	-0.0313	74.0	0.0365	160.66	240.48
51094E8	0.00438	1396.866	3033.412	46993.12	167.376	-0.0536	-0.0321	1.0	-0.0313	166.53	239.70
51094E8	0.00438	1396.866	3033.412	46993.12	167.376	-0.0536	-0.0321	2.5	-0.0301	168.45	239.70
51094E8	0.00438	1396.866	3033.412	46993.12	167.376	-0.0536	-0.0321	4.0	-0.0288	179.04	239.70
51094E8	0.00438	1396.866	3033.412	46993.12	167.376	-0.0536	-0.0321	5.5	-0.0276	182.13	239.70
51094E8	0.00438	1396.866	3033.412	46993.12	167.376	-0.0536	-0.0321	7.0	-0.0264	189.77	239.70
51094E8	0.00438	1396.866	3033.412	46993.12	167.376	-0.0536	-0.0321	9.0	-0.0247	191.03	239.70
51094E8	0.00438	1396.866	3033.412	46993.12	167.376	-0.0536	-0.0321	11.0	-0.0230	193.43	239.70
51094E8	0.00438	1396.866	3033.412	46993.12	167.376	-0.0536	-0.0321	13.0	-0.0214	191.84	239.70
51094E8	0.00438	1396.866	3033.412	46993.12	167.376	-0.0536	-0.0321	15.0	-0.0197	190.04	239.70
51094E8	0.00438	1396.866	3033.412	46993.12	167.376	-0.0536	-0.0321	17.0	-0.0181	188.15	239.70
51094E8	0.00438	1396.866	3033.412	46993.12	167.376	-0.0536	-0.0321	19.0	-0.0164	185.96	239.70
51094E8	0.00438	1396.866	3033.412	46993.12	167.376	-0.0536	-0.0321	21.0	-0.0148	182.15	239.70
51094E8	0.00438	1396.866	3033.412	46993.12	167.376	-0.0536	-0.0321	24.0	-0.0123	178.84	239.70
51094E8	0.00438	1396.866	3033.412	46993.12	167.376	-0.0536	-0.0321	27.0	-0.0098	175.41	239.70
51094E8	0.00438	1396.866	3033.412	46993.12	167.376	-0.0536	-0.0321	30.0	-0.0073	174.04	239.70
51094E8	0.00438	1396.866	3033.412	46993.12	167.376	-0.0536	-0.0321	33.0	-0.0048	172.15	239.70
51094E8	0.00438	1396.866	3033.412	46993.12	167.376	-0.0536	-0.0321	36.0	-0.0023	169.93	239.70
51094E8	0.00438	1396.866	3033.412	46993.12	167.376	-0.0536	-0.0321	39.0	0.0001	168.63	239.70
51094E8	0.00438	1396.866	3033.412	46993.12	167.376	-0.0536	-0.0321	42.0	0.0026	168.22	239.70
51094E8	0.00438	1396.866	3033.412	46993.12	167.376	-0.0536	-0.0321	45.0	0.0051	167.69	239.70
51094E8	0.00438	1396.866	3033.412	46993.12	167.376	-0.0536	-0.0321	48.0	0.0076	166.53	239.70
51094E8	0.00438	1396.866	3033.412	46993.12	167.376	-0.0536	-0.0321	51.0	0.0101	165.44	239.70
51094E8	0.00438	1396.866	3033.412	46993.12	167.376	-0.0536	-0.0321	54.0	0.0126	163.96	239.70
51094E8	0.00438	1396.866	3033.412	46993.12	167.376	-0.0536	-0.0321	59.0	0.0167	162.31	239.70
51094E8	0.00438	1396.866	3033.412	46993.12	167.376	-0.0536	-0.0321	62.0	0.0192	161.50	239.70
51094E8	0.00438	1396.866	3033.412	46993.12	167.376	-0.0536	-0.0321	65.0	0.0217	159.41	239.70
51094E8	0.00438	1396.866	3033.412	46993.12	167.376	-0.0536	-0.0321	68.0	0.0241	158.79	239.70
51094E8	0.00438	1396.866	3033.412	46993.12	167.376	-0.0536	-0.0321	74.0	0.0291	155.03	239.70

APPENDIX D FLUID PROPERTIES

This appendix presents the equations of the thermophysical properties employed in the property subroutines used in the present study. A computer property code, known as the UO code, was originally developed by Wong et al. [1990] for the prediction of the thermophysical properties of nonpolar fluids as a function of pressure and temperature. Since then, several revised versions of the code have been presented by this author et al. [1990, 1991, 1992, 1993a, 1993b].

The UO code predicts the properties for subcooled and saturated liquid and for saturated and superheated vapour. It uses simple equations to calculate fluid properties. The equations were chosen based on accuracy and simplicity. Each fluid of interest requires 21 constants for property evaluation. A list of such constants for 24 fluids is given in a data block. The list of the 24 fluids is presented in Table D.1, with their properties and computer code names listed in Table D.2.

To improve the prediction accuracy of the properties, some special codes (each special code contains many subprograms) are used. In the property code, the general code will first predict the properties based on input pressure (in kPa) and temperature (in °C). If the special code is also available for the same pressure and temperature, its prediction will replace that of the general code. Note that the special code is normally valid over narrower ranges of pressure and temperature.

The subprograms from the special codes, which are listed in Table D.3, come from various sources. The subprograms of Freon-12 are based on AECL's saturated Freon-12 code. The saturated property prediction equations for Freon-12 suitable for direct application are given in section D.1.

The subprograms of Freon-22 come from Hammouda et al. [1993b]. The property equations for Freon-22 suitable for direct application are presented in section D.2. The subprograms for Freon-134a [Tain, 1994] and water [Cheng and Nguyen, 1989] have been added recently. Note that the special code for Freon-134a only covers saturation properties. The property equations for Freon-134a suitable for direct application are given in section D.3.

D.1 Prediction for Freon-12

D.1.1 General

This section presents property equations for Freon-12 suitable for direct application. All these equations were correlated based on experimental data. Comparison of property predictions with data showed excellent agreement.

D.1.2 Equations for Freon-12

Properties at saturation state evaluated at given pressure, P, in psia.

Saturation temperature, T_{Sat}, in deg. F:

For $0.13798 \le P < 1.428$ psia (i.e., for $-152 \le T_{Sat} < -100$ deg. F):

$$T_{sat} = -176.263522614+P*(237.462921795+P*(-548.622683 678+P*(857.994126381+P*(-783.548641145+P*(377.5 08914902+P*(-73.8224707068))))))) \quad (D.1.1)$$

For $1.428 \le P < 11.999$ psia (i.e., for $-100 \le T_{Sat} < -30$ deg. F):

$$T_{Sat} = -142.954546734+P*(47.5915844277+P*(-17.8888115563 +P*(5.11021247291+P*(-0.97166793420 9+P*(0.11888900 229+P*(-8.95297916875*10^{-3}+P*(3.76356147704*10^{-4}+ P*(-6.74342777188*10^{-6})))))))) \quad (D.1.2)$$

For $11.999 \le P < 24.878$ psia (i.e., $-30 \le T_{Sat} < +20$ deg. F):

$$T_{Sat} = -92.7194787086+P*(7.85524442314+P*(-0.292384879075 +P*(6.95535302851*10^{-3}+P*(-7.00611732877*10^{-5})))) \quad \text{(D.1.3)}$$

For $24.878 \le P < 596.9$ psia (i.e., $20 \le T_{Sat} < 233.6$ deg. F):

$$T_{Sat} = -74.478213270+P*(4.9712143458+P*(-0.117963337711 +P*(2.33173933938*10^{-3}+P*(-3.35718303592*10^{-5}+ P*(3.49759386133*10^{-7}+P*(-2.64902090007*10^{-9}+P* (1.45735440830*10^{-11}+P*(-5.73540235865*10^{-14}+P* (1.53590443102*10^{-16}+P*(-2.33869100104*10^{-19}+P* (-2.40821607020*10^{-23}+P*(1.09481805154*10^{-24}+P* (-2.88734550572*10^{-27}+P*(4.16893939433*10^{-30}+P* (-3.65200076898*10^{-33}+P*(1.82778030481*10^{-36}+P* (-4.03446488348*10^{-40})))))))))))))))) \quad \text{(D.1.4)}$$

Saturated vapour density, ρ_g, in lb/ft^3:

$\rho_g = 1/v_g$

For $0.13799 \le P < 4.6139$ psia

$$v_g = 28/(3.77105107327*10^{-3}+P*(1.04176772388+P*(-0.37 3597959077+P*(0.579576771419+P*(-0.689987638743+P* (0.571928414136+P*(-0.325790743895+P*(0.126598786965 +P*(-0.0328896654168+P*(5.45257110029*10^{-3}+P*(-5.205 66217067*10^{-4}+P*(2.17404531850*10^{-5})))))))))) \quad \text{(D.1.5)}$$

For $4.6139 \le P < 599.6$ psia

$v_g =$ 28/(0.172763727605+P*(0.806426878669+P*(-7.157899
09373*10^{-3}+P*(2.62147759713*10^{-4}+P*(-6.88012584993
10^{-6}+P(1.28714755264*10^{-7}+P*(-1.73216357935*10^{-9}+
P*(1.70640147556*10^{-11}+P*(-1.24862295869*10^{-13}+P*
(6.8525331818268*10^{-16}+P*(-2.83302783541*10^{-18}+P*(
8.81145121352*10^{-21}+P*(-2.04503250164*10^{-23}+P*(3.48
102465857*10^{-26}+P*(-4.21220414110*10^{-29}+P*(3.42590
693940*10^{-32}+P*(-1.67743692232*10^{-35}+P*(3.733593764
28*10^{-39})))))))))))))))))) (D.1.6)

Saturated liquid density, ρ_f, in lb/ft^3:

For 0.13798 ≤ P < 6.19 psia

$\rho_f =$ 106.280318974+P*(-16.4217111170+P*(31.3091640919
+P*(-43.2640254469+P*(39.8820117805+P*(-25.0402351683
+P*(10.9826065154+P*(-3.42740736768+P*(0.768489261471
+P*(-0.123836710572+P*(0.0141864828679+P*(-1.12526
499869*10^{-3}+P*(5.86478749173*10^{-5}+P*(-1.80395931054
10^{-6}+P(2.47813340279*10^{-8})))))))))))))) (D.1.7)

For 6.19 ≤ P < 7.12 psia

$\rho_f =$ -0.50537664*(P-6.19)+96.086 (D.1.8)

For 7.12 ≤ P < 8.15 psia

$\rho_f =$ -0.461165049*(P-7.12)+95.616 (D.1.9)

For 8.15 ≤ P < 9.31 psia

$\rho_f =$ -0.413793103*(P-8.15)+95.141 (D.1.10)

For $9.31 \leq P < 10.59$ psia

$\rho_f =$ -0.37734375*(P-9.31)+94.661 (D.1.11)

For $10.59 \leq P < 12.0$ psia

$\rho_f =$ -0.346099291*(P-10.59)+94.178 (D.1.12)

For $12.0 \leq P < 112.85$ psia

$\rho_f =$ $1.27404928207*10^{-6}+P*(44.1899469527+P*(-9.090050$
$16705+P*(1.10640504984+P*(-0.0902071398492+P*(5.24$
$426005297*10^{-3}+P*(-2.25626791621*10^{-4}+P*(7.35359$
$934779*10^{-6}+P*(-1.84191563468*10^{-7}+P*(-5.37901438$
$240*10^{-11}+P*(6.25954740104*10^{-13}+P*(-5.57166656983*$
$10^{-15}+P*(3.71992320136*10^{-17}+P*(-1.80178722859*10^{-19}$
$+P*(5.97455512510*10^{-22}+P*(-1.21254259664*10^{-24}+$
$P*(1.13546000013*10^{-27}))))))))))))))))$ (D.1.13)

For $112.85 \leq P < 499.53$ psia

$\rho_f =$ $155.305869416+P*(-3.18375337234+P*(0.0655269135950$
$+P*(-8.16089413159*10^{-4}+P*(6.62551439091*10^{-6}+P*$
$(-3.66845838498*10^{-8}+P*(1.41230158780*10^{-10}+P*(-3.78$
$102978635*10^{-13}+P*(6.90293115835*10^{-16}+P*(-8.1925709$
$0230*10^{-19}+P*(5.69519082318*10^{-22}+P*(-1.75901054$
$409*10^{-25}))))))))))$ (D.1.14)

For $499.53 \leq P < 524.43$ psia

$$\rho_f = -0.089879518*(P-499.53)+54.908 \quad \text{(D.1.15)}$$

For $524.43 \leq P < 550.26$ psia

$$\rho_f = -0.108478513*(P-524.43)+52.67 \quad \text{(D.1.16)}$$

For $550.26 \leq P < 577.03$ psia

$$\rho_f = -0.153828913*(P-550.26)+49.868 \quad \text{(D.1.17)}$$

For $577.03 \leq P < 596.9$ psia

$$\rho_f = -0.549068948*(P-577.03)+45.75 \quad \text{(D.1.18)}$$

Saturated enthalpy of liquid, H_f, in Btu/lb:

For $0.13798 \leq P < 6.1874$ psia

$$H_f = -28.0014797151+P*(48.0814955383+P*(-114.047211707 +P*(198.721187457+P*(-234.490500010+P*(190.374555 781+P*(-108.674681103+P*(44.3252652847+P*(-13.023 5037422+P*(2.75443940397+P*(-0.414499420791+P*(0.0 432026773050+P*(-2.95859557113*10^-3+P*(1.1953108 7209*10^-4+P*(-2.15549805628*10^-6)))))))))))) \quad \text{(D.1.19)}$$

For $6.1874 \leq P < 7.1168$ psia

$$H_f = 1.126102862*(P-6.1874)-3.1477 \quad \text{(D.1.20)}$$

For $7.1168 \leq P < 8.154$ psia

$$H_f = 1.01156961*(P-7.1168)-2.1011 \quad \text{(D.1.21)}$$

For $8.154 \leq P < 9.3076$ psia

$H_f =$ 0.911841193*(P-8.154)-1.0519 (D.1.22)

For $9.3076 \leq P < 122.7$ psia

$H_f =$ -1.13167334348*10^-5+P*(-3.62522639648+P*(1.025977
34821+P*(-0.128136246969+P*(0.0100347449575+P*(-5.4
0169189446*10^-4+P*(2.09346992313*10^-5+P*(-6.002473
29108*10^-7+P*(1.29374223809*10^-8+P*(-2.11235020751
10^-10+P(2.61373414672*10^-12+P*(-2.43307707556*10^-14
+P*(1.67518275292*10^-16+P*(-8.26761806537*10^-19+P
*(2.76465698794*10^-21+P*(-5.60779245574*10^-24+P*
(5.20734379678*10^-27)))))))))))))))) (D.1.23)

For $122.7 \leq P < 577.6$ psia

$H_f =$ 41.3981095624+P*(-1.14023578681+P*(0.0231970262353
+P*(-2.23213745055*10^-4+P*(1.23029176847*10^-6+P*(
-3.61392785512*10^-9+P*(1.70067619699*10^-12+P*(2.9
3164028946*10^-14+P*(-1.23520100058*10^-16+P*(2.558
61661620*10^-19+P*(-3.05711161193*10^-22+P*(2.013781
75655*10^-25+P*(-5.68596985575*10^-29)))))))))))) (D.1.24)

For $577.6 \leq P < 596.9$ psia

$H_f =$ 0.300301963*(P-577.03)+72.893 (D.1.25)

Saturated enthalpy of vapour, H_g, in Btu/lb:

For $0.13798 \leq P < 2.4371$ psia

$H_g =$ 57.8788395419+P*(28.4905272162+P*(-82.4027673779+

P*(180.284189681+P*(-268.474549375+P*(271.713433642

+P*(-187.775189384+P*(88.2508653095+P*(-27.6497911

973+P*(5.51074961042+P*(-0.630400778420+P*(0.0314

402100777)))))))))) (D.1.26)

For $2.4371 \leq P < 2.8807$ psia

$H_g =$ 1.253381425*(P-2.4371)+67.911 (D.1.27)

For $2.8807 \leq P < 3.3879$ psia

$H_g =$ 1.096214511*(P-2.8807)+68.467 (D.1.28)

For $3.3879 \leq P < 3.9651$ psia

$H_g =$ 0.965003465*(P-3.3879)+69.023 (D.1.29)

For $3.9651 \leq P < 26.4831$ psia

$H_g =$ -13.7654027517+P*(110.666316597+P*(-68.9836961733+

P*(26.2771330037+P*(-6.78185302553+P*(1.25687412567

+P*(-0.173151609295+P*(0.0181063406891+P*(-1.45405

167773*10^{-3}+P*(9.00762979012*10^{-5}+P*(-4.29500488317

10^{-6}+P(1.56142314932*10^{-7}+P*(-4.24721565013*10^{-9}

+P*(8.36459338876*10^{-11}+P*(-1.12590215007*10^{-12}+P

*(9.26246942795*10^{-15}+P*(,-3.51140463941

*10^{-17})))))))))))))))) (D.1.30)

For $26.4831 \leq P < 100.36$ psia

$H_g =$ 68.5986374649+P*(0.607114097508+P*(-0.0153106504501

$$+P*(2.76789032964*10^{-4}+P*(-3.03608668810*10^{-6}+P*$$

$$(1.80375348525*10^{-8}+P*(-4.44104801657*10^{-11}))))) \quad \text{(D.1.31)}$$

For $100.36 \leq P < 368.11$ psia

$$H_g = 74.5518451586+P*(0.181784956782+P*(-1.09198802529*$$

$$10^{-3}+P*(4.60114805776*10^{-6}+P*(-1.23054826672*10^{-8}+P*$$

$$(1.81839587497*10^{-11}+P*(-1.14047681262*10^{-14}))))) \quad \text{(D.1.32)}$$

For $368.11 \leq P < 596.9$ psia

$$H_g = -5.18585141540*10^{5}+P*(9.08187740769*10^{3}+P*(-69.346$$

$$5178504+P*(0.301598859586+P*(-8.17172316322*10^{-4}+P*$$

$$(1.41248628461*10^{-6}+P*(-1.52108009242*10^{-9}+P*(9.330658$$

$$75679*10^{-13}+P*(-2.49630448664*10^{-16})))))) \quad \text{(D.1.33)}$$

Properties at saturation state evaluated at given temperature, T, in deg. F.

Saturation pressure, P_{Sat}, in psia:

For $-152.0 \leq T < 233.6$ deg. F

$$P_{Sat} = 23.8474771675+T*(0.505686173058+T*(4.13244154148*10^{-3}$$

$$+T*(1.50071838344*10^{-5}+T*(8.45884908379*10^{-9}+T*(-9$$

$$.42046493402*10^{-11}+T*(2.03848722652*10^{-12}+T*(1.39$$

$$469997838*10^{-14}+T*(-2.89934189203*10^{-16}+T*(-1.2641$$

$$7218264*10^{-18}+T*(2.30886481481*10^{-20}+T*(5.3250345$$

$$1183*10^{-23}+T*(-1.04296231671*10^{-24}+T*(-5.776341566$$

$$21*10^{-28}+T*(2.51897200970*10^{-29}+T*(-2.26791951857*$$

$$10^{-32}+T*(-2.53161813616*10^{-34}+T*(5.20591913666*$$

10^{-37})))))))))))))))))) (D.1.34)

Saturated density of vapour, ρ_g, in lb/ft^3:

For $-152.0 \leq T < 233.6$ deg. F

$\rho_g = 1/v_g$

$v_g =$ 1.60889392619+T*(-0.0320420932480+T*(3.91933021908*10^{-4}+T*(-3.80288857908*10^{-6}+T*(3.18684351762*10^{-8}+T*(-2.32066367608*10^{-10}+T*(1.49588321844*10^{-12}+T*(-1.12014214107*10^{-14}+T*(9.22629175633*10^{-17}+T*(-3.39923358647*10^{-19}+T*(-1.34216492763*10^{-21}+T*(-4.0087165557*10^{-24}+T*(2.75174964776*10^{-25}+T*(-1.31568921132*10^{-27}+T*(-4.65047535478*10^{-30}+T*(4.33281845259*10^{-32}+T*(3.93283836837*10^{-35}+T*(-1.10327737869*10^{-36}+T*(3.50987135310*10^{-39}+T*(-3.64256288634*10^{-42})))))))))))))))))))) (D.1.35)

Saturated density of liquid, ρ_f, in lb/ft^3:

For $-152.0 \leq T < 180.0$ deg.

$\rho_f =$ 90.6588224624+T*(-0.104176422903+T*(-1.11704093841*10^{-4}+T*(-2.40358880585*10^{-7}+T*(-5.71568355488*10^{-10}+T*(-2.64964231015*10^{-12}+T*(-1.84311238669*10^{-14}+T*(2.07742029206*10^{-17}+T*(4.03211496283*10^{-19}+T*(-1.51782291547*10^{-21}+T*(-9.14638823988*10^{-24}))))))))))) (D.1.36)

For $180.0 \leq T < 233.6$ deg. F

$$\rho_f = -3.48162947673*10^{8}+T*(1.37215635520*10^{7}+T*(-2.36358786709*10^{5}+T*(2.32418856010*10^{3}+T*(-14.2699035937+T*(0.0560172111850+T*(-1.37300989848*10^{-4}+T*(1.92114728274*10^{-7}+T*(-1.17489732796*10^{-10}))))))) \quad (D.1.37)$$

Saturated enthalpy of liquid, H_f, in Btu/lb:

For $-152.0 \leq T < 128.0$ deg. F

$$H_f = 8.52073270945+T*(0.215604069050+T*(7.07513161682*10^{-5}+T*(1.83175468158*10^{-7}+T*(9.00221153814*10^{-10}+T*(3.82386287*10^{-12}+T*(-2.80330584345*10^{-15}+T*(1.25842080396*10^{-17}+T*(1.46184758115*10^{-19}))))))) \quad (D.1.38)$$

For $128.0 \leq T < 233.6$ deg. F

$$H_f = 7.67424370353*10^{6}+T*(-4.52529819*10^{5}+T*(1.19526354931*10^{4}+T*(-186.219709674+T*(1.89516884165+T*(-0.0131646473516+T*(6.32138370499*10^{-5}+T*(-2.07192400564*10^{-7}+T*(4.43644301266*10^{-10}+T*(5.60402145588*10^{-13}+T*(3.17135606571*10^{-16})))))))))) \quad (D.1.39)$$

Saturated enthalpy of vapour, H_g, in Btu/lb:

For $-152.0 \leq T < 185.0$ deg. F

$$H_g = 77.2698402307+T*(0.106906015628+T*(-5.992179296900*10^{-5}+T*(-2.43333530471*10^{-7}+T*(-2.41688211436*10^{-10}+$$

$T*(-7.01771241246*10^{-12}+T*(-6.23759758832*10^{-15}+T*$

$(1.77314230978*10^{-16}+T*(-1.65473748681*10^{-19}+T*(-3$

$.54604965071*10^{-21}))))))))$ (D.1.40)

For $185.0 \leq T < 233.6$ deg. F

$H_g =$ $3.55379815382*10^{7}+T*(-1.21030434948*10^{6}+T*(1.7649$

$3429831*10^{4}+T*(-142.856094962+T*(0.693154890464+T$

$*(-2.01615823079*10^{-3}+T*(3.25506617470*10^{-6}+T*(-2.$

$25026610183*10^{-9}))))))$ (D.1.41)

Saturated viscosity of liquid, μ_f, in Btu/(ft*hr):

$\mu_f =$ $(-1.8908E-03)*T + 0.6713.$ (D.1.42)

valid within the temperature range 60 to 160 deg. F.

To convert the British units into the international system of units, the following coefficients have to be applied:

$P\ [kPa] = P\ [psia] * 6.8947,$ (D.1.43)

$T\ [C] = 5/9 * (T\ [deg.F] - 32),$ (D.1.44)

$v\ [m^3/kg] = v\ [ft^3/lb] * 0.0624298,$ (D.1.45)

$\rho\ [kg/m^3] = \rho\ [lb/ft^3] * 16.018,$ (D.1.46)

$H\ [kJ/kg] = H\ [Btu/lb] * 2.326,$ (D.1.47)

$\mu\ [kg/(ms)] = \mu\ [lb/(ft*hr)] * 4.1338*10^{-4}.$ (D.1.48)

D.2 Prediction for Freon-22

D.2.1 General

Property predictions of Freon-22 are based on available semi-empirical equations from the

literature, theoretical relations based on an equation of state and the correlations curve fitted to the data. Specifically, the saturation properties of Freon-22 are approximated by semi-empirical equations and correlations curve fitted to the available data. Freon-22 properties at the subcooled liquid state are approximated by the saturation properties at the same temperature, except for the density and the viscosity, where semi-empirical equations are employed instead. Adachi et al.'s [1983] equation of state is chosen for the prediction of the thermodynamic properties of Freon-22 at the superheated vapour state.

D.2.2 Equations for Freon-22

Equation of state:

$$P=\frac{8314.3T}{86.469x10^{6}\ v-50.6275}-\frac{0.86557[1+0.69737(1-T_r^{1/2})]^2}{(86.469v-22.9230x10^{-6})(86.469v+113.858x10^{-6})} \qquad \text{(D.2.1)}$$

where

P is in MPa, T in degree kelvin and v in m^3/kg

$T_r=T/T_c$

$T_c=369.33$ K

Saturation pressure and temperature, P_{sat}, in MPa, T_{sat}, in kelvin:

$$P_{sat}=4.99\exp(5.92714-6.09648\,T_r^{-1}-1.28862\,lnT_r+0.16934\,T_r^{6} +0.221\,(15.2518-15.6875\,T_r^{-1}-13.4721\,lnT_r+0.43577\,T_r^{6}) \qquad \text{(D.2.2)}$$

The saturation temperature, T_{sat}, in Eq. (D.2.2) is expressed implicitly, hence for a given pressure an iteration process is required to find T_{sat}.

Saturated liquid density, ρ_f, in kg/m^3:

$$\rho_f = 513\,[1.869358\,\tau^{1/3} + 0.555972\,\tau^{2/3} + 0.3563298\,\tau^{5/3}] + 513 \qquad \textbf{(D.2.3)}$$

where

$$\tau = 1 - T/T_c$$

Subcooled liquid density, ρ_l, in kg/m^3:

$$\rho_l = \frac{1}{v_l} \qquad \textbf{(D.2.4)}$$

$$v_l = 1.8931\,x10^{-3} V_R^{(o)} [1 - f V_R^{(\delta)}] \left(1 - c \ln \frac{\beta + P}{\beta + P_{vp}} \right) \qquad \textbf{(D.2.5)}$$

For $0.25 < T_r < 0.95$

$$V_R^{(0)} = 1 + g\,\tau^{1/3} + h\,\tau^{2/3} + i\,\tau + j\,\tau^{4/3} \qquad \textbf{(D.2.6)}$$

For $0.25 < T_r < 1.0$

$$V_R^{(\delta)} = \frac{k + l T_r + m T_r^2 + n T_r^3}{(T_r - 1.00001)} \qquad \textbf{(D.2.7)}$$

with

$$\beta = 4.97[-1 + a(1-T_r)^{1/3} + b(1-T_r)^{2/3} + d(1-T_r) + e(1-T_r)^{4/3}]$$

$$P_{vp} = 4.97 \exp\{(1-\tau)^{-1}[-6.99913\tau + 1.23014\tau^{1.5} - 2.49377\tau^3 - 2.21052\tau^6]\}$$

a=-9.070217 b=62.45326 c=0.093779 d=-135.1102 e=135.28026

f=0.2215 g=-1.52816 h=1.43907

i=-0.81446 j=0.190454 k=-0.296123 l=0.386914

m=-0.0427258 n=-0.0480645.

Saturated vapour density, ρ_g, in kg/m^3:

$\rho_g = 1/v$

v is obtained from Eq. (D.2.1) by iteration.

Saturated liquid specific enthalpy, h_f, in J/kg:

a) Temperature correlations

For $232 \leq T \leq 273$ K

$$h_f = (-264.151 + 1.132128\ T) \times 10^3 \qquad \text{(D.2.8)}$$

For $273 \leq T \leq 358$ K

$$h_f = (45.564322 \exp(0.005428\ T) - 154.65) \times 10^3 \qquad \text{(D.2.9)}$$

For $358 \leq T \leq 369$ K

$$h_f = (13.206339 \exp(0.008888\ T) - 154.65) \times 10^3 \qquad \text{(D.2.10)}$$

b) Pressure correlations

For $0.1 \leq P \leq 2$ MPa

$$h_f = (-17.3039 + 197.2856\ P - 186.2100\ P^2 + 99.0557\ P^3 - 19.7531\ P^4) \times 10^3 \qquad \text{(D.2.11)}$$

For $2 \leq P \leq 4.5$ MPa

$$h_f = (57.26080 + 26.93866\ P) \times 10^3 \qquad \text{(D.2.12)}$$

Subcooled liquid specific enthalpy, h_f, in J/kg:

The specific enthalpy of the subcooled liquid state is approximated by the temperature correlations of the saturated liquid specific enthalpy at the same temperature.

Latent heat of vaporization, h_{fg}, in J/kg:

a) Temperature correlations

For $232 \leq T \leq 291$ K

$$h_{fg} = (245.0076 + 516.176 \times 10^{-3}\, T - 2.430 \times 10^{-3}\, T^2) \times 10^3 \qquad \text{(D.2.13)}$$

For $291 \leq T \leq 328$ K

$$h_{fg} = (1099.006 - 7.42441\, T + 0.018397\, T^2 - 4.28 \times 10^{-8}\, T^4) \times 10^3 \qquad \text{(D.2.14)}$$

For $328 \leq T \leq 365$ K

$$h_{fg} = (25715.06 - 201.455\, T + 0.448554\, T^2 - 6.694 \times 10^{-7}\, T^4) \times 10^3 \qquad \text{(D.2.15)}$$

b) Pressure correlations

For $0.1 \leq P \leq 1.0$ MPa

$$h_{fg} = (247.3175 - 156.9500\, P + 232.6786\, P^2 - 219.1150\, P^3 + 80.2338\, P^4) \times 10^3 \qquad \text{(D.2.16)}$$

For $1.0 \leq P \leq 4.0$ MPa

$$h_{fg} = (224.4585 - 47.1949\, P + 7.6643\, P^2 - 1.0791\, P^3) \times 10^3 \qquad \text{(D.2.17)}$$

For $4.0 \leq P \leq 4.9$ MPa

$$h_{fg} = (-11719.700 + 11154.770\, P - 3934.670\, P^2 + 616.1727\, P^3 - 36.2908\, P^4) \times 10^3 \qquad \text{(D.2.18)}$$

Superheated vapour specific enthalpy, h_v, J/kg:

$$h_v=[(h_p-h^\circ)_T-(h_{Pref}-h^\circ)_{Tref}]/M+\int_{T_{ref}}^{T} C_p^\circ dT+h_{fg,ref} \qquad \text{(D.2.19)}$$

$$\frac{(h-h^\circ)_T}{RT_c}=(Z-1)T_r+\frac{1}{(B_2+B_3)}\left[A(T_r)-T_r\frac{dA(T_r)}{dT_r}\right]\ln\left[\frac{Z-B_2P_r/T_r}{Z+B_3P_r/T_r}\right] \qquad \text{(D.2.20)}$$

with

$B_2 = 0.03725$

$B_3 = 0.18502$

$A(T_r) = 0.45806[1 + 0.69737(1 - T_r^{1/2})]^2$

$Z = (PV)/(10^6RT)$

$M = 86.469$

$h_{fg,ref}(J/kg) = RT_c(Z_g - Z_f)/M[6.09648 - 1.28862\,T_r + 1.016082\,T_r^7$

$+ 0.221(15.6875 - 13.4721\,T_r + 2.61462\,T_r^7)]$

$P_{ref}(MPa) = P_c \exp[5.92714-6.09648/T_r -1.28862\ln(T_r) +0.169347T_r^6$

$+0.221(15.2518 - 15.6875/T_r -13.4721\ln(T_r)$

$+0.43577T_r)]$

$Z_g = (P_{ref}V_g)/(10^6RT_{ref})$

$Z_f = (P_{ref}V_f)/(10^6RT_{ref})$

$C_p^\circ(J/kg.K) = 200.07 + 1.8711\,T - 1.35308\times10^{-3}\,T^2$

$+ 3.53652\times10^{-7}\,T^3$

Saturated liquid specific heat, C_{pf}, in J/kg.K:

For 120 ≤ T ≤ 260 K

$$C_{P_f} = 1117.82 + 1.34991\,x10^{-1}\,T - 8.07980\,x10^{-3}\,T^2 + 3.03989\,x10^{-5}\,T^3 \qquad \textbf{(D.2.21)}$$

For 260 ≤ T ≤ 350 K

$$C_{P_f} = -14044.5 + 163.93\,T - 5.96758\,x10^{-1}\,T^2 + 7.34454\,x10^{-4}\,T^3 \qquad \textbf{(D.2.22)}$$

Subcooled liquid specific heat:

The specific heat of the subcooled liquid is approximated by the saturated liquid equations at the same temperature.

Saturated vapour specific heat, C_{pg}, in J/kg.K:

For 200 ≤ T ≤ 340 K

$$C_{P_g} = -6769.23 + 87.4138\,x10^{-2}\,T - 3.52504\,x10^{-1}\,T^2 + 4.86108\,x10^{-4}\,T^3 \qquad \textbf{(D.2.23)}$$

For T<200 K or T>340 K, the superheated vapour specific heat equation (Eq. (D.2.24)) can be used to evaluate C_{pg}.

Superheated vapour specific heat, C_{pv}, in J/kg.K:

$$C_{P_v} - C_p^{\circ} = -\frac{1}{(b_2+b_3)} T \frac{d^2a(T)}{dT^2} \ln\left(\frac{V-b_2}{V+b_3}\right) - R + D\left[\frac{RT}{V-b_1} - T\frac{da(T)}{dT}\frac{1}{(V-b_2)(V+b_3)}\right] \qquad \textbf{(D.2.24)}$$

where

$a(T) = 0.86557x10^{-6}[1+0.69737(1 - T_r^{1/2})]^2$

$b_1 = 50.6275x10^{-6}$

$b_2 = 22.9230x10^{-6}$

b_3 = 113.858x10^{-6}

V=86.469v

v is the specific volume in m^3/kg

$$D=\frac{\frac{R}{V-b_1}-\frac{da(T)}{dT}\left(\frac{1}{(V-b_2)(V+b_3)}\right)}{\frac{RT}{(V-b_1)^2}-\frac{a(T)}{(b_2+b_3)}\left(\frac{1}{(V-b_2)^2}-\frac{1}{(V+b_3)^2}\right)} \qquad \textbf{(D.2.25)}$$

and

Saturated liquid viscosity, μ_f, in N.s/m^2:

For 170 ≤ T ≤ 310 K

$$\mu_f\,(10^{-3}N.s/m^2)=\exp(-3.39554+532.855/T) \qquad \textbf{(D.2.26)}$$

For 310 ≤ T ≤ 360 K

$$\mu_f\,(10^{-3}N.s/m^2)=-1.65108+1.24147\,x10^{-2}\,T-2.09286\,x10^{-5}\,T^2 \qquad \textbf{(D.2.27)}$$

Subcooled liquid viscosity, μ_l, in N.s/m^2:

For 0.9≤ P ≤6.0 MPa and 283≤ T ≤363 K

$$\mu_l=1.2277401\quad\exp(-0.10893/T_r)(P_r)^{0.064329}\,\mu_f \qquad \textbf{(D.2.28)}$$

Saturated and superheated vapour viscosity:

For 230≤ T ≤350 K

$$\mu_g\ (10^{-3} N.s/m^2) = -0.031501 + 4.20115\ x10^{-4}\ T - 1.50840\ x10^{-6}\ T^2 + 2.02506\ x10^{-9}\ T^3 \qquad \textbf{(D.2.29)}$$

For T >350 K or T < 230 K and $P_r < (-0.125+0.1875T_r)$

$$\mu^o_{(g,v)}(10^{-7}\ N.s/m^2) = [4.610\ T_r^{0.618} - 2.04\ \exp(-0.449\ T_r) + 1.94\ \exp(-4.058\ T_r) + 0.1]/\xi \qquad \textbf{(D.2.30)}$$

where

$$\xi = 0.217 T_c^{1/6} M^{-1/2} P_c^{-2/3}$$

For T >350 K and T < 230 K and $P_r > (-0.125+0.1875T_r)$

$$\mu_{(g,v)} = ([1.0230 + 0.23364\ \rho_r + 0.58533\ \rho_r^2 - 0.40758\ \rho_r^3 + 0.093324\ \rho_r^4]^4 - 1)/\xi + \mu^o_{(g,v)} \qquad \textbf{(D.2.31)}$$

where

$\mu_{(g,v)}$ is in micropoise ($=10^{-7}$ N.s/m^2).

Saturated liquid thermal conductivity, k_f, in W/m.K:

For $144 \leq T \leq 350$ K

$$k_f = 0.23531 - 0.000495\ T \qquad \textbf{(D.2.32)}$$

Subcooled liquid thermal conductivity:

The liquid thermal conductivity of the subcooled state is approximated by the saturated liquid thermal conductivity at the same temperature.

Saturated and superheated vapour thermal conductivity, k_g, in W/m.K, $k_{(g,v)}$, in W/m.k:

For $225 \leq T \leq 325$K

$$k_g(W/m.K) = -0.007605 + 6.2306 \times 10^{-5} T \quad \textbf{(D.2.33)}$$

For T >325 K or T < 225 K and $P_r < (-0.125+0.1875T_r)$

$$k^{\circ}_{(g,v)} = (C_p{}^{\circ} + 120.19)\mu^{\circ}_{(g,v)} \quad \textbf{(D.2.34)}$$

with

$$C_p{}^{\circ} = 0.20007 + 1.8711 \times 10^{-3} T - 1.35308 \times 10^{-6} T^2 + 3.53652 \times 10^{-10} T^3$$

and $\mu^{\circ}_{(g,v)}$ is given by Eq. (E.2.30)

For T >325 K or T < 225 K and $P_r > (-0.125+0.1875T_r)$:

for $\rho_r < 0.5$

$$k_{(g,v)} = 2.287 \times 10^{-2}[\exp(0.535\,\rho_r) - 1] + k^{\circ}_{(g,v)} \quad \textbf{(D.2.35)}$$

for $0.5 < \rho_r < 2.0$

$$k_{(g,v)} = 2.137 \times 10^{-2}[\exp(0.67\,\rho_r) - 1.069] + k^{\circ}_{(g,v)} \quad \textbf{(D.2.36)}$$

for $2.0 < \rho_r < 2.8$

$$k_{(g,v)} = 4.873 \times 10^{-3}[\exp(1.155\,\rho_r) + 2.016] + k^{\circ}_{(g,v)} \quad \textbf{(D.2.37)}$$

where

$\rho_r = \rho_{(g,v)} / \rho_c$

$\rho_c = 513$ kg/m^3

Surface tension, σ, in N/m:

$$\sigma = B(\sigma_o)^*(1-T_r)^n \qquad \textbf{(D.2.38)}$$

where

$(\sigma_o)^* = 12.35$

B= 5.024×10^{-3} (N/m)

n= 1.249

D.3 Prediction for Freon-134a

D.3.1 General

This section presents the saturation property equations for Freon-134a suitable for direct application. All these equations were correlated based on the data of McLinden et al. [1989] and Diller et al. [1991].

D.3.2 Equations for Freon-134a

Critical temperature, T_c, in °C:

$$T_c = 101.15\,°C \qquad \textbf{(D.3.1)}$$

Saturation Pressure, P_{sat}, in kPa:

for $-40 \le T \le 100$ °C

$$P_{sat} = 292.1935 + 10.62572\,T + 0.15203\,T^2 + 0.00087\,T^3 - 4.8597 \times 10^{-7}\,T^4 + 2.7245 \times 10^{-8}\,T^5 \qquad \textbf{(D.3.2)}$$

Saturation temperature, T_{sat}, in °C:

for $52 \le P \le 3971$ kPa

$$T_{sat} = -84.9841 - 0.01335\ P + 14.19546\ P^{1/2} - 240.661\ P^{1/3} + 744.1678\ P^{1/4} - 524.819\ P^{1/5} \quad \textbf{(D.3.3)}$$

Saturated liquid density, ρ_f, in kg/m^3:

for -40 ≤ T ≤ 100°C

$$\rho_f = 1535.119 + 47.58204\ TN + 0.445156\ TN^2 - 108.87\ TN^{2/3} - 3.34549\ TN^{5/3} - 1.0823 \times 10^{-8}\ TN^5 \quad \textbf{(D.3.4)}$$

where

$$TN = T + 45 \quad \textbf{(D.3.5)}$$

Saturated vapour density, ρ_g, in kg/m^3:

for -40 ≤ T ≤ 100°C

$$\rho_g = 515.3 \times e^{a_1} \quad \textbf{(D.3.6)}$$

with

$$a_1 = -3.47966\ TA^{0.34} + 9.34904\ TA^{2/3} - 0.40186\ TA + 28.09001\ TA^{4/3} + 31.91004 \ln\left(\frac{T + 273.15}{T_c + 273.15}\right) \quad \textbf{(D.3.7)}$$

and

$$TA = 1 - \frac{T + 273.15}{T_c + 273.15} \quad \textbf{(D.3.8)}$$

Saturated liquid enthalpy, h_f, in J/kg:

for -40 ≤ T ≤ 100°C

$$h_f = (48.8174 + 1.319583\ T + 0.003524\ T^2 - 4.8\times10^{-6} T^3 - 6.4045\times10^{-7} T^4 + 7.08406\times10^{-9} T^5)\times 1000 \quad \textbf{(D.3.9)}$$

Saturated vapour enthalpy, h_g, in J/kg:

for $-40 \le T < 50$°C

$$h_g = (247.7652 + 0.585009\ T - 0.00089\ T^2 - 9.6373\times10^{-6} T^3 - 1.0605\times10^{-7} T^4)\times 1000 \quad \textbf{(D.3.10)}$$

for $50 \le T \le 100$°C

$$h_g = (-73.5242 + 19.95118\ T - 0.43351\ T^2 + 0.004245\ T^3 - 1.57109\times10^{-5} T^4)\times 1000 \quad \textbf{(D.3.11)}$$

Latent heat of Vaporization, h_{fg}, in J/kg:

$$h_{fg} = h_g - h_f \quad \textbf{(D.3.12)}$$

Saturated liquid specific heat, Cp_f, in J/kg/°C:

for $-40 \le T \le 50$°C

$$C_{p_f} = (1.32009 + 0.004544\ T - 4.5971\times10^{-6} T^2 + 1.7032\times10^{-7} T^3 + 3.6307\times10^{-9} T^4)\times 1000 \quad \textbf{(D.3.13)}$$

for $50 < T \le 100$°C

$$C_{p_f} = (1.429998 + 1.95723\times10^{-43} e^{T} + 7.436\times10^{-9} e^{T/5} - 6.4739\times10^{-5} e^{T/10} + 0.012937\ e^{T/20})\times 1000 \quad \textbf{(D.3.14)}$$

Saturated vapour specific heat, Cp_g, in J/kg/°C:

for $-40 \le T \le 60$°C

$$C_{p_g} = (0.889972 + 0.00439\ T + 1.9844 \times 10^{-5} T^2 + 2.863 \times 10^{-7} T^3 + 5.9531 \times 10^{-9} T^4) \times 1000 \quad \textbf{(D.3.15)}$$

for $60 < T \leq 100°C$

$$C_{p_g} = (1.000027 + 2.6644 \times 10^{-43} e^{T} + 9.355 \times 10^{-9} e^{T/5} - 3.2555 \times 10^{-5} e^{T/10} + 0.01902\ e^{T/20}) \times 1000 \quad \textbf{(D.3.16)}$$

Surface tension, σ, in N/m:

for $-40 \leq T < 30°C$

$$\sigma = 0.011714 - 0.00014\ T + 1.4393 \times 10^{-7} T^2 - 4.2338 \times 10^{-10} T^3 + 1.4501 \times 10^{-11} T^4 \quad \textbf{(D.3.17)}$$

for $30 < T \leq 65°C$

$$\sigma = 0.012621 - 0.00021\ T + 1.8878 \times 10^{-6} T^2 - 1.8913 \times 10^{-8} T^3 + 8.4796 \times 10^{-11} T^4 \quad \textbf{(D.3.18)}$$

for $65 < T \leq 100°C$

$$\sigma = -0.007457 + 0.000663\ T - 1.1996 \times 10^{-5} T^2 + 7.6262 \times 10^{-8} T^3 - 1.5151 \times 10^{-10} T^4 \quad \textbf{(D.3.19)}$$

Saturated liquid viscosity, μ_f, in kg/m/s:

for $-22.2 \leq T \leq 70.15°C$

$$\mu_f = \frac{e^{\left[-3.3528 + \frac{714.25}{T + 273.15} - 0.0019969(T + 273.15)\right]}}{1000} \quad \textbf{(D.3.20)}$$

Table D.1 List of 24 Fluids

Computer Code	Name	Chemical Formula
ISUB = 1	Water	H_2O
ISUB = 2	R-11	CCl_3F
ISUB = 3	R-12	CCl_2F_2
ISUB = 4	R-13	$CClF_3$
ISUB = 5	R-21	$CHCl_2F$
ISUB = 6	R-22	$CHClF_2$
ISUB = 7	R-113	$C_2Cl_3F_3$
ISUB = 8	R-114	$C_2Cl_2F_4$
ISUB = 9	R-115	C_2ClF_5
ISUB = 10	Carbon Dioxide	CO_2
ISUB = 11	Benzene	C_6H_6
ISUB = 12	Ammonia	NH_3
ISUB = 13	Methanol	CH_4O
ISUB = 14	Isopropanol	C_3H_8O
ISUB = 15	Acetone	C_3H_6O
ISUB = 16	Ethanol	C_2H_6O
ISUB = 17	Hydrazine	N_2H_4
ISUB = 18	Oxygen	O_2
ISUB = 19	R-152a	$C_2H_4F_2$
ISUB = 20	R-134a	CH_2FCF_3
ISUB = 21	Nitrogen	N_2
ISUB = 22	R-123	$CHCl_2CF_3$
ISUB = 23	R-142b	$C_2H_3ClF_2$
ISUB = 24	C318	C_4F_8 (CYCLIC)

Table D.2 List of Properties and Their Computer Code Names

Specific Volume	v_f(VF)	v_g(VG)	v_l(VL)	v_v(VL)
Density	ρ_f(RHOF)	ρ_g(RHOG)	ρ_l(RHOL)	ρ_v(RHOL)
Specific Enthalpy	h_f(HF)	h_g(HG)	h_l(HL)	h_v(HL)
Specific Heat	Cp_f(CPF)	Cp_g(CPG)	Cp_l(CPL)	Cp_v(CPL)
Viscosity	μ_f(UF)	μ_g(UG)	μ_l(UL)	μ_v(UL)
Thermal Conductivity	k_f(AKF)	k_g(AKG)	k_l(AKL)	k_v(AKL)
Prandtl Number	Pr_f(PRF)	Pr_g(PRG)	Pr_f(PRL)	Pr_v(PRL)
Latent heat, Pressure, Temperature	h_{fg}(HFG)	P_{sat}(PSAT)	T_{sat}(TSAT)	
Critical Pressure, Critical Temperature	P_c(PC)	T_c(TC)		
Specific Entropy	s_f(SF)	s_g(SG)	s_l(SL)	s_v(SL)
Surface Tension, Latent entropy	σ(SIGMA)	s_{fg}(SFG)		

Table D.3 List of Subprograms

Subprogram names	Predicted Properties
R-12 Subprograms	VG, RHOF, HF, HG, UF, PSAT and TSAT
R-22 Subprograms	VF, VL, RHOF, RHOL, HF, HL, CPF, CPG, CPL, UF, UG, UL, AKF, AKG, AKL, HFG and SIGMA
R-123 Subprograms	RHOF, RHOG, HF, HG, CPF, CPG, UF, HFG, PSAT, TSAT and SIGMA
R-134a Subprograms	RHOF, RHOG, HF, HG, CPF, CPG, UF, HFG, PSAT, TSAT and SIGMA
Water Subprograms	VF, VG, VL, RHOF, RHOG, RHOL, HF, HG, HL, CPF, CPL, UF, UG, UL, AKF, AKL, PRF, PRG, PRL, HFG, PSAT, TSAT and SIGMA